Copyright is owned by the Author of the thesis. Permission is given for a copy to be downloaded by an individual for the purpose of research and private study only. The thesis may not be reproduced elsewhere without the permission of the Author.

Investigating HDAC4 aggregation in a *Drosophila* model of neuronal development

A dissertation presented in partial fulfilment of the requirements for the degree of

Doctor of Philosophy
in
Biochemistry

at Massey University, Manawatū, New Zealand

Hannah Rose Hawley
2024

Parts of the work conducted in this thesis have been included in the following publications:

Hawley, H. R., Roberts, C. J., & Fitzsimons, H. L. (2023). Comparison of neuronal GAL4 drivers along with the AGES (auxin-inducible gene expression system) and TARGET (temporal and regional gene expression targeting) systems for fine tuning of neuronal gene expression in *Drosophila*. *MicroPublication Biology*, *2023*. https://doi.org/10.17912/micropub.biology.000885

Tan, W. J., **Hawley, H. R.**, Wilson, S. J., & Fitzsimons, H. L. (2024). Deciphering the roles of subcellular distribution and interactions involving the MEF2 binding region, the ankyrin repeat binding motif and the catalytic site of HDAC4 in *Drosophila* neuronal morphogenesis. *BMC Biology, 22*(1), 2. https://doi.org/10.1186/s12915-023-01800-1

Where this data is presented, the appropriate acknowledgement of its publication is included.

All data that is published has been done so under the Creative Commons Licence (version 4.0) and is acknowledged accordingly (CC BY 4.0).

Abstract

Histone deacetylase four (HDAC4) is essential in neuronal development and function, and dysregulation of HDAC4 has been observed in a number of neurodevelopmental and neurodegenerative diseases, including Alzheimer's and Parkinson's diseases. In particular, its aberrant nuclear accumulation is a common feature among these diseases, and it has been observed that upon upregulation or accumulation in the nucleus, HDAC4 forms punctate foci in neuronal nuclei. Previous research in a *Drosophila* model determined that overexpression of HDAC4 disrupted both neuronal development and long-term memory, and this was largely mediated by the nuclear pool of HDAC4. Based on these data, it was hypothesised that aggregates of HDAC4 are responsible for the neurotoxicity that leads to disrupted neurodevelopment and memory. Therefore, this study aimed to determine whether the presence of HDAC4 nuclear aggregates correlated with neurodevelopmental deficits in a *Drosophila* model of neurodevelopment, and if so, how they mediate their toxic effects.

The N-terminus of HDAC4 forms homo-oligomers in solution, and it was hypothesised that full-length HDAC4 similarly oligomerises, and that this is required for its aggregation in neuronal nuclei. Mutations predicted to prevent oligomerisation were introduced into the N-terminus of HDAC4 and were shown to significantly reduce aggregation of HDAC4 in *Drosophila* neurons. Furthermore, their presence also reduced the severity of HDAC4 overexpression-induced impairments in neurodevelopment. Conversely, stabilisation of oligomerisation increased aggregation and the severity of neurodevelopmental phenotypes, together indicating that aggregation positively correlates with the severity of neurodevelopmental deficits.

HDAC4 aggregates have been previously shown to sequester the transcription factor MEF2, and further investigation revealed that the presence of MEF2 stabilised aggregation and increased the severity of defects in neuronal development. Importantly, targeting the interaction between HDAC4 and MEF2 reduced the severity of these defects. Other than MEF2, the composition of HDAC4 aggregates is unknown, and therefore immunoprecipitation-coupled mass spectrometry was performed on nuclear HDAC4 to identify candidate interactors of aggregates. This revealed a number of proteins with roles in neuronal development and function, as well as those involved in splicing and protein homeostasis, suggesting that aggregates may be impairing these processes to mediate toxicity.

Together these data indicate that nuclear aggregation of HDAC4 impairs neurodevelopment, and may constitute a novel biomarker of disease or therapeutic target. Given the overlap in aetiology between neurodevelopmental and neurodegenerative diseases, further investigation of whether HDAC4 aggregation contributes to the severity and/or progression of neurodegenerative disorders is warranted.

Acknowledgements

I think this is of the hardest parts of a thesis to write. Not only because of the terror of forgetting someone, rambling on for too long, or not having something witty or insightful to say, but it is difficult because it signals that this chapter is really coming to a close. The last few years have been an absolute blast, and that's largely because of the people that listened, helped, consoled, and celebrated with me every step of the way.

I am immensely grateful to have had the opportunity to work in the lab of Dr Helen Fitzsimons, my main supervisor. The culture Helen creates in the lab is one that makes you excited to turn up every single day, even if it is early and you're not a morning person. Thank you for your patience, guidance, excitement, encouragement, and support, both inside and outside of the lab, it really means a lot. Thanks also for all the cat pictures and cool cakes!

To my co-supervisors, A/Prof Andrew Sutherland-Smith, and A/Prof Evelyn Sattlegger, thank you for your expertise, advice, and reassurance in areas I was not as confident in, it has been invaluable. Thanks also to Trevor Loo for assistance with IP-MS, and your willingness to help troubleshoot even the most troubled experiments.

To the staff at MMIC, thank you for your patience and assistance, and for the maintenance of the microscopes, especially keeping the 'old confocal' alive for just long enough to finish this work. Thanks also to Dr Matthew Savoian for letting me in early, as well as your advice and camaraderie. Thanks also to the wider support staff within the School, especially Ann and Cynthia, for keeping everything running so smoothly.

To the members of the Massey Neurogenetics lab: Ana, Wei, Sarah, Celestine, and Raoul, thanks for sharing the ups and downs of every day. A special thanks to Sarah for putting up with me, day in, day out. Thanks also to Aseel, the honorary lab member, for testing your baking skills on us.

To everyone that has been part of the 'lunch club', especially Cathy, Kelli, Ruby, Jennifer, Sean, Cat, Rayén, and Hannah, thanks for your constant judgement of my lunches and making me feed myself better (your friendship is valued too I guess…).

To my friends and family, thank you for your constant support and kindness. Cathy, thank you for always lending an ear and being a voice of reason. Mum, thank you for always being my number one supporter. Binley, thanks for always being by my side and harassing me into going for walks. And Layla, thank you for always being yourself, and being the most fun to play with, Tully is lucky to have the bestest big sister.

This research was funded by the Royal Society of New Zealand Marsden fund

Abbreviations

Aβ	Amyloid beta
AD	Alzheimer's disease
ANKRA2	Ankyrin repeat family A member 2
AT	Ataxia telangiectasia
ATM	Ataxia telangiectasia mutated serine/threonine kinase
ATF4	Activating transcription factor 4
BDMR	Brachydactyly mental retardation syndrome
BDSC	Bloomington *Drosophila* Stock Centre
bp	Base pairs
BSA	Bovine serum albumin
CaMK	Calcium/calmodulin-dependent protein kinase
CD	Circular dichroism
CDKL5	Cyclin dependent kinase-like 5
CMA	Chaperone-mediated autophagy
CS	Canton-Special
CtBP	C-terminal binding protein
CyO	Curly of Oster
dH_2O	Deionised water
DAPI	4′,6-diamidino-2-phenylindole
DAVID	Database for Annotation, Visualization and Integrated Discovery
Dm	*Drosophila melanogaster*
DMSO	Dimethyl sulfoxide
DNA	Deoxyribonucleic acid
DSHB	Developmental Studies Hybridoma Bank
elav	*Embryonic lethal abnormal vision*
ERG	Early response gene
F65A	*Drosophila* HDAC4 hydrophobic core mutant
F93D	Human HDAC4 hydrophobic core mutant
FasII	Fasciclin II
FBgn	FlyBase ID
FDR	False discovery rate
GAL80ts	Temperature sensitive mutant of GAL80
GFP	Green fluorescent protein
GMR	*Glass multimer reporter*
GOterm	Gene Ontology term
GWAS	Genome-wide association studies
h	Human
H97F	Human HDAC4 superstable mutant
HA	Hemagglutinin
HAT	Histone acetyltransferase
HCl	Hydrochloric acid
HD	Huntington's disease

HDAC	Histone deacetylase
HP1	Heterochromatin protein 1
HPLC	High-performance liquid chromatography
HTT	Huntingtin
IDR	Intrinsically disordered region
IP	Immunoprecipitation
IP-MS	Immunoprecipitation-coupled mass spectrometry
KC	Kenyon cell
kDa	Kilodalton
L	Litre
LTM	Long-term memory
M	Molar
Mb	Megabases
MB	Mushroom body
MEF2	Myocyte enhancer factor 2
mg	Milligram
mL	Millilitre
mM	Millimolar
MMIC	Manawatu Microscopy and Imaging Centre
mRNA	Messenger RNA
NCI	National Cancer Institute
NCoR	Nuclear receptor corepressor
NES	Nuclear export sequence
NLS	Nuclear localisation sequence
P	Phosphorylated residue
PBS	Phosphate-buffered saline
PBT	Phosphate-buffered saline with triton X-100
PD	Parkinson’s disease
PKIA	Protein kinase inhibitor alpha
PP2A	Protein phosphatase 2A
RCSB PDB	Research Collaboratory for Structural Bioinformatics Protein Data Bank
RFXANK	Regulatory factor X associated ankyrin containing protein
RIPA	Radioimmunoprecipitation assay buffer
RNA	Ribonucleic acid
RNAi	RNA interference
RNApol	RNA polymerase
ROS	Reactive oxygen species
RUNX2	Runt-related transcription factor 2
S69F	*Drosophila* HDAC4 oligomerisation mutant
Sb	Stubble
SCA1	Spinocerebellar ataxia type 1
SDS-PAGE	Sodium dodecyl sulfate- polyacrylamide gel electrophoresis
SEC-MALS	Size exclusion chromatography coupled to multiangle light scattering
SEM	Standard error of the mean

shRNA	Short hairpin RNA
SIK	Salt-inducible kinase
SMRT	Silencing mediator of retinoic acid and thyroid hormone receptor
SRF	Serum response factor
STRING	Search Tool for the Retrieval of Interacting Genes/Proteins
SUMO	Small ubiquitin-like modifier
SV40t	Simian virus 40 large T antigen
TARGET	Temporal and regional gene expression targeting
TBS	Tris-buffered saline
TBST/TBS-T	Tris-buffered saline with Tween-20
TF	Transcription factor
UAS	Upstream activating sequence
UPS	Ubiquitin proteasome system
V	Volts
VDRC	Vienna *Drosophila* Resource Centre
w(CS10)	White Canton-Special
WT	Wild-type
YFP	Yellow fluorescent protein
α	Alpha
β	Beta
γ	Gamma
ΔMEF2	*Drosophila* HDAC4 MEF2-binding domain mutant
ΔNES	*Drosophila* HDAC4 nuclear export sequence domain mutant
µg	Microgram
µl	Microlitre
µm	Micrometre
°C	Degree Celsius
3SA	*Drosophila* HDAC4 nuclear mutant
9QA	*Drosophila* HDAC4 stabilisation mutant
9QAΔQ	*Drosophila* HDAC4 stabilisation mutant with additional polyglutamine deletion

Table of Contents

Abstract v

Acknowledgements vii

Abbreviations ix

Table of Contents xiii

List of Figures xxi

List of Tables xxvii

1. Introduction 2

1.1. Neurodevelopmental and neurodegenerative disease 2

1.1.1. Neurodegenerative disease aetiology: Protein aggregation is a common factor 3

1.2. *Drosophila melanogaster* as a model for neuroscientific discovery 5

1.2.1. Introduction to *Drosophila* genetics 6

1.2.2. Nomenclature used in this thesis 8

1.2.3. Spatial and temporal control of gene expression in *Drosophila* 8

1.3. *Drosophila* development 11

1.3.1. The *Drosophila* brain 12

1.3.2. The *Drosophila* eye 14

1.4. Epigenetic regulation of gene expression 16

1.4.1. Histone acetylation and deacetylation 18

1.4.2. Histone deacetylases 19

1.5. Histone deacetylase four (HDAC4): structure and function 20

1.5.1. Regulation of HDAC4 subcellular distribution 22

1.5.1.1. NLS and NES-dependent regulation of HDAC4 nucleocytoplasmic shuttling 23

1.5.1.2. MEF2 mediates dynamic nuclear import of HDAC4 24

1.5.1.3. 14-3-3 proteins mediate dynamic nuclear export of HDAC4 26

1.5.1.4. Regulation of HDAC4 distribution via cleavage 27

1.5.1.5. Regulation of HDAC4 distribution in neuronal cells 28

1.6. Roles of HDAC4 in neuronal development, function, and neurodegenerative disease 28

1.6.1. HDAC4 is essential in neuronal development and function 28

1.6.2. HDAC4 dysregulation is observed in neuronal disease 32

1.7. The roles of MEF2 in neuronal development and disease 39

1.8. Oligomerisation and aggregation of HDAC4 40

1.8.1. Mechanism of tetramerisation 42

2. Aims & Objectives 46

3. Materials & Methods 52

3.1. *Drosophila melanogaster* strains 52
3.1.1. Generation of transgenic *Drosophila* 52
3.1.2. Maintenance of *Drosophila* stocks 54
3.1.3. Genetic crosses 55
3.2. Protein analyses 57
3.2.1. Modelling of the HDAC4 tetramer 57
3.2.2. Total protein isolation from fly heads 57
3.2.3. Subcellular fractionation from fly heads 58
3.2.4. Immunoprecipitation 59
3.2.5. SDS-PAGE 60
3.2.6. Western blotting 60
3.2.7. Quantification of western blots 61
3.2.8. Colloidal Coomassie staining 62
3.2.9. In-gel tryptic digestion 62
3.2.10. Mass spectrometry 63
3.2.11. Proteomic data analysis 65
3.3. DNA analyses 66
3.3.1. Isolation of genomic DNA from whole flies 66
3.3.2. PCR amplification 66
3.3.3. Agarose gel electrophoresis 67
3.3.4. DNA sequencing 67
3.4. Immunohistochemistry 68
3.4.1. *Drosophila* adult brain isolation 68
3.4.2. *Drosophila* larval eye disc isolation 68
3.4.3. *Drosophila* adult eye isolation 68
3.4.4. Immunostaining 69
3.4.5. Immunofluorescence 70
3.4.6. Quantification of HDAC4 aggregates 70
3.4.7. Quantification of mushroom body development 71
3.4.8. Quantification of MEF2 intensity 72
3.5. Evaluation of adult eye morphology 72
3.5.1. Light microscopy 72
3.5.2. Scanning electron microscopy 73

4. Characterisation of the role of HDAC4 oligomerisation in HDAC4 aggregation and its effects on neuronal development in *Drosophila* 76

4.1. Characterisation of the expression patterns and levels of neuronal GAL4 drivers 77

4.2. Overexpression of HDAC4 induces nuclear aggregation in Kenyon cells 81

4.3. Development and validation of HDAC4 oligomerisation mutants 84

4.3.1. Design of HDAC4 oligomerisation mutants 84

4.3.2. Expression of HDAC4 oligomerisation mutants in *Drosophila* 87

4.3.3. HDAC4 oligomerisation mutants are altered in oligomerisation capacity 89

4.4. HDAC4 oligomerisation is required for nuclear aggregation 92

4.4.1. Validation of method of quantification of HDAC4 aggregates in Kenyon cell nuclei 92

4.4.2. HDAC4 oligomerisation mutants are altered in aggregation in Kenyon cells 93

4.4.3. HDAC4 oligomerisation mutants are altered in aggregation in the larval eye disc 97

4.5. HDAC4 aggregation correlates with neurodevelopmental phenotypes in *Drosophila* 103

4.5.1. HDAC4 oligomerisation mutants reduce severity of mushroom body phenotypes arising from HDAC4 overexpression 103

4.5.2. HDAC4 oligomerisation mutants reduce the severity of eye phenotypes arising from HDAC4 overexpression 107

4.6. Combination of HDAC4^{9QA} and HDAC4^{F65A} mutations does not further reduce aggregation or HDAC4 overexpression-induced phenotypes 113

4.6.1. Expression of HDAC4$^{9QA\text{-}F65A}$ in *Drosophila* 114

4.6.2. HDAC4$^{9QA\text{-}F65A}$ does not further reduce aggregation in Kenyon cells 115

4.6.3. HDAC4$^{9QA\text{-}F65A}$ expression does not result in less severe mushroom body defects than the single mutants 117

4.6.4. HDAC4$^{9QA\text{-}F65A}$ expression results in an eye phenotype equivalent to HDAC4^{F65A} 119

4.7. Discussion 121

4.7.1. Oligomerisation of HDAC4 contributes to higher order multimerisation and subsequent aggregation of HDAC4 122

4.7.1.1. The oligomerisation domain of human and *Drosophila* HDAC4 is highly conserved 122

4.7.1.2. Limitations of analyses in the presence of endogenous HDAC4 124

4.7.2. Glutamine residues are critical to maintaining protein levels of HDAC4 127

4.7.3. HDAC4 aggregation appears to correlate tightly with HDAC4-overexpression induced defects in neuronal development in *Drosophila* 129

4.7.3.1. The differential requirement for MEF2 in HDAC4-overexpression induced neurodevelopmental phenotypes 132

4.7.4. HDAC4 oligomerisation may have a role in the regulation of its subcellular distribution 133

4.7.5. How does tetramerisation of HDAC4 result in aggregation? 134

4.7.6. How do HDAC4 aggregates mediate neurotoxicity? 137

5. Examination of the relationship between HDAC4 oligomerisation and subcellular distribution, and how this affects HDAC4 aggregation and neuronal development 140

5.1. HDAC4 oligomerisation mutants are altered in subcellular distribution in Kenyon cells .141

5.2. Enforced nuclear localisation of oligomerisation mutants affects aggregation and related phenotypes 146

5.2.1. Expression of nuclear-restricted HDAC4 oligomerisation mutants in *Drosophila* 148

5.2.2. Confirmation of nuclear localisation of HDAC4 oligomerisation mutants 149

5.2.3. Nuclear-restricted HDAC4 mutants are altered in oligomerisation capacity 155

5.2.4. Enforced nuclear localisation increases aggregation of HDAC4 oligomerisation mutants 156

5.2.5. Enforced nuclear localisation differentially impacts the ability of HDAC4 oligomerisation mutants to confer mushroom body phenotypes 159

5.2.6. Enforced nuclear localisation differentially impacts the ability of HDAC4 oligomerisation mutants to disrupt eye development 163

5.2.7. $HDAC4^{3SA\text{-}F65A}$ has different aggregation characteristics between Kenyon cells and basal cells of the larval eye disc 166

5.3. Overexpression of HDAC4 increases the abundance of MEF2 in Kenyon cells 167

5.3.1. Overexpression of HDAC4 increases MEF2 intensity in Kenyon cells 168

5.3.2. Mutation of the MEF2 binding site prevents the HDAC4-induced increase of MEF2 in Kenyon cells 170

5.3.3. HDAC4 oligomerisation mutants differentially impact MEF2 intensity in Kenyon cells 172

5.4. MEF2 and the MEF2 binding site within HDAC4 promote nuclear localisation and stabilise aggregation of HDAC4 173

5.4.1. The MEF2 binding site stabilises but is not required for aggregation of HDAC4 in Kenyon cells 174

5.4.2. MEF2 overexpression increases nuclear localisation of HDAC4 in Kenyon cells 176

5.4.3. MEF2 overexpression increases the severity of HDAC4-overexpression induced β-lobe fusion of the mushroom body 178

5.4.4. Mutation of the MEF2 binding site alters HDAC4 subcellular distribution in the larval eye disc 180

5.4.5. Endogenous MEF2 protein is detected in the adult eye 183

5.4.6. MEF2 overexpression impairs eye development 184

5.5. The *Drosophila* HDAC4 nuclear export sequence is functional, and mutations of this region induce nuclear localisation, aggregation, and neuronal phenotypes 185

5.5.1. Mutation of the nuclear export sequence within HDAC4 results in nuclear accumulation in Kenyon cells 187

5.5.2. $HDAC4^{\Delta NES}$ has different aggregation characteristics to $HDAC4^{3SA}$ 189

5.5.3. $HDAC4^{\Delta NES}$ induces severe β-lobe fusion similarly to $HDAC4^{3SA}$ 191

5.5.4. $HDAC4^{\Delta NES}$ induces more severe defects in eye development than $HDAC4^{3SA}$ 193

5.6. Discussion 196

5.6.1. Oligomerisation and dose of HDAC4 regulate its subcellular distribution 197

5.6.2. Restriction of HDAC4 localisation to the nucleus increases aggregate load 200

5.6.3. Differential phenotypic effects of HDAC4 oligomerisation mutants when localised to the nucleus. 203
5.6.4. The role of MEF2 and the MEF2 binding domain within HDAC4 in the *Drosophila* eye 204
5.6.5. The role of MEF2 in promoting and stabilising aggregation of HDAC4 206
5.6.6. The role of serine residues and the HDAC4 nuclear export sequence in nuclear localisation and aggregation dynamics 211

6. Characterisation of the composition of HDAC4 positive aggregates resulting from overexpression of nuclear restricted HDAC4 218

6.1. Identification of interactors of nuclear-restricted HDAC4 in the *Drosophila* brain 219
6.1.1. Overview of experimental approach 219
6.1.2. Optimisation of immunoprecipitation 220
6.1.3. Interactors detected via IP-MS from whole head lysates of flies expressing HDAC4^{3SA} under the control of *elav-GAL4* 222
6.2. Determining an approach to enrich for nuclear interactors of HDAC4 227
6.3. Identification of interactors of nuclear-restricted HDAC4 in Kenyon cells.....229
6.3.1. IP-MS on nuclear lysates expressing HDAC4^{3SA} in Kenyon cells 229
6.4. Discussion.....235
6.4.1. Evaluation of the strategy to determine HDAC4 aggregate composition.....235
6.4.1.1. Limitations of the current dataset..... 237
6.4.2. Pathway analyses reveal processes that HDAC4 aggregates disrupt to mediate neurotoxicity ...239
6.4.2.1. Candidate HDAC4^{3SA} interactors have roles in neuronal development and function 239
6.4.2.2. Candidate HDAC4^{3SA} interactors are involved in splicing..... 242
6.4.2.3. Enrichment of proteins involved in the protein homeostasis network..... 245
6.4.3. How do HDAC4 aggregates mediate neurotoxicity?.....247
6.4.3.1. HDAC4 may stochastically sequester proteins with common functions to mediate neurotoxicity..... 247
6.4.3.2. HDAC4 aggregates may disrupt proteostasis to mediate neurotoxicity 249

7. Investigation of a mechanism to alter HDAC4 aggregate formation 252

7.1. A strategy to disrupt HDAC4 aggregation and neurotoxicity 252
7.1.1. Design of HDAC4$^{N\text{-}term}$ constructs to disrupt oligomerisation of full-length HDAC4^{WT} 253
7.2. Characterisation of the expression of HDAC4$^{N\text{-}term}$.....256
7.2.1. HDAC4$^{N\text{-}term}$ constructs are expressed in *Drosophila* 256
7.2.2. HDAC4$^{N\text{-}term}$ constructs have different subcellular distributions in the adult brain 258
7.2.3. Sequencing confirms the identity of HDAC4$^{N\text{-}term}$ constructs 263
7.3. Characterisation of the neurodevelopmental effects of expression of HDAC4$^{N\text{-}term}$ 263
7.3.1. HDAC4$^{N\text{-}term}$ expression does not affect mushroom body development 264
7.3.2. HDAC4$^{N\text{-}term}$ expression does not affect eye development.....265

7.4. Characterisation of co-expression of HDAC4^{WT} and HDAC4$^{N\text{-}term}$ 270
7.4.1. HDAC4$^{N\text{-}term}$ expression affects the subcellular distribution and aggregation of HDAC4^{WT} in Kenyon cells 270
7.4.2. HDAC4$^{N\text{-}term}$ constructs differentially modulate HDAC4^{WT}-induced defects in mushroom body development 274
7.4.3. HDAC4$^{N\text{-}term}$ constructs differentially modulate HDAC4^{WT}-induced defects in eye development 277
7.5. Discussion 284
7.5.1. The N-terminal region of HDAC4 stabilises aggregation of full-length HDAC4 in neuronal nuclei 286
7.5.1.1. Implications of HDAC4 aggregate stabilisation in a disease context 288
7.5.2. Targeting the interaction between HDAC4 and MEF2 may be of therapeutic benefit 289
7.5.3. Modulating the subcellular distribution of HDAC4 may be of therapeutic benefit 292

8. Summary, reflections, & future directions 296

8.1. The utility of *Drosophila* as a model organism 296
8.1.1. It is essential to consider performing structure-function studies in more than one neuronal cell type 297
8.2. HDAC4 aggregation is dependent on oligomerisation, dose, and nuclear localisation 298
8.3. HDAC4 aggregation correlates with defects in neuronal development 300
8.4. Towards understanding the mechanism of how HDAC4 aggregates mediate toxicity 302
8.5. Targeting the interaction between HDAC4 and MEF2 may be of therapeutic benefit in neuronal disease 304
8.6. Conclusion 306

9. References 308

10. Appendix 344

10.1. Supplementary methods 344
10.1.1. *Drosophila* lines used in this study 344
10.1.2. Full-length *Drosophila* HDAC4-Myc sequence with mutations characterised in this thesis 346
10.1.3. N-terminal *Drosophila* HDAC4 sequences 347
10.1.4. Full-length *Drosophila* MEF2-HA sequence 350
10.1.5. Generation of transgenic flies 350
10.1.6. Crossing schemes used to combine transgenes 353
10.1.7. Details of tissue-specific immunofluorescent imaging 359

10.2. Supplementary data corresponding to Chapter 4 360
10.2.1. Generation of the HDAC4::GFP protein trap line 360
10.2.2. Protein sequence alignment of *Drosophila* and Human HDAC4 with annotation of key residues important for hHDAC4 function 361
10.2.3. Western blots of HDAC4^{mutant} expression used for intensity quantification 364
10.2.4. Changes in HDAC4^{mutant} intensity in the mushroom body 367
10.2.5. Replication of co-immunoprecipitation assays to examine oligomerisation of HDAC4 368
10.2.6. Full western blots of co-immunoprecipitation assays to examine oligomerisation of HDAC4 369
10.2.7. Optimisation of immunohistochemistry to visualise HDAC4 aggregates 370
10.2.8. Validation of the specificity of the endogenous MEF2 antibody 371
10.2.9. Confirmation that the circadian clock does not affect HDAC4 aggregation in Kenyon cells 372
10.2.10. Images of *Drosophila* eyes resulting from expression of HDAC4 from one genomic insertion 374
10.3. Supplementary data corresponding to Chapter 5 376
10.3.1. Further investigation and verification of HDAC4$^{3SA\text{-}F65A}$ 376
10.3.2. Full western blots of subcellular fractionation and co-immunoprecipitation performed on heads of flies expressing HDAC4 mutants 382
10.3.3. Eye phenotypes resulting from expression of nuclear-restricted HDAC4 oligomerisation mutants from one genomic insertion 386
10.3.4. Images of female eyes expressing HDAC4$^{\Delta NES}$ 388
10.4. Supplementary data corresponding to Chapter 6 390
10.4.1. Identification of interactors of nuclear-restricted HDAC4 in the *Drosophila* brain 390
10.4.2. Preliminary investigation into HDAC4^{3SA} candidate interactors 392
10.4.3. Optimisation of protocols for IP-MS analysis 395
10.4.3.1. Optimisation of the immunoprecipitation protocol 395
10.4.3.2. Optimisation and validation of the subcellular fractionation protocol 399
10.4.3.3. Immunoprecipitation of HDAC4^{3SA} from nuclear lysates 401
10.4.4. Selection of the driver and conditions in which to raise flies for IP-MS analysis 403
10.4.4.1. HDAC4 aggregation characteristics alter significantly with increased dose 403
10.4.4.2. *OK107-GAL4* drives higher total expression of HDAC4^{3SA} compared to *elav-GAL4* 410
10.4.4.3. Addition of the TARGET system does not significantly alter the levels or subcellular distribution of HDAC4^{3SA} 412
10.4.4.4. Comparison of HDAC4^{3SA} distribution in the brain and aggregate formation in Kenyon cells resulting from expression under the control of *elav-GAL4* or *OK107-GAL4* in the presence and absence of the TARGET system 414
10.4.4.5. Aggregates in Kenyon cells resulting from HDAC4^{3SA} expression under the control of *OK107-GAL4* +TARGET are within nuclei 418
10.4.5. Identification of interactors of nuclear-restricted HDAC4 in Kenyon cells 420
10.5. Supplementary data corresponding to Chapter 7 434
10.5.1. Western blots of HDAC4$^{N\text{-}term}$ expression used for intensity quantification 434
10.5.2. Verification of *HDAC4$^{N\text{-}term}$* 435
10.5.3. HDAC4$^{N\text{-}term}$ and HDAC4^{WT} distribution in Kenyon cells 445

List of Figures

Figure 1.1 Example of a genetic cross depicting the inheritance of the curly wing marker in *Drosophila* 6
Figure 1.2 The UAS-GAL4 system 9
Figure 1.3 The TARGET system 11
Figure 1.4 The structure of the adult *Drosophila* mushroom body 13
Figure 1.5 The organisation of the adult *Drosophila* eye 14
Figure 1.6 The *Drosophila* eye develops from the eye-antennal disc 15
Figure 1.7 DNA associates with histone proteins to form nucleosomes 17
Figure 1.8 Modification of histones by histone acetyltransferases and deacetylases impacts chromatin compaction and transcription 18
Figure 1.9 Domain alignment of the human zinc-dependent histone deacetylases 19
Figure 1.10 Domain structure and characterised binding partners of human HDAC4 21
Figure. 1.11 HDAC4 undergoes dynamic regulation of its subcellular distribution 23
Figure 1.12 HDAC4 co-localises with MEF2 in nuclear aggregates in the *Drosophila* brain 41
Figure 1.13 Tetramerisation of the glutamine-rich N-terminus of HDAC4 42
Figure 2.1 Strategy to investigate the relationship between HDAC4 aggregation and neuronal development in *Drosophila* 49
Figure 3.1 Standard crossing schemes used to generate progeny that express transgenes using the UAS/GAL4 system 56
Figure 4.1 *elav-GAL4* and *OK107-GAL4* mediate different expression patterns of mCD8::GFP in the adult brain 77
Figure 4.2 *OK107-GAL4* drives higher expression of mCD8::GFP in the lobes of the mushroom body than *elav-GAL4* 79
Figure 4.3 Schematic diagrams used in this thesis to convey driver selection and conditions under which flies were raised 80
Figure 4.4 Overexpression of HDAC4 results in the redistribution and co-aggregation of endogenous HDAC4 with transgene HDAC4 in neuronal nuclei 82
Figure 4.5 Sequence alignment and schematic diagram of HDAC4 tetramerisation mutants 85
Figure 4.6 Comparison of the AlphaFold predicted *Drosophila* HDAC4 N-terminal structure when modelled as a tetramer with the human HDAC4 crystal structure 86
Figure 4.7 HDAC4 oligomerisation mutants are altered in protein levels compared to wild-type HDAC4 in *Drosophila* 88
Figure 4.8 Schematic diagram of the co-immunoprecipitation workflow to assess changes in HDAC4 oligomerisation 90
Figure 4.9 HDAC4 tetramerisation mutants are altered in their ability to oligomerise 91
Figure 4.10 HDAC4 oligomerisation mutants are altered in aggregation and recruitment of MEF2 to aggregates in Kenyon cell nuclei 94
Figure 4.11 The number of HDAC4-containing aggregates in neuronal nuclei is altered by mutations that affect oligomerisation of HDAC4 96
Figure 4.12 Endogenous MEF2 is not detected in the developing eye disc 98
Figure 4.13 Expression pattern of endogenous and transgene HDAC4 in the larval eye disc 100
Figure 4.14 HDAC4 oligomerisation mutants are altered in aggregation and subcellular distribution in basal cells of the third instar larval eye disc 102
Figure 4.15 Mushroom body phenotypes observed upon HDAC4 overexpression 104

Figure 4.16 HDAC4 oligomerisation mutants alter the severity of β-lobe fusion of the mushroom body..... 105
Figure 4.17 Comparison of β-lobe fusion phenotypes at 18 °Cand 22 °C illustrates a subtle increase in severity associated with expression of HDAC4^{S69F} compared to HDAC4^{WT}..... 106
Figure 4.18 Overexpression of HDAC4 oligomerisation mutants alters *Drosophila* eye development..... 108
Figure 4.19 Increased dose of HDAC4 exacerbates differences in disruption of eye development between HDAC4 oligomerisation mutants..... 111
Figure 4.20 Implementation of a scoring system to characterise HDAC4-overexpression induced deficits in eye development resulting from expression of oligomerisation mutants..... 113
Figure 4.21 Combination of 9QA and F65A mutations does not significantly alter protein levels of HDAC4.. 114
Figure 4.22 Combination of 9QA and F65A mutations does not further reduce aggregation of HDAC4 in Kenyon cells..... 116
Figure 4.23 Combination of 9QA and F65A mutations does not further reduce the severity of β-lobe fusion in the mushroom body..... 118
Figure 4.24 Combination of 9QA and F65A mutations reduces the severity of the eye defects to that of HDAC4^{F65A}..... 120
Figure 4.25 HDAC4 tetramerisation is a requirement of its aggregation *in vivo*..... 124
Figure 4.26 Implications of the presence of endogenous/wild-type HDAC4 for the characterisation of HDAC4 tetramerisation mutants..... 125
Figure 4.27 Schematic diagram depicting the correlation between aggregation of HDAC4 and defects in neuronal development in *Drosophila*..... 130
Figure 4.28 3D reconstruction of a DmHDAC4 tetramer based on the AlphaFold prediction of the structure of DmHDAC4 and the crystal structure of the N-terminus of hHDAC4..... 135
Figure 4.29 HDAC4 aggregates may aberrantly sequester proteins to induce defects in neuronal development and function..... 137
Figure 5.1 Examination of HDAC4^{WT} and HDAC4^{mutant} subcellular distribution in the mushroom body lobes and cell bodies surrounding the suboesophageal ganglion and antennal lobe in the adult *Drosophila* brain..... 143
Figure 5.2 The capacity of HDAC4 to oligomerise affects its subcellular distribution in Kenyon cells..... 145
Figure 5.3 Sequence alignment and schematic diagram of nuclear-restricted HDAC4 oligomerisation mutants147
Figure 5.4 HDAC4$^{3SA-9QA}$ is reduced in protein levels compared to nuclear-restrcited HDAC4 in *Drosophila*. 149
Figure 5.5 The 3SA mutations increase the nuclear distribution of HDAC4 oligomerisation mutants..... 151
Figure 5.6 Oligomerisation of HDAC4 regulates its nuclear localisation in Kenyon cells..... 153
Figure 5.7 The 3SA mutations do not affect oligomerisation of HDAC4 mutants..... 156
Figure 5.8 Nuclear-restricted HDAC4 oligomerisation mutants alter redistribution of MEF2 to aggregates and the number of aggregates in Kenyon cells..... 157
Figure 5.9 Nuclear-restricted HDAC4 oligomerisation mutants alter the severity of β-lobe fusion of the mushroom body..... 161
Figure 5.10 Comparison of the β-lobe fusion phenotype resulting from expression of nuclear-restricted HDAC4 oligomerisation mutants at 22 °C and 18 °C..... 162
Figure 5.11 Increased dose of HDAC4 exacerbates differences in disruption of eye development between the nuclear-restricted HDAC4 oligomerisation mutants..... 164
Figure 5.12 Implementation of a scoring system to characterise HDAC4-overexpression induced deficits in eye development resulting from expression of nuclear-restricted oligomerisation mutants..... 165
Figure 5.13 HDAC4$^{3SA-F65A}$ has different aggregation characteristics between Kenyon cells and the basal cells of the larval eye disc..... 167
Figure 5.14 Increased expression of HDAC4^{WT} causes a dose-dependent increase in MEF2 in Kenyon cells .. 169

Figure 5.15 HDAC4 overexpression-induced increased MEF2 intensity in Kenyon cells is dependent on an intact MEF2 binding site....171
Figure 5.16 HDAC4 oligomerisation mutants differentially alter MEF2 intensity in Kenyon cells....173
Figure 5.17 The MEF2 binding site within HDAC4 is not required for aggregation but stabilises and increases aggregate number....175
Figure 5.18 MEF2 overexpression increases nuclear localisation of HDAC4^{WT} in Kenyon cells....177
Figure 5.19 MEF2 overexpression exacerbates β-lobe fusion mediated by HDAC4^{WT} but not by HDAC4$^{\Delta MEF2}$ 179
Figure 5.20 Mutation of the MEF2 binding site alters HDAC4 subcellular distribution in the larval eye disc ...182
Figure 5.21 MEF2 is expressed in the adult eye....183
Figure 5.22 Overexpression of MEF2 affects *Drosophila* eye development 185
Figure 5.23 Sequence alignment of human and *Drosophila* HDAC4 identifies conservation of the nuclear export sequence....186
Figure 5.24 Mutation of the nuclear export sequence within HDAC4 results in nuclear accumulation in Kenyon cells 188
Figure 5.25 HDAC4$^{\Delta NES}$ has different nuclear aggregation characteristics compared to HDAC4^{3SA}....190
Figure 5.26 Nuclear localisation of HDAC4 impairs β-lobe development 192
Figure 5.27 Eye phenotypes resulting from enforcing nuclear localisation of HDAC4 via 3SA and ΔNES mutations....194
Figure 5.28 Implementation of a scoring system to compare deficits in eye development resulting from enforcing nuclear localisation of HDAC4 via the 3SA and ΔNES mutations 195
Figure 5.29 A model of the potential interplay between oligomerisation of HDAC4, association of MEF2 and 14-3-3, and regulation of subcellular distribution....199
Figure 5.30 Reducing the effective volume in which HDAC4 is distributed increases its ability to aggregate...201
Figure 5.31 A model depicting how dimerisation of MEF2 may facilitate formation of higher order oligomers of HDAC4 that stabilise aggregation 207
Figure 5.32 Higher order oligomerisation of HDAC4 may be facilitated by the interaction of HDAC4-MEF2 oligomers....209
Figure 5.33 Comparison of potential MEF2 binding for 3SA and ΔNES mutants of HDAC4....213
Figure 5.34 Model of the effects of 14-3-3 or MEF2 binding on HDAC4 nuclear aggregation....214
Figure 4.29 HDAC4 aggregates may aberrantly sequester proteins to induce defects in neuronal development and function 218
Figure 6.1 Schematic representation of immunoprecipitation-coupled mass spectrometry workflow to identify HDAC4 aggregate binding partners....219
Figure 6.2 Optimised co-immunoprecipitation of GFP-HDAC4^{WT} with HDAC4^{WT}-Myc (Protocol 1)....221
Figure 6.3 Six proteins were common between IP-MS studies....230
Figure 6.4 HDAC4^{3SA} aggregates may sequester components of the splicing machinery to mediate neurotoxicity 243
Figure 6.5 HDAC4^{3SA} aggregation may disrupt the proteostasis network 246
Figure 6.6 HDAC4 aggregates may stochastically sequester proteins to mediate defects in neuronal development and function 248
Figure 7.1 Expression of a minimal fragment of HDAC4 including the tetramerisation domain may alter tetramerisation and aggregation of full-length HDAC4 253
Figure 7.2 N-terminal constructs of HDAC4....254
Figure 7.3 HDAC4$^{N\text{-}term}$ constructs are expressed in *Drosophila melanogaster* 257
Figure 7.4 Distribution of HDAC4$^{N\text{-}term}$ constructs in the lobes of the adult mushroom body....260

Figure 7.5 Distribution of HDAC4$^{N\text{-}term}$ constructs in the cell bodies of Kenyon cells 262
Figure 7.6 HDAC4$^{N\text{-}term}$ constructs do not induce β-lobe fusion of the mushroom body 265
Figure 7.7 Overexpression of HDAC4$^{N\text{-}term}$ mutants does not alter *Drosophila* eye development 266
Figure 7.8 Increased dose of HDAC4$^{N\text{-}term}$ does not induce defects in eye development 268
Figure 7.9 Implementation of a scoring system to characterise HDAC4$^{N\text{-}term}$ induced defects in eye development 269
Figure 7.10 Co-expression of HDAC4$^{N\text{-}term}$ differentially affects the subcellular distribution of HDAC4^{WT} in the mushroom body 271
Figure 7.11 Co-expression of HDAC4$^{N\text{-}term}$ affects the aggregation of HDAC4^{WT} in Kenyon cells 273
Figure 7.12 Co-expression of HDAC4$^{M1\text{-}L285}$ but no other HDAC4$^{N\text{-}term}$ construct reduces β-lobe fusion induced by HDAC4^{WT} overexpression 277
Figure 7.13 Co-expression of HDAC4$^{N\text{-}term}$ increases the severity of HDAC4^{WT}-induced defects in *Drosophila* eye development 279
Figure 7.14 Implementation of a scoring system to characterise the modulation of HDAC4^{WT} phenotypes in the adult eye by co-expression of HDAC4$^{N\text{-}term}$ 280
Figure 7.15 Expression of HDAC4$^{N\text{-}term}$ does not significantly alter *Drosophila* eye development in the presence of HDAC4^{F65A} 282
Figure 7.16 Implementation of a scoring system to characterise the modulation of HDAC4^{F65A} phenotypes in the adult eye by co-expression of HDAC4$^{N\text{-}term}$ 283
Figure 7.17 HDAC4$^{N\text{-}term}$ has little intrinsic ability to aggregate, but stabilises aggregation of HDAC4^{WT} 287
Figure 10.1 Generation of transgenic flies by PhiC31-mediated site-specific integration 351
Figure 10.2 Physical map of pUASTattB DmHDAC4-WT 352
Figure 10.3 Physical map of pUASTattB DmMEF2-WT 353
Figure 10.4 Crossing scheme to combine *OK107-GAL4* and *HDAC4^{WT}-Myc* into a single fly line 354
Figure 10.5 Crossing scheme to recombine *GFP-HDAC4^{WT}* and *HDAC4-Myc* transgenes 355
Figure 10.6 Crossing scheme to combine *GMR-GAL4* and *HDAC4* transgenes into a single fly line 356
Figure 10.7 Crossing scheme to combine *MEF2-HA* and *HDAC4-Myc* transgenes into a single fly line 357
Figure 10.8 Crossing scheme to combine *elav-GAL4* and *HDAC4-Myc* into a single fly line 358
Figure 10.9 Simplified schematic diagram of the generation of the *HDAC4::GFP* protein trap 360
Figure 10.10 Full western blots of HDAC4^{mutant} expression used for intensity quantification in Figure 4.7 365
Figure 10.11 Full western blots of HDAC4^{mutant} expression used for intensity quantification in Figure 4.21 and Figure 5.4 366
Figure 10.12 HDAC4^{9QA} and HDAC4$^{9QA\Delta Q}$ signal is reduced in the mushroom body compared to HDAC4^{WT} 367
Figure 10.13 Replication of the HDAC4 co-immunoprecipitation assay to assess oligomerisation 368
Figure 10.14 Full western blots of the co-immunoprecipitation assay in Figure 4.9 369
Figure 10.15 Fixation of brains prior to dissection improves the specificity of detection of HDAC4 aggregates containing MEF2 in Kenyon cells 370
Figure 10.16 The endogenous MEF2 antibody specifically detects MEF2 in Kenyon cells 371
Figure 10.17 The number of nuclear HDAC4-MEF2-containing aggregates does not change with the circadian clock 373
Figure 10.18 Eye phenotypes resulting from of HDAC4$^{9QA\text{-}F65A}$ expression from one genomic insertion 375
Figure 10.19 Plasmid map of pUASTattB HDAC4$^{3SA\text{-}F65A}$ 377
Figure 10.20 Gel electrophoresis of PCR products that span *HDAC4$^{3SA\text{-}F65A}$* show no difference in size compared to *HDAC4^{WT}* 379

Figure 10.21 Sequence alignment of *HDAC4^{3SA}* expected, plasmid, and genomic sequences shows no mutations near the N-terminus....380
Figure 10.22 Full-length and C-terminal cleavage products of HDAC4$^{3SA\text{-}F65A}$ are reduced in apparent molecular weight....381
Figure 10.23 Full western blots of the subcellular fractionation assays in Figure 5.5 383
Figure 10.24 Full western blots of the subcellular fractionation assays in Figure 5.6 384
Figure 10.25 Full western blots of the co-immunoprecipitation assay in Figures 5.7 and 10.13 386
Figure 10.26 Overexpression of nuclear-restricted HDAC4 oligomerisation mutants differentially impacts *Drosophila* eye development 387
Figure 10.27 Eye phenotypes resulting from enforcing nuclear restriction of HDAC4 via 3SA and ΔNES mutations in females 388
Figure 10.28 STRING interaction network of 27 HDAC4^{3SA} candidate interactors....391
Figure 10.29 Armadillo does not co-localise with HDAC4^{3SA} in Kenyon cell nuclear aggregates 393
Figure 10.30 NinaC does not co-localise with HDAC4^{3SA} in nuclear aggregates....395
Figure 10.31 Confirming the efficacy and specificity of new protein A/G and anti-Myc beads and respective immunoprecipitation protocols (Protocol 2)....396
Figure 10.32 Final optimisation of the GFP-HDAC4^{WT} and HDAC4^{WT}-Myc co-immunoprecipitation (Protocol 2) 398
Figure 10.33 Comparison of protocols for subcellular fractionation from *Drosophila* heads....400
Figure 10.34 Optimisation of wash conditions for effective subcellular fractionation from *Drosophila* heads ..401
Figure 10.35 Colloidal Coomassie gel of anti-Myc immunoprecipitates from nuclear fractions 402
Figure 10.36 HDAC4^{WT} forms aggresome-like inclusions in Kenyon cells upon increased dose 404
Figure 10.37 3D rendering of an aggresome-like HDAC4 inclusion shows HDAC4^{WT} displacement of DAPI staining....405
Figure 10.38 Aggresome-like inclusions of HDAC4^{WT} are localised within the nuclear envelope 407
Figure 10.39 Aggresome-like inclusions of HDAC4^{WT} sequester and co-localise with MEF2 409
Figure 10.40 Nuclear HDAC4^{3SA} protein levels are increased under the control of *OK107-GAL4* compared to *elav-GAL4* 411
Figure 10.41 There is no significant change in total HDAC4^{3SA} level or subcellular distribution in the presence of the TARGET system....413
Figure 10.42 Distribution of HDAC4^{3SA} and MEF2 in the anterior of the adult brain....415
Figure 10.43 Distribution of HDAC4^{3SA} and MEF2 in the posterior of the adult brain....417
Figure 10.44 HDAC4^{3SA} aggregates are within the bounds of the nuclear envelope in Kenyon cells 419
Figure 10.45 Full western blots of HDAC4$^{N\text{-}term}$ expression used for intensity quantification 435
Figure 10.46 Plasmid maps of pUAST used to generate *HDAC4$^{N\text{-}term}$* constructs and notation of primer annealing sites for PCR amplification....439
Figure 10.47 Agarose gel electrophoresis of *HDAC4$^{N\text{-}term}$* PCR products....440
Figure 10.48 Verification *of HDAC4$^{N\text{-}term}$ NLS/NES*-containing construct sequences from genomic DNA 444
Figure 10.49 Co-expression of HDAC4$^{N\text{-}term}$ differentially affects the subcellular distribution of HDAC4^{WT} in Kenyon cells....446

List of Tables

Table 3.1 HDAC4 mutants used in this study....53
Table 3.2 Primary antibodies used for western blotting....61
Table 3.3 Secondary antibodies used for western blotting....61
Table 3.4 Mass spectrometry instrument configuration....64
Table 3.5 Mass spectrometry parameters....64
Table 3.6 Proteome Discoverer search parameters....65
Table 3.7 Thermocycling conditions....67
Table 3.8 Primary antibodies used for immunohistochemistry....69
Table 3.9 Secondary antibodies used for immunohistochemistry....70
Table 3.10 Semi-quantitative scoring system for the evaluation of rough eye phenotypes....73
Table 4.1. DmHDAC4 mutants characterised in this chapter....87
Table 4.2 Frequency of mushroom body phenotypes resulting from HDAC4 transgene expression at 22 °C and 18 °C....104
Table 4.3 Frequency of mushroom body phenotypes resulting from the combination of 9QA and F65A mutations at 22°C....118
Table 5.1. DmHDAC4 mutants characterised in this chapter....148
Table 5.2 Frequency of mushroom body phenotypes resulting from the expression of nuclear-restricted HDAC4 oligomerisation mutants at 22 °C and 18 °C....160
Table 5.3 Frequency of mushroom body phenotypes resulting from the expression of HDAC4 in the presence and absence of MEF2 overexpression....180
Table 5.4 Frequency of mushroom body phenotypes resulting from overexpression of HDAC4$^{\Delta NES}$....191
Table 6.1 DAVID functional annotation clustering of candidate HDAC4^{3SA} interactors from initial mass spectrometry analysis....225
Table 6.2 DAVID functional annotation clustering of candidate HDAC4^{3SA} interactors....232
Table 6.3 DAVID functional annotation chart: GOTERM: Cellular Component....233
Table 6.4 Summary of candidate HDAC4^{3SA} interactors for which disruption has led to defects in the development of the mushroom body and/or eye, and/or impairments in memory....241
Table 7.1 DmHDAC4$^{N\text{-}term}$ constructs characterised in this chapter....256
Table 7.2 Frequency of mushroom body phenotypes resulting from HDAC4$^{N\text{-}term}$ expression at 22 °C.....264
Table 7.3 Frequency of mushroom body phenotypes resulting from the co-expression of HDAC4$^{N\text{-}term}$ and HDAC4^{WT} at 22°C....276
Table 7.4 Summary of the data presented in this chapter....285
Table 10.1. *Drosophila* lines used in this study....344
Table 10.2 Primers used for PCR amplification of regions spanning HDAC4$^{3SA\text{-}F65A}$....378
Table 10.3 Candidate interactors of HDAC4^{3SA} from initial mass spectrometry analysis....390
Table 10.4 Candidate interactors of HDAC4^{3SA} from the secondary mass spectrometry analysis....420
Table 10.5 HDAC4^{3SA} candidate interactors with annotations relating to HDAC4 overexpression-induced phenotypes....429
Table 10.6 HDAC4^{3SA} candidate interactors with annotations relating to splicing....431
Table 10.7 HDAC4^{3SA} candidate interactors with annotations relating to protein homeostasis....432
Table 10.8 Primers used for PCR amplification of *HDAC4$^{N\text{-}term}$*....435

Chapter One

Introduction

1. Introduction

1.1. Neurodevelopmental and neurodegenerative disease

Neurodevelopmental diseases refer to a group of disorders most frequently diagnosed in childhood that have a range of presentations including intellectual disability, difficulty with communication, learning impairments, and motor disorders (American Psychiatric Association, 2013). In contrast, the key characteristic of neurocognitive, or neurodegenerative disorders is acquired cognitive decline (American Psychiatric Association, 2013). Neurocognitive disorders are frequently described as age-related neurodegenerative diseases due to increased prevalence in the ageing population, and clinical manifestations include declines in executive function, learning, memory, and perceptual-motor ability. A subclassification of these is the dementias, which include Alzheimer's, Parkinson's, and neuronal intranuclear inclusion diseases. Despite evidence of a strong genetic basis for many neurodevelopmental diseases (Mitchell, 2011), and identification of genetic risk factors for neurodegenerative diseases (Bertram & Tanzi, 2005), the underlying mechanisms of pathology are largely unknown (Bergbaum & Ogilvie, 2016). The overlapping presentations of these diseases, notwithstanding differences in time of onset, suggest similarities in underlying disease aetiology, therefore a greater understanding of the molecular pathways involved in neurodevelopment will aid in deciphering how they dysfunction during neurodegeneration.

Estimates suggest a prevalence of neurodevelopmental disorders in New Zealand children of between 3-10% (Saraf & Marks, 2019). A wide panel of screening tools are available and effective intervention following diagnosis is possible (Saraf & Marks, 2019), nevertheless, a greater understanding of the mechanisms of disease will contribute to advancements in both screening and intervention, with a focus on improved quality of life. In 2020 an estimated 8% of the population aged over 65 lived with dementia in New Zealand, costing almost $52,000 per patient (Ma'u *et al.*, 2021). The number of people with dementia is increasing, expected to double in New Zealand and triple worldwide by 2050 (Ma'u *et al.*, 2021; Patterson, 2018). Indeed New Zealand also has an increasing ageing population (*National population projections: 2022(base)-2073*, 2022), and the pace of population ageing around the globe is also increasing (*Ageing and health*, 2022), due in part to an increase in the accessibility of healthcare (Roser *et al.*, 2013). The estimated incidence of dementia in New Zealand in 2020 ranged from 0.8% in the 65-69 year old bracket, to 33.9% in ages 95+ (Cheung *et al.*, 2022). Māori are also disproportionately burdened by dementia in New Zealand, being 8.5 years

younger than Pākeha when diagnosed (Cullum *et al.*, 2018), and having increased incidence compared to New Zealand Europeans in the 60+ and 80+ age categories by 21% and 24% respectively (Cheung *et al.*, 2022). It is therefore critical that New Zealand research focuses on how to effectively diagnose and manage the increasing number of dementia patients, for both their wellbeing as well as that of those around them. To achieve this, targeted research toward understanding biomarkers of disease onset and progression as well as development of therapeutic treatments is imperative.

1.1.1. Neurodegenerative disease aetiology: Protein aggregation is a common factor

It has been well established that progressive loss of neuronal cells, which occurs in all neurodegenerative diseases, is causative of disease, but the specific mechanisms through which neuronal loss occurs beyond induction of cell death remain unclear (Moujalled *et al.*, 2021). Our understanding of the underlying aetiologies of neurological diseases is increasing; there is evidence of genetic contributions to these diseases, such as mutations within APOE being associated with Alzheimer's disease (reviewed by Yamazaki *et al.* (2019)), and PINK1 in Parkinson's disease (reviewed by Quinn *et al.* (2020)), but these findings have not yet led to the development of revolutionary treatments. This is exemplified by the amyloid cascade hypothesis, which describes that growing accumulations of amyloid-β (Aβ), produced by cleavage of the amyloid precursor protein, are causative of AD pathology, specifically dementia (Karran *et al.*, 2011). However, there are a number of criticisms of the hypothesis, including that a significant population of aged but otherwise healthy individuals have high burdens of Aβ without dementia symptoms (reviewed in Kepp *et al.* (2023)), highlighting that the disease process is far more complex than first thought (Herrup, 2015). While the amyloid hypothesis remains illustrious in AD research, it is essential to focus on mechanisms beyond this to progress knowledge in the field of neurodegeneration, specifically to identify novel markers of disease progression for diagnostics, which may also be therapeutic targets if they are found to be causative of disease.

Given the overlapping phenotypes of neurodegenerative diseases, specifically dementia, it is important to look at common molecular features to begin to elucidate mechanisms of pathogenicity. One such feature is protein aggregation (Ross & Poirier, 2004; Takalo *et al.*, 2013), which refers to the accumulation and clumping of proteins within a cell, thought to occur

following protein misfolding. Typically, when a protein is natively folded the hydrophobic regions of the structure are buried within the interior, attaining the most thermodynamically favourable state (Wang *et al.*, 2010). If this process is disrupted, such as by a mutation, increase in protein level, or change in environment, the hydrophobic regions of a protein remain exposed and thus interact between proteins to reach a thermodynamically favourable conformation, resulting in aggregation (Balch *et al.*, 2008; Housmans *et al.*, 2023). Such an occurrence is not uncommon, and cells are able to respond to this via quality control mechanisms (reviewed by Ross and Poirier (2005) and Tyedmers *et al.* (2010)). The first line of defence is the induction of protein refolding via chaperone proteins, which minimises further aggregation. This allows targeting of aggregates for degradation via either the ubiquitin proteasome system (UPS) or autophagy. However, where these processes fail to match the rate of protein aggregation, extreme protective measures occur such as deposition into amyloid fibrils or aggresomes (Fink, 1998; Kopito, 2000).

There is contention around the role of these aggregates in disease onset and progression, highlighted by the above described caveat in the amyloid hypothesis; there appears to be a broad correlation between level of protein accumulation and severity of disease, but this does not address whether the aggregates themselves are causative of disease (Kepp *et al.*, 2023). Proposed mechanisms of pathogenicity of these aggregates include loss of function as well as toxic gain of function (Ogen-Shtern *et al.*, 2016). However, it has also been proposed that the overwhelm and impairment of the protein quality control machinery and clearance systems, instead of the aggregates themselves, is causative of disease (Gorman, 2008). This highlights that although different genetic contributions to neurodegenerative diseases have been identified, similar mechanisms may underlie the pathogenesis of these (i.e. dysfunction of protein homeostasis).

In light of this, it remains essential that research focuses on the whole story of protein aggregation. This includes understanding which proteins are susceptible to aggregation, how these aggregates form, the genetic contributions to aggregation susceptibility, correlations with neuronal dysfunction, and the cellular response to these aggregates. This will enable targeted approaches for preventing aggregate formation and protecting protein homeostasis, which may stop the onset and/or progression of neurodegenerative disease. This begins with fundamental studies of a protein's wild-type function to understand how such dysregulation may drive aggregation.

Finally, many genes involved in neurodegeneration also have roles in neurodevelopment (Magnin, 2021; Schor & Bianchi, 2021; Shabani & Hassan, 2023). Examining the roles genes have in neurodevelopment provides foundational understanding of their normal function, and aids in identification of what pathways may be disrupted in both neurodevelopmental and neurodegenerative diseases. Critically, understanding of roles in neurodevelopment and neuronal homeostasis will give a better understanding of how biomarkers may change over time, and enable appropriately timed targeting for therapeutics.

1.2. *Drosophila melanogaster* as a model for neuroscientific discovery

Drosophila melanogaster has long been used as a model to investigate neurodevelopmental and neurodegenerative disease (Gatto & Broadie, 2011; McGurk *et al.*, 2015). A large number of widely accepted concepts in developmental biology and genetics were elucidated in *Drosophila* models, including the chromosome theory of inheritance (Bridges, 1916; Morgan, 1910) and the molecular pathways that underpin embryonic development (Nüsslein-Volhard & Wieschaus, 1980). Importantly, approximately 75% of disease-causing genes in humans are conserved in *Drosophila* (Pandey & Nichols, 2011; Reiter *et al.*, 2001). This has allowed the development of *Drosophila* models of neurodegenerative disorders such as Parkinson's, Alzheimer's and polyglutamine diseases, resulting in increasing understanding of the molecular pathways involved in such diseases, as well as revealing potential therapeutic targets (Cao *et al.*, 2008; Crowther *et al.*, 2005; Feany & Bender, 2000; Fernandez-Funez *et al.*, 2000; Warrick *et al.*, 1998). In addition to the ease of culturing *Drosophila* and their short lifespan, their appeal owes largely to the genetic toolkit which has been developed to manipulate gene expression *in vivo,* as well as easily monitored developmental phenotypes (reviewed in Jeibmann and Paulus (2009)). This is complemented by the existence of FlyBase, a database which compiles genetic and genomic data, including *Drosophila* genes (with approved names and symbols to enable consistency in the literature), their associated phenotypes, and tools that are available to examine them (Gramates *et al.*, 2022).

Drosophila have a relatively small non-redundant genome of approximately 180 Mb (Adams *et al.*, 2000) encoding >17,800 genes (R6.55, Gramates *et al.* (2022)) over four chromosomes (Bridges, 1916). Established techniques enable the stable transformation of *Drosophila* via site-specific genomic integration of transgenes (Appendix 10.1.5), and insertion of regulatory

elements allows fine spatiotemporal control of gene expression via the UAS-GAL4 and TARGET systems (Section 1.2.3). Mutant and transgenic lines are widely available from stock centres including the Vienna *Drosophila* Resource Centre (VDRC), Bloomington *Drosophila* Stock Centre (BDSC) and Kyoto Stock Centre.

1.2.1. Introduction to *Drosophila* genetics

The genome of *Drosophila* is arranged across four pairs of chromosomes, consisting of the X/Y pair, the second, third and fourth chromosomes (Roote & Prokop, 2013). Like humans, *Drosophila* is diploid and the rules of classical genetics apply; genes undergo equal segregation and thus one copy of each gene is inherited from either parent. It is this that allows the design of genetic crosses (Figure 1.1), which are used to represent the inheritance of traits/genes of interest when using *Drosophila*.

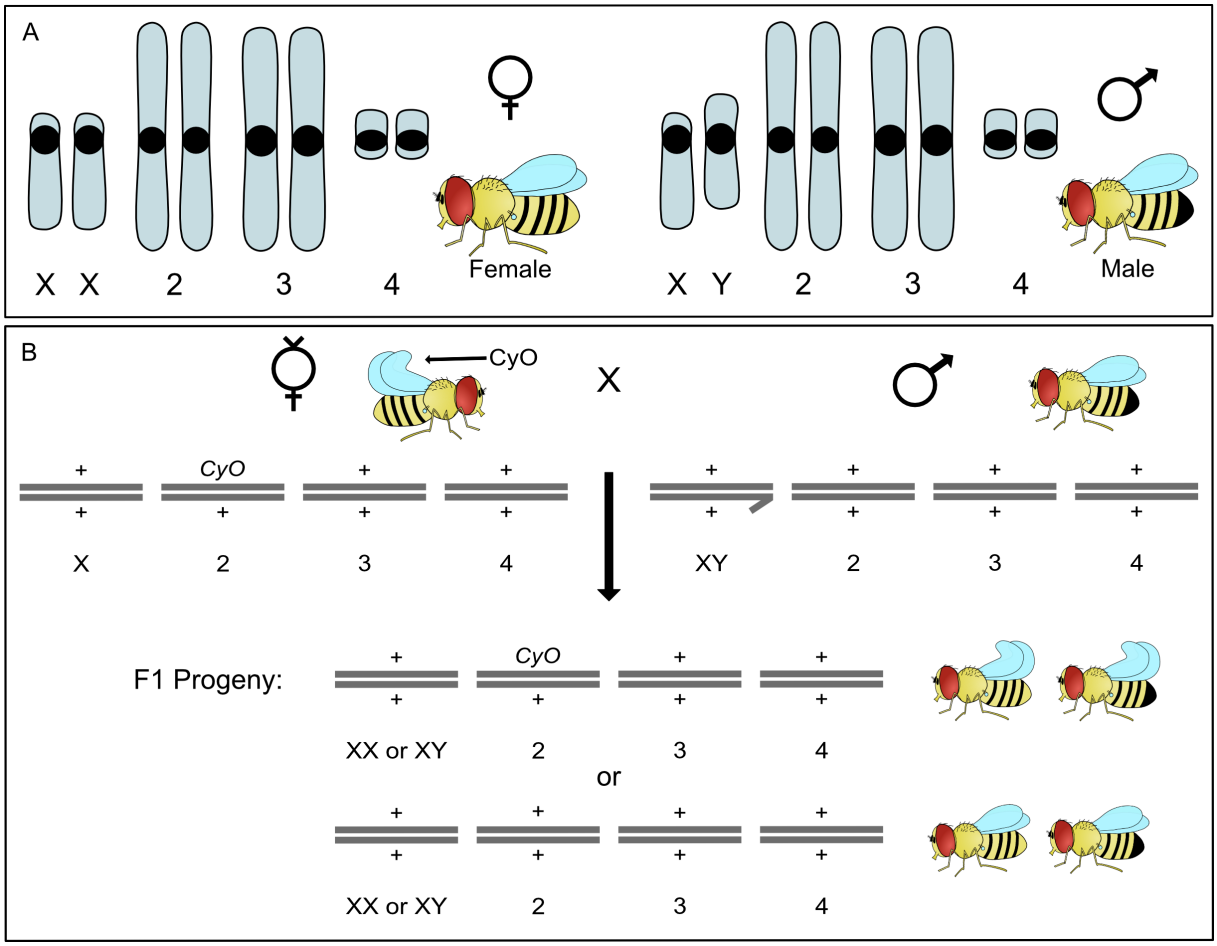

Figure 1.1 Example of a genetic cross depicting the inheritance of the curly wing marker in *Drosophila*

(A) Schematic depiction of the arrangement of the *Drosophila* genome across four chromosomes. Females are XX and males are XY. (B) Genetic cross in which females that are heterozygous for the dominant curly wing marker (*CyO*) on the second chromosome are crossed to wild-type males. Wild-type chromosomes are represented by a +. Half of the F1 progeny of this cross receive the *CyO*-containing chromosome from the maternal parent and thus have curly wings, while the other half receive the wild-type chromosome from both parents and thus have no visible phenotype. The number of each chromosome is noted. The V on the head of the female symbol denotes that this parent was a virgin (i.e. all eggs from this female will only be fertilised by the male used in this cross). *This figure is an original artwork created with reference to Hales et al. (2015).*

Genetic crosses have been designed to facilitate studies in this thesis and are included in the Methods (Section 3.1.3) and Appendix (Section 10.1.6). These follow the above conventions as described in Roote and Prokop (2013); chromosomes are drawn in order with the X/Y chromosome representing the first pair (the X chromosome is also referred to as the first chromosome). Chromosomes are represented by a line and the genes/markers of interest (which may or may not contain mutations) on each chromosome are noted above/below. A plus (+) is used to indicate a wild-type chromosome. In the F1 progeny the top chromosome is inherited from the female parent and the bottom from the male parent.

Balancer chromosomes are a key tool for ensuring accuracy of genotypes in complex genetic crossing schemes that continue over several generations (Roote & Prokop, 2013). Balancer chromosomes contain dominant mutations that act as visible markers, and their inheritance can be traced through progeny. For example, *CyO* in Figure 1.1B corresponds to the Curly of Oster marker, present within a balancer chromosome, and flies with this chromosome have curly wings. These chromosomes contain mutations that are homozygous lethal (i.e. are recessive lethal), and hence can be kept as a stable heterozygous population when balancing a homozygous lethal gene of interest. Balancer chromosomes also contain inverted repeats, which prevent unwanted recombination events with the target gene, and are essential in maintaining multiple genes of interest on a single chromosome in heterozygotes (Hales *et al.*, 2015).

Unlike humans however, *Drosophila* sex determination differs, and males undergo dosage compensation (reviewed in Gelbart and Kuroda (2009)). That is, in males (XY) transcription from the X chromosome is upregulated by approximately two-fold to match that of females (XX). This is an important consideration in this study as the endogenous *Drosophila HDAC4* gene is found on the X-chromosome, and therefore crosses with the *HDAC4::GFP* line

(introduced in Section 4.2) must consider both the directionality of the cross (i.e. males do not pass on an X chromosome to sons) as well as the offspring examined to ensure equal dosage of *HDAC4::GFP*. Moreover, the *elav-GAL4* driver (introduced in Section 4.1) is also on the X-chromosome, and therefore progeny must similarly be considered for level of *GAL4* expression. Finally, dosage compensation in *Drosophila* also results in slight differences in wild-type eye colour between males and females due to the presence of the *white* gene on the X chromosome (Hazelrigg *et al.*, 1984), which encodes a membrane transporter required for pigment synthesis (Sullivan & Sullivan, 1975). Males have increased expression of *white* resulting in more intense eye pigmentation.

1.2.2. Nomenclature used in this thesis

As the experiments performed in this thesis are grounded in the *Drosophila* model, all nomenclature follows the convention as set out in FlyBase, (Gramates *et al.* (2022), https://wiki.flybase.org/wiki/FlyBase:Nomenclature), and approved *Drosophila* gene names and gene symbols are used throughout this thesis. Gene names and genotypes are italicised, and protein names and phenotypes named after a genotype are non-italic. Protein names are not approved by FlyBase and therefore follow the consensus of the literature; the first letter of proteins named after a gene is capitalised, and protein names that are an abbreviation (such as HDAC4, short for histone deacetylase four) are entirely capitalised. Superscript is used to denote the allele of a gene, named after the amino-acid substitution or mutation within the protein. Superscript WT denotes the wild-type allele. A plus (+) is used to denote wild-type chromosomes. When referring to non-*Drosophila* genes and proteins, the nomenclature follows the consensus in the literature.

1.2.3. Spatial and temporal control of gene expression in *Drosophila*

Drosophila is described as the gold standard for precise tissue-specific and temporal regulation of gene expression (Ogienko *et al.*, 2022). Many systems are available that have been designed to allow manipulation of both endogenous and exogenous gene expression in any tissue at any stage of development (reviewed in del Valle Rodríguez *et al.* (2011) and Xu *et al.* (2019)). The most common and elegant system for such manipulation is the bipartite UAS-GAL4 system (Brand and Perrimon (1993), Figure 1.2).

GAL4 'driver' fly lines govern the tissue specificity of the bipartite system (Brand & Perrimon, 1993). These consist of genomic insertions of the yeast *GAL4* transcriptional activator (Ma & Ptashne, 1987), the expression of which is dependent on nearby regulatory elements. Many established collections of *GAL4* lines were developed using enhancer traps generated by transposon mutagenesis, whereby a transposon carrying *GAL4* is randomly inserted into the genome and the expression pattern of *GAL4* governed by nearby enhancers is determined using a GAL4-responsive reporter (Brand & Perrimon, 1993; O'Kane & Gehring, 1987). Alternatively, driver lines are also generated with high specificity from genomic integration of plasmids in which promoter fragments with known tissue specificity are cloned upstream of the *GAL4* coding sequence (Brand & Perrimon, 1993; Jenett *et al.*, 2012). The location of *GAL4* insertion in these lines is known, reducing genomic positional effects (Pfeiffer *et al.*, 2010).

The GAL4 DNA binding site is known as the upstream activating sequence (*UAS*) (Webster *et al.*, 1988). The *UAS* is not responsive to endogenous *Drosophila* transcriptional activators, therefore the *UAS-transgene* construct is not constitutively expressed (Fischer *et al.*, 1988). Crossing of flies harbouring the *GAL4* driver line with flies harbouring the *UAS-transgene* line yields F1 progeny that inherit both components of this system and therefore express GAL4 in a tissue-specific manner, which activates transgene expression in this pattern (Figure 1.2).

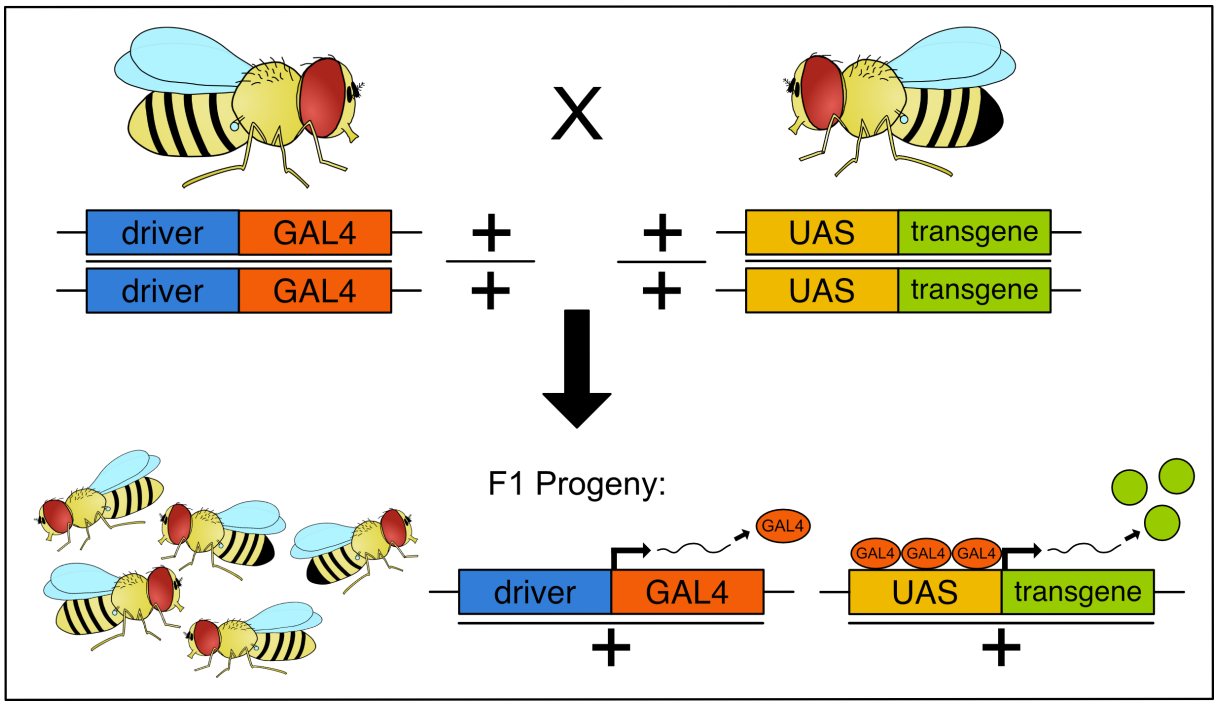

Figure 1.2 The UAS-GAL4 system

Schematic diagram depicting the inheritance and activation of the UAS-GAL4 system in *Drosophila*. Two parental lines homozygous for the *driver-GAL4* and *UAS-transgene* on chromosomes 2 and 3, respectively, are shown. When crossed together, the F1 progeny inherit both components of the system, and are heterozygous for each of the *driver-GAL4* and *UAS-transgene*-containing chromosomes. Wild-type chromosomes are indicated by +. F1 progeny express the GAL4 transcriptional activator in a tissue specific manner (governed by the 'driver' regulatory elements), which binds to the *UAS* (upstream activating sequence) and activates transgene expression in target cells. *This figure is an original artwork created with reference to Brand and Perrimon (1993).*

In addition to transgene expression to facilitate overexpression studies, inverted repeat or short hairpin RNAs (shRNA) can also be designed and expressed under GAL4 control to target endogenous mRNA for RNA interference (RNAi), resulting in tissue-specific knockdown (Dietzl *et al.*, 2007). More recently, the CRISPR-Cas9 system has been adapted for use in *Drosophila* alongside the UAS-GAL4 system, allowing spatially restricted highly specific mutagenesis (Gratz *et al.*, 2013; Port *et al.*, 2020).

The temporal and regional gene expression targeting (TARGET) system is an adaptation of the UAS-GAL4 system that enables the addition of temporal control (reviewed in McGuire *et al.* (2004)). GAL80 is a repressor of GAL4 (Lee & Luo, 1999; Yun *et al.*, 1991), and GAL80ts, which is a temperature sensitive mutant of GAL80, enables temperature sensitive repression (McGuire *et al.* (2003), Figure 1.3). *GAL80ts* is typically placed under the control of the *tubulin* promoter, and thus is expressed ubiquitously. At permissive temperatures (18°C), GAL80ts binds GAL4, preventing interaction with the *UAS* and restricting transgene expression. Temperature increases result in the degradation of GAL80ts, therefore at non-permissive temperatures (30°C) GAL4 is no longer repressed, resulting in activation of transgene expression. The temperature at which flies are raised can be manipulated to restrict or enable transgene expression as required, governing temporal specificity. This is particularly advantageous in deciphering the role of a gene during development compared to in adult life, and becomes especially important in teasing apart the function of genes in the brain, as those involved in neurodevelopment usually also have roles in learning, memory and neurodegeneration (Magnin, 2021). Moreover, in the presence of GAL80ts, GAL4 undergoes linear temperature-dependent increases in activity between 18 °C and 30 °C (McGuire *et al.*, 2004; Schwartz *et al.*, 2016), allowing further fine-tuning of the level of transgene expression (Hawley *et al.*, 2023; Tan *et al.*, 2024).

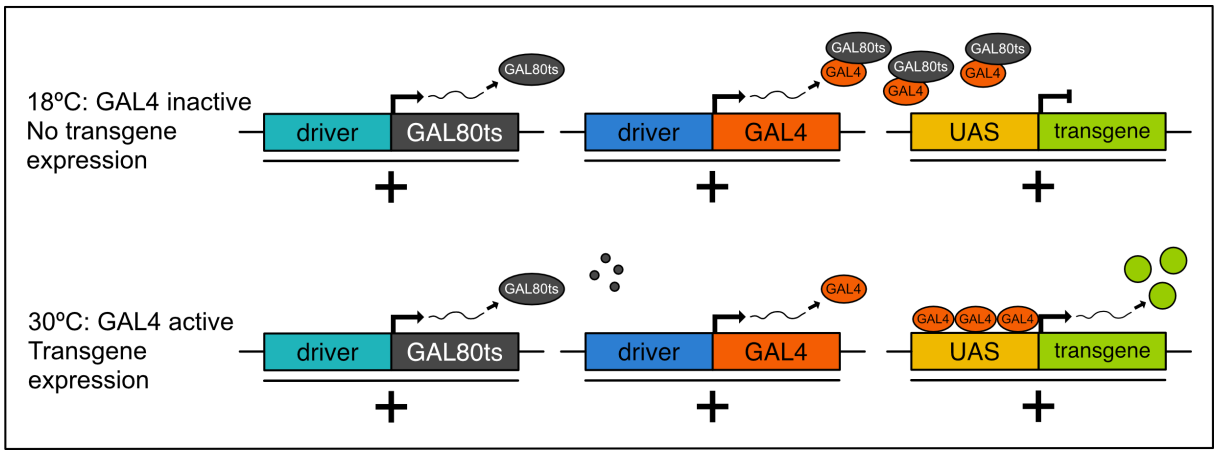

Figure 1.3 The TARGET system
Schematic diagram representing the TARGET system. An example *Drosophila* genotype is depicted (heterozygotes, *transgene/+*), with chromosomes 2-4 containing each component of the system. To restrict transgene expression to adulthood, flies are raised at the restrictive temperature (18°C) where a temperature sensitive mutant of GAL80, GAL80ts, binds to GAL4 to prevent *UAS* binding. Once emerged, flies are transferred to the permissive temperature (30°C) where GAL80ts is degraded and no longer binds GAL4, thus transgene expression is activated. *This figure is an adaptation from that found in Hawley et al. (2023) (doi: 10.17912/micropub.biology.000885), which is distributed under CC BY 4.0.*

1.3. *Drosophila* development

A major advantage of *Drosophila* as a model organism is their ease of culturing (Methods 3.1.2), quick generation of a large number of progeny for functional characterisation, and short lifespan (Hales *et al.*, 2015). *Drosophila* is a typical invertebrate that undergoes metamorphosis, with a lifecycle involving four distinct stages; embryo, larva, pupa, and adult (reviewed in Hales et al. (2015)). Many structures in the adult fly develop from imaginal discs, which are epithelial sacs of undifferentiated cells with determined developmental fates reserved from a small cluster of cells early in embryonic development (reviewed in Blair (1999)). The precise regulation of gene expression that occurs during *Drosophila* development is well understood and demonstrates conservation with vertebrate development; determination of the dorsoventral axes of *Drosophila* and vertebrate embryos as well as limb patterning are highly similar processes (Holley *et al.*, 1995; Johnson & Tabin, 1997). Taken together, these features position *Drosophila* as an excellent model to explore the molecular function of human homologues in development.

1.3.1. The *Drosophila* brain

The *Drosophila* brain (Figure 1.4) is a compact yet highly complex organised structure, significantly smaller than its human counterpart, with an estimated 100,000 neurons (Simpson, 2009). *Drosophila* share the same neurotransmitter systems as vertebrates, and furthermore, the neuronal genes and molecular pathways involved in neuronal function are highly conserved (Pandey & Nichols, 2011), making *Drosophila* an excellent small-scale model for the human brain. The brain is easily isolated from the fly head and immunohistochemistry enables visualisation of the gross structure as well as *in vivo* protein characterisation (Helfrich-Forster, 2007; Wu & Luo, 2006), a valuable tool in applied neurobiology for both understanding and treating neurological disease (Pandey & Nichols, 2011). This value is extended by the array of pre-characterised neuronal GAL4-driver lines available (Aso *et al.*, 2009).

The *Drosophila* mushroom body is a key integration centre for sensory information and shares many architectural features with the vertebrate cerebellum (Li *et al.*, 2020). The bundled neuropile structure (Figure 1.4B) receives both olfactory and non-olfactory inputs essential in learning and memory (de Belle & Heisenberg, 1994; Dubnau *et al.*, 2001; Heisenberg *et al.*, 1985; McBride *et al.*, 1999). Kenyon cells (KCs), similar to granule cells of the vertebrate brain (Li *et al.*, 2020), are the intrinsic neurons of the mushroom body. There are between 2,000-2,500 KCs per hemisphere (Aso *et al.*, 2009; Balling *et al.*, 1987), born from four neuroblasts (Ito *et al.*, 1997). KC bodies are positioned in the posterior of the brain (Figure 1.4C), spatially organised by the neuroblast from which they arose (Li *et al.*, 2020), and project their axons anteriorly into a bundled fibre termed the peduncle, before dividing into lobes (Heisenberg *et al.*, 1985). Dendritic processes of KCs arborise in the calyx, where they receive olfactory inputs (Yasuyama *et al.*, 2002). KCs are separated into three subtypes governed by their lobe organisation; at the anterior point of the peduncle, alpha/beta (α/β) and alpha prime/beta prime (α'/β') KC axons bifurcate into dorsal and medial lobes, while gamma (γ) axons only extend medially (Figure 1.4D) (Crittenden *et al.*, 1998). The projection of KCs into the mushroom body occurs in a defined, sequential pattern involving neuron birth, pruning and axon degeneration (Lee *et al.*, 1999).

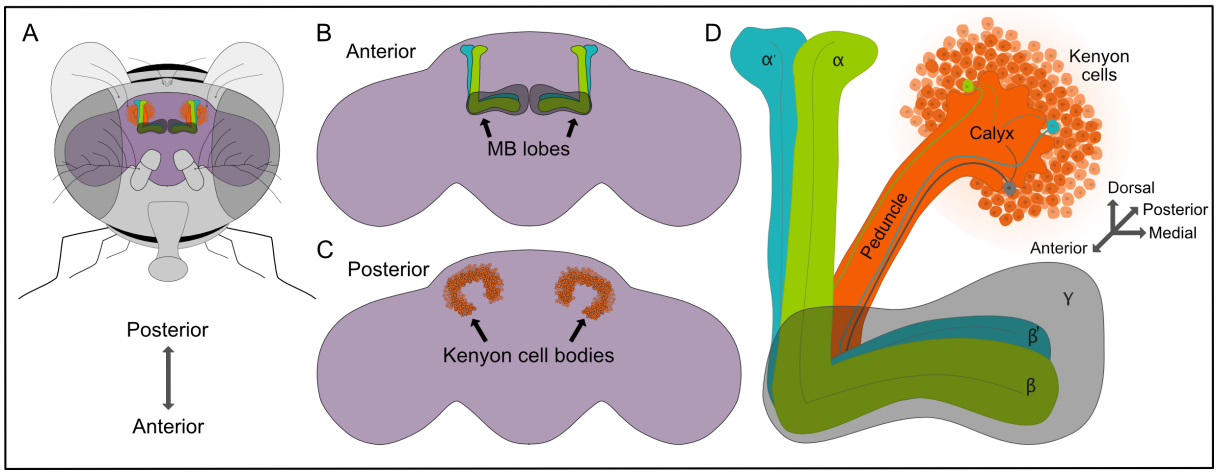

Figure 1.4 The structure of the adult *Drosophila* mushroom body
(A) Schematic depiction of a fly viewed from the anterior, with the brain coloured in purple. (B) Anterior view of the mushroom body lobes within the *Drosophila* brain. (C) Posterior view of the Kenyon cell bodies within the *Drosophila* brain. (D) Axons of the three types of Kenyon cells (α/β, α'/β' and γ) project from the cell bodies (posterior) through the peduncle (orange) and branch to form the lobes of the mushroom body. Dendrites project to form the calyx. A single neuron of each cell type is depicted, projecting through the peduncle as well as into the calyx; α/β, green; α'/β' teal; γ, grey. *This figure is an adaptation from that found in Tan et al. (2024) (doi: 10.1186/s12915-023-01800-1), which is distributed under CC BY 4.0.*

Consisting of bundles of axons, the mushroom body is an effective model to assess defects in axon morphogenesis. The development of the mushroom body can be readily assessed via immunohistochemistry; Fasciclin II (FasII) is a neuronal cell adhesion molecule expressed in the α-, β- and γ-lobes of the mushroom body (Crittenden *et al.*, 1998). Immunostaining with anti-FasII therefore highlights the mushroom body, and neurodevelopmental phenotypes can be scored using standard parameters (Freymuth & Fitzsimons, 2017; Main *et al.*, 2021; Palmer & Fitzsimons, 2023; Schwartz *et al.*, 2023; Tan *et al.*, 2024). Axon bundles of the β-lobes typically terminate prior to the midline, leaving a gap between the left and right lobes, however if they are defective in termination, these axons cross the midline, appearing as β-lobe fusion. This can be characterised as mild if a subset of axons cross the midline, or severe if the majority cross the midline (Tan *et al.*, 2024). Similarly, where a subset of axons fail to elongate, lobes appear thin, or may be entirely absent if all display defects in elongation. Lobes may also be misdirected as a result of deficits in axon guidance.

1.3.2. The *Drosophila* eye

The adult *Drosophila* eye is a highly organised lattice of between 700-800 bundles of photoreceptors, termed ommatidia (Cagan & Ready, 1989; Ready *et al.*, 1976) (Figure 1.5A). Each ommatidium consists of a cluster of eight photoreceptors (R1-R8), as well as four non-neuronal accessory cone cells, and two primary pigment cells (Figure 1.5B) (Ready *et al.*, 1976). These clusters are further surrounded by shared insulating secondary and tertiary pigment cells (Burnet *et al.*, 1968; Tomlinson, 2012), and mechanosensory bristles intersperse ommatidia at opposing vertices (Cagan & Ready, 1989). Together, this comprises an incredibly precise arrangement of ommatidia and bristles that evenly cover the visual field.

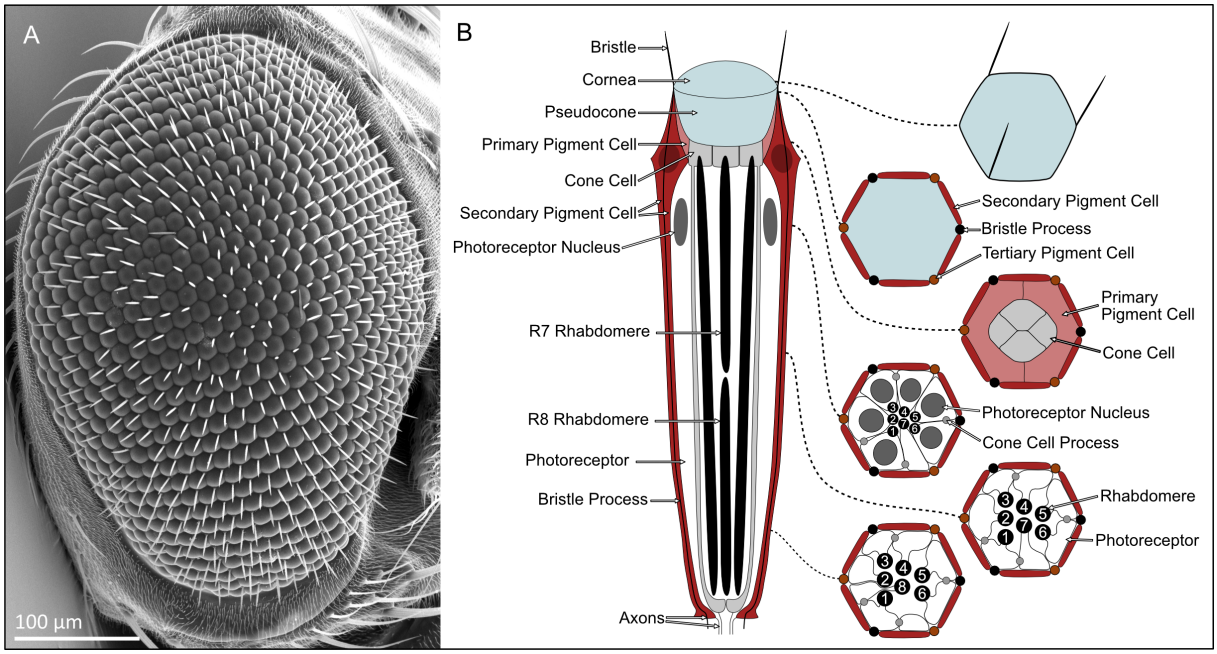

Figure 1.5 The organisation of the adult *Drosophila* eye
(A) Scanning electron microscopy image of a wild-type *Drosophila* eye. (B) Schematic diagram depicting a cross section of an adult ommatidium. Single sections at right angles to the cross section on the left are shown at indicated depths to further demonstrate the organisation of cells within an ommatidium. Each ommatidium contains eight photoreceptor cells (R1-R8), four cone cells and two primary pigment cells, and shares secondary and tertiary pigment cells and bristles with neighbouring ommatidia. The lens (cornea) is at the apical most surface. *This figure is an original artwork created with reference to Wolff and Ready (1993) and Nie et al. (2015).*

Developmental perturbation or neurodegeneration of the neurocrystalline array is readily visualised, and as the eye is not required for survival (Halder *et al.*, 1995; Richards & Furrow, 1925) this provides a useful model for the study of neurodevelopmental and neurodegenerative pathways (Cao *et al.*, 2008; St Johnston, 2002). Genetic modifier screens in the eye most

famously aided in the elucidation of the receptor tyrosine kinase and Ras signalling pathways (Karim *et al.*, 1996; Simon *et al.*, 1991). More recently, the eye has been used for modelling genetic diseases and screening personalised cancer therapeutics (Kasai & Cagan, 2010). While these screens are performed using light microscopy and visualise the adult eye, complementary immunohistochemistry can be performed on the developing eye; third instar eye discs are easily isolated and imaged (Spratford & Kumar, 2014) (Figure 1.6A), allowing for analysis of the effects of gene expression on early eye development.

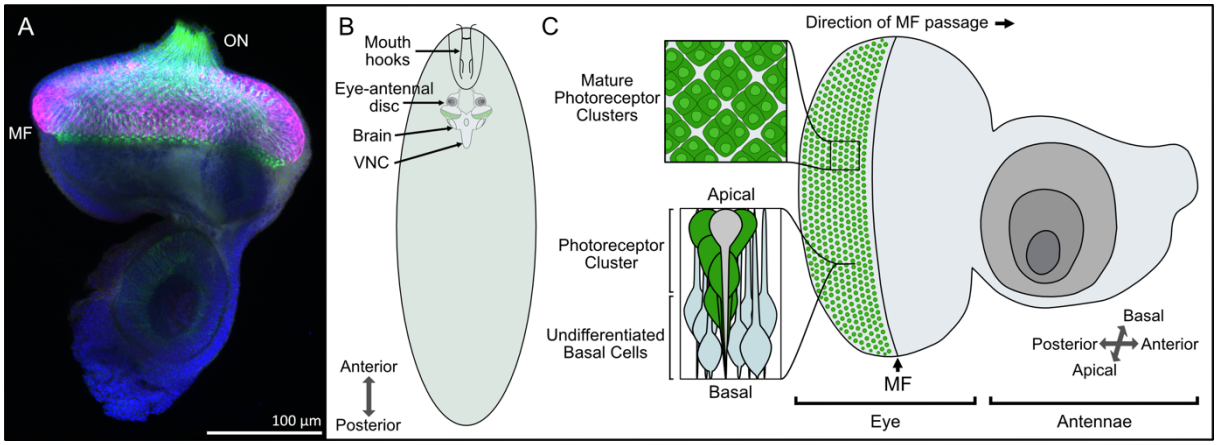

Figure 1.6 The *Drosophila* eye develops from the eye-antennal disc
(A) Maximum projection image of a third instar larval eye disc; photoreceptor axons are shown in green, postmitotic photoreceptor cells in magenta, and nuclei across the disc in blue. ON, optic nerve; MF, morphogenetic furrow. (B) Schematic diagram of a third instar larva depicting the position of the brain, eye-antennal discs, and mouth hooks. VNC, ventral nerve cord. (C) Schematic diagram of the third instar larval eye disc. Eye disc has been rotated 90° relative to in (B). Arrows indicate directionality; basal is into the page and apical is out of the page. Upper panel: mature photoreceptor clusters are found at the apical surface and are observed in a square array. Lower panel: a cross section through the disc showing recruitment of photoreceptor cells into clusters at the apical surface (green) and undifferentiated cells remaining at the basal surface. Photoreceptor cells posterior to the MF in (B) and (C) are labelled green. *This figure is an original artwork created with reference to Spratford and Kumar (2014), Ready et al. (1976), and Fan and Bergmann (2008).*

The precise development and patterning of the *Drosophila* eye initiates early in larval development. The adult visual field forms from the eye-antennal disc (Figure 1.6A, C) which develops in a defined sequence (reviewed in Cagan (2009)). Asynchronous cell division increases the population of precursor cells (Meserve & Duronio, 2017) before a morphogenetic front advances from posterior to anterior of the disc, leaving a wake of differentiated photoreceptors posterior to the morphogenetic furrow by the end of the third instar (Ready *et al.*, 1976). It is during this time in which the defined pattern of photoreceptors emerge; following the passage of the furrow, photoreceptor cells are progressively recruited to the apical

clusters (Figure 1.6C, green) from posterior to anterior of the disc (Fristrom & Rickoll, 1982), while undifferentiated cells remain at the basal surface (Fan & Bergmann, 2008). At this stage the photoreceptor clusters are observed as a square array at the apical surface (containing R1-8) and their axons project through the basal cells to the basement membrane, where growth cones direct posterior growth and bundle into the optic nerve, which innervates the optic lobe of the larval brain (Tomlinson, 1985). Throughout late larval development cone cells are also recruited to the apical surface (Tomlinson, 1985), and the remaining cells that occupy the basal side of the disc are undifferentiated accessory cells, including pigment and bristle cells, which are organised later in pupal development (Ready *et al.*, 1976). In early pupal development, the eye disc unfolds and everts resulting in exposure of the developed eye tissue, and recruitment of the pigment and bristle cells to the ommatidium completes the hexagonal lattice (Cagan & Ready, 1989); 48 hours after pupal formation the patterning is identical to that in adult retina (Ready *et al.*, 1976). Cell death occurs throughout pupal development and refines the organisation of the lattice, in particular by removing excess interommatidial cells (Wolff & Ready, 1991).

Disruption to the expression of genes important in development (Thomas & Wassarman, 1999) often results in widespread disorganisation of the array of ommatidia and bristles, as well as fusion of ommatidia, which is commonly referred to as a "rough" eye phenotype. This disorganisation can result from defects in patterning, occurring as early as during passage of the morphogenetic furrow, until 55 hours after pupal formation at which time pattern formation is complete (Wolff & Ready, 1991). Therefore, examination of the larval eye is of interest to visualise changes in protein localisation that may induce defects in adult eye morphology.

1.4. Epigenetic regulation of gene expression

Epigenetic regulation of gene expression refers to the heritable changes in genome function that occur independent of changes in the sequence of DNA (Handy *et al.*, 2011). Examples of epigenetic modifications include DNA methylation and histone modification, however DNA methylation in *Drosophila* is low compared to in mammals (Dunwell & Pfeifer, 2014), and therefore most epigenetic regulation in *Drosophila* is via histone modification. In the nucleus, the genetic material is arranged into a tightly packed structure known as chromatin, composed of DNA and histone proteins (reviewed in Campos and Reinberg (2009)). Four histone proteins

form a core octamer (H2A, H2B, H3 and H4), and 147 base pairs (bp) of DNA wrap around this core to form the nucleosome (Richmond and Davey (2003), Figure 1.7). Histone H1 associates on the surface of the core nucleosome, binding the DNA entry/exit sites, and facilitates compaction of chromatin into higher-order structures (reviewed in Hergeth and Schneider (2015)). Core histones have a globular head domain and an N-terminal tail that protrudes from the nucleosome (Mariño-Ramírez *et al.*, 2005). Covalent modification of histone tails alters the accessibility of chromatin to the transcription machinery, and various combinations of post-translational modifications differentially mediate access to the DNA, known as the histone code (Jenuwein & Allis, 2001). Major modifications on histone tails include acetylation, methylation, and phosphorylation, and are dynamically regulated by enzymes that catalyse either addition or removal, therefore the careful balance of the activities of these proteins is critical for controlled gene expression (Verdin & Ott, 2015).

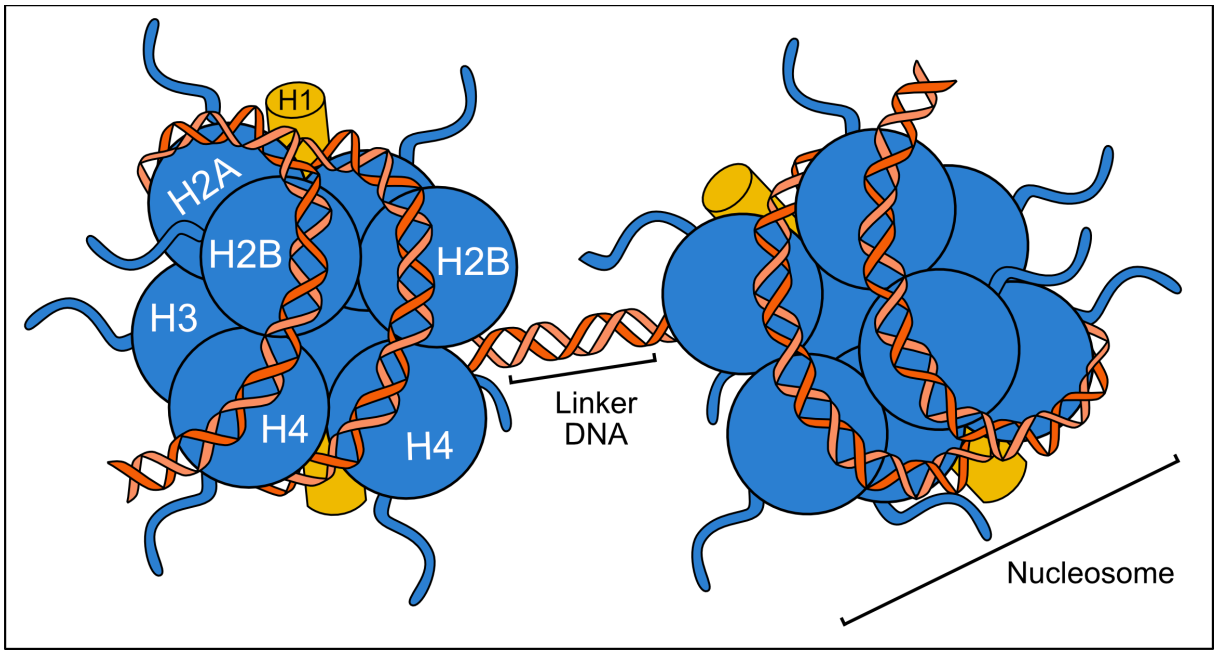

Figure 1.7 DNA associates with histone proteins to form nucleosomes
Schematic diagram depicting the organisation of DNA and histone proteins into nucleosomes. Each nucleosome consists of eight core histones (H2A, H2B, H3 and H4) around which 147 bp of DNA is wound. Linker DNA separates sequential nucleosomes. Histone H1 binds linker DNA and stabilises nucleosome formation and compaction. *This figure is an adaptation from that found in Caputi et al. (2017) (doi: 10.5772/intechopen.69566), which is distributed under CC BY 3.0.*

1.4.1. Histone acetylation and deacetylation

Reversible histone acetylation occurs on ε-lysine residues within the N-terminal tail of histone proteins (Allfrey *et al.*, 1964), catalysed by histone acetyltransferases (HATs) (reviewed in Struhl (1998)) (Figure 1.8). Unmodified histone tails carry a net positive charge, resulting in their interaction with the negatively charged phosphate groups within DNA (Mariño-Ramírez *et al.*, 2005). Addition of an acetyl group neutralises this and reduces the affinity of the histone tail for DNA (Hong *et al.*, 1993), resulting in an open chromatin conformation referred to as euchromatin (Norton *et al.*, 1989). In an acetylated open conformation, bromodomain containing proteins recognise acetyl groups and create an environment conducive to gene expression through further histone modification, modulation of the chromatin architecture, and recruitment of the transcription machinery (Fujisawa & Filippakopoulos, 2017; Jacobson *et al.*, 2000). The action of HATs is antagonised by histone deacetylases (HDACs), which remove acetyl groups, increasing the affinity of histone tails for DNA and reducing accessibility in a conformation known as heterochromatin (reviewed in Seto and Yoshida (2014)). Despite the name, phylogenetic analysis determined that HDACs precede the evolution of histone proteins (Gregoretti *et al.*, 2004) and act on a number of non-histone proteins to induce changes in protein stability, enzymatic activity, and protein-protein interactions, ultimately modifying their function (Narita *et al.*, 2019).

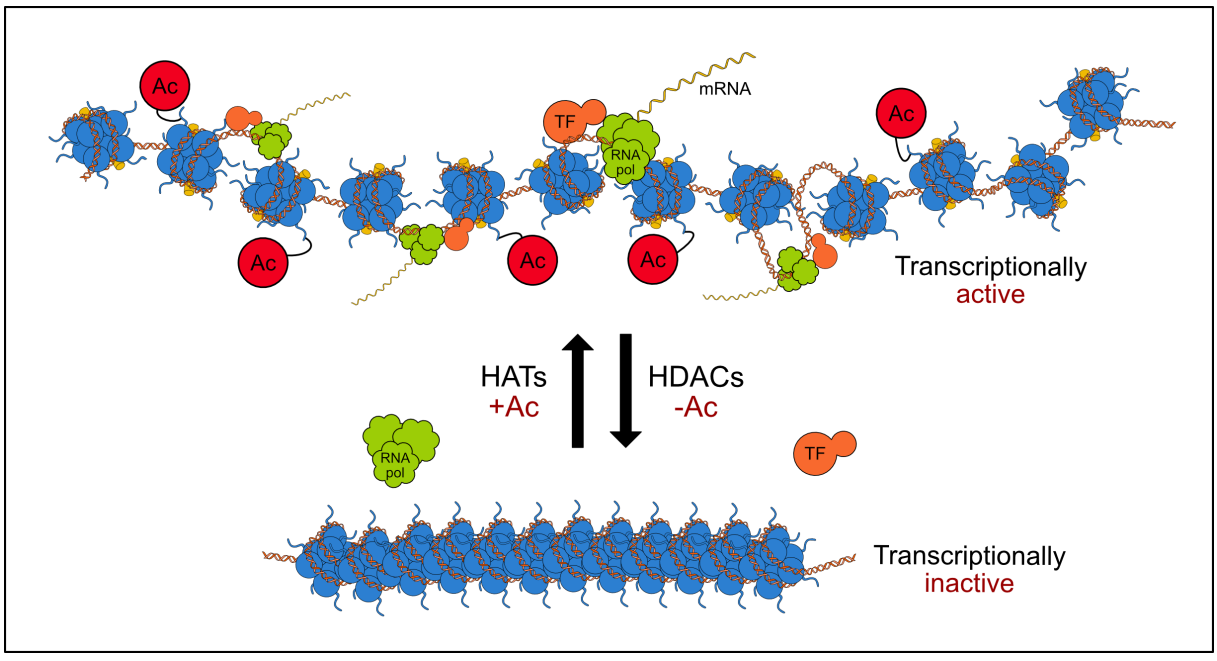

Figure 1.8 Modification of histones by histone acetyltransferases and deacetylases impacts chromatin compaction and transcription

Schematic diagram depicting the effect of histone acetylation on chromatin compaction and transcription. Histone acetyltransferases (HATs) add acetyl groups to the tails of core histone proteins which results in an open chromatin conformation, enabling association of transcription factors (TF) and RNA polymerase (RNApol) with DNA that results in transcription of mRNA. Histone deacetylases (HDACs) remove acetyl groups from the tails of core histones, resulting in compaction of chromatin and preventing association of transcription factors and RNA polymerase. *This figure is an original artwork created with reference to Verdin and Ott (2015).*

1.4.2. Histone deacetylases

HDACs are a highly conserved family of proteins that are divided into four classes based on sequence homology and phylogenetic analysis (Seto & Yoshida, 2014). With the exception of fungi, all classes are found in fully-sequenced eukaryotes (Gregoretti *et al.*, 2004), therefore some functional overlap may occur between classes, but each must have an essential non-redundant function. The four classes (I-IV) are homologous to the yeast histone deacetylases *Rpd3*, *HDA1*, *Sir2* and *Hos3* respectively (Park & Kim, 2020). All zinc-dependent classes are depicted in Figure 1.9.

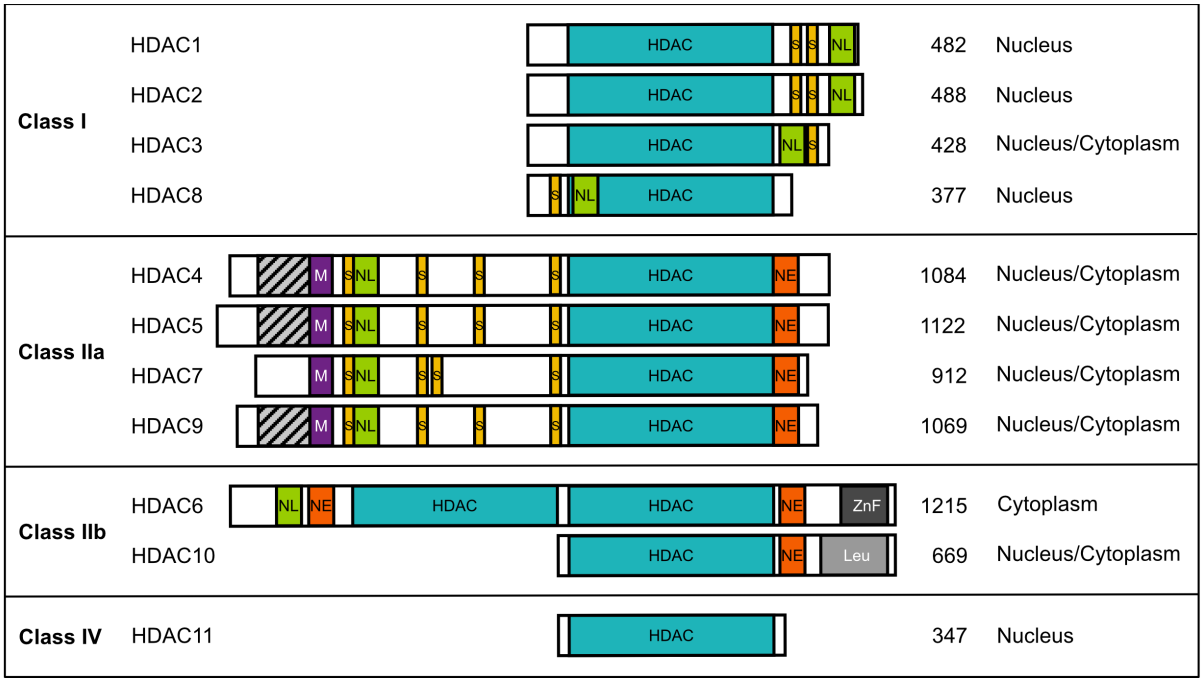

Figure 1.9 Domain alignment of the human zinc-dependent histone deacetylases
Schematic diagram depicting the domain structure of the zinc-dependent family of HDACs (class III, the Sirtuins, is not shown). The number of residues comprising each of the predominant human isoforms is noted alongside the accepted subcellular distribution. NL, nuclear localisation signal, green; M, MEF2 binding site, purple; S, serine residues that mediate 14-3-3 binding, yellow, NE, nuclear export signal, orange; HDAC, histone deacetylase domain, teal; ZnF, zinc finger motif, dark grey; Leu, leucine rich region, light grey. Shaded area depicts the α-helix/coiled-coil domain. *This figure is an original artwork created with reference to Haberland et al. (2009), Kwon et al. (2020), Liu et al. (2012), Milazzo et al. (2020), Yang and Seto (2008), Yang et al. (2018), Xu et al. (2012).*

Class I HDACs (HDACs 1, 2, 3 & 8) are catalytically active and are responsible for the majority of deacetylase activity *in vivo* (Fischle *et al.,* 2001; Lahm *et al.*, 2007). Class I HDACs are ubiquitously expressed and predominantly nuclear (Park & Kim, 2020), however their subcellular localisation differs between tissues (reviewed in Moser *et al.* (2014) and Seto and Yoshida (2014)). In contrast, with the exception of HDAC6, which is exclusively cytoplasmic (Hubbert *et al.*, 2002), class II HDACs undergo dynamic nucleocytoplasmic shuttling, thought to be important in regulating their activity (Section 1.5.1). Class II is further divided into subclass IIa (HDACs 4, 5, 7 & 9), and IIb (HDACs 6 & 10). All class II HDACs have a conserved deacetylase domain, while IIa have an N-terminal extension critical in transcription factor binding (Section 1.5) and homo- and hetero-oligomerisation (Section 1.8), and IIb have a C-terminal tail domain (Park & Kim, 2020). While the above mentioned HDACs are Zn^{2+} dependent, Class III HDACs, also known as sirtuins, exhibit NAD dependent deacetylase activity (Imai *et al.*, 2000) and are widely expressed and differ in their subcellular localisation (Herskovits & Guarente, 2013; Nakagawa & Guarente, 2011). Relatively little is known about class IV HDACs in comparison, HDAC11 being the sole member; it is predominantly nuclear (Gao *et al.*, 2002) and has a novel role in fatty acid metabolism in skeletal muscle (Hurtado *et al.*, 2020).

1.5. Histone deacetylase four (HDAC4): structure and function

Histone deacetylase four (*HDAC4*) was first identified in 1999 by homology to the yeast class II HDAC *Hda1p* (Grozinger *et al.*, 1999; Miska *et al.*, 1999; Wang *et al.*, 1999). It is highly conserved; human and *Drosophila* HDAC4 share 57% identity and 84% similarity through the C-terminal domain, and 35% identity and 59% similarity overall (Fitzsimons *et al.*, 2013). The domain structure of human HDAC4 (hHDAC4) is illustrated in Figure 1.10; sequence similarity and mutagenesis studies suggest conservation of each of these domains in *Drosophila,* and these are essential to HDAC4 function (Tan *et al.*, 2024), however less is known about the conservation of binding partners.

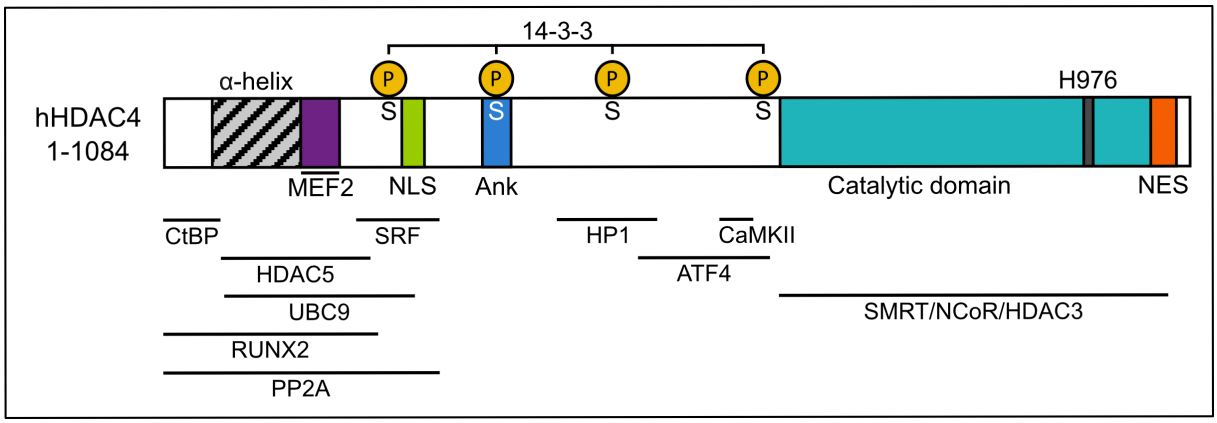

Figure 1.10 Domain structure and characterised binding partners of human HDAC4
Domain structure of human HDAC4 (hHDAC4) (GenBank accession NP_006028) is shown. The N-terminal domain of HDAC4 consists of an α-helix, nuclear localisation sequence (NLS, green) and ankyrin-repeat binding domain (Ank, blue), while the C-terminal region consists of the catalytic domain (teal) and the nuclear export sequence (NES, orange). The MEF2 binding domain (purple) is also present within the N-terminus of HDAC4 and mediates binding of myocyte enhancer factor two (MEF2, Wang and Yang (2001)). Four serine residues are shown (S) that when phosphorylated (yellow circle with P) mediate binding of 14-3-3 (Grozinger & Schreiber, 2000; McKinsey *et al.*, 2000; Wang *et al.*, 2000; Xu *et al.*, 2012). Histidine 976, which is associated with low catalytic activity (Lahm *et al.*, 2007) is also noted in grey. A number of additional proteins interact with hHDAC4 upstream of the catalytic domain including c-terminal binding protein (CtBP, Zhang *et al.* (2001)), histone deacetylase five (HDAC5, Backs *et al.* (2008)), SUMO-enzyme UBC9 (Zhao *et al.*, 2005), Runt-related transcription factor two (RUNX2, Vega *et al.* (2004)), protein phosphatase 2 alpha (PP2A, Paroni *et al.* (2008)), serum response factor (SRF, Backs *et al.* (2011)), heterochromatin protein 1 (HP1, Zhang *et al.* (2002)), activating transcription factor four (ATF4, (Zhang *et al.*, 2014)), calcium/calmodulin-dependent kinase II (CaMKII, Backs *et al.* (2006)). Silencing mediator of retinoic acid and thyroid hormone receptor (SMRT), nuclear coreceptor corepressor (NCoR) and histone deacetylase three (HDAC3) associate via the catalytic domain (Kim *et al.*, 2015). Lines indicate the approximate binding regions. *This figure is an adaptation from that found in Tan et al. (2024) (doi: 10.1186/s12915-023-01800-1), which is distributed under CC BY 4.0.*

Early studies identified that HDAC4 has high sequence conservation with catalytically active HDACs (Hassig *et al.*, 1998) and deacetylase activity *in vitro* (Grozinger *et al.,* 1999). Indeed, point mutation analysis of *HDAC4* based on sequence homology to human *HDAC1* reduced catalytic activity (Hassig *et al.*, 1998; Miska *et al.*, 1999; Wang *et al.*, 1999). However, it was later determined that the catalytic site of HDAC4 confers extremely low intrinsic deacetylase activity due to a tyrosine-histidine substitution (Lahm *et al.*, 2007) and that it 'borrows' its catalytic power from HDAC3 via interaction with the NCoR/SMRT repressor complex (Fischle *et al.*, 2001; Fischle *et al.*, 2002; Huang *et al.*, 2000), mediated by residues within the catalytic rim (Bottomley *et al.*, 2008; Kim *et al.*, 2015). It is noted that this substitution is not conserved in *Drosophila,* and it is therefore likely that DmHDAC4 has intrinsic deacetylase activity (Fitzsimons *et al.*, 2013), however this activity does not appear to be required for its ability to

impair neuronal development and learning and memory upon overexpression (Section 1.6.1, Fitzsimons *et al.* (2013), Main *et al.* (2021), Tan *et al.* (2024)).

The N-terminal extension of HDAC4 contains binding sites for a number of transcription factors (Figure 1.10), allowing it to act as a hub for regulation of a number of biological processes. Ultimately, this affords HDAC4 roles in development and learning and memory (Section 1.6.1), as well as significant roles in cell-cycle regulation and cancer (Bodily *et al.*, 2011; Majdzadeh *et al.*, 2008; Zhang *et al.*, 2019). Figure 1.10 provides a comprehensive but not exhaustive summary of characterised binding partners and approximate binding locations within human HDAC4. Domains that mediate subcellular shuttling and homo-tetramerisation are also indicated and are further discussed in Section 1.5.1 and Section 1.8 respectively.

1.5.1. Regulation of HDAC4 subcellular distribution

Dynamic nucleocytoplasmic shuttling regulates the activity of HDAC4 (Miska *et al.*, 1999). The subcellular distribution of HDAC4 varies between cell types and is not typically restricted to either the nucleus or cytoplasm; nuclear export and import processes are in a dynamic equilibrium (reviewed in Fitzsimons (2015)). Human HDAC4 harbours an N-terminal nuclear localisation signal (NLS), and a C-terminal hydrophobic nuclear export sequence (NES) (Wang & Yang, 2001). While these mediate traditional mechanisms of nuclear import and export, the subcellular distribution of HDAC4 is also modulated by additional binding partners including MEF2 and 14-3-3, resulting in highly dynamic regulation (Figure 1.11).

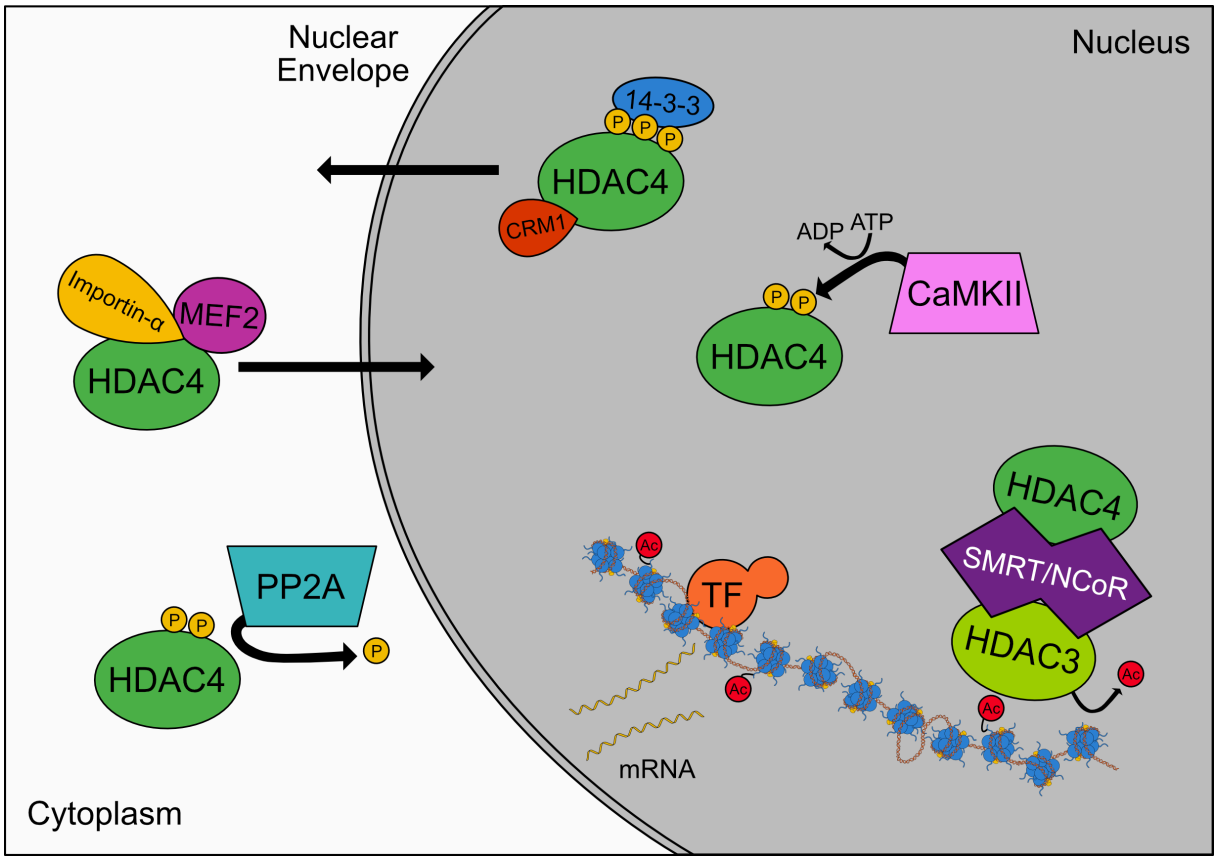

Figure. 1.11 HDAC4 undergoes dynamic regulation of its subcellular distribution
Schematic diagram depicting the regulation of HDAC4 subcellular distribution. Nuclear import of HDAC4 is mediated by importin-α and myocyte enhancer factor 2 (MEF2), while nuclear export is mediated by 14-3-3 and the exportin chromosomal maintenance 1 (CRM1). Calcium/calmodulin-dependent protein kinase II (CamKII) acts to phosphorylate (P) HDAC4 in the nucleus while protein phosphatase 2A (PP2A) dephosphorylates HDAC4 in the cytoplasm, and this modulates 14-3-3 binding. In the nucleus HDAC4 interacts with silencing mediator of retinoic acid and thyroid hormone receptor (SMRT) and nuclear receptor corepressor (N-CoR) to facilitate deacetylation of histone H3 tails (Ac) via histone deacetylase 3 (HDAC3). *This figure is an original artwork created with reference to* Backs *et al.* (2006)*, Fitzsimons (2015), Grozinger and Schreiber (2000); Guenther et al. (2001), Miska et al. (1999); Paroni et al. (2008), Wang and Yang (2001), McKinsey et al. (2001).*

1.5.1.1. NLS and NES-dependent regulation of HDAC4 nucleocytoplasmic shuttling

The balance of nuclear import and nuclear export of a given protein governs its subcellular distribution, and this is typically mediated by intrinsic nuclear localisation (NLS) and nuclear export signals (NES) (reviewed in Xu *et al.* (2010)). These are regions with conserved features that encode binding sites for receptors (importins and exportins) that mediate transport through the nucleopore complex. Via extensive deletion mutant analysis of hHDAC4 expressed in cell culture, Wang and Yang (2001) demonstrated the presence of an authentic tripartite NLS within HDAC4. Alone this region was sufficient to mediate nuclear import of GFP, and this was dependent on the presence of arginine/lysine clusters. Nuclear import via this region is thought

to be mediated by interaction with importin-α, which physically interacts with HDAC4 (Grozinger & Schreiber, 2000). hHDAC4 also contains an authentic NES, located downstream of the catalytic domain, which mediates CRM1-dependent nuclear export (McKinsey *et al.*, 2001; Wang & Yang, 2001). This region is hydrophobic and alone it was capable of maintaining GFP in the cytoplasm (Wang & Yang, 2001). However, the NLS was insufficient to mediate nuclear localisation of full length HDAC4, which was instead largely dependent on MEF2 binding. Moreover, a second region within hHDAC4 also mediated cytoplasmic localisation in a CRM1-independent manner, and further mutational analysis identified this to be the site of 14-3-3 binding (Wang & Yang, 2001), essential in nuclear export and cytoplasmic anchoring of HDAC4.

The distribution of HDAC4 is modulated by the availability of the NLS and NES for importin/exportin binding. Interaction of 14-3-3 with HDAC4 masks the NLS, preventing nuclear import (Grozinger & Schreiber, 2000; Wang & Yang, 2001). Similarly, it is hypothesised that the NES is masked by binding of SMRT to HDAC4 (McKinsey *et al.*, 2001), where overexpression of SMRT drives nuclear accumulation and aggregation of HDAC4 (Wu *et al.*, 2001). Moreover, HDAC4 has been demonstrated to undergo conformational changes in a redox dependent manner; exposure to H_2O_2 or mutation of two cysteine residues within the catalytic domain of HDAC4 prevented interaction of the HDAC domain with the NES, resulting in its exposure and CRM-1 dependent nuclear export (Ago *et al.*, 2008).

1.5.1.2. MEF2 mediates dynamic nuclear import of HDAC4

Myocyte enhancer factor two (MEF2) proteins are transcription factors known for their roles in regulation of development, and are encoded by four genes in humans (*MEF2A-D*) (reviewed by Pon and Marra (2016)). The MEF2 protein is comprised of a MADS domain that mediates dimerisation, a MEF2-domain that is important in DNA-binding and cofactor interaction, and a transcription activation domain (McKinsey *et al.*, 2002). Despite being known for its role in regulation of myogenesis (Bour *et al.*, 1995; Breitbart *et al.*, 1993), MEF2 also plays roles in neuronal development (Section 1.7). Invertebrates have a single MEF2 gene (Lilly *et al.*, 1994), and are therefore ideal to investigate its conserved function.

MEF2 transcriptional activity is inhibited via direct interaction with class IIa HDACs, including HDAC4 (Miska *et al.*, 1999; Sparrow *et al.*, 1999; Wang *et al.*, 1999). Homology with the MEF2 interacting transcription repressor (MITR, later classified as HDAC9) narrowed the interaction domain within HDAC4 to the N-terminus between residues 166-184 (Miska *et al.*, 1999; Sparrow *et al.*, 1999; Wang & Yang, 2001), and among others Leu175 was identified as a key MEF2 binding residue (Wang & Yang, 2001). HDAC4 was shown to repress MEF2-dependent transcription in a dose-dependent manner (Chan *et al.*, 2003), and this required only the N-terminus of HDAC4 (Backs *et al.*, 2011). The interaction of HDAC4 with MEF2 did not interfere with DNA binding (Lu *et al.*, 2000), and repression was sensitive to the HDAC inhibitor trichostatin A, which preferentially targets class I HDACs (Furumai *et al.*, 2001). HDAC4-dependent repression of MEF2 is thought to be mediated by complex formation with catalytically active HDACs including HDAC1 (Chan *et al.*, 2003), HDAC3 (Grozinger & Schreiber, 2000), and SIRT1 (Zhao *et al.*, 2005), resulting in local histone deacetylation.

The interaction between HDAC4 and MEF2 is most curious; although HDAC4 represses MEF2-dependent transcription (Miska *et al.*, 1999; Wang *et al.*, 1999), MEF2 facilitates nuclear import of HDAC4 (Borghi *et al.*, 2001; Wang & Yang, 2001). That is to say, MEF2 mediates nuclear import of its own repressor. Overexpression of MEF2 induced nuclear import of HDAC4 (Borghi *et al.*, 2001; Wang & Yang, 2001), and deletion of the N-terminus of HDAC4 including the MEF2 binding site (but excluding the NLS) of HDAC4 rendered it cytoplasmic in the presence of MEF2 overexpression (Wang & Yang, 2001) (see Figure 1.10 for order of domains). This cytoplasmic localisation was a result of the loss of MEF2 binding and not deletion of upstream regions as a point mutant of HDAC4 with abrogated MEF2 binding was also cytoplasmic (Wang & Yang, 2001). Mutation of the MEF2-binding domain of HDAC4, specifically residue Leu175, altered HDAC4 distribution in *Drosophila* (Main *et al.*, 2021; Tan *et al.*, 2024). Finally, in further support of this, small drugs that target the interaction between MEF2 and HDAC4 altered the localisation of HDAC4 (Jayathilaka *et al.*, 2012).

MEF2-dependent nuclear import of HDAC4 requires the NLS within MEF2 (Borghi *et al.*, 2001) and not that within HDAC4 (Wang & Yang, 2001), alluding to redundancy within the import mechanisms of HDAC4, potentially influencing tissue- and condition-specific regulation. Furthermore, residues upstream of the MEF2 binding site within HDAC4 appear to be important in mediating MEF2-dependent nuclear import (Borghi *et al.*, 2001; Wang & Yang, 2001). This domain has since been identified as important in mediating oligomerisation of

HDAC4 via its N-terminal α-helix (Guo *et al.* (2007), Section 1.8), and a mutation that disrupts tetramerisation of HDAC4 prevented repression of MEF2 dependent transcription *in vitro* (Guo *et al.*, 2007). Together these data suggest a role for tetramerisation in regulation of MEF2-dependent nuclear import of HDAC4.

1.5.1.3. 14-3-3 proteins mediate dynamic nuclear export of HDAC4

The 14-3-3 family consists of seven proteins in humans (Fu *et al.*, 2000). They are highly conserved between species, and while they carry out diverse roles, six have been demonstrated to interact with HDAC4 (Miska *et al.*, 2001; Paroni *et al.*, 2008; Xu *et al.*, 2012). *Drosophila* only have two 14-3-3 proteins (Darling *et al.*, 2005) and are therefore again an excellent model for studying the conserved function of this protein family. Overexpression of 14-3-3 in mammalian cell culture induced cytoplasmic localisation of HDAC4 (Grozinger & Schreiber, 2000), but interestingly, in the absence of either its NES or 14-3-3 binding sites, HDAC4 remained nuclear (McKinsey *et al.*, 2001; Wang & Yang, 2001), therefore both the NES and 14-3-3 binding are required for nuclear export and cytoplasmic retention. It is hypothesised that 14-3-3 binding to HDAC4 results in conformational changes that reveal its NES, enabling CRM-1 dependent nuclear export (McKinsey *et al.*, 2001). In addition to mediating nuclear export, interaction of 14-3-3 with HDAC4 facilitates cytoplasmic anchoring; the HDAC4 NLS is flanked by 14-3-3 binding sites (McKinsey *et al.* (2001), Figure 1.10) and binding of 14-3-3 blocks this, inhibiting the association of importin-α and therefore sequestering HDAC4 in the cytoplasm (Grozinger & Schreiber, 2000; Wang *et al.*, 2000).

The interaction between HDAC4 and 14-3-3, and thus nucleocytoplasmic trafficking of HDAC4, is modulated in a phosphorylation-dependent manner (Grozinger & Schreiber, 2000). When phosphorylated, four serine residues within HDAC4 (S246, S350, S467 and S632 of hHDAC4) facilitate its interaction with 14-3-3 (Grozinger & Schreiber, 2000; McKinsey *et al.*, 2000; Wang *et al.*, 2000; Xu *et al.*, 2012); substitution of three of these residues for alanine (3SA) or treatment with kinase inhibitors reduced the interaction between HDAC4 and 14-3-3 and resulted in nuclear localisation (Grozinger & Schreiber, 2000). Consequently, HDAC4 distribution is sensitive to the activity of protein phosphatases and kinases. Protein phosphatase 2 alpha (PP2A) is the key phosphatase that facilitates nuclear import of HDAC4 (Paroni *et al.*, 2008). Inhibition of PP2A with okadaic acid, a potent inhibitor of protein phosphatases

(Swingle *et al.*, 2007), or RNAi-mediated knockdown, resulted in cytoplasmic localisation of HDAC4 in mammalian cell culture (Paroni *et al.*, 2008). In contrast, calcium/calmodulin dependent kinases (CaMKs) are responsible for phosphorylation of HDAC4 (McKinsey *et al.*, 2000). Constitutively active CaMKIV increased the cytoplasmic localisation of HDAC4 in myoblasts and reduced the ability of HDAC4 to repress MEF2-dependent transcription (Miska *et al.*, 2001). While it is tempting to speculate that this directly induces the HDAC4-14-3-3 interaction, the association of HDAC4 and 14-3-3 was first required for CaMKIV association, and it is therefore suggested that CaMKIV then stimulates efficient nuclear export (Zhao *et al.*, 2001). It is thought that CaMKI and/or CaMKII may be the first required kinase, as constitutively active forms of these caused complete export of HDAC4 to the cytoplasm (Backs *et al.*, 2006). SIK2 and SIK3 kinases (salt-inducible kinases) also regulate the distribution of HDAC4 (Walkinshaw *et al.*, 2013; Wang *et al.*, 2011). Overexpression of constitutively active SIK3 induced phosphorylation and cytoplasmic redistribution of HDAC4 (Wang *et al.*, 2011). SIK2 overexpression impaired the ability of $HDAC4^{WT}$ to repress MEF2-dependent transcription, and interestingly, SIK3 expression also increased cytoplasmic aggregation of HDAC4 (Walkinshaw *et al.*, 2013). Since these discoveries, the 3SA mutation has been widely used to enforce nuclear localisation and thus examine the nuclear activities of HDAC4 (Ago *et al.*, 2008; Backs *et al.*, 2006; Bolger & Yao, 2005; Chawla *et al.*, 2003; Chen & Cepko, 2009; Cohen *et al.*, 2009; Cohen *et al.*, 2007; Grozinger & Schreiber, 2000; Li *et al.*, 2012; Litke *et al.*, 2018; Litke *et al.*, 2022; Main *et al.*, 2021; McKinsey *et al.*, 2000; McKinsey *et al.*, 2001; Nishino *et al.*, 2008; Paroni *et al.*, 2008; Penrod *et al.*, 2018; Sando *et al.*, 2012; Schlumm *et al.*, 2013; Schwartz *et al.*, 2016; Tan *et al.*, 2024; Vega *et al.*, 2004; Wang *et al.*, 2000; Wang & Yang, 2001; Q. Wu *et al.*, 2016; Wu *et al.*, 2001; Zhao *et al.*, 2001; Zhu *et al.*, 2019).

1.5.1.4. Regulation of HDAC4 distribution via cleavage

In mammalian cells, HDAC4 undergoes caspase-dependent cleavage to produce an N-terminal fragment ($HDAC4^{1-289}$) that translocates to the nucleus and is capable of repressing MEF2-dependent transcription, while the C-terminal product remains cytoplasmic and is rapidly degraded (Paroni *et al.*, 2004). Nuclear translocation of $HDAC4^{1-289}$ induced release of cytochrome C from mitochondria, indicative of activation of the intrinsic apoptotic pathway, and promoted UV-induced apoptosis (Liu *et al.*, 2004; Paroni *et al.*, 2004). HDAC4 N-terminal cleavage products have also been observed in the context of cardiometabolism, in which they appear to have a protective effect (Jebessa *et al.*, 2019; Kronlage *et al.*, 2019; Lehmann *et al.*,

2018) and were produced in response to oxidative stress (Zhang *et al.*, 2014). HDAC4 also undergoes protein kinase A-dependent proteolysis to yield a shorter N-terminal product (cleaved at Y201) that localised to the nucleus and inhibited cardiomyocyte hypertrophy via interaction with MEF2 (Backs *et al.*, 2011). Together these data demonstrate that the N-terminus of HDAC4 has novel roles independent of its deacetylase domain.

1.5.1.5. Regulation of HDAC4 distribution in neuronal cells

HDAC4 subcellular distribution varies widely among neuronal subtypes (Section 1.6.1), and this is controlled in part via neuronal activity. Both protein levels and the subcellular distribution of HDAC4 are responsive to synaptic signalling; HDAC4 undergoes nuclear export in response to electrical activities, where inhibition of L-type calcium channels, sodium channels, and NMDA receptors results in nuclear accumulation of HDAC4, regulated in part by its interaction with 14-3-3 and CaMKs (Chawla *et al.*, 2003; Chen *et al.*, 2014; Litke *et al.*, 2018; Sando *et al.*, 2012; Schlumm *et al.*, 2013).

1.6. Roles of HDAC4 in neuronal development, function, and neurodegenerative disease

HDAC4 is expressed in the brain and has key roles in neuronal development and function. Consequently, HDAC4 must be carefully regulated with respect to its subcellular distribution, as numerous studies have observed aberrant nuclear accumulation of HDAC4 in neurodevelopmental and neurodegenerative diseases. Evidence of the roles of HDAC4 in neuronal development and function are presented in this section, as well as evidence of dysregulation in disease.

1.6.1. HDAC4 is essential in neuronal development and function

Expression and distribution of HDAC4 in the brain

HDAC4 is widely expressed in humans with transcripts enriched in the brain, heart, and skeletal muscle (Grozinger *et al.*, 1999; Wang *et al.*, 1999) and plays key roles in neuronal and skeletal development. Expression of HDAC4 has been detected in all brain regions examined in the human protein atlas (Sjöstedt *et al.*, 2020). Comprehensive studies have shown widespread

distribution of HDAC4 in the rodent brain (Broide *et al.*, 2007; Darcy *et al.*, 2010) with high expression in the cerebrum and cerebellum of mice and predominant localisation to the cytoplasm in both adult and neonatal neurons (Bolger & Yao, 2005). During early postnatal development, HDAC4 is significantly upregulated in the mouse cortex, concomitant with massive synaptogenesis (Sando *et al.*, 2012). Despite predominant cytoplasmic localisation, as aforementioned, HDAC4 undergoes dynamic regulation of its subcellular distribution (Section 1.5.1) and as such its localisation has been observed to differ depending on the neuronal subtype in which it is expressed (Darcy *et al.*, 2010). It is likely that this results from the differential availability of HDAC4 binding partners between these tissues as well as variation in levels of HDAC4 expression.

In particular, in the mouse cerebellum HDAC4 distribution has been observed to vary significantly; in some cells it was exclusively cytoplasmic, while in others it was more predominantly nuclear or pancellular (Darcy *et al.*, 2010). Fine immunoreactive puncta of HDAC4 were also observed in the cytoplasm of neurons in all brain regions examined, but these puncta were most strongly associated with the postsynaptic density (Darcy *et al.*, 2010). Given that HDAC4 distribution is altered by synaptic activity (Chawla *et al.*, 2003; Chen *et al.*, 2014; Sando *et al.*, 2012; Schlumm *et al.*, 2013), these data suggest that HDAC4 may shuttle between postsynaptic sites and the nucleus in response to neuronal activity.

In *Drosophila*, HDAC4 is expressed highly in the mushroom body (Fitzsimons *et al.*, 2013), a key integration centre for sensory information similar to the vertebrate cerebellum (Li *et al.*, 2020) (Section 1.3.1). HDAC4 localises to the lobes (bundled axons) of the mushroom body in the anterior of the brain (Fitzsimons *et al.*, 2013), but its subcellular distribution in Kenyon cell bodies in the posterior is unknown. Further characterisation of HDAC4 distribution in the *Drosophila* brain is therefore required.

Loss of HDAC4 impairs skeletal and brain development

Significant defects in skeletal development were observed in *HDAC4* null mice, which died early after birth (Vega *et al.*, 2004). No change in expression of the remaining class IIa HDACs was detected in these mice, nor was the phenotype exacerbated upon null mutation of HDACs 5 and 9, suggesting that *HDAC4* is the sole class IIa contributor toward regulation of skeletogenesis. Brains of newborn *HDAC4* null mice were approximately 40% smaller than controls (Majdzadeh *et al.*, 2008) but no changes in histone acetylation were detected compared

to wild-type controls, and few transcriptional changes were observed (Mielcarek, Seredenina, *et al.*, 2013), suggesting that HDAC4 acts through non-transcriptional mechanisms in the brain. Conditional knockout of *HDAC4* in the mouse forebrain was viable, but mice had impairments in motor coordination, spatial learning and memory, and associative long-term memory, implicating HDAC4 in each of these processes (Kim *et al.*, 2012). The same impairments were not recapitulated upon conditional *HDAC5* knockout, again illustrating that the role of HDAC4 is non-redundant. Loss of *HDAC4* also reduced long-term potentiation, suggesting a role in synaptic plasticity (Kim *et al.*, 2012). Such impairments were associated with a lack of changes in transcription via microarray analysis, again indicating that HDAC4 is likely acting through non-transcriptional processes.

Regulation of HDAC4 distribution in the brain is critical for neuronal function

HDAC4 is mainly cytoplasmic in the postnatal forebrain and in cultured cortical neurons, and this is reinforced by glutamatergic inputs that trigger nuclear export of HDAC4 in the brain as deletion of Syb2 (synaptobrevin-2, essential for neurotransmitter exocytosis) or knockdown of NMDA (N-methyl-D-aspartate, a glutamate receptor) receptor subunit NR1 resulted in HDAC4 nuclear accumulation (Sando *et al.*, 2012). Expression of nuclear-localised HDAC4^{3SA} (which mutates three serine residues that when phosphorylated result in binding of 14-3-3 and nuclear export, Section 1.5.1.3) but not wild-type HDAC4 in cultured neurons repressed genes essential for synaptic function, including those involved in neurotransmitter reception and release, as well as signalling molecules implicated in plasticity and memory formation. In contrast, knockdown of HDAC4 in mixed cortical cultures resulted in loss of all neuronal cell types (Sando *et al.*, 2012). Expression of wild-type HDAC4 rescued such loss, and this was dependent on its cytoplasmic distribution as expression of two nuclear-localised mutants of HDAC4, HDAC4^{3SA} or HDAC4 with a deleted NES, failed to rescue neuronal loss. Rescue was also independent of the deacetylase domain, implicating cytoplasmic HDAC4 in neuronal survival independent of its catalytic activity.

Interestingly, translocation of HDAC4 to nuclei in the somatosensory cortex, hippocampus, and dentate gyrus has been observed following contextual fear conditioning in mice (Zhu *et al.*, 2019). This resulted in a reduction in immunoreactivity of Fos in these neurons, an early response gene (ERG) that is important in memory storage (Minatohara *et al.*, 2016). Expression of nuclear localised (3SA) but not wild-type HDAC4 in cultured cortical neurons similarly repressed *Fos* expression as well as that of other classical ERGs, demonstrating that careful

regulation of class IIa HDACs is necessary for spatiotemporal control of ERG programs during memory formation. Moreover, drug-induced expression of HDAC4^{3SA} prior to learning strongly impaired associative fear memory in mice, but had no effect on pre-conditioned animals, suggesting a deleterious effect of nuclear HDAC4 in memory acquisition but not recall (Zhu *et al.*, 2019).

Dysregulation of HDAC4 impairs neuronal development and memory in *Drosophila*

Overexpression of HDAC4 during *Drosophila* development impairs neuronal morphogenesis as assessed by the morphology of the mushroom body and the adult eye (Main *et al.*, 2021; Schwartz *et al.*, 2016; Tan *et al.*, 2024). In the mushroom body, this manifested as defects in axon elongation and termination, observed as thinning and absence of lobes, as well as overgrowth of the β-lobe, which appears fused (Main *et al.*, 2021; Tan *et al.*, 2024). In the eye, there was significant disruption to the uniform array, which became misaligned, as well as fusion of ommatidia and loss of pigmentation (Main *et al.*, 2021; Schwartz *et al.*, 2016; Tan *et al.*, 2024). These phenotypes appear to be dose dependent, and are largely attributed to the nuclear pool of HDAC4 as severity significantly increased upon increased dose or induction of nuclear localisation by the 3SA mutation. HDAC4 overexpression restricted to the adult brain also impaired long-term memory (LTM) without affecting learning or short-term memory (Fitzsimons *et al.*, 2013), and again the deleterious effect was ascribed to the nuclear pool of HDAC4 (Main *et al.*, 2021). HDAC4 knockdown similarly impaired LTM (Fitzsimons *et al.*, 2013). Together these data demonstrate that HDAC4 plays an essential role in LTM, but also underscore the need for precise regulation of HDAC4 expression and distribution in this process.

As earlier mentioned (Section 1.5), the amino acid substitution within the catalytic domain of human HDAC4 that renders it inactive is not present in *Drosophila* HDAC4 (Fitzsimons *et al.*, 2013), suggesting that deacetylase activity may be responsible for overexpression-induced defects in *Drosophila*. However, overexpression of DmHDAC4 with the conserved inactivating tyrosine to histidine mutation (Y1142H) resulted in the same defects in mushroom body development as wild-type HDAC4 (Tan *et al.*, 2024), and similarly, overexpression of a different catalytic mutant of HDAC4 (H968A) still impaired LTM (Fitzsimons *et al.*, 2013). Together these data suggest that HDAC4 interferes with these processes independent of its deacetylase activity, analogous to human HDAC4. Consistent with impairments independent of its catalytic domain, few global transcriptional changes were observed upon overexpression

of HDAC4 in *Drosophila* (Main *et al.*, 2021; Schwartz *et al.*, 2016), further implicating HDAC4 in the regulation of non-transcriptional processes. Interestingly, a reduction in the severity of the eye phenotype was observed upon Y1142H inactivating mutation (Tan *et al.*, 2024), however this was not absolute, suggesting HDAC4 may act through both deacetylase dependent and independent activities to disrupt eye development upon overexpression. It is acknowledged however that this mutation may impact binding of other proteins at the deacetylase domain (Figure 1.10) and therefore the effect of the Y1142H mutation may also be independent of intrinsic deacetylation activity.

Together these data demonstrate that correct regulation of HDAC4 expression levels and subcellular distribution is crucial in both neuronal development and function. Specifically, increased abundance of HDAC4 and aberrant nuclear accumulation contributes to defects in neuronal development as well as neuronal dysfunction. Curiously, the catalytic domain is consistently not required for the effects that HDAC4 mediates, reinforcing that a pool of HDAC4 acts predominantly through non-transcriptional mechanisms that are not yet understood.

1.6.2. HDAC4 dysregulation is observed in neuronal disease

It is evident that careful regulation of HDAC4 expression and distribution is essential in correct neuronal development and function. Changes in the regulation of HDAC4 distribution have been observed in neurodevelopmental and neurodegenerative disease, commonly featuring nuclear accumulation of HDAC4, which results in formation of punctate aggregates. Studies of diseases in which HDAC4 distribution is disrupted are described herein, with an emphasis on those in which HDAC4 nuclear accumulation is significant.

2q37 deletion syndrome

Synonymous with its name, 2q37 deletion syndrome (formerly brachydactyly mental retardation syndrome (BDMR)) is a neurodevelopmental disorder correlated with deletions within the 2q37 region of chromosome two, which includes *HDAC4* (Williams *et al.*, 2010), and is characterised by intellectual disability, developmental delays, autism spectrum disorder, and craniofacial and skeletal abnormalities (Aldred *et al.*, 2004; Falk & Casas, 2007). New cases of 2q37 deletion syndrome are continually identified, the majority of which involve

deletions encompassing *HDAC4* (Gavril *et al.*, 2023), and thus haploinsufficiency of *HDAC4* is thought to be the primary contributor to disease phenotypes as deletions result in significantly reduced mRNA levels (Le *et al.*, 2019; Williams *et al.*, 2010). The 2q37 phenotype exhibits variable penetrance however, with some patients harbouring entire deletions of *HDAC4* presenting with brachydactyly type E but no cognitive impairment (Wheeler *et al.*, 2014), suggesting contribution from other genes (Le *et al.*, 2019; Moretti *et al.*, 2020).

In support of haploinsufficiency, the severity of 2q37 deletion phenotypes appears to correlate with levels of *HDAC4* expression; a patient with 23% expression of *HDAC4* relative to healthy controls had significant cognitive impairment and brachydactyly, while their parent had increased *HDAC4* expression (67%) and mild brachydactyly with no cognitive impairment (Morris *et al.*, 2012). Further mutations associated with 2q37 deletion syndrome have also been mapped within *HDAC4;* the +C nonsense mutation was identified in one individual, which results in a truncation at Gly801, resulting in loss of the catalytic domain and nuclear export signal (Williams *et al.*, 2010). HDAC4^{+C} had an increased nuclear distribution in cultured neurons compared to wild-type, and a similar truncation mutant acted as a transcriptional repressor and impaired spatial learning and memory in mice as assessed by the Barnes maze (Sando *et al.*, 2012).

De novo missense mutations have also been observed within the 14-3-3 binding site of HDAC4 in seven unrelated individuals presenting with intellectual disability without brachydactyly (Wakeling *et al.*, 2021). These mutations reduced the affinity of HDAC4 for 14-3-3β by approximately two-fold in cultured cells; it is hypothesised that as a result these patients have increased nuclear abundance of HDAC4, contributing to the 2q37 phenotype. A further mutation near the catalytic site of HDAC4 has also been identified in a family with 2q37 deletion syndrome (Takeyari *et al.*, 2023), which may affect complex formation involving HDAC4. Given that HDAC4 distribution is influenced by its interaction with numerous proteins, it is likely that many mutations to HDAC4 affect the regulation of its distribution and therefore activity, which may contribute to the 2q37 deletion phenotype.

Ataxia telangiectasia

Ataxia telangiectasia (AT) is a neurodegenerative disease characterised by progressive loss of coordination and poor immune function which results from mutations in the ATM protein (Rothblum-Oviatt *et al.*, 2016). Nuclear abundance of HDAC4 is increased in Purkinje neurons

of the cerebellar cortex in AT patients (Li *et al.*, 2012), and in Purkinje neurons and fibroblasts in an *ATM* null mouse model (Ricci *et al.*, 2020). *ATM* null mice also had poor motor coordination as assessed by rotarod performance (Li *et al.*, 2012). This performance was increased by replacement of endogenous HDAC4 with a cytoplasmic-localised mutant, but not by nuclear-localised HDAC4, which instead resulted in further impairments (Li *et al.*, 2012). ATM is a regulator of PP2A activity (Li *et al.*, 2012), and PP2A regulates the subcellular distribution of HDAC4 (Section 1.5.1.3); PP2A was upregulated in *ATM*-null mice, and this correlated with decreased phosphorylation of HDAC4, reduced 14-3-3 association, and increased binding of MEF2 resulting in nuclear accumulation (Li *et al.*, 2012). This suggests that ATM typically represses PP2A, thus maintaining the phosphorylated state of HDAC4 and 14-3-3-dependent cytoplasmic retention.

CDKL5 disorder

CDKL5 disorder is a neurodevelopmental disease characterised by severe intellectual disability and motor impairment, correlated with mutations in *Cyclin-dependent kinase like 5* (*CDKL5*) (Fehr *et al.*, 2013), which encodes a serine/threonine kinase that directly targets HDAC4 to promote cytoplasmic retention (Trazzi *et al.*, 2016). Neuronal proliferation and maturation are impaired in *CDKL5* null mice (Trazzi *et al.*, 2016); phosphorylation of HDAC4 was reduced and nuclear accumulation increased in neuronal precursor cells as well as hippocampal cultures and neocortical neurons. This correlated with increased repression of MEF2-dependent transcription compared to wild-type mice, suggesting that HDAC4 may be acting through MEF2 to mediate impairments. Treatment with the class II HDAC inhibitor LMK235 (Marek *et al.*, 2013) decreased nuclear accumulation of HDAC4 in *CDKL5* null mice and *HDAC4* siRNA or LMK235 treatment restored MEF2-dependent transcription and impairments in neuronal proliferation and maturation (Trazzi *et al.*, 2016), directly implicating dysregulation of HDAC4 in CDKL5 pathogenesis.

Alzheimer's Disease

Alzheimer's disease (AD) is the most common cause of dementia (Schneider *et al.*, 2009), characterised by slow but progressive cognitive decline (Breijyeh & Karaman, 2020). An initial study in *Drosophila* implicated HDAC4 in AD pathology, where an *HDAC4* loss of function mutant enhanced amyloid beta (Aβ) aggregate induced neurodegeneration in the eye and increased accumulation of soluble Aβ peptides (Cao *et al.*, 2008), which are understood to disrupt cognitive function (Cleary *et al.*, 2005). In the 5xFAD mouse model of AD, HDAC4

protein was increased by 63% in whole left hemispheres compared to wild-type mice (Anderson *et al.*, 2015). HDAC4 was subsequently identified as a top predicted upstream regulator of changes in hippocampal membrane protein abundance between wild-type and AD model (5xFAD) mice, which correlated with a decline in contextual fear memory (Neuner *et al.*, 2017). The same study also identified HDAC4 as a regulator of age-related memory impairment independent of familial Alzheimer's mutations, further demonstrating that HDAC4 modulates memory defects in both aging and disease contexts.

Examination of CA1 pyramidal cells in post-mortem brains from individuals with AD demonstrated that nuclear HDAC4 increased as AD-related cognitive impairment advanced in severity (Herrup *et al.*, 2013). Increased nuclear accumulation and subsequent aggregation of HDAC4 has also been observed in the midfrontal gyrus, hippocampus, frontal cortex, and locus coeruleus of post-mortem brains of patients diagnosed with Alzheimer's Disease (AD) (Shen *et al.*, 2016). The extent of accumulation correlated with Braak staging (which quantifies neurofibrillary tangle/tau presence) and clinical severity, while HDAC4 was almost exclusively cytoplasmic in individuals without clinical or pathological signs of AD, suggesting that nuclear translocation occurs early but is ongoing during the progression of AD. Interestingly, hippocampal neurons also showed reduced ATM levels (Shen *et al.*, 2016), characteristic of AT patients, demonstrating overlapping aetiologies that are often alluded to, but not often established between neurodevelopmental and neurodegenerative disease.

Nuclear accumulation of HDAC4 in hippocampal pyramidal neurons has been observed in three different mouse models of AD (Shen *et al.*, 2016). Further examination of the 3xTG model demonstrated that endogenous HDAC4 was typically cytoplasmic in wild-type mice but accumulated in nuclei of CA1 and CA3 hippocampal neurons from 3xTG mice (Colussi *et al.*, 2023). Treatment of cultured hippocampal neurons from wild-type mice with purified Aβ or tau protein also induced nuclear accumulation of HDAC4 and decreased dendritic localisation. This was associated with reduced dendritic length, which was rescued by overexpression of cytoplasmically-localised HDAC4, suggesting that nuclear accumulation may further contribute to pathogenesis by depletion of the cytoplasmic pool of HDAC4 (Colussi *et al.*, 2023). In contrast, increasing concentrations of Aβ oligomers increased protein levels of HDAC4 in SH-SY5Y cells, but HDAC4 remained cytoplasmic (Chen *et al.*, 2021), demonstrating the cell-specific effect of Aβ on HDAC4 distribution.

Apolipoprotein E4 (ApoE4) has been identified as the strongest genetic risk factor for AD (Sadigh-Eteghad *et al.*, 2012). Expression of ApoE4 in cholesterol-treated neuroblastoma cells induced nuclear translocation of HDAC4, and ApoE4 transgenic mice had a higher abundance of nuclear HDAC4 in hippocampal neurons compared to control mice (Sen *et al.*, 2015), further supporting the role of nuclear HDAC4 in AD pathology. ApoE4 is thought to induce nuclear accumulation by repressing PKCε (Sen *et al.*, 2015), important in maintaining the cytoplasmic HDAC4 pool (Nishino *et al.*, 2008).

One mechanism through which nuclear abundance of HDAC4 may be increased in AD is via SIK3, which promotes phosphorylation of HDAC4 resulting in 14-3-3 dependent nuclear export (Section 1.5.1.3). *SIK3* transcripts were reduced in both the 5xFAD mouse model of AD as well as in the temporal cortex of AD patients (Dai *et al.*, 2023), and this correlated with a reduction in the phosphorylation of HDAC4 in the dorsal hippocampus of the mouse model. Knockdown of *SIK3* in cell culture resulted in nuclear accumulation of HDAC4, while overexpression reinforced its cytoplasmic distribution. Importantly, adeno-associated viral expression of a truncated SIK3 rescued cognitive impairments in the 5xFAD mice, as measured by the Morris Water Maze, and restored phosphorylated HDAC4 levels. Together these data implicate SIK3 as an effector of HDAC4 distribution in AD.

Spinocerebellar Ataxia

Spinocerebellar ataxia type 1 (SCA1) is a neurodegenerative disease that predominantly affects the cerebellum, resulting in progressive ataxia due to polyglutamine expansion within Ataxin-1 (abbreviated as both ATXN1 and SCA1, but for clarity between the protein and the disease ATXN1 will be used here) (Sullivan *et al.*, 2019). Expression of human polyglutamine-expanded *ATXN1* in mice resulted in progressive ataxia (Burright *et al.*, 1995), but this was not dependent on its nuclear aggregation, as mutation of the self-aggregation domain of ATXN1 prevented aggregation but did not improve ataxia in mice (Klement *et al.*, 1998). Instead, mutation of the ATXN1 NLS reduced ataxia, suggesting that it is not aggregation of ATXN1 but another nuclear activity that is responsible for this phenotype (Klement *et al.*, 1998).

Transfection of cerebellar granule neurons with polyglutamine-expanded ATXN1 resulted in nuclear accumulation of HDAC4, which was sequestered alongside MEF2 in ATXN1 aggregates (Bolger *et al.*, 2007). Importantly, this occurred in a polyglutamine-independent manner (Bolger *et al.*, 2007). S776A mutation of ATXN1 abrogated its interaction with

HDAC4 and reduced cell death associated with its expression in Cos-7 cells (Bolger *et al.*, 2007), and interestingly, this also reduced the rate of nuclear aggregate formation (Chen *et al.*, 2003; Emamian *et al.*, 2003), which no longer sequestered HDAC4 (Bolger *et al.*, 2007). Moreover, S776A mutation prevented 14-3-3 association with ATXN1 (Chen *et al.*, 2003; Emamian *et al.*, 2003), therefore it is possible that nuclear accumulation of HDAC4 is forced by ATXN1-dependent sequestration of 14-3-3. Together these data suggest that it is not the ATXN1 aggregates that mediate toxicity, but the enforced nuclear localisation of HDAC4 and its interaction with ATXN1.

Parkinson's Disease

HDAC4 has also been observed to accumulate in neuronal nuclei in models of Parkinson's disease (PD) (Lang *et al.*, 2019; Q. Wu *et al.*, 2016), a neurodegenerative disease characterised by increasing tremor, cognitive decline, and dementia, as well as the presence of cytoplasmic inclusions of α-synuclein (Poewe *et al.*, 2017). Using induced pluripotent stem cell-derived dopamine neurons from PD patients with the GBA-N370S risk variant, Lang *et al.* (2019) identified that HDAC4 mislocalised to nuclei and downregulated a subset of genes, which led to defects in regulation of autophagy and lysosomal activity. Similar nuclear localisation was also observed in idiopathic PD patients, suggesting changes in HDAC4 distribution may not be limited to a small subset of familial mutations associated with PD.

The A53T mutation in α-synuclein is associated with strong genetic risk of PD (Spira *et al.*, 2001), and nuclear accumulation of HDAC4 has been observed in dopaminergic cells of the substantia nigra in mice expressing the A53T mutant of α-synuclein upon treatment with MPTP (Q. Wu *et al.*, 2016), a drug used to model PD by inducing motor defects via generation of reactive oxygen species (ROS) (Gerlach *et al.*, 1991). The same was not observed in wild-type mice, suggesting that expression of A53T α-synuclein sensitises neurons to ROS-induced nuclear accumulation of HDAC4. Interestingly, loss of viability in cell culture of A53T-expressing neurons in the presence of MPTP was specifically mediated via HDAC4 as this was rescued upon HDAC4 knockdown (Q. Wu *et al.*, 2016). Furthermore, viability of cells co-expressing A53T and nuclear-localised HDAC4 but not $HDAC4^{WT}$ was decreased, specifically implicating the nuclear pool of HDAC4 in regulation of A53T cell viability.

HDAC4 transcripts are also upregulated in brains of PD patients, specifically in the locus coeruleus and substantia nigra (Wang *et al.*, 2023). It is possible that HDAC4 has a role in α-synuclein accumulation, as knockdown of HDAC4 or inhibition with MC1568, which induces proteasome-dependent degradation of HDAC4 (Scognamiglio *et al.*, 2008), suppressed rotenone-induced accumulation of α-synuclein in SH-SY5Y cells (Wang *et al.*, 2023).

HDAC4 in cytoplasmic aggregates in neuronal disease

In addition to disease-induced nuclear accumulation of HDAC4, cytoplasmic aggregation of HDAC4 has been observed in neuronal disease, and this may mediate similar disruptions to cellular homeostasis as nuclear aggregation. Huntington's disease (HD) is a progressive neurodegenerative disease associated with involuntary choreiform movements and dementia which results from polyglutamine expansions within *huntingtin (HTT)* (Tabrizi *et al.*, 2020). In a mouse model of HD, HDAC4 interacted with mutant HTT protein in a polyglutamine length-dependent manner, and co-localised with cytoplasmic HTT aggregates (Mielcarek, Landles*, et al.*, 2013). Heterozygous knockout of HDAC4 reduced HTT aggregation and increased solubility, and this was associated with improved rotarod performance, delayed HD pathogenesis and improved synaptic function (Mielcarek, Landles*, et al.*, 2013). Proteomic analysis of cytoplasmic HDAC4 binding partners in the whole brain and striatum of HD mice identified proteins involved in vesicle trafficking, synaptic function and cytoskeletal regulation (Federspiel *et al.*, 2019), supporting the rescue of synaptic plasticity observed upon HDAC4 reduction (Mielcarek, Landles*, et al.*, 2013). Overexpression of HDAC4 alongside polyglutamine expanded HTT in HeLa cells also increased HTT aggregation, whereas RNAi of *HDAC4* reduced aggregate number, suggesting HDAC4 may stabilise HTT aggregation (Yue *et al.*, 2015).

HDAC4 also co-localises with α-synuclein and 14-3-3 in ubiquitinated Lewy bodies (Takahashi-Fujigasaki & Fujigasaki, 2006), which are cytoplasmic inclusions associated with Parkinson's disease and Lewy Body Dementia. Lewy bodies are thought to be a protective response to aberrant protein aggregation, collecting misfolded proteins in a single unit termed an aggresome (Tanaka *et al.*, 2004), which represents overwhelm of the cellular protein degradation systems (Johnston *et al.*, 1998).

From the above summarised studies, it is evident that dysregulation of HDAC4, and particularly its subcellular shuttling, is a common feature of neurodevelopmental and neurodegenerative disease. As the degree of HDAC4 dysregulation appears to correlate with severity of disease, this positions HDAC4 as an interesting candidate for further investigation of both the potential for use as a diagnostic marker, as well as a therapeutic target.

1.7. The roles of MEF2 in neuronal development and disease

Given the interaction between HDAC4 and MEF2 (Section 1.5.1.2) and the sequestration of MEF2 in HDAC4 aggregates in Kenyon cells (Section 1.8), the roles of MEF2 in neuronal development and disease are also of interest and are briefly summarised. MEF2 is expressed in the brain (Leifer *et al.*, 1993; McDermott *et al.*, 1993; Yu *et al.*, 1992), its target genes are enriched for expression in the central nervous system (Flavell *et al.*, 2008), and consequently MEF2 has a significant role in neuronal development, plasticity, and survival (Dietrich, 2013). In an activity-dependent manner, MEF2 promoted neuronal survival in the developing rat cerebral cortex (Mao *et al.*, 1999), and negatively regulated excitatory synapse number and function in hippocampal neurons (Barbosa *et al.*, 2008; Flavell *et al.*, 2006). MEF2 also negatively regulated neuronal plasticity in learning-induced memory formation in mice (Cole *et al.*, 2012) and has a significant role in *Drosophila* mushroom body development (Crittenden *et al.*, 2018). Specifically, MEF2 is expressed in the α, β and γ lobes, but not the α' or β' lobes, and is required for embryonic mushroom body development where null mutants had reduced numbers of differentiated mushroom body neurons (Crittenden *et al.*, 2018). Moreover, overexpression but not knockdown of MEF2 impaired mushroom body development (Main *et al.*, 2021; Tan *et al.*, 2024).

Genome wide association studies (GWAS) have identified MEF2C as a susceptibility locus for AD (Lambert *et al.*, 2013; Ruiz *et al.*, 2014) and the c.1250C/T (P279L) polymorphism in *MEF2A* is associated with increased risk of late onset AD, the frequency of which was increased in patients who were also ApoEε4 carriers (González *et al.*, 2007). Expression of MEF2C was significantly reduced in temporal and frontal lobes of AD patients, as well as in a mouse model of Aβ deposition, and MEF2 levels negatively correlated with Aβ levels, suggesting that the decrease in MEF2C may be due to deposition of Aβ or vice versa (Ren *et al.*, 2022).

Knockdown of *MEF2C* increased Aβ aggregation in the mouse model via increased expression of BACE1 (Ren *et al.*, 2022), responsible for production of toxic Aβ (Cole & Vassar, 2007), whilst further impairing spatial learning and memory and increasing apoptosis and oxidative stress.

Intriguingly, the opposite is observed in PD where MEF2D levels are significantly increased in brains of PD patients (Yang *et al.*, 2009). MEF2 typically undergoes chaperone-mediated autophagy (CMA) where it is translocated to the cytoplasm for degradation, however this was attenuated upon overexpression of wild-type or A53T mutant α-synuclein in a serum deprivation model in neuronal cell culture, and cytoplasmic MEF2 was increased in an A53T mouse model and in PD patients (Yang *et al.*, 2009). Oxidative stress induced by 6-OHDA (6-hydroxydopamine, which causes PD-like symptoms in animal models) caused oxidative modification of MEF2D, resulting in increased CMA and degradation of MEF2D in a dopaminergic neuronal cell line (Gao *et al.*, 2014). Oxidised levels of MEF2D were also increased in post-mortem PD brains as well as in a rodent PD model (Gao *et al.*, 2014), suggesting that MEF2D undergoes oxidative modification during PD onset that should induce CMA, but upon overwhelm, MEF2D accumulates in the neuronal cytoplasm. MEF2D undergoes caspase cleavage which generates a dominant negative fragment (Li *et al.*, 2001); cytoplasmic accumulation of MEF2D may favour this aberrant processing, contributing toward PD phenotypes.

GWAS also identified that genes that were differentially expressed upon *MEF2C* deletion in the adult mouse brain were enriched for genes with variants associated with schizophrenia, intelligence and educational attainment (Cosgrove *et al.*, 2021). Moreover, there is evidence of enrichment of MEF2-binding sites in promoters of genes whose expression positively correlated with cognitive function (Barker *et al.*, 2021).

1.8. Oligomerisation and aggregation of HDAC4

HDAC4 is observed to form nuclear aggregates under certain conditions, including upon overexpression or shift of nucleocytoplasmic equilibrium either by nuclear restriction (Main *et al.*, 2021; Tan *et al.*, 2024) or by altered expression or regulation of binding partners (Borghi *et*

al., 2001; Chan *et al.*, 2003; Miska *et al.*, 1999; Paroni *et al.*, 2004; Wang *et al.*, 2000). In addition to aggregation of HDAC4 in cultured cells, HDAC4 aggregates have been observed in post-mortem brains of AD, PD, and neuronal intranuclear inclusion disorder patients (Herrup *et al.*, 2013; Shen *et al.*, 2016; Takahashi-Fujigasaki *et al.*, 2006; Takahashi-Fujigasaki & Fujigasaki, 2006), and it is hypothesised that these aggregates may have a role in disease onset and/or pathogenesis. Indeed in *Drosophila*, overexpression of nuclear-localised HDAC4 increased the severity of developmental phenotypes compared to wild-type HDAC4, and this correlated with an increase in the number of nuclear aggregates (Main *et al.*, 2021; Tan *et al.*, 2024). In both cultured mammalian cells and the *Drosophila* brain, HDAC4 commonly associates with MEF2 when sequestered in nuclear aggregates (Figure 1.12) (Borghi *et al.*, 2001; Chan *et al.*, 2003; Fitzsimons *et al.*, 2013; Main *et al.*, 2021; Miska *et al.*, 1999; Tan *et al.*, 2024). HDAC4 aggregates have been colloquially termed "speckles" despite no evidence of enrichment in pre-mRNA splicing factors, which are typically a feature of aggregates classified as speckles (Lamond & Spector, 2003), therefore herein these will be described as aggregates.

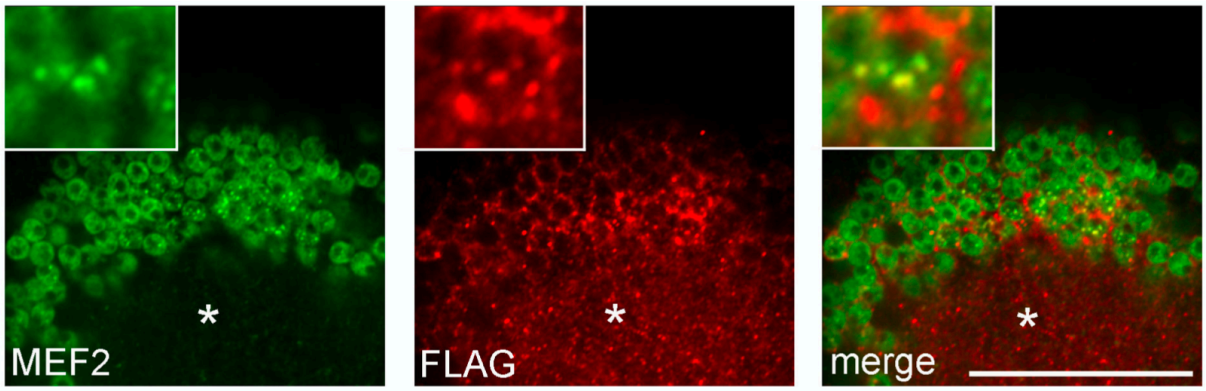

Figure 1.12 HDAC4 co-localises with MEF2 in nuclear aggregates in the *Drosophila* brain
Confocal microscopy of Kenyon cells within the *Drosophila* brain expressing FLAG-tagged HDAC4^{WT} (red) which co-localises with endogenous MEF2 (green) in punctate foci within nuclei. * denotes location of the calyx. Scale bar = 25 µm. *This figure is reproduced from Fitzsimons et al. (2013) (doi: 10.1371/journal.pone.0083903.g005), which is distributed under CC BY 4.0.*

Kirsh *et al.* (2002) determined that the N-terminus of HDAC4 is necessary for its aggregation upon overexpression in HeLa cells. While the N-terminus alone did not form aggregates, these could be induced under certain conditions, such as MEF2-overexpression (Chan *et al.*, 2003) and excess caspase cleavage (Paroni *et al.*, 2004). However, the mechanism through which

HDAC4 forms these aggregates is poorly understood, owing in part to the inaccessibility of structural and biophysical analyses due to insolubility (Guo *et al.*, 2007; Smialowski *et al.*, 2007). This limits studies to use of peptide fragments, preventing assessment of other contributing domains and limiting traditional structural analyses.

1.8.1. Mechanism of tetramerisation

HDAC4 has a unique N-terminal extension rich in glutamine residues (Figure 1.13C), and regions such as these are a feature frequently associated with proteins that form intranuclear neuronal inclusions (Chen *et al.*, 2001), further demonstrating the relevance of this region to the ability of HDAC4 to aggregate. Indeed, it was determined that this region alone formed homo-tetramers in solution (Figure 1.13A) (Guo *et al.*, 2007). Informed by circular dichroism (CD) spectroscopy and crystal structure analysis, residues 62-129 of human HDAC4 constitute a single α-helix, and this tetramerised in solution via the formation of a four-helix-bundle (Guo *et al.*, 2007). The helices were arranged in antiparallel with three two-fold axes of symmetry (Figure 1.13A).

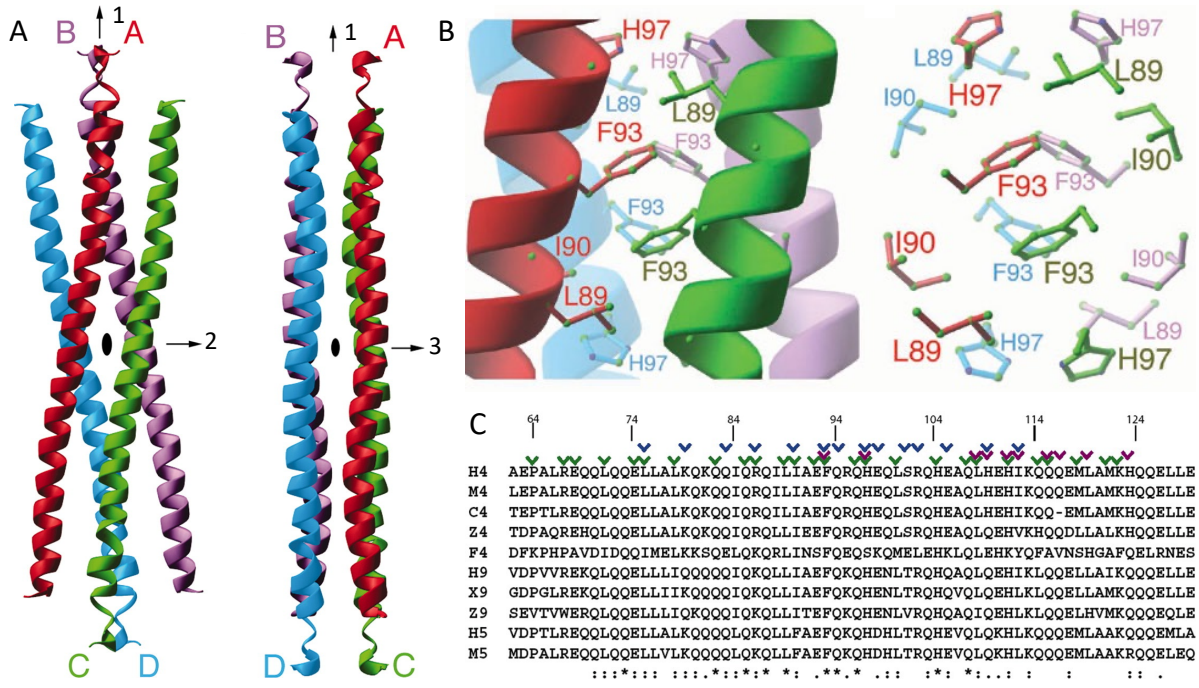

Figure 1.13 Tetramerisation of the glutamine-rich N-terminus of HDAC4
(A) The N-terminal region of HDAC4 tetramerises through the formation of a four-helix bundle where two pairs of antiparallel helices (A & C, B & D) stack onto each other with a crossing angle of 23°. Three perpendicular twofold axes of symmetry are indicated by arrows (labelled 1-3), intercepting (oval) at the hydrophobic core. (B) Three nonpolar residues from each helix form a small hydrophobic core (L89, I90, F93) stabilised by a double helical network of hydrophobic residues (F93 and H97). (C)

Sequence alignment of HDAC4 shows conservation between species and class. H4, human HDAC4; M4, mouse HDAC4; C4, chicken HDAC4; Z4, zebrafish HDAC4; F4, *Drosophila* HDAC4; H9, human HDAC9; X9, *Xenopus* HDAC9; Z9, zebrafish HDAC9; H5, human HDAC5; and M5, mouse HDAC5. Numbering is according to human HDAC4. Arrows indicate interhelical interactions: magenta A/B, green A/C, blue A/D. *Reproduced from Guo et al. (2007) (doi: 10.1073/pnas.0608041104). Copyright (2007) National Academy of Sciences. Permission for the reproduction of this content was granted by PNAS.*

Kirsh *et al.* (2002) suggested that the N-terminus of HDAC4 may aggregate via a coiled-coil domain. These are over-represented in polyglutamine-rich proteins, and interestingly, mutations that enhance the propensity to form coiled-coils promote protein aggregation (Fiumara *et al.*, 2010). Coiled-coil domains traditionally mediate interactions between two α-helices, and are thought of as rope-like structures; helices intertwine to minimise the interaction of the hydrophobic stripes present on each helix which arise due to the heptad repeat arrangement ('a-b-c-d-e-f-g'), where hydrophobic residues occupy 'a' and 'd' residues, and are interspersed with glutamine or arginine residues (Parry, 1982). Unusually however, due to an absence of this characteristic repeat, only a small hydrophobic core mediated tetramerisation of HDAC4 (Figure 1.13B) (Guo *et al.*, 2007). Furthermore, there was an absence of traditional "knobs into holes" interactions due to inflexibility of the helices, and instead stability along the length of the straight helix was governed by the contribution of glutamine residues to intra- and interhelical polar interaction networks. As observed in Figure 1.13C, the residues that mediate the stabilising interhelical interactions (arrows) are highly conserved across both species and isoforms of HDACs, suggesting they are essential to function.

Guo *et al.* (2007) conducted studies concentrating on the formation of the hydrophobic core and its impact on the dynamics of tetramerisation. In solution, HDAC4 N-terminal tetramers were highly dynamic and too unstable to analyse by size exclusion chromatography alone, however, in tandem with multiangle light scattering, an equilibrium between monomeric and tetrameric species was demonstrated. Substitution of a single residue within the hydrophobic core (F93D) abolished tetramerisation, shifting the equilibrium to the monomeric species, while substitution to extend the hydrophobic core (H97F) shifted the equilibrium to tetrameric species. These data demonstrate that the core is essential to tetramer formation in solution, and that this can be modulated to alter the dynamics of tetramerisation.

Given the requirement of the N-terminal domain for aggregation (Kirsh *et al.*, 2002) it was hypothesised that the hydrophobic core is critical for transient tetramerisation of full-length HDAC4 *in vivo*, and that this tetramerisation contributes to aggregation of HDAC4 in neuronal nuclei (Hawley, 2020). Preliminary proof of principle studies in *Drosophila* supported this hypothesis, as well as that tetramerisation of HDAC4 is required for aggregate formation in neuronal nuclei (Hawley, 2020). This pilot study examined the role of tetramerisation of HDAC4 in its aggregation in Kenyon cell nuclei; expression of the *Drosophila* equivalent of F93D, F65A ($HDAC4^{F65A}$), was associated with reduced aggregation of HDAC4 in Kenyon cells compared to $HDAC4^{WT}$. A second mutant was also generated, which substituted nine conserved glutamine residues important in formation of polar interaction networks, for alanine, 9QA ($HDAC4^{9QA}$), and this also reduced nuclear aggregation. This was independent of the additional polyglutamine stretch found downstream of the α-helix in *Drosophila* HDAC4 (which is not conserved in humans), as deletion of this alongside the 9QA mutation, 9QAΔQ ($HDAC4^{9QAΔQ}$) reduced aggregation similarly to $HDAC4^{9QA}$ alone.

Importantly, these preliminary studies also examined how HDAC4 aggregation disrupts neuronal development using *Drosophila* models of neurodevelopment in the eye and brain (Hawley, 2020). Overexpression of $HDAC4^{WT}$ in the developing eye or brain impairs correct development of these tissues (Section 1.6.1), and the phenotypes resulting from this are easily visualised and quantified (Main *et al.*, 2021; Schwartz *et al.*, 2016; Tan *et al.*, 2024). In the eye, overexpression of $HDAC4^{WT}$ typically induces misalignment and fusion of ommatidia, while in the mushroom body, overexpression of $HDAC4^{WT}$ typically interferes with axon termination resulting in fusion of the β-lobes. All mutants examined in the preliminary study reduced the severity of HDAC4 overexpression-induced defects in both mushroom body and eye development, suggesting a correlation between aggregation and impairment of neuronal development (Hawley, 2020). Together, these preliminary studies provided confidence of a viable avenue for further exploration in this thesis.

Chapter Two

Aims & Objectives

2. Aims & Objectives

Dysregulation of HDAC4, specifically increased nuclear abundance and aggregation, has been observed in a number of neurodevelopmental diseases including CDKL5 disorder and 2q37 deletion syndrome (Trazzi *et al.*, 2016; Wakeling *et al.*, 2021) as well as neurological diseases including Alzheimer's, Parkinson's and neuronal intranuclear inclusion diseases (Lang *et al.*, 2019; Shen *et al.*, 2016; Takahashi-Fujigasaki & Fujigasaki, 2006), however **it is unclear whether the presence of these aggregates is related to disease pathogenesis.** This study therefore seeks to examine the relationship between aggregation of HDAC4 and defects in neuronal function in a *Drosophila* model.

Drosophila are an excellent model for these studies as they can be genetically manipulated with ease, facilitating overexpression of wild-type and mutant HDAC4 with spatial and temporal specificity (Section 1..2.3). Moreover, aggregates of HDAC4 in Kenyon cells are easily visualised (Fitzsimons *et al.*, 2013), and the development of the mushroom body and eye can be reproducibly quantified (Main *et al.*, 2021; Tan *et al.*, 2024). Therefore, both aggregation and impairments in development can be quantified in the same cell types, and correlations between the two can be examined.

Previous studies demonstrated that overexpression of HDAC4 in *Drosophila* induces neurodevelopmental phenotypes as well as defects in memory, and HDAC4 was observed to aggregate in nuclei (Fitzsimons *et al.*, 2013; Main *et al.*, 2021; Tan *et al.*, 2024). Importantly, these defects increased in severity upon nuclear restriction of HDAC4, which also increased aggregation (Main *et al.*, 2021; Tan *et al.*, 2024). In light of this, **it is hypothesised that nuclear aggregation of HDAC4 correlates with impairments in neuronal function in *Drosophila*.**

The N-terminus of human HDAC4 tetramerises in solution (Guo *et al.*, 2007) and this region of HDAC4 was also required for nuclear aggregation of HDAC4 upon overexpression (Kirsh *et al.*, 2002). Together these data lead to **the hypothesis that aggregation of HDAC4 is dependent on tetramer formation.** Tetramer formation in solution was dependent on a single residue that forms a hydrophobic core, and mutation of this prevented tetramerisation (Guo *et al.*, 2007). **It is therefore proposed that disrupting the formation of the hydrophobic core of HDAC4 will disrupt its aggregation *in vivo*.**

To that end, the aim of this project is to investigate the aggregation of HDAC4 in neuronal nuclei, and the effects of this on *Drosophila* neurodevelopment, with the overall intention of delineating the mechanism of neurotoxicity. This is to be achieved via the characterisation of various mutant HDAC4 constructs that are hypothesised to alter tetramer stability and/or subcellular distribution, identification of the composition of HDAC4 aggregates, and testing strategies to reduce aggregation of HDAC4.

The specific objectives of this project will be addressed in separate chapters as follows:

1. **Characterise the relationship between oligomerisation and aggregation of HDAC4, and the effect this has on *Drosophila* neurodevelopment.**

Transgenic flies harbouring HDAC4 constructs with mutations F65A, 9QA and 9QAΔQ which are hypothesised to reduce tetramerisation were previously generated (Hawley, 2020) as was wild-type HDAC4 (Main *et al.*, 2021). A further mutant that is hypothesised to stabilise tetramerisation will be generated here (S69F) alongside a double mutant (F65A-9QA), which is hypothesised to maximally destabilise tetramerisation. Optimisation and validation of the experimental conditions for quantification of HDAC4 aggregation and overexpression-induced phenotypes will then be performed. Specifically, this involves optimisation of MEF2 and HDAC4 immunohistochemistry and subsequent quantification of HDAC4 aggregation in Kenyon cells, as well as optimisation of imaging of eyes, and production a consistent scoring system for both mushroom body and eye development. Following this, all of the HDAC4 mutants will be characterised as a group to allow direct comparisons. Each of the HDAC4 mutants will be examined with respect to their expression level, ability to oligomerise and capacity to form aggregates in neuronal nuclei compared to wild-type HDAC4. This will then be correlated with the ability of each of these mutants to mediate HDAC4 overexpression-induced defects in the development of the mushroom body and eye.

2. **Examine the interaction between HDAC4 oligomerisation and regulation of subcellular distribution and how this affects HDAC4 aggregation and neuronal development.**

Changes in the subcellular distribution of the HDAC4 oligomerisation mutants outlined in Objective 1 will be examined. New mutants will then be generated that are restricted to the nucleus to assess changes in oligomerisation, aggregation, and ability to confer neurodevelopmental phenotypes independent of changes in distribution. An additional mutant that is predicted to be reduced in MEF2 binding will also be characterised. Following these studies the roles of MEF2 and 14-3-3 in regulation of subcellular distribution, aggregation, and neurotoxicity of HDAC4 will then be further investigated.

3. **Identify the composition of HDAC4 aggregates associated with overexpression of nuclear-localised HDAC4.**

Immunoprecipitation-coupled mass spectrometry (IP-MS) will be performed on whole-cell lysates from heads of flies expressing nuclear-localised HDAC4 to identify proteins that are sequestered in HDAC4 aggregates. This involves further characterisation of the dynamics of HDAC4 aggregation and determination of the appropriate experimental conditions to isolate and identify binding partners of nuclear HDAC4.

4. **Investigate mechanisms to reduce aggregation of HDAC4.**

Truncations of the N-terminus of HDAC4 will be examined for their ability to aggregate in neuronal nuclei, followed by their effect on neuronal development upon overexpression. The effect of these constructs on the aggregation of full-length wild-type HDAC4 will then be examined to determine whether they alter aggregation, followed by investigation of whether they modulate HDAC4 overexpression-induced neurotoxicity.

The strategy for objectives 1, 2, and 4 involves examining the consistency of the correlation between aggregation of HDAC4 in neuronal nuclei, and defects in *Drosophila* neurodevelopment. This is summarised in Figure 2.1.

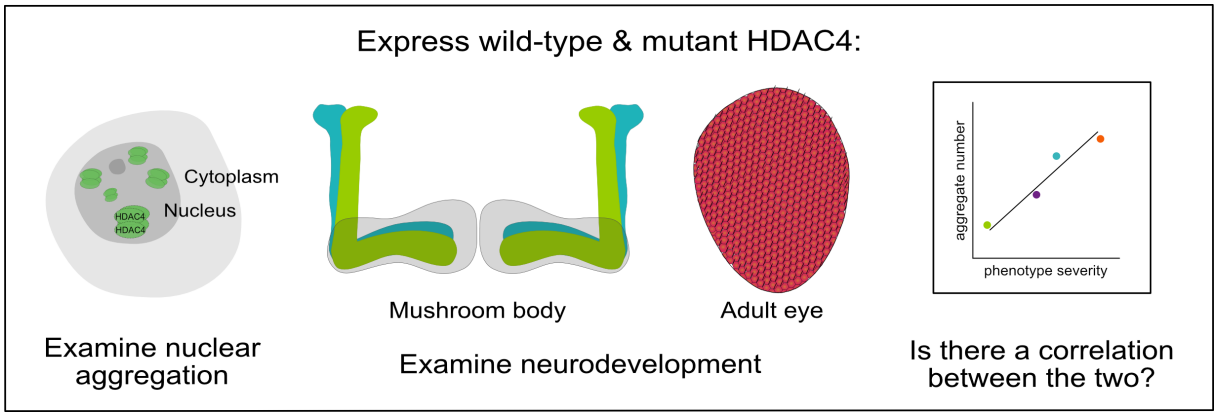

Figure 2.1 Strategy to investigate the relationship between HDAC4 aggregation and neuronal development in *Drosophila*
Schematic diagram demonstrating that upon expression of wild-type or mutant HDAC4, its ability to form nuclear aggregates will be correlated with the effect its expression has on development of the *Drosophila* mushroom body and eye to examine the role of HDAC4 aggregation in disruption of *Drosophila* development. *This figure is an original artwork.*

Chapter Three

Materials & Methods

3. Materials & Methods

3.1. *Drosophila melanogaster* strains

Drosophila strains used are listed in Appendix 10.1.1 Shorthand names used throughout this document are noted alongside genotype. Nomenclature is described in Section 1.2.2.

3.1.1. Generation of transgenic *Drosophila*

The open reading frame of wild-type *Drosophila HDAC4 (HDAC4^{WT})* was previously synthesised (nucleotides 461–4216, NCBI NM_132640) with a C-terminal 6x Myc tag (Main *et al.*, 2021), and mutagenesis performed to obtain *HDAC4* mutants listed in Table 3.1. The following *HDAC4$^{N\text{-}term}$* mutants were synthesised with a C-terminal 3x HA tag: *HDAC4$^{M1\text{-}L285}$* nucleotides 461–1315, *HDAC4$^{M1\text{-}Q143}$* nucleotides 461–889, *HDAC4$^{P37\text{-}Q143}$* nucleotides 569–889, NCBI NM_132640. Nuclear localisation and export sequences added to HDAC4$^{P37\text{-}Q143}$ were from Shiga *et al.* (1996) and Bajusz *et al.* (2021) respectively. *MEF2^{WT}* was previously synthesised (nucleotides 1057–2601, NM_057670.5) with a C-terminal 3x HA tag (Main *et al.*, 2021). Sequences for each of these are found in Appendix 10.1.2-10.1.4. Flanking NotI and XbaI sites allowed the subcloning of *HDAC4* and *MEF2* constructs into the pUASTattB vector (Groth *et al.*, 2004) for generation of transgenic flies (Appendix 10.1.5). Synthesis, mutagenesis and subcloning was carried out by GenScript (New Jersey, USA). Plasmids were prepared for germline transformation using the PureLink HiPure Plasmid Midiprep Kit (Invitrogen) as per manufacturer's instructions. Restriction digests were performed to confirm the presence of the insert. HDAC4 transgenic fly lines were generated using the P2 injection strain, with constructs inserted into the attP site on chromosome 3L at 68A4, and the VK22 injection strain was used to make the MEF2 line, inserted into chromosome 2R at 57F5. Transgenic flies were generated by GenetiVision (Houston, TX). Point mutations were confirmed via PCR and sanger sequencing. HDAC4^{WT} and the following mutants were confirmed by Ana Claasen: 3SA, ΔMEF2, 9QA, 9QAΔQ, F65A, S69F and 3SA-ΔMEF2. EPA approval is in place for the import and development of transgenic *Drosophila* (approval numbers GMD100518, GMD100517 GMC001092).

Table 3.1 HDAC4 mutants used in this study

Name	Mutation	Hypothesised effect of mutation	Template	Reference
HDAC4^{WT}	-	-	-	Main *et al.* (2021)
HDAC4^{3SA}	3x serine residues substituted for alanine: S239A, S573A, S748A	Prevent phosphorylation and 14-3-3 binding, resulting in nuclear accumulation of HDAC4	HDAC4^{WT}	Main *et al*. (2021)
HDAC4$^{\Delta MEF2}$	3x amino acid substitutions: K165A, L168A, I172A	Prevent binding of MEF2 resulting in cytoplasmic accumulation of HDAC4	HDAC4^{WT}	Tan *et al.* (2024)
HDAC4^{9QA}	9x glutamine residues substituted for alanine: Q45A, Q46A, Q54A, Q57A, Q59A, Q66A, Q68A, Q71A, Q79A	Destabilise tetramer formation; nine residues conserved between human and *Drosophila* HDAC4 are important in tetramer stability in solution (Guo *et al.*, 2007)	HDAC4^{WT}	This study
HDAC4$^{9QA\Delta Q}$	9QA mutation plus deletion of residues Q112-Q143	Destabilise tetramer formation; additional deletion of poly-Q stretch present in *Drosophila* but not human HDAC4	HDAC4^{9QA}	This study
HDAC4^{F65A}	1x phenylalanine residue substituted for alanine: F65A	Destabilise tetramer formation; homologous to F63D in human HDAC4 which destabilises tetramerisation in solution (Guo *et al.*, 2007)	HDAC4^{WT}	This study
HDAC4^{S69F}	1x serine residue substituted for phenylalanine: S69F	Stabilise tetramer formation; homologous to H97F in human HDAC4 which stabilises tetramer formation in solution (Guo *et al.*, 2007)	HDAC4^{WT}	This study
HDAC4$^{9QA-F65A}$	Combination of 9QA and F65A mutations	Maximally destabilise tetramer formation	HDAC4^{9QA}	This study
HDAC4$^{3SA-9QA}$	Combination of 3SA and 9QA mutations	Prevent phosphorylation and 14-3-3 binding, resulting in nuclear accumulation of HDAC4 with destabilised tetramer formation	HDAC4^{9QA}	This study
HDAC4$^{3SA-F65A}$	Combination of 3SA and F65A mutations	Prevent phosphorylation and 14-3-3 binding, resulting in nuclear accumulation of HDAC4 with destabilised tetramer formation	HDAC4^{3SA}	This study
HDAC4$^{3SA-\Delta MEF2}$	Combination of 3SA and ΔMEF2 mutations	Prevent 14-3-3 and MEF2 binding	HDAC4^{3SA}	Tan *et al.* (2024)
HDAC4$^{3SA-F65A-\Delta MEF2}$	Combination of 3SA-F65A and ΔMEF2 mutations	Prevent tetramerisation and binding of 14-3-3 and MEF2	HDAC4$^{3SA-F65A}$	This study

Name	Mutation	Hypothesised effect of mutation	Template	Reference
$HDAC4^{\Delta NES}$	4x amino acid substitutions: M1225A, L1228A, M1230A, M1233A	Prevent association of CRM1 and nuclear export of HDAC4	$HDAC4^{WT}$	This study/Tan *et al.* (2024)
$HDAC4^{M1\text{-}L285}$	Residues M1 to L285 of DmHDAC4. Ser239 mutated to alanine.		Synthesised new	This study
$HDAC4^{M1\text{-}Q143}$	Residues M1-Q143 of DmHDAC4		Synthesised new	This study
$HDAC4^{P37\text{-}Q143}$	Residues P37-Q143 of DmHDAC4		Synthesised new	This study
$HDAC4^{NLS\text{-}P37\text{-}Q143}$	Residues P37-Q143 of DmHDAC4 with an N-terminal NLS		Synthesised new	This study
$HDAC4^{P37\text{-}Q143\text{-}NLS}$	Residues P37-Q143 of DmHDAC4 with a C-terminal NLS		Synthesised new	This study
$HDAC4^{NES\text{-}P37\text{-}Q143}$	Residues P37-Q143 of DmHDAC4 with an N-terminal NES		Synthesised new	This study
$HDAC4^{P37\text{-}Q143\text{-}NES}$	Residues P37-Q143 of DmHDAC4 with a C-terminal NES		Synthesised new	This study

3.1.2. Maintenance of *Drosophila* stocks

Drosophila stocks were maintained on standard medium (per litre of dH_2O: 10 g agar, 40 g yeast, 110 g ground cornmeal, 20 mL molasses, 130 g sugar, 3.3 g methyl 4-hydroxybenzoate (Sigma Aldrich) and 37 mL 95% ethanol) with a 12 hour light dark cycle at 22°C. Stocks were turned onto fresh food every three weeks, adults emptied approximately four days after turning, and vials were checked for dryness and watered at least once per week. For all experiments stocks were expanded and crosses were set as in Section 3.1.3; the temperature at which crosses were set and flies were raised was specifically optimised for each experimentand is noted in the results. To encourage egg laying, media was topped with yeast.

3.1.3. Genetic crosses

Genetic crosses for functional analyses were performed using virgin females. These were collected by clearing bottles of adults in the morning and collecting any females that emerged within eight hours of clearing, as adult *Drosophila* do not mate within ten hours of eclosion at 25 °C (Greenspan, 2004). In the morning, flies with visible meconium through the abdomen, which indicates recent emergence, were also collected.

Crosses were set in 30 mL vials (LabServ) with 8 mL of media or bottles (Schott) with 40 mL of media. Vials were set with five virgin females and five males, and bottles were set with a minimum of ten virgin females and eight males. Adults were removed before progeny emerged. F1 progeny were collected and used for analyses unless otherwise stated.

Standard genetic crosses used in this thesis are presented in Figure 3.1 Crossing schemes to combine transgenes into a single fly line are presented in Appendix 10.1.6, and the combined lines are noted in the stock list in Table 10.1. Flies generated using the crossing schemes depicted in Figures 10.7 and 10.8 were made by Dr Helen Fitzsimons, as were those involving $HDAC4^{WT}$, $HDAC4^{F65A}$, $HDAC4^{9QA}$, $HDAC4^{9QA\Delta Q}$, $HDAC4^{S69F}$, and $HDAC4^{3SA\text{-}F65A}$ in Figures 10.5 and 10.6.

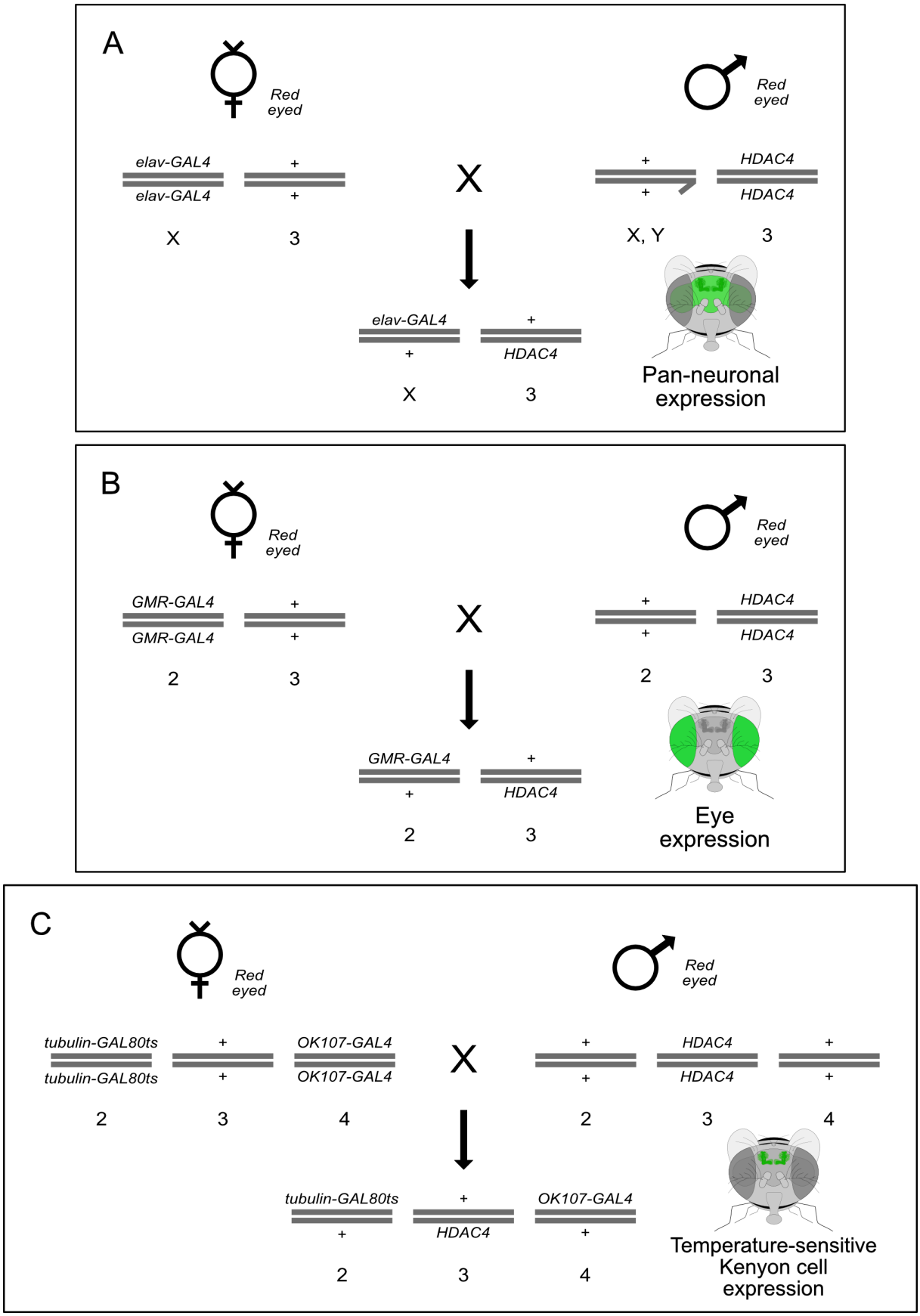

Figure 3.1 Standard crossing schemes used to generate progeny that express transgenes using the UAS/GAL4 system

(A-B) Female virgin *GAL4* driver line flies (*elav-GAL4* in (A), *GMR-GAL4* in (B)) are crossed to males that harbour the *HDAC4* transgene. F1 progeny inherit both components of the UAS-GAL4 system and express the transgene in the spatiotemporal pattern governed by the driver regulatory region as in Figure 1.2. The genotype of the progeny from this cross is noted as *driver-GAL4/+; HDAC4/+*, where flies are heterozygous for both the driver and the transgene. HDAC4 refers to both full-length and N-terminal constructs of HDAC4. Please note that $MEF2^{WT}$-HA is also expressed using these drivers, and is on the second chromosome. (C) Female virgin *tubulin-GAL80ts; OK107-GAL4* (driver line) flies are crossed to males that harbour the *HDAC4* transgene. F1 progeny inherit both components of the UAS-GAL4 system as well as the TARGET system and the transgene is expressed with spatiotemporal control as in Figure 1.3; the pattern in which the transgene is expressed is governed by *OK107-GAL4* and temporal control of gene expression is governed by *tubulin-GAL80ts. This figure is an original artwork.*

3.2. Protein analyses

3.2.1. Modelling of the HDAC4 tetramer

An *in silico* model of the DmHDAC4 tetramer was generated based on the crystal structure obtained by Guo *et al.* (2007). The structure of the hHDAC4 N-terminal tetramer (2h8n, version 1.2, Guo *et al.* (2007)) was downloaded from the Research Collaboratory for Structural Bioinformatics Protein Data Bank (RCSB PDB, Berman *et al.* (2000)) and the predicted structure of DmHDAC4 (Q9VYF3, corresponding to NP_572868.3, accessed on 10/01/2024) was downloaded from AlphaFold (Jumper *et al.*, 2021; Varadi *et al.*, 2021). Both were imported into ChimeraX* (Meng *et al.* (2023), version 1.7) and the matchmaker command (Meng *et al.*, 2006) was then used to superimpose four monomers of DmHDAC4 onto the hHDAC4 tetramer under the default settings; this involved pairwise sequence alignment followed by fitting of the aligned residue pairs. Chains were then coloured according to Guo *et al.* (2007) and the indicated residues are displayed.

*UCSF ChimeraX was developed by the Resource for Biocomputing, Visualization, and Informatics at the University of California, San Francisco, with support from National Institutes of Health R01-GM129325, the Office of Cyber Infrastructure and Computational Biology, and the National Institute of Allergy and Infectious Diseases.

3.2.2. Total protein isolation from fly heads

Flies were anaesthetised using CO_2 before freezing 50-100 whole flies in 15 mL tubes (Greiner) at -80 °C. Heads were snapped from bodies by vortexing and sorted over a small sheet of acetate on dry ice before homogenising in buffer (western blotting: RIPA buffer (150 mM NaCl, 0.1%

Triton X-100, 0.5% sodium deoxycholate, 0.1% SDS, 50 mM Tris HCl pH 8.0, 1X cOmplete EDTA-free Protease Inhibitor Cocktail (Roche)). Immunoprecipitation: IP-buffer (50 mM NaCl, 30 mM Na pyrophosphate, 50 mM NaF, 10% glycerol, 0.5% Triton X-100, 0.5 mM PMSF, 25 mM Tris, pH 7.05, 1X cOmplete mini EDTA-free Protease Inhibitor Cocktail (Roche))) for 45 seconds using a disposable mortar and pestle to produce a crude lysate. Head capsule debris were pelleted by centrifugation at 13,000 g for 2 minutes at 4 °C. All supernatant was collected and subject to protein quantification by Pierce BCA Protein assay as per the manufacturer's instructions (ThermoFisher Scientific).

3.2.3. Subcellular fractionation from fly heads

Subcellular fractionation was performed using the NE-PER Nuclear and Cytoplasmic extraction reagents (ThermoFisher Scientific) using a protocol modified from Maitra *et al.* (2019) and Wilson (2021). Flies were anaesthetised using CO_2 and incubated on ice until no longer moving. Heads were manually removed using a scalpel blade and collected in chilled 1.7 mL microcentrifuge tubes. Protease inhibitors (cOmplete EDTA free Protease Inhibitor Cocktail (Roche)), were added to cytoplasmic buffer 1 (C1) and the nuclear extraction buffer. Whilst held in ice, 50 heads were homogenised in 25 µL of C1 for 10 seconds, followed by addition of 75 µL of C1 and homogenisation for 20 seconds, then incubation on ice for 10 minutes. 5.5 µL of cytoplasmic buffer 2 (C2) was then added, the lysate resuspended, and centrifuged for 5 minutes at 4C, 10,000 x g. The supernatant was collected as the cytoplasmic fraction and the pellet washed twice as follows: resuspend in 50 µL of C1, incubate on ice for 10 minutes, resuspend in 2.75 µL of C2, centrifuge for 5 mins minutes at 4 °C, 10,000 x g, discard supernatant. The pellet was then resuspended in 50 µL of nuclear extraction reagent, incubated on ice for 40 minutes, and centrifuged for 10 mins minutes at 4 °C, 10,000 x g, and the supernatant collected as the nuclear fraction.

For fractionation prior to immunoprecipitation-coupled mass spectrometry, preparations were scaled up. Flies were snap frozen at -80 °C in 15 mL tubes and vortexed to separate heads from bodies before sieving over dry ice. Approximately 100 heads were placed into a 1.7 mL tube and fractionation performed as above but using double the volume of each reagent. Nuclear pellets were resuspended in 50 µL of IP-buffer. Ten fractionations were prepared per genotype and the nuclear lysate pooled for quantification.

3.2.4. Immunoprecipitation

Two protocols for immunoprecipitation were used in this thesis. The first was optimised and used for the initial mass spectrometry (Section 6.1) and the co-immunoprecipitation experiment in Appendix 10.2.5. Extended use of this protocol determined that the agarose beads were susceptible to batch-to-batch variation therefore a protocol using alternative magnetic beads was optimised and used for all other applications. Extra precautions were taken to minimise keratin contamination for immunoprecipitation-coupled mass spectrometry; gloves were worn at all times and all equipment was cleaned with 70% ethanol before use. Fresh reagents were prepared for each run.

Protocol 1:

All incubations and washes were performed with end-over-end mixing followed by centrifugation at 4 °C, 1,000 x g. Protein A/G PLUS agarose beads (Santa Cruz) were twice washed with IP-buffer before blocking with 0.1 µg/µL BSA and 75 ng/µL salmon sperm DNA in IP-buffer (1:1 volume of beads to blocking buffer) for one hour at room temperature. Whole cell lysate (2 mg) was diluted to 500 µL in IP-buffer and pre-cleared by incubated with 20 µL of pre-blocked beads for one hour at 4 °C. The supernatant was then collected and incubated overnight at 4 °C with pulldown antibody (2 µL α-Myc, ab9106 or 0.2 µL α-GFP, ab290) to form the immune complex. To capture the immune complex, 30 µL of pre-blocked beads were added and incubated for one hour at 4 °C. Non-captured proteins in the supernatant were collected to determine the efficiency of the pulldown, and the beads were washed 4 x 5 min with IP-buffer. For co-immunoprecipitation studies, protein was eluted from the beads by heating to 90 °C in 40 µL of 1X elution sample buffer (0.02% SDS, 15% 2-mercaptoethanol, 6% glycerol, 0.02% bromophenol blue, 125 mM Tris HCl pH 6.8), or for mass spectrometry analyses in 20 µL of 2X elution sample buffer. Total eluate was loaded for SDS-PAGE (Section 3.2.5), and two pulldowns were loaded per lane for mass spectrometry.

Protocol 2:

Protein A/G magnetic beads (ThermoFisher Scientific, 25 µL) were resuspended and washed in 1 mL of filter-sterilised TBS-T (20 mM Tris, 150 mM NaCl, filter sterilised + 0.05% Tween-20) before incubation with 2 µL of immunoprecipitation antibody (α-Myc, ab9106 or α-GFP, ab290) for one hour at room temperature with end over end mixing. Whole cell lysate (2 mg) was diluted to 300 µL and added to the antibody-bead mixture and incubated overnight at 4 °C

with end-over end mixing. Beads were then magnetised and non-captured proteins collected to determine the efficiency of the pulldown, followed by three washes of the beads in 1 mL of TBS-T. Captured proteins were eluted by incubation with 38 µL of 1X sample buffer (2% SDS, 5% 2-mercaptoethanol, 10% glycerol, 0.01% bromophenol blue, 60 mM Tris HCl pH 6.8) for 10 minutes at room temperature with end-over end mixing. Beads were magnetised and the supernatant collected and incubated at 95 °C for 5 minutes to denature proteins. For mass spectrometry analyses, all steps were the same apart from the following: 50 µL of beads were used per reaction, incubated with 4 µL of immunoprecipitation antibody in a final volume of 200 µL, and 2 mg of nuclear lysate was added to a final volume of 1 mL.

3.2.5. SDS-PAGE

Whole cell lysate (30 µg), nuclear lysate (20 µg), or cytoplasmic lysate (20 µg) was denatured in 1X Laemmli buffer (2% SDS, 5% 2-mercaptoethanol, 10% glycerol, 0.01% bromophenol blue, 60 mM Tris HCl pH 6.8) at 95 °C for five minutes. Immunoprecipitation samples were prepared as per Section 3.2.4. All samples were cooled on ice and centrifuged before gel loading alongside the PageRuler Prestained NIR Protein Ladder (ThermoFisher Scientific). Precast gels (Mini-PROTEAN TGX Precast Protein gels (Bio-Rad), general purpose: 4-20% gradient with 25 µL wells, immunoprecipitation: 10% with 50 µL wells) were run at constant voltage (200 V) for 30-40 minutes in 1X Running buffer (25 mM Tris, 190 mM glycine, 0.1% SDS).

3.2.6. Western blotting

Protein was blotted to a nitrocellulose membrane (GE Life Sciences) in Transfer buffer (1X Running buffer, 20% methanol) for one hour at 4 °C. Ponceau staining (0.1% Ponceau-S, 5% acetic acid) confirmed successful protein transfer and enabled band visualisation for membrane cutting, which was followed by incubation in 5% blocking buffer (5% skim milk powder, TBST) for one hour at room temperature. Membranes were washed in TBST (20mM Tris, 150mM NaCl, pH 7.6, 0.1% Tween-20) before incubation overnight in primary antibody (Table 3.2) in 1% blocking buffer at 4 °C, followed by secondary antibody (Table 3.3) for one hour at room temperature. Amersham ECL Prime detection reagent (GE Life Sciences) was used as per manufacturer's instructions, and chemiluminescence recorded using the Azure Biosystems C600 imaging system.

Table 3.2 Primary antibodies used for western blotting

Antibody	Host	Clonality	Source	Catalogue number	Antibody Registry ID	Dilution
Anti-alpha-tubulin	Mouse	Monoclonal	DSHB*	12G10	AB_1157911	1:500
Anti-GFP	Rabbit	Polyclonal	Abcam	Ab290	AB_303395	1:4,000
Anti-HA	Rat	Monoclonal	Roche	3F10	AB_2687407	1:1,000
Anti-lamin (Dm0)	Mouse	Monoclonal	DSHB*	ADL67.10	AB_528336	1:1,000
Anti-Myc	Rabbit	Polyclonal	Abcam	Ab9106	AB_307014	1:1,000

*Developmental Studies Hybridoma Bank. The following antibodies were obtained from the DSHB, created by the NICHD of the NIH and maintained at The University of Iowa, Department of Biology, Iowa City, IA 52242, USA:
12G10 (anti-alpha-tubulin) was deposited to the DSHB by Frankel, J. / Nelsen, E.M.
ADL67.10 (anti-lamin Dm0) was deposited to the DSHB by Fisher, P. A.

Table 3.3 Secondary antibodies used for western blotting

Antibody	Host	Source	Catalogue number	Antibody Registry ID	Dilution
Anti-Mouse HRP	Sheep	Sigma Aldrich	NA931VS		1:20,000
Anti-Rabbit HRP	Donkey	Sigma Aldrich	NA934VS		1:40,000
Anti-Rat HRP	Goat	Abcam	Ab97057	AB_10680316	1:10,000
VeriBlot*		Abcam	Ab131366	AB_2892718	1:4,000

*VeriBlot for IP Detection Reagent (HRP); this reagent preferentially detects native (non-reduced) antibodies to minimise detection of heavy and light chains following immunoprecipitation.

3.2.7. Quantification of western blots

Quantification of western blots was performed using the Gel Analyzer plugin within ImageJ (Schneider *et al.*, 2012). Whole cell lysate signal was normalised to that of tubulin. For fractionation samples, nuclear fractions were normalised to lamin and cytoplasmic to tubulin. To normalise band intensity, a normalisation factor was first calculated for each lane:

$$Lane\ normalisation\ factor = \frac{observed\ signal\ of\ tubulin\ or\ lamin}{the\ highest\ observed\ signal\ of\ tubulin\ or\ lamin}$$

Which was then used to calculate the normalised signal for each band of interest:

$$Normalised\ signal = \frac{observed\ experimental\ signal}{lane\ normalisation\ factor}$$

For each blot, the fold change of the normalised signal was then calculated, relative to the indicated sample, and plotted. Statistical significance was calculated using a one sample t-test with a hypothetical mean of 1.

As the HDAC4$^{N\text{-}term}$ proteins were of different molecular weights, quantification could not be performed using Gel Analyzer, and therefore was performed in ImageJ as follows. A rectangle was drawn around the widest band using rectangle selection, and then moved to the leftmost band. The intensity within this box was measured using the measure function, as well as the intensity of background immediately below each band. The mean grey value was recorded, all values were inverted (255-value), and then the background subtracted from each band, before normalising HDAC4$^{N\text{-}term}$-HA signal to tubulin. Statistical significance was calculated using a one-way ANOVA with post-hoc Tukey's HSD test with significance set at α=0.05.

3.2.8. Colloidal Coomassie staining

Following SDS-PAGE (Section 3.2.5), gels were fixed with 40% (v/v) ethanol, 10% (v/v) acetic acid for 30 minutes then washed three times for 10 minutes in dH_2O. Gels were stained overnight in fresh Colloidal Coomassie stain (0.08% (w/v) Coomassie Brilliant Blue G-250, 1.6% (v/v) orthophosphoric acid, 8% (w/v) ammonium sulfate, 20% (v/v) methanol); a stock solution excluding methanol was made at least 24 hours prior to use, and methanol added immediately before use. Prior to imaging gels were destained in dH_2O until the background was clear, or in 1% acetic acid for mass spectrometry application. Gels were stored in dH_2O until use.

3.2.9. In-gel tryptic digestion

All methods were performed wearing gloves to minimise keratin contamination and equipment was cleaned with 70% ethanol before use. All solutions were made using mass spectrometry grade reagents. Each lane of the Colloidal Coomassie stained gel was excised on a glass plate using a clean scalpel blade and cut into seven slices. Each slice was processed as a separate sample, alongside a sample of bovine serum albumin (BSA) to assess digestion efficiency.

Slices were cut into fine pieces with a cleaned scalpel, placed into LoBind microcentrifuge tubes (Protein LoBind, Eppendorf), and destained in 50 mM ammonium bicarbonate (1X ABC), 50% methanol at 50 °C. The destain solution was changed frequently until gel pieces were colourless (approx. three hours), then gel pieces were dehydrated in 80% acetonitrile (ACN) and dried using a centrifugal evaporator (Savant SpeedVac™ Vacuum Concentrator model SPD131DDA, ThermoFisher Scientific). Following dehydration gel pieces were rehydrated and reduced in 10 mM DTT in 1X ABC for one hour at 42 °C, washed in 1X ABC, dehydrated in 80% ACN, dried, and then alkylated in 20 mM iodoacetamide in 1X ABC for 20 minutes in darkness. Gel pieces were then washed in 1X ABC and twice dehydrated in 80% ACN, with the wash and dehydration repeated followed by vacuum centrifugation until completely dry.

Gel pieces were allowed to swell in digestion solution (Trypsin (SOLu-Trypsin EMS004, Sigma Aldrich) + 1 mM $CaCl_2$ at 20 ng/µL in 1X ABC) for 10 minutes on ice, then excess digestion solution was removed and replaced with enough 1X ABC to keep gel pieces hydrated during overnight incubation at 37 °C. The following day gel pieces were sonicated and centrifuged, and the supernatant of the digestion was carefully added to new LoBind tubes. Peptides were then extracted in two stages by washing first with 5% formic acid, 50% ACN then 0.1% formic acid, 80% ACN. Gel pieces were sonicated and centrifuged between each extraction step and the supernatants pooled with that from digestion. The volume was then reduced to ~30 µL by vacuum centrifugation and samples centrifuged at 16,000 x g for 15 minutes, before the top two thirds was loaded into MS sample vials, avoiding gel debris.

3.2.10. Mass spectrometry

Samples were subjected to liquid chromatography with tandem mass spectrometry (LC-MS/MS) at the Massey University Mass Spectrometry facility by Trevor Loo. All mass spectrometry instrument configurations are listed in Table 3.4. Samples underwent reversed-phase liquid chromatography separation using a nanoLC system with peptide trap and analytical columns for desalting/enrichment and peptide separation respectively, before eluted peptides were analysed by mass spectrometry using a data-dependent tandem MS acquisition. Scans were acquired over a mass range of 370-1700 *m/z* at a resolution of 70,000. Full settings are found in Table 3.5.

Table 3.4 Mass spectrometry instrument configuration

nanoLC system	Dionex Ultimate 3000 Binary RSLCnano LC system (ThermoFisher Scientific)
Mass spectrometer	Q Exactive™ Plus Hybrid Quadrupole-Orbitrap™ (ThermoFisher Scientific)
Ionisation source	Nanospray Flex™ (ThermoFisher Scientific)
Trapping column	Acclaim™ PepMap™ 100 C_{18}, 3 µm particle size, 75 µm inner diameter, 2 cm length (ThermoFisher Scientific)
Analytical column	Acclaim™ PepMap™ C_{18}, 2 µm particle size, 75 µm inner diameter, 50 cm length (ThermoFisher Scientific)
Flow rates	Trap: 15 µL/min Analytical: 300 nL/min
Column oven temperature	50 °C
Gradient	3-30% MeCN in 0.1% formic acid over 60 minutes
Buffers	Trap loading: 0.1% trifluoracetic acid / 2% MeCN / H_2O Analytical A: 0.1% formic acid / 2% MeCN / H_2O Analytical B: 0.1% formic acid / 98% MeCN / H_2O

Table 3.5 Mass spectrometry parameters

Capillary temperature (°C)	250
S-Lens RF level (%)	50
Polarity	Positive
Source voltage (kV)	1.5
AGC target	Full MS 3 x 106, MS2 (HCD) 1 x 105
Maximum injection times (ms)	Full MS 100 ms, MS2 (HCD) 110 ms
Full MS mass range	370-1700 m/z
Resolution settings	Full MS 70,000, MS2 (HCD) 17,500
Number of micro-scans	1
Isolation width	1.4 m/z
Loop count (TopN)	10
MSX count	1
Collision energy	28
Charge exclusion	Unassigned, 1, >6
Peptide match	Preferred
Exclude isotopes	On
Dynamic exclusion (s)	6
Spectrum data type	Centroid

3.2.11. Proteomic data analysis

LC-MS data was acquired via the Xcalibur™ (ThermoFisher Scientific) software. Raw data was imported into Proteome Discoverer™ 2.4 SP1 (ThermoFisher Scientific) and searched within *Drosophila melanogaster* (TaxID7227, NCBI database downloaded 10 February 2022), Trypsin, and contaminant databases. Full search parameters are found in Table 3.6. The sequence for DmHDAC4^{3SA} was also included. Only data mapping to *Drosophila melanogaster* was retained for further analyses.

Table 3.6 Proteome Discoverer search parameters

Search engine	Proteome Discoverer™ v2.4.1.15
Databases	Non-redundant NCBI compiled on 10/02/2022 + contaminant from The Global Proteome Machine
Taxonomy	*Drosophila melanogaster*
Enzyme	Trypsin
Maximum number of missed cleavages	2
Minimum/Maximum peptide length	6 /144
Precursor mass tolerance	10 ppm
Fragment mass tolerance	0.02 Da
Decoy database search	Enabled (default)
Static modifications	Carbamidomethyl / +57.021 Da (C)
Variable modifications	Peptides: Oxidation / +15.995 Da (M), Deamidated / +0.984 Da (N, Q). Protein terminus: Acetylation / +42.011 Da (N-Terminus), Met-loss / -131.040 Da (M), Met-loss + Acetylation / -89.030 Da (M).
False discovery rate (FDR)	≤1%

Independent searches were made for each gel piece processed (seven per genotype) and the resulting data was exported into Excel and compiled. Only peptides that had a high protein FDR confidence (FDR ≤ %1) and at least two unique peptides were further analysed as per publication guidelines. Accessions were mapped to FlyBase using the ID Validator tool and consolidated. Gene symbols, names, annotation symbols, gene summaries and FlyBase IDs

were extracted using Batch Download. Where accessions were not matched automatically in ID Validator, these were converted to FlyBase IDs by manually searching NCBI.

Where an ID had matches to both control and HDAC4^{3SA} samples, only those with ≥2-fold higher number of peptide spectrum matches in HDAC4^{3SA} were retained. It is noted that this is very conservative, and that a higher degree of specificity could be conferred by a more stringent parameter; a four-fold cut-off has been used previously (Mukherjee *et al.*, 2014), however two-fold is appropriate here for pathway analysis, and has also been used previously (Gaucherand *et al.*, 2019).

FlyBase IDs were submitted to DAVID (DAVID 2021, knowledgebase v2023q2, (Dennis *et al.*, 2003; Huang *et al.*, 2009; Sherman *et al.*, 2022)) and STRING (database version 12.0, (Szklarczyk *et al.*, 2023)) databases for further analyses using default settings.

3.3. DNA analyses

3.3.1. Isolation of genomic DNA from whole flies

Whole flies (25) were added to a 1.7 mL Eppendorf tube and homogenised in solution A (0.1 M EDTA, 1% SDS, 0.1 M Tris-HCl pH 9.0) over ice. Following incubation for 30 minutes at 70 °C, 35 µL of KAc (8 M) was added and samples were incubated on ice for a further 30 minutes before centrifugation for 15 minutes at 13,000 g. The supernatant was collected and added in equal volume to Phenol-Chloroform (1:1), shaken, and centrifuged for 5 minutes at 13,000 g. This step was repeated, the resulting supernatant collected, 150 µL isopropanol added, and after further centrifugation the pellet was retained, washed in 70% ethanol, vacuum dried, then resuspended in 100 µL of TE (10 mM Tris-HCl, 0.1 mM EDTA pH 8.0).

3.3.2. PCR amplification

Primers were previously designed by Dr Helen Fitzsimons and synthesised by Sigma Aldrich (Appendix 10.3.1, Table 10.2 and Appendix 10.5.2, Table 10.8). PCR was performed using OneTaq 2X master mix (New England Biolabs) as per manufacturer's instructions. Reactions were prepared using 10 µM forward primer, 10 µM reverse primer, 100 ng template DNA, 1X

OneTaq master mix, and nuclease free water to a final volume of 25 µL. Thermocycling conditions were as per Table 3.7.

Table 3.7 Thermocycling conditions

Step	Temperature (°C)	Time
30 cycles:		
Denature	94	30 seconds
Anneal	49-50	15-30 seconds
Extend	68	15-30 seconds
Final extension	68	1.5 minutes (1 min/kb)
Hold	4-10	5 minutes

3.3.3. Agarose gel electrophoresis

PCR products (9 µL in 1 µL of 10X loading buffer, final concentration of 4% (v/v) glycerol, 0.05% (w/v) SDS, 0.1 mM EDTA, 0.025% (w/v) bromophenol blue, 0.025% (w/v) xylene cyanol) were electrophoresed on a 1% agarose (Bio-Rad) gel containing 5% ethidium bromide (cast in an Owl Separation Systems Buffer Puffer gel system) in 1X TAE (Tris-base, acetic acid, 0.5 M EDTA, with 10 µL ethidium bromide added once poured into tank) alongside the 1 Kb Plus DNA Ladder (Invitrogen) for 1 hour and 45 minutes at 100 V. The gel was imaged using the black platform of a Gel Doc XR (Bio-Rad) imaging apparatus.

3.3.4. DNA sequencing

PCR products were purified using the DNA Clean & Concentrator-5 kit (Zymo Research) as per manufacturer's instructions. DNA was eluted in 20 µL TE buffer. DNA concentration was measured using a Denovix DS-11 spectrophotometer. Purified PCR products were submitted for ABI sanger sequencing (BigDye Terminator v3.1) at the Massey University Genome Service. Sequencing results were imported into Geneious R9 (Biomatters), read ends trimmed using default settings and pairwise alignment of sequences performed.

3.4. Immunohistochemistry

3.4.1. *Drosophila* adult brain isolation

For mushroom body analysis, adult flies were anaesthetised with CO_2 and placed on ice prior to dissection. For all other analyses adult flies were pre-fixed in PFAT-DMSO (4% paraformaldehyde, PBS, 0.1% Triton X-100, 5% DMSO) for one hour at room temperature, followed by washing in PBT (10 mM phosphate buffer, pH 7.4 (Sigma Aldrich), 0.5% Triton X-100). Brains were dissected from the head capsule in PBT using Dumont #5 forceps under a stereomicroscope. Brains were incubated with 55% heptane and 1.4% formaldehyde in PBT and the heptane and upper aqueous phases discarded to remove debris, before post-fixing in PFAT-DMSO for 20 minutes at room temperature, and washing and storing in 100% methanol at -20 °C. For immunohistochemistry using the HDAC4::GFP line, which is on the X chromosome, only males were dissected to maximise expression of the GFP-tagged form of HDAC4. For all other analyses, equal numbers of males and females were dissected.

3.4.2. *Drosophila* larval eye disc isolation

Third instar crawling larvae were picked from the sides of vials using a PBS (10 mM phosphate buffer, pH 7.4 (Sigma Aldrich)) soaked paintbrush, and washed in PBS to remove any residual food. Using Dumont #5 forceps, the mouth hooks, eye antennal discs, and brain hemispheres were isolated from larvae as a single unit under a stereomicroscope before fixing in PFAT-DMSO for 20 minutes at room temperature, and washing and storing in 100% methanol at -20 °C.

3.4.3. *Drosophila* adult eye isolation

Adult flies were pre-fixed in PFAT-DMSO for one hour at room temperature, followed by washing in PBT. The retina was dissected from the head and brain in PBT using Dumont #5 forceps under a stereomicroscope. Retina were incubated in 4% formaldehyde in PBT for 30 minutes at room temperature, and stored in 100% methanol at -20 °C.

3.4.4. Immunostaining

Tissues were rehydrated in 50% methanol/PBT before washing in PBT and blocking for three hours at room temperature in immunobuffer (5% normal goat serum in PBT). For retina this incubation was shortened to 90 minutes. Primary antibody (Table 3.8) was diluted in immunobuffer, and tissues incubated overnight at room temperature. Tissues were then washed in PBT and incubated in secondary antibody (Table 3.9) in immunobuffer overnight at 4 °C.

Table 3.8 Primary antibodies used for immunohistochemistry

Antibody	Host	Clonality	Source	Catalogue number	Antibody Registry ID	Dilution
Anti-Armadillo	Mouse	Monoclonal	DSHB*	N2 7A1	AB_528089	1:200
Anti-Bruchpilot	Mouse	Monoclonal	DSHB*	nc82	AB_2314866	1:100
Anti-FasII	Mouse	Monoclonal	DSHB*	1D4	AB_528235	1:20
Anti-GFP	Rabbit	Polyclonal	Abcam	Ab290	AB_303395	1:20,000
Anti-HA	Rat	Monoclonal	Sigma Aldrich	3F10	AB_2687407	1:500
Anti-HA	Rabbit	Monoclonal	Cell Signaling	C29F4	AB_1549585	1:200
Anti-Lamin (Dm0)	Mouse	Monoclonal	DSHB*	ADL67.10	AB_528336	1:200
Anti-MEF2	Rabbit	Polyclonal	NCI†	n/a		1:500
Anti-Myc	Rabbit	Polyclonal	Abcam	Ab9106	AB_307014	1:100
Anti-Myc	Mouse	Monoclonal	DSHB*	9E 10	AB_2266850	1:100
Anti-NinaC	Mouse	Polyclonal	C.M§	Zb551		1:250
Anti-Polychaetoid2	Mouse	Monoclonal	DSHB*	PYD2	AB_2618043	1:50

*Developmental Studies Hybridoma Bank. The following antibodies were obtained from the DSHB, created by the NICHD of the NIH and maintained at The University of Iowa, Department of Biology, Iowa City, IA 52242, USA:
nc82 (anti-Bruchpilot) was deposited to the DSHB by Buchner, E.
1D4 (anti-Fasciclin II) was deposited to the DSHB by Goodman, C
9E 10 (anti-Myc) was deposited to the DSHB by Bishop, J.M.
ADL67.10 (anti-Lamin) was deposited to the DSHB by Fisher, P. A.
N2 7A1 Armadillo was deposited to the DSHB by Wieschaus, E.
†Gift from Bruce Paterson, National Cancer Institute, Bethesda, MD, USA.
§Gift from Craig Montell, University of California, Santa Barbara, CA, USA.

Table 3.9 Secondary antibodies used for immunohistochemistry

Antibody	Host	Source	Catalogue number	Antibody Registry ID	Dilution
Anti-rat Alexa 555	Goat	Invitrogen	A-21434	AB_2535855	1:500
Anti-mouse Alexa 555	Goat	Invitrogen	A-21422	AB_2535844	1:500
Anti-rabbit Alexa 555	Goat	Invitrogen	A-21428	AB_2535849	1:500
Anti-rabbit Alexa 647	Goat	Invitrogen	A-21244	AB_2535812	1:500

Following further washing all tissues were mounted in Antifade (90% glycerol, 0.2% n-propyl gallate, PBT) and secured by a coverslip sealed with nail polish. Brains and retina were mounted on a microscope slide in a well created by two coverslips sealed one centimetre apart by nail polish. Eye discs were dissected from the brain and mouth hooks in PBT, and mounted on a microscope slide. For DAPI staining, tissues were washed in PBT before incubation with DAPI (1:20,000 in PBT), and then washed further and mounted in Antifade.

Brains were positioned anterior-up for all mushroom body analyses, and posterior up for examination of Kenyon cells.

3.4.5. Immunofluorescence

Brains, retina, and eye discs were imaged at the Manawatu Microscopy and Imaging Centre using a Leica TCS SP5 DM6000B Confocal Microscope. Files were imported into ImageJ (Schneider *et al.*, 2012) using the Bio Formats plugin (Linkert *et al.*, 2010). Tissue-specific imaging is described in Appendix 10.1.7.

3.4.6. Quantification of HDAC4 aggregates

HDAC4 aggregates in Kenyon cell nuclei were counted using the Cell Counter plugin in ImageJ. This quantification was of brains for which immunohistochemistry was performed to detect HDAC4-Myc and MEF2 (endogenous). For quantification, the HDAC4 channel was set to green and MEF2 to magenta. The colour balance was kept constant between samples. Aggregates were counted as discrete white puncta on merge images that were also visible on individual HDAC4-Myc and MEF2 channels.

To distinguish between HDAC4-MEF2 co-localising and HDAC4-only aggregates (Figure 5.17), quantification was further optimised as described in Tan *et al.* (2024). For effective visualisation of aggregates, the MEF2 channel was set to grey and HDAC4 to the red/green lookup table. The colour-balance was kept constant between samples. Aggregates of HDAC4-Myc and MEF2 were counted on merged channels as those that co-localised, as well as appeared as distinct aggregates in both HDAC4-Myc and MEF2 channels. Aggregates that only contained HDAC4 were then counted; only HDAC4 aggregates that overlapped with MEF2 staining but did not induce redistribution of MEF2 were counted to reduce inclusion of cytoplasmic aggregates.

In both instances, aggregates in ten serial optical sections at 1 μm increments were counted, beginning at the first emergence of the calyx. Four brains were counted per genotype. To ensure the same aggregate was not counted twice, labels from the previous section were kept for the following section and examined for co-localisation, and each aggregate only counted once. For comparisons of two genotypes, an unpaired t-test was performed. For comparisons of greater than two genotypes, statistical significance was assessed using a one-way ANOVA with post-hoc Tukey's HSD test with significance set at α=0.05.

3.4.7. Quantification of mushroom body development

A scoring system to assess changes in mushroom body morphology was devised and implemented by a blinded scorer, which considered the structure of the α- and β-lobes. Defects in axon elongation, termination and guidance were scored, characterised by thinning or absence of the α- and β-lobes, β-lobe fusion, or altered positioning of lobes (guidance) (Freymuth & Fitzsimons, 2017; Main *et al.*, 2021; Schwartz *et al.*, 2016) (Figure 4.15). β-lobe fusion was scored as mild if axons measuring less than half the width of the lobe crossed the midline of the brain, or as severe if axons measuring more than half the width of the lobe crossed the midline. For analyses in Sections 5.4.3 and 5.5.3, β-lobe fusion was scored as per Tan *et al.* (2024); minor was scored if only a few axons crossed the midline, moderate if this was for axons measuring less than half the lobe width, or severe if this was for axons measuring more than half the lobe width (Figure 5.19). Statistical significance was assessed using the Fisher's exact test.

3.4.8. Quantification of MEF2 intensity

MEF2 intensity was quantified in ImageJ (Schneider *et al.*, 2012). Maximum projection images were generated from serial optical sections through the Kenyon cell layer, and the intensity of the MEF2 signal in these was measured using the Measure function. Statistical significance was assessed using a one-way ANOVA with post-hoc Tukey's HSD test with significance set at α=0.05.

3.5. Evaluation of adult eye morphology

3.5.1. Light microscopy

Light microscopy was performed using an Olympus SZX16 Stereo Zoom microscope and cellSens Dimension (Olympus) imaging software. Flies were frozen at -20 °C before thawing and imaging at 110 x magnification. Constant light intensity and exposure was used. Images were imported into Adobe Photoshop (versions 2021-2024), Z-axis drift accounted for using the Auto-Align Layers function, and optical sections stacked using the Auto-Blend Layers function. A scoring system was developed to assess severity of defects in morphology (Table 3.10) and was implemented by a blinded scorer. Scores for each phenotype were summed, giving a maximum score of 12 per eye, which was then converted to % severity.

Table 3.10 Semi-quantitative scoring system for the evaluation of rough eye phenotypes

		Phenotype description		
Key word	**Score**	**Bristles**	**Ommatidia**	**Pigmentation**
None	**0**	All bristles present and correctly placed	Ommatidia correctly aligned and no fusion	No changes in pigmentation
Mild	**1**	Most correct, a few missing or extra	Alignment of ommatidia altered but no fusion	Occasional entire ommatidium missing pigment
Moderate	**2**	Presence of bristles but not necessarily the right amount or in the right places. Large loss of bristles at edges of the eye.	Ommatidia alignment perturbed, altered depth of ommatidia boundary but no fusion	Many ommatidia with only pigment at the boundary
Major	**3**	Presence of bristles but very few (stubby)	Ommatidia alignment perturbed and fusion	Only pigmentation around the edge of the eye
Severe	**4**	Complete absence of bristles	Complete absence of ommatidia (total fusion)	Little to no pigmentation

This scoring system considered three facets of eye development: bristles, ommatidia and pigmentation, each being scored from 0-4, giving a total score range from 0-12.

As the final score is represented as % severity, the data was arcsine transformed and statistical significance was assessed by one-way ANOVA with post-hoc Tukey's HSD test with significance set at α=0.05. If the data did not satisfy the assumptions of the ANOVA test (i.e. the data was not normally distributed or with equal variance) the Kruskal-Wallis test was performed on non-transformed data with significance set at α=0.05. Multiple comparisons were determined using the Dunn's post-hoc test with a Bonferroni-corrected α.

3.5.2. Scanning electron microscopy

Prior to fixation, adult flies were incubated overnight on a damp paper towel, and their natural grooming behaviours (Zhang *et al.*, 2020) cleaned the eyes of any food debris. The following day, adults were anaesthetised using FlyNap (Carolina Biologicals) and immersed in primary modified Karnovsky's fixative (3% glutaraldehyde, 2% formaldehyde, 0.1 M sodium phosphate buffer) with Triton X-100 before vacuum infiltration and washing with 0.1 M sodium phosphate buffer. After subjection to a graded ethanol series (25%, 50%, 75%, 95%, 100%, 15

minutes each) with a final one-hour incubation in 100% ethanol, flies were critical point dried (Polaron E3000 series II drying apparatus), heads were separated from bodies and mounted onto aluminium stubs, and sputter coated with gold (Bal-Tec SCD 050 sputter coater). Images were obtained using an FEI Quanta 200 environmental scanning electron microscope (20.00 kV, spot 4.0 nm). Scanning electron microscopy was performed at the Manawatu Microscopy and Imaging Centre, and vacuum filtration through to critical point drying was performed by Raoul Solomon (MMIC).

Chapter Four

Characterisation of HDAC4 oligomerisation, aggregation, and its effects on neurodevelopment

4. Characterisation of the role of HDAC4 oligomerisation in HDAC4 aggregation and its effects on neuronal development in *Drosophila*

Increased nuclear abundance of HDAC4 is commonly observed in both neurodevelopmental and neurodegenerative diseases (Section 1.6.2). Small nuclear aggregates of HDAC4 have been observed in the brains of patients with Alzheimer's (Shen *et al.*, 2016) and neuronal intranuclear inclusion diseases (Takahashi-Fujigasaki *et al.*, 2006), however, it is unclear whether accumulation of nuclear HDAC4 and/or HDAC4 aggregates are pathogenic. While these diseases are neurodegenerative, HDAC4 has also been implicated in neurodevelopmental disease, including 2q37 deletion syndrome, in which the *HDAC4* locus is deleted (Sando *et al.*, 2012; Williams *et al.*, 2010). Moreover, HDAC4 mutations that are predicted to result in nuclear retention also result in neurodevelopmental deficits (Wakeling *et al.*, 2021). HDAC4 has also been demonstrated to be essential for normal rodent brain development (Majdzadeh *et al.*, 2008; Vega *et al.*, 2004).

To begin to understand the specific roles of HDAC4 in neuronal development and function, a *Drosophila* model was characterised (Fitzsimons *et al.*, 2013). Both increased and reduced expression of HDAC4 impaired long-term memory (Fitzsimons *et al.*, 2013) and development of the mushroom body (Main *et al.*, 2021; Tan *et al.*, 2024), and these impairments had a strong correlation with nuclear localisation of HDAC4. It is therefore evident that careful regulation of HDAC4 distribution is essential to correct neuronal function, however the role that HDAC4 aggregates specifically play in these effects, and the mechanisms through which they form remain unclear.

This chapter examines the mechanisms through which HDAC4 aggregates form. This includes establishing effective experimental conditions and methods for reliable quantification of nuclear aggregation of HDAC4, and the severity of HDAC4-overexpression induced defects in the development of the mushroom body and eye (the development of these tissues is discussed in Section 1.3). Transgenic flies harbouring HDAC4 with mutations hypothesised to disrupt or stabilise tetramerisation were generated and assessed for their ability to oligomerise, aggregate, and induce neurodevelopmental phenotypes in *Drosophila*. These data establish that oligomerisation of HDAC4 promotes its nuclear aggregation, and that HDAC4 aggregation positively correlates with impaired neurodevelopment.

4.1. Characterisation of the expression patterns and levels of neuronal GAL4 drivers

It is important to be able to precisely control the level of transgene expression when conducting experiments involving overexpression. In the UAS-GAL4 system (Section 1.2.3), the level of transgene expression is dependent on protein levels of the transcriptional activator GAL4, and this is facilitated largely by the regulatory elements upstream of GAL4, which determine spatial expression. To aid in effective selection of drivers for each experiment performed herein, the expression patterns and levels of two drivers commonly used to promote transgene expression in the brain were characterised. *elav-GAL4* is derived from the promoter of *embryonic lethal abnormal vision* (*elav*), which facilitates transgene expression in all postmitotic neuronal cells including Kenyon cells (Robinow & White, 1988), while for the *OK107-GAL4* driver, *GAL4* expression is controlled by an enhancer of the *eyeless* gene, and predominantly mediates strong expression in Kenyon cells (Connolly *et al.*, 1996). Each driver was crossed to UAS-mCD8::GFP, a membrane-targeted GFP marker (Lee & Luo, 1999) that allows for easy visualisation of axonal and dendritic processes as well as cell bodies, and the expression pattern examined in the adult brain (Figure 4.1).

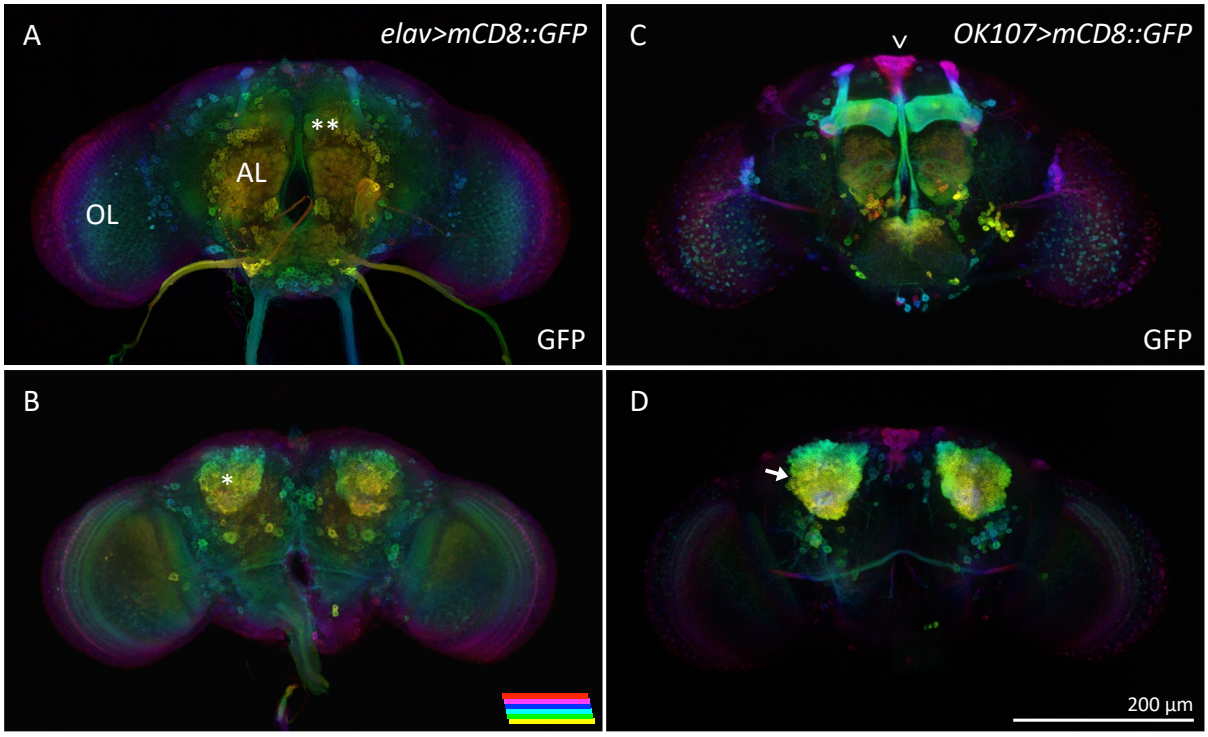

Figure 4.1 *elav-GAL4* and *OK107-GAL4* mediate different expression patterns of mCD8::GFP in the adult brain
Maximum projections through the anterior (A, C) and posterior (B, D) of the brain expressing mCD8::GFP under the control of *elav-GAL4* (A-B) or *OK107-GAL4* (C-D). Flies were raised at 25 °C.

AL, antennal lobe; OL, optic lobe; ** γ-lobe of the mushroom body; * calyx; arrowhead, insulin producing cells; arrow, Kenyon cell bodies. The applied colour illustrates the depth through the brain as per the bar in (B); magenta is deeper and yellow is shallower. *This figure is an adaptation from that found in Hawley et al. (2023) (doi: 10.17912/micropub.biology.000885), which is distributed under CC BY 4.0.*

elav-GAL4 mediated widespread expression of mCD8::GFP in the anterior (Figure 4.1A) and posterior (Figure 4.1B) of the brain, including in the antennal and optic lobes, as well as in the mushroom body as previously described (Armstrong *et al.*, 2011). In contrast, *OK107-GAL4*-mediated expression was much restricted, localising largely to the mushroom body, as observed in the lobes (Figure 4.1C), the Kenyon cell bodies (Figure 4.1D), and within the optic lobes, which is consistent with previous observations (Aso *et al.*, 2009). Strong expression was also observed in the insulin producing cells. To examine relative levels of expression mediated by both drivers in Kenyon cells, the intensity of mCD8::GFP expression in each of the lobes of the mushroom body was quantified (Figure 4.2). The neural cell adhesion molecule fasciclin II (FasII) is expressed strongly in the α- and β-lobes, and weakly in the γ-lobes of the mushroom body (Crittenden *et al.* (1998), Figure 4.2A) and is thus an ideal marker to outline the lobes and to use as a calibration control to account for any variability in staining. The FasII signal was used to trace each of the lobes in a single optical section. The expression of GAL4 did not affect FasII intensity, which was consistent across all lobes of all genotypes, confirming its suitability as a marker to normalise mCD8::GFP intensity. *OK107-GAL4* drove between 2.6- and 3.9-fold higher expression of mCD8::GFP in all lobes compared to *elav-GAL4* (Figure 4.2B).

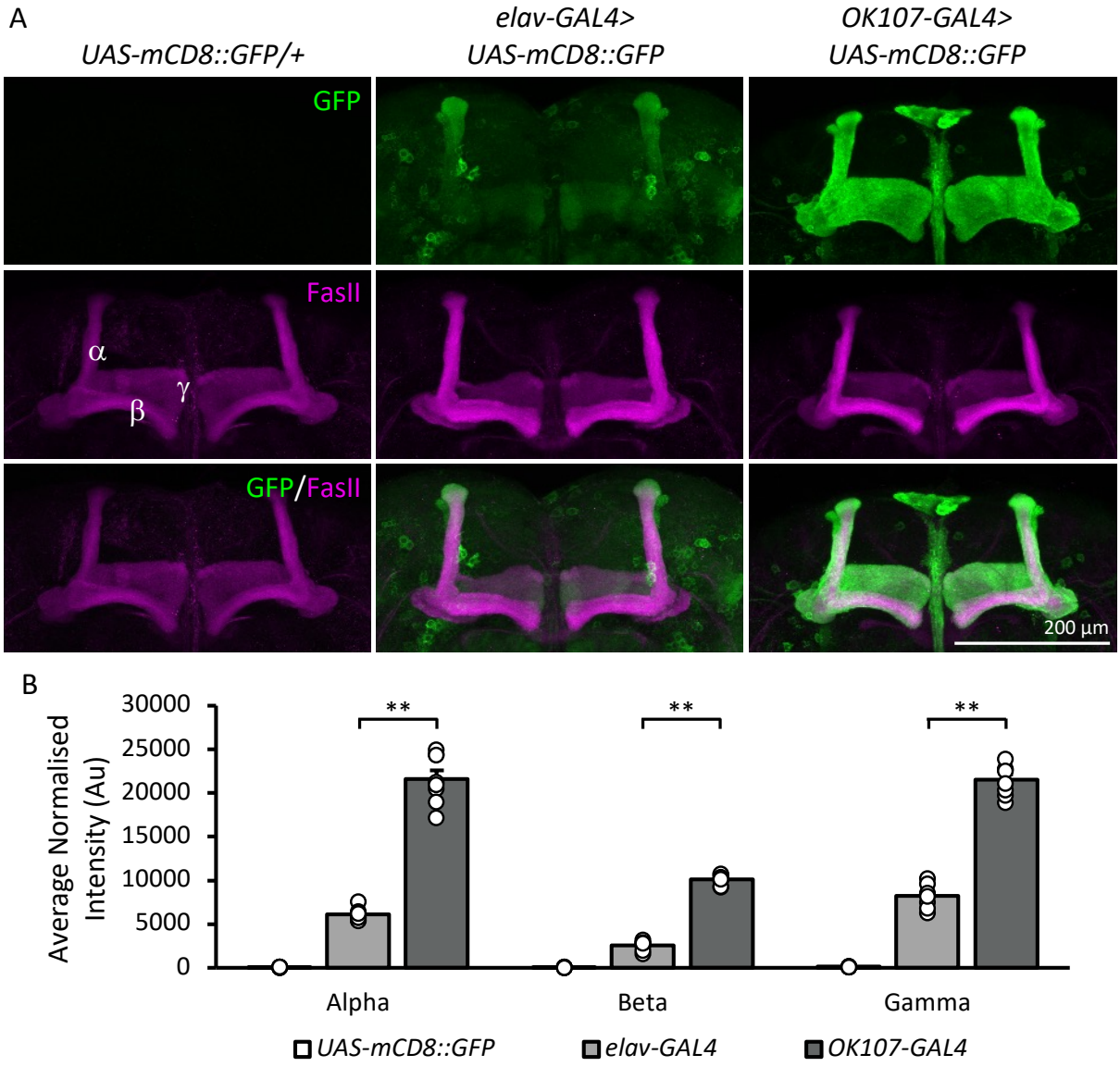

Figure 4.2 *OK107-GAL4* drives higher expression of mCD8::GFP in the lobes of the mushroom body than *elav-GAL4*

(A) Maximum projections through the anterior of the brain of flies expressing mCD8::GFP (green) under the control of *elav-GAL4* and *OK107-GAL4*. Flies were raised at 25 °C. Adult brains were counterstained with anti-FasII (magenta) to label the alpha (α), beta (β), and gamma lobes (γ). (B) Quantification of mCD8::GFP intensity in the lobes of the mushroom body. Lobes (α, β and γ) were traced on a single optical section (FasII channel), then the intensity of mCD8::GFP was measured and normalised to the FasII intensity. The mCD8::GFP signal outside of the α, β, and γ lobe outlines provided by FasII counterstaining was not recorded. *OK107-GAL4>mCD8::GFP* intensity was significantly increased compared to *elav-GAL4>mCD8::GFP* in each of the α, β, and γ lobes (ANOVA, α $F_{(3,28)}$=128, p<0.001; β $F_{(3,28)}$=251, p<0.001; γ $F_{(3,28)}$=182, p<0.001; post-hoc Tukey's HSD, **p<0.01). Mean ±SEM is shown, n=8 lobes/genotype. *This figure is an adaptation from that found in Hawley et al. (2023) (doi: 10.17912/micropub.biology.000885), which is distributed under CC BY 4.0.*

These data provide a valuable resource for understanding the relative distribution pattern of each of the *OK107-GAL4* and *elav-GAL4* drivers, as well as the level of expression each mediates in Kenyon cells, allowing for an informed choice as to which driver is most appropriate to answer each biological question. Figure 4.3 summarises icons that are included in the figures herein to quickly orient the reader to the driver used in each experiment. While not discussed above, this includes the eye-specific driver *GMR-GAL4* (derived from the promoter of the *glass multimer reporter*), the expression of which begins posterior to the morphogenetic furrow in the larval eye disc and continues throughout the eye in adulthood (Figure 4.3 C (Escobedo *et al.*, 2021; Freeman, 1996)). Schematics are also used to indicate the conditions under which flies were raised (Figure 4.3D, E). While the TARGET system is primarily used to facilitate temporal control of transgene expression (McGuire *et al.*, 2004), it is often used to tailor the level of transgene expression. The presence of GAL80ts allows for linear increases in transgene expression in a temperature sensitive manner (Hawley *et al.*, 2023; Schwartz *et al.*, 2016). The icons depicted in Figure 4.3E will be used to indicate if GAL80ts is present, and the relative level of GAL4 activity based on the temperature at which flies were raised. Representative crossing schemes are also included in the methods, (Section 3.1.3) and correspond to each of the distributions described here.

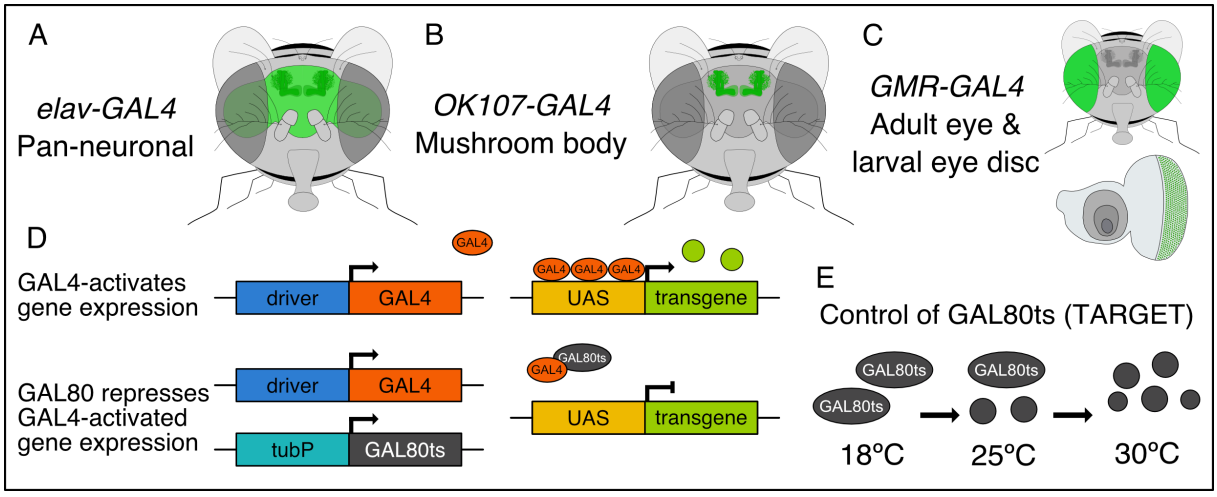

Figure 4.3 Schematic diagrams used in this thesis to convey driver selection and conditions under which flies were raised

(A-C) Schematic diagram representing the distribution of transgene expression mediated by each driver in the adult fly and larval eye disc. Transgene expression is represented in green. *elav-GAL4*-mediated expression is seen in the whole brain (pan-neuronal), (A) while *OK107-GAL4*-mediated expression is predominantly observed in the mushroom body (B). *GMR-GAL4* mediates expression in the adult eye and third instar larval eye disc. (D-E) Modulation of GAL4 activity via the TARGET system. (D) In the UAS-GAL4 system, GAL4 expression is spatiotemporally controlled by the regulatory regions upstream (driver). Transgene expression is mediated by GAL4 binding to the upstream activating region (*UAS*), initiating transcription in the same pattern in which GAL4 is expressed. GAL80 is a repressor of GAL4,

and GAL80ts is a temperature sensitive mutant of GAL80. Expression of GAL80ts under the control of the tubP (tubulin promoter) regulatory elements results in ubiquitous expression of GAL80ts and repression of GAL4 and subsequent transgene expression. (E) GAL80ts stability is modulated by temperature; increasing temperature correlates with increasing degradation of GAL80ts and de-repression of GAL4-dependent transcription. *This figure is an adaptation from that found in Hawley et al. (2023) (doi: 10.17912/micropub.biology.000885), which is distributed under CC BY 4.0.*

4.2. Overexpression of HDAC4 induces nuclear aggregation in Kenyon cells

Previous studies in *Drosophila* demonstrated that overexpression of HDAC4 in Kenyon cells induces nuclear accumulation and aggregation, resulting in sequestration of the transcription factor MEF2 (Fitzsimons *et al.*, 2013; Main *et al.*, 2021; Tan *et al.*, 2024). Each of these studies were performed in the presence of endogenous HDAC4, which is expected to co-aggregate via oligomerisation with overexpressed HDAC4. This could have implications for deciphering the role of oligomerisation in aggregation of HDAC4, therefore the effect of $HDAC4^{WT}$ overexpression on the distribution and aggregation of endogenous HDAC4 was first characterised.

Since there is no antibody currently available that detects HDAC4 in *Drosophila* tissue, endogenous HDAC4 was visualised via the *HDAC4::GFP* protein trap fly line. This line harbours a GFP-tag within the endogenous HDAC4 gene, which was generated by incorporation of an artificial exon containing the *EGFP* open reading frame flanked by splice donor and acceptor sites within the second intron of *HDAC4,* resulting in an internal fusion of GFP (Buszczak *et al.*, 2007) (Appendix 10.2.1). HDAC4::GFP expression (green) was observed widely throughout the brain (Figure 4.4). In the anterior of the brain (Figure 4.4A), HDAC4::GFP localised strongly to the antennal lobes as well as the lobes of the mushroom body (Figure 4.4B); localisation was observed in each of the α, α', β and β' lobes, and was most notable in the γ lobe (Figure 4.4D-E). In the posterior of the brain (Figure 4.4G), HDAC4::GFP was observed in the Kenyon cell bodies (Figure 4.4H) in a predominantly cytoplasmic punctate pattern, but also appeared to localise to nuclei in a subset of cells (Figure 4.4I-J). The distribution of HDAC4::GFP across the brain is consistent with that previously observed by Fitzsimons *et al.* (2013) using HDAC4 enhancer trap lines to drive expression of fluorescent proteins. The subcellular distribution of HDAC4::GFP is also similar to that seen in several areas of the mammalian brain where HDAC4 is detected in the cell bodies, axons, and dendrites, but only in subsets of nuclei (Bolger & Yao, 2005; Darcy *et al.*, 2010).

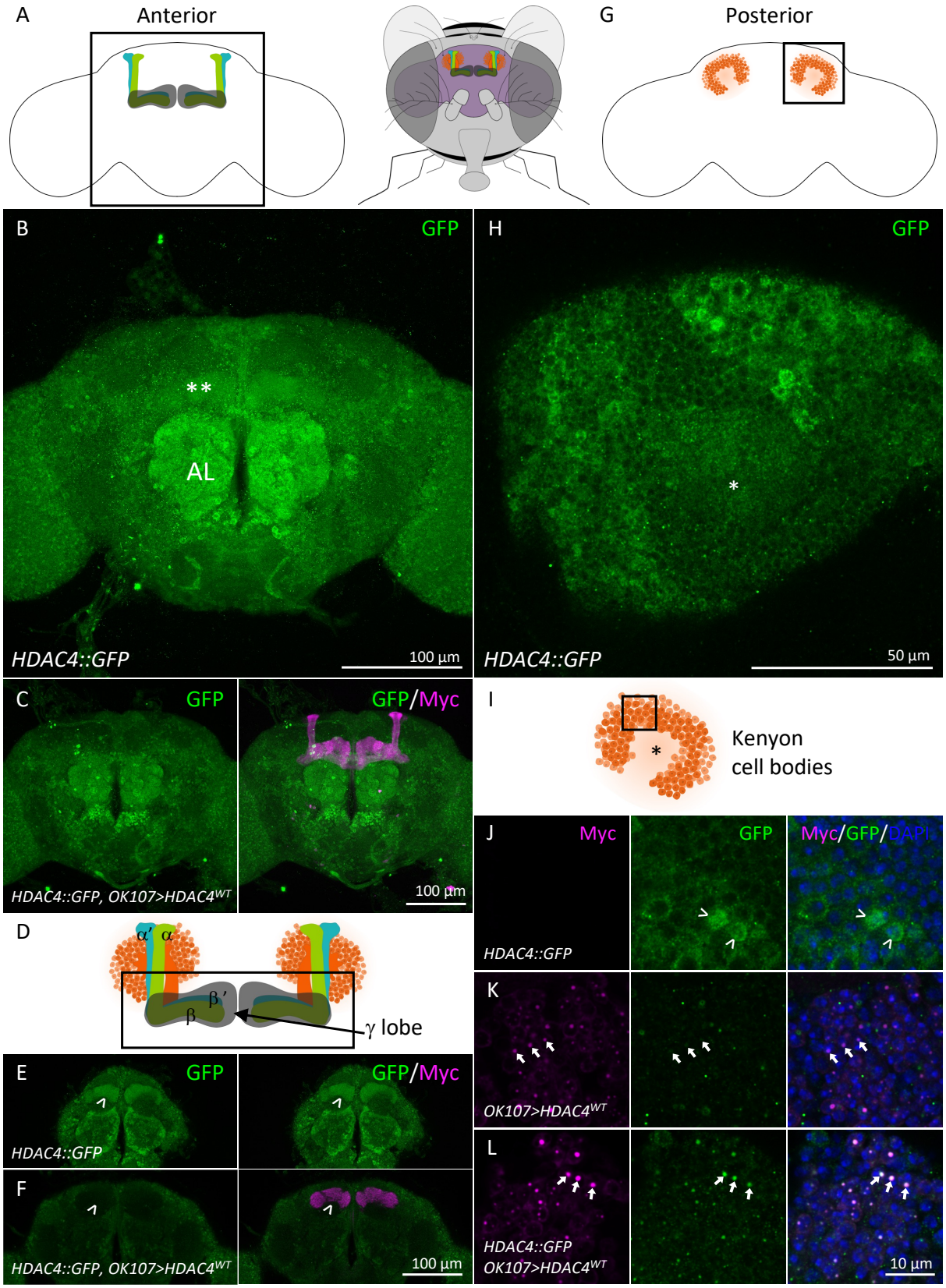

Figure 4.4 Overexpression of HDAC4 results in the redistribution and co-aggregation of endogenous HDAC4 with transgene HDAC4 in neuronal nuclei

HDAC4::GFP distribution was altered by co-expression of HDAC4^{WT}-Myc. (A) Schematic diagram illustrating the location of the mushroom body lobes as observed by imaging the anterior of the adult *Drosophila* brain. The boxed region is depicted in (B-C) which are maximum projections of the anterior

of brains expressing HDAC4::GFP (green) in its endogenous expression pattern (B), which was altered by co-expression of HDAC4^{WT} (magenta) under the control of *OK107-GAL4* (C). AL, antennal lobe; **, γ-lobe of the mushroom body. (D) Schematic diagram of the mushroom body showing Kenyon cells (orange) in the posterior, the axons of which bundle in the pedunculus and project anteriorly to form the α/β (green), α'/β' (teal) and γ (grey) lobes of the mushroom body. (E-F) Single optical sections (0.5 µm) as per the boxed area in (D) demonstrate the distribution of HDAC4::GFP within the γ-lobe (arrowhead, E) which was lost upon co-expression of HDAC4^{WT} (F). (G) Schematic diagram illustrating the location of the Kenyon cell bodies as observed by imaging the posterior of the adult *Drosophila* brain. The boxed region is depicted in (H), which is a single optical section (0.5 µm) through the Kenyon cell layer in the posterior of the brain. HDAC4::GFP was observed in the nucleus and cytoplasm of the Kenyon cells with distribution varying between cells, as well as in the dendritic field (calyx, *). (I) Schematic diagram of the Kenyon cell layer depicting localisation of the Kenyon cell bodies surrounding the calyx (*). The boxed region is depicted in (J-L), which are magnified single optical sections (0.5 µm) of the Kenyon cell layer above the calyx. DAPI (blue) highlights nuclei. (J) HDAC4::GFP (green) localised to the nucleus and cytoplasm of Kenyon cells, with punctate staining observed in some cells (arrowhead). (K) HDAC4^{WT} (magenta) expressed under the control of *OK107-GAL4* formed aggregates in nuclei in the absence of HDAC4::GFP (arrow). (L) HDAC4^{WT} aggregates sequestered HDAC4::GFP (arrow). All flies were raised at 25 °C. *This figure is an adaptation from that found in Tan et al. (2024) (doi: 10.1186/s12915-023-01800-1), which is distributed under CC BY 4.0.*

The UAS-GAL4 system (Section 1.2.3) was used to facilitate expression of the *HDAC4^{WT}-Myc* transgene under the control of the *OK107-GAL4* driver in the mushroom body. This experiment was performed to test the hypothesis that HDAC4^{WT}-Myc and HDAC4::GFP interact, owing to HDAC4's ability to homo-oligomerise. HDAC4^{WT}-Myc localised strongly to the lobes of the mushroom body in the anterior of the brain as expected (Figure 4.4C), as well as to the Kenyon cells in the posterior, forming large nuclear aggregates (Figure 4.4K). Overexpression of HDAC4 resulted in a significant depletion of endogenous HDAC4::GFP from the γ-lobes (Figure 4.4F) and sequestration into aggregates in Kenyon cell nuclei (Figure 4.4L). It is noted that the HDAC4^{WT} transgene contains a 6x Myc tag that significantly amplifies antibody detection compared to the single internal GFP tag within HDAC4::GFP, which is likely to account for the comparatively brighter signal observed, especially in the mushroom body lobes.

These data demonstrate that endogenous HDAC4(::GFP) co-aggregates with overexpressed transgenic HDAC4, highlighting that endogenous HDAC4 and its ability to oligomerise with transgene (either wild-type or mutant) HDAC4 must be kept in mind when interpreting studies involving overexpression, and particularly in the assessment of the role of oligomerisation in HDAC4 nuclear aggregation, which is the focus of this chapter. Given the shift in distribution of HDAC4::GFP from the mushroom body lobes to the Kenyon cell nuclei that was observed when the total amount of HDAC4 was increased (i.e. upon expression of HDAC4^{WT}-Myc), these data also suggest that HDAC4 may undergo dose-dependent regulation of subcellular distribution, whereby increased levels of HDAC4 results in increased nuclear accumulation.

4.3. Development and validation of HDAC4 oligomerisation mutants

The N-terminus of human HDAC4 (hHDAC4) tetramerises in solution through the formation of a small hydrophobic core (Section 1.8). Guo *et al.* (2007) performed mutagenesis studies to delineate key residues involved in core formation; a destabilised mutant was developed that abolished tetramerisation in solution, while conversely a superstable mutant was created that stabilised tetrameric species (Figure 1.13). It was also noted that polar interaction networks form between each of the helices, mediated predominantly by glutamine residues, and these are thought to contribute to tetramer stability. It was hypothesised that the findings of Guo *et al.* (2007) constitute the mechanism of transient tetramerisation of full-length HDAC4 *in vivo*.

To determine whether tetramerisation of HDAC4 contributes to aggregation *in vivo*, mutant *Drosophila* HDAC4 constructs targeting the hydrophobic core and glutamine residues were developed and transgenic flies were generated (Section 3.1.1). These constructs are broadly described as HDAC4^{mutant}, while wild-type HDAC4 is referred to as HDAC4^{WT}. Expression of each of these was validated, followed by the assessment of HDAC4 protein levels and oligomerisation status. Studies assessed oligomer and aggregate formation, which may represent dimers, trimers, tetramers, or higher order oligomers of HDAC4. For this reason the terms oligomers and oligomerisation are used broadly to encompass the effects of these mutations, and the terms tetramers/tetramerisation will be reserved for specific cases where this has been empirically determined.

4.3.1. Design of HDAC4 oligomerisation mutants

Protein sequence alignment of human and *Drosophila* HDAC4 (DmHDAC4) shows relatively high conservation with 35% identity and 59% similarity across the whole protein (Fitzsimons *et al.*, 2013). A local alignment of hHDAC4 and DmHDAC4 is provided in Appendix 10.2.2, with annotations of key residues within hHDAC4 important for function, and these are conserved with DmHDAC4. Indeed within the N-terminus of HDAC4, residues important in formation of the hydrophobic core and stabilising polar interaction networks that mediate tetramerisation are also conserved among species (Guo *et al.*, 2007), including in *Drosophila* (Figure 4.5) suggesting that they are critical to function.

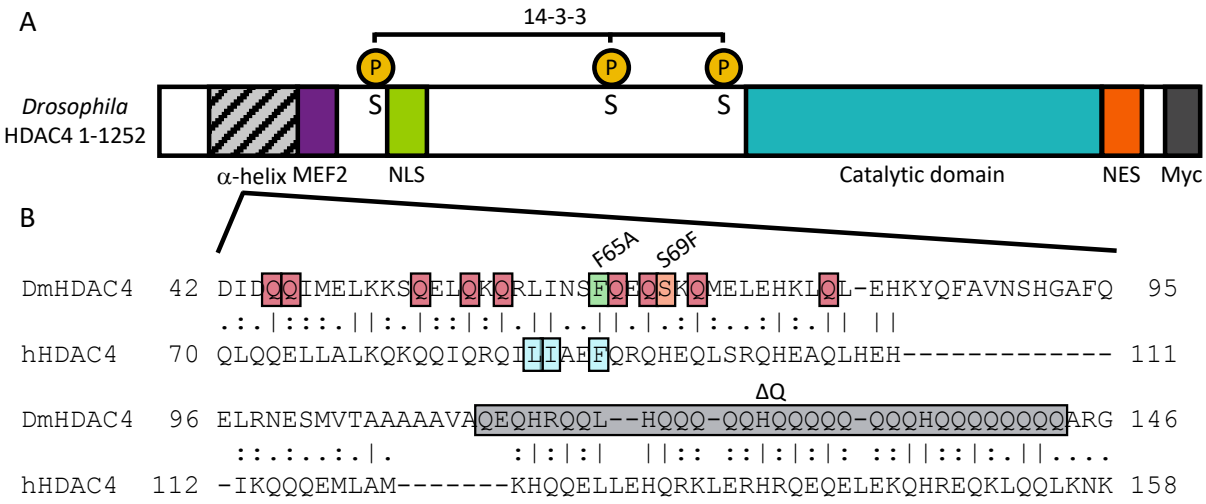

Figure 4.5 Sequence alignment and schematic diagram of HDAC4 tetramerisation mutants

(A) Schematic diagram of the domain structure of DmHDAC4. (B) EMBOSS Water alignment of the glutamine-rich N-terminus of human HDAC4 (hHDAC4, GenBank accession NP_006028), and *Drosophila* HDAC4 (DmHDAC4, GenBank accession NP_572868) demonstrates high conservation of the N-terminus. The hydrophobic core of hHDAC4 (L89, I90, F93) is indicated by blue boxes. *Drosophila* tetramerisation mutation sites are indicated by coloured boxes: 9QA, red; F65A, green; S69F, orange; 9QAΔQ, red and grey. *This figure is an adaptation from that found in Tan et al. (2024) (doi: 10.1186/s12915-023-01800-1), which is distributed under CC BY 4.0.*

To examine whether the mechanism of tetramerisation of *Drosophila* HDAC4 may be similar to that of human HDAC4, the AlphaFold (Jumper *et al.*, 2021; Varadi *et al.*, 2021) predicted structure of the N-terminus of *Drosophila* HDAC4 was aligned to the crystal structure of the human HDAC4 tetramer (Guo *et al.*, 2007) (Methods 3.2.1). Residues 62-129 of human and 37-101 of *Drosophila* HDAC4 are shown in Figure 4.6; both N-terminal regions form an α-helix and assemble into the four-helix bundle similarly (Figure 4.6A-B). The hydrophobic core appears to be conformationally conserved (Figure 4.6C), as does the position of the side chains of most of the glutamine residues identified in the sequence alignment (Figure 4.6A-B) suggesting that the mechanism of tetramerisation of *Drosophila* and human HDAC4 may be conserved.

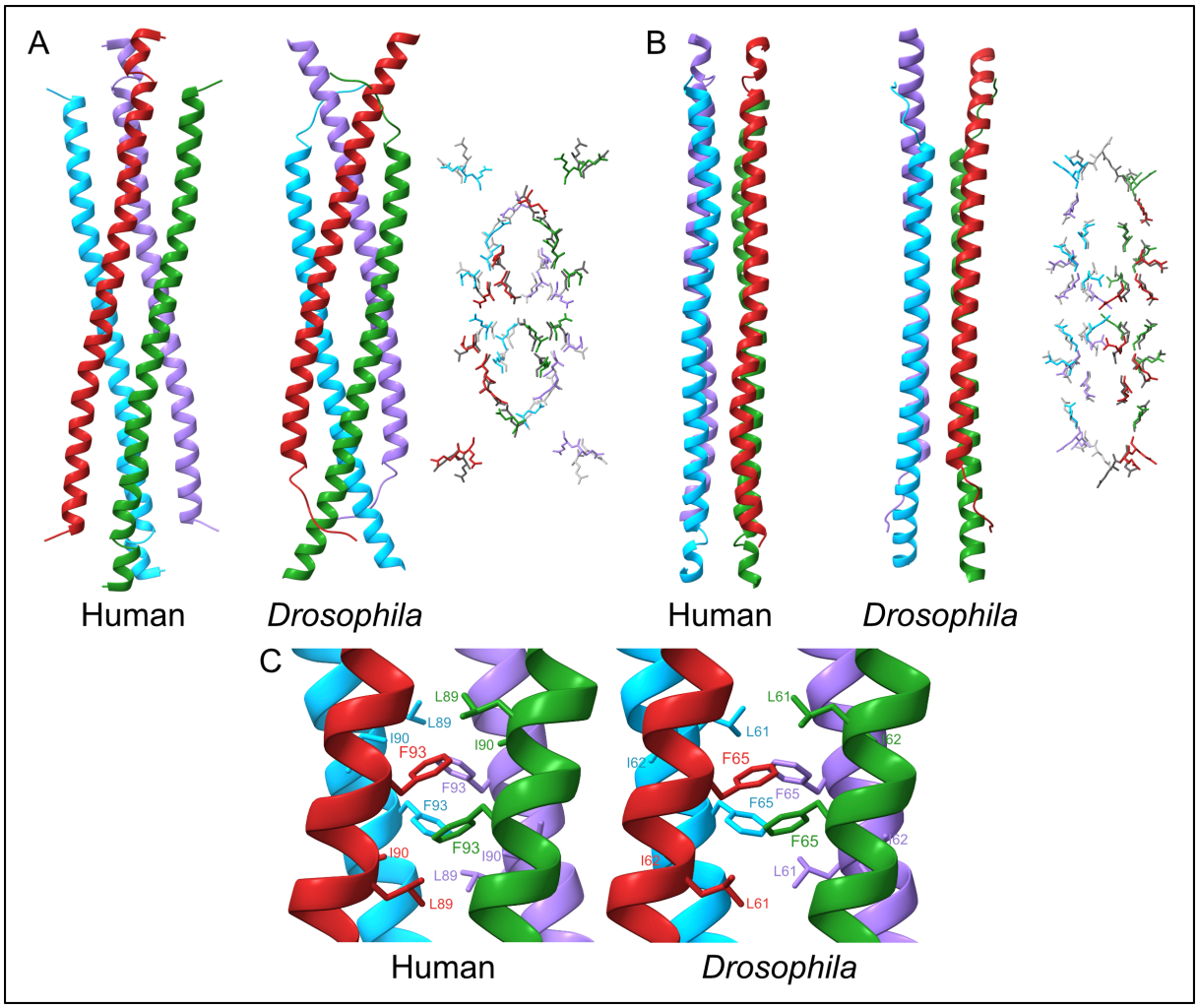

Figure 4.6 Comparison of the AlphaFold predicted *Drosophila* HDAC4 N-terminal structure when modelled as a tetramer with the human HDAC4 crystal structure
The AlphaFold predicted structure of the N-terminus of *Drosophila* HDAC4 was aligned to the structure of the N-terminal four helix bundle of human HDAC4 as presented by Guo *et al.* (2007) (Methods 3.2.1). Orientations in (A-B) show residues 62-129 of human and 37-101 of *Drosophila* HDAC4, and demonstrate that the *Drosophila* HDAC4 model tetramer forms similarly to that of human HDAC4. The right-hand side of (A) and (B) shows an overlay of the position of the side chains (stick representation) of the nine glutamine residues conserved between hHDAC4 (grey) and DmHDAC4 (coloured), which appear to be largely conserved. (C) The hydrophobic core of *Drosophila* HDAC4 also appears to be structurally conserved. Key residues in core formation are labelled. The orientations of the helices and hydrophobic core are presented with the same alignment to the images presented by Guo *et al.* (2007), and permission for the reproduction of these was sought as per Figure 1.13

The small hydrophobic core at the centre of the hHDAC4 tetramer consists of three nonpolar residues: Leu-89, Ile-90, and Phe-93, all of which are conserved in *Drosophila* (Figure 4.5B, Figure 4.6C). Substitution of hHDAC4 Phe-93 for a polar amino acid previously abolished tetramerisation in solution (Guo *et al.*, 2007). It is therefore hypothesised that substituting Phe-65 in DmHDAC4 (HDAC4^{F65A}) will reduce aggregation if aggregation is dependent on tetramerisation of HDAC4 via an equivalent hydrophobic core region. The N-terminus of both

hHDAC4 and DmHDAC4 are glutamine rich; glutamine residues mediate 28 intrahelical and 12 interhelical hydrogen bonds within the hHDAC4 tetramer (Guo *et al.*, 2007). This includes nine glutamine residues that are conserved in DmHDAC4 (Figure 4.5B, 4.6A-B), and it is hypothesised that substitution of these for alanine ($HDAC4^{9QA}$) will decrease tetramerisation, similarly to the F65A mutation. DmHDAC4 harbours an extended polyglutamine stretch that is not present in hHDAC4 (Figure 4.5B). Given the role that polyglutamine regions have in protein aggregation (Michalik & Van Broeckhoven, 2003), deletion of this (ΔQ) was combined with the 9QA mutations ($HDAC4^{9QAΔQ}$) to determine the contribution of this region to HDAC4 aggregation. Guo *et al.* (2007) also developed a superstable tetramer mutant by the substitution of hHDAC4 His-97 for Phe, extending the central hydrophobic core without causing significant structural changes to the HDAC4 tetramer (Section 1.8). It is hypothesised that substitution of Ser-69 in DmHDAC4 for Phe ($HDAC4^{S69F}$) will similarly extend the hydrophobic core and stabilise tetramerisation, and thus will increase aggregation. The mutants that are characterised in this chapter are summarised in Table 4.1.

Table 4.1. DmHDAC4 mutants characterised in this chapter

Name	Predicted consequence of mutation
$HDAC4^{WT}$	-
$HDAC4^{9QA}$	Disrupts polar interaction networks important in tetramerisation
$HDAC4^{9QAΔQ}$	Disrupts polar interaction networks important in tetramerisation and prevents aggregation mediated by the polyglutamine stretch
$HDAC4^{F65A}$	Disrupts the hydrophobic core required for tetramerisation
$HDAC4^{S69F}$	Stabilises the hydrophobic core required for tetramerisation
$HDAC4^{9QA\text{-}F65A}$	Double mutant of $HDAC4^{9QA}$ and $HDAC4^{F65A}$

Transgenic flies harbouring each of these constructs were generated and each are expressed in *Drosophila* under the control of GAL4.

4.3.2. Expression of HDAC4 oligomerisation mutants in *Drosophila*

Transgenic flies harbouring the Myc epitope tagged $HDAC4^{mutant}$ constructs under UAS-control were generated (Section 3.1.1). The UAS-GAL4 system (Section 1.2.3) was used to govern pan-neuronal expression of HDAC4 oligomerisation mutants via the *elav-GAL4* driver, whereby males harbouring the Myc-tagged *HDAC4* constructs were crossed to virgin female

flies carrying *elav-GAL4* to yield progeny expressing *HDAC4* in the brain (Figure 3.1A). Western blotting was performed on whole cell lysates generated from heads of the progeny which confirmed expression of each HDAC4 mutant (Figure 4.7A). Blotting using antibodies against the Myc tag demonstrated that both HDAC4^{WT} and HDAC4^{mutant} are expressed and present at the expected size of 144 kDa with the exception of HDAC4$^{9QA\Delta Q}$, which migrated slightly faster due to the deletion of 32 amino acids. No bands of similar size were detected in the negative control of lysates generated from the progeny of *elav-GAL4* females crossed to males of the same genetic background as the *HDAC4* constructs. Band intensity of HDAC4^{9QA} and HDAC4$^{9QA\Delta Q}$ mutants was consistently lower than HDAC4^{WT}, and quantification demonstrated that each were reduced by approximately half in comparison to HDAC4^{WT}, while HDAC4^{F65A} and HDAC4^{S69F} were not significantly different to HDAC4^{WT} (Figure 4.7B). The slight increase and decrease noted for HDAC4^{F65A} and HDAC4^{S69F} respectively is likely due to changes in subcellular distribution (Further investigated in Chapter 5) coupled with inefficient nuclear lysis. Immunohistochemistry was also performed on whole brains dissected from progeny of the same crosses, and revealed that the intensity of HDAC4^{9QA} and HDAC4$^{9QA\Delta Q}$ in the mushroom body of the adult brain was also markedly reduced compared to HDAC4^{WT} (Appendix 10.2.4). These data confirm the expression of each of the HDAC4^{mutant} constructs. The reduced level of protein in 9QA and 9QAΔQ containing mutants of HDAC4 has important ramifications for interpretation of dose-dependent phenotypes, which is discussed in Section 4.7.2.

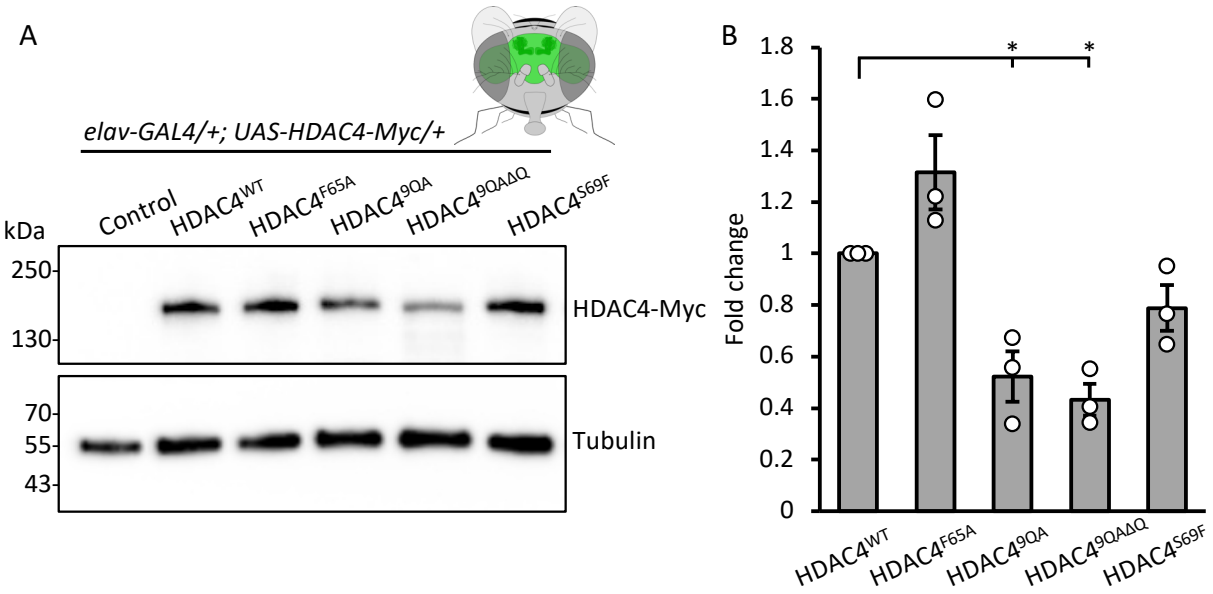

Figure 4.7 HDAC4 oligomerisation mutants are altered in protein levels compared to wild-type HDAC4 in *Drosophila*

(A) Western blot of *elav-GAL4*-driven expression of HDAC4^{WT} and HDAC4^{mutant} in head whole-cell lysates (30 µg) using anti-Myc and anti-alpha-tubulin antibodies. Flies were raised at 25 °C. Control is *elav-GAL4/+*. The protein bands were of the expected size of ~144 kDa, with the exception of HDAC4$^{9QA\Delta Q}$, which has an expected size of ~140 kDa. (B) Quantification of HDAC4 band intensity. HDAC4-Myc intensity was measured and normalised to tubulin (n=3 blots). The average fold change relative to HDAC4^{WT} is plotted, with individual data points represented as circles. Error bars indicate the SEM. HDAC4^{9QA} and HDAC4$^{9QA\Delta Q}$ were significantly reduced compared to HDAC4^{WT} (one sample t-test compared to HDAC4^{WT}: HDAC4^{F65A} $t_{(2)}$=2.2021, p=0.1586; HDAC4^{9QA} $t_{(2)}$=4.8747, p=0.0396; HDAC4$^{9QA\Delta Q}$ $t_{(2)}$=9.1283, p=0.0118; HDAC4^{S69F} $t_{(2)}$=2.3819, p=0.1401). Full blots used for quantification are found in Appendix 10.2.3, Figure 10.10.

4.3.3. HDAC4 oligomerisation mutants are altered in oligomerisation capacity

To assess the capacity of each of the HDAC4 tetramerisation mutants to oligomerise, a co-immunoprecipitation approach was employed (Figure 4.8). This involves co-expression of two differentially tagged HDAC4 transgenes: *GFP-HDAC4^{WT}*, which carries an N-terminal fusion of GFP and has been previously characterised (Main *et al.*, 2021), and the C-terminally tagged *HDAC4^{WT}-Myc* (Tan *et al.*, 2024). It is hypothesised that tetramerisation of GFP-HDAC4^{WT} and HDAC4^{WT}-Myc will be unaffected by their epitope tags, and therefore upon immunoprecipitation of one, the other should be co-immunoprecipitated and be detected via western blotting, thus providing a measure of their ability to oligomerise. *HDAC4^{WT}-Myc* and *HDAC4^{mutant}-Myc* constructs were each crossed into the same line as *GFP-HDAC4^{WT}* for co-expression (Appendix Section 10.1.6, Figure 10.5). Both *GFP-HDAC4^{WT}* and *HDAC4^{WT}-Myc* are under UAS-GAL4 control (Main *et al.*, 2021; Main, 2019), and were therefore expressed at the same levels in the same tissues dependent on driver selection. A standard genetic cross was performed between flies harbouring the *elav-GAL4* driver and both *HDAC4* constructs, and *HDAC4* expression was induced in the brains of progeny (Figure 4.8A). GFP-tagged HDAC4 was immunoprecipitated from whole-head lysates and western blotting was performed to detect HDAC4-Myc to assess oligomerisation status. The blot was also probed with anti-GFP to confirm successful immunoprecipitation. Optimisation and validation of this protocol is detailed in Chapter 6 (Appendix 10.4.3.1).

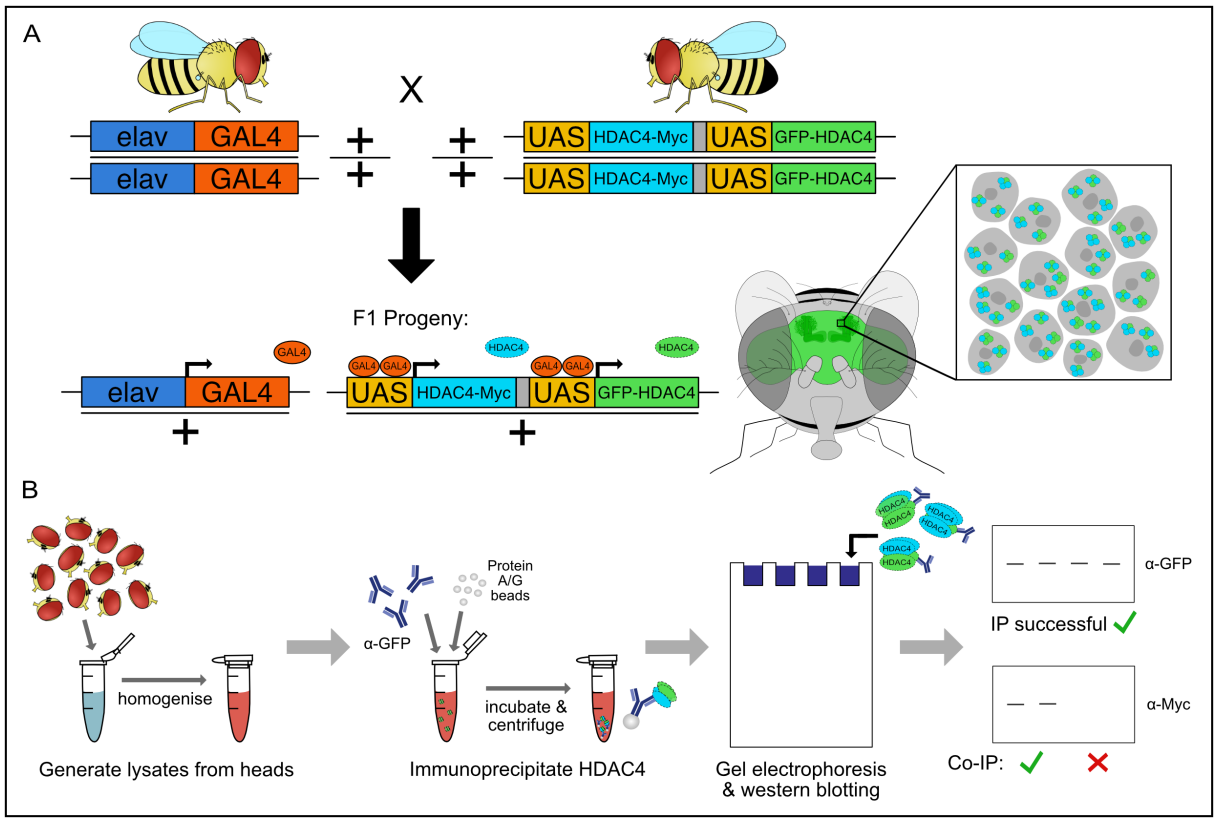

Figure 4.8 Schematic diagram of the co-immunoprecipitation workflow to assess changes in HDAC4 oligomerisation
(A) Flies were raised by crossing *elav-GAL4* virgin females to males harbouring both *HDAC4-Myc* and *GFP-HDAC4*^{WT}, resulting in progeny expressing both transgenes pan-neuronally. (B) Heads of progeny were homogenised and GFP-HDAC4^{WT} immunoprecipitated. The immunoprecipitate was electrophoresed and western blotting performed to detect confirm successful immunoprecipitation (IP, GFP-HDAC4) and co-immunoprecipitation (Co-IP, HDAC4-Myc). *This figure is an original artwork.*

Immunoprecipitation of GFP-HDAC4^{WT} resulted in co-immunoprecipitation of HDAC4^{WT}-Myc (Figure 4.9, lane 3), supporting the hypothesis that GFP-HDAC4^{WT} and HDAC4^{WT}-Myc form oligomers *in vivo*. This was a specific interaction as HDAC4^{WT}-Myc was not immunoprecipitated in the absence of GFP-HDAC4^{WT}. In contrast, HDAC4^{F65A}, HDAC4^{9QA} and HDAC4$^{9QA\Delta Q}$ were all significantly reduced in co-immunoprecipitation yield compared to HDAC4^{WT}, with only faint bands being observed, suggesting a severely reduced capacity to oligomerise. GFP-HDAC4^{WT} was successfully immunoprecipitated in each sample in which it was present, indicating that the lack of co-immunoprecipitation is due to changes in oligomerisation (Figure 4.9, lanes 4-6). The residual immunoprecipitation of these mutants is likely a result of stabilisation of oligomerisation by GFP-HDAC4^{WT} (further discussed in Section 4.7.1.2). HDAC4^{S69F} did not appear to be increased in co-immunoprecipitation yield compared to HDAC4^{WT} (Figure 4.9, lane 7), however the immunoprecipitation yield of GFP-

HDAC4^{WT} was considerably lower, suggesting that HDAC4^{S69F} may be increased in oligomer stability compared to HDAC4^{WT}. These findings were also replicated using immunoprecipitation protocol 1, demonstrating the specificity of the interaction (Appendix 10.2.5). Together, these data show that the regions of the N-terminus of HDAC4 that mediate oligomerisation of hHDAC4 (Guo *et al.*, 2007) are also required for oligomerisation of DmHDAC4. These mutants can therefore next be used to test whether their reduced capacity to oligomerise also results in reduced aggregate formation and reduced disruption to neurodevelopment upon overexpression.

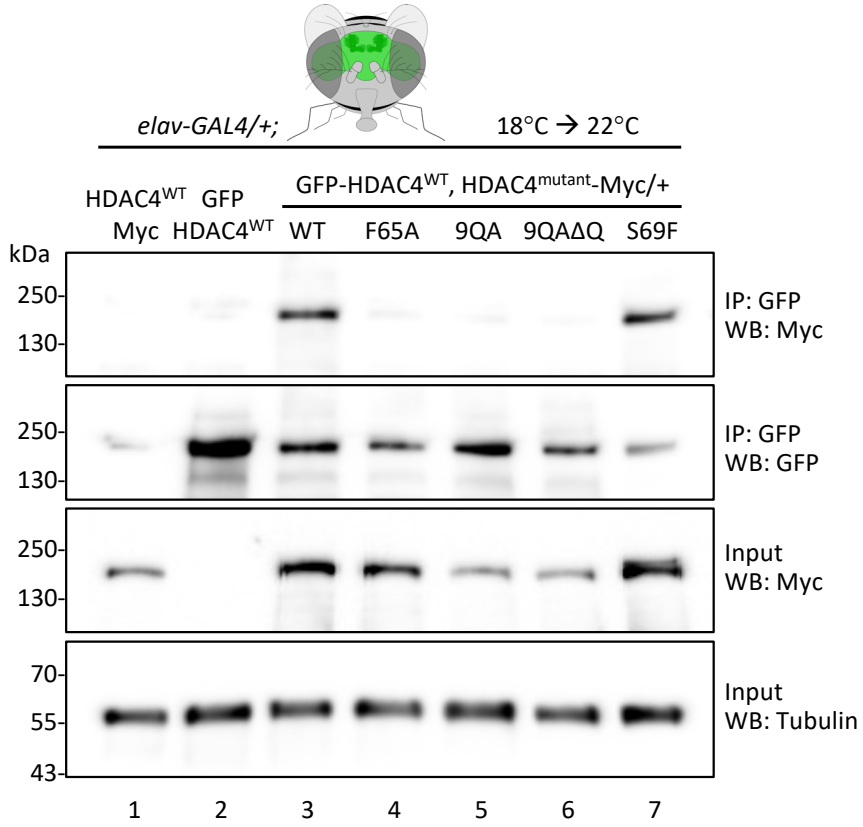

Figure 4.9 HDAC4 tetramerisation mutants are altered in their ability to oligomerise
Co-immunoprecipitation experiments to examine the ability of HDAC4^{mutant} to bind HDAC4^{WT} to assess oligomerisation capacity. The indicated transgenes were expressed pan-neuronally in *Drosophila* under the control of *elav-GAL4*. Flies were raised at 18 °C until adulthood and then moved to 22 °C for five days to increase the level of transgene expression before harvesting and generation of whole-head lysates. Anti-GFP conjugated magnetic beads were used to immunoprecipitate GFP-HDAC4^{WT} from all samples, followed by probing for HDAC4-Myc. HDAC4^{WT} and HDAC4^{S69F} co-immunoprecipitated with GFP-HDAC4^{WT} while HDAC4^{F65A}, HDAC4^{9QA} and HDAC4^{9QAΔQ} did not despite comparable immunoprecipitation of GFP-HDAC4^{WT} from all samples. Input samples were 30 µg of whole-cell lysate and the level of transgene expression was consistent with previous quantification (Figure 4.7). Protocol 2 (Methods 3.2.4) was used for this experiment.

4.4. HDAC4 oligomerisation is required for nuclear aggregation

Overexpression of HDAC4^{WT} in *Drosophila* Kenyon cells results in the formation of small nuclear aggregates (Fitzsimons *et al.*, 2013; Main *et al.*, 2021; Tan *et al.*, 2024). It is hypothesised that these aggregates result from tetramerisation of HDAC4 and subsequent formation of higher order structures, as deletion of the N-terminus of HDAC4 prevents nuclear aggregate formation (Kirsh *et al.*, 2002). In this section, the optimisation and validation of a method to quantify nuclear aggregation of HDAC4 was performed, and aggregation of each of the HDAC4 oligomerisation mutants was examined in Kenyon cell nuclei in the brain, as well as within the third instar larval eye disc.

4.4.1. Validation of method of quantification of HDAC4 aggregates in Kenyon cell nuclei

Nuclear aggregates of HDAC4 are observed to sequester the transcription factor MEF2 in mammalian cells (Chan *et al.*, 2003; Miska *et al.*, 1999) as well as in *Drosophila* Kenyon cells (Fitzsimons *et al.*, 2013; Main *et al.*, 2021; Tan *et al.*, 2024). Co-localisation of MEF2 in HDAC4^{WT} aggregates in Kenyon cells is invariable and thus can be used as a counterstain for quantification of HDAC4 aggregation (Fitzsimons *et al.*, 2013). To provide a consistent comparison with previous studies (Fitzsimons *et al.*, 2013; Tan *et al.*, 2024) *HDAC4* transgene expression was driven by *OK107-GAL4* in the presence of the TARGET system (Figure 3.1C) for all analyses that quantify aggregation in Kenyon cells unless otherwise stated. The TARGET system (Section 1.2.3) was used to restrict *HDAC4* expression to adulthood to simulate the increase in nuclear HDAC4 abundance that has been observed during the onset of some neurodegenerative diseases (Q. Wu *et al.*, 2016), and mitigate any developmental effects that may arise as a result of transgene expression. Flies were raised at 18°C until adulthood, where they were transferred to 30°C for three days to induce transgene expression. The optimisation of the fixation and staining protocol is described in Appendix 10.2.7. Following this the specificity of the MEF2 antibody was validated (Appendix 10.2.8). In addition, the subcellular distribution of MEF2 is also regulated in a circadian manner in a subset of cells within the brain (Blanchard *et al.*, 2010; Sivachenko *et al.*, 2013), therefore the role of the circadian clock was also examined with respect to HDAC4 aggregation (Appendix 10.2.9). No significant difference in aggregation was observed between flies processed in the morning or

the afternoon, confirming that differences observed between HDAC4 oligomerisation mutants are unlikely to be affected by the time of day these samples were processed.

4.4.2. HDAC4 oligomerisation mutants are altered in aggregation in Kenyon cells

Following the validation of a method to quantify HDAC4 aggregation in Kenyon cell nuclei, the ability of each oligomerisation mutant to aggregate was investigated. HDAC4^{WT} and HDAC4^{mutant} expression was induced during adulthood under the control of *OK107-GAL4* via the TARGET system (Figure 3.1C), and brains dissected (Section 3.4.1) and immunostained with antibodies against both the Myc tag and endogenous MEF2 (Figure 4.10). Imaging of whole brains expressing HDAC4^{WT} confirmed the robust expression of HDAC4 in Kenyon cells (Figure 4.10A). HDAC4^{WT} was present in the nucleus and the cytoplasm, as well as in the lobes (bundled axons) and in the calyx, the region where dendrites of Kenyon cells arborise (Yasuyama *et al.*, 2002). Minimal Myc staining was observed elsewhere in the brain, consistent with the expression pattern of OK107-GAL4 (Figure 4.1). Imaging of Kenyon cells from control brains confirmed that in the absence of overexpression of HDAC4, MEF2 was evenly distributed across nuclei (Figure 4.10B), as previously observed (Fitzsimons *et al.*, 2013), with the exception of one to two regions per nucleus where MEF2 was absent. Counterstaining with DAPI performed subsequently suggested that these are regions of heterochromatin (Section 10.4.4.1). Upon expression of HDAC4^{WT}, MEF2 was redistributed into small discrete aggregates that contained HDAC4 (Figure 4.10C-E). These aggregates were visualised as white punctate foci on merged images. The number of these aggregates decreased upon expression of HDAC4^{F65A}, HDAC4^{9QA}, and HDAC4$^{9QA\Delta Q}$ when compared to HDAC4^{WT} (Figures 4.10F-H). In contrast, the number of aggregates increased upon expression of HDAC4^{S69F} (Figure 4.10I).

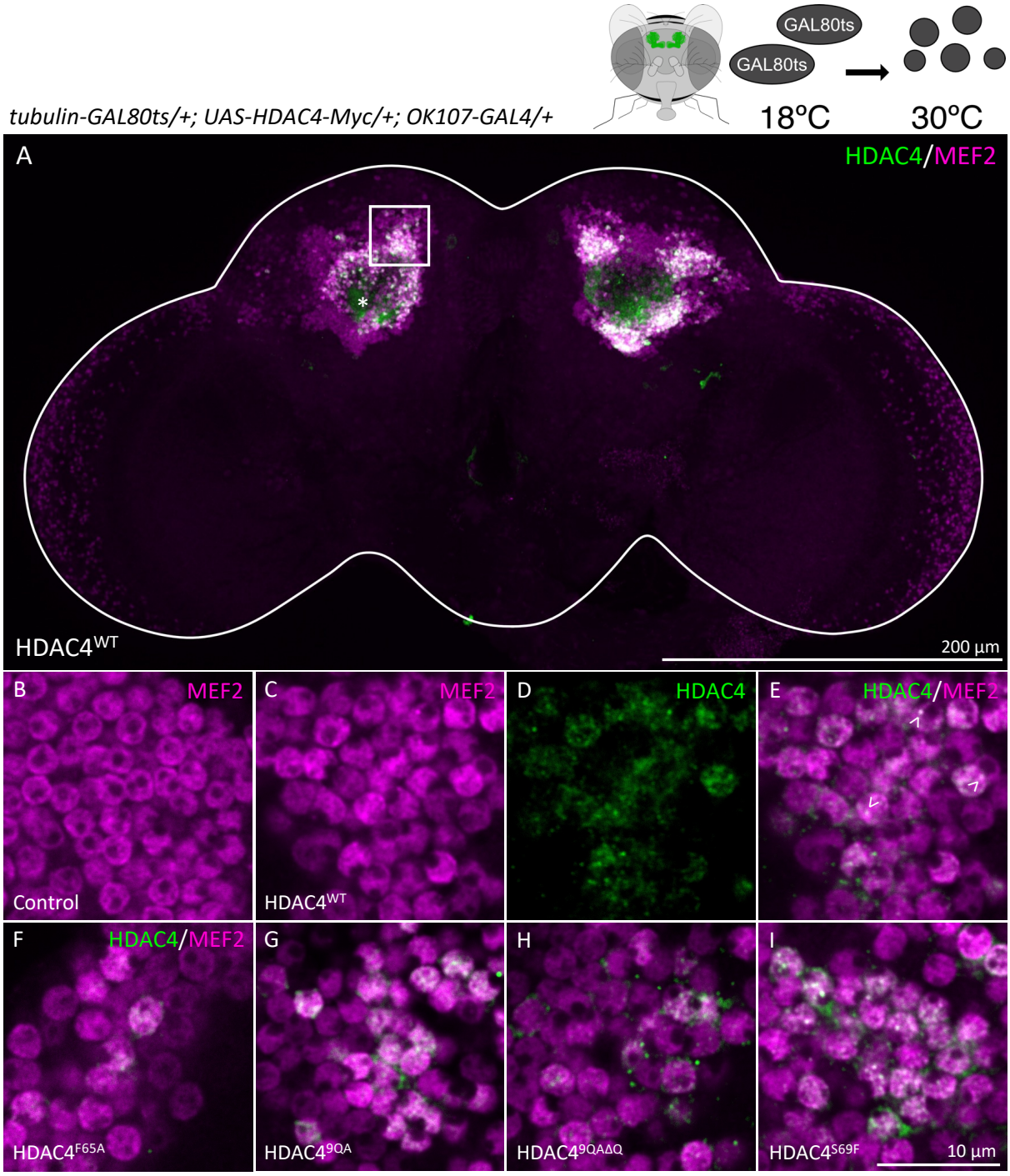

Figure 4.10 HDAC4 oligomerisation mutants are altered in aggregation and recruitment of MEF2 to aggregates in Kenyon cell nuclei

(A) Typical distribution of endogenous MEF2 and *OK107-GAL4* driven expression of HDAC4^{WT} in the posterior of the brain. Maximum projection of optical sections through the posterior of the whole-brain of flies expressing HDAC4^{WT} under the control *OK107-GAL4* in the presence of the TARGET system. Flies were raised at 18 °C until eclosion, where adults were transferred to 30 °C for three days to induce HDAC4 expression. HDAC4^{WT} (green) was observed in Kenyon cell nuclei where endogenous MEF2 (magenta) was present, white indicates co-localisation. HDAC4^{WT} was also localised to dendrites in the calyx (*). Boxed area of the calyx and surrounding Kenyon cells in (A) is depicted as a single optical section (0.5 µm) in (B-I). (B) In control brains (*+; tubulin-GAL80ts/+; +; OK107-GAL4/+*) MEF2 was relatively uniformly distributed in nuclei in the absence of HDAC4 overexpression. (C-E) When HDAC4^{WT} was expressed, small punctate foci (arrowheads) containing both MEF2 and HDAC4 were

formed in nuclei. (F-I) Mutations to the N-terminus of HDAC4 altered the formation of aggregates. Expression of HDAC4^{F65A} (F), HDAC4^{9QA} (G), and HDAC4$^{9QA\Delta Q}$ (H) reduced the presence of aggregates compared to HDAC4^{WT} (E), whereas they were increased upon expression of HDAC4^{S69F} (I).

HDAC4 aggregation following expression of either HDAC4^{WT} or HDAC4^{mutant} was quantified through the Kenyon cell layer (Figure 4.11, Methods 3.4.6). Expression of HDAC4^{WT} led to an average of 82 aggregates per section, which was significantly increased upon expression of HDAC4^{S69F} to 157 per section (Figure 4.11F). In contrast, expression of HDAC4^{F65A}, HDAC4^{9QA} and HDAC4$^{9QA\Delta Q}$ significantly reduced the number of aggregates to 31, 41, and 30 per section respectively. As observed in Figure 4.4, endogenous HDAC4 is sequestered in transgene HDAC4 aggregates, and it is therefore hypothesised that endogenous HDAC4 stabilises aggregation of HDAC4^{mutant}. Oligomers of HDAC4 will likely contain monomers of both HDAC4^{mutant} and endogenous HDAC4, and oligomers with a higher proportion of endogenous HDAC4 are likely to be more stable than those that contain just HDAC4^{mutant} as they can better form the hydrophobic core and stabilising interaction networks required for tetramerisation (Guo *et al.*, 2007). As a result, endogenous HDAC4 will facilitate oligomerisation and thus aggregation of HDAC4^{mutant} may not be possible in the absence of endogenous HDAC4. For HDAC4^{F65A}, HDAC4^{9QA} and HDAC4$^{9QA\Delta Q}$, this would result in an overestimation of their ability to aggregate. Together, these data show that oligomerisation of HDAC4 contributes to its aggregation in Kenyon cell nuclei.

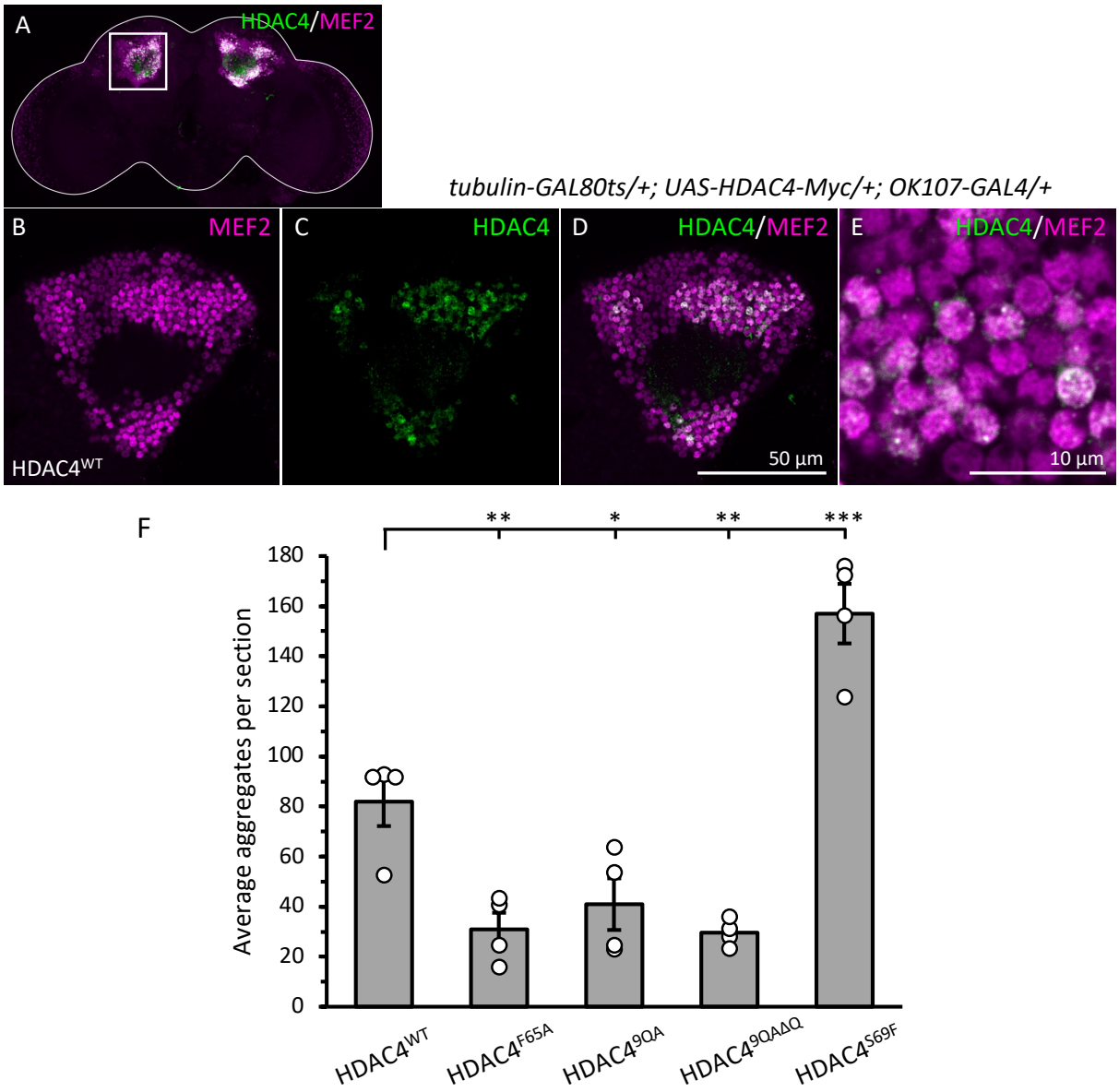

Figure 4.11 The number of HDAC4-containing aggregates in neuronal nuclei is altered by mutations that affect oligomerisation of HDAC4

(A) Replicated image from Figure 4.10A of the distribution of endogenous MEF2 (magenta) and HDAC4^{WT} (green) driven by *OK107-GAL4* in the presence of the TARGET system in the posterior of the brain. Boxed region of the Kenyon cell layer is depicted as a single optical section (0.5 µm) in (B-D). This is presented to show the area through the Kenyon cell layer that was quantified in (F). (E) Magnified image of HDAC4^{WT} aggregates. (F) Quantification of HDAC4 aggregates. The indicated HDAC4 transgene was expressed under the control of *OK107-GAL4* in the presence of the TARGET system. Flies were raised at 18 °C until eclosion, where adults were transferred to 30 °C for three days to induce HDAC4 expression. HDAC4 aggregates that co-localised with MEF2 (visualised as white foci) were counted through the Kenyon cell layer (as seen in B-D) for 10 optical sections spaced 1 µm apart as per Section 3.4.6, n=4 brains per genotype. The mean is plotted, and the average number of aggregates per section per brain are plotted as individual points. Error bars indicate the SEM. Aggregate number was significantly reduced by each of HDAC4^{F65A}, HDAC4^{9QA} and HDAC4^{9QAΔQ} compared to HDAC4^{WT}, and significantly increased by HDAC4^{S69F} (ANOVA, $F(4,15)=36.88$, $p<0.0001$, post-hoc Tukey's HSD *$p<0.05$, **$p<0.01$, ***$p<0.001$. HDAC4^{WT} vs HDAC4^{F65A}, $p=0.007801$; vs HDAC4^{9QA}, $p=0.0365$; vs HDAC4^{9QAΔQ}, $p=0.006189$; vs HDAC4^{S69F}, $p<0.001$. There was no significant difference between each of HDAC4^{F65A}, HDAC4^{9QA} and HDAC4^{9QAΔQ}).

4.4.3. HDAC4 oligomerisation mutants are altered in aggregation in the larval eye disc

Thus far, nuclear aggregation of HDAC4 resulting from its overexpression in *Drosophila* has only been examined in Kenyon cells of the mushroom body. The rationale for analysis of Kenyon cell aggregates and correlation with mushroom body phenotypes was based on the observation that increased expression of HDAC4 in the mushroom body disrupts its development (Main *et al.*, 2021; Tan *et al.*, 2024). It was therefore hypothesised that the presence of nuclear HDAC4 aggregates may be responsible for these defects. Moreover the mushroom body is essential for memory in *Drosophila* (de Belle & Heisenberg, 1994; Dubnau *et al.*, 2001; Heisenberg *et al.*, 1985; McBride *et al.*, 1999), thus examining this brain region also has relevance to neurodegenerative diseases associated with cognitive dysfunction.

Increased HDAC4 also disrupts eye development in *Drosophila* (Main *et al.*, 2021; Schwartz *et al.*, 2016; Tan *et al.*, 2024), yet it is unknown whether HDAC4 forms aggregates in other types of neuronal cells, including those involved in the development of the adult eye, and whether this contributes to the overexpression-induced phenotype. To that end, HDAC4 distribution and aggregation was also assessed in the third instar larval eye disc (the development of which is described in Section 1.3.2). MEF2 provides an excellent counterstain to visualise HDAC4 aggregates in Kenyon cells. However, since it was unclear whether MEF2 is expressed in photoreceptor neurons at this stage of development, the expression of endogenous MEF2 in the larval eye disc was first characterised. Eye discs were dissected from third instar larvae (Section 3.4.2) in which *Drosophila* MEF2 with a C-terminal HA epitope tag was overexpressed (*UAS-MEF2^{WT}-HA*, Main *et al.* (2021)) under the control of the *GMR-GAL4* eye driver (Figure 3.1B), and immunohistochemistry was then performed using antibodies against endogenous MEF2 and the HA tag (Figure 4.12). The antibody against endogenous MEF2 detected MEF2^{WT}-HA, and an overlapping pattern was detected with anti-HA, confirming the ability to detect MEF2 by immunohistochemistry in the eye disc (Figure 4.12B-D). However, in the absence of MEF2^{WT}-HA (control, *GMR-GAL4/+*), the endogenous MEF2 antibody appeared to bind non-specifically across the eye disc (Figure 4.12A), suggesting an absence of MEF2 expression. This therefore indicates that MEF2 is not an appropriate counterstain for the visualisation of HDAC4 aggregates in the developing eye.

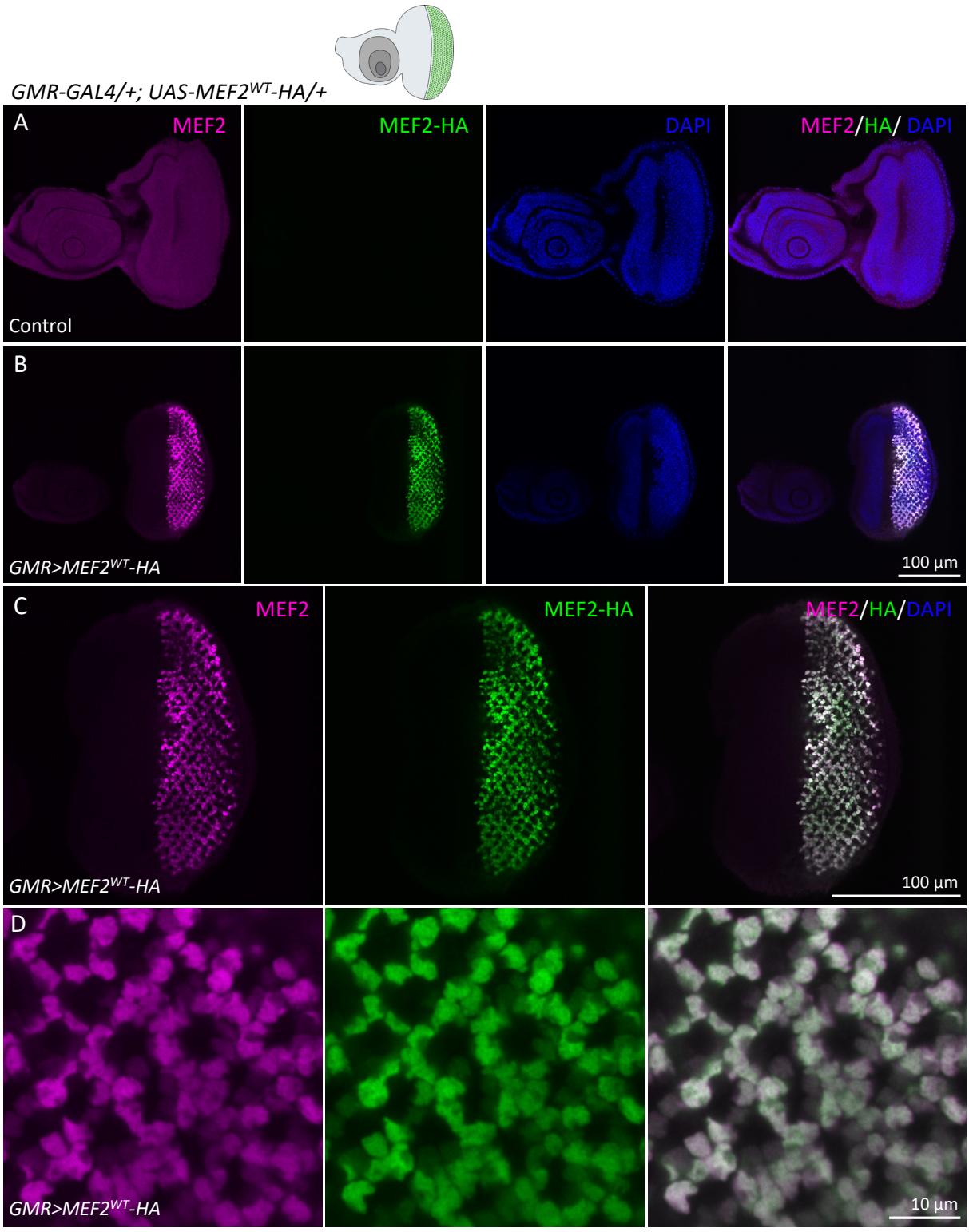

Figure 4.12 Endogenous MEF2 is not detected in the developing eye disc

(A-B) Single optical sections (0.5 µm) through the third instar larval eye disc depicting the binding pattern of the MEF2 antibody. (A) In the absence of MEF2, the MEF2 antibody (magenta) bound non-specifically across the whole eye disc while no signal in the HA channel (green) was observed. DAPI (blue) highlights nuclei across the disc. (B) Expression of MEF2^{WT}-HA driven by *GMR-GAL4* resulted in specific binding of the MEF2 antibody to MEF2^{WT}-HA, as verified by co-localisation with MEF2-HA signal, and loss of non-specific MEF2 antibody binding across the eye disc. (C) Single optical section (0.5 µm) depicting the pattern of MEF2-HA^{WT} in the apical side of the eye disc. This is magnified in (D). Control is *GMR-GAL4/+*. Images were obtained using constant settings. *This figure is an*

adaptation from that found in Tan et al. (2024) (doi: 10.1186/s12915-023-01800-1), which is distributed under CC BY 4.0.

HDAC4 distribution and aggregation in the larval eye disc was assessed in combination with 4′,6-diamidino-2-phenylindole (DAPI) staining, which binds double stranded DNA, to highlight nuclei (Kapuscinski, 1995). *UAS-GFP.nls* was also co-expressed with *HDAC4*^{WT} to label nuclei in which *GMR-GAL4* mediates expression (Shiga *et al.*, 1996). GFP.nls and HDAC4^{WT} were observed posterior to the morphogenetic furrow (Figure 4.13A), consistent with the known expression pattern of *GMR-GAL4* (Freeman, 1996). In a cross section of the disc (Figure 4.13B), the distribution of HDAC4^{WT} differed between apical and basal cells (described in Figure 1.6); small nuclear aggregates were only observed in basal cells and HDAC4^{WT} was not localised to apical nuclei. Further examination in single sections corroborated this, where HDAC4^{WT} was predominantly cytoplasmic in both the apical and basal cells (Figure 4.13C-D), with aggregates only observed in a subset of the nuclei of basal cells. The distribution of HDAC4^{WT} is consistent with that of endogenous HDAC4 (HDAC4::GFP, Figure 4.13E-F) which was punctate and predominantly cytoplasmic in both apical and basal cells.

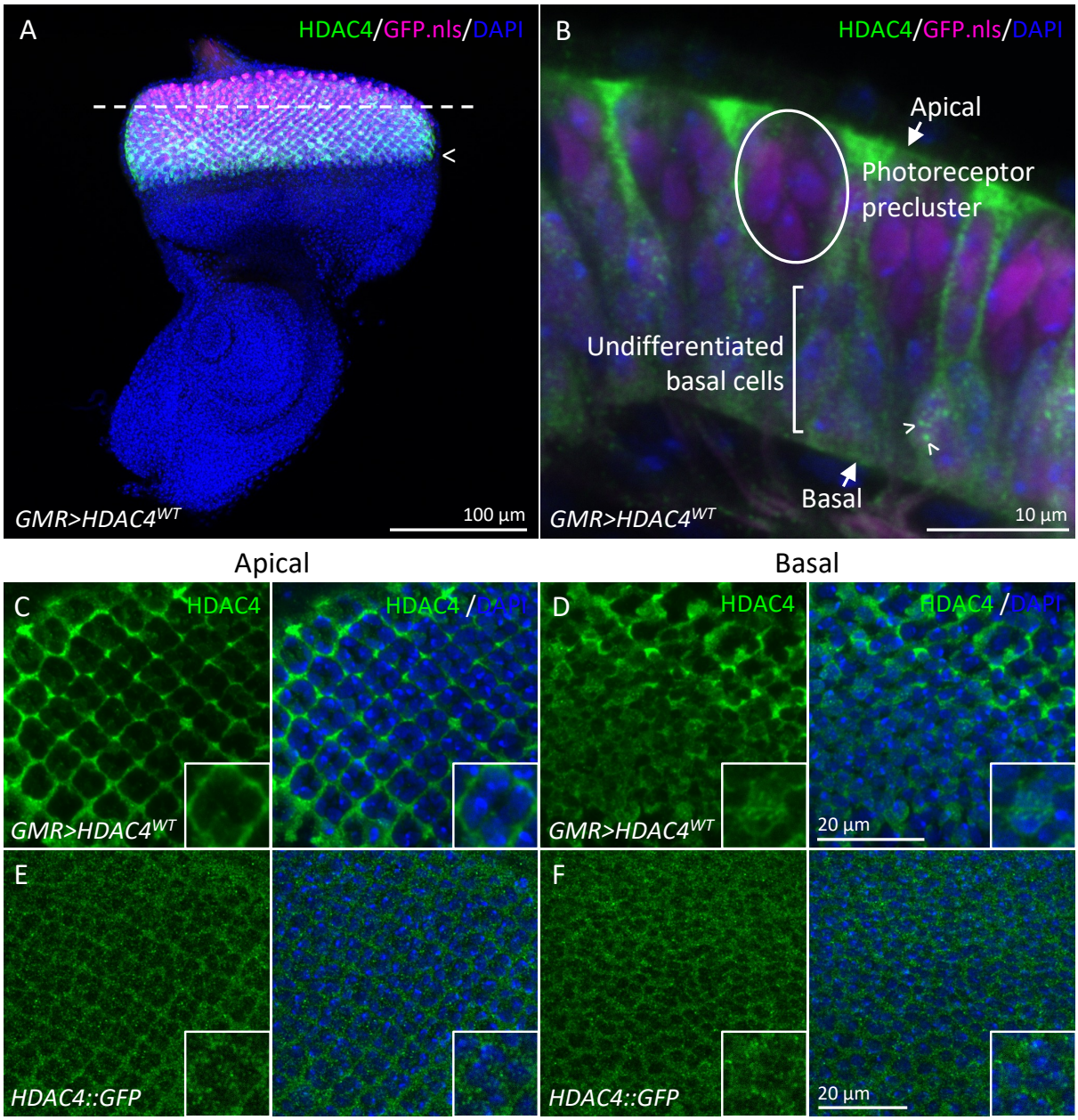

Figure 4.13 Expression pattern of endogenous and transgene HDAC4 in the larval eye disc

(A) Maximum projection of a third instar larval eye disc expressing HDAC4^{WT} (green) and GFP.nls (magenta) under the control of *GMR-GAL4.* Flies were raised at 25 °C. Expression of both HDAC4^{WT} and GFP.nls was observed posterior to the morphogenetic furrow (arrowhead). DAPI (blue) highlights nuclei across the whole disc. The dashed line indicates the location of the cross section depicted in (B). (B) HDAC4^{WT} localised to both apical and basal cells of the disc and formed small nuclear aggregates (arrows) in undifferentiated basal cells. A photoreceptor precluster which forms one ommatidium is circled in the apical surface, where HDAC4 aggregates were not observed. (C-F) Single optical sections (0.5 µm) of the apical (C, E) and basal (D, F) cells of the eye disc. Under the control of *GMR-GAL4,* HDAC4^{WT} localised primarily to the cytoplasm of apical cells (C) and was found in cytoplasmic haloes and nuclear aggregates in basal cells (D). (E-F) The endogenous distribution of HDAC4 (HDAC4::GFP) was similar to HDAC4^{WT} distribution. The inset shows a magnified image of several cells demonstrating that HDAC4 is present in both the nucleus and the cytoplasm to varying degrees in each cell type.

Cells found on the apical side of the third instar larval eye disc are differentiated photoreceptor clusters; recruitment and arrangement of photoreceptors continues throughout the third instar stage and therefore the clusters contain up to eight cells (Section 1.3.2). In contrast, basal cells are those that become accessory cells or are yet to be recruited as photoreceptors and are less regularly arranged. As aggregates of $HDAC4^{WT}$ were found in basal cells, and errors in division, differentiation and clearance of accessory cells give rise to adult eye phenotypes (Kumar, 2012), the distribution and ability of $HDAC4^{mutants}$ to aggregate was examined in these cells (Figure 4.14). As observed in Figure 4.13, $HDAC4^{WT}$ formed cytoplasmic haloes and nuclear aggregates in a large proportion of basal cells (Figure 4.14B). In comparison, $HDAC4^{F65A}$, $HDAC4^{9QA}$, and $HDAC4^{9QA\Delta Q}$ were all more strongly localised to cytoplasmic haloes than $HDAC4^{WT}$, and nuclear aggregates were rarely detected (Figure 4.14C-E). The shift in distribution of $HDAC4^{F65A}$ was particularly striking as little was observed within nuclei and no aggregates were detectable. Small nuclear aggregates were infrequently detected for each of $HDAC4^{9QA}$ and $HDAC4^{9QA\Delta Q}$, however the distribution also appeared punctate within the cytoplasm. In contrast, $HDAC4^{S69F}$ was increased in both nuclear distribution and aggregate formation compared to $HDAC4^{WT}$ (Figure 4.14F).

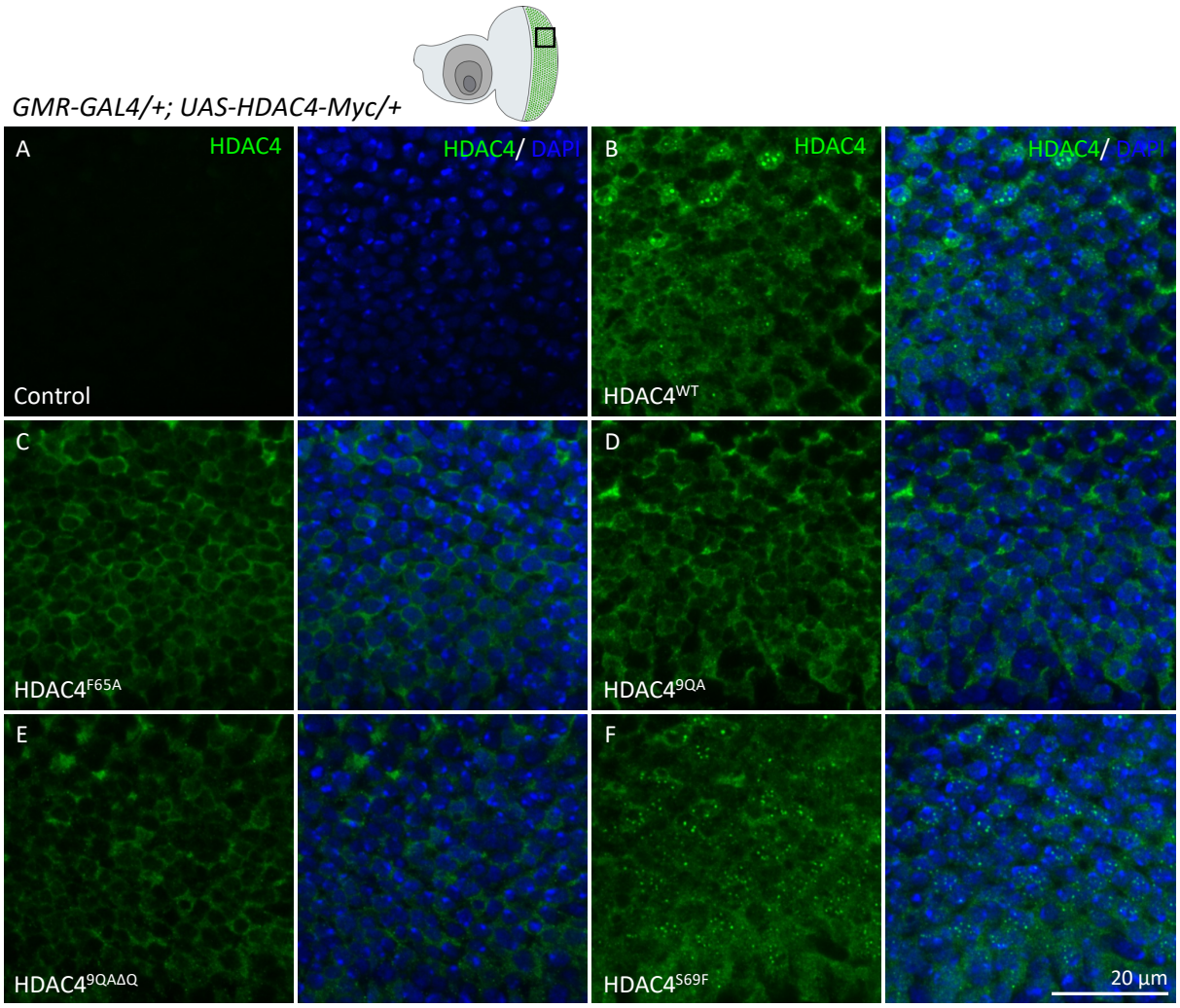

Figure 4.14 HDAC4 oligomerisation mutants are altered in aggregation and subcellular distribution in basal cells of the third instar larval eye disc
(A-F) Single optical sections (0.5 µm) of basal cells of the larval eye disc expressing HDAC4^{WT} and HDAC4^{mutant} (green) under the control of *GMR-GAL4*. Flies were raised at 25 °C. Control is *GMR-GAL4/+*. Nuclei were labelled with DAPI (blue). HDAC4^{WT} and HDAC4^{S69F} formed many nuclear aggregates, while few were observed for HDAC4^{F65A}, HDAC4^{9QA}, and HDAC4^{9QAΔQ}.

Together these data demonstrate that in two independent neuronal cell types, both the Kenyon cells of the adult brain and the basal cells of the larval eye disc, mutations to the N-terminus of HDAC4 impact its subcellular distribution and its ability to form nuclear aggregates.

4.5. HDAC4 aggregation correlates with neurodevelopmental phenotypes in *Drosophila*

It is now established that mutation of residues predicted to be required for the tetramerisation of HDAC4 reduces its aggregation in neuronal nuclei. Therefore, to examine the correlation between oligomerisation and aggregation of HDAC4 and HDAC4-overexpression induced phenotypes, the effect that each mutation has on HDAC4 overexpression-induced defects in mushroom body and eye development was investigated.

4.5.1. HDAC4 oligomerisation mutants reduce severity of mushroom body phenotypes arising from HDAC4 overexpression

Upon overexpression of HDAC4^{WT}, a number of defects are observed in the development of the *Drosophila* mushroom body and the most prominent defect is β-lobe fusion, the severity of which is increased when HDAC4 is restricted to the nucleus (Main *et al.*, 2021; Tan *et al.*, 2024). It was hypothesised that there would be a positive correlation between aggregation and severity of β-lobe fusion, and that mutations that decrease oligomerisation and aggregation of HDAC4 would decrease the severity of β-lobe fusion. Conversely, as expression of HDAC4^{S69F} increased the number of aggregates in Kenyon cell nuclei compared to HDAC4^{WT}, it was also hypothesised that it would also increase the severity of neurodevelopmental defects observed in the mushroom body.

HDAC4^{WT} and HDAC4^{mutant} were pan-neuronally expressed throughout development with *elav-GAL4*. Adult flies were then dissected and brains were immunostained for FasII, which strongly labels the α- and β-lobes (Figure 4.2) and is commonly used for assessment of mushroom body development (Fitzsimons *et al.*, 2013; Main *et al.*, 2021; Palmer & Fitzsimons, 2023; Schwartz *et al.*, 2016; Schwartz *et al.*, 2023; Tan *et al.*, 2024). Brains were imaged from the anterior, and maximum projections through the mushroom body lobes were generated and then scored for developmental defects using standard parameters (Main *et al.*, 2021; Tan *et al.*, 2024). These examine the formation of the α- and β-lobes, considering axon extension, termination, and guidance (Figure 4.15). As observed previously when raised at 22°C, overexpression of HDAC4^{WT} predominantly impaired β-lobe development, where axons extended past the mid-line appearing as one extended β-lobe (Figure 4.15F-G), which is commonly referred to as β-lobe fusion (Table 4.2).

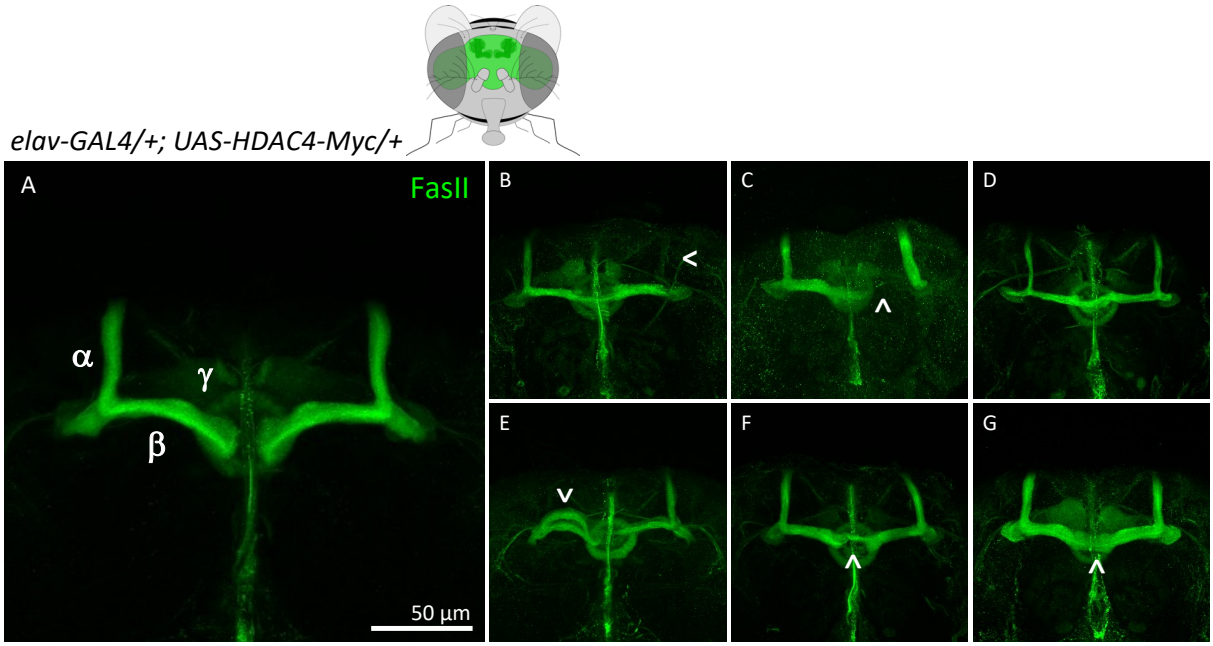

Figure 4.15 Mushroom body phenotypes observed upon HDAC4 overexpression
(A-G) Maximum projections of optical sections through the anterior of the adult brain. Anti-FasII immunostaining (green) labels the alpha (α), beta (β) and gamma (γ) lobes of the mushroom body. Defects (arrowhead) resulting from HDAC4 overexpression included missing α lobe (B), missing β-lobe (C), lobe thinning (D), guidance defect (E), mild β-lobe fusion (F) and severe β-lobe fusion (G). β-lobe fusion was also observed in (B) and (D).

Table 4.2 Frequency of mushroom body phenotypes resulting from HDAC4 transgene expression at 22 °C and 18 °C

		22 °C					18 °C	
(% of brains)	**Con**	**HDAC4 WT**	**HDAC4 F65A**	**HDAC4 9QA**	**HDAC4 9QAΔQ**	**HDAC4 S69F**	**HDAC4 WT**	**HDAC4 S69F**
α thinning	0	6	0	8	0	26	5	10
α missing	0	0	0	4	0	5	0	0
β thinning	0	3	0	8	0	13	11	3
β missing	0	0	0	0	0	3	5	0
β fusion	**5**	**94**	**68**	**54**	**32**	**95**	**84**	**100**
Mild	5	9	23	19	18	3	42	28
Severe	0	84	45	35	14	92	42	72
Guidance	0	3	0	0	4	0	5	0
n	44	32	31	26	22	39	19	29

Expression of each denoted *HDAC4* transgene was driven by *elav-GAL4*; virgin *elav-GAL4* female flies were crossed to males harbouring the *HDAC4* transgene and adult progeny of this cross were dissected and their brains immunostained for FasII to assess mushroom body lobe development. Flies were raised at 18 °C and 22 °C as indicated. Instances of defects in morphology were scored for n≥19 brains per genotype as per Section 3.4.7 and are displayed as the % of brains with the indicated phenotype. Control (con) is *elav-GAL4/+*. Percentages may not sum to 100 due to rounding.

β-lobe fusion was characterised as either mild (Figure 4.15F), where less than half the width of the lobe crossed the centre line (i.e. appeared fused) on one or both sides of the brain, or severe (Figure 4.15G), where more than half the lobe appeared fused. HDAC4^{WT} induced severe β-lobe fusion in 84% of brains analysed (Figure 4.16). Expression of each of the tetramerisation mutants HDAC4^{F65A}, HDAC4^{9QA}, and HDAC4^{9QAΔQ} significantly reduced the incidence and severity of β-lobe fusion compared to HDAC4^{WT}. Incidence and severity of β-lobe fusion mediated by HDAC4^{9QAΔQ} was reduced compared to HDAC4^{9QA}, however this was not statistically significant (incidence, p=0.15, severe fusion, p=0.18). Conversely, expression of HDAC4^{S69F} increased severe β-lobe fusion penetrance to 92%, however this increase was not statistically significant. Both α- and β-lobe thinning were also increased, albeit not significantly, in HDAC4^{S69F} compared to HDAC4^{WT} (p=0.053 and 0.21 respectively).

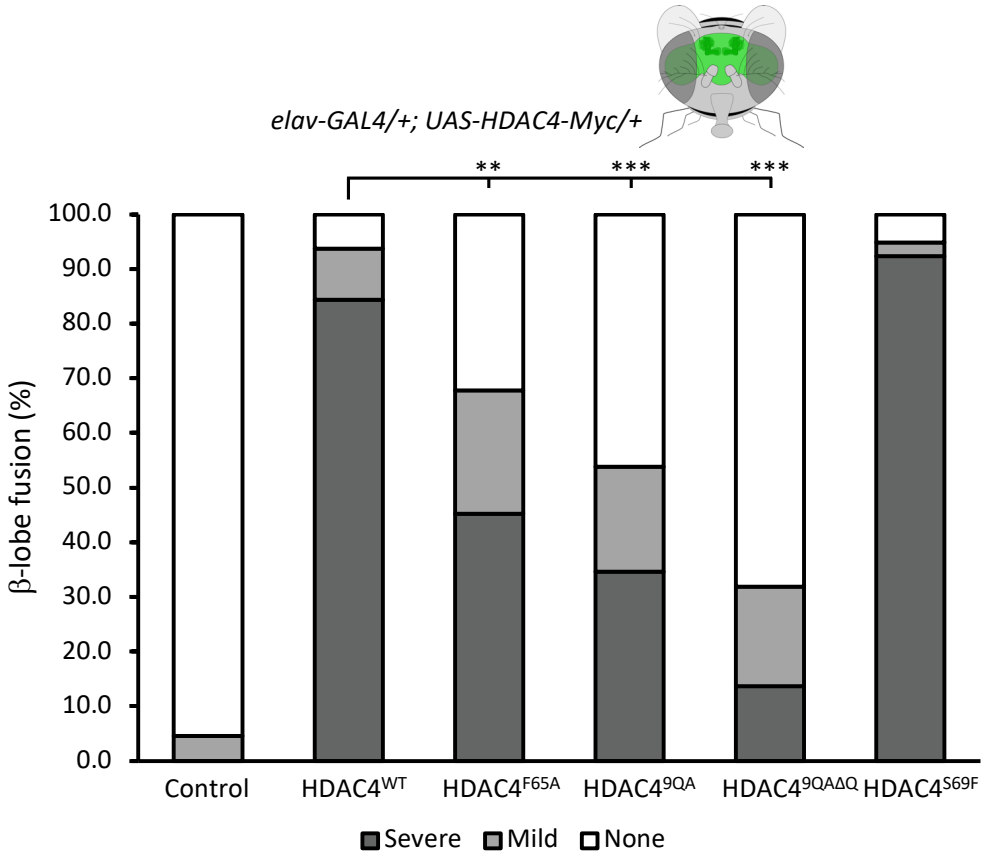

Figure 4.16 HDAC4 oligomerisation mutants alter the severity of β-lobe fusion of the mushroom body

Quantification of β-lobe fusion resulting from HDAC4 overexpression. HDAC4 expression was driven by *elav-GAL4* at 22°C, adult brains were processed for anti-FasII immunohistochemistry, and β-lobe fusion was scored. Control is *elav-GAL4/+*. n≥19 brains per genotype. HDAC4^{F65A}, HDAC4^{9QA} and HDAC4^{9QAΔQ} mutants each significantly reduced the severity of β lobe fusion compared to HDAC4^{WT} (Fisher's exact test, severe β-lobe fusion, * p<0.05, ** p<0.01, *** p<0.001). There was no significant difference between HDAC4^{WT} and HDAC4^{S69F} (p=0.4536).

To tease apart potentially subtle phenotypic differences between HDAC4^{WT} and HDAC4^{S69F}, flies were instead raised at 18°C, at which temperature GAL4 is less active and transgene expression is reduced (Duffy, 2002). Accordingly, the difference in β-lobe fusion between HDAC4^{WT} and HDAC4^{S69F} was exacerbated (Table 4.2, Figure 4.17). Total β-lobe fusion had 100% penetrance for HDAC4^{S69F}, compared to 84% for HDAC4^{WT}. Severe β-fusion was present in 72% of HDAC4^{S69F} brains, and only 42% of HDAC4^{WT} brains. While these differences are not statistically significant, the increase in severity for HDAC4^{S69F} compared to HDAC4^{WT} correlates with the increased number of aggregates in Kenyon cell nuclei. These data illustrate the antagonistic involvement of HDAC4 aggregation in correct β-lobe development, and that this effect is dose-dependent.

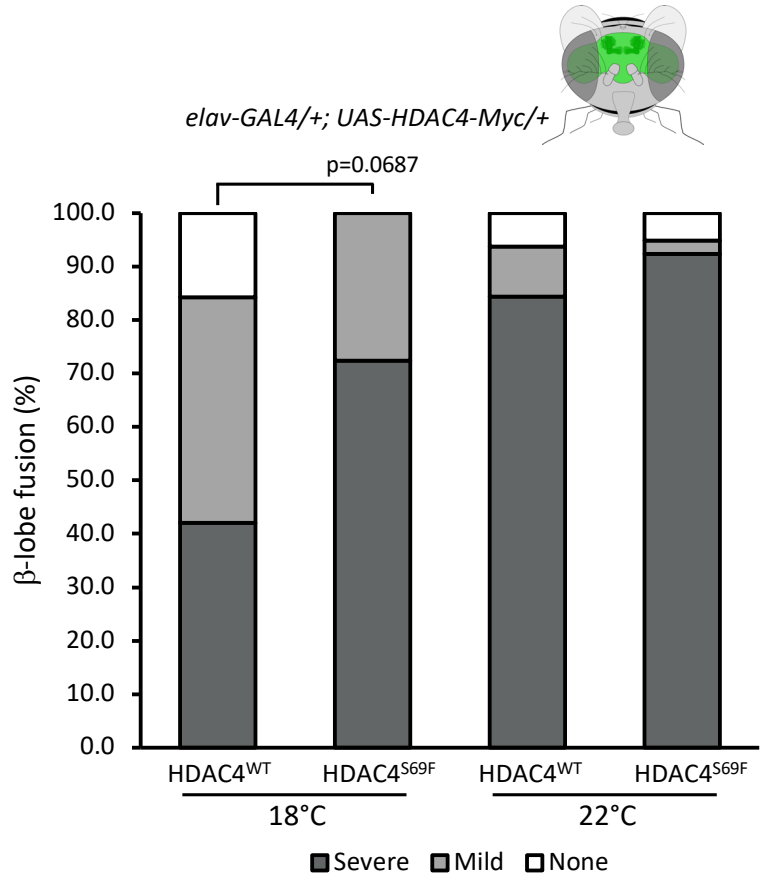

Figure 4.17 Comparison of β-lobe fusion phenotypes at 18 °Cand 22 °C illustrates a subtle increase in severity associated with expression of HDAC4^{S69F} compared to HDAC4^{WT}

Quantification of β-lobe fusion resulting from HDAC4 overexpression. HDAC4 expression was driven by *elav-GAL4* at either 18°C or 22°C, adult brains were processed for anti-FasII immunohistochemistry, and β-lobe fusion was scored. Severe and total β-fusion was not significantly increased by HDAC4^{S69F} expression (Fisher's exact test, severe β lobe fusion, n≥19 brains per genotype, p=0.0687 and p=0.056 respectively). The data at 22°C was previously displayed in Figure 4.16.

4.5.2. HDAC4 oligomerisation mutants reduce the severity of eye phenotypes arising from HDAC4 overexpression

Overexpression of HDAC4 in post-mitotic photoreceptors using the *GMR-GAL4* driver disrupts the development of the eye, resulting in what is termed a mild 'rough-eye phenotype', which is characterised by the disorganisation of ommatidia and bristles, as well as fusion and loss of pigmentation (Main *et al.*, 2021; Schwartz *et al.*, 2016; Tan *et al.*, 2024). This increases in severity upon restriction of HDAC4 to the nucleus (Main *et al.*, 2021; Tan *et al.*, 2024). To examine whether there is a correlation between nuclear aggregation and severity of eye phenotypes resulting from HDAC4 overexpression, $HDAC4^{WT}$ and $HDAC4^{mutant}$ were expressed using *GMR-GAL4* (Figure 3.1B) and their effect on eye development was examined (Figure 4.18).

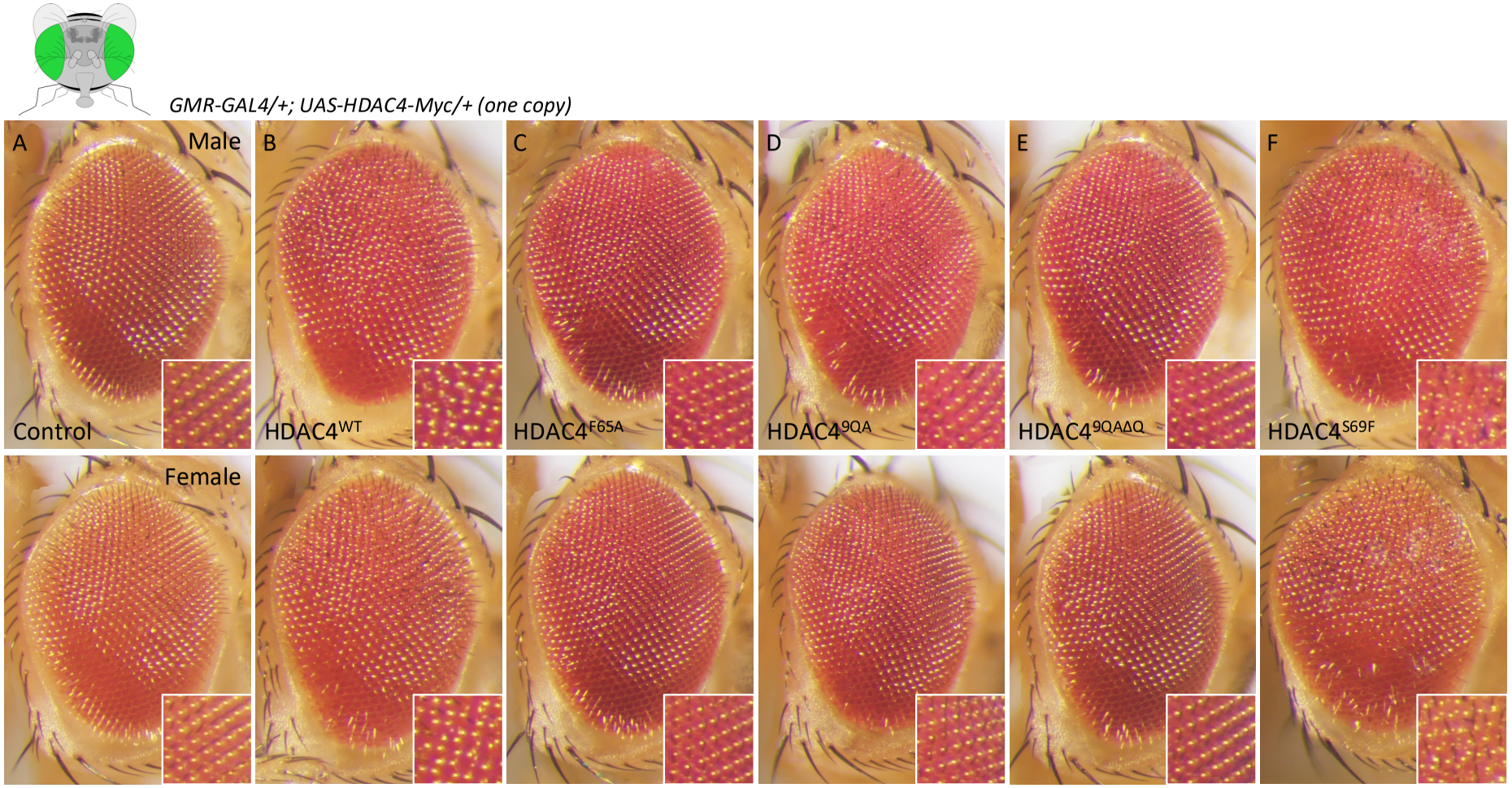

Figure 4.18 Overexpression of HDAC4 oligomerisation mutants alters *Drosophila* eye development
(A-F) Light microscopy images (110x magnification) of *Drosophila* eyes raised at 25°C. Top row, males; bottom row, females. Inset shows a magnified image of ommatidia. (A) Control is *GMR-GAL4/+*. (B-F) Flies harboured one copy of the driver (*GMR-GAL4/+*) and one copy of the transgene (*UAS-HDAC4/+*). (B) HDAC4^{WT} overexpression induced mild perturbation of the organisation of the adult eye, characterised by misalignment of ommatidia and bristles, which was reduced for HDAC4^{F65A} (C), HDAC4^{9QA} (D), and HDAC4^{9QAΔQ} (E). There was little difference between HDAC4^{WT} and HDAC4^{S69F} (F).

Both female and male eyes are presented in Figure 4.18. Eye colour is determined by a locus found on the X-chromosome; dosage compensation in *Drosophila* results in increased expression of genes on the X-chromosome in males, therefore an increase in pigmentation is observed in males (Section 1.2.1). Similarly, the *white* gene (*mini-white*) is included in these transgenic flies as a marker for selection of successful transgene incorporation, which is selected for by the presence of orange to red eyes (Section 10.1.5). The control flies presented in this figure are in the *wCS10* genetic background, in which flies carry a null mutation in the *white* gene, resulting in white eyes. Control flies are the progeny of *wCS10* white-eyed males crossed to red-eyed *GMR-GAL4* females, and therefore they only have one copy of *white* from the female parent, and as a result have a lower dosage of white expression compared to flies with the HDAC4 transgene, which have one copy of *white* from the female parent and one copy of *mini-white* with the HDAC4 transgene. Therefore, changes in eye colour between the control and HDAC4 flies are a result of transgene incorporation rather than HDAC4-Myc expression.

HDAC4^{WT} overexpression resulted in a mild rough eye phenotype compared to controls (Figure 4.18A-B), consisting of misalignment of ommatidia and misplacement of bristles, as previously observed (Schwartz *et al.*, 2016; Tan *et al.*, 2024). The severity of this was significantly reduced in HDAC4^{F65A}, HDAC4^{9QA} and HDAC4$^{9QA\Delta Q}$ expressing eyes, restoring the alignment of ommatidia to almost that of controls. The rescue mediated by HDAC4^{F65A} was particularly striking with no defects in alignment observed. In contrast, expression of HDAC4^{S69F} caused a rough eye phenotype, however this did not appear to differ significantly to that observed with HDAC4^{WT}.

As demonstrated in the mushroom body (Section 4.5.1) HDAC4^{WT} overexpression-induced phenotypes are dose-dependent, where severity increases upon increased transgene expression, as increasing the dose of HDAC4 overexpression by increasing the number of genomic insertions of the HDAC4 transgene exacerbated the eye phenotype (Schwartz *et al.*, 2016). Eyes shown in Figure 4.18 are from flies which harboured one genomic insertion each of the *GMR-GAL4* driver and *UAS-HDAC4-Myc* transgene, and only show subtle changes in severity, therefore to discern differences between each of the mutants, the level of HDAC4 expression was increased. Excessive expression of GAL4 results in a rough eye phenotype (Kramer & Staveley, 2003), which would interfere with determining any effect HDAC4-overexpression may have on eye development, therefore flies were generated that harboured only one copy of

the *GMR-GAL4* driver, and two of the *UAS-HDAC4-Myc* transgene (Appendix Section 10.1.6, Figure 10.6).

The severity of the HDAC4^{WT} overexpression-induced phenotype was significantly increased in the presence of two copies of the transgene compared to one (Figure 4.19D compared to 4.18B). Eyes presented with widespread fusion of ommatidia and absence of bristles, as well as loss of pigmentation, which was observed only at the boundary of the eye and edges of ommatidia (Figure 4.19B). Scanning electron microscopy revealed loss of structural integrity toward the centre of each ommatidium, appearing as a dimple, and emphasised the absence of boundaries between ommatidium (Figure 4.19E-F). Accordingly, the phenotypes resulting from expression of each of the mutants were also increased in severity upon increased copy number, except for HDAC4^{F65A} (Figure 4.19G-I), which appeared remarkably indistinguishable from control eyes. Ommatidial disorganisation increased for HDAC4^{9QA} and HDAC4$^{9QA\Delta Q}$, with increased loss of pigmentation and bristle organisation as well as central ommatidial dimpling (Figure 4.19J-O). Interestingly, ommatidia were not fused but the depth of the boundary between ommatidia was consistently shallower for HDAC4^{9QA} and HDAC4$^{9QA\Delta Q}$ compared to HDAC4^{F65A}. HDAC4$^{9QA\Delta Q}$ appeared to have more defined ommatidial boundaries compared to HDAC4^{9QA}, however no other significant differences between the two were evident. Scanning electron microscopy also demonstrated the severity of bristle disorganisation with occasions of up to three bristles emerging from the same pore. Eye development was significantly disrupted by 9QA-containing mutants compared to HDAC4^{F65A}. Increased copy number also exacerbated the difference between HDAC4^{WT} and HDAC4^{S69F}, where HDAC4^{S69F} had widespread ommatidial fusion and loss of pigmentation, as well as significant loss of bristles (Figure 4.19P-R). SEM revealed the severity of fusion, with dimpling of ommatidia still present and appearing to increase into holes toward the posterior of the eye.

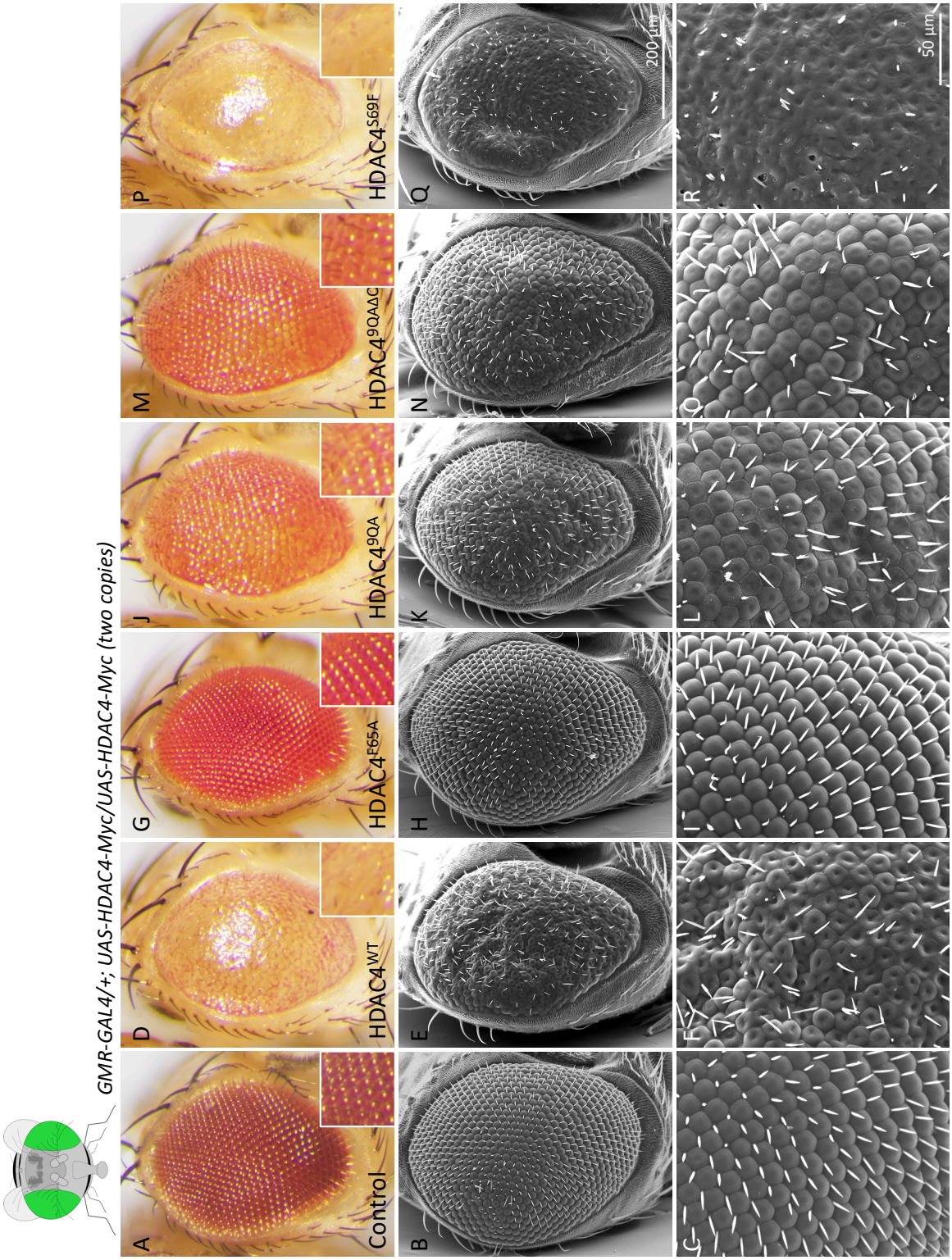

Figure 4.19 Increased dose of HDAC4 exacerbates differences in disruption of eye development between HDAC4 oligomerisation

Light microscopy (110x magnification) and scanning electron microscopy (250x and 800x magnification) images of *Drosophila* eyes raised at 25°C. Inset shows a magnified image of ommatidia. (A-C) Control is *GMR-GAL4/+; +/+*. Control eyes were uniformly aligned with respect to ommatidia and bristles, with wild-type pigmentation. (D-R) Flies harboured one copy of the driver (*GMR-GAL4/+*) and two copies of the transgene (*UAS-HDAC4/UAS-HDAC4*). HDAC4^{WT} overexpression induced severe widespread disorganisation of the adult eye, characterised by ommatidial fusion and loss of pigmentation (D-F), which was reduced for HDAC4^{F65A} (G-I), HDAC4^{9QA} (J-L), and HDAC4$^{9QA\Delta Q}$ (M-Q). Fusion was increased upon expression of HDAC4^{S69F} (P-R). Please note the control scanning electron microscopy images were obtained at a different time to the remainder of HDAC4-overexpression images, but under the same experimental conditions.

To quantify changes in the rough eye phenotype, a scoring system was generated and implemented (Methods Section 3.5.1, Table 3.10). This considered three key facets of eye development that can be reproducibly analysed using light microscopy, including bristle formation, ommatidia alignment and fusion, and pigmentation. Each eye could obtain a maximum score of 12, and these scores were calculated for each phenotype before converting to percentage severity (% severity) and averaging (Figure 4.20). Flies expressing HDAC4^{WT} scored 73% severity, and expression of HDAC4^{S69F} significantly increased this to 86%. F65A mutation strikingly reduced the rough eye phenotype with a score of 0%, compared to HDAC4^{9QA} and HDAC4$^{9QA\Delta Q}$ which scored 42% and 45% respectively. While HDAC4^{9QA} and HDAC4$^{9QA\Delta Q}$ both significantly reduced the wild-type overexpression induced phenotype, the difference between their scores was not statistically significant, confirming that the polyglutamine stretch (ΔQ) present in *Drosophila* HDAC4 does not have a particular role in disrupting eye development. These data suggest that the severity of HDAC4 overexpression-induced phenotypes in the *Drosophila* eye positively correlates with the ability of HDAC4 to oligomerise and form nuclear aggregates.

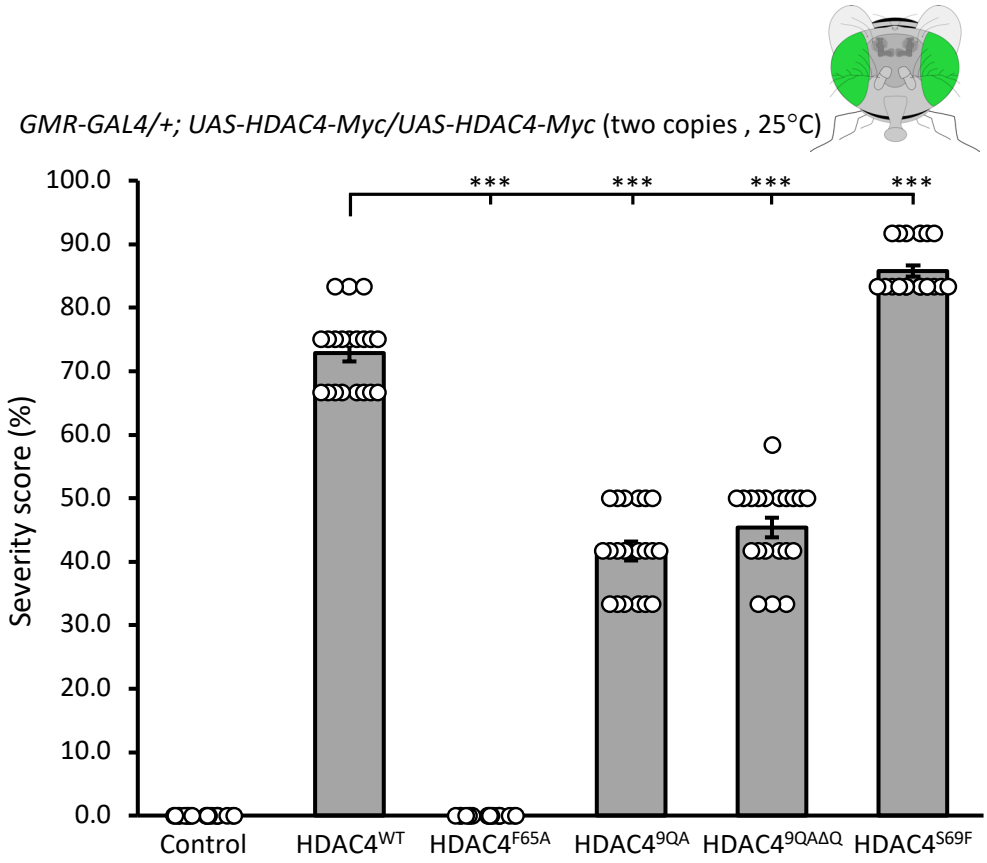

Figure 4.20 Implementation of a scoring system to characterise HDAC4-overexpression induced deficits in eye development resulting from expression of oligomerisation mutants

The severity of eye phenotypes resulting from HDAC4 expression under the control of *GMR-GAL4* at 25°C was scored as per Section 3.5.1. Flies were heterozygous for *GMR-GAL4* and homozygous for *HDAC4* (*GMR-GAL4/+, UAS-HDAC4/UAS-HDAC4*). Control is *GMR-GAL4/+; +/+*. Severity scores were converted to % severity and the average is displayed. Individual data points are represented as circles, and error bars indicate the SEM. n≥18 eyes per genotype. Severity was significantly reduced for each of HDAC4^{F65A}, HDAC4^{9QA} and HDAC4^{9QAΔQ} compared to HDAC4^{WT}, and severity was increased for HDAC4^{S69F} compared to HDAC4^{WT} (ANOVA, $F(5,112)=1642.19$, $p<0.0001$, post-hoc Tukey's HSD, ***$p<0.001$). There was no significant difference between HDAC4^{9QA} and HDAC4^{9QAΔQ} ($p=0.2507$).

4.6. Combination of HDAC4^{9QA} and HDAC4^{F65A} mutations does not further reduce aggregation or HDAC4 overexpression-induced phenotypes

While each of the F65A and 9QA mutations result in reduced aggregation of HDAC4 and less severe overexpression-induced developmental phenotypes, some aggregation in Kenyon cells was still observed. Aside from the complete rescue of the eye phenotype by HDAC4^{F65A}, expression of these mutants still resulted in mild developmental defects in the mushroom body

and eye. The HDAC4 hydrophobic core (addressed by the F65A mutation) and glutamine residues (addressed by the 9QA mutations) contribute differentially to tetramerisation (Section 1.8.1). Hydrophobic core formation via Phe-93 is required for hHDAC4 tetramer formation, while a number of glutamine residues contribute to stability of the tetramer surrounding the core (Guo *et al.*, 2007). Therefore, to further examine the contribution of Phe-65 and the nine glutamine residues to tetramerisation, an additional DmHDAC4 mutant was generated in which F65A and 9QA mutations were combined in the double mutant HDAC4$^{9QA\text{-}F65A}$, which was hypothesised to maximally destabilise tetramer formation and thus further reduce neurodevelopmental phenotypes which result from aggregate formation.

4.6.1. Expression of HDAC4$^{9QA\text{-}F65A}$ in *Drosophila*

Transgenic flies harbouring the Myc epitope-tagged *HDAC4$^{9QA\text{-}F65A}$* construct under UAS-control were generated (Section 3.1.1). As HDAC4^{9QA} was shown to have reduced total protein levels compared to HDAC4^{WT} (Section 4.3.2), protein levels of HDAC4$^{9QA\text{-}F65A}$ were assessed. Transgenes were pan-neuronally expressed with *elav-GAL4* and western blotting performed as previously described (Section 4.3.2). The HDAC4$^{9QA\text{-}F65A}$ double mutant migrated at the expected size of 144 kDa alongside the single mutants (Figure 4.21A). While HDAC4^{9QA} intensity remained reduced compared to HDAC4^{WT} (although in this case it did not quite reach significance), protein levels of the double mutant were variable, but on average similar to HDAC4^{WT} (Figure 4.21B).

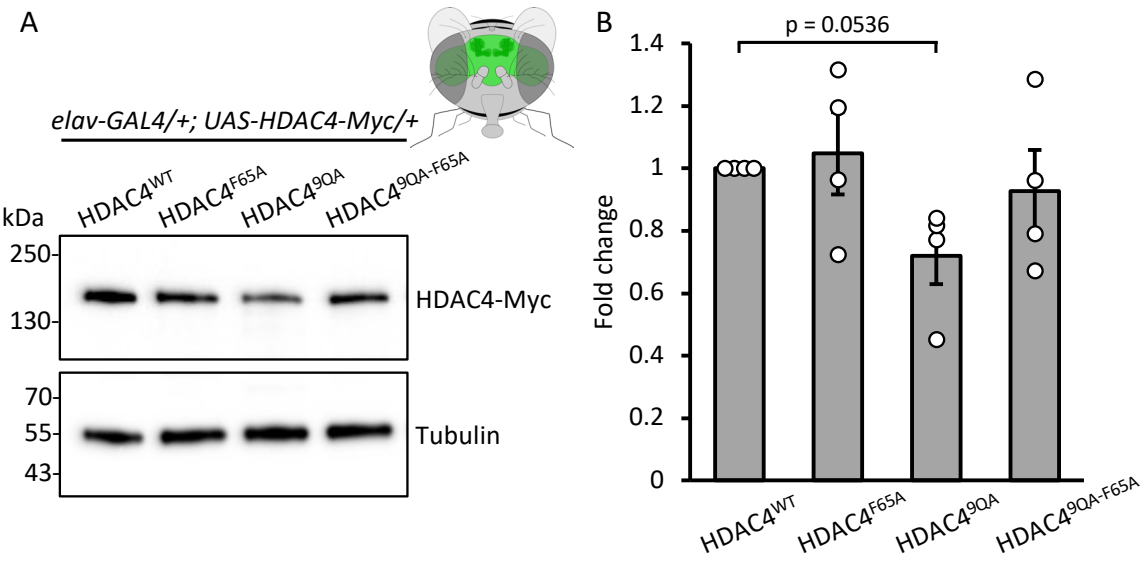

Figure 4.21 Combination of 9QA and F65A mutations does not significantly alter protein levels of HDAC4

(A) Western blot of *elav-GAL4* driven expression of $HDAC4^{WT}$ and $HDAC4^{mutant}$ in head whole-cell lysates (30 µg) using anti-Myc and anti-alpha-tubulin antibodies. Flies were raised at 25 °C. The protein bands were of the expected size of ~144 kDa. (B) Quantification of HDAC4 band intensity normalised to tubulin (n=4 blots). The average fold change relative to $HDAC4^{WT}$ is displayed, with individual data points represented as circles. Error bars indicate the SEM. $HDAC4^{9QA}$ was almost significantly reduced compared to $HDAC4^{WT}$, while there was no difference between each of $HDAC4^{F65A}$ and $HDAC4^{9QA\text{-}F65A}$ compared to $HDAC4^{WT}$ (One sample t-test compared to $HDAC4^{WT}$, $HDAC4^{9QA}$ $t_{(3)}$=3.0915, p=0.0536; $HDAC4^{F65A}$ $t_{(3)}$=0.3717, p=0.7348; $HDAC4^{9QA\text{-}F65A}$ $t_{(3)}$=0.5502, p=0.6205). Full blots used for quantification are found in Appendix 10.2.3, Figure 10.11.

4.6.2. $HDAC4^{9QA\text{-}F65A}$ does not further reduce aggregation in Kenyon cells

The ability of $HDAC4^{9QA\text{-}F65A}$ to aggregate in Kenyon cell nuclei was assessed as previously described (Section 4.4.2). $HDAC4^{WT}$ and $HDAC4^{mutant}$ expression was induced during adulthood under the control of *OK107-GAL4* via the TARGET system, and brains dissected and immunostained with antibodies against the Myc tag, and endogenous MEF2 (Figure 4.22). While $HDAC4^{9QA\text{-}F65A}$ localised to both nuclei and cytoplasm of Kenyon cells as well as the calyx (Figure 4.22D), nuclear staining was less intense and cytoplasmic haloes were observed more frequently compared to each of $HDAC4^{9QA}$ (Figure 4.22B), $HDAC4^{F65A}$ (Figure 4.22C), and $HDAC4^{WT}$ (Figure 4.22A). Despite this, quantification demonstrated no significant reduction in co-localisation of $HDAC4^{9QA\text{-}F65A}$ and MEF2 in nuclear aggregates compared to each single mutant alone, with an average of 31 aggregates per section compared to 41 and 37 for $HDAC4^{9QA}$ and $HDAC4^{F65A}$ respectively (Figure 4.22I). It is noted that the intensity of $HDAC4^{9QA}$ and $HDAC4^{9QA\text{-}F65A}$ in Figure 4.22B and D are reduced compared to $HDAC4^{WT}$; given that $HDAC4^{9QA\text{-}F65A}$ had similar protein levels to $HDAC4^{WT}$ in Figure 4.21, this may be reflective of an increase in axonal distribution of $HDAC4^{9QA\text{-}F65A}$ and $HDAC4^{9QA}$, where localisation to the axon bundles of the mushroom body in the anterior of the brain reduces intensity in the Kenyon cell bodies in the posterior.

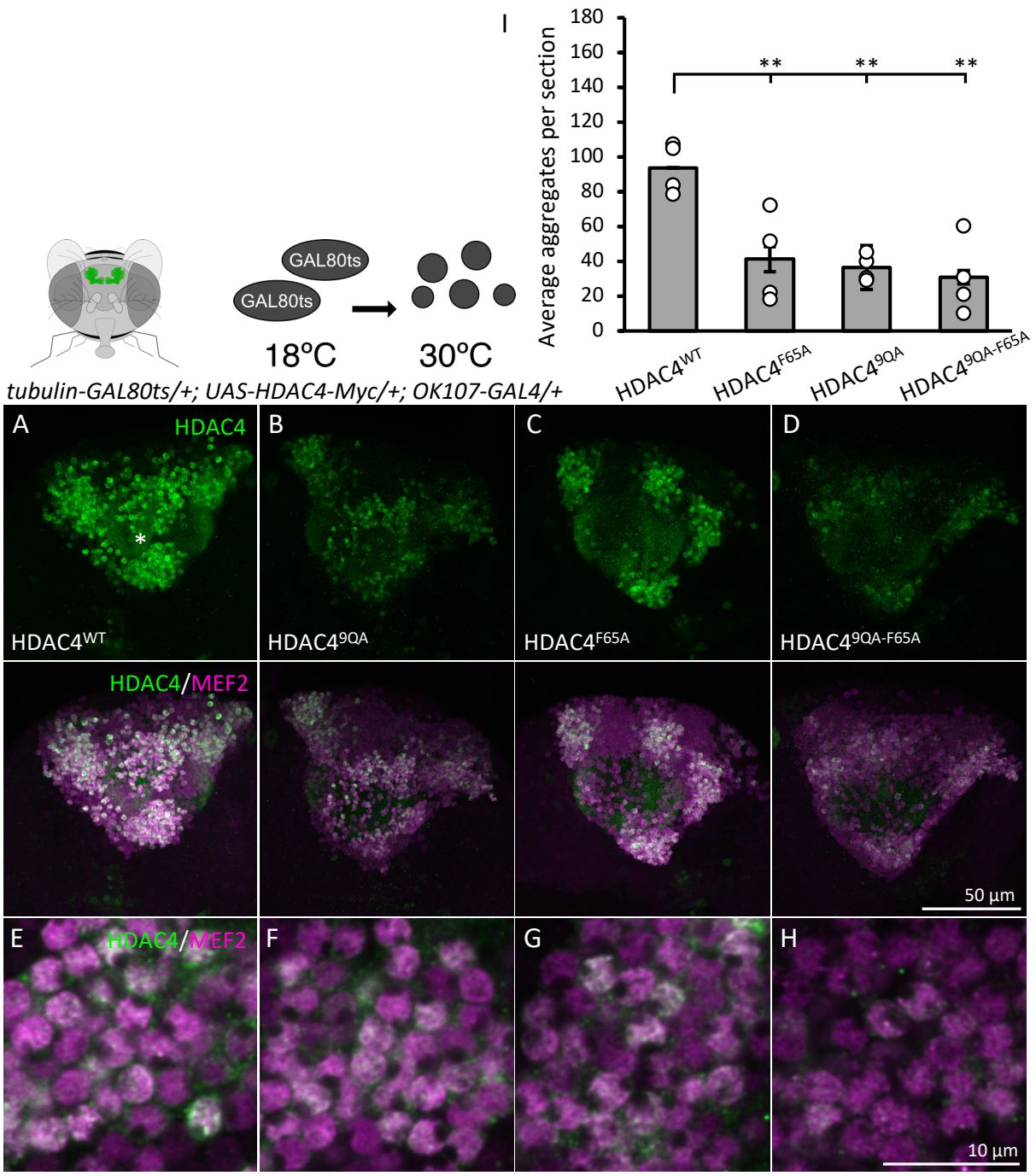

Figure 4.22 Combination of 9QA and F65A mutations does not further reduce aggregation of HDAC4 in Kenyon cells

(A-D) Maximum projections of optical sections through the Kenyon cell layer in the posterior of the whole-brain of flies expressing HDAC4^{WT} or HDAC4^{mutant} under the control of *OK107-GAL4* in the presence of the TARGET system. Flies were raised at 18 °C until eclosion, where adults were transferred to 30 °C for three days to induce HDAC4 expression. HDAC4^{WT} (green) was observed in Kenyon cell nuclei where endogenous MEF2 (magenta) was present, white indicates co-distribution. HDAC4^{WT} was also localised to dendrites, observed in the calyx (*). HDAC4^{9QA} and HDAC4$^{9QA-F65A}$ were observed at a reduced intensity compared to HDAC4^{WT} and HDAC4^{F65A} but still localised to the nucleus and cytoplasm of Kenyon cells as well as the calyx. (E-H) Single optical sections (0.5 µm) of Kenyon cells. Aggregation of each of HDAC4^{9QA}, HDAC4^{F65A}, and HDAC4$^{9QA-F65A}$ was reduced compared to HDAC4^{WT}, observed as fewer instances of white punctate foci of HDAC4 and MEF2. (I) Aggregates of HDAC4 that co-localised with MEF2 were counted through the Kenyon cell layer (as seen in A-D) for

10 optical sections spaced 1µm apart as per Section 3.4.6, n=4 brains per genotype. The mean is plotted, and the average number of aggregates per section per brain are plotted as individual points. Error bars indicate the SEM. Aggregate number was not further reduced for HDAC4$^{9QA\text{-}F65A}$ compared to each of HDAC4^{9QA} and HDAC4^{F65A} (ANOVA, F(3,12)=9.7956, p=0.00151, post-hoc Tukey's HSD, p=0.8533 and p=0.9716 respectively. **p<0.01). There was no significant difference between each of HDAC4^{9QA}, HDAC4^{F65A}, and HDAC4$^{9QA\text{-}F65A}$.

4.6.3. HDAC4$^{9QA\text{-}F65A}$ expression does not result in less severe mushroom body defects than the single mutants

Despite no significant reduction in aggregation in Kenyon cells, neurodevelopmental phenotypes resulting from HDAC4$^{9QA\text{-}F65A}$ overexpression were still assessed. Mushroom body phenotypes resulting from expression of HDAC4$^{9QA\text{-}F65A}$ were examined as previously described (Section 4.5.1). HDAC4$^{9QA\text{-}F65A}$ was expressed pan-neuronally throughout development under the control of *elav-GAL4* at 22°C; adult flies were dissected and brains were immunostained for FasII and imaged from the anterior orientation. As previously observed, the dominant phenotype resulting from HDAC4^{WT} overexpression was β-lobe fusion (Table 4.3, Figure 4.23). β-lobe fusion was observed in 60% of brains expressing HDAC4$^{9QA\text{-}F65A}$ which was intermediate between HDAC4^{9QA} and HDAC4^{F65A}, each presenting with 80% and 50% respectively. In contrast, severe fusion was increased to 45% with the double mutant compared to 30% and 25% for HDAC4^{9QA} and HDAC4^{F65A} individually. However, these changes in level of severity of β-lobe fusion are subtle and none reached statistical significance. All three mutants significantly reduced severe fusion compared to HDAC4^{WT}.

Table 4.3 Frequency of mushroom body phenotypes resulting from the combination of 9QA and F65A mutations at 22°C

(% of brains)	Con	HDAC4^{WT}	HDAC4^{9QA}	HDAC4^{F65A}	HDAC4$^{9QA\text{-}F65A}$
α thinning	0	35	0	10	0
α missing	0	0	0	0	0
β thinning	0	25	5	0	0
β missing	0	0	5	5	5
β fusion	**0**	**95**	**80**	**50**	**60**
Mild	0	0	50	25	15
Severe	0	95	30	25	45
Guidance	0	0	10	5	5
n	20	20	20	20	20

Expression of each denoted *HDAC4* transgene was driven by *elav-GAL4*; virgin *elav-GAL4* female flies were crossed to males harbouring the *HDAC4* transgene and adult progeny of this cross were dissected and their brains immunostained for FasII to assess mushroom body lobe development. Flies were raised at 22 °C. Instances of defects in morphology were scored for n=20 brains per genotype as per Section 3.4.7 and are displayed as the % of brains with the indicated phenotype. Control (con) is *elav-GAL4/+*. Percentages may not sum to 100 due to rounding.

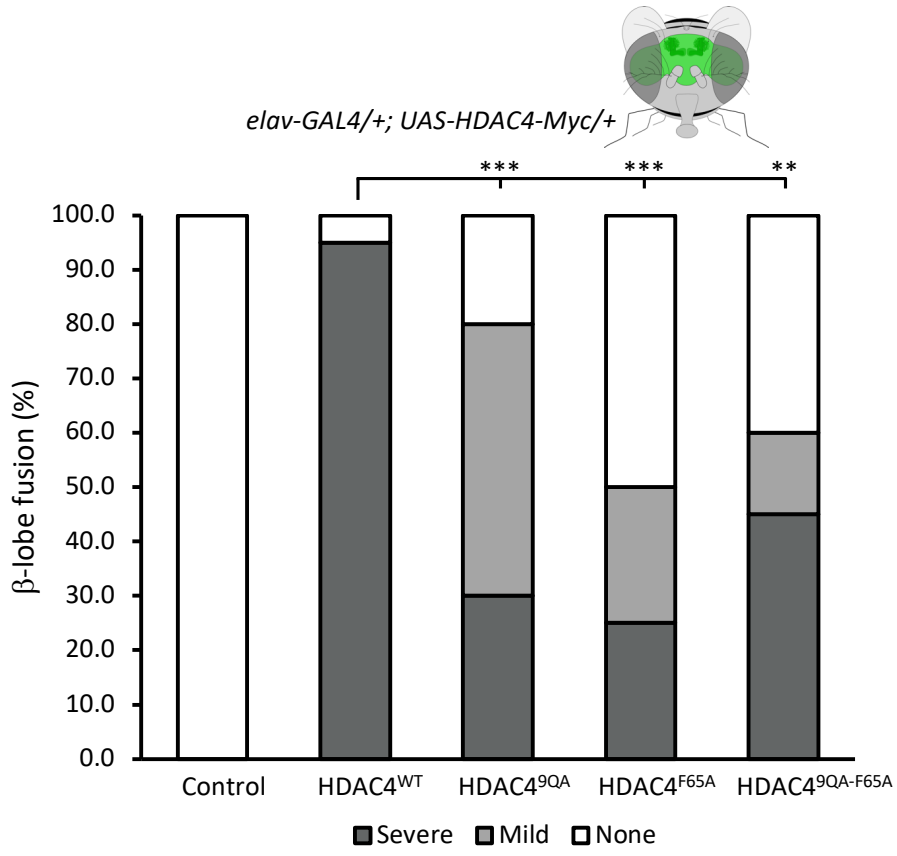

Figure 4.23 Combination of 9QA and F65A mutations does not further reduce the severity of β-lobe fusion in the mushroom body

Quantification of β-lobe fusion resulting from HDAC4 overexpression. HDAC4 expression was driven by *elav-GAL4* at 22°C, adult brains were processed for anti-FasII immunohistochemistry, and β-lobe fusion was scored. Control is *elav-GAL4/+*. n=20 brains per genotype. There was no statistically significant difference in severe β-lobe fusion associated with expression of $HDAC4^{9QA-F65A}$ compared to each of $HDAC4^{9QA}$ and $HDAC4^{F65A}$ (Fisher's exact test, severe β-lobe fusion, **p<0.01, ***p<0.0001. p=0.5145 and p=0.3203 respectively).

4.6.4. $HDAC4^{9QA-F65A}$ expression results in an eye phenotype equivalent to $HDAC4^{F65A}$

The impact of expression of $HDAC4^{9QA-F65A}$ on eye development in comparison to the two single mutants was examined as previously described (Section 4.5.2). No significant difference between each of $HDAC4^{9QA}$, $HDAC4^{F65A}$ and $HDAC4^{9QA-F65A}$ was observed in flies harbouring one insertion of the HDAC4 transgene (Appendix 10.2.10, Figure 10.18). Upon expression from two genomic insertions, $HDAC4^{9QA}$ resulted in a loss of pigmentation and significant disorganisation of ommatidia (Figure 4.24C), with both effects less severe upon expression of $HDAC4^{9QA-F65A}$ (Figure 4.24E), which had a phenotype comparable to $HDAC4^{F65A}$ expression (Figure 4.24D, F).

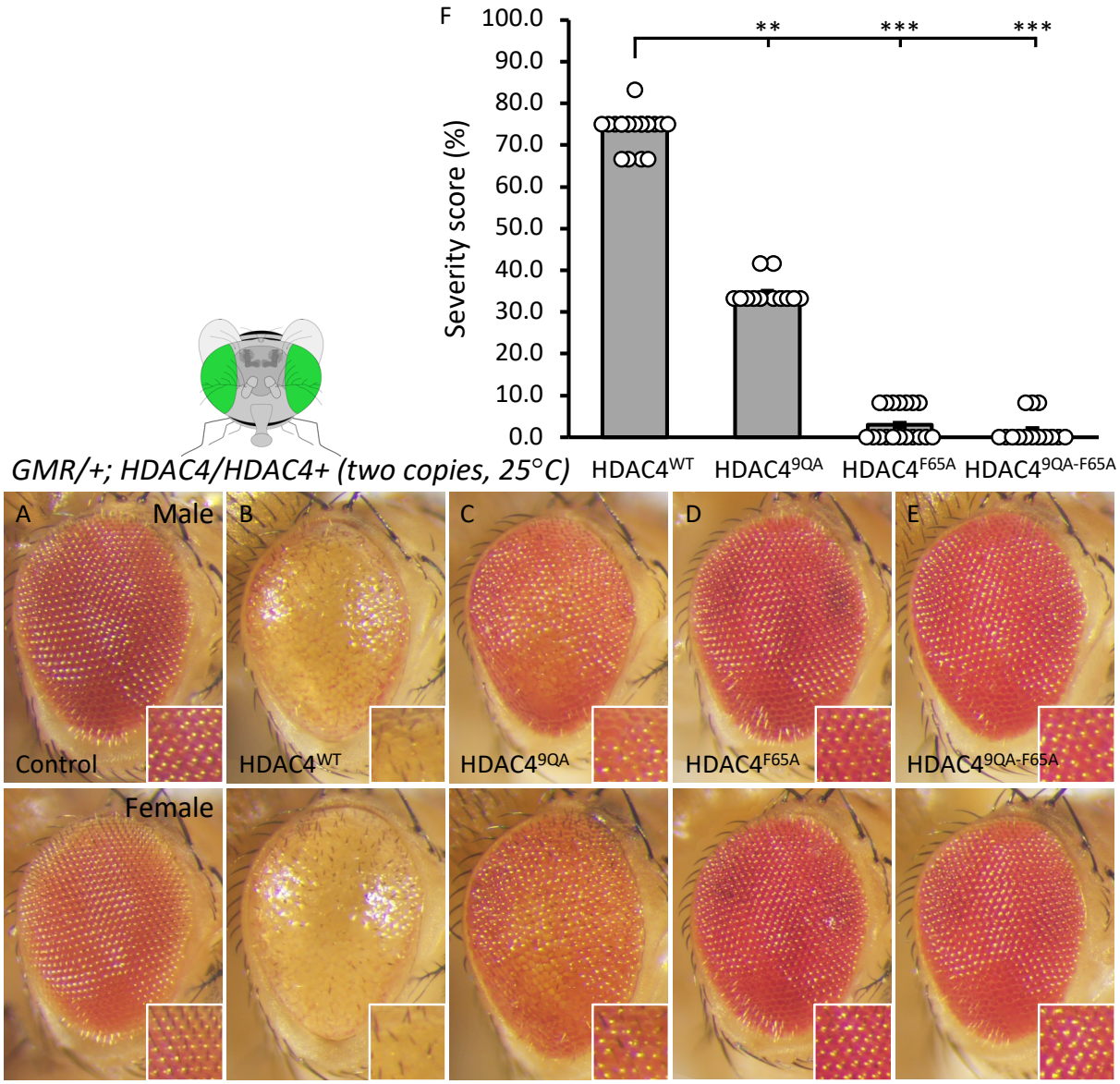

Figure 4.24 Combination of 9QA and F65A mutations reduces the severity of the eye defects to that of HDAC4^{F65A}

(A-E) Light microscopy (110x magnification) images of *Drosophila* eyes raised at 25°C. Flies harboured one copy of the driver and two copies of the *HDAC4* transgene *(GMR-GAL4/+; UAS-HDAC4/UAS-HDAC4*). HDAC4^{WT} overexpression induced severe widespread disorganisation of the adult eye, characterised by ommatidial fusion and loss of pigmentation (B), which was reduced by varying degrees by each of HDAC4^{9QA} (C), HDAC4^{F65A} (D), and HDAC4$^{9QA-F65A}$ (E). Top row, males; bottom row, females. Inset shows a magnified image of ommatidia. (F) Quantification of severity of eye phenotypes as per Methods 3.5.1. Severity scores were converted to % severity and the average is displayed. Individual data points are represented as circles, and error bars indicate the SEM. n≥19 eyes per genotype. There was no significant difference between HDAC4^{F65A} and HDAC4$^{9QA-F65A}$ (Kruskal-Wallis test, $H_{(3)}$=72.21, p<0.001, post-hoc Dunn's test, p=0.5719. **p<0.01, ***p<0.001).

4.7. Discussion

Dysregulation of HDAC4 subcellular distribution is observed in a number of neurological diseases, typically resulting in increased nuclear localisation of HDAC4 (Section 1.6.2), however it is unknown whether this distribution is causative of neuronal dysfunction. In a *Drosophila* model, HDAC4 overexpression impaired long-term memory and the development of the adult eye and mushroom body (Fitzsimons *et al.*, 2013; Main *et al.*, 2021; Schwartz *et al.*, 2016; Tan *et al.*, 2024). These phenotypes appeared to be a result of a nuclear activity of HDAC4, as nuclear restriction increased phenotype severity (Main *et al.*, 2021; Tan *et al.*, 2024), and this was not an effect of HDAC4 overexpression as knockdown of endogenous HDAC4 and replacement with the nuclear-localised mutant still resulted in significant defects in the development of the mushroom body (Tan *et al.*, 2024). In both cases, small nuclear aggregates of HDAC4 were observed that sequestered the transcription factor MEF2 (Fitzsimons, 2015; Main *et al.*, 2021; Tan *et al.*, 2024), and moreover, aggregate number correlated with phenotype severity (Tan *et al.*, 2024), suggesting that HDAC4 aggregates may be mediating defects in neuronal development.

This chapter aimed to address this correlation and used a *Drosophila* model to investigate oligomerisation and aggregation of HDAC4 in neurons, and whether this correlated with errors in neuronal development in two different tissues. HDAC4 forms tetramers in solution (Guo *et al.*, 2007) and the region that mediates this is highly conserved. Deletion of the N-terminus of HDAC4 including this region prevented aggregation of HDAC4 in HeLa cells (Kirsh *et al.*, 2002), therefore it was hypothesised that tetramerisation via the N-terminal helix is a requirement of aggregation *in vivo*. Mutations predicted to destabilise tetramerisation reduced oligomerisation and aggregation of HDAC4, and this correlated with a reduction in the severity of HDAC4 overexpression-induced phenotypes. Conversely, the S69F mutation which was hypothesised to stabilise tetramerisation increased aggregation and severity of phenotypes. The data presented here therefore show that HDAC4 aggregation is dependent on its ability to oligomerise, and this is positively correlates with the severity of HDAC4 overexpression-induced disruption of neuronal development.

4.7.1. Oligomerisation of HDAC4 contributes to higher order multimerisation and subsequent aggregation of HDAC4

4.7.1.1. The oligomerisation domain of human and *Drosophila* HDAC4 is highly conserved

Expression of both human and *Drosophila* HDAC4 results in aggregate formation in Kenyon cell nuclei (Fitzsimons *et al.*, 2013; Main *et al.*, 2021; Tan *et al.*, 2024) and similar aggregates of HDAC4 and MEF2 have been observed in cell culture (Chan *et al.*, 2003; Miska *et al.*, 1999), together suggesting a conserved mechanism of aggregation. A dimerisation domain was previously localised to the N-terminus of hHDAC4 via *in vitro* binding assays (Wang & Yang, 2001), and deletion of this region prevented nuclear aggregation in HeLa cells (Kirsh *et al.*, 2002), suggesting that aggregation is mediated by the N-terminus of hHDAC4. Guo *et al.* (2007) described the tetramerisation of the N-terminus of hHDAC4 in solution, however it was unclear whether tetramerisation persisted *in vivo*, and whether this contributed to aggregation.

Computational analysis suggested that the dimerisation domain formed a coiled coil structure (Kirsh *et al.*, 2002), and indeed this region forms an α-helix (Guo *et al.*, 2007), however it oligomerises in an unusual way; the four helix bundle consists of two antiparallel helices that associate via the formation of a small hydrophobic core (Figure 1.13). This core involves three residues that are conserved across species, suggesting it is crucial to HDAC4 function. Importantly, substitution of a single phenylalanine residue within the core abolished tetramer formation in solution, and conversely, substitution of a nearby residue for phenylalanine extended the core and stabilised tetramerisation. It was hypothesised that tetramerisation of HDAC4 was a prerequisite of aggregate formation *in vivo*, and therefore a series of mutants were developed based on this study to examine the oligomerisation and aggregation of HDAC4 in *Drosophila*.

Two of these mutants examined the contribution of the hydrophobic core, with F65A orthologous to the mutation that destabilised, and S69F orthologous to the mutation that stabilised HDAC4 tetramerisation in solution (Guo *et al.*, 2007). In addition to the hydrophobic core, numerous intra-helical and inter-helical polar interactions occur between glutamine residues, which are also thought to stabilise tetramer formation (Guo *et al.*, 2007). The 9QA mutation substituted nine glutamines conserved between *Drosophila* and human HDAC4 for alanine, and was hypothesised to destabilise the interactions required for α-helix formation, as well as tetramerisation. The *Drosophila* HDAC4 sequence has an additional polyglutamine

stretch C-terminal to the hydrophobic core region that is not conserved in human HDAC4. Similar glutamine repeat sequence regions have been shown to induce protein aggregation, and are frequently observed in neurodegenerative disease, particularly arising from CAG expansions (Michelitsch & Weissman, 2000). Therefore this region in DmHDAC4 was deleted in addition to the 9QA mutation (9QAΔQ) to determine its contribution to aggregation. As demonstrated by co-immunoprecipitation assays with wild-type GFP-tagged HDAC4, each of the F65A, 9QA and 9QAΔQ mutations decreased, and S69F increased oligomerisation, confirming that the mechanism of tetramerisation is conserved and persists with full-length HDAC4.

Changes in oligomerisation correlated with changes in aggregation; mutations that reduced oligomerisation reduced nuclear HDAC4 aggregation in the Kenyon cells of the adult brain and the basal cells of the larval eye disc, while oligomer stabilisation increased aggregation. These data confirm that oligomerisation of HDAC4 contributes significantly to its aggregation *in vivo*. It is noted that the reduced protein levels of 9QA-containing mutants may confound these findings, and this is further discussed in Section 4.7.2. Furthermore, 9QA-containing mutants had a punctate distribution within the cytoplasm of basal cells of the larval eye disc compared to HDAC4^{F65A}, which was relatively uniform. This result suggests that HDAC4 may form cytoplasmic aggregates, which have previously been observed before under various conditions in cell culture (Cernotta *et al.*, 2011; Fischle *et al.*, 2002; Grégoire & Yang, 2005; Grozinger & Schreiber, 2000; Kirsh *et al.*, 2002; Mielcarek, Landles*, et al.*, 2013; Paroni *et al.*, 2004; Wang *et al.*, 2000; Wang & Yang, 2001). In addition, this suggests that the 9QA-containing mutants may not reduce HDAC4 nuclear aggregation exclusively via changes in oligomerisation, but may in part be mediated by changes in dose and/or subcellular distribution. This is further discussed in Section 4.7.2.

These data support a model wherein HDAC4 tetramerisation facilitates the formation of higher order homo-oligomers that subsequently aggregate in nuclei (Figure 4.25). While it is evident that the hydrophobic core and glutamine residues are important in aggregate formation, the specific mechanism through which aggregates form beyond oligomerisation remains unclear. This is further discussed in Section 4.7.5. Moreover, it is unclear whether the native fold of HDAC4 as well as its tetramer state, is maintained in aggregates. Given the significant reduction in aggregate formation for the oligomerisation mutants, it is likely that tetramerisation

is a precursor event to aggregate formation, and therefore targeting HDAC4 tetramerisation is likely to reduce nuclear aggregation of HDAC4.

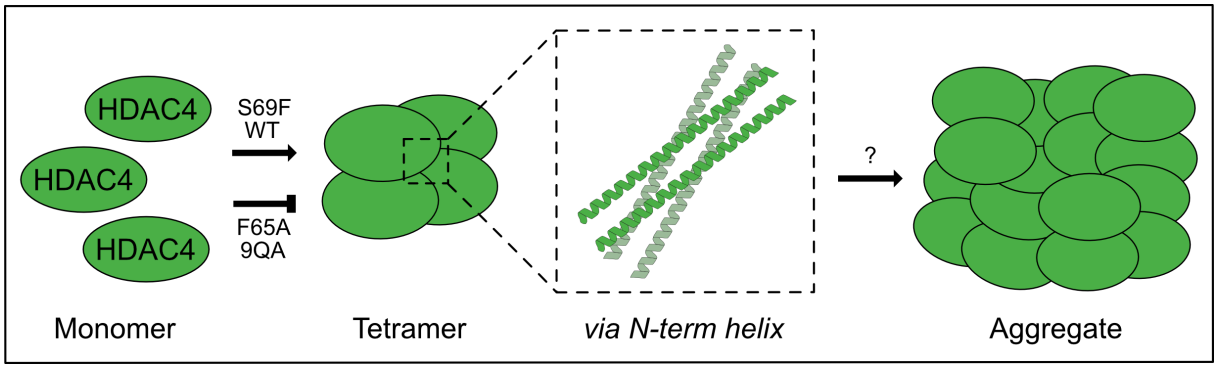

Figure 4.25 HDAC4 tetramerisation is a requirement of its aggregation *in vivo*
Schematic diagram of a model demonstrating that tetramerisation of HDAC4 via its N-terminal α-helix is a precursor event to aggregate formation. Wild-type HDAC4 or the S69F mutant can form tetramers, and therefore aggregate, while F65A and 9QA mutations prevent tetramer formation and subsequent aggregation. *This figure is an original artwork.*

Following the completion of these experiments, a follow-up study to that by Guo *et al.* (2007) was published (Dai *et al.*, 2024). This study used structural, biochemical, and mutagenesis assays to determine that when the N-terminus of hHDAC4 is bound by the HDAC-interacting domain of MEF2, HDAC4 forms a dimer that facilitates chromatin looping (Dai *et al.*, 2024). Dimerisation of HDAC4 was mediated through the formation of a hydrophobic core involving Phe-93, identical to that which mediates tetramerisation (Guo *et al.*, 2007). As Phe-93 is important in core formation for both the HDAC4 dimer and tetramer, this study remains consistent with the findings presented here, where F65A mutation disrupts oligomerisation of HDAC4, whether that be dimerisation or tetramerisation. Interestingly, Dai *et al.* (2024) observed a second dimerisation interface, and they hypothesised that this may facilitate formation of tetramer or higher-order complexes of HDAC4 when bound to MEF2. The mechanism of this interface was not further delineated, but it is possible that this may facilitate aggregation of HDAC4 *in vivo*. This is further discussed in Section 5.6.5.

4.7.1.2. Limitations of analyses in the presence of endogenous HDAC4

An important limitation of the current study is the presence of endogenous HDAC4. Upon overexpression in Kenyon cells, nuclear aggregates of HDAC4^{WT}-Myc sequestered endogenous HDAC4 (visualised with HDAC4::GFP). The association of transgene and

endogenous HDAC4 together in aggregates suggests that endogenous (wild-type) HDAC4 may be able to stabilise aggregation of mutant HDAC4 (Figure 4.26). This significantly limits the functional analyses of HDAC4 oligomerisation that can be performed *in vivo*, as absolute shifts from oligomeric/aggregated to monomeric species of HDAC4 will not be observed in the presence of endogenous wild-type HDAC4.

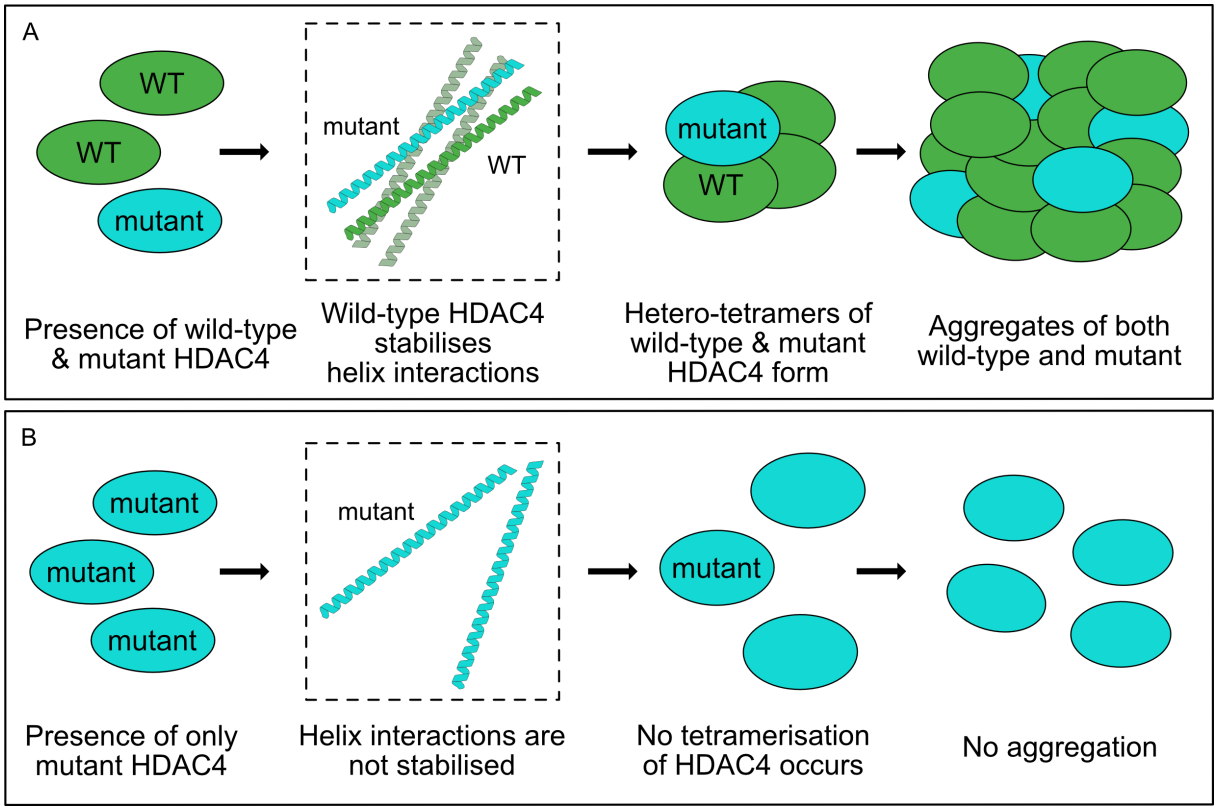

Figure 4.26 Implications of the presence of endogenous/wild-type HDAC4 for the characterisation of HDAC4 tetramerisation mutants
Schematic diagram of a model demonstrating that (A) the presence of endogenous (wild-type) HDAC4 stabilises aggregation of mutant HDAC4. (B) In the absence of a pool of wild-type HDAC4, mutant HDAC4 (i.e. F65A, 9QA or 9QAΔQ) is unable to tetramerise and therefore form aggregates. *This figure is an original artwork.*

In agreeance with this, low level co-immunoprecipitation of HDAC4^{F65A}, HDAC4^{9QA} and HDAC4^{9QAΔQ} with wild-type GFP-HDAC4^{WT} was detected, and this was consistent with the reduction in co-immunoprecipitation of hHDAC4^{F93D}-Myc with FLAG-hHDAC4^{WT} compared to hHDAC4^{WT}-Myc observed by Dai *et al.* (2024). Accordingly, absolute loss of aggregation in Kenyon cells was also not observed upon expression of these three mutants. It is likely that the small aggregates observed in brains of flies expressing the HDAC4 oligomerisation mutants consist of both endogenous HDAC4 and HDAC4^{mutant}; these aggregates arise from

multimerisation of HDAC4 tetramers, and it is hypothesised that these tetramers consist predominantly of endogenous HDAC4 (Figure 4.26A). As endogenous HDAC4 is capable of hydrophobic core formation as well as forming stabilising polar interaction networks, it is able to support inclusion of HDAC4^{mutant} within oligomers, enabling its sequestration within aggregates. Conversely in the absence of endogenous HDAC4, it is hypothesised that HDAC4^{mutant} tetramers would not be able to form sufficient interactions to oligomerise, and no aggregates would be observed (Figure 4.26B). Therefore, in this system the ability of each mutant to oligomerise and aggregate is likely overestimated. This is further confirmed by the 9QA-F65A mutant; it was hypothesised that if residual aggregation is instead a result of more transient tetramerisation that this mutant would maximally destabilise tetramer formation and thus further reduce aggregation, however no significant reduction in aggregation was observed.

To overcome these limitations, an obvious solution would be to generate HDAC4 knockout flies and replace endogenous wild-type HDAC4 with mutant transgene HDAC4, however RNAi-mediated knockdown of HDAC4 is largely embryonic lethal in *Drosophila* (Zeremski *et al.* (2003); Dr Helen Fitzsimons, unpublished data). Conditional knockout of HDAC4 in the mouse forebrain is viable (Kim *et al.*, 2012), suggesting that a conditional knockout in the brain of flies may be viable, however this does not allow for differentiation between developmental and degenerative effects of HDAC4 loss. Due to these limitations, a study performed in parallel with this study in this laboratory used genetic tools to deplete endogenous HDAC4, and replaced it with transgene HDAC4 in a spatially and temporally controlled manner, which enabled functional dissection of HDAC4 (Tan *et al.*, 2024). This was technically challenging requiring significant optimisation to tailor levels of gene expression as well as a sustained effort to combine many transgenes into a single fly line. The conditions required to successfully replace endogenous HDAC4 with transgene HDAC4 have now been established and could be used to further validate the data presented here. Alternatively, an HDAC4 CRIMIC line which utilises the T2A-GAL4 system (Lee *et al.*, 2018) has since been developed (CR70828) and would be a more effective way to determine the changes in oligomerisation and aggregation of HDAC4 in the absence of endogenous HDAC4. The T2A-GAL4/CRIMIC system involves insertion of GAL4 within an early coding region of a gene of interest such that it effectively knocks out the gene, and expresses GAL4 under the control of its endogenous regulatory regions (Lee *et al.*, 2018). Expression of HDAC4^{mutants} in these conditions would enable examination of aggregation in the absence of endogenous HDAC4, and characterisation of the endogenous role of tetramerisation of HDAC4. Importantly, understanding the role

tetramerisation plays in canonical HDAC4 function will inform on the viability of targeting tetramerisation for the development of therapeutics that reduce HDAC4 aggregation.

Finally, while this section focuses on the limitations of an overexpression model in the presence of endogenous HDAC4, this model also recapitulates some aspects of events occurring in a human disease context. Seven individuals presenting with 2q37 deletion syndrome were identified to have heterozygous *de novo* missense mutations within the 14-3-3 binding site of HDAC4 (Wakeling *et al.*, 2021). It has widely been observed that mutations within the 14-3-3 binding site of HDAC4 result in nuclear accumulation (Section 1.5.1.3). While only half of the HDAC4 protein produced in these individuals is expected to have increased nuclear localisation, given the nuclear accumulation of HDAC4::GFP upon overexpression of $HDAC4^{WT}$ it is hypothesised that mutant HDAC4 may induce nuclear accumulation of wild-type in these patients, exacerbating the severity of phenotypes in a dominant negative manner. Similarly, another case presented with an insertion that resulted in a truncated HDAC4 without a nuclear export sequence, and this accumulated in nuclei (Sando *et al.*, 2012; Williams *et al.*, 2010); it is likely that this truncated form also sequesters wild-type HDAC4 in nuclei. It is therefore essential to consider dominant negative effects that may amplify phenotypic severity associated with mutations that alter the subcellular distribution and potentially aggregation of HDAC4 in heterozygous individuals.

4.7.2. Glutamine residues are critical to maintaining protein levels of HDAC4

An unexpected finding was the reduced protein levels of HDAC4 associated with the 9QA mutation. The same reduction was not observed for F65A or S69F mutations, suggesting it is an effect independent of HDAC4 oligomerisation. It is unlikely that the reduced protein level is a result of transcriptional regulation, as expression of both wild-type and mutant HDAC4 was mediated by the UAS/GAL4 system. It is also unlikely that the reduction was a result of the introduction of a novel mutation during the generation of transgenic flies, as it occurred in two independently generated lines ($HDAC4^{9QA}$ and $HDAC4^{9QA\Delta Q}$). Interestingly, the combination of 9QA and F65A mutations did not significantly decrease protein levels compared to $HDAC4^{WT}$, suggesting that there may be a biological explanation for the reduction in protein levels that is modulated in part by oligomerisation of HDAC4.

While it appears that HDAC4^{9QA} and HDAC4$^{9QA\Delta Q}$ reduce aggregation of HDAC4, such aggregation is likely to be dose dependent as aggregate number increased with increased nuclear localisation (Tan *et al.*, 2024), and expression of HDAC4^{WT} induced aggregation of endogenous HDAC4. The reduced protein level of each of HDAC4^{9QA} and HDAC4$^{9QA\Delta Q}$ therefore confounds determination of the effect of these mutations on HDAC4 aggregation, and as a result no conclusions can yet be made about the effect of glutamine residues on oligomerisation and aggregation of HDAC4. It is possible that these mutations are destabilising the N-terminal α-helix, resulting in a conformational change within HDAC4 that increases its turnover rate. Human HDAC4 contains a PEST sequence (a sequence region with a high density of proline, glutamine, serine and threonine amino acids bounded by basic residues; 43% of the indicated region in hHDAC4) that acts as a phosphodegron; phosphorylated Ser298 mediates association of E3 ligases resulting in polyubiquitination and HDAC4 degradation by the proteasome (Cernotta *et al.*, 2011). The region containing this PEST sequence is conserved in *Drosophila* (45% of the aligned region contains the indicated residues) including the serine residues (Ser294 in *Drosophila,* Appendix 10.2.2) suggesting it too may undergo degradation regulated by this region. Given the close proximity of Ser294 to the glutamine-rich region in *Drosophila* HDAC4 it is possible that 9QA mutation may induce conformational changes that increase the susceptibility of this region to phosphorylation and subsequent degradation.

Alternatively, reduced protein levels may be a more direct effect of the substitution and deletion of glutamine residues. Proteins with long polyglutamine tracts are not as readily degraded by the proteasome; polyglutamine-rich regions are released during proteolysis (Holmberg *et al.*, 2004; Venkatraman *et al.*, 2004) and are instead degraded by lysosomal proteases (Bhutani *et al.*, 2012; Menzies *et al.*, 2010). It is therefore possible that HDAC4^{9QA} and HDAC4$^{9QA\Delta Q}$ are inherently degraded faster by the proteasome than HDAC4^{WT}. These mutations might also cause non-specific HDAC4 misfolding, resulting in increased subsequent degradation.

In vitro studies replicating those performed by Guo *et al.* (2007) on human HDAC4 are currently underway to assess *Drosophila* HDAC4 protein folding, oligomerisation and stability. These include comparison of recombinantly-expressed and purified mutant HDAC4 proteins presented in this chapter via CD spectroscopy, cross-linking analysis, and size exclusion chromatography coupled to multiangle light scattering (SEC-MALS). Given that glutamine residues mediate interhelical interactions that promote tetramerisation as well as stabilise individual α-helices of HDAC4 (Guo *et al.*, 2007), it is of interest to determine whether the

9QA mutation affects α-helix formation. CD spectroscopy will be used to analyse the predominant secondary structure of the N-terminus of *Drosophila* HDAC4 and the contribution the nine glutamine residues make to this. It would also be interesting to directly compare *Drosophila* and human HDAC4 to determine whether the polyglutamine stretch within DmHDAC4 confers additional tetramer stability. Crosslinking studies and SEC-MALS will determine the effect of each mutant on tetramerisation in the absence of any other cellular protein binding partners that may mediate aggregation, and will shed light on whether glutamine residues stabilise tetramerisation *in vitro*.

4.7.3. HDAC4 aggregation appears to correlate tightly with HDAC4-overexpression induced defects in neuronal development in *Drosophila*

Previous studies demonstrated that HDAC4 overexpression in *Drosophila* induced defects in the development of the mushroom body of the adult brain and the adult eye (Main *et al.*, 2021; Schwartz *et al.*, 2016; Tan *et al.*, 2024). These defects appear to correlate with aggregate number as restricting HDAC4 localisation to the nucleus increased aggregation and phenotypic severity (Tan *et al.*, 2024). However it was unclear whether these developmental phenotypes were a direct result of increased aggregation or another effect of increased nuclear localisation. To address this, HDAC4 oligomerisation mutants were overexpressed during development and morphology of the mushroom body and eye examined. Overexpression of mutants that reduced aggregation reduced the severity of β-lobe fusion in the mushroom body as well as the severity of the rough eye phenotype in the adult eye, whereas phenotype severity was increased with increased aggregate load. Given the parallels in each of the eye and mushroom body, comprised of independent neuronal cell types, these data suggest that there is a correlation between aggregation of HDAC4 and defects in neuronal development (Figure 4.27) and that HDAC4 aggregates are affecting major converging pathways.

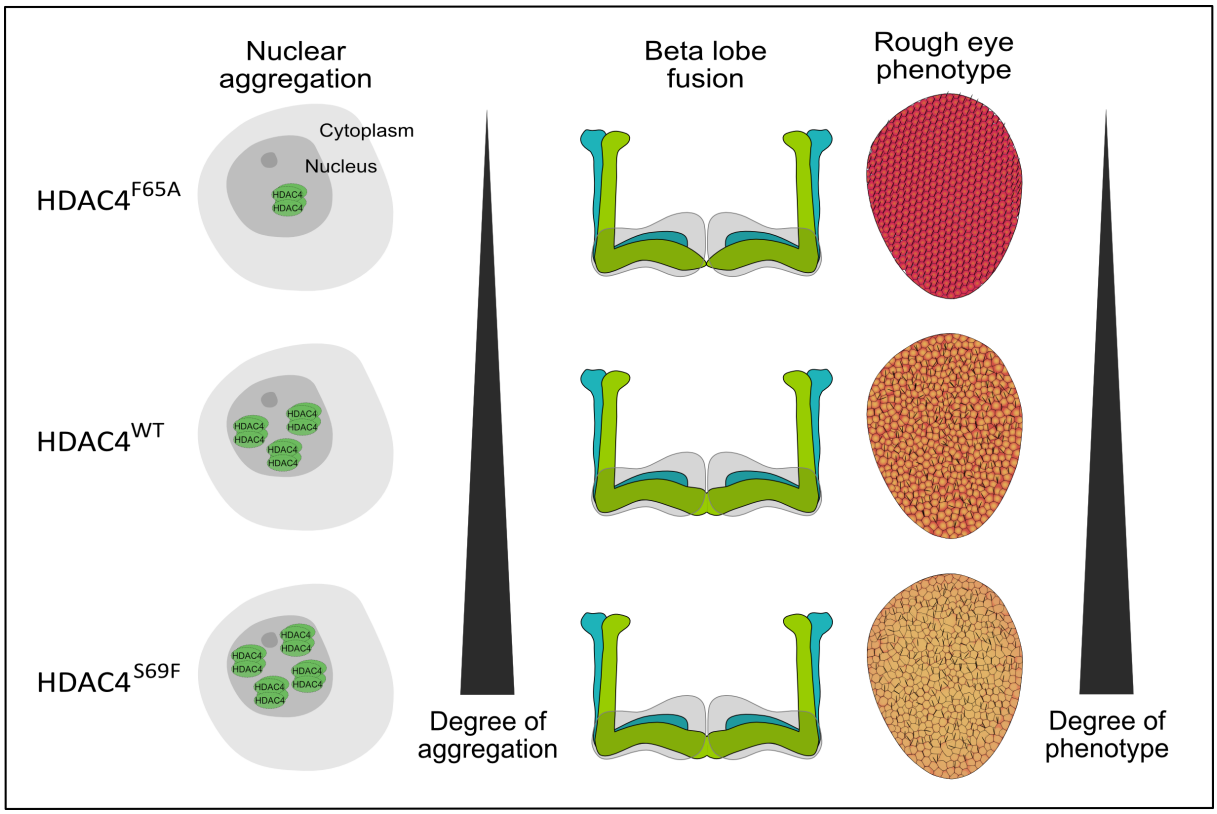

Figure 4.27 Schematic diagram depicting the correlation between aggregation of HDAC4 and defects in neuronal development in *Drosophila*

Schematic diagram representing that HDAC4^{WT} overexpression results in nuclear aggregation, β-lobe fusion of the mushroom body, and a rough eye phenotype. Mutations that destabilise aggregation (F65A) reduce the severity of β-lobe fusion and eye overexpression-induced phenotypes, while mutations that stabilise aggregation (S69F) increase the severity of β-lobe fusion and eye overexpression-induced phenotypes. *This figure is an original artwork.*

Overexpression of HDAC4 in the developing brain results in morphological defects in the mushroom body (Main *et al.*, 2021; Tan *et al.*, 2024). These include lobe thinning and guidance defects, which likely result from defects in axon extension and pathfinding, however the most prominent phenotype was β-lobe fusion where axons of each medial lobe cross the midline of the brain. It is likely that lobe fusion results from defects in axon elongation and termination, as well as similar defects in axon pathfinding, as no significant differences in the number of Kenyon cells have been observed, suggesting it is not a change in cell body and thus axon number. Reducing aggregation of HDAC4 by F65A mutation reduced the severity of β-lobe fusion, where fewer axons appeared to cross the midline compared to HDAC4^{WT}. Given that HDAC4^{F65A} mutation reduces but does not completely abolish aggregate formation in this system, it is likely that nuclei of axons that cross the midline in HDAC4^{F65A} expressing brains contain the few nuclear aggregates observed. Reducing aggregation of HDAC4 by 9QA or

9QAΔQ mutation also reduced the severity of β-lobe fusion, however western blotting determined that 9QA-containing proteins were present at a lower level compared to HDAC4^{WT}. As this phenotype is dose-dependent, it is likely that the reduction in severity mediated by these mutants is due to a lower level of total HDAC4. Increasing aggregation by the S69F mutation did not significantly increase phenotype severity, however it is acknowledged that under these experimental conditions the phenotype resulting from HDAC4^{WT} overexpression was already severe, and increases in severity were therefore hard to quantify. The temperature at which flies were raised was reduced to reduce GAL4 activity (Duffy, 2002) however this only revealed a subtle increase in severity associated with the S69F mutation. Additional experiments could be performed utilising the TARGET system to further reduce GAL4 activity and reduce the level of transgene expression to examine subtle differences in severity between HDAC4^{WT} and HDAC4^{S69F}.

In this project, HDAC4 aggregation in Kenyon cells of the adult brain was compared to the morphology of the adult mushroom body, however it is acknowledged that developmental processes are responsible for the defects observed in adulthood. Further experiments should be performed to examine the distribution of HDAC4^{WT} in the larval brain and whether aggregation occurs, and whether this is reduced by the F65A mutation. The structure of the larval mushroom body could also be examined at different developmental stages to pinpoint the critical time during which HDAC4 aggregation disrupts axonal projection.

Overexpression of HDAC4 in the developing eye also results in morphological defects in adults (Main *et al.*, 2021; Schwartz *et al.*, 2016; Tan *et al.*, 2024). In eyes of HDAC4^{9QA} and HDAC4^{9QAΔQ}-expressing flies, the widespread fusion of ommatidia and alignment was largely restored compared to HDAC4^{WT}, however loss of pigmentation and mild dimpling was still observed. Strikingly, eyes of HDAC4^{F65A} expressing flies were completely normal. All three of the mutants abolished nuclear aggregation in basal cells of the larval eye disc, however punctate cytoplasmic distribution persisted in HDAC4^{9QA} and HDAC4^{9QAΔQ} discs. It is unclear whether mutations predicted to affect oligomerisation also affect regulation of the subcellular distribution of HDAC4, and this is further discussed in Section 4.7.4. It is possible that the 9QA mutation reduces nuclear aggregation due to reduced nuclear import, resulting in persistence of cytoplasmic aggregates that impair eye development. In support of this, the combination of the 9QA and F65A mutations reduced the severity of the eye phenotype compared to the 9QA

mutation alone. These data support the idea that F65A and 9QA act in different but possibly overlapping mechanisms to reduce HDAC4 aggregation and phenotypic severity.

It is also noted that this project focuses on the role of HDAC4 aggregation in neuronal development, yet a large majority of diseases in which aberrant nuclear accumulation and aggregation of HDAC4 is observed are neurodegenerative (Section 1.6.2). While we cannot directly infer the implications for neurodegenerative disease from HDAC4 function in neuronal development, these studies provide an important basis to justify more intensive studies of the role of HDAC4 in neuronal function. Moreover, it is important to have an understanding of the developmental role HDAC4 plays in case this may be related to degeneration. $HDAC4^{WT}$ overexpression in *Drosophila* impairs long-term memory (Fitzsimons *et al.*, 2013) and this is predominantly via the actions of nuclear HDAC4 (Main *et al.*, 2021), suggesting that aggregates may impair neuronal function independent of development. Work is currently underway to determine the effect $HDAC4^{F65A}$ overexpression has on long-term memory in *Drosophila*. Furthermore, if the HDAC4 CRIMIC line described in Section 4.7.1.2 is successfully rescued by expression of $HDAC4^{WT}$, and expression of $HDAC4^{F65A}$ is viable, this can be utilised to examine the role that oligomerisation of HDAC4 has in its function in long-term memory, as well as in neuronal development. This work would highlight the implications of targeting HDAC4 oligomerisation for the development of therapeutics.

4.7.3.1. The differential requirement for MEF2 in HDAC4-overexpression induced neurodevelopmental phenotypes

The previous section described the correlation between HDAC4 aggregation in both Kenyon cells and basal cells of the larval eye disc, and phenotypes in the mushroom body and eye. However there is a striking difference for the F65A mutant; in the mushroom body the reduction in severity is only ~50% of $HDAC4^{WT}$, compared to 100% in the eye. While a possible explanation for this may be that the relative level of overexpression in the mushroom body may be higher than in the eye, resulting in a higher baseline of severity, this is also likely reflective of differences in the functional proteome between different cell types.

Differences in the availability of binding partners of HDAC4 is essential to consider in a model where HDAC4 aggregates sequester proteins and prevent their wild-type function to disrupt neuronal processes (discussed in Section 4.7.4). This is highlighted by the absence of MEF2 in

the larval eye disc. While this result was surprising given the presence of HDAC4 aggregates, MEF2 transcript expression has only been detected at relatively low levels in the larval eye-antennal disc, lower than endogenous HDAC4, and expression appeared predominantly anterior to the morphogenetic furrow (Mishra *et al.*, 2016; Quiquand *et al.*, 2021). This is further supported by mutagenesis studies performed by Tan *et al.* (2024); mutation of the MEF2 binding site within HDAC4 completely reduces HDAC4-overexpression induced defects in the mushroom body, but has little effect in the eye, suggesting that HDAC4-induced disruption of eye development is largely independent of MEF2. It is important to note that an absence of MEF2 protein at the late third instar larval stage does not preclude its expression later in development; the absence of MEF2 protein during the larval stage of development may account for the minimal effect mutation of the MEF2 binding site has on the HDAC4 overexpression induced phenotype in the eye (i.e. the small reduction governed by mutation of the MEF2 binding site in the eye may occur during later development where MEF2 expression begins). These data highlight the importance of considering multiple models to infer the roles of proteins in neuronal development. The role of MEF2 in mediating HDAC4-overexpression induced phenotypes is further investigated in the following chapter.

4.7.4. HDAC4 oligomerisation may have a role in the regulation of its subcellular distribution

In basal cells of the larval eye disc, it appears that reductions in the nuclear aggregation of HDAC4 are accompanied by an increase in cytoplasmic distribution. The same is not overly evident in Kenyon cells, for which there may be many explanations. As Kenyon cells are the intrinsic cells of the mushroom body, their cell bodies pinch to form the axons that bundle to form the mushroom body lobes (Section 1.3.1). This results in a very small area of cytoplasm around Kenyon cell nuclei, which makes visualisation of cytoplasmic aggregation difficult. It was also demonstrated that *OK107-GAL4* drives strong transgene expression in Kenyon cells relative to *elav-GAL4*, therefore it is hypothesised that subtle changes in distribution may be masked by the dose of HDAC4 overexpression.

A key piece of evidence from the literature that suggests that HDAC4 distribution may be regulated in part by oligomerisation is that H97F mutation (orthologous to S69F) of hHDAC4 increased HDAC4-dependent transcriptional repression of MEF2 *in vitro* (Guo *et al.*, 2007), and F93D mutation (orthologous to F65A) prevented HDAC4-mediated repression of MEF2-

dependent transcription (Dai *et al.*, 2024), suggesting a relationship between oligomerisation of HDAC4 and MEF2 binding and/or repression capacity. It is well established that HDAC4 binds MEF2 (Wang & Yang, 2001), and this results in repression of MEF2-dependent transcription (Miska *et al.*, 1999). The association of HDAC4 and MEF2 is most curious as MEF2 mediates nuclear import of HDAC4 (Borghi *et al.*, 2001; Wang & Yang, 2001), and mutations of the MEF2 binding domain within HDAC4 result in cytoplasmic localisation of HDAC4 in Kenyon cells (Main *et al.*, 2021; Tan *et al.*, 2024). It is therefore possible that changes in oligomerisation may affect MEF2 binding and subsequently nuclear import of HDAC4. Again this may not have been observed in Kenyon cells here due to the high level of HDAC4 overexpression. The following chapter will therefore examine the subcellular distribution of each oligomerisation mutant resulting from expression under the control of *elav-GAL4* or *OK107-GAL4* to aid in understanding the role that oligomerisation plays in the regulation of HDAC4 subcellular distribution.

4.7.5. How does tetramerisation of HDAC4 result in aggregation?

The data presented and discussed herein suggests that tetramerisation of full-length HDAC4 is mediated within the N-terminus, and this is required in part to form nuclear aggregates. However, it remains unclear how HDAC4 tetramers multimerise to form higher order structures and eventually nuclear aggregates. Guo *et al.* (2007) determined the tetrameric structure of the N-terminal helix, however this does not consider how the remainder of the HDAC4 protein associates within a tetramer. Therefore, to begin to understand the mechanism of aggregation an *in silico* model was generated. This involved alignment of the AlphaFold prediction of the structure of *Drosophila* HDAC4 (Figure 4.28A-C) to the crystal structure of the N-terminal tetramer of human HDAC4 (Guo *et al.*, 2007) (Figure 4.28D-E).

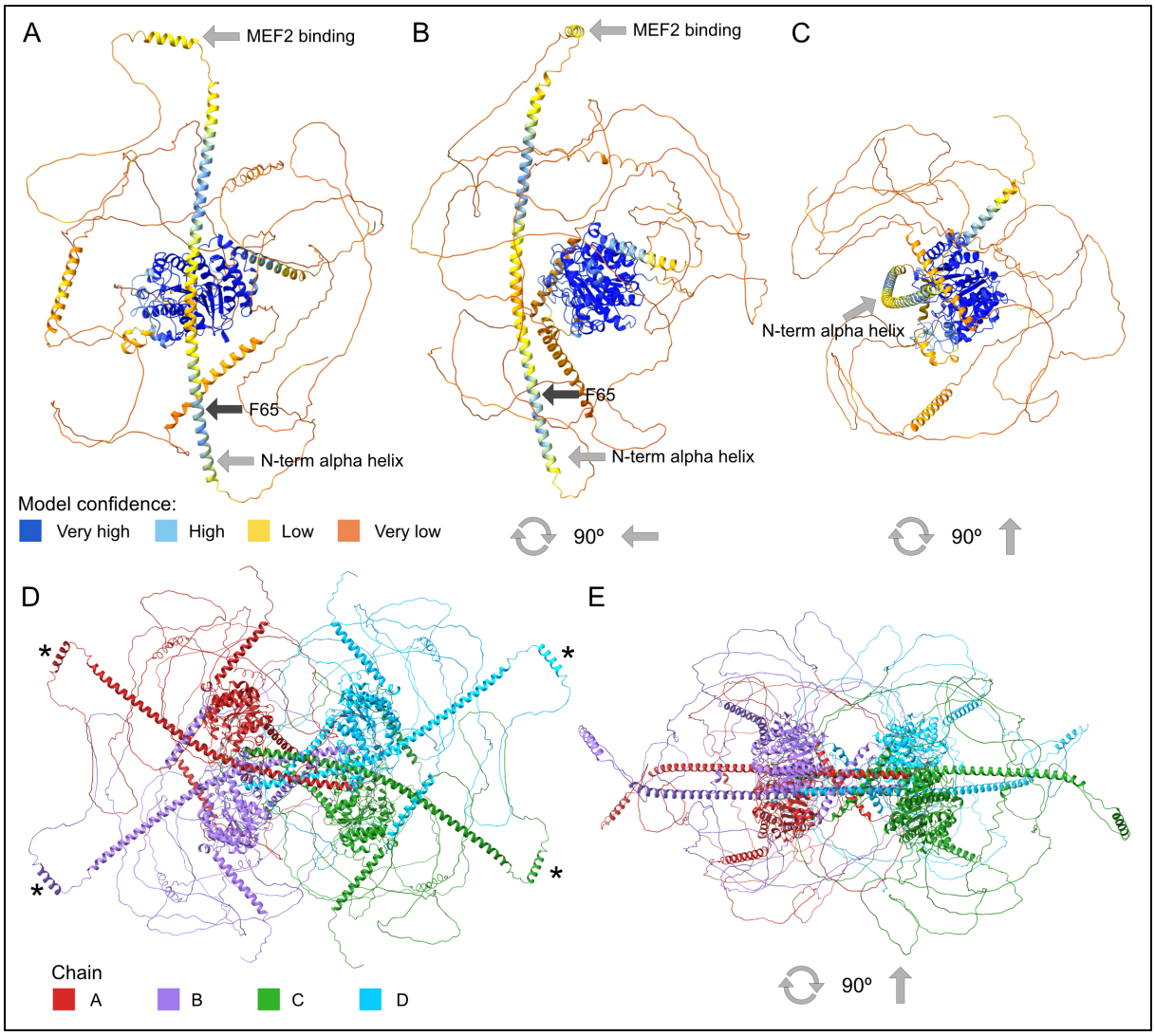

Figure 4.28 3D reconstruction of a DmHDAC4 tetramer based on the AlphaFold prediction of the structure of DmHDAC4 and the crystal structure of the N-terminus of hHDAC4

(A-C) A monomer of DmHDAC4 as predicted by AlphaFold (UniProt Q9VYF3, accessed 10/01/2024)(Jumper *et al.*, 2021; Varadi *et al.*, 2021). The monomer in (A) is rotated 90° about the Y axis in (B). The monomer in (B) is rotated 90° about the X axis in (C). Colours in (A-C) are based on model confidence (assigned as pLDDT scores as per Varadi *et al.* (2021)). (D-E) Assembly of four DmHDAC4 monomers into a tetramer. The tetramer was assembled in ChimeraX using the matchmaker function as per Section 3.2.1. Chains are coloured as per Guo *et al.* (2007). Tetramer in (D) is rotated 90° about the X axis in (E). * indicates the MEF2 binding region.

The AlphaFold predicted structures in Figure 4.28A-C are coloured by pLDDT score, which is a measure of local accuracy of the model's prediction (Varadi *et al.*, 2021). The catalytic domain is coloured in dark blue, indicating a high confidence, due to a number of crystal structures available for the HDAC4 catalytic domain (Bottomley *et al.*, 2008; Bürli *et al.*, 2013; Luckhurst *et al.*, 2019; Park *et al.*, 2018). The N-terminal α-helix is coloured in light blue

toward the bottom of Figure 4.28A and B, which corresponds to the region of the helix determined by structural analyses by Guo *et al.* (2007), including the hydrophobic core, suggesting a high confidence of prediction. The majority of the remainder of the protein is predicted with little secondary structure and low confidence. The important consideration here is that the predicted conformation of the DmHDAC4 monomer places the N-terminal helix of HDAC4 toward the outside of its structure. Therefore, when modelled as a tetramer, the orientation of the catalytic domains is complementary to one another and regions that overlap are disordered loop regions of the model with low prediction confidence (i.e. defined structural regions do not clash when assembled as a tetramer). This supports the biological data wherein the F65A mutation reduces full-length HDAC4 oligomerisation.

The helix that binds MEF2 (Wang & Yang, 2001) is situated on the outside of the tetramer (Figure 4.28D, noted by *), consistent with MEF2 being able to be recruited to HDAC4 tetramers and subsequent aggregates. This is likely to have functional significance as repression of MEF2 is lost upon destabilisation of HDAC4 tetramerisation (Guo *et al.*, 2007). It is also possible that binding of MEF2 in this way may also stabilise HDAC4 aggregation. To address this, the effect that mutation of the MEF2 binding region has on aggregate formation of nuclear-restricted HDAC4 is examined and discussed in the following chapter. It is also noted that more data is now available on the relationship between HDAC4 oligomerisation and MEF2 binding (Dai *et al.*, 2024) and this is also discussed in the following chapter.

While this model provides an interesting discussion about the interactions mediated via monomeric vs tetrameric HDAC4, it is still unclear how higher order aggregates form, and whether these aggregates maintain native HDAC4 folding. Further investigation of this should be pursued, and include staining with thioflavin S/T to examine amyloid formation and determine whether HDAC4 aggregates through β-sheet association (Biancalana & Koide, 2010), as well as examination of co-localisation of aggregates with other typical markers of nuclear accumulations. The oligomerisation domain of HDAC4 is further characterised in Chapter 7, as well as potential mechanisms to disrupt aggregation of HDAC4.

4.7.6. How do HDAC4 aggregates mediate neurotoxicity?

The specific mechanism through which HDAC4 aggregates mediate neurotoxicity remains unknown. The association of MEF2 with nuclear HDAC4 aggregates has been widely observed (Borghi *et al.*, 2001; Chan *et al.*, 2003; Fitzsimons *et al.*, 2013; Main *et al.*, 2021; Miska *et al.*, 1999; Tan *et al.*, 2024), and human HDAC4 has a number of additional binding partners that may co-localise (Figure 1.10). It is therefore possible that HDAC4 may be sequestering proteins within these aggregates, preventing their wild-type function, and inducing errors in neuronal development and function (Figure 4.29). Such interactions may involve proteins directly responsible for processes observed to be dysregulated upon HDAC4 overexpression, such as those involved in β-lobe extension and termination, as well as proteins critical for normal eye development and long-term memory formation. Characterisation of the composition of HDAC4 positive aggregates is therefore imperative to identify potential mechanisms of neurotoxicity. This is addressed in Chapter 6.

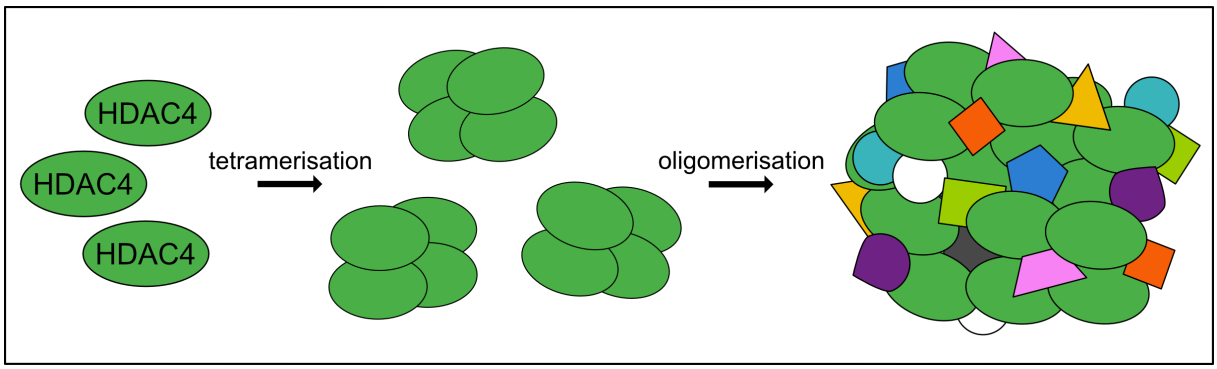

Figure 4.29 HDAC4 aggregates may aberrantly sequester proteins to induce defects in neuronal development and function
Schematic diagram of a model depicting that tetramerisation of HDAC4 results in higher order oligomerisation into aggregates, which sequester additional proteins. *This figure is an original artwork.*

Chapter Five

Regulation of HDAC4 subcellular distribution, oligomerisation, and aggregation

5. Examination of the relationship between HDAC4 oligomerisation and subcellular distribution, and how this affects HDAC4 aggregation and neuronal development

The previous chapter demonstrated a relationship between oligomerisation of HDAC4 and aggregation *in vivo*, and a correlation between aggregation and HDAC4-overexpression induced phenotypes, where decreasing aggregation decreased the severity of phenotypes and vice versa. Oligomerisation of full-length HDAC4 was disrupted by the F65A mutation, hypothesised to reduce formation of the hydrophobic core that is essential for tetramerisation *in vitro* (Guo *et al.*, 2007), and this prevented aggregation in nuclei of both Kenyon cells and the basal cells of the larval eye disc. In contrast, the S69F mutation, which is hypothesised to extend the hydrophobic core, increased nuclear aggregation. However, while carrying out these experiments it was observed that there appeared to be subtle shifts in the subcellular distribution of the tetramerisation mutants in the larval eye disc. This could potentially confound interpretation of the results as it cannot be firmly concluded that the reduced aggregation and the associated decrease in developmental defects are a result of reduced oligomerisation of HDAC4 in the nucleus, or whether they are due to reduced nuclear entry of HDAC4. In other words, the changes observed in severity of developmental defects could potentially be elicited by the tetramerisation mutants independently of aggregation, as if oligomerisation promotes nuclear entry, there would be less of the tetramerisation mutants present in the nucleus to impair development.

Evidence that oligomerisation may regulate nuclear entry is described by Guo *et al.* (2007), where mutations that reduce tetramerisation of the HDAC4 N-terminus in solution reduce the ability of HDAC4 to repress MEF2-dependent transcription, suggesting that the tetramerisation mutants may bind MEF2 less efficiently. MEF2 binding is required for efficient nuclear entry of HDAC4 (Borghi *et al.*, 2001; Wang & Yang, 2001)(Section 1.5.1.2), and in *Drosophila,* mutations that affect MEF2 binding affect the subcellular distribution and propensity of HDAC4 to mediate neurodevelopmental phenotypes (Main *et al.*, 2021; Tan *et al.*, 2024). Therefore, this chapter focuses on the relationship between HDAC4 subcellular distribution and oligomerisation and the contribution of the MEF2 binding site as well as other domains within HDAC4 to the regulation of its distribution and aggregation.

Specifically, the following analyses were undertaken:

To examine the contribution of oligomerisation to the regulation of HDAC4 subcellular localisation, the distribution of $HDAC4^{WT}$ and $HDAC4^{mutant}$ was examined in the adult brain by immunohistochemistry, as well as in the whole head by subcellular fractionation followed by western blotting.

To assess the impact of oligomerisation on aggregation and associated disruption of mushroom body and eye development independently of subcellular distribution, mutants were developed that sequestered each of the oligomerisation mutants in the nucleus, and aggregation and neurotoxicity associated with these was compared to nuclear-localised HDAC4.

Co-immunoprecipitation was carried out to determine if the 3SA mutation that promotes nuclear accumulation alters the ability of the mutants to oligomerise.

The impact of increased expression of MEF2 on the regulation of HDAC4 subcellular distribution and aggregation was assessed to determine the role of MEF2 in HDAC4 overexpression-induced neurodevelopmental phenotypes.

The NES within HDAC4 was mutated to examine its contribution to nuclear localisation and whether this differentially affects aggregation of HDAC4 and disruption of mushroom body and eye development compared to the 3SA mutation.

5.1. HDAC4 oligomerisation mutants are altered in subcellular distribution in Kenyon cells

HDAC4 distribution was examined in the adult brain by overexpression with *elav-GAL4*, which mediates pan-neuronal expression in the adult brain (Section 4.1). In contrast to *OK107-GAL4*, *elav-GAL4* drives wider expression (Figure 4.1), allowing for the examination of HDAC4 subcellular distribution in other cell-types. *elav-GAL4* also mediates a considerably lower level of transgene expression in the mushroom body compared to *OK107-GAL4* (Figure 4.2), and this is modest in comparison to total levels of endogenous HDAC4 in the brain (Tan *et al.*,

2024), allowing for examination of the contribution of dose of overexpression to the regulation of HDAC4 subcellular distribution. Flies were raised in the absence of the TARGET system, therefore transgene expression was activated during development. Adult brains were dissected and prepared for immunohistochemistry. To observe the ultrastructure of the brain, an antibody against Bruchpilot, a cytoskeletal protein important in the structural integrity of pre-synaptic active zones (Wagh *et al.*, 2006), was used in addition to anti-Myc to visualise HDAC4.

In the anterior of the central brain, HDAC4^{WT} localised strongly to the axons of the α-, β-, and γ-lobes of the mushroom body, as well in as cells surrounding the antennal lobes and the suboesophageal ganglion (Figure 5.1B). In the latter cells, HDAC4^{WT} was predominantly cytoplasmic, with haloes surrounding nuclei that were largely devoid of staining (Figure 5.1G). Each of the oligomerisation mutants were also present in the α-, β-, and γ-lobes of the mushroom body (Figure 5.1C-F), however the intensity within the mushroom body lobes was markedly reduced for HDAC4^{9QA}, HDAC4$^{9QA\Delta Q}$ and HDAC4^{S69F}. The reduction in intensity observed for HDAC4^{9QA} and HDAC4$^{9QA\Delta Q}$ is likely a result of lower total protein levels (Section 4.3.2), whereas the reduction observed with HDAC4^{S69F} in the mushroom body may result from increased localisation to Kenyon cell nuclei in the posterior. There was no change in subcellular localisation in the cells surrounding the antennal lobe and the suboesophageal ganglion for any of the mutants in comparison to HDAC4^{WT} (Figure 5.1G-K).

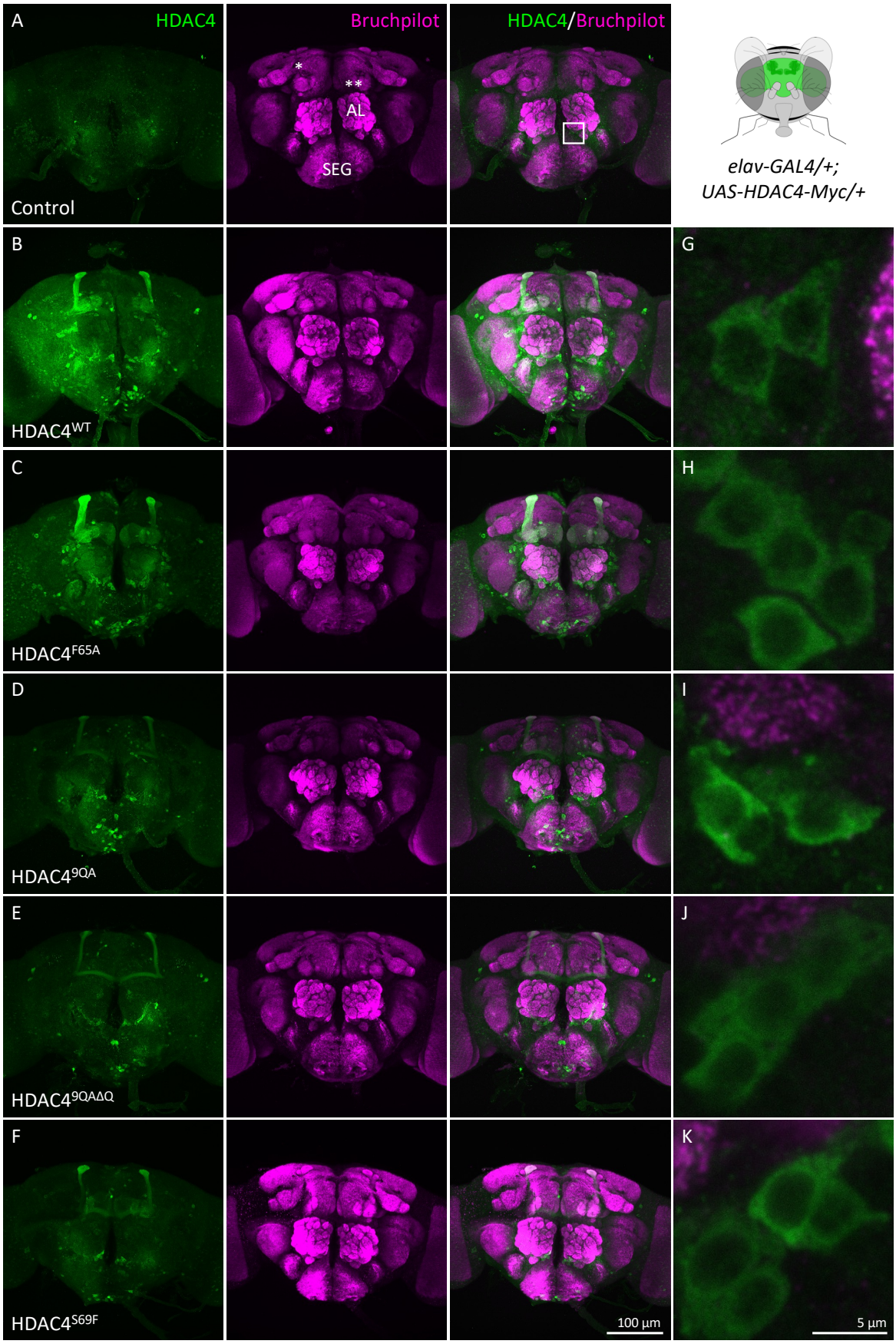

Figure 5.1 Examination of HDAC4^{WT} and HDAC4^{mutant} subcellular distribution in the mushroom body lobes and cell bodies surrounding the suboesophageal ganglion and antennal lobe in the adult *Drosophila* brain

(A-F) Maximum projections through the anterior of the central brain expressing HDAC4^{WT} or HDAC4^{mutant} (green) under the control of *elav-GAL4*. Flies were raised at 25 °C. Bruchpilot (magenta) highlights the ultrastructure of the brain. AL, antennal lobe; SEG, suboesophageal ganglion. Asterisks denote the approximate locations of the α- (*) and β-/γ- (**) lobes. The box below antennal lobe denotes approximate location of images in (G-K). Control is *elav-GAL4/+*. (G-K) Magnified single optical section (0.5 μm) of HDAC4 in the cells surrounding the antennal lobe and suboesophageal ganglion.

When imaged from the posterior of the brain, HDAC4^{WT} expression was most notable in the Kenyon cells (Figure 5.2B), present in both the nucleus and cytoplasm (Figure 5.2G), as well as localising to dendrites in the calyx (Figure 5.2B, asterisk). Within Kenyon cell nuclei, HDAC4^{WT} had a relatively uniform distribution, with similarly small aggregates compared to when it was expressed with *OK107-GAL4* in the presence of the TARGET system (compare Figure 5.2G to Figure 4.10). Strikingly, localisation of HDAC4^{F65A} to nuclei was reduced compared to HDAC4^{WT}, which was predominantly observed as cytoplasmic haloes (Figure 5.2C, H). HDAC4^{9QA} and HDAC4$^{9QA\Delta Q}$ also appeared less nuclear compared to HDAC4^{WT} (Figure 5.2D-E, I-J). In contrast, while still forming cytoplasmic haloes, HDAC4^{S69F} formed more and larger punctate nuclear aggregates than HDAC4^{WT} (Figure 5.2F, K). These were significantly increased in size compared to those in Figure 4.10 when HDAC4^{S69F} was expressed under the control of *OK107-GAL4* in the presence of the TARGET system, further suggesting that dose and/or length of time of overexpression is an important factor in the aggregation of HDAC4.

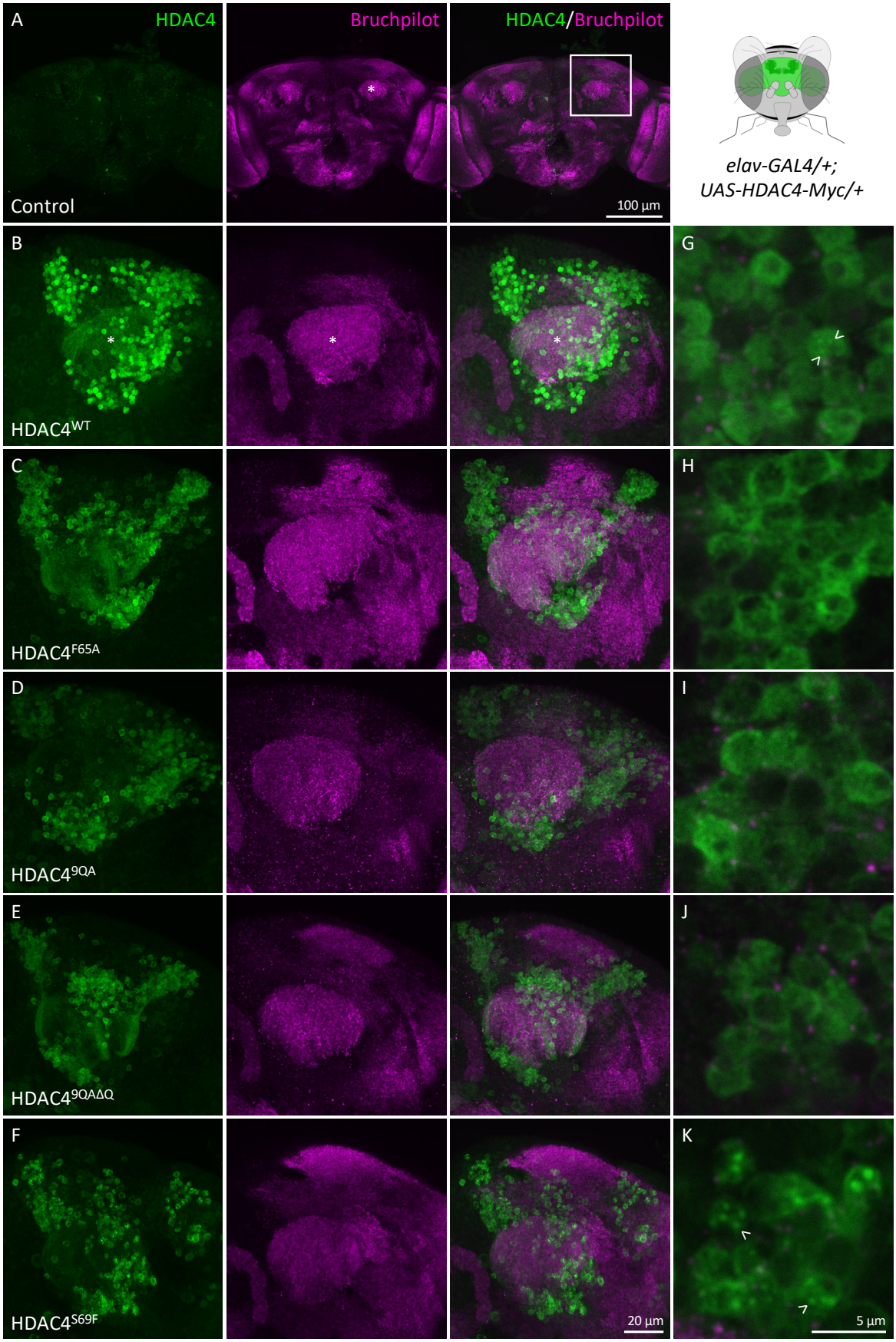

Figure 5.2 The capacity of HDAC4 to oligomerise affects its subcellular distribution in Kenyon cells

(A-F) Maximum projections through the posterior of the brain expressing HDAC4^{WT} or HDAC4^{mutant} (green) under the control of *elav-GAL4*. Flies were raised at 25 °C. Bruchpilot (magenta) highlights the ultrastructure of the brain. Control is *elav-GAL4/+*. (A) Maximum projection through the central region of control brains. Boxed region is magnified in (B-F). * denotes the calyx. (G-K) Magnified single optical section (0.5 μm) of HDAC4 in Kenyon cells above the calyx. Arrowheads point to nuclear aggregates of HDAC4.

Together these data demonstrate that when expressed under the control of *elav-GAL4* during development, mutations that affect oligomerisation of HDAC4 impact its subcellular distribution in Kenyon cells. As the same changes were not observed when expressed at a higher level with *OK107-GAL4* (Figure 4.10), these data also support the idea that HDAC4 undergoes dose-dependent regulation of its subcellular distribution. To further investigate this, the relative levels of nuclear and cytoplasmic HDAC4 were quantified by subcellular fractionation followed by western blotting in Section 5.2.2 of this chapter.

5.2. Enforced nuclear localisation of oligomerisation mutants affects aggregation and related phenotypes

As changes in the subcellular distribution of HDAC4 alter HDAC4 overexpression-induced phenotypes (Tan *et al.*, 2024), and each of the oligomerisation mutants display altered subcellular distribution compared to HDAC4^{WT} in Kenyon cells (Section 5.1) as well as in the eye disc (Section 4.4.3), it is not clear whether the reduction of phenotypes by the F65A and 9QA mutations is a function of reduced aggregation, or a result of reduced nuclear localisation. Therefore, to further investigate the role of HDAC4 aggregation independent of changes in subcellular distribution, a new set of HDAC4 oligomerisation mutants was generated with additional mutations that together restrict their subcellular localisation to the nucleus (Figure 5.3, Table 5.1).

Nuclear exit and cytoplasmic anchoring of HDAC4 is mediated by the chaperone protein 14-3-3, and mutation of the three serine residues (3SA) within HDAC4 that mediate phosphorylation-dependent 14-3-3 binding results in nuclear localisation (Section 1.5.1.3). Therefore, to induce nuclear localisation of the HDAC4 oligomerisation mutants, mutagenesis was performed on the original HDAC4^{9QA}- or HDAC4^{F65A}-Myc constructs to incorporate the 3SA mutations (substituting Ser239, Ser573 and Ser748 with alanine, Figure 5.3C), previously demonstrated

to result in nuclear localisation of DmHDAC4^{3SA} in the *Drosophila* brain (Tan *et al.*, 2024). While it is hypothesised that HDAC4$^{3SA-F65A}$ will have significantly increased nuclear localisation compared to HDAC4^{F65A}, restriction of localisation to the nucleus may increase its ability to aggregate due to a higher local protein concentration (i.e. being confined within a smaller space). Importantly, MEF2 is also exclusively nuclear (Figure 10.39), and its binding to HDAC4$^{3SA-F65A}$ may support aggregation as it was earlier suggested that binding of MEF2 may stabilise oligomerisation and aggregation of HDAC4 (Section 4.7.5). Therefore, a further mutant, HDAC4$^{3SA-F65A-\Delta MEF2}$, was generated that includes mutations of the MEF2-binding site within HDAC4, as these mutations (ΔMEF2) were previously suggested to reduce MEF2 binding (Tan (2022), Figure 5.3D). It is hypothesised that if MEF2 does indeed stabilise aggregation of HDAC4, then nuclear aggregation will be maximally destabilised by HDAC4$^{3SA-F65A-\Delta MEF2}$. HDAC4$^{3SA-\Delta MEF2}$ was previously generated (Tan *et al.*, 2024) and was examined alongside HDAC4$^{3SA-F65A-\Delta MEF2}$ to specifically delineate the role of oligomerisation of nuclear HDAC4. Transgenic flies were generated harbouring each of these constructs (Section 3.1.1) and their expression confirmed and characterised. The mutants that are characterised in this chapter are summarised in Table 5.1.

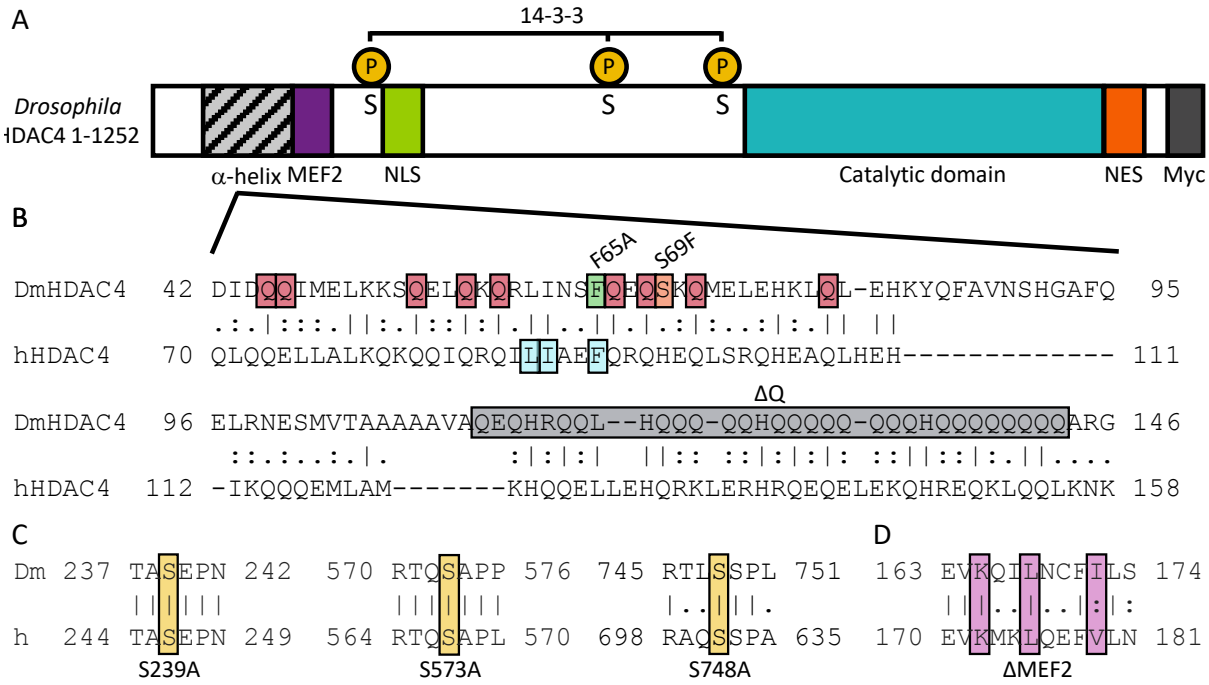

Figure 5.3 Sequence alignment and schematic diagram of nuclear-restricted HDAC4 oligomerisation mutants

(A) Schematic diagram of the domain structure of DmHDAC4. (B) EMBOSS Water alignment of the glutamine-rich N-terminus of human HDAC4 (hHDAC4, GenBank accession NP_006028), and *Drosophila* HDAC4 (DmHDAC4, GenBank accession NP_572868) demonstrates high conservation of the N-terminus. The hydrophobic core of hHDAC4 (L89, I90, F93) is indicated by blue boxes.

Drosophila tetramerisation mutants are indicated by coloured boxes: 9QA, red; F65A, green; S69F, orange; 9QAΔQ, red and grey. (C-D) Alignment of human (h) and *Drosophila* (Dm) HDAC4 shows conservation of the three serine residues critical for 14-3-3 binding (Grozinger & Schreiber, 2000) and MEF2 binding (Wang & Yang, 2001). The HDAC4^{3SA} mutation sites are indicated by yellow boxes (C) and the HDAC4$^{\Delta MEF2}$ mutation sites are indicated by purple boxes (D) where each of these residues were mutated to alanine. Alignment for (C) and (D) is derived from that in Tan *et al.* (2024). Please note parts (A) and (B) of this figure are reproduced from Figure 4.5 for clarity.

Table 5.1. DmHDAC4 mutants characterised in this chapter

Name	Predicted consequence of mutation
HDAC4^{WT}	-
HDAC4^{3SA}	Prevents 14-3-3 binding, resulting in nuclear localisation
HDAC4^{9QA}	Disrupts the polar interaction networks important in tetramerisation
HDAC4^{F65A}	Disrupts the hydrophobic core required for tetramerisation
HDAC4$^{3SA-9QA}$	Double mutant of HDAC4^{3SA} and HDAC4^{9QA}
HDAC4$^{3SA-F65A}$	Double mutant of HDAC4^{3SA} and HDAC4^{F65A}
HDAC4$^{\Delta MEF2}$	Prevents MEF2 binding resulting in cytoplasmic localisation via loss of MEF2-dependent nuclear import
HDAC4$^{3SA-\Delta MEF2}$	Double mutant of HDAC4^{3SA} and HDAC4$^{\Delta MEF2}$
HDAC4$^{3SA-F65A-\Delta MEF2}$	Triple mutant of HDAC4^{3SA} and HDAC4^{F65A} HDAC4$^{\Delta MEF2}$
HDAC4$^{\Delta NES}$	Prevent association of exportin (CRM1) and nuclear export of HDAC4

Transgenic flies harbouring each of these constructs were generated and each are expressed in *Drosophila* under the control of GAL4.

5.2.1. Expression of nuclear-restricted HDAC4 oligomerisation mutants in *Drosophila*

The nuclear-restricted HDAC4 oligomerisation mutants were expressed in the brain under the control of *elav-GAL4*, and western blotting was performed to confirm expression. HDAC4^{3SA} was expressed and present at the expected size of 144 kDa (Figure 5.4A). HDAC4$^{3SA-9QA}$, HDAC4$^{3SA-\Delta MEF2}$ and HDAC4$^{3SA-F65A-\Delta MEF2}$ all also migrated at the same rate, however HDAC4$^{3SA-F65A}$ appeared at a lower molecular weight. Quantification of band intensity demonstrated that HDAC4$^{3SA-F65A}$ and HDAC4$^{3SA-F65A-\Delta MEF2}$ protein levels were similar to HDAC4^{3SA}, while HDAC4$^{3SA-9QA}$ was significantly reduced (Figure 5.4B). This was the same

pattern as observed for HDAC4^{9QA} relative to HDAC4^{WT}, which further supports the idea that the glutamine residues within the N-terminus of HDAC4 are important in protein stability, and that this stability is likely independent of subcellular distribution. The cause of the different migratory rate for HDAC4$^{3SA\text{-}F65A}$ was investigated further in Appendix 10.3.1, however this remains unresolved.

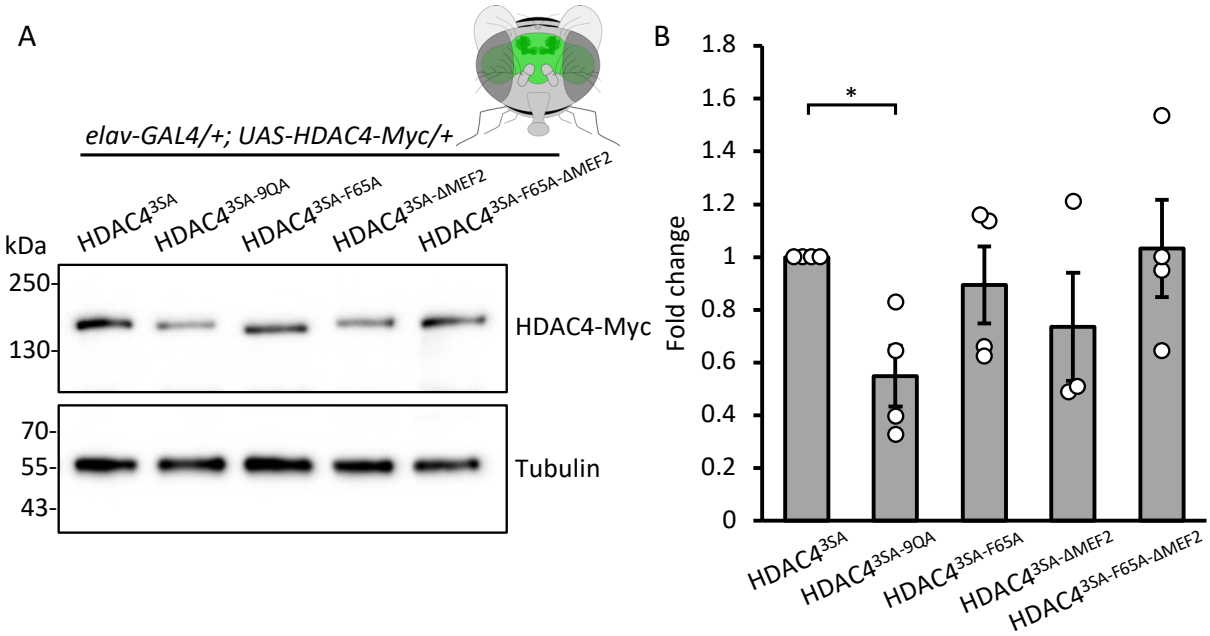

Figure 5.4 HDAC4$^{3SA\text{-}9QA}$ is reduced in protein levels compared to nuclear-restrcited HDAC4 in *Drosophila*

(A) Western blot of *elav-GAL4* driven expression of HDAC4^{3SA} and HDAC4$^{3SA\text{-}mutant}$ in head whole-cell lysates (30 µg) using anti-Myc and anti-alpha-tubulin antibodies. Flies were raised at 25 °C. The protein bands were of the expected size of ~144 kDa with the exception of HDAC4$^{3SA\text{-}F65A}$. (B) Quantification of HDAC4 band intensity normalised to tubulin (n=4 blots). Note that HDAC4$^{3SA\text{-}\Delta MEF2}$ was only quantified for three blots as it was not included on the fourth. The average fold change relative to HDAC4^{3SA} is plotted, with individual data points represented as circles. Error bars indicate the SEM. HDAC4$^{3SA\text{-}9QA}$ was significantly reduced compared to HDAC4^{3SA} (One sample t-test compared to HDAC4^{3SA}, HDAC4$^{3SA\text{-}9QA}$ $t_{(3)}$=3.9078, p=0.0298; HDAC4$^{3SA\text{-}F65A}$ $t_{(3)}$=0.7172, p=0.525; HDAC4$^{3SA\text{-}\Delta MEF2}$ $t_{(2)}$=1.1155, p=0.3807; HDAC4$^{3SA\text{-}F65A\text{-}\Delta MEF2}$ $t_{(3)}$=0.1755, p=0.8719). Full blots used for quantification are found in Appendix 10.2.3, Figure 10.11.

5.2.2. Confirmation of nuclear localisation of HDAC4 oligomerisation mutants

To compare the distribution of the original oligomerisation mutants to their nuclear-enforced counterparts, subcellular fractionation was performed on the heads of flies expressing each transgene under the control of *elav-GAL4* (Figure 5.5A). Myc intensity was quantified and normalised to either lamin or tubulin for nuclear and cytoplasmic fractions respectively. Total

normalised Myc intensity was then calculated to determine the relative proportion of nuclear and cytoplasmic HDAC4 (Figure 5.5B). It is important to note that in all cases, a small amount of tubulin was detected in the nuclear fractions, suggesting that they contain a low level of cytoplasmic contamination. Therefore, the amount of nuclear HDAC4 observed here is likely an overestimation. HDAC4^{WT} was 25% nuclear, and the 3SA mutations increased this to 80%. The nuclear proportion of HDAC4$^{\Delta MEF2}$, HDAC4^{9QA} and HDAC4^{F65A} was similar to HDAC4^{WT}, whereas their 3SA counterparts were increased in nuclear distribution with proportions comparable to HDAC4^{3SA}.

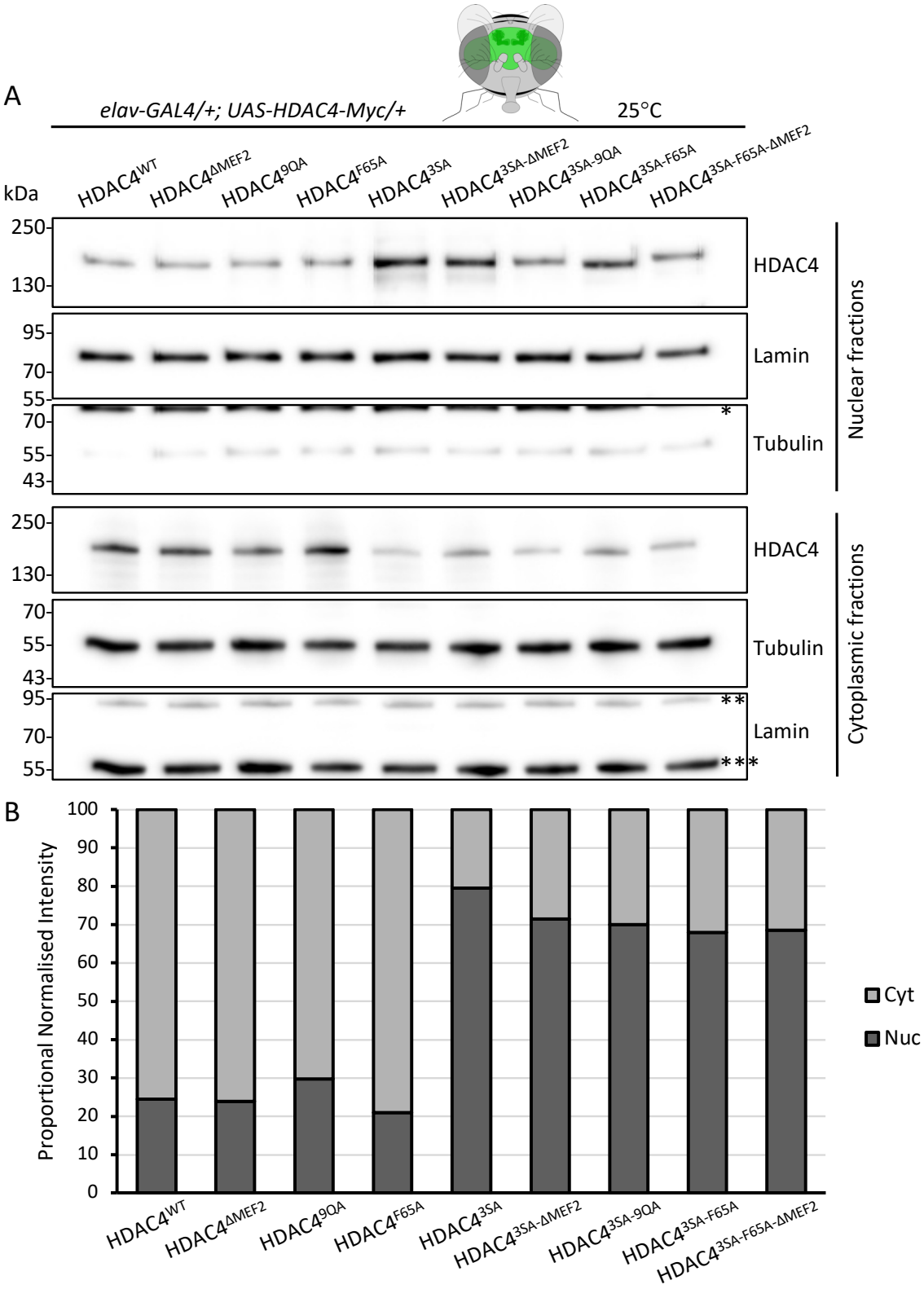

Figure 5.5 The 3SA mutations increase the nuclear distribution of HDAC4 oligomerisation mutants

Subcellular fractionation was performed on the heads of flies expressing HDAC4^{WT} and HDAC4^{mutant} under the control of *elav-GAL4*. Flies were raised at 25 °C. (A) Total protein was loaded (20 µg) for both nuclear and cytoplasmic fractions, and each was probed with anti-Myc to detect HDAC4, and anti-lamin and anti-alpha-tubulin to assess nuclear and cytoplasmic abundance respectively in each lysate. Lamin was observed at ~71 kDa and tubulin at ~55 kDa. * indicates residual detection of lamin due to

re-probing. ** indicates residual detection of the ~95 kDa non-specific band, previously characterised for the anti-Myc antibody, due to re-probing. *** indicates residual detection of tubulin due to re-probing. No lamin was observed in the cytoplasmic fractions. Blots were exposed for the same amount of time for each antibody detection and underwent the same adjustments in brightness and contrast between nuclear and cytoplasmic membranes. (B) Nuclear and cytoplasmic HDAC4 were quantified and normalised to lamin and tubulin respectively. Total normalised HDAC4 intensity was calculated, and the proportion of nuclear and cytoplasmic distribution is displayed. Cyt, cytoplasmic; Nuc, nuclear. Full blots are found in Appendix 10.3.2, Figure 10.23.

The lack of difference in distribution between HDAC4^{WT} and HDAC4$^{\Delta MEF2}$ is curious given the striking change in distribution observed previously in Kenyon cells (Tan *et al.*, 2024). *elav-GAL4* drives widespread expression of *HDAC4*, whereas endogenous *MEF2* is predominantly expressed in Kenyon cells (compare Figure 4.1B to Figure 4.10A), which comprise approximately 2% of the neurons in the brain (Aso *et al.*, 2009; Balling *et al.*, 1987; Ito *et al.*, 1997). Given that the majority of neurons in the brain do not express MEF2, or express it at very low levels, the distribution of HDAC4 may not be altered by the ΔMEF2 mutation in these cells, meaning that any changes to HDAC4 distribution in Kenyon cells will be diluted. Therefore, to determine the effect that each of these mutations have on the subcellular distribution of HDAC4, specifically in Kenyon cells in the presence of MEF2, the mutants were expressed under the control of the mushroom body driver *OK107-GAL4*. To directly compare HDAC4 distribution determined by subcellular fractionation to the immunohistochemistry performed in Section 4.4.2 and 5.2.4, the conditions in which flies were raised was replicated. That is, transgene expression was driven by *OK107-GAL4* in the presence of the TARGET system; flies were raised at 18 °C until eclosion, and adults were transferred to 30 °C for three days to induce expression, after which time the flies were harvested and fractionation performed on heads (Figure 5.6).

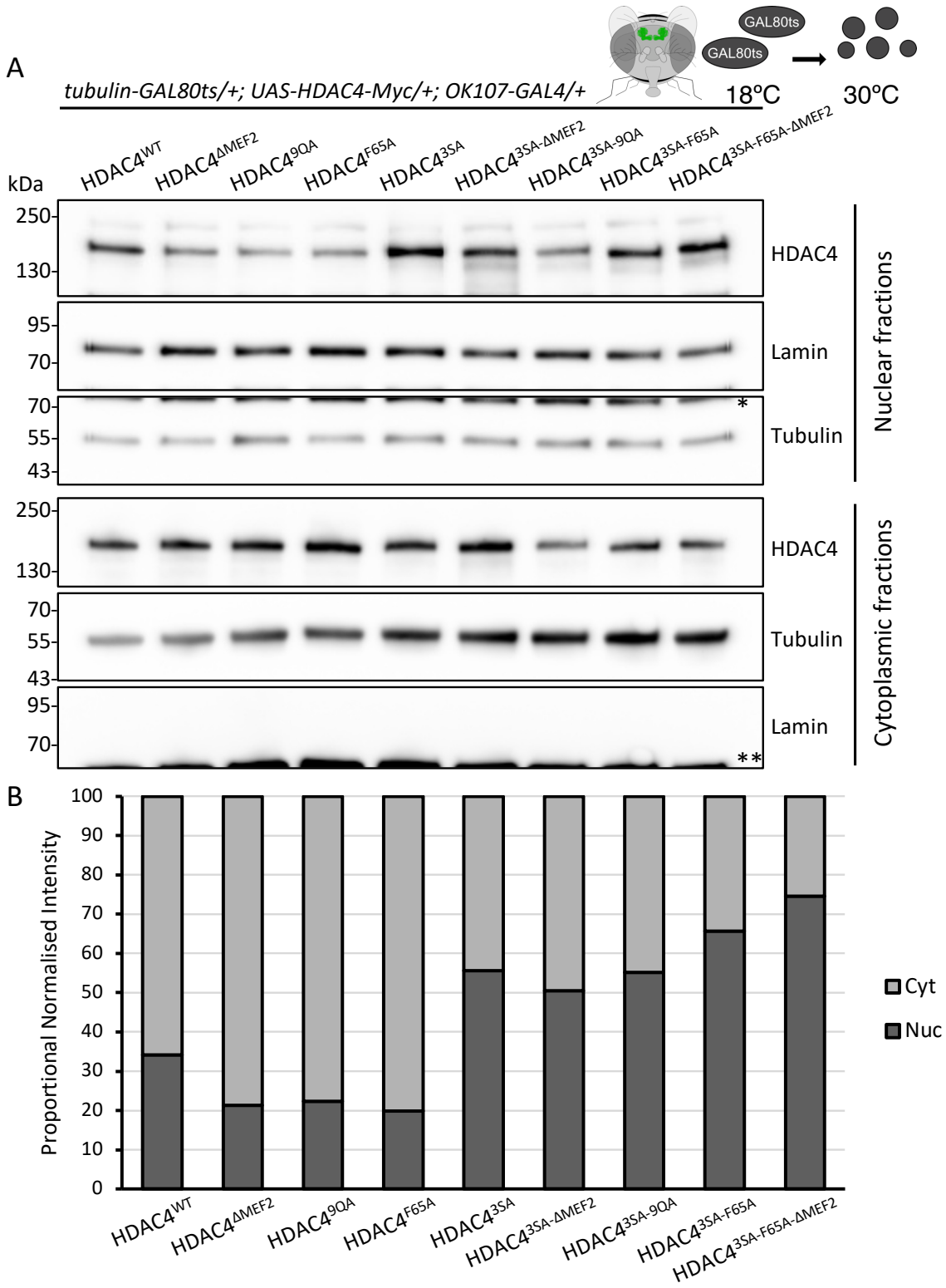

Figure 5.6 Oligomerisation of HDAC4 regulates its nuclear localisation in Kenyon cells
Subcellular fractionation was performed on the heads of flies expressing *HDAC4*^{WT} and *HDAC4*^{mutant} under the control of *OK107-GAL4* in the presence of the TARGET system. Flies were raised at 18 °C until eclosion, and adults were transferred to 30 °C for three days to induce expression. (A) Total protein was loaded (20 µg) for both nuclear and cytoplasmic fractions, and each was probed with anti-Myc to detect HDAC4, and anti-lamin and anti-alpha-tubulin to assess nuclear and cytoplasmic abundance respectively in each lysate. Lamin was observed at ~71 kDa and tubulin at ~55 kDa. * indicates residual detection of lamin due to re-probing. ** indicates residual detection of tubulin due to re-probing. No

lamin was observed in the cytoplasmic fractions. Blots were exposed for the same amount of time for each antibody detection and underwent the same adjustments in brightness and contrast between nuclear and cytoplasmic membranes. (B) Nuclear and cytoplasmic HDAC4 were quantified and normalised to lamin and tubulin respectively. Total normalised HDAC4 intensity was calculated, and the proportion of nuclear and cytoplasmic distribution is displayed. Cyt, cytoplasmic; Nuc, nuclear. Full blots are found in Appendix 10.3.2, Figure 10.24.

The proportion of cytoplasmic contamination of the nuclear fraction increased in Figure 5.6 compared to Figure 5.5, therefore the proportional distribution cannot be directly compared between the two. Under the control of *OK107-GAL4* in Kenyon cells, HDAC4^{WT} was 34% nuclear, while HDAC4^{3SA} was 56% nuclear. Notably, HDAC4$^{\Delta MEF2}$ was decreased in nuclear distribution compared to HDAC4^{WT} at 21%, suggesting that this protocol is sensitive enough to detect MEF2-dependent changes in distribution in Kenyon cells. Interestingly, HDAC4^{9QA} and HDAC4^{F65A} nuclear distribution was also reduced to 23% and 20% respectively compared to HDAC4^{WT}. HDAC4$^{3SA\text{-}F65A}$ and HDAC4$^{3SA\text{-}F65A\text{-}\Delta MEF2}$ were also increased in nuclear abundance compared to HDAC4^{3SA} at 66% and 75% respectively. While the 3SA mutation prevents 14-3-3 dependent nuclear export and thus induces nuclear localisation, the ΔMEF2 mutation counters this by preventing MEF2-dependent nuclear import (Main *et al.*, 2021; Tan *et al.*, 2024; Wang & Yang, 2001). As a result, the nuclear import of HDAC4 constructs with both the 3SA and ΔMEF2 mutations is facilitated by the NLS of HDAC4, as well as by oligomerisation with endogenous HDAC4, and prevention of nuclear exit by the 3SA mutation results in nuclear localisation.

These data therefore confirm that the 3SA mutation increases the nuclear localisation of HDAC4 oligomerisation mutants, and these can now be used to assess the impact of the F65A and 9QA mutations on HDAC4 overexpression-induced phenotypes independent of changes in subcellular distribution. These data also support the immunohistochemistry shown in Figure 5.1 and 5.2 wherein both F65A and 9QA mutations (in the absence of the 3SA mutation) decrease nuclear localisation of HDAC4 in Kenyon cells, together supporting the hypothesis that oligomerisation of HDAC4 promotes nuclear entry. Moreover, these data support that oligomerisation and distribution of HDAC4 appears to be regulated in a cell-type specific manner, illustrating the importance of informed driver selection to appropriately address the biological question at hand. While the proportional distribution has been quantified and reported in these experiments, these were calculated from a single data set and further replication is essential.

5.2.3. Nuclear-restricted HDAC4 mutants are altered in oligomerisation capacity

14-3-3 binding sites have been linked to the regulation of protein aggregation, whereby the introduction of 14-3-3 binding sites into aggregation-prone proteins reduces their aggregation and increases their solubility (Segal *et al.*, 2023). It is therefore possible that addition of the 3SA mutation to the HDAC4 tetramerisation mutants may induce aggregation, and thus oligomerisation of HDAC4, independent of the hydrophobic core and stabilising glutamine residues. Moreover, it is possible that the increased nuclear localisation may also alter aggregation of these mutant proteins. To determine whether the 3SA mutation impacts the intrinsic oligomerisation of HDAC4, co-immunoprecipitation was again performed to assess the ability of each nuclear-localised Myc-tagged oligomerisation mutant to interact with wild-type GFP-HDAC4^{WT} as performed previously (Section 4.3.3). Immunoprecipitation of GFP-HDAC4^{WT} was successful in all samples, and resulted in co-immunoprecipitation of HDAC4^{WT}-Myc (Figure 5.7A-B, lane 3). In further confirmation of the previous co-immunoprecipitation experiment (Figure 4.9), neither HDAC4^{9QA} nor HDAC4^{F65A} significantly co-immunoprecipitated with GFP-HDAC4^{WT} (Figure 4.9A, lanes 4-5; B, lanes 4 and 6) indicating a markedly reduced ability to oligomerise. Incorporation of the 3SA mutation did not alter this as neither HDAC4$^{3SA\text{-}9QA}$ nor HDAC4$^{3SA\text{-}F65A}$ co-immunoprecipitated with GFP-HDAC4^{WT} (Figure 4.9A, lane 6, B, lane 5, respectively). These data indicate that the 3SA mutation does not further reduce the intrinsic ability of HDAC4^{F65A} or HDAC4^{9QA} to fail to form oligomers with GFP-HDAC4. It is important to note that these experiments were performed using whole-cell lysates, and therefore nuclei were lysed early on in the protocol. It is hypothesised that HDAC4 oligomerisation is dynamic, and therefore these experiments do not directly address whether nuclear-localisation affects the oligomerisation of HDAC4, rather these experiments address whether the 3SA mutation alters oligomerisation in a whole-cell lysate, which may be independent of subcellular localisation.

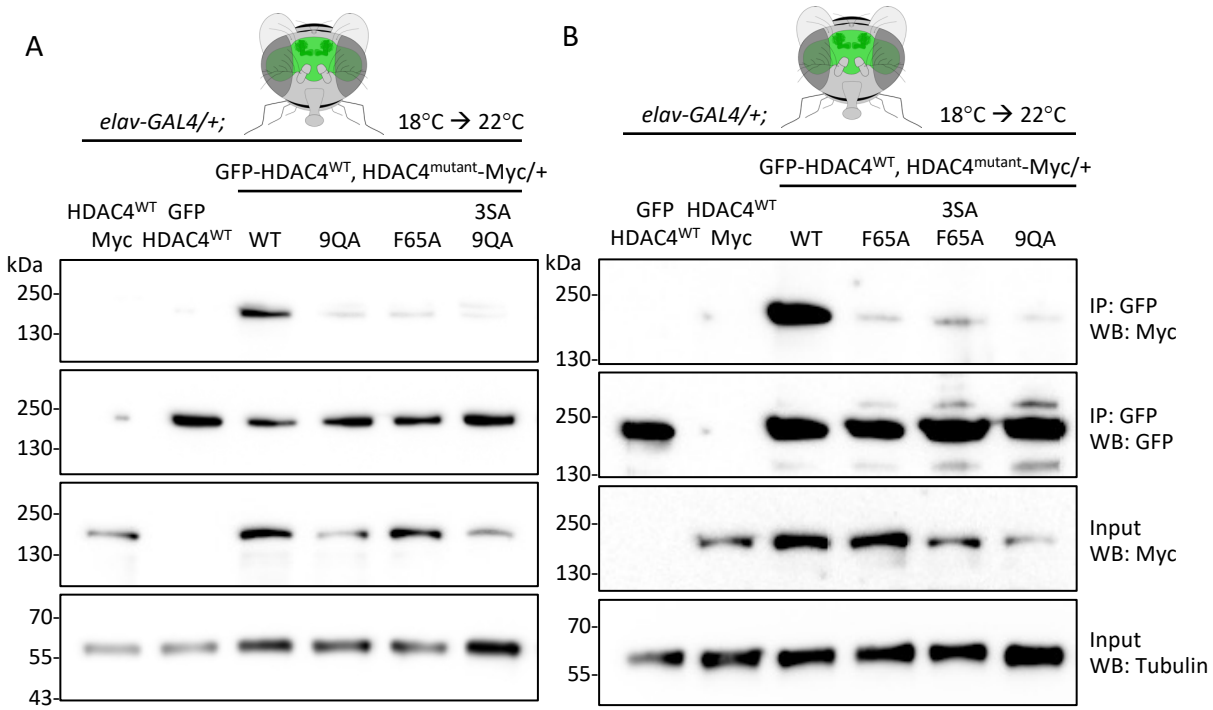

Figure 5.7 The 3SA mutations do not affect oligomerisation of HDAC4 mutants
(A, B) Co-immunoprecipitation experiments to examine the ability of HDAC4^{mutant} to bind HDAC4^{WT} to assess oligomerisation capacity. The indicated transgenes were expressed pan-neuronally in *Drosophila* under the control of *elav-GAL4*. Flies were raised at 18 °C until adulthood and adults were moved to 22 °C for five days to increase level of transgene expression before harvesting and generation of whole-head lysates. Anti-GFP conjugated beads were used to immunoprecipitate GFP-HDAC4^{WT} from all samples, followed by probing for HDAC4-Myc. HDAC4^{WT} co-immunoprecipitated with GFP-HDAC4^{WT} while HDAC4^{9QA}, HDAC4^{F65A}, HDAC4$^{3SA-9QA}$ and HDAC4$^{3SA-F65A}$ did not do so significantly despite comparable immunoprecipitation of GFP-HDAC4^{WT} from all samples. Input samples were 30 µg of whole-cell lysate, and the level of transgene expression is consistent with previously quantification (Figures 4.7 and 5.4). Protocol 2 was used for the data shown in (A), and protocol 1 for the data shown in (B) (Section 3.2.4).

5.2.4. Enforced nuclear localisation increases aggregation of HDAC4 oligomerisation mutants

Next, the ability of each nuclear-restricted oligomerisation mutant to aggregate in Kenyon cell nuclei was examined as performed previously (Section 4.4.2). HDAC4^{3SA} and HDAC4$^{3SA-mutant}$ expression was induced during adulthood under the control of *OK107-GAL4* via the TARGET system, and brains were dissected and immunostained with antibodies against the Myc tag, and endogenous MEF2 (Figure 5.8). Imaging of Kenyon cells in the posterior of the brain confirmed the co-localisation of HDAC4^{3SA} and MEF2 in nuclei (Figure 5.8 A-B). HDAC4^{3SA} formed many nuclear aggregates that sequestered MEF2. HDAC4$^{3SA-9QA}$ still formed many aggregates (Figure 5.8C) however these were smaller than those formed upon expression of HDAC4^{3SA} (Figure 5.8B). In contrast HDAC4$^{3SA-F65A}$ (Figure 5.8D) and HDAC4$^{3SA-\Delta MEF2}$ (Figure 5.8E)

were massively reduced in aggregate size and number, and few aggregates of HDAC4$^{3SA\text{-}F65A\text{-}\Delta MEF2}$ (Figure 5.8F) were detected.

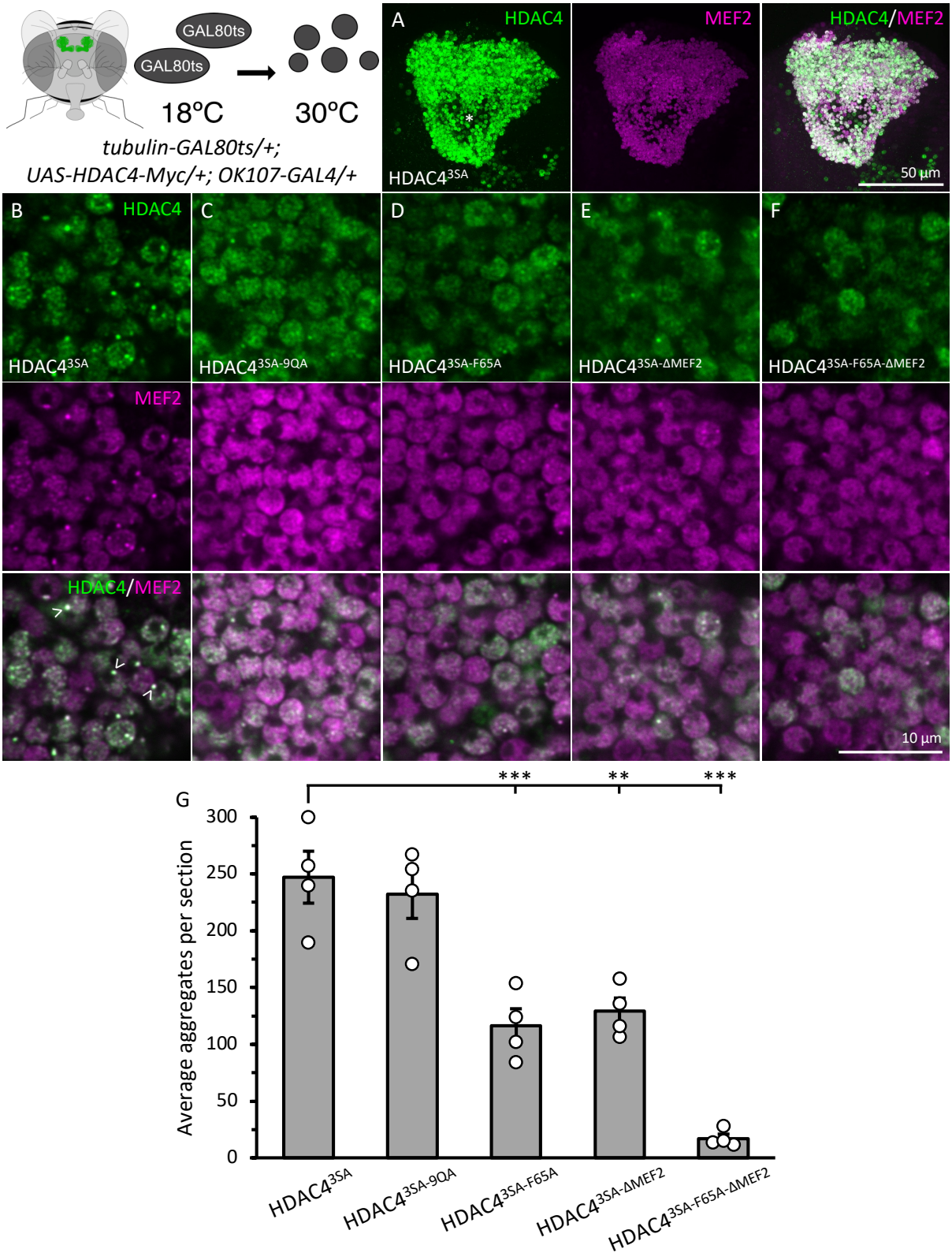

Figure 5.8 Nuclear-restricted HDAC4 oligomerisation mutants alter redistribution of MEF2 to aggregates and the number of aggregates in Kenyon cells

(A) Maximum projection of optical sections through the Kenyon cell layer in the posterior of the brain of flies expressing HDAC4^{3SA} or HDAC4$^{3SA\text{-}mutant}$ under the control of *OK107-GAL4* in the presence of the TARGET system. Flies were raised at 18 °C until eclosion, where adults were transferred to 30 °C for three days to induce HDAC4 expression. HDAC4 (green) was observed in Kenyon cell nuclei where endogenous MEF2 (magenta) was present, white indicates co-distribution. HDAC4^{3SA} was absent from dendrites in the calyx (*). (B-F) Magnified single optical section (0.5 µm) depicting the distribution and aggregation of HDAC4^{3SA} and HDAC4$^{3SA\text{-}mutant}$ in Kenyon cells. (B) HDAC4^{3SA} was nuclear and formed large aggregates that sequestered MEF2 (arrowheads). (C-F) Mutations to the N-terminus of HDAC4 reduced the formation of HDAC4-containing aggregates. (G) Quantification of HDAC4 aggregates. Aggregates of HDAC4 that co-localised with MEF2 were counted through the Kenyon cell layer (as seen in A) for 10 optical sections spaced 1µm apart as per Section 3.4.6, n=4 brains per genotype. The mean is plotted, and the average number of aggregates per section per brain are plotted as individual points. Error bars indicate the SEM. Aggregate number was significantly reduced for each of HDAC4$^{3SA\text{-}F65A}$, HDAC4$^{3SA\text{-}\Delta MEF2}$, and HDAC4$^{3SA\text{-}F65A\text{-}\Delta MEF2}$ compared to HDAC4^{3SA} (ANOVA, $F(4,15)=32.65$, $p<0.0001$, post-hoc Tukey's HSD **$p<0.01$, ***$p<0.001$). HDAC4$^{3SA\text{-}F65A\text{-}\Delta MEF2}$ was significantly reduced compared to HDAC4$^{3SA\text{-}F65A}$ ($p=0.005262$). There was no significant difference between HDAC4^{3SA} and HDAC4$^{3SA\text{-}9QA}$ ($p=0.9681$) or HDAC4$^{3SA\text{-}F65A}$ and HDAC4$^{3SA\text{-}\Delta MEF2}$ ($p=0.9785$).

Quantification of aggregates containing both HDAC4 and MEF2 corroborated these observations (Figure 5.8G). However, it should be reiterated that this quantification does not consider aggregate size, and therefore significant increases in aggregation which result in aggregate coalescence are underestimated. Expression of HDAC4^{3SA} resulted in an average of 247 aggregates per section, and this was slightly but insignificantly reduced to 232 by HDAC4$^{3SA\text{-}9QA}$. Aggregate number was significantly reduced by approximately half upon expression of either HDAC4$^{3SA\text{-}F65A}$ or HDAC4$^{3SA\text{-}\Delta MEF2}$ to 116 and 129 aggregates per section respectively, and this was further reduced to 17 aggregates per section upon combination of these mutations in HDAC4$^{3SA\text{-}F65A\text{-}\Delta MEF2}$. This experiment was performed in parallel with that in Figure 4.22, therefore the numbers of aggregates can be directly compared; HDAC4$^{3SA\text{-}9QA}$ and HDAC4$^{3SA\text{-}F65A}$ were significantly increased in aggregate number compared to HDAC4^{9QA} and HDAC4^{F65A}, which had an average of 41 and 37 aggregates per section respectively. These data demonstrate that enforced nuclear localisation increases the aggregation of HDAC4 oligomerisation mutants, and that compared to nuclear HDAC4^{3SA}, the F65A or ΔMEF2 mutations significantly reduced both the number and size of aggregates. The total number of HDAC4$^{3SA\text{-}9QA}$ aggregates was not significantly reduced compared to HDAC4^{3SA}, however they were smaller, which indicates a reduced capacity to aggregate. The role of MEF2 in aggregate stabilisation is further investigated in Section 5.4.

5.2.5. Enforced nuclear localisation differentially impacts the ability of HDAC4 oligomerisation mutants to confer mushroom body phenotypes

Overexpression of HDAC4^{WT} induces defects in the development of the mushroom body (Main *et al.*, 2021; Tan *et al.*, 2024), and mutations that reduce oligomerisation of HDAC4 reduce the severity of β lobe fusion (Section 4.5.1). Mutations that reduce nuclear distribution of HDAC4 also reduce the severity of β-lobe fusion, and these phenotypes are dependent on interaction of HDAC4 with MEF2 (Main *et al.*, 2021; Tan *et al.*, 2024). Therefore, the nuclear-restricted oligomerisation mutants were assessed for their ability to impair mushroom body development. Expression of each HDAC4$^{3SA\text{-}mutant}$ construct was driven by *elav-GAL4* throughout development and immunostaining against FasII was performed on adult brains. Consistent with previous results from our laboratory (Tan *et al.*, 2024), the predominant phenotype resulting from expression of nuclear-restricted HDAC4 was severe β-lobe fusion, which occurred in 100% of brains examined (Table 5.2, Figure 5.9). Guidance defects were also present in 50% of brains upon expression of HDAC4^{3SA}. Interestingly, when restricted to the nucleus, HDAC4$^{3SA\text{-}9QA}$ significantly reduced severe β-lobe fusion to 60% compared to 100% for HDAC4^{3SA}, but the same level of reduction was not observed for HDAC4$^{3SA\text{-}F65A}$, which only decreased severe β-lobe fusion to 80%. Strikingly, no severe β-lobe fusion was observed for HDAC4$^{3SA\text{-}\Delta MEF2}$ or HDAC4$^{3SA\text{-}F65A\text{-}\Delta MEF2}$, and total fusion was reduced to 30% and 11% respectively. These data support the hypothesis that β-lobe fusion resulting from HDAC4-overexpression is largely dependent on an intact MEF2 binding site.

Table 5.2 Frequency of mushroom body phenotypes resulting from the expression of nuclear-restricted HDAC4 oligomerisation mutants at 22 °C and 18 °C

	22°C									18°C				
(% of brains)	Con	HDAC4 WT	HDAC4 9QA	HDAC4 F65A	HDAC4 3SA	HDAC4 3SA-9QA	HDAC4 3SA-F65A	HDAC4 3SA-ΔMEF2	HDAC4 3SA-F65A-ΔMEF2	Con	HDAC4 WT	HDAC4 3SA	HDAC4 F65A	HDAC4 3SA-F65A
α thinning	0	35	0	10	50	27	35	5	0	0	10	40	0	10
α missing	0	0	0	0	6	24	0	0	0.0	5	0	5	0	0
β thinning	0	25	5	0	13	9	5	0	6	0	0	10	0	15
β missing	0	0	5	5	13	0	5	5	11	0	0	5	10	5
β fusion	**0**	**95**	**80**	**50**	**100**	**82**	**100**	**30**	**11**	**20**	**100**	**100**	**65**	**100**
Mild	0	0	50	25	0	24	20	30	11	20	15	10	60	50
Severe	0	95	30	25	100	59	80	0	0	0	85	90	5	50
Guidance	0	0	10	5	50	32	45	10	11	5	0	50	15	40
n	20	20	20	20	16	34	20	20	18	20	20	20	20	20

Expression of each denoted *HDAC4* transgene was mediated by *elav-GAL4*; virgin *elav-GAL4* female flies were crossed to males harbouring the *HDAC4* transgene, and adult progeny of this cross were dissected and their brains immunostained for FasII to assess mushroom body lobe development. Flies were raised at 18°C or 22°C as indicated. Instances of defects in morphology were scored for n=20 brains per genotype as per Section 3.4.7, and are displayed as the % of brains with the indicated phenotype. Control (con) is *elav-GAL4*/+. This experiment was performed concurrently with the examination of $HDAC4^{9QA\text{-}F65A}$, therefore samples for each of control, $HDAC4^{WT}$, $HDAC4^{9QA}$ and $HDAC4^{F65A}$ at 22°C are the same between this table and Table 4.3, and are repeated here for ease of comparison. Percentages may not sum to 100 due to rounding.

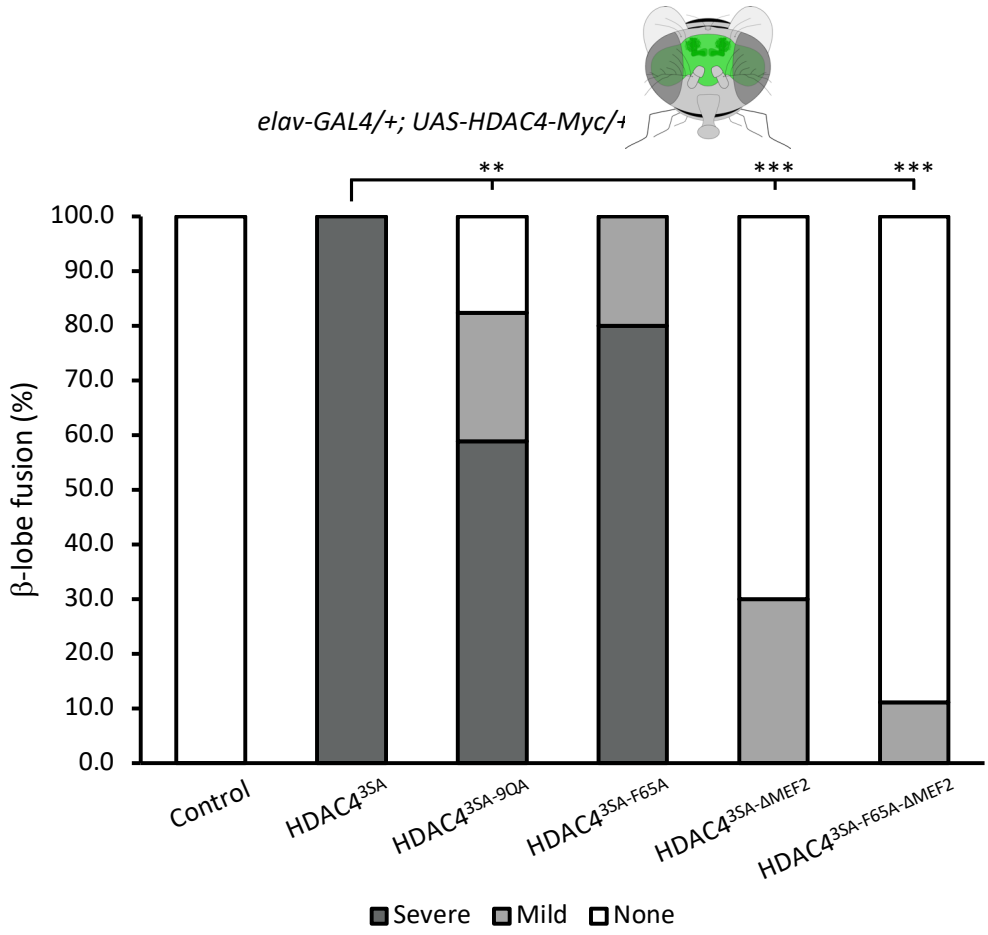

Figure 5.9 Nuclear-restricted HDAC4 oligomerisation mutants alter the severity of β-lobe fusion of the mushroom body

Quantification of β-lobe fusion resulting from HDAC4 overexpression. HDAC4 expression was driven by *elav-GAL4* at 22°C, adult brains were processed for anti-FasII immunohistochemistry, and β-lobe fusion was scored. Control is *elav-GAL4/+*. n≥16 brains per genotype. $HDAC4^{3SA-9QA}$, $HDAC4^{3SA-\Delta MEF2}$, and $HDAC4^{3SA-F65A-\Delta MEF2}$ mutants each significantly reduced severe β-lobe fusion compared to $HDAC4^{3SA}$ (Fisher's exact test, severe β-lobe fusion, p=0.0019, p<0.0001, and p<0.0001 respectively. **p<0.01, ***p<0.001). There was no significant difference in severe fusion between $HDAC4^{3SA}$ and $HDAC4^{3SA-F65A}$ (p=0.1131, severe fusion).

As HDAC4-overexpression induced β-lobe fusion is dose dependent (Section 4.5.1), the level of expression of HDAC4 was reduced to determine whether there was a significant difference between $HDAC4^{3SA}$ and $HDAC4^{3SA-F65A}$. To achieve this, *HDAC4* overexpression was driven by *elav-GAL4* and flies were raised at 18°C to induce a lower level of GAL4 activity and thus a lower level of HDAC4 expression (Table 5.2, Figure 5.10). At 18°C, $HDAC4^{WT}$ induced severe β-lobe fusion in 85% of brains, and this was reduced to 5% by the F65A mutation. A similar reduction was observed for the nuclear-restricted mutants; $HDAC4^{3SA}$ induced severe β-lobe fusion in 90% of brains and this was reduced to 50% by $HDAC4^{3SA-F65A}$. Together these

data demonstrate that mutations that reduce oligomerisation of HDAC4 results in a reduction in β-lobe fusion phenotypes regardless of subcellular distribution.

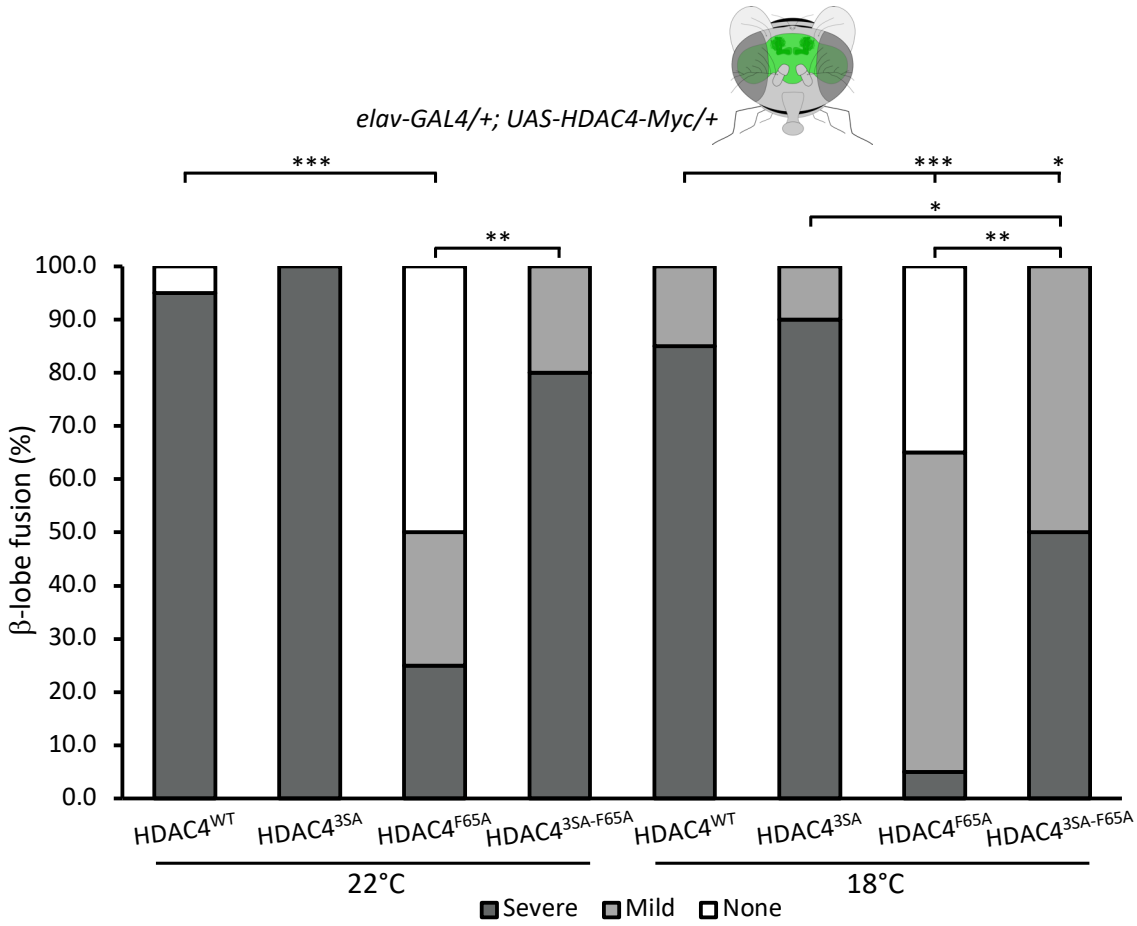

Figure 5.10 Comparison of the β-lobe fusion phenotype resulting from expression of nuclear-restricted HDAC4 oligomerisation mutants at 22 °C and 18 °C

Quantification of β-lobe fusion resulting from HDAC4 overexpression. HDAC4 expression was driven by *elav-GAL4* at either 18°C or 22°C, adult brains were processed for anti-FasII immunohistochemistry, and β-lobe fusion was scored. n≥16 brains per genotype. At 22°C, severe β-lobe fusion was reduced for $HDAC4^{F65A}$ compared to $HDAC4^{3SA-F65A}$ (Fisher's exact test, severe β-lobe fusion, p=0.0012. *p<0.05, **p<0.01, ***p<0.001), but the difference between $HDAC4^{3SA}$ and $HDAC4^{3SA-F65A}$ was not significant (p=0.1131). Severe β-lobe fusion was also reduced for $HDAC4^{F65A}$ compared to $HDAC4^{WT}$ (p<0.0001). At 18°C severe β-lobe fusion was significantly reduced for $HDAC4^{3SA-F65A}$ compared to $HDAC4^{3SA}$ (p=0.0138). $HDAC4^{3SA-F65A}$ severity was increased compared to $HDAC4^{F65A}$ (p=0.0033). Severe β-lobe fusion was reduced for $HDAC4^{F65A}$ and $HDAC4^{3SA-F65A}$ compared to $HDAC4^{WT}$ (p<0.0001 and p=0.0407 respectively). Please note that the data at 22°C is reproduced from that in Figure 5.9 and Figure 4.23.

5.2.6. Enforced nuclear localisation differentially impacts the ability of HDAC4 oligomerisation mutants to disrupt eye development

Overexpression of HDAC4^{WT} in the *Drosophila* eye significantly impacts its development; adult eyes present with severe fusion of ommatidia and loss of pigmentation (Main *et al.*, 2021; Tan *et al.*, 2024). As shown in Section 4.5.2, the presence of either the F65A or 9QA mutations significantly reduced these phenotypes, although to varying degrees; F65A completely rescued the eye defects, and while the fusion defects were reduced by 9QA, the pigmentation defects remained. Both HDAC4^{F65A} and HDAC4^{9QA} were also reduced in nuclear distribution in the larval eye disc compared to HDAC4^{WT} (Section 4.4.3). It is therefore of interest to reassess eye phenotypes with the nuclear-restricted tetramerisation mutants to examine the effect of reduced oligomerisation without the confounding effect of reduced nuclear localisation.

HDAC4 expression was driven in post-mitotic photoceptors under the control of *GMR-GAL4* and adult eyes imaged. In the presence of one insertion of each of *GMR-GAL4* and the *HDAC4^{3SA}* transgene, there was a mild phenotype consisting of occasional fusion and misalignment of ommatidia, and loss of pigmentation (Appendix Section 10.3.3, Figure 10.26). This was completely reduced by each of HDAC4$^{3SA\text{-}9QA}$, HDAC4$^{3SA\text{-}F65A}$, and HDAC4$^{3SA\text{-}F65A\text{-}\Delta MEF2}$, but not HDAC4$^{3SA\text{-}\Delta MEF2}$. Therefore, to further tease out the difference between each of these mutations, the dose of HDAC4 was increased as previously shown (Section 4.5.2). Increasing the dose of HDAC4^{3SA} increased the severity of the overexpression-induced phenotype (Figure 5.11B). Flies harbouring one insertion of *GMR-GAL4* and two of *HDAC4^{3SA}* (*GMR-GAL4/+; HDAC4^{3SA}-Myc*) presented with complete fusion of ommatidia, loss of pigmentation, and loss of bristles. Eyes also appeared shrunken toward the ventral side, and necrosis was observed. Expression of HDAC4$^{3SA\text{-}9QA}$ slightly reduced the severity of the phenotype with only small spots of necrosis, but widespread fusion of ommatidia was still evident as well as loss of pigmentation (Figure 5.11C). In a stark contrast, HDAC4$^{3SA\text{-}F65A}$ was significantly reduced in severity of the phenotype; individual ommatidia could be located and pigmentation was increased, but fusion and disorganisation persisted (Figure 5.11D). Combination of the MEF2 binding site mutations further reduced the severity of this, where HDAC4$^{3SA\text{-}F65A\text{-}\Delta MEF2}$ appeared largely wild-type with red pigmentation and no fusion of ommatidia, however in males ommatidial alignment was still slightly disrupted (Figure 5.11F). In contrast, HDAC4$^{3SA\text{-}\Delta MEF2}$ barely reduced the severity of the phenotype compared to HDAC4^{3SA} (Figure 5.11E).

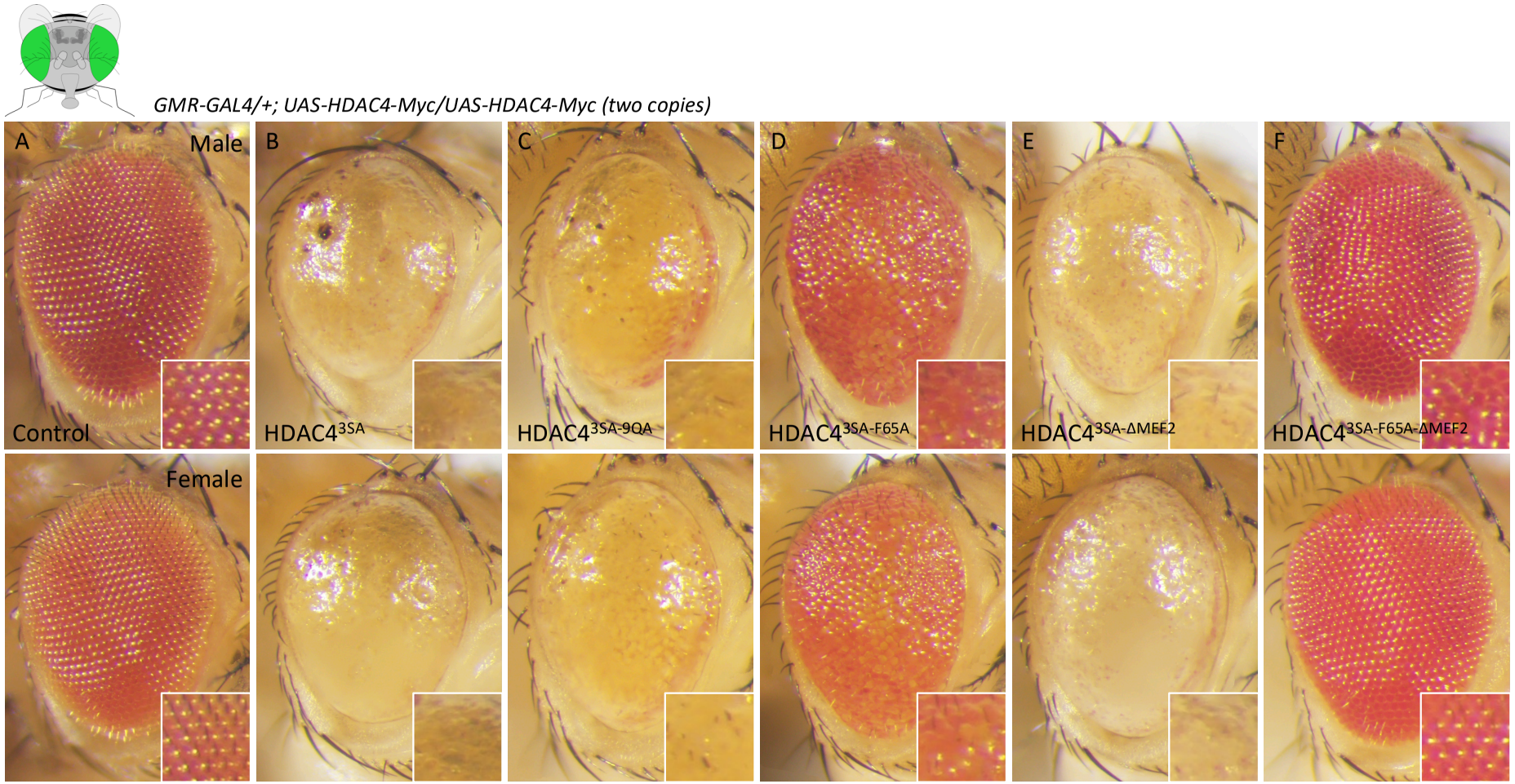

Figure 5.11 Increased dose of HDAC4 exacerbates differences in disruption of eye development between the nuclear-restricted HDAC4 oligomerisation mutants

Light microscopy (110x magnification) images of *Drosophila* eyes raised at 25°C. Top row, males; bottom row, females. Inset shows a magnified image of ommatidia. (A) Control is *GMR-GAL4/+; +/+*. (B-F) Flies harboured one copy of the driver (*GMR-GAL4/+*) and two copies of the transgene (*UAS-HDAC4/UAS-HDAC4*). (B) HDAC4^{3SA} overexpression induced severe fusion of all ommatidia across the eye with complete loss of pigmentation and bristles, and small spots of necrosis. Only a small amount of pigmentation was rescued upon expression of HDAC4$^{3SA-9QA}$ (B) while the eye increased in size with HDAC4$^{3SA-\Delta MEF2}$ (E). Both HDAC4$^{3SA-F65A}$ (D) and HDAC4$^{3SA-F65A-\Delta MEF2}$ (F) significantly reduced severity, and HDAC4$^{3SA-F65A-\Delta MEF2}$ was largely the same as

the control.

Implementation of the semi-quantitative scoring system (Section 3.5.1) supported these observations (Figure 5.12); HDAC4^{3SA} had the most severe phenotype with a score of 100%, and this was only slightly reduced to 87% for HDAC4$^{3SA\text{-}9QA}$. Phenotypes resulting from expression of HDAC4$^{3SA\text{-}F65A}$ and HDAC4$^{3SA\text{-}F65A\text{-}\Delta MEF2}$ were significantly reduced to 55% and 4% respectively compared to HDAC4^{3SA}. Despite no significant reduction by HDAC4$^{3SA\text{-}\Delta MEF2}$ compared to HDAC4^{3SA}, combination of the ΔMEF2 mutation into HDAC4$^{3SA\text{-}F65A\text{-}\Delta MEF2}$ significantly reduced the severity compared to HDAC4$^{3SA\text{-}F65A}$. There was no significant difference between the eyes of controls and HDAC4$^{3SA\text{-}F65A\text{-}\Delta MEF2}$ expressing flies. Together these data indicate that Phe65 plays a critical role in nuclear HDAC4-induced disruption to eye development, and that this acts synergistically with the MEF2-binding site to impede development.

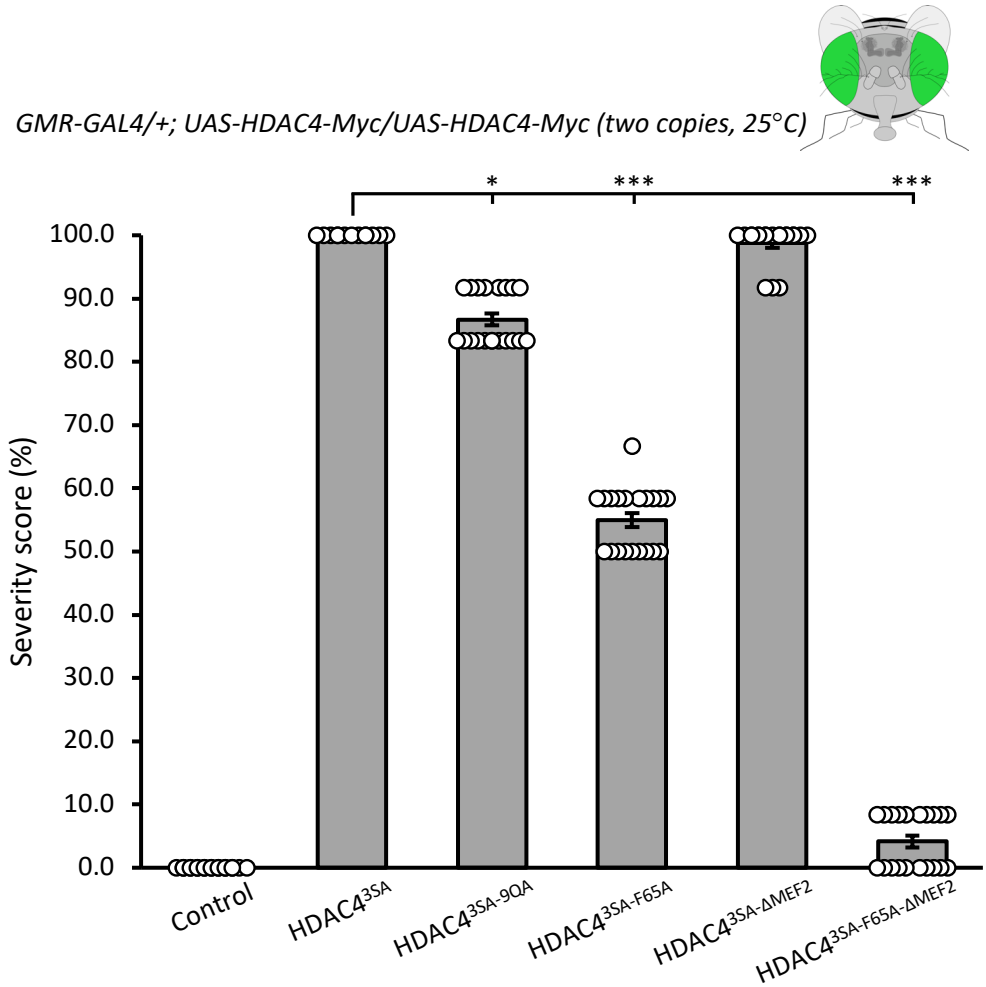

Figure 5.12 Implementation of a scoring system to characterise HDAC4-overexpression induced deficits in eye development resulting from expression of nuclear-restricted oligomerisation mutants

The severity of eye phenotypes resulting from HDAC4 expression under the control of *GMR-GAL4* at 25°C was scored as per Section 3.5.1. Flies were heterozygous for *GMR-GAL4* and homozygous for *HDAC4* (*GMR-GAL4/+, UAS-HDAC4/UAS-HDAC4*). Control is *GMR-GAL4/+; +/+*. Severity scores were converted to % severity and the average is displayed. Individual data points are represented as circles, and error bars indicate the SEM. n≥13 eyes per genotype. Significant differences between $HDAC4^{3SA}$ and $HDAC4^{3SA\text{-}mutant}$ were observed (Kruskal-Wallis test, $H_{(5)}=106.92$, $p<0.001$, post-hoc Dunn's test, **$p<0.01$, ***$p<0.001$. $HDAC4^{3SA}$ vs $HDAC4^{3SA\text{-}9QA}$, $p=0.01561$; vs $HDAC4^{3SA\text{-}F65A}$, $p<0.001$; vs $HDAC4^{3SA\text{-}\Delta MEF2}$, $p=0.07861$; vs $HDAC4^{3SA\text{-}F65A\text{-}\Delta MEF2}$ $p<0.001$. $HDAC4^{3SA\text{-}F65A}$ vs $HDAC4^{3SA\text{-}F65A\text{-}\Delta MEF2}$ $p=0.01387$. Control vs $HDAC4^{3SA\text{-}F65A\text{-}\Delta MEF2}$ $p=0.3387$).

5.2.7. $HDAC4^{3SA\text{-}F65A}$ has different aggregation characteristics between Kenyon cells and basal cells of the larval eye disc

In comparison to the expression of $HDAC4^{WT}$, the expression of $HDAC4^{F65A}$ reduced severe β-lobe fusion in the mushroom body (Section 4.5.1) as well as defects in adult eye development (Section 4.5.2), however the same pattern of rescue was not as prominent upon restriction of localisation to the nucleus with $HDAC4^{3SA\text{-}F65A}$, and observing reductions in the severity of β-lobe fusion required a reduced dose of expression. It was hypothesised that this was a result of increased severity due to nuclear localisation inherently increasing the ability of HDAC4 to aggregate. Therefore, the aggregation characteristics of $HDAC4^{3SA\text{-}F65A}$ were further examined in the Kenyon cells of the adult brain, and the basal cells of the larval eye disc (Figure 5.13). These data were collected in parallel with that in Figure 5.2 and Figure 4.14, and therefore can be directly compared. Pan-neuronal expression of $HDAC4^{3SA\text{-}F65A}$ was driven throughout development with *elav-GAL4*, and its distribution in Kenyon cells compared to $HDAC4^{3SA}$ (Figure 5.13A-B). Under these conditions in Kenyon cells, $HDAC4^{3SA}$ formed large punctate aggregates in nuclei. $HDAC4^{3SA\text{-}F65A}$ remained localised to nuclei and formed aggregates, however these were reduced in size and intensity. In comparison, in the basal cells of the larval eye disc, when expressed under the control of *GMR-GAL4*, $HDAC4^{3SA}$ formed large aggregates in nuclei (Figure 5.13C) whereas $HDAC4^{3SA\text{-}F65A}$ rarely formed punctate foci and instead had a granular nuclear distribution (Figure 5.13D). These data demonstrate different aggregation characteristics of $HDAC4^{3SA\text{-}F65A}$ in a tissue-specific manner; aggregation of $HDAC4^{3SA\text{-}F65A}$ appears more significant in Kenyon cells than in the basal cells of the larval eye disc. This may explain the differences in severity of the developmental phenotypes, and supports that Phe65 is more important for the mechanism through which HDAC4 disrupts development of the eye compared to the mushroom body.

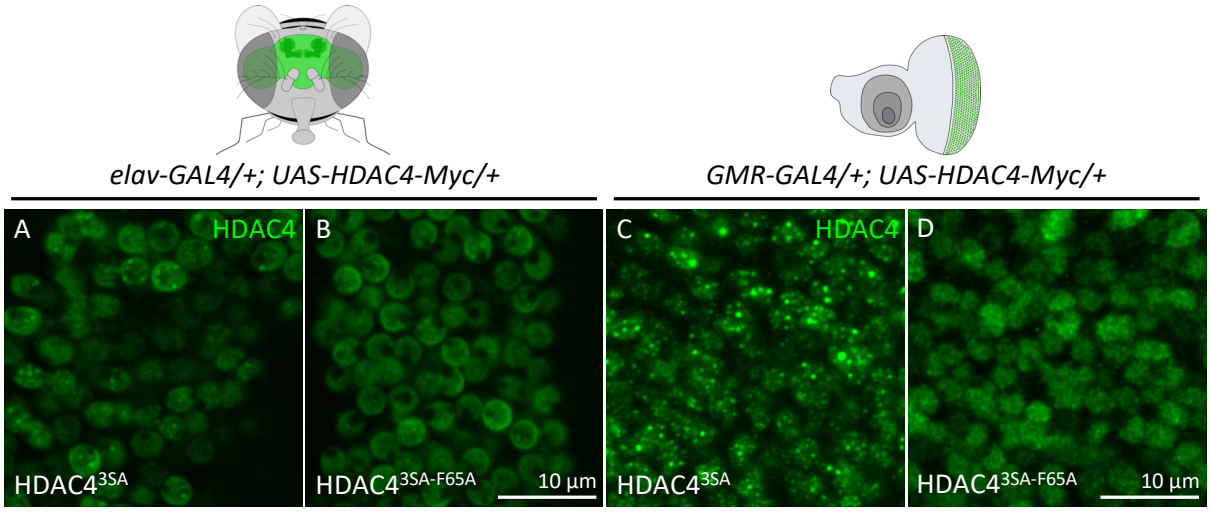

Figure 5.13 HDAC4$^{3SA-F65A}$ has different aggregation characteristics between Kenyon cells and the basal cells of the larval eye disc
(A-B) Single optical sections (0.5 µm) of Kenyon cells in the posterior of the adult brain expressing HDAC4^{3SA} or HDAC4$^{3SA-F65A}$ (green) under the control of *elav-GAL4*. Flies were raised and maintained at 25 °C until dissection. HDAC4^{3SA} formed larger and more intense aggregates than HDAC4$^{3SA-F65A}$, however punctate aggregates were still visible. (C-D) Single optical sections (0.5 µm) of basal cells of the larval eye disc expressing HDAC4^{3SA} and HDAC4$^{3SA-F65A}$ (green) under the control of *GMR-GAL4*. Flies were raised at 25 °C. HDAC4^{3SA} formed significant nuclear aggregates while HDAC4$^{3SA-F65A}$ had a largely granular distribution with few punctate aggregates.

5.3. Overexpression of HDAC4 increases the abundance of MEF2 in Kenyon cells

The findings in Section 5.2 are in agreement with previous studies that determined that the nuclear pool of HDAC4 is responsible for the majority of β-lobe fusion induced by overexpression of HDAC4 (Main *et al.*, 2021; Tan *et al.*, 2024). The importance of MEF2 binding to HDAC4 function is clear; mutation of the MEF2 binding site within HDAC4 (ΔMEF2) almost completely prevents β-lobe fusion regardless of whether HDAC4 is restricted to nuclei (Tan *et al.*, 2024), and knockdown of MEF2 in the presence of HDAC4^{3SA} also reduces the severity of β lobe fusion (Main *et al.*, 2021). Consistent with this, combination of the ΔMEF2 mutations with HDAC4$^{3SA-F65A}$ almost completely abolished β-lobe fusion (Section 5.2.5). However, it is unknown how HDAC4 acts through MEF2 to mediate defects in β-lobe development. Interestingly, during the imaging of Kenyon cells for assessment of aggregation of HDAC4 in Sections 4.4.2, 4.6.2, and 5.2.4, it was noted that MEF2 intensity appeared higher upon overexpression of HDAC4 than in control brains, and it was hypothesised that the defects resulting from increased HDAC4 may be a result of upregulation or stabilisation of MEF2.

5.3.1. Overexpression of HDAC4 increases MEF2 intensity in Kenyon cells

To analyse the change in MEF2 protein levels upon $HDAC4^{WT}$ overexpression, it was first determined whether the increase in MEF2 intensity in Kenyon cells occurred in a dose-dependent manner. The TARGET system can be used to tailor the dose of transgene expression in a temperature-dependent manner (Hawley *et al.*, 2023; Schwartz *et al.*, 2016) therefore $HDAC4^{WT}$ expression was driven under the control of *OK107-GAL4* in the presence of the TARGET system, and the temperature at which expression was induced was varied to modulate the dose of *HDAC4*. All flies were raised at 19 °C until eclosion, where they were transferred to either 25 °C or 30 °C for three days to induce expression, or were maintained at 19 °C. Images were then taken through the Kenyon cell layer and MEF2 intensity was measured (Figure 5.14). At 19 °C, minimal $HDAC4^{WT}$ expression was detected in only a few Kenyon cells. This is consistent with leaky transgene expression observed previously in the presence of the TARGET system at 19 °C (Hawley *et al.*, 2023). The number of cells in which $HDAC4^{WT}$ was detected increased with increasing temperature, consistent with increasing activation of GAL4, and this positively correlated with an increase in the amount of endogenous MEF2.

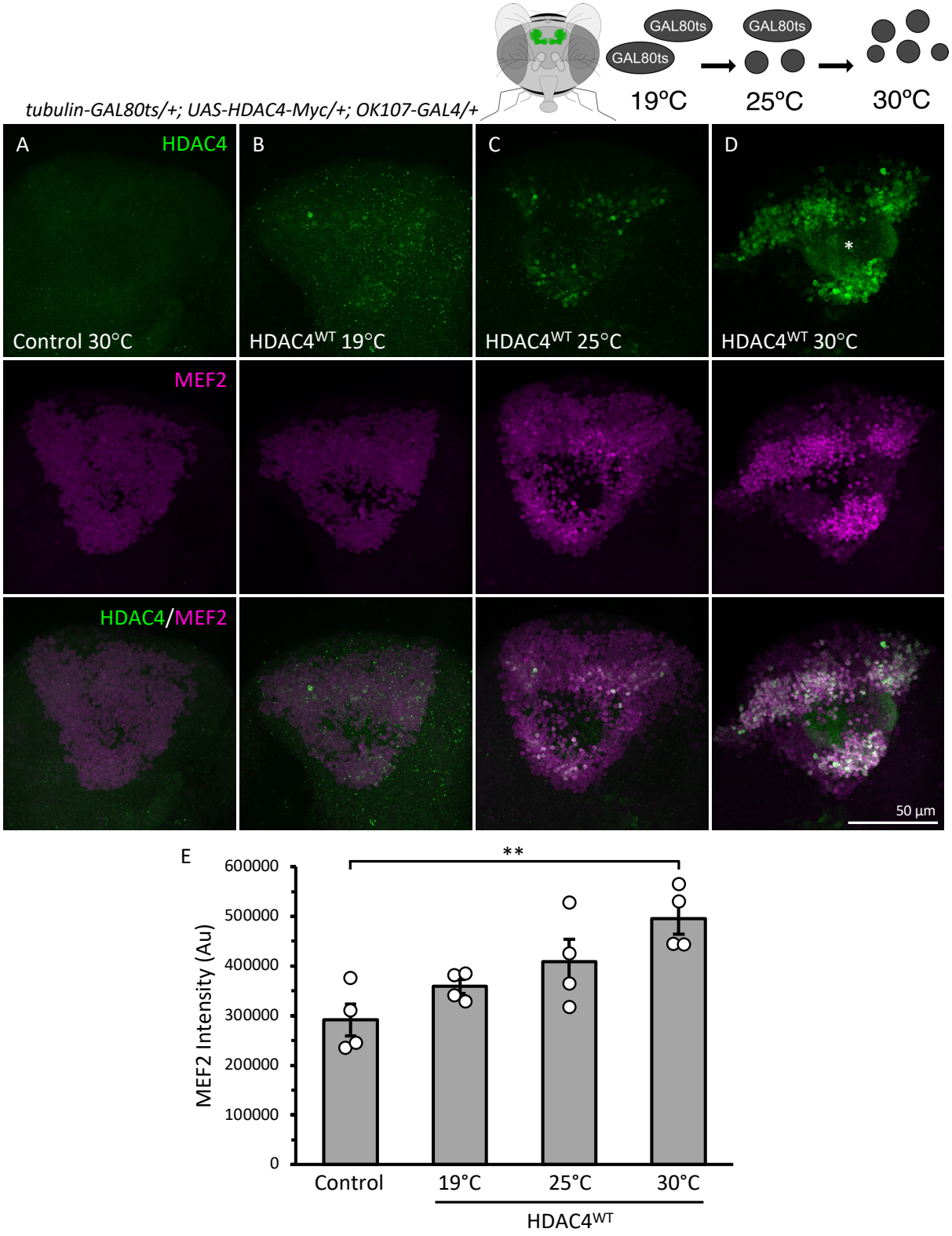

Figure 5.14 Increased expression of HDAC4^{WT} causes a dose-dependent increase in MEF2 in Kenyon cells

(A-D) Maximum projection of optical sections through the Kenyon cell layer in the posterior of the brain of flies expressing *HDAC4^{WT}* under the control of *OK107-GAL4* in the presence of the TARGET system (*tubulin-GAL80ts/+; HDAC4^{WT}-Myc/+; OK107-GAL4/+*); flies were raised at 19 °C until eclosion, where adults were transferred to either 25 °C or 30 °C for three days to induce expression, or maintained at 19 °C. HDAC4 (green) was increasingly observed in Kenyon cells surrounding the calyx

(*) with increasing temperature. Endogenous MEF2 (magenta) also localised to nuclei around the calyx. Co-localisation of MEF2 and HDAC4 appeared white, and in cells where $HDAC4^{WT}$ was strongly expressed, the intensity of MEF2 increased. (E) Quantification of MEF2 intensity through the Kenyon cell layer. n=4 brains per genotype. Mean is plotted with individual data points represented as circles. Error bars indicate the SEM. MFE2 intensity increased with increasing $HDAC4^{WT}$ dose (ANOVA, $F(3,11)=6.896$, $p<0.01$, post-hoc Tukey's HSD $p=0.004086$. **$p<0.01$).

5.3.2. Mutation of the MEF2 binding site prevents the HDAC4-induced increase of MEF2 in Kenyon cells

It is unclear how increased expression of HDAC4 results in increased MEF2 protein in Kenyon cells. To address this, it was investigated whether this effect is dependent on the MEF2 binding site within HDAC4 by expression of the ΔMEF2 mutants. HDAC4 was expressed under the control of *OK107-GAL4* in the presence of the TARGET system, with flies being raised at 19 °C until eclosion, and adults were transferred to 30 °C for three days to induce expression. The distribution of $HDAC4^{WT}$, $HDAC4^{\Delta MEF2}$, $HDAC4^{3SA}$ and $HDAC4^{3SA\text{-}\Delta MEF2}$ (Figure 5.15A-E) was consistent with previous studies (Main *et al.*, 2021; Tan *et al.*, 2024); $HDAC4^{WT}$ localised to both the nucleus and cytoplasm, as well as dendrites of the calyx, $HDAC4^{\Delta MEF2}$ shifted to a more cytoplasmic distribution while $HDAC4^{3SA}$ and $HDAC4^{3SA\text{-}\Delta MEF2}$ were restricted to the nucleus. MEF2 intensity was significantly increased upon the expression of $HDAC4^{WT}$ but not $HDAC4^{\Delta MEF2}$. (Figure 5.15F). Expression of $HDAC4^{3SA}$ also increased MEF2 intensity, however this was not as significant as $HDAC4^{WT}$. It is hypothesised that this is due in part to the crude method of intensity quantification (Section 3.4.8); expression of $HDAC4^{3SA}$ resulted in a tighter sequestration of MEF2 into aggregates, disturbing the usually uniform distribution of MEF2 within nuclei, whereas $HDAC4^{WT}$ was reduced in aggregate size and number (compare Figures 5.8B, 4.10E, and 4.22E), leading to a more uniform distribution of MEF2 and higher average intensity. MEF2 intensity was reduced by expression of $HDAC4^{3SA\text{-}\Delta MEF2}$ compared to $HDAC4^{3SA}$, but this was not statistically significant. However, the increase mediated by $HDAC4^{3SA\text{-}\Delta MEF2}$ was also not significantly increased compared to controls. Together these data demonstrate that the increase in MEF2 intensity mediated by HDAC4 overexpression is dependent on an intact MEF2 binding site within HDAC4.

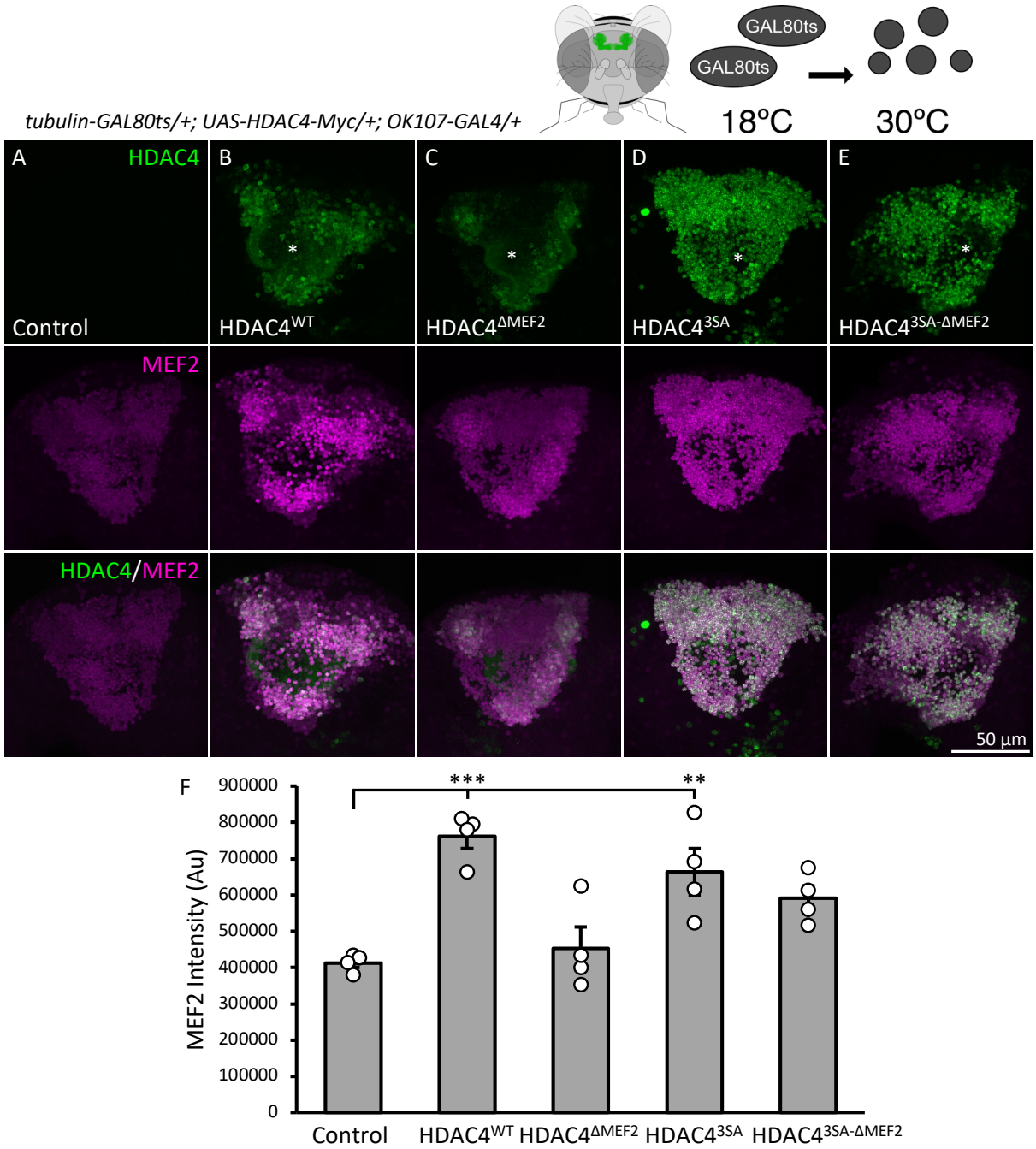

Figure 5.15 HDAC4 overexpression-induced increased MEF2 intensity in Kenyon cells is dependent on an intact MEF2 binding site

(A-E) Maximum projection of optical sections through the Kenyon cell layer in the posterior of the brain of flies expressing HDAC4^{WT} or HDAC4^{mutant} under the control of *OK107-GAL4* in the presence of the TARGET system. Flies were raised at 19 °C until eclosion where adults were transferred to 30 °C for three days to induce expression. Control is *tubulin-GAL80ts/+; +; OK107-GAL4/+*. Expression of HDAC4 (green) induced an increase in endogenous MEF2 (magenta) intensity, dependent on the MEF2 binding region within HDAC4. * denotes the calyx. (F) Quantification of MEF2 intensity through the Kenyon cell layer. n=4 brains per genotype. Mean is plotted with individual data points represented as circles. Error bars indicate the SEM. Expression of HDAC4^{WT} and HDAC4^{3SA} significantly increased MEF2 intensity compared to controls (ANOVA, $F(4,15)=10.41$, $p<0.001$, post-hoc Tukey's HSD, $p<0.001$ and $p=0.009603$ respectively. **$p<0.01$, ***$p<0.001$). Expression of HDAC4$^{\Delta MEF2}$ did not result in a significant increase compared to controls ($p=0.968$). MEF2 intensity of HDAC4$^{3SA-\Delta MEF2}$ expressing flies was reduced compared to HDAC4^{3SA}, however this did not reach statistical significance

(p=0.7743). There was no significant difference between HDAC4$^{3SA-\Delta MEF2}$ expressing flies and controls (p=0.08591). *This figure is an adaptation from that found in Tan et al. (2024) (doi: 10.1186/s12915-023-01800-1), which is distributed under CC BY 4.0.*

5.3.3. HDAC4 oligomerisation mutants differentially impact MEF2 intensity in Kenyon cells

To determine whether the increases in endogenous MEF2 intensity in Kenyon cells are due to sequestration in nuclear aggregates, the effect was assessed upon expression of the HDAC4 oligomerisation mutants (Figure 5.16). Each were expressed under the control of *OK107-GAL4* in the presence of the TARGET system, where crosses were set and raised at 18 °C until flies emerged, and adults were transferred to 30 °C for three days to induce HDAC4^{WT} and HDAC4^{mutant} expression. Consistent with the previous experiments (Sections 5.3.1 and 5.3.2), expression of HDAC4^{WT} (Figure 5.16C) significantly increased MEF2 intensity compared to controls (Figure 5.16B). This was not altered by the F65A mutation (Figure 5.16D). Flies expressing HDAC4^{9QA} (Figure 5.16E) or HDAC4$^{9QA-F65A}$ (Figure 5.16D) did not display a significant increase in MEF2 intensity compared to controls, however since HDAC4^{9QA} is reduced in protein levels compared to HDAC4^{WT} (Section 4.3.2) it is likely that this is a result of reduced dose. While these data suggest that oligomerisation of HDAC4 is not required for increases in nuclear intensity of MEF2, it is possible that this may be an effect of endogenous HDAC4 (discussed in Section 5.6.5).

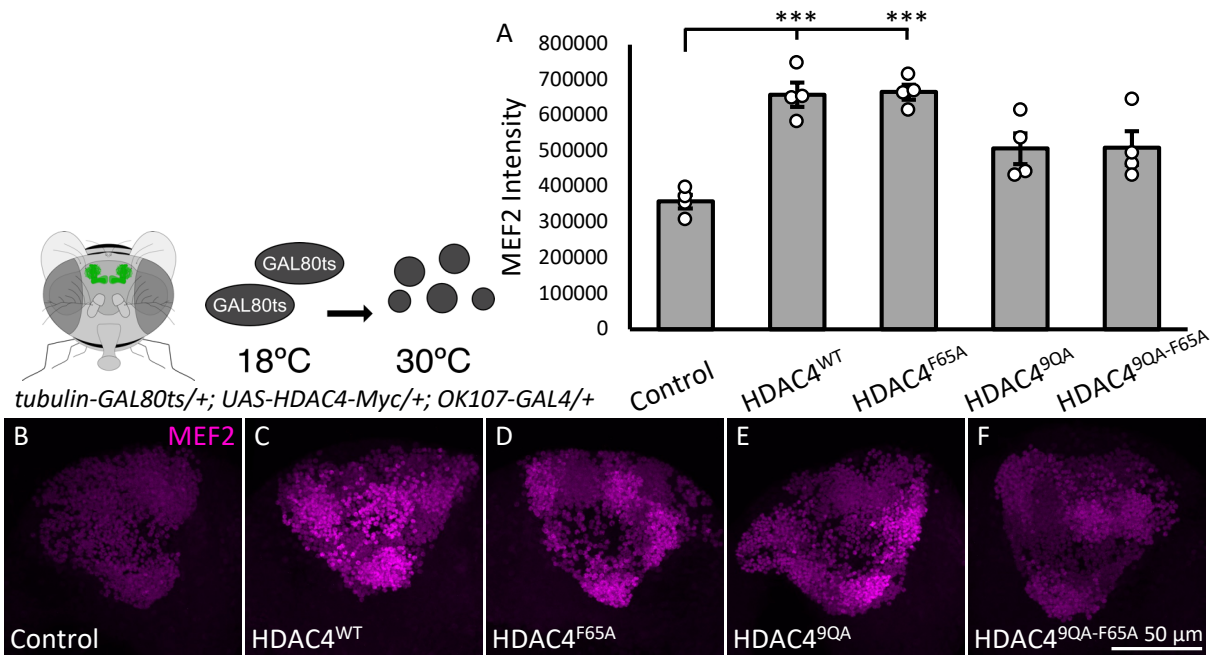

Figure 5.16 HDAC4 oligomerisation mutants differentially alter MEF2 intensity in Kenyon cells

(A) Quantification of MEF2 intensity through the Kenyon cell layer. n=4 brains per genotype. Mean is plotted with individual data points represented as circles. Error bars indicate the SEM. Each of HDAC4^{WT} and HDAC4^{F65A} were significantly increased compared to control (ANOVA, $F(4,15)=10.41$, $p<0.001$, post-hoc Tukey's HSD ***$p<0.001$.). There was no significant increase between control and HDAC4^{9QA} or HDAC4$^{9QA\text{-}F65A}$ ($p=0.057748$ and 0.0524 respectively). (B-F) Maximum projection of optical sections through the Kenyon cell layer in the posterior of the brain of flies expressing HDAC4^{WT} or HDAC4^{mutant} under the control of *OK107-GAL4* in the presence of the TARGET system; flies were raised at 19 °C until eclosion where adults were transferred to 30 °C for three days to induce expression. Control is *tubulin-GAL80ts/+; +; OK107-GAL4/+*. Expression of HDAC4 induced an increase in endogenous MEF2 (magenta) intensity regardless of the presence of mutations that affect oligomerisation. Please note that some panels displayed here are the MEF2 channel that is displayed in conjunction with HDAC4 in Figure 4.22.

5.4. MEF2 and the MEF2 binding site within HDAC4 promote nuclear localisation and stabilise aggregation of HDAC4

In combination with the previous study (Tan *et al.*, 2024), the data herein makes a strong case that the MEF2 binding site within HDAC4 is a key element in mediating defects in β-lobe development in an aggregation-dependent manner. It was confirmed that this is through an interaction with MEF2, rather than another protein binding this site, as overexpression of HDAC4 combined with MEF2 RNAi also reduces the severity of β-lobe fusion (Main *et al.*, 2021). Moreover, it appears that HDAC4 may stabilise protein levels of MEF2 (Section 5.3). It remains unclear however whether the interaction with MEF2 is important for stabilisation of HDAC4 aggregation. Expression of HDAC4$^{\Delta MEF2}$ resulted in a reduced number of aggregates

compared to HDAC4^{WT} (Tan *et al.*, 2024), however MEF2 also mediates nuclear import of HDAC4 (Borghi *et al.*, 2001; Wang & Yang, 2001), therefore the reduced aggregation observed for HDAC4$^{\Delta MEF2}$ is likely largely due to reduced nuclear localisation of MEF2. The following section therefore addresses the role of MEF2, and how it affects aggregation and function of HDAC4 in the nucleus.

5.4.1. The MEF2 binding site stabilises but is not required for aggregation of HDAC4 in Kenyon cells

As aforementioned, it is unclear whether HDAC4 aggregation is altered by MEF2 binding independent of changes in subcellular distribution. To address this, the aggregation characteristics of HDAC4$^{\Delta MEF2}$ and HDAC4$^{3SA-\Delta MEF2}$ were compared with HDAC4^{WT} and HDAC4^{3SA}. Expression of *HDAC4* transgenes was facilitated by *OK107-GAL4* in the presence of the TARGET system, and flies were raised at 18 °C until adulthood where they were raised for three days at 30 °C before brains were dissected and immunohistochemistry performed for HDAC4-Myc and endogenous MEF2 (Figure 5.17). Consistent the previous data (Figure 4.10, 4.22 and 5.8) HDAC4^{WT} localised both to nuclei, co-localising with MEF2, as well as cytoplasmic haloes, and formed white punctate aggregates in merged sections (Figure 5.17A), while HDAC4^{3SA} localised exclusively to nuclei and formed aggregates that were increased in size (Figure 5.17C). HDAC4$^{\Delta MEF2}$ was relatively devoid from Kenyon cell nuclei (Figure 5.17B), while HDAC4$^{3SA-\Delta MEF2}$ was almost entirely nuclear (Figure 5.17D), consistent with that observed by Tan *et al.* (2024). Nuclear aggregates in the Kenyon cell layer were counted as described in Section 3.4.6; HDAC4$^{\Delta MEF2}$ and HDAC4$^{3SA-\Delta MEF2}$ were significantly reduced in total aggregate number with an average of 90 and 287 aggregates per section respectively, compared to 204 and 443 for HDAC4^{WT} and HDAC4^{3SA}, respectively. To determine the contribution of MEF2 to these, the number of aggregates containing both HDAC4 and MEF2 (MEF2 positive), or HDAC4 only (MEF2 negative) were counted (Figures 5.17E-F). Interestingly, for both HDAC4$^{\Delta MEF2}$ and HDAC4$^{3SA-\Delta MEF2}$, the number of HDAC4 aggregates negative for MEF2 was unchanged compared to HDAC4^{WT} and HDAC4^{3SA} respectively, however the number of MEF2-containing aggregates was significantly reduced by ΔMEF2 mutation. Moreover, the ΔMEF2 mutation significantly reduced the size of aggregates observed. Together these data suggest that the MEF2 binding site within HDAC4 is not required for aggregation of HDAC4, but an intact site stabilises and promotes aggregation, increasing both aggregate number and size.

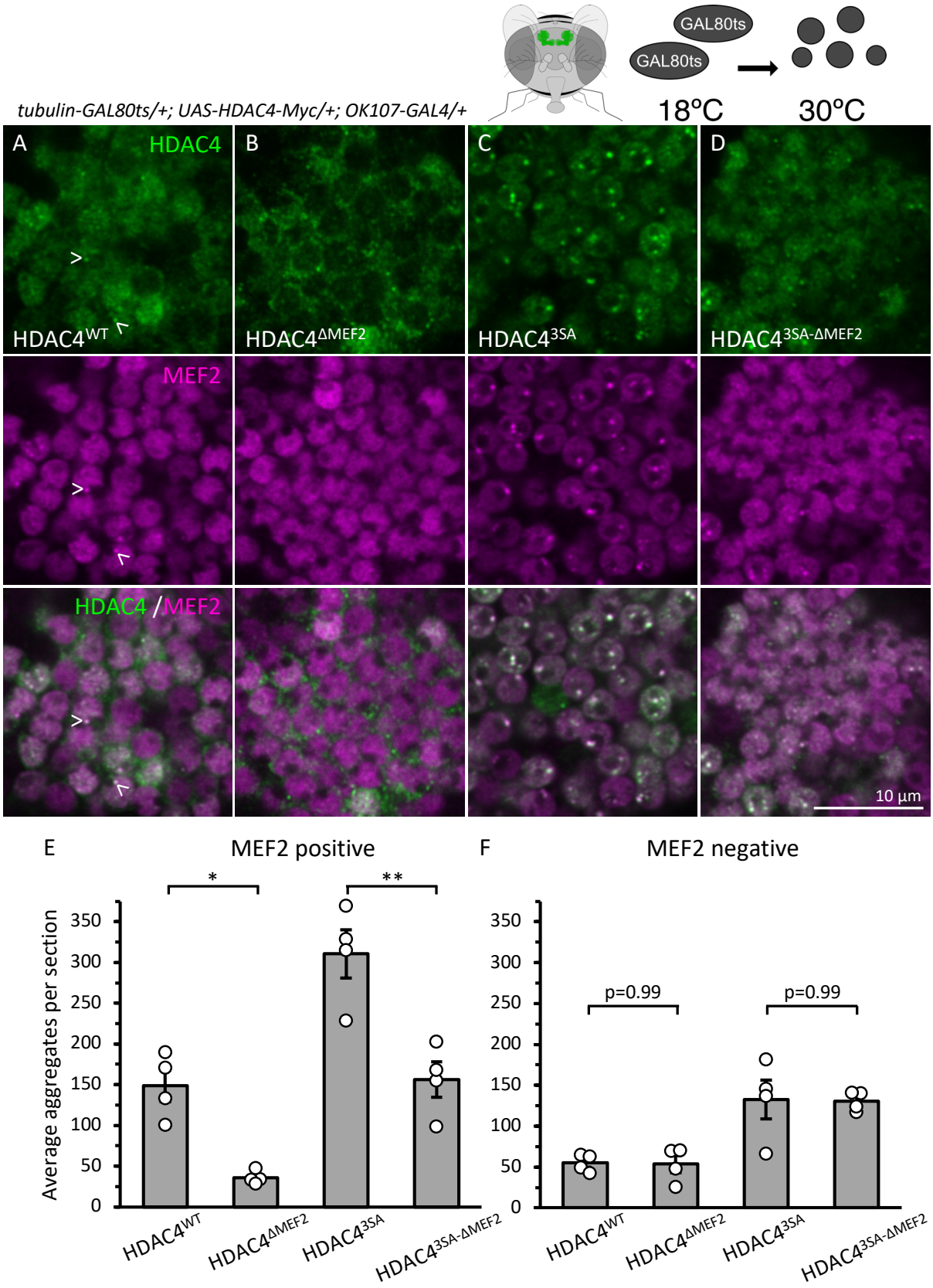

Figure 5.17 The MEF2 binding site within HDAC4 is not required for aggregation but stabilises and increases aggregate number

(A-D) Magnified single optical sections (0.5 µm) depicting the distribution and aggregation of HDAC4^{WT} and HDAC4^{mutant} in Kenyon cells. HDAC4 expression was mediated by *OK107-GAL4* in the presence of the TARGET system; flies were raised at 18 °C until eclosion, where adults were transferred

to 30 °C for three days to induce HDAC4 expression. HDAC4^{WT} (green) formed nuclear aggregates (arrows) that co-localised with MEF2 (magenta) (A), which were increased in size upon restriction of localisation to the nucleus in HDAC4^{3SA} (C). Mutation of the MEF2 binding site reduced nuclear localisation for HDAC4$^{\Delta MEF2}$ (B) and nuclear aggregation for HDAC4$^{3SA\text{-}\Delta MEF2}$ (D). (E-F) Quantification of HDAC4 aggregates. Aggregates of HDAC4 that were MEF2 positive or MEF2 negative were counted through the Kenyon cell layer for 10 optical sections spaced 1 µm apart, n=4 brains per genotype as per Section 3.4.6. MEF2-positive aggregates were counted as those that were visible as distinct foci on both HDAC4-Myc and MEF2 channels independently, while MEF2-negative aggregates were only visible on the HDAC4-Myc channel. The average number of aggregates per section per brain are plotted as individual points. Error bars indicate the SEM. Presence of the MEF2 binding site significantly increased the total number of MEF2-positive aggregates, but had no effect on MEF2-negative aggregate formation (MEF2-positive: ANOVA, $F(3,12)=28.93$, $p<0.0001$, post-hoc Tukey's HSD *$p<0.05$*, **$p<0.01$. HDAC4^{WT} vs HDAC4$^{\Delta MEF2}$, $p=0.01155$; HDAC4^{3SA} vs HDAC4$^{3SA\text{-}\Delta MEF2}$, $p=0.001095$. MEF2-negative: ANOVA, $F(3,12)=10.60$, $p<0.01$, post-hoc Tukey's HSD. HDAC4^{WT} vs HDAC4$^{\Delta MEF2}$, $p=0.9999$; HDAC4^{3SA} vs HDAC4$^{3SA\text{-}\Delta MEF2}$, $p=0.9997$). *This figure is an adaptation from that found in Tan et al. (2024) (doi: 10.1186/s12915-023-01800-1), which is distributed under CC BY 4.0.*

5.4.2. MEF2 overexpression increases nuclear localisation of HDAC4 in Kenyon cells

As an intact MEF2 binding site within HDAC4 promotes its aggregation in Kenyon cell nuclei, it was hypothesised that overexpression of MEF2 should promote the nuclear localisation and aggregation of HDAC4. Therefore, HDAC4^{WT} was overexpressed in Kenyon cells under the control of *OK107-GAL4* +TARGET in the presence and absence of *MEF2^{WT}* overexpression (Figure 5.18). To achieve this, HDAC4^{WT}and MEF2^{WT} transgenes were combined into a single fly line (Appendix 10.1.6, Figure 10.7), which was performed by Dr Helen Fitzsimons. Brains were prepared for immunohistochemistry using antibodies to detect both the Myc-tag of the HDAC4 transgene, as well as an antibody that detects MEF2 (both endogenous and transgene). HDAC4^{WT} localised to both the nucleus and cytoplasm of Kenyon cells, forming prominent cytoplasmic haloes as well as small nuclear aggregates (Figure 5.18A). Upon MEF2^{WT} overexpression, HDAC4^{WT} localised primarily to nuclei and the incidence of cytoplasmic haloes was reduced (Figure 5.18B). Nuclear aggregates also appeared larger and were more frequent. These data further support the hypothesis that MEF2 increases nuclear localisation of HDAC4 and stabilises aggregate formation.

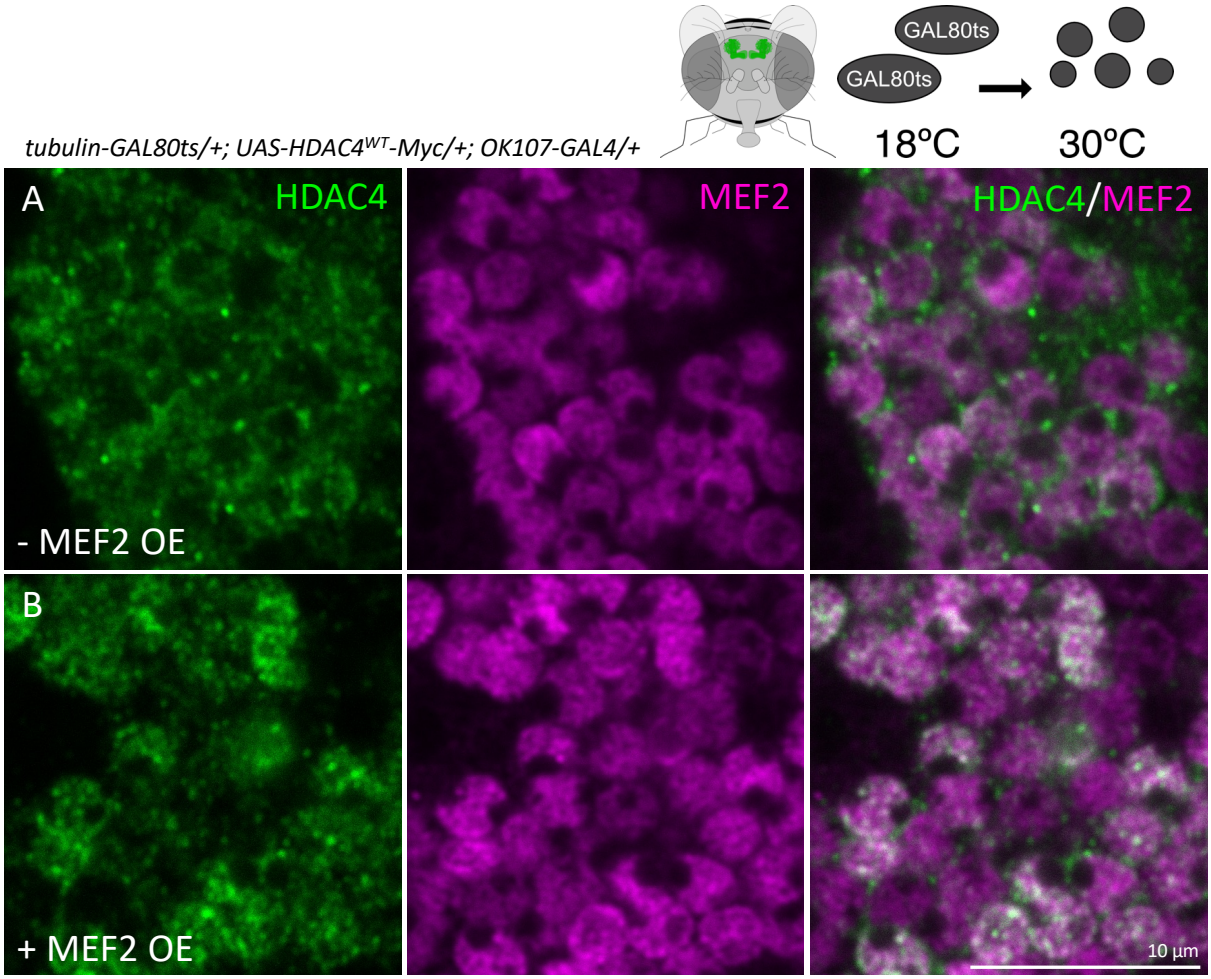

Figure 5.18 MEF2 overexpression increases nuclear localisation of HDAC4^{WT} in Kenyon cells

Magnified single optical section (0.5 µm) depicting the distribution and aggregation of HDAC4^{WT} in Kenyon cells in the absence (-MEF2 OE, A) and presence (+MEF2 OE, B) of MEF2^{WT} overexpression. HDAC4^{WT} and MEF2^{WT} expression was mediated by *OK107-GAL4* in the presence of the TARGET system; flies were raised at 18 °C until eclosion, where adults were transferred to 30 °C for three days to induce transgene expression. Anti-Myc and anti-MEF2 immunohistochemistry was performed to detect HDAC4 and MEF2, being both endogenous and transgene MEF2. (A) In the absence of MEF2 overexpression, HDAC4^{WT} formed nuclear aggregates that sequestered endogenous MEF2, and was also observed in cytoplasmic haloes. (B) In the presence of MEF2 overexpression, HDAC4^{WT} formed larger and more numerous nuclear aggregates and the intensity of cytoplasmic haloes was reduced. *This figure is an adaptation from that found in Tan et al. (2024) (doi: 10.1186/s12915-023-01800-1), which is distributed under CC BY 4.0.*

5.4.3. MEF2 overexpression increases the severity of HDAC4-overexpression induced β-lobe fusion of the mushroom body

As there is a correlation between nuclear localisation of HDAC4 and the severity of β-lobe fusion (Tan *et al.*, 2024), as well as a requirement of an intact MEF2 binding site for nuclear localisation and aggregation, it was hypothesised that MEF2 overexpression would increase the severity of β-lobe fusion mediated by $HDAC4^{WT}$ overexpression. Under the conditions previously used in this thesis (*elav-GAL4* driver, flies raised at 18-22 °C) $HDAC4^{WT}$ overexpression resulted in close to 100% β-lobe fusion, therefore any increase in severity could not be assessed. To that end, to determine the effect of $MEF2^{WT}$ overexpression in the presence of $HDAC4^{WT}$, expression was driven by *OK107-GAL4* +TARGET and flies were raised at 25 °C to yield an intermediate transgene expression level (Hawley *et al.*, 2023; Tan *et al.*, 2024), followed by assessment of β-lobe fusion. Brains were dissected and processed for immunohistochemistry to detect FasII and observe the structure of the mushroom body. Three levels of β-lobe fusion were scored, with minor fusion resulting from only a few axons, moderate being axons measuring less than half the width of the lobe, or severe being axons measuring more than half the lobe width crossing the midline (Figure 5.19). $HDAC4^{WT}$ overexpression alone resulted in β-lobe fusion in 58% of brains, with 35% of these displaying moderate or severe fusion (Table 5.3). $MEF2^{WT}$ overexpression alone induced minor fusion in only 24% of brains. When $HDAC4^{WT}$ and $MEF2^{WT}$ were co-expressed, β-lobe fusion increased to 100%, with 75% of brains displaying moderate or severe fusion. To confirm the specificity of this synergistic interaction, $MEF2^{WT}$ was also co-expressed with $HDAC4^{\Delta MEF2}$; if the increase in severity is dependent on the specific interaction between MEF2 and HDAC4 this should be lost upon ΔMEF2 mutation of HDAC4. Alone $HDAC4^{\Delta MEF2}$ overexpression resulted in β-lobe fusion in 36% of brains, with a significant reduction in moderate and severe fusion compared to $HDAC4^{WT}$ at only 7%. Upon $MEF2^{WT}$ co-expression there was a modest but insignificant increase to 57% total fusion. Together these data demonstrate that MEF2 overexpression induces nuclear localisation and aggregation of HDAC4, and increases the severity of β-lobe fusion, dependent on an intact MEF2 binding site.

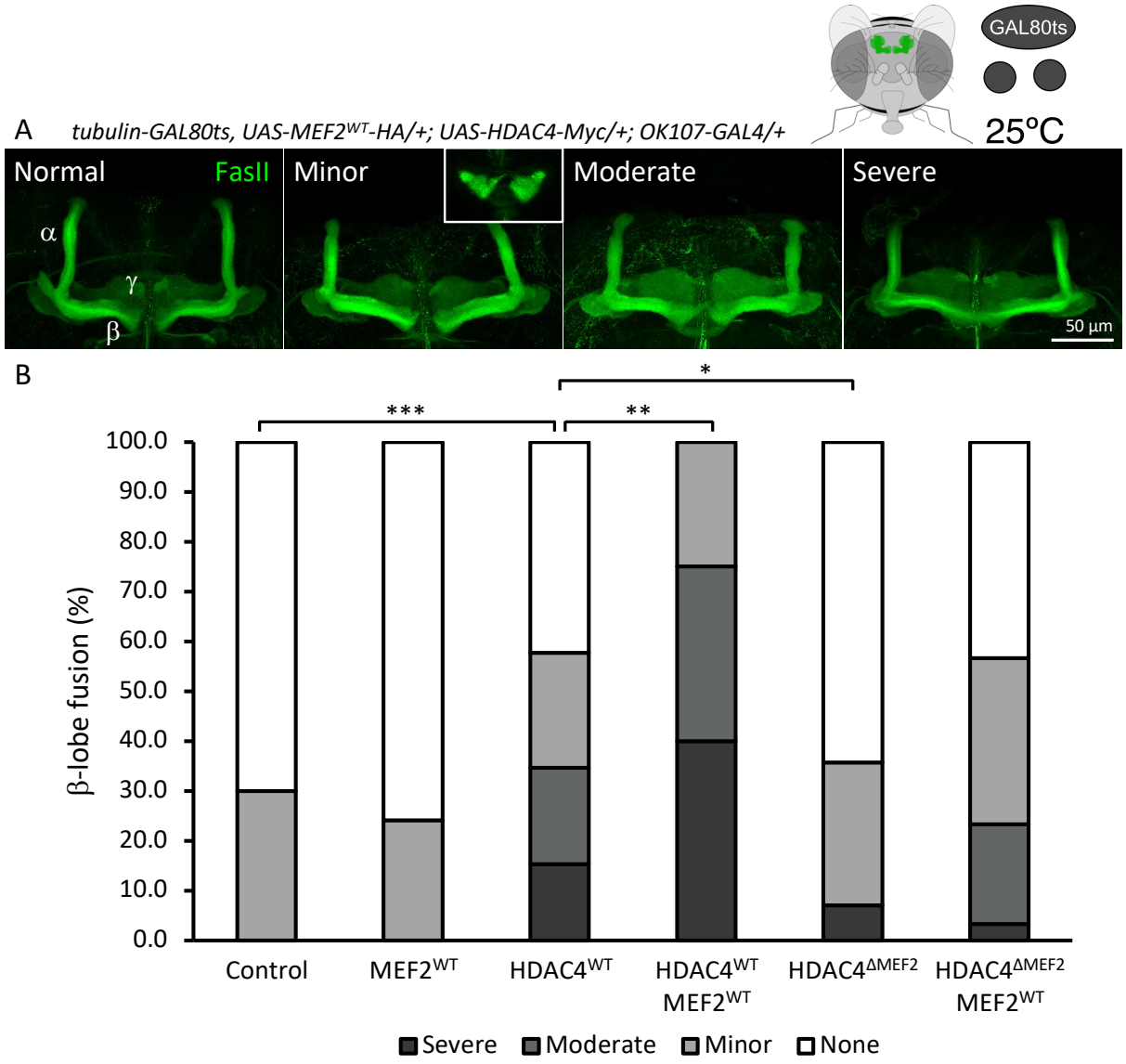

Figure 5.19 MEF2 overexpression exacerbates β-lobe fusion mediated by HDAC4^{WT} but not by HDAC4$^{\Delta MEF2}$

(A) Maximum projections of optical sections through the anterior of the adult brain. Anti-FasII immunostaining labels the alpha (α), beta (β) and gamma (γ) lobes of the mushroom body. β-lobe fusion resulting from HDAC4-overexpression was classified as either minor, resulting from midline crossing of only a few axons only observable in a single optical section (inset, 1 µm), moderate, where axons measuring less than half of the lobe width crossed the midline, or severe, where axons measuring more than half the lobe width crossed the midline. (B) Quantification of β-lobe fusion resulting from HDAC4 overexpression in the presence and absence of MEF2 overexpression. HDAC4 and MEF2^{WT} expression was driven by *OK107-GAL4* in the presence of the TARGET system at 25°C throughout development. Adult brains were processed for anti-FasII immunohistochemistry and β-lobe fusion was scored. Control is *tubulin-GAL80ts/+; +; OK107-GAL4/+*. n≥20 brains per genotype. MEF2 overexpression alone did not induce a significant increase in total fusion compared to controls, and HDAC4^{WT} but not HDAC4$^{\Delta MEF2}$ overexpression was exacerbated in the presence of MEF2 overexpression (Fisher's exact test, moderate and severe β-lobe fusion, *p<0.05, **p<0.01, ***p<0.001. Control vs HDAC4^{WT}, p<0.001. HDAC4^{WT} vs HDAC4$^{\Delta MEF2}$, p=0.0411. HDAC4^{WT} vs HDAC4^{WT} + MEF2^{WT} p=0.0037. HDAC4$^{\Delta MEF2}$ vs HDAC4$^{\Delta MEF2}$ + MEF2^{WT} p=0.1468). *This figure is an adaptation from that found in Tan et al. (2024) (doi: 10.1186/s12915-023-01800-1), which is distributed under CC BY 4.0.*

Table 5.3 Frequency of mushroom body phenotypes resulting from the expression of HDAC4 in the presence and absence of MEF2 overexpression

(% of brains)	Con	$MEF2^{WT}$	$HDAC4^{WT}$	$HDAC4^{WT}$ + $MEF2^{WT}$	$HDAC4^{\Delta MEF2}$	$HDAC4^{\Delta MEF2}$ + $MEF2^{WT}$
α thinning	0	0	0	0	0	0
α missing	0	0	0	0	0	0
β thinning	0	0	0	0	0	0
β missing	0	0	0	0	0	0
β fusion	**30**	**24**	**58**	**100**	**36**	**57**
Minor	30	24	23	25	29	33
Moderate	0	0	19	35	0	20
Severe	0	0	15	40	7	3
n	30	29	26	20	28	30

Expression of each denoted *HDAC4* or *$MEF2^{WT}$* transgene was mediated by *OK107-GAL4* in the presence of the TARGET system; virgin *tubulin-GAL80ts; OK107-GAL4* female flies were crossed to males harbouring the *HDAC4* and/or *MEF2* transgenes and adult progeny of this cross were dissected and their brains immunostained for FasII to assess mushroom body lobe development. Flies were raised at 25 °C. Instances of defects in morphology were scored for n≥20 brains per genotype as per Section 3.4.7, and are displayed as the % of brains with the indicated phenotype. Control (con) is *tubulin-GAL80ts/+; OK107-GAL4/+*. Percentages may not sum to 100 due to rounding. *These data are also presented in Tan et al. (2024) (doi: 10.1186/s12915-023-01800-1), which is distributed under CC BY 4.0.*

5.4.4. Mutation of the MEF2 binding site alters HDAC4 subcellular distribution in the larval eye disc

While the MEF2 binding site is required for HDAC4 overexpression-induced defects in the development of the mushroom body, the role of this site in manifestation of eye phenotypes remains unclear. It was previously determined that $HDAC4^{WT}$ overexpression induces a severe rough eye phenotype (Main *et al.*, 2021; Schwartz *et al.*, 2016; Tan *et al.*, 2024), which is exacerbated upon restriction of localisation to the nucleus (Sections 4.5.2 and 5.2.6) (Tan *et al.*, 2024), similarly to the mushroom body. Interestingly, mutation of the MEF2 binding site did not reduce the severity of this phenotype as significantly as the effect observed in the mushroom body (Tan *et al.*, 2024), suggesting that the eye phenotype resulting from HDAC4 overexpression is not mediated through the MEF2-binding site, and this is supported by the lack of MEF2 in the developing eye (Figure 4.12). Moreover, it was observed that F65A

mutation completely prevented HDAC4 overexpression-induced defects in eye development (Section 4.5.2), but the effect of this was significantly reduced upon nuclear localisation (Section 5.2.6). Interestingly, expression of HDAC4$^{3SA\text{-}F65A\text{-}\Delta MEF2}$ also resulted in no defects, while HDAC4$^{3SA\text{-}\Delta MEF2}$ was not reduced in severity compared to HDAC4^{3SA}, suggesting a specific role for the MEF2 domain in regulation of HDAC4-overexpression induced defects in eye development in conjunction with Phe65. It remains unclear how this domain regulates the function of HDAC4 in the eye, and whether this is through MEF2 given that MEF2 protein was unable to be detected in the larval eye disc.

Patterning of the ommatidial lattice begins in the third instar with the formation of photoreceptor preclusters (Ready *et al.*, 1976), Section 1.3.2). Therefore, to investigate the role of the MEF2 site within HDAC4 during eye development, the distribution of HDAC4 in the larval eye disc was further characterised and compared to adult eye phenotypes (Figure 5.20). HDAC4 expression was driven in the developing eye under the control of *GMR-GAL4* and eye discs of third instar larvae processed for immunohistochemistry. HDAC4^{WT} was present in both the nucleus and cytoplasm of basal cells of the eye disc, and frequently formed nuclear aggregates (Figure 5.20A) as observed previously (Figure 4.14). The adult eye presented with widespread fusion of ommatidia and loss of pigmentation as previously shown (Section 4.5.2, (Tan, 2022; Tan *et al.*, 2024))(Figure 5.20E). HDAC4^{3SA} was absent from cytoplasmic haloes and localised exclusively to basal cell nuclei, forming large nuclear aggregates (Figure 5.20C). The increase in aggregation correlated with an increase in the severity of the adult eye phenotype with complete loss of pigmentation and the development of necrosis (Figure 5.20G). In contrast, HDAC4$^{\Delta MEF2}$ was excluded from nuclei and only observed in cytoplasmic haloes (Figure 5.20B), and the severity of the eye phenotype was reduced compared to HDAC4^{WT}, with less fusion of ommatidia (Figure 5.20F). Combination of the 3SA and ΔMEF2 mutations resulted in a less severe adult eye phenotype than HDAC4^{3SA} alone (Figure 5.20H). This is interesting given that MEF2 protein was not detected in the eye disc (Section 4.4.3). It is possible that another protein may bind at the MEF2 site to regulate the subcellular distribution of HDAC4 in the developing eye and restrain the severity of HDAC4 overexpression induced phenotypes in the adult eye. It is also possible that MEF2 expression may be induced later in development.

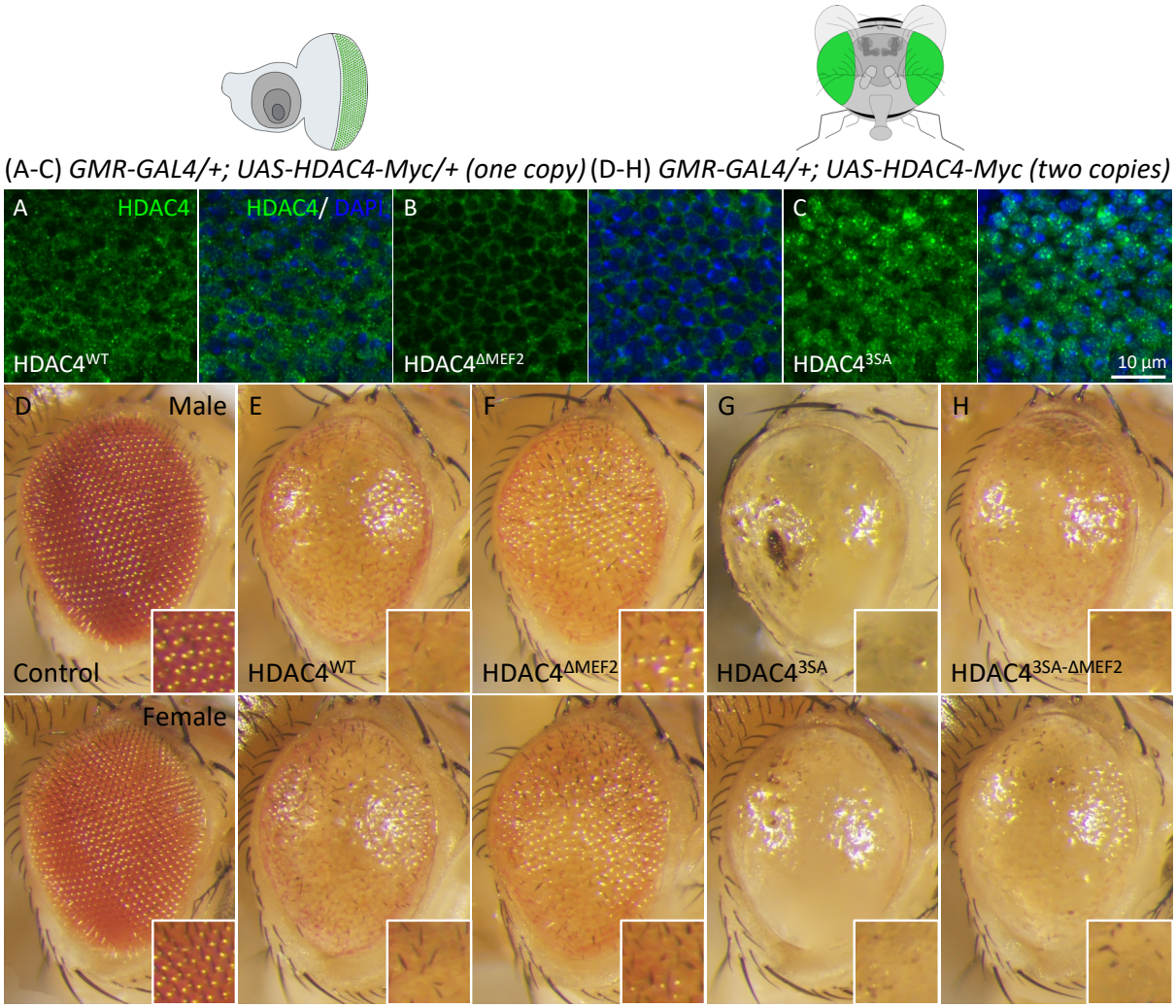

Figure 5.20 Mutation of the MEF2 binding site alters HDAC4 subcellular distribution in the larval eye disc

(A-C) Single optical sections (0.5 µm) of basal cells of the larval eye disc expressing $HDAC4^{WT}$ and $HDAC4^{mutant}$ (green) under the control of *GMR-GAL4*, co-labelled with DAPI (blue), which highlights nuclei. (D-H) Light microscopy images (110x magnification) of *Drosophila* eyes raised at 25°C. Top row, males; bottom row, females. Inset shows a magnified image of ommatidia. (D) Control is *GMR-GAL4/+*. (E-H) Flies harboured one copy of the driver (*GMR-GAL4/+*) and two copies of the transgene (*UAS-HDAC4/UAS-HDAC4*). $HDAC4^{WT}$ overexpression induced severe widespread disorganisation of the adult eye, characterised by ommatidial fusion and loss of pigmentation (E), the severity of which was reduced by $HDAC4^{\Delta MEF2}$ (F) and increased by $HDAC4^{3SA}$ (G). Combination of 3SA and ΔMEF2 mutations in $HDAC4^{3SA\text{-}\Delta MEF2}$ resulted in a phenotype with intermediate severity compared to each mutation individually (H). *This figure is an adaptation from that found in Tan et al. (2024) (doi: 10.1186/s12915-023-01800-1), which is distributed under CC BY 4.0.*

5.4.5. Endogenous MEF2 protein is detected in the adult eye

Many proteins bind within the N-terminus of HDAC4, some sites of which overlap with the MEF2 binding site (Figure 1.10). While it is possible that these proteins may mediate the modest reduction in severity of eye phenotypes associated with ΔMEF2 mutants, MEF2 remains an obvious candidate for mediating effects via HDAC4 later in eye development. To determine whether MEF2 expression is detected at a later stage of development, immunohistochemistry was performed on eyes of adult flies (Figure 5.21). A single optical section at the approximate depth of the photoreceptor nuclei (Figure 1.5) in the centre of the adult eye is presented in Figure 5.21. MEF2 was detected in a uniform pattern in circular clusters of approximately six cells (Figure 5.21A), and this specific staining was reduced upon co-expression of MEF2 RNAi (Figure 5.21B-C), verified by two independent RNAi lines. While not specifically counterstained for, the characteristic bundle of six circles are likely nuclei of photoreceptor cells (as depicted in Figure 1.5). These data demonstrate that MEF2 is expressed in the adult eye. It remains unclear at what stage MEF2 expression is initiated, and further experiments should be done in the pupal eye to determine this.

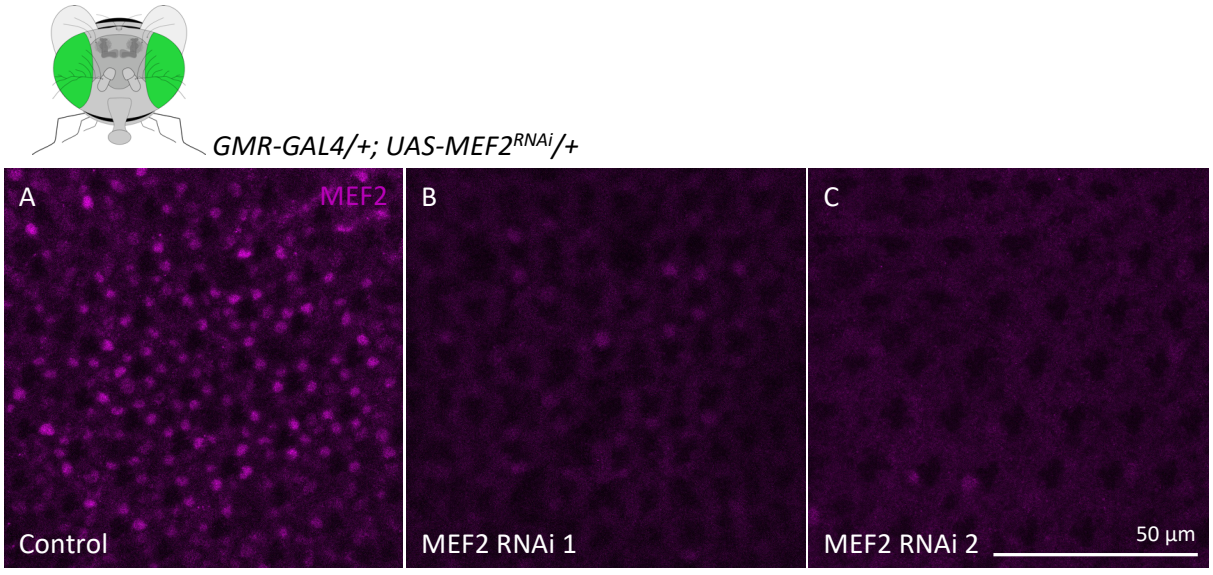

Figure 5.21 MEF2 is expressed in the adult eye
Adult eyes were dissected and immunostained for endogenous MEF2 (magenta). (A-C) Single optical sections (0.5 µm) through the centre of the eye at the approximate depth of the photoreceptor nuclei. Control is *GMR-GAL4/+*. *MEF2 RNAi* was driven by *GMR-GAL4* and MEF2 RNAi #1 and #2 were two independent RNAi lines. MEF2 signal was detected in control eyes (A), while the intensity of staining was significantly reduced upon MEF2 knockdown (B-C), confirming the specificity of detection.

5.4.6. MEF2 overexpression impairs eye development

Given that expression of HDAC4$^{\Delta MEF2}$ mutants results in a modest and major reduction in severity of adult eye and mushroom body phenotypes, respectively, and MEF2 overexpression increases the severity of HDAC4-overexpression induced β-lobe fusion, it was hypothesised that the same may occur in the eye. Therefore, the effect of MEF2 overexpression in the presence and absence of HDAC4^{WT} overexpression on eye development was investigated. However, *MEF2^{WT}* overexpression under the control of *GMR-GAL4* alone resulted in a severe eye phenotype with complete fusion of ommatidia and loss of pigmentation, reduction in eye size, and necrosis (Figure 5.22D). When raised at 25 °C, the majority of flies did not emerge from their pupal case; eyes of these flies were developed, but with increased severity of the phenotype, and it is hypothesised the lack of emergence was due to 'sticking' of the surface of the eye to the pupal cuticle. Consequently, overexpression of both MEF2^{WT} and HDAC4^{WT} at 25 °C was lethal, and progeny died as pupae. At the lower temperature of 18 °C, MEF2 overexpression still significantly impaired eye development, resulting in widespread misalignment, fusion, and necrosis of ommatidia (Figure 5.22B). These data demonstrate that aberrant expression of MEF2 significantly impairs eye development. The interaction between HDAC4 and MEF2 in the eye requires further investigation.

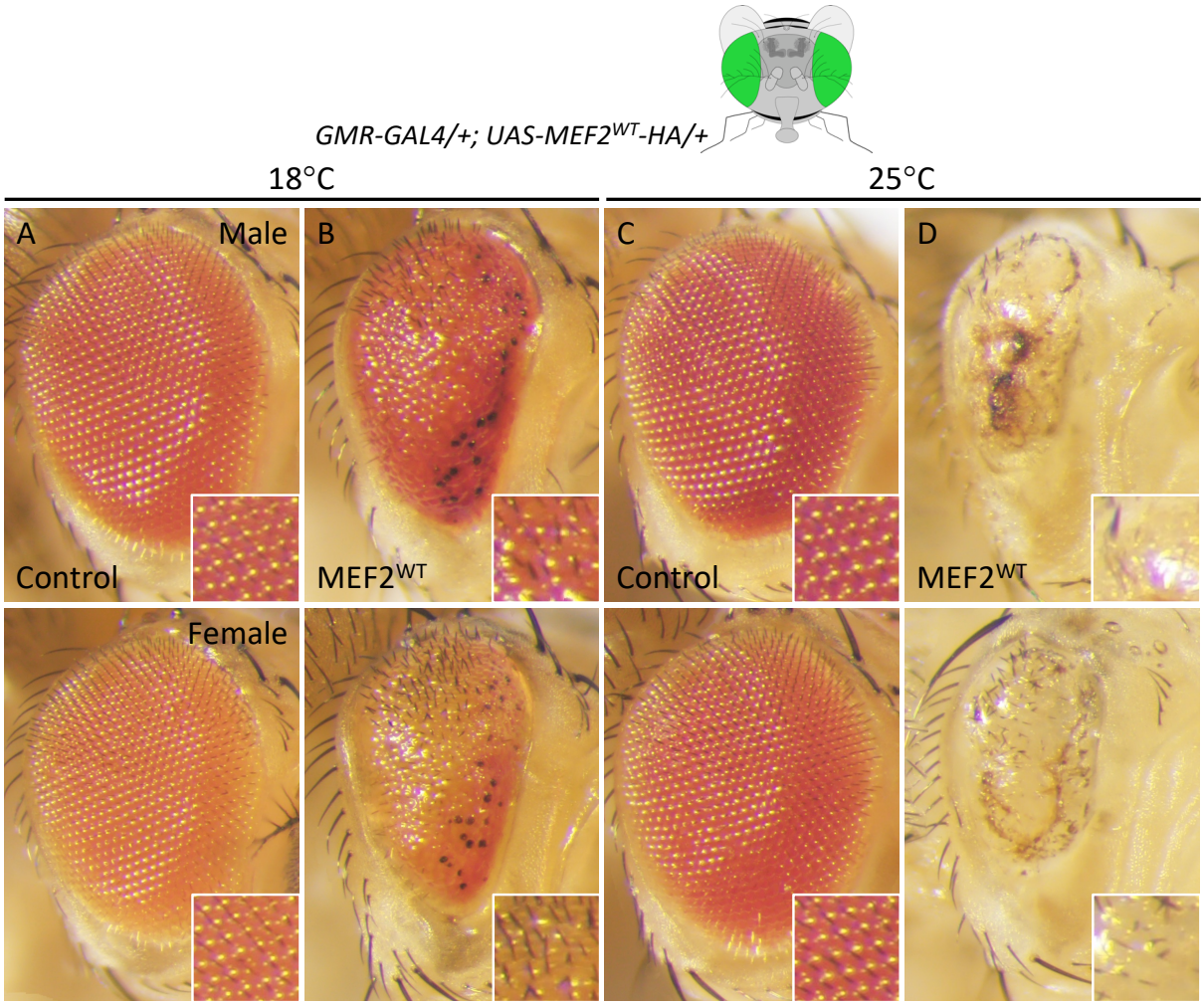

Figure 5.22 Overexpression of MEF2 affects *Drosophila* eye development
Light microscopy (110x magnification) images of *Drosophila* eyes raised at 18 °C (A-B) or 25°C (C-D). Top row, males; bottom row, females. Inset shows a magnified image of ommatidia. (A, C) Control is *GMR-GAL4/+*. (B, D) Flies harboured one copy of the driver (*GMR-GAL4/+*) and one copy of the *MEF2^{WT}* overexpression construct (*UAS-MEF2^{WT}/+*). MEF2^{WT} overexpression severely impaired eye development regardless of the dose of expression, resulting in misalignment, fusion, and necrosis of ommatidia when flies were raised at 18 °C (B) and complete fusion of all ommatidia with necrotic patches that peeled when raised at 25 °C (D).

5.5. The *Drosophila* HDAC4 nuclear export sequence is functional, and mutations of this region induce nuclear localisation, aggregation, and neuronal phenotypes

In functional studies of HDAC4, its subcellular distribution is typically altered not by mutation of its intrinsic nuclear import or export signals, but by altering binding sites for other factors that regulate its distribution (Sections 1.5.1.2 and 1.5.1.3). The most frequently used mutation is 3SA, which substitutes three serine residues that when phosphorylated typically allow

binding of 14-3-3 chaperone proteins resulting in cytoplasmic localisation (Section 1.5.1.3). This substitution has a striking effect on HDAC4 subcellular localisation, resulting in nuclear accumulation in many cell types. However, 14-3-3 has functions other than its typical role in mediating nuclear exit. It was recently determined that 14-3-3 binding to a wide range of proteins regulates their dynamics of protein aggregation (Segal *et al.*, 2023). Mutations that reduced 14-3-3 interaction resulted in nuclear foci formation, while engineering 14-3-3 binding sites into aggregation-prone proteins reduced nuclear aggregation. This suggests that in addition to reinforcing nuclear localisation of HDAC4, the 3SA mutation may independently affect nuclear aggregation.

To address the role of 14-3-3 binding in the nuclear aggregation of HDAC4, the DmHDAC4 nuclear export sequence was investigated. It was previously suggested that the nuclear export sequence within hHDAC4 was absent in DmHDAC4 (Main *et al.*, 2021), but upon closer inspection, another PhD student in this laboratory, Dr Wei Jun Tan, observed conservation of key residues that constitute the nuclear export sequence of human HDAC4 (Wang & Yang, 2001), in an alignment of human and *Drosophila* HDAC4 (Figure 5.23). Therefore, these were mutated to alanine to generate HDAC4$^{\Delta NES}$.

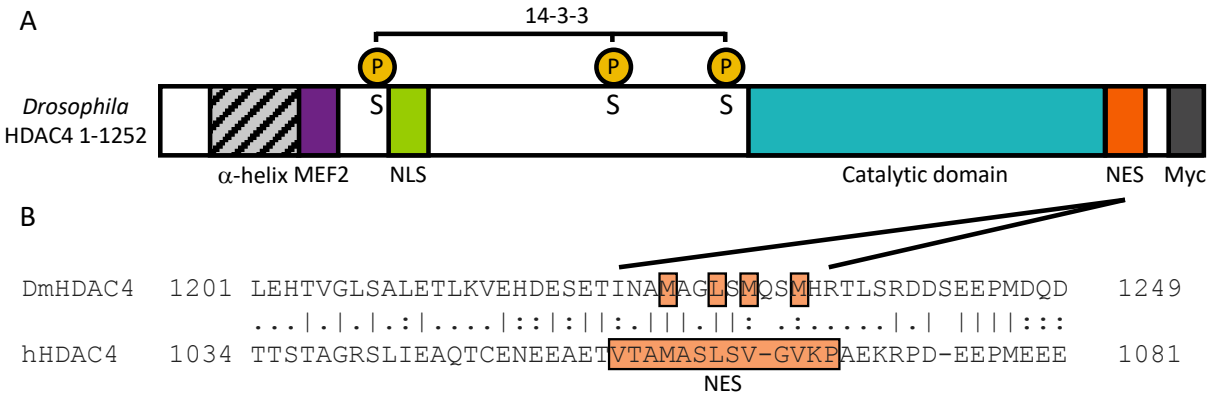

Figure 5.23 Sequence alignment of human and *Drosophila* HDAC4 identifies conservation of the nuclear export sequence
(A) Schematic diagram of the domain structure of DmHDAC4. (B) EMBOSS Water alignment of the C-terminus of human HDAC4 (hHDAC4, GenBank accession NP_006028), and *Drosophila* HDAC4 (DmHDAC4, GenBank accession NP_572868) demonstrates high conservation of the C-terminus and nuclear export sequence (NES). The region of the NES annotated on hHDAC4 (orange) is as per Wang and Yang (2001), and residues essential in mediating nuclear export are M1059, L1062, V1064 and V1066. The boxed residues M1225, L1228, M1230 and M1233 of DmHDAC4 are either strictly or functionally conserved with those important for nuclear export in hHDAC4, and were mutated to alanine in the HDAC4$^{\Delta NES}$ mutant. Please note that part (A) of this figure is reproduced from that found in Figure 4.5 for clarity.

5.5.1. Mutation of the nuclear export sequence within HDAC4 results in nuclear accumulation in Kenyon cells

The localisation of HDAC4$^{\Delta NES}$ was first investigated in the mushroom body and Kenyon cells (Figure 5.24). To remain consistent with the previous characterisation of HDAC4 distribution in the mushroom body (Tan *et al.*, 2024), HDAC4 expression was driven by *OK107-GAL4* +TARGET; flies were raised at 18 °C until emerging and then transferred to 30 °C to induce transgene expression. HDAC4^{WT} was observed in the lobes of the mushroom body and in axons within the antennal lobe in the anterior of the brain and localised to Kenyon cell bodies in the posterior as well as within the calyx (Figure 5.24B, E). In contrast, HDAC4$^{\Delta NES}$ was absent from the lobes of the mushroom body and only observed when the gain was significantly increased (Figure 5.24C, inset). When imaged from the anterior, HDAC4$^{\Delta NES}$ was also only observed in nuclei surrounding the antennal lobe and the suboesophageal ganglion, and in nuclei medial to the optic lobe, and was absent from axons in the antennal lobe. When imaged from the posterior, HDAC4$^{\Delta NES}$ localised to Kenyon cell nuclei and was absent from cytoplasmic haloes and the calyx (Figure 5.24F). Expression of both HDAC4^{WT} and HDAC4$^{\Delta NES}$ increased the intensity of MEF2 staining in Kenyon cells compared to control. These data confirm that the DmHDAC4 NES is functional, and mutation of this sequence motif results in nuclear accumulation.

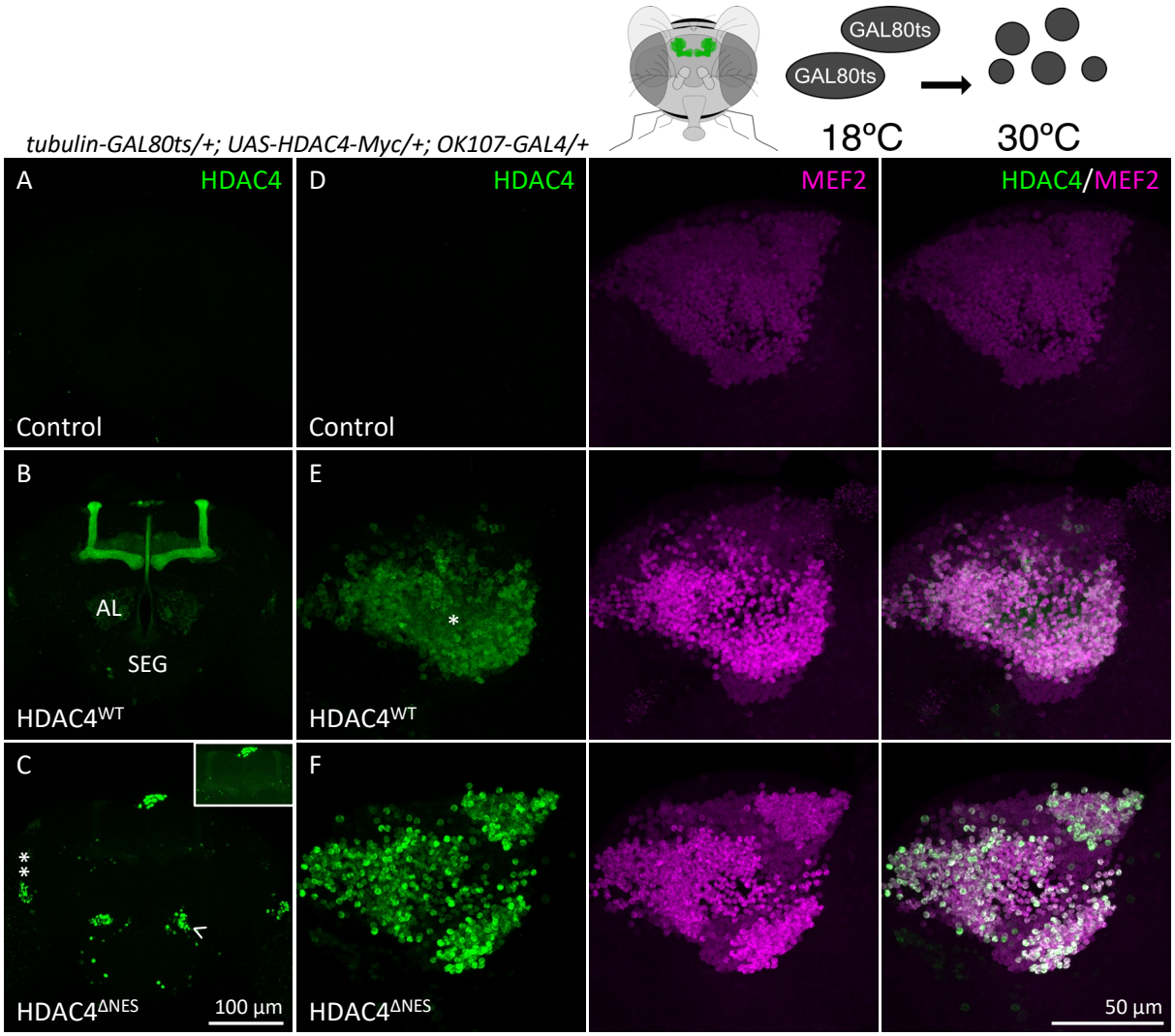

Figure 5.24 Mutation of the nuclear export sequence within HDAC4 results in nuclear accumulation in Kenyon cells

Maximum projections of optical sections through the central brain in the anterior (A-C), or Kenyon cell layer in the posterior (D-F), of the brain expressing HDAC4^{WT} or HDAC4$^{\Delta NES}$ (green) under the control of *OK107-GAL4* in the presence of the TARGET system. Flies were raised at 18 °C until eclosion, where adults were transferred to 30 °C for three days to induce HDAC4 expression. MEF2 (magenta) is included as a counterstain. Control is *OK107-GAL4/+*. HDAC4^{WT} was detected in the lobes of the mushroom body (B) while HDAC4$^{\Delta NES}$ was largely absent from these (C), and only observed upon an increase in microscope gain (inset). Arrowheads in (C) indicate the nuclear localisation of HDAC4$^{\Delta NES}$ in cells surrounding the antennal lobe (AL) and suboesophageal ganglion (SEG), the location of which are noted in (B). * in (C) indicates nuclear localisation of HDAC4$^{\Delta NES}$ in cells medial to the optic lobe. HDAC4^{WT} localised to nuclei and cytoplasmic haloes of Kenyon cells as well as the calyx (*, E) while HDAC4$^{\Delta NES}$ was absent from haloes as well as from the calyx (F). *This figure is an adaptation from that found in Tan et al. (2024) (doi: 10.1186/s12915-023-01800-1), which is distributed under CC BY 4.0.*

5.5.2. HDAC4$^{\Delta NES}$ has different aggregation characteristics to HDAC4^{3SA}

Given that HDAC4$^{\Delta NES}$ is increased in nuclear localisation similarly to HDAC4^{3SA}, it was hypothesised that its nuclear aggregation would be similar unless 14-3-3 binding alters aggregate dynamics as suggested by Segal *et al.* (2023). As above, HDAC4 expression was driven by *OK107-GAL4* +TARGET with flies being raised at 18 °C until emerging, which were then transferred to 30 °C to induce transgene expression. Figure 5.25 shows the distribution of HDAC4^{3SA} and HDAC4$^{\Delta NES}$ in Kenyon cells across two independent experiments. HDAC4^{WT} distribution is similar between the two therefore this comparison is appropriate. In both Figure 5.25A and C HDAC4^{WT} localised to the nucleus and cytoplasm, and formed small punctate foci in nuclei that sequestered MEF2. HDAC4^{3SA} was sequestered in nuclei, and as a result there was a significant increase in aggregate number and size compared to HDAC4^{WT} (Figure 5.25B). Interestingly, while HDAC4$^{\Delta NES}$ was excluded from cytoplasmic haloes, the aggregation dynamics were significantly altered compared to HDAC4^{3SA} (Figure 5.25D). HDAC4$^{\Delta NES}$ accumulated at the nuclear periphery and redistributed MEF2 to this region. Fewer aggregates were observed than for HDAC4^{3SA}, both in total per brain as well as the number per nucleus. It is unclear whether there was a significant difference in the number of aggregates between HDAC4^{WT} and HDAC4$^{\Delta NES}$, and whether the composition of these were altered. These data suggest that in addition to mediating nuclear export of HDAC4, 14-3-3 binding to HDAC4 may regulate aggregation dynamics.

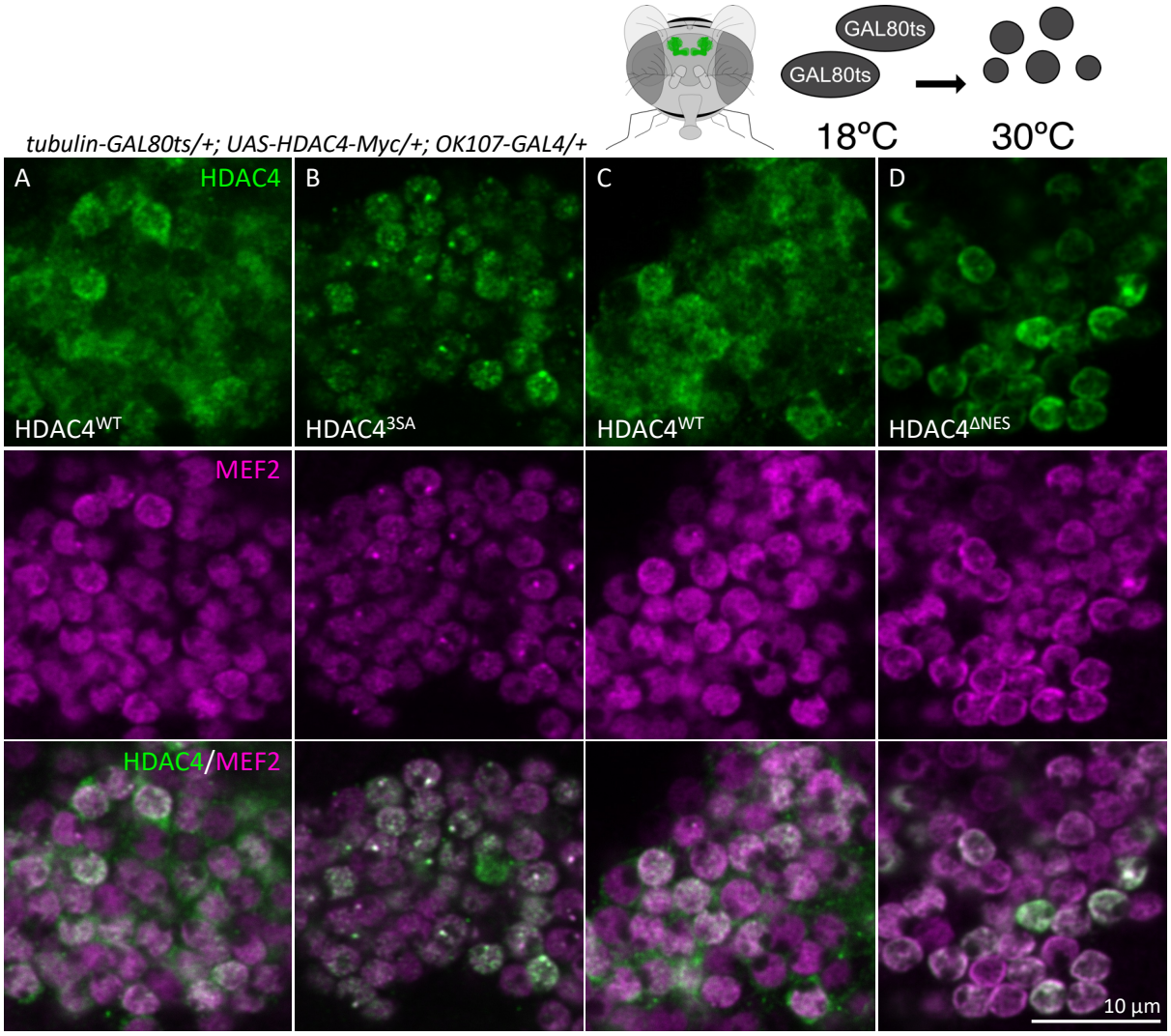

Figure 5.25 HDAC4$^{\Delta NES}$ has different nuclear aggregation characteristics compared to HDAC4^{3SA}

(A-D) Single optical sections (0.5 µm) of HDAC4 (green) expression under the control of *OK107-GAL4* in the presence of the TARGET system in Kenyon cells. Flies were raised at 18 °C until eclosion, where adults were transferred to 30 °C for three days to induce HDAC4 expression. (A-B) and (C-D) are from two independent experiments, therefore the distribution of HDAC4^{WT} is displayed for both. (A, C) HDAC4^{WT} localised to both cytoplasmic haloes and the nucleus where it formed small aggregates that co-localised with MEF2 (magenta). (B) HDAC4^{3SA} was not observed in cytoplasmic haloes and had an increased frequency of nuclear aggregates compared to HDAC4^{WT}. (D) In comparison, HDAC4$^{\Delta NES}$ was not observed in cytoplasmic haloes, formed fewer but larger aggregates than HDAC4^{3SA}, and accumulated at the nuclear periphery. *This figure is an adaptation from that found in Tan et al. (2024) (doi: 10.1186/s12915-023-01800-1), which is distributed under CC BY 4.0.*

5.5.3. HDAC4$^{\Delta NES}$ induces severe β-lobe fusion similarly to HDAC4^{3SA}

Compared to HDAC4^{3SA}, the aggregation dynamics of HDAC4$^{\Delta NES}$ are significantly altered. Overexpression of HDAC4^{WT} impaired mushroom body development in a dose-dependent manner, and this was increased in severity upon expression of either HDAC4^{3SA} or HDAC4^{S69F}, both of which increase the nuclear localisation and aggregation of HDAC4 (Sections 4.4.2 and 5.2.4). It is unclear however whether this different aggregation profile, despite similar nuclear accumulation of HDAC4$^{\Delta NES}$, affects the HDAC4 overexpression-induced β-lobe fusion phenotype. To determine changes in the severity of β-lobe fusion compared to HDAC4^{WT} and HDAC4^{3SA}, expression was driven under the control of *OK107-GAL4* +TARGET, and flies were raised at 25 °C to yield an intermediate expression level as previously (Section 5.4.3). Brains were dissected and processed for immunohistochemistry to detect FasII and observe the structure of the mushroom body, where three levels of β-lobe fusion severity were scored (Table 5.4).

Table 5.4 Frequency of mushroom body phenotypes resulting from overexpression of HDAC4$^{\Delta NES}$

(% of brains)	Con	HDAC4^{WT}	HDAC4^{3SA}	HDAC4$^{\Delta NES}$
α thinning	0	0	0	0
α missing	0	0	0	0
β thinning	0	0	0	0
β missing	0	0	0	0
β fusion	**55**	**83**	**100**	**89**
Minor	45	66	58	44
Moderate	5	14	38	33
Severe	5	3	4	11
n	20	29	24	27

Expression of each denoted transgene was mediated by *OK107-GAL4* in the presence of the TARGET system; virgin *tubulin-GAL80ts; OK107-GAL4* female flies were crossed to males harbouring the *HDAC4* transgene and adult progeny of this cross were dissected and their brains immunostained for FasII to assess mushroom body lobe development. Flies were raised at 25 °C. Instances of defects in morphology were scored for n≥20 brains per genotype as per Section 3.4.7, and are displayed as the % of brains with the indicated phenotype. Control (con) is *tubulin-GAL80ts/+; OK107-GAL4/+*. Percentages may not sum to 100 due to rounding. *These data are also presented in Tan et al. (2024) (doi: 10.1186/s12915-023-01800-1), which is distributed under CC BY 4.0.*

Overexpression of HDAC4^{WT} resulted in β-lobe fusion in 83% of brains, of which only 17% were moderate or severe (Figure 5.26). Overexpression of either HDAC4^{3SA} or HDAC4$^{\Delta NES}$ resulted in an increase in β-lobe fusion to 100% and 89%, with an increase in moderate or severe fusion to 42% and 44% respectively. There was no statistically significant difference in moderate and severe β-lobe fusion between HDAC4^{3SA} and HDAC4$^{\Delta NES}$. These data reinforce that increased nuclear localisation of HDAC4 is responsible for β-lobe axon overgrowth resulting in fusion.

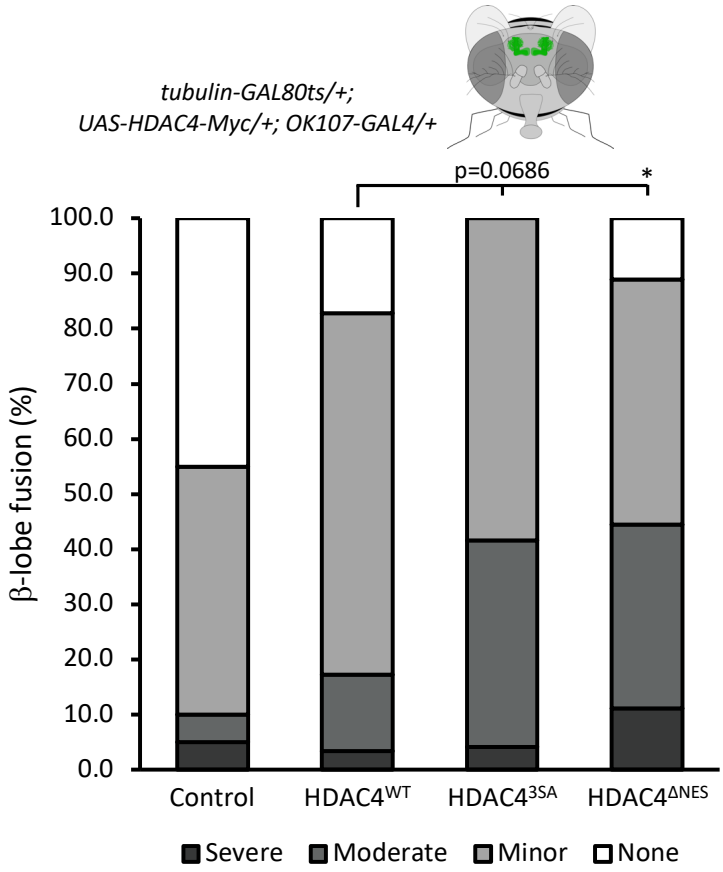

Figure 5.26 Nuclear localisation of HDAC4 impairs β-lobe development
Quantification of β-lobe fusion resulting from HDAC4$^{\Delta NES}$ overexpression. HDAC4 expression was driven by *OK107-GAL4* in the presence of the TARGET system at 25°C throughout development. Adult brains were processed for anti-FasII immunohistochemistry, and β-lobe fusion was scored. n≥20 brains per genotype. Moderate and severe β-lobe fusion was significantly increased by HDAC4$^{\Delta NES}$ compared to HDAC4^{WT} (Fisher's exact test, moderate and severe β-lobe fusion, p=0.0415), but not quite by HDAC4^{3SA} (p=0.0686). There was no statistically significant difference in fusion between HDAC4^{3SA} and HDAC4$^{\Delta NES}$ (p=1). *This figure is an adaptation from that found in Tan et al. (2024) (doi: 10.1186/s12915-023-01800-1), which is distributed under CC BY 4.0.*

5.5.4. HDAC4$^{\Delta NES}$ induces more severe defects in eye development than HDAC4^{3SA}

Overexpression of HDAC4^{WT} impairs eye development in a dose-dependent manner, and this is increased in severity upon expression of either HDAC4^{3SA} or HDAC4^{S69F}, both of which increase the nuclear localisation and aggregation of HDAC4 (Sections 4.4.2 and 5.2.4). To examine how the different aggregation dynamics of HDAC4$^{\Delta NES}$ impact eye development, the eye phenotype resulting from expression driven by *GMR-GAL4* was examined (Figure 5.27 and Appendix 10.3.4, Figure 10.27). Flies harbouring one insertion of *GMR-GAL4* and one of *HDAC4^{WT}* (*GMR-GAL4/+; HDAC4^{WT}-Myc*/+) presented with mild disorganisation of ommatidia and bristles (Figure 5.27B) as observed previously (Section 4.5.2). Restriction of HDAC4 localisation to the nucleus via the 3SA mutations resulted in loss of pigmentation and increased disorganisation of ommatidia (Figure 5.27C) but interestingly, nuclear localisation via the ΔNES mutations resulted in a phenotype similar to that of HDAC4^{WT}, with only mild disorganisation of ommatidia (Figure 5.27C).

As it was difficult to discern any changes in phenotype severity between HDAC4^{WT} overexpression and HDAC4$^{\Delta NES}$, the dose of HDAC4 expression was increased. When raised at 25 °C (Figure 5.27I-L), harbouring two copies of *HDAC4$^{\Delta NES}$* and one of *GMR-GAL4* (*GMR-GAL4/+; HDAC4$^{\Delta NES}$-Myc*) was largely lethal; flies did not emerge from their pupal cases and had small eyes with large necrotic patches. Flies that did emerge had small smooth eyes with patches of necrosis (Figure 5.27L). In comparison, flies expressing HDAC4^{3SA} and HDAC4^{WT} were viable and had phenotypes similar in severity to that observed previously (compare Figure 5.27J to 4.19D, and 5.27K to 5.11B). Therefore, to score changes in severity between these genotypes the temperature at which they were raised was reduced to 22 °C to reduce the level of transgene expression (Figure 5.27E-H). Under these conditions, both HDAC4^{WT} and HDAC4^{3SA} presented with loss of pigmentation, disorganisation of ommatidia, and occasional instances of ommatidial fusion (Figure 5.27F-G), while HDAC4$^{\Delta NES}$ expressing eyes had complete fusion of ommatidia, loss of pigmentation, and loss of bristles. When scored for severity as per Section 3.5.1, this demonstrated that flies expressing HDAC4$^{\Delta NES}$ were significantly increased in phenotype severity compared to flies expressing HDAC4^{WT} and HDAC4^{3SA} (Figure 5.28). These data reinforce that increased nuclear localisation of HDAC4 is responsible for increasing severity of defects in eye development.

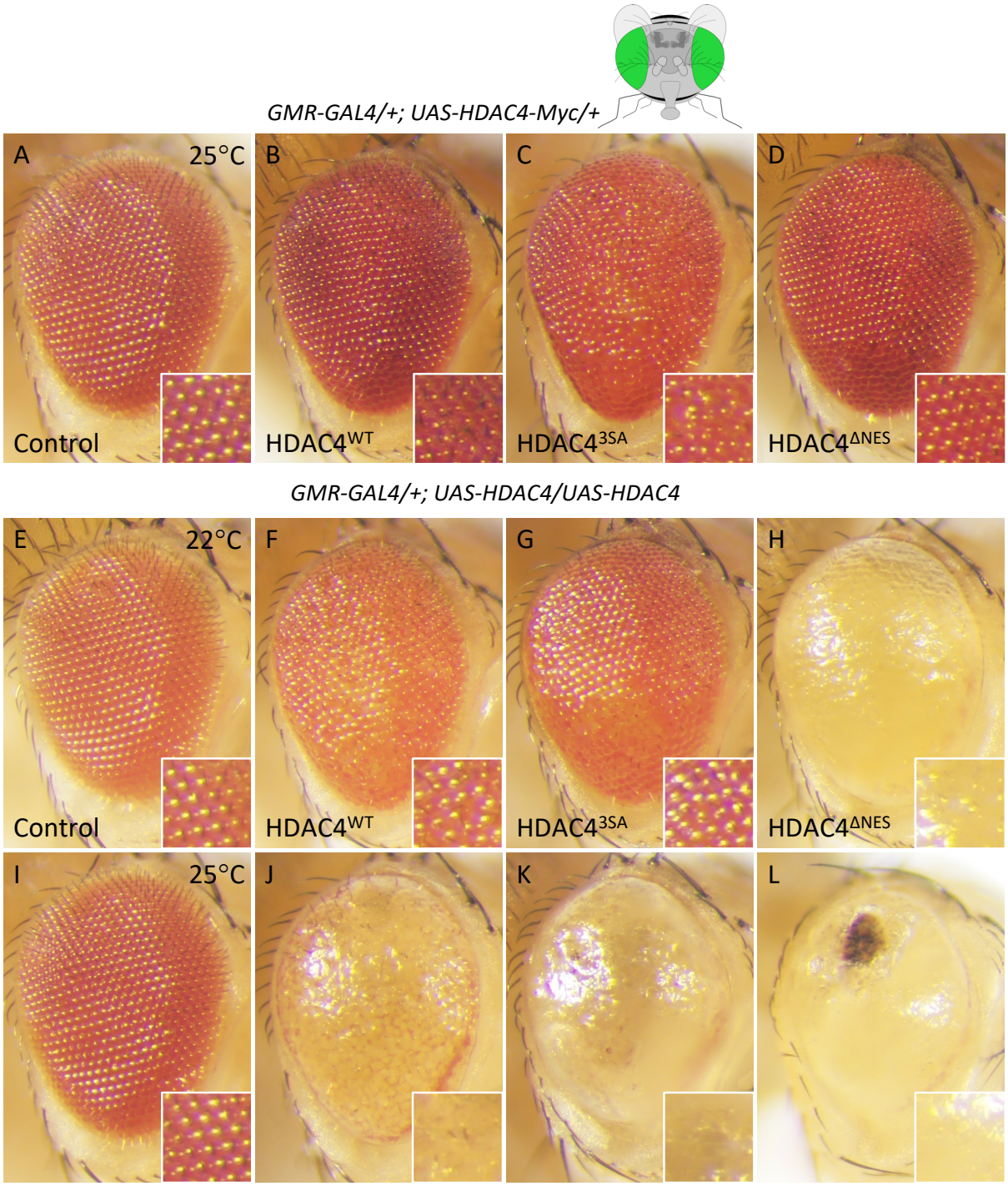

Figure 5.27 Eye phenotypes resulting from enforcing nuclear localisation of HDAC4 via 3SA and ΔNES mutations

Light microscopy images of *Drosophila* eyes raised at the indicated temperatures. All eyes shown are from male flies. Females are presented in Appendix 10.3.4, Figure 10.27. Inset shows a magnified image of ommatidia. (A, E, I) Control is *GMR-GAL4/+*. (B-D) Flies harboured one copy of the driver (*GMR-GAL4/+*) and one copy of $HDAC4^{WT}$ or $HDAC4^{mutant}$ (*UAS-HDAC4/+*) and were raised at 25 °C. (B) $HDAC4^{WT}$ overexpression induced disorganisation of bristles and ommatidia. This phenotype was increased in severity upon expression of $HDAC4^{3SA}$ (C) which resulted in loss of pigmentation and occasional fusion of ommatidia as well as disorganisation. (D) Expression of $HDAC4^{\Delta NES}$ did not increase phenotype severity compared to $HDAC4^{WT}$. (F-H) Flies harboured one copy of the driver (*GMR-GAL4/+*) and two copies of $HDAC4^{WT}$ or $HDAC4^{mutant}$ (*UAS-HDAC4/UAS-HDAC4*) and were raised at 22 °C. (F) Increasing the dose of $HDAC4^{WT}$ overexpression increased the severity of the eye

phenotype, with increased loss of pigmentation and fusion of ommatidia, similarly to that of HDAC4^{3SA} (G). (H) Expression of HDAC4$^{\Delta NES}$ resulted in complete fusion of ommatidia and loss of pigmentation. (J-L) Flies harboured one copy of the driver (*GMR-GAL4/+*) and two copies of *HDAC4^{WT}* or *HDAC4^{mutant}* (*UAS-HDAC4/UAS-HDAC4*) and were raised at 25 °C. Increasing the temperature at which flies were raised increased the severity of the phenotype. (J) HDAC4^{WT} expressing eyes presented with fusion of ommatidia, and pigment was largely only observed at the edges of the eye. HDAC4^{3SA} expressing eyes (K) presented with total fusion and loss of pigmentation, with necrotic patches. (L) Expression of HDAC4$^{\Delta NES}$ was largely lethal as flies remained in their pupal cases; of the flies that emerged their eyes were small, smooth, and had necrotic patches.

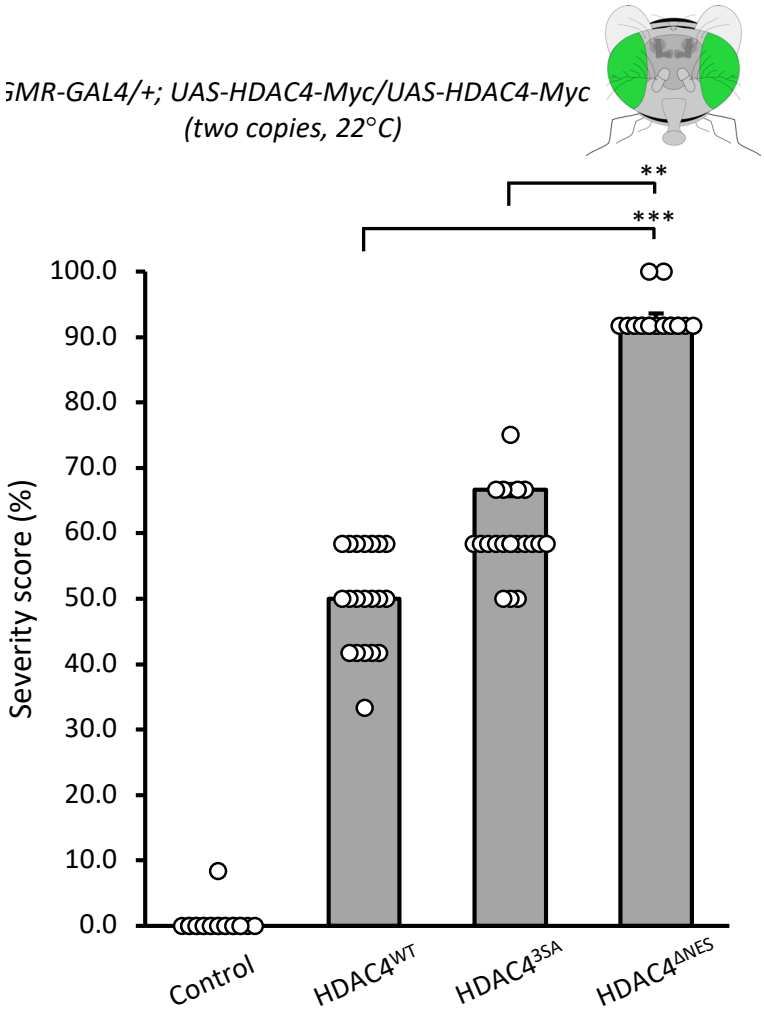

Figure 5.28 Implementation of a scoring system to compare deficits in eye development resulting from enforcing nuclear localisation of HDAC4 via the 3SA and ΔNES mutations

The severity of eye phenotypes resulting from HDAC4 expression under the control of *GMR-GAL4* at 22°C was scored as per Section 3.5.1. Flies were heterozygous for *GMR-GAL4* and homozygous for *HDAC4* (*GMR-GAL4/+, UAS-HDAC4/UAS-HDAC4*). Control is *GMR-GAL4/+; +/+*. Severity scores were converted to % severity and the mean is plotted with individual data points represented as circles. Error bars indicate the SEM. n=20 eyes per genotype. Nuclear localisation via ΔNES mutations induced a more severe eye phenotype than nuclear localisation induced by 3SA mutations (Kruskal-Wallis test, $H_{(3)}=72.56$, $p<0.001$, post-hoc Dunn's test, **$p<0.01$, ***$p<0.001$. HDAC4^{WT} vs HDAC4^{3SA}, $p=0.07887$; vs HDAC4^{NES}, $p<0.001$. HDAC4^{3SA} vs HDAC4$^{\Delta NES}$, $p=0.001$).

5.6. Discussion

The previous chapter identified a correlation between the oligomerisation/aggregation of HDAC4 and its ability to disrupt neuronal development in *Drosophila*. It remained unclear however if oligomerisation of HDAC4 contributes to the regulation of its subcellular distribution, and whether this inherently alters its ability to aggregate in the nucleus. This chapter demonstrated that in Kenyon cells, oligomerisation of HDAC4 affects its subcellular distribution, and mutations that reduce oligomerisation of HDAC4 reduce its nuclear accumulation. As a result, it was unclear whether the reduction in severity of neuronal phenotypes mediated by the oligomerisation mutants described in the previous chapter was a result of decreased aggregation by decreased oligomerisation, or a function of reduced nuclear localisation as this was previously determined to mediate reductions in severity (Main *et al.*, 2021; Tan *et al.*, 2024).

Restriction of HDAC4 oligomerisation mutants to the nucleus by combination with the 3SA mutations confirmed that each of the F65A and 9QA mutations reduced aggregation independently of changes in subcellular distribution, as aggregates were fewer and smaller, and this again correlated with a reduction in the severity of neuronal phenotypes. MEF2 is key in regulating the ability of HDAC4 to disrupt mushroom body development, and in agreement with Main *et al.* (2021) and Tan *et al.* (2024), this disruption was dependent on both the MEF2 protein and the MEF2 binding site within HDAC4. In contrast, Phe65 within HDAC4 was required for manifestation of eye phenotypes resulting from HDAC4-overexpression, and this acted synergistically with the MEF2 binding domain. It was also determined that MEF2 protein stabilises HDAC4 aggregation, whereas 14-3-3 may antagonise and alter the dynamics of HDAC4 aggregates. These data significantly increase understanding of HDAC4 aggregates, how they form, and how they mediate neuronal dysfunction. Moreover, these data demonstrate a complex interaction between HDAC4 dose, subcellular distribution, and aggregation, and that this varies between neuronal cell-types, highlighting that HDAC4 aggregation results in different effects dependent on the function of the cell in which it is dysregulated. Together these data illustrate that HDAC4 aggregation can affect different cells through different mechanisms. These data also progress knowledge of how HDAC4 aggregates form, and the role that oligomerisation plays in regulation of HDAC4 subcellular distribution.

5.6.1. Oligomerisation and dose of HDAC4 regulate its subcellular distribution

HDAC4 undergoes complex regulation of its subcellular distribution in an activity-dependent manner in neuronal cells (Section 1.5.1). Histone deacetylases are typically thought of as nuclear proteins due to their name, where it is assumed their primary function is to deacetylate histone proteins, however it is becoming increasingly clear that HDACs have alternative critical functions (reviewed in Fitzsimons (2015)). HDAC4 in particular is unusual as it is predominantly localised to the cytoplasm in the brain (Darcy *et al.*, 2010), however its main function here remains unknown. Importantly, in neurological disease aberrant nuclear accumulation of HDAC4 is frequently observed, and in some instances, it is found to form nuclear aggregates (Section 1.6.2). Given the positive correlation between nuclear aggregation of HDAC4 and defects in neuronal development in *Drosophila* (Chapter 4), in AD manifestation (Shen *et al.*, 2016), and that increased nuclear localisation of HDAC4 increases aggregation and phenotypic severity (Tan *et al.*, 2024), it is essential to understand the mechanisms through which HDAC4 subcellular distribution is regulated.

Human HDAC4 has functional nuclear import and export signals, however its distribution is dynamically regulated by other binding partners, including MEF2 and 14-3-3 (Section 1.5.1). The interaction with MEF2 is particularly novel, whereby MEF2 mediates the nuclear import of HDAC4 (Borghi *et al.*, 2001; Wang & Yang, 2001), and binding of HDAC4 to MEF2 results in repression of MEF2-dependent transcription (Miska *et al.*, 1999; Wang *et al.*, 1999), thus MEF2 imports its own repressor to the nucleus. Guo *et al.* (2007) and Dai *et al.* (2024) observed that mutations that affect oligomerisation of HDAC4 alter its ability to repress MEF2-dependent transcription, suggesting that oligomerisation of HDAC4 may affect MEF2 binding and subsequent nucleocytoplasmic shuttling. Indeed, mutations that destabilised oligomerisation reduced the nuclear localisation of HDAC4 in Kenyon cells while the inverse was seen for the stabilising S69F mutation. These changes in subcellular distribution also appear to be dose-dependent, as marked changes in nuclear localisation were observed in Kenyon cells under the control of *elav-GAL4*, but all oligomerisation mutants were more nuclear when expressed at a higher level in the mushroom body by *OK107-GAL4*. However, as HDAC4^{9QA} and HDAC4$^{9QA\Delta Q}$ are reduced in protein levels compared to HDAC4^{WT}, changes in distribution for these mutants could result from changes in oligomerisation or reduced protein level. In addition, changes in distribution were not observed for F65A, 9QA and 9QAΔQ mutants relative to HDAC4^{WT} in cells surrounding the antennal lobe. Together these data

highlight that HDAC4 distribution can be modulated by oligomerisation in a dose-dependent manner, and that this is differentially regulated between cell types.

Regulation of HDAC4 subcellular distribution in a dose-dependent manner is interesting in the context of neuronal disease and mental disorders as dysregulation of HDAC4 expression has been widely noted (Y. Wu *et al.*, 2016). Upregulation of HDAC4 has been observed at the mRNA level in patients with autism spectrum disorder (Nardone *et al.*, 2014) and depressive states of bipolar disorder (Hobara *et al.*, 2010) as well as in mouse models of AD (Chen *et al.*, 2021). In light of the dose-dependent distribution in Kenyon cells it is likely that HDAC4 may become increasingly nuclear in these cases where its expression is upregulated. Increased nuclear abundance of HDAC4 results in repression of genes essential for synaptic function (Sando *et al.*, 2012), impaired long-term memory in *Drosophila* (Main *et al.*, 2021), and impaired memory acquisition in mice (Zhu *et al.*, 2019). Moreover, nuclear HDAC4 abundance correlated with Alzheimer's disease severity as assessed by Braak staging in post-mortem brains of patients (Shen *et al.*, 2016), directly correlating disease progression with the nuclear abundance of HDAC4. These data further suggest a correlation between nuclear HDAC4 and neuronal dysfunction. This provides an interesting avenue of investigation whereby increases in HDAC4 expression may increase its nuclear distribution, resulting in loss of canonical HDAC4 activity in the cytoplasm as well as gain of function in the nucleus, together resulting in impaired neuronal function. Further characterisation of the expression levels and subcellular distribution of HDAC4 in normal, diseased, and ageing brains may shed light on mechanisms of aberrant nuclear accumulation of HDAC4.

The question of how oligomerisation of HDAC4 regulates its subcellular distribution remains unanswered. Section 4.7.5 presented a 3D model of the HDAC4 tetramer that placed the MEF2 binding site externally. In combination with the finding that the F65A mutation (which destabilises oligomerisation) reduces both repression of MEF2-dependent transcription (Guo *et al.*, 2007), and the nuclear localisation of HDAC4, both of which require MEF2 binding, it is hypothesised that tetramerisation of HDAC4 favours the binding of MEF2. However, it remains unclear what effect MEF2 binding has on the interaction of 14-3-3 with HDAC4; it is possible that binding of MEF2 and 14-3-3 to HDAC4 is mutually exclusive, and therefore 14-3-3 binding may be favoured by the monomeric state of HDAC4, thus inducing nuclear export and reinforcing cytoplasmic localisation of monomeric HDAC4. Moreover, it is possible that 14-3-3 binding is not compatible with oligomerisation of HDAC4 as binding sites are buried in the

oligomer. Together this hypothesis is presented as a model in Figure 5.29, where 14-3-3 binding may be favoured by monomeric HDAC4, preventing MEF2 association and retaining HDAC4 in the cytoplasm, while in contrast, tetramerisation favours the binding of MEF2, resulting in the nuclear import of HDAC4. This model may provide an explanation for the reduced nuclear distribution of HDAC4^{F65A} observed within the basal cells of the larval eye disc compared to HDAC4^{WT} (Figure 4.14), where HDAC4^{F65A} favours the monomeric form and allows binding of 14-3-3 to facilitate export from the nucleus. It is also possible that HDAC4 aggregation inherently prevents its nuclear export as aggregates are too large to be transported through the nuclear pore complex. This may contribute to the severity of aggregation and phenotypes associated with HDAC4^{S69F}. Further investigation into the dynamics of HDAC4 aggregation, as well as the role of oligomerisation in MEF2 and 14-3-3 binding, will shed light on the relative contribution of each to the subcellular distribution of HDAC4.

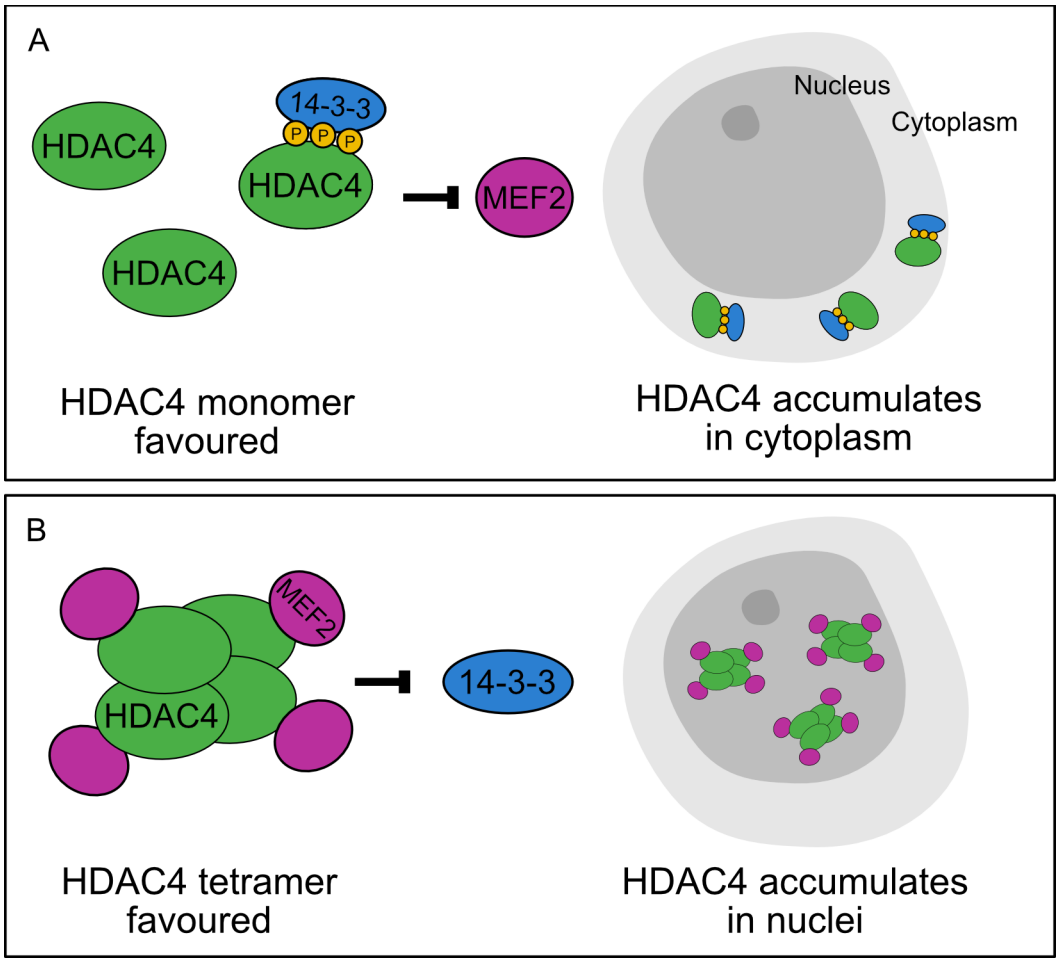

Figure 5.29 A model of the potential interplay between oligomerisation of HDAC4, association of MEF2 and 14-3-3, and regulation of subcellular distribution
Schematic diagram depicting a model in which HDAC4 tetramerisation modulates its interaction with proteins that regulate its subcellular distribution. (A) In the monomeric state, binding of 14-3-3 to HDAC4 is favoured, and binding of MEF2 is impaired, resulting in cytoplasmic localisation of HDAC4.

(B) In the tetrameric state binding of MEF2 to HDAC4 is favoured, and binding of 14-3-3 is impaired, resulting in nuclear localisation of HDAC4. *This figure is an original artwork.*

It is acknowledged that although this model poses tetramerisation of HDAC4 as the factor that governs the preference of either MEF2 or 14-3-3 binding, this may more broadly represent oligomerisation of HDAC4. That is, the formation of dimer, trimer, tetramer, or higher order species of HDAC4 may prevent 14-3-3 binding and favour MEF2 association and vice versa. This model is complementary to the recent findings that the N-terminus of HDAC4 dimerises in solution, and appears to form higher order networks with MEF2 (Dai *et al.*, 2024).

5.6.2. Restriction of HDAC4 localisation to the nucleus increases aggregate load

Tan *et al.* (2024) demonstrated that nuclear aggregation of HDAC4 increases upon 3SA mutation. The 3SA mutation is widely used to induce nuclear localisation of HDAC4. For wild-type HDAC4, phosphorylation of these three serine residues mediates binding of 14-3-3 and subsequent nuclear export (Wang *et al.*, 2000), in conjunction with the HDAC4 nuclear export sequence (McKinsey *et al.*, 2001). Binding of 14-3-3 at this site also reinforces cytoplasmic localisation as the NLS is masked, which inhibits association of importin-α (Grozinger & Schreiber, 2000). To examine how nuclear aggregation changes upon F65A or 9QA mutation independent of changes in distribution, HDAC4^{F65A} and HDAC4^{9QA} were directed to the nucleus by incorporation of the 3SA mutation. HDAC4$^{3SA\text{-}F65A}$ and HDAC4$^{3SA\text{-}9QA}$ were both localised to nuclei, but interestingly, only HDAC4$^{3SA\text{-}F65A}$ was significantly reduced in nuclear aggregate number compared to HDAC4^{3SA}. While aggregate number did not decrease for HDAC4$^{3SA\text{-}9QA}$, the size of aggregates was significantly reduced. Given the increase in aggregate size between HDAC4^{WT} and HDAC4^{3SA} it is hypothesised that when HDAC4 aggregates become more numerous, they coalesce to form larger aggregates, and consequently the total number of aggregates per nucleus is reduced, resulting in underestimation of aggregation when quantification is carried out via counting of aggregates. Following this hypothesis, these data suggest that 9QA mutation may destabilise aggregate coalescence, but not sufficiently enough to reduce aggregate number. It is again unclear however if this is a direct result of changes in oligomerisation, or is a function of reduced dose, as similarly to HDAC4^{9QA}, HDAC4$^{3SA\text{-}9QA}$ was reduced in protein levels compared to HDAC4^{3SA}.

The aggregation of HDAC4$^{3SA\text{-}F65A}$ was increased compared to HDAC4^{F65A}, suggesting there is a change in aggregation dynamics upon restriction of HDAC4 subcellular localisation to the nucleus. In support of this, HDAC4$^{3SA\text{-}F65A}$ aggregation was also increased compared to HDAC4^{WT}. It is hypothesised that confinement to a single subcellular compartment reduces the space in which HDAC4 is distributed, and therefore increases the chance of aggregate formation and aggregate coalescence (Figure 5.30). The presence of endogenous HDAC4 may aid in reinforcing this; as expression of HDAC4^{WT} increased the nuclear localisation of endogenous HDAC4 such that it accumulated in aggregates within Kenyon cell nuclei (Section 4.2), it is possible that HDAC4$^{3SA\text{-}F65A}$ may increase the nuclear localisation of endogenous HDAC4, which may in turn stabilise aggregation of HDAC4$^{3SA\text{-}F65A}$, contributing toward increased aggregate number. However, increased nuclear aggregation of HDAC4$^{3SA\text{-}F65A}$ relative to HDAC4^{F65A} may also be a function of decreased 14-3-3 binding, as mutation of 14-3-3 sites has been observed to promote aggregation of a number of proteins (Segal *et al.*, 2023), which is further discussed in Section 5.6.6.

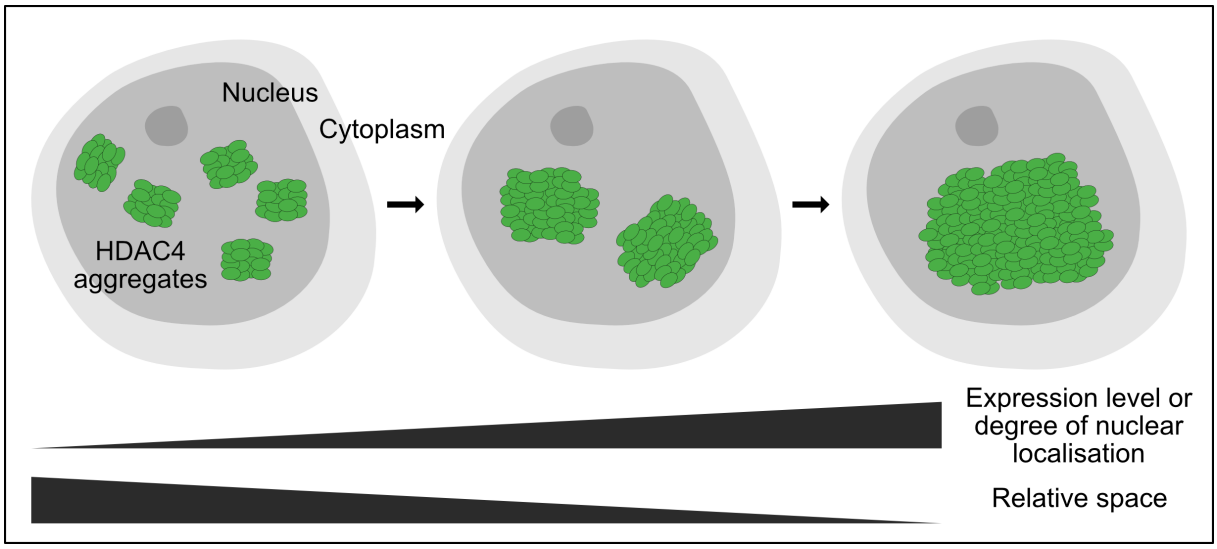

Figure 5.30 Reducing the effective volume in which HDAC4 is distributed increases its ability to aggregate
Schematic diagram depicting a model in which HDAC4 aggregation is increased upon changes in the relative space in which HDAC4 can aggregate. As HDAC4 expression or nuclear localisation is increased, the relative volume in which HDAC4 is distributed is decreased, which increases the effective concentration of HDAC4. This increase in concentration results in increased aggregate formation and coalescence. *This figure is an original artwork.*

It is noted that there was a reduction in the apparent molecular weight of HDAC4$^{3SA\text{-}F65A}$ compared to both HDAC4^{3SA} and HDAC4^{F65A}. This is curious as neither F65A nor 3SA mutations involve deletions that may account for a change in size. HDAC4^{F65A} and HDAC4^{3SA}

migrate at the same molecular weight as HDAC4^{WT}, suggesting it is not a biological effect of one of the mutations. HDAC4$^{3SA\text{-}F65A\text{-}\Delta MEF2}$ was generated via mutagenesis of the plasmid containing HDAC4$^{3SA\text{-}F65A}$, and was found to migrate at the same molecular weight on SDS-PAGE as HDAC4^{WT}, suggesting it is unlikely that there is any additional mutation within the HDAC4$^{3SA\text{-}F65A}$ plasmid that would cause production of a smaller protein. Further investigation of the cause of this was sought in Appendix 10.3.1. PCR amplification of regions spanning the HDAC4 insert from genomic DNA of flies harbouring the HDAC4$^{3SA\text{-}F65A}$ construct revealed no deletions compared to HDAC4^{WT}, suggesting it is unlikely that a deletion was introduced during phi-C31-mediated integration of the pUASTattB-HDAC4$^{3SA\text{-}F65A}$ plasmid into the fly genome. Sequencing also confirmed that no mutations were present in either the plasmid DNA or genomic DNA near the translation start site, suggesting there is no reason for favouring of an alternative start site. Overexposure of membranes detected with anti-Myc showed smaller HDAC4 C-terminal products that were shifted in size for HDAC4$^{3SA\text{-}F65A}$ compared to other HDAC4 constructs, and this was localised to approximately 50-70 kDa from the C-terminus, suggesting a C-terminal modification may be lost, or an in-frame internal deletion is occurring. It remains unclear why HDAC4$^{3SA\text{-}F65A}$ migrates with a smaller molecular weight. It is possible that the combination of 3SA and F65A mutations may favour some biological occurrence such as enzymatic cleavage by a change in protein binding or conformation that may reveal a cleavage site, or site creation by the combination of these mutations. However, it is difficult to reason how this would result in an internal deletion, and be reversed upon addition of the ΔMEF2 mutations. It is more likely that there is a change in post-translational modification of HDAC4$^{3SA\text{-}F65A}$ that is differentially regulated compared to each of HDAC4^{3SA}, HDAC4^{F65A}, and HDAC4$^{3SA\text{-}F65A\text{-}\Delta MEF2}$. Further investigation of this is required.

It is possible that the change in molecular weight associated with HDAC4$^{3SA\text{-}F65A}$ may confer some change in function not attributed to 3SA or F65A mutations alone, for example by altering sequestration of specific proteins within nuclear aggregates. However, there were no instances where phenotypic severity was unexpectedly altered (Section 5.6.3), therefore this mutant still provides proof of principle that reducing the nuclear aggregation of HDAC4 reduces aggregate load and severity of neuronal phenotypes. Further clarification as to the cause of the reduced protein size may be pertinent if oligomerisation of HDAC4 within the nucleus is investigated as a therapeutic target, and this should begin with re-generation of the pUASTattB-HDAC4$^{3SA\text{-}F65A}$ plasmid and generation of a new line of transgenic flies if investigation in the *Drosophila* model is continued.

5.6.3. Differential phenotypic effects of HDAC4 oligomerisation mutants when localised to the nucleus

A major finding of this chapter is that even when subcellular distribution is controlled for, oligomerisation mutants of HDAC4 form fewer and smaller nuclear aggregates, and are associated with reduced developmental defects, therefore oligomerisation is an important step in mediating HDAC4-induced defects in neurodevelopment. It is again important to consider the presence of endogenous HDAC4 in these findings, which is likely present in HDAC4 oligomers and therefore contributes to oligomer stability, aggregation, and subsequent phenotypes (Section 4.7.1.2).

The similarities between HDAC4^{F65A} and HDAC4^{9QA} mutations were highlighted in the previous chapter. Both are hypothesised to destabilise tetramerisation, albeit by different mechanisms, where F65A mutation directly destabilises the hydrophobic core that is essential for tetramerisation (Guo *et al.*, 2007), whereas the 9QA mutations were designed to disrupt hydrophilic interactions surrounding the core that stabilise the HDAC4 tetramer. Both mutants reduced the severity of HDAC4 overexpression-induced β-lobe fusion in the mushroom body and defects in adult eye development compared to HDAC4^{WT}. However, upon restriction of localisation to the nucleus, HDAC4$^{3SA\text{-}9QA}$ reduced severe β-lobe fusion more than HDAC4$^{3SA\text{-}F65A}$, whereas HDAC4$^{3SA\text{-}F65A}$ reduced the severity of the eye phenotype more than HDAC4$^{3SA\text{-}9QA}$. It is essential to consider however that reductions mediated by HDAC4^{9QA} and HDAC4$^{3SA\text{-}9QA}$ cannot solely be attributed to oligomerisation-dependent changes in HDAC4 aggregation, as both mutant proteins are present at a lower level than HDAC4^{WT}, and HDAC4-overexpresion induced phenotypes are dose-dependent. For this reason, only the effect of the F65A mutation is further discussed.

HDAC4$^{3SA\text{-}F65A}$ aggregation was increased compared to HDAC4^{WT}, and consequently HDAC4$^{3SA\text{-}F65A}$ did not decrease the severity of β-lobe fusion in the mushroom body compared to either HDAC4^{WT} or HDAC4^{3SA} under the original experimental conditions. However, upon lowering the dose of HDAC4 overexpression by reducing the temperature at which flies were raised, the level of severe β-lobe fusion induced by HDAC4$^{3SA\text{-}F65A}$ was significantly reduced compared to both HDAC4^{WT} and HDAC4^{3SA}. Lowering the dose of HDAC4 expression likely reduced aggregate number (Figure 5.30), and subsequently decreased the severity of phenotypes. These data could be further extended by comparing aggregation of HDAC4$^{3SA\text{-}F65A}$

and HDAC4^{WT} in Kenyon cells at a lower level of expression, to determine whether there is a sudden shift in nuclear aggregate formation associated with the F65A mutation.

The role of the 3SA-F65A mutations in the adult eye differs to that in the brain as there was a more significant reduction in phenotype severity compared to HDAC4^{3SA} in the eye than that in the mushroom body when comparing phenotypes in the original experimental conditions. Interestingly, the degree of severity correlated with nuclear aggregation. In Kenyon cells, HDAC4$^{3SA-F65A}$ still formed nuclear puncta comparable in size compared to HDAC4^{3SA}, while in the eye disc HDAC4$^{3SA-F65A}$ nuclear distribution was largely granular and significantly fewer aggregates were observed. While many factors are likely to contribute to these differences in aggregation, it is important to consider the dose of overexpression and the presence of endogenous HDAC4 and MEF2. The relative level of expression driven by *elav-GAL4* in Kenyon cells compared to *GMR-GAL4* in the eye disc is unknown. If one drives a higher level of expression, this would likely result in a higher level of aggregate formation (Figure 5.30). The relative level of endogenous HDAC4 may also differ between these cell types; if there is a lower level of endogenous HDAC4 in the eye disc than in Kenyon cells, there may be comparatively less stabilisation of oligomerisation, thus resulting in a decrease in aggregation. Similarly, the lack of MEF2 in the eye disc may result in reduced stabilisation of aggregation compared to that in Kenyon cells. These data highlight the importance of the investigation of protein function in different cell types, where a different interactome will be present.

5.6.4. The role of MEF2 and the MEF2 binding domain within HDAC4 in the *Drosophila* eye

There is little known about the role of MEF2 in the development and function of the *Drosophila* eye. MEF2 was not detected in the developing third instar larval eye disc (Figure 4.12), however MEF2 expression has been detected in the optic lobes (Schulz *et al.* (1996), Figure 4.10) and subsequent investigation revealed that MEF2 is present in the adult eye. It is unclear at what stage MEF2 expression begins in *Drosophila*; as the ommatidial array emerges during larval development and is refined during the pupal stage (Section 1.3.2), MEF2 protein expression would be expected to begin at a relatively early stage if it is involved in these processes. Studies in mice demonstrated that MEF2A and MEF2D protein was detected in the developing retina (Andzelm *et al.*, 2015), *MEF2C* transcripts were observed at birth (Wolf *et al.*, 2017) and protein levels increased with age (Andzelm *et al.*, 2015). MEF2D plays a critical role in retinal

development in mice as its knockout induced defects in the maturation of rod and cone cells and prevented correct retinal development, leading to impaired visual response and photoreceptor degeneration (Andzelm *et al.*, 2015; Omori *et al.*, 2015). Comparatively, RNAi mediated knockdown of *MEF2* under the control of *GMR-GAL4* had a subtle effect on adult eye morphology (Schwartz *et al.*, 2016), suggesting it does play a role in *Drosophila* eye development, albeit a small one.

Overexpression of $HDAC4^{WT}$ results in widespread fusion of ommatidia and loss of pigmentation, the severity of which is slightly reduced by the ΔMEF2 mutation (Tan *et al.*, 2024). Similarly, the severity of eyes of $HDAC4^{3SA}$ and $HDAC4^{3SA\text{-}F65A}$ mutants is reduced by mutation of the MEF2 binding site, suggesting that binding of MEF2 at this site enhances HDAC4-overexpression induced toxicity. However, this is in conflict with the genetic screen data; if MEF2 enhances HDAC4-overexpression induced toxicity through the MEF2 domain within HDAC4, it would be expected that knockdown of MEF2 would suppress the HDAC4-overexpression induced eye phenotype, but the opposite was observed (Schwartz *et al.*, 2016). These data suggest that binding of another protein at this site may be responsible for enhancing HDAC4-overexpression induced defects. In support of this, mutation of the MEF2 binding site in $HDAC4^{WT}$ had a striking effect on subcellular distribution in basal cells of the larval eye disc, yet MEF2 protein was not detected in this tissue.

PP2A is another regulator of nucleocytoplasmic shuttling of HDAC4 (Section 4.5.1.3). Dephosphorylation of HDAC4 by PP2A results in loss of 14-3-3 binding, reducing the efficiency of nuclear export and cytoplasmic anchoring (Paroni *et al.*, 2008). The PP2A binding site within HDAC4 is at the N-terminus, and it has been suggested that PP2A and MEF2 bind at the same domain (Paroni *et al.*, 2008). It is therefore conceivable that the ΔMEF2 mutation within HDAC4 may affect PP2A binding, maintaining phosphorylation of serine residues critical for 14-3-3 binding, resulting in an increase in cytoplasmic localisation compared to $HDAC4^{WT}$. This shift in distribution may mediate changes in severity of the eye phenotype associated with ΔMEF2 mutation.

A third interactor of HDAC4 is SRF, the orthologue of which in *Drosophila* is blistered (Affolter *et al.*, 1994). Similarly to MEF2, SRF belongs to the MADS-box family of DNA binding transcription factors and contains a MADS domain of which blistered shares 93% sequence identity (Affolter *et al.*, 1994). The N-terminus of HDAC4 represses SRF-dependent

transcription (Paroni *et al.*, 2007) and the binding region within human HDAC4 has been narrowed to residues 201-289 (Backs *et al.*, 2011). This region is just downstream of the MEF2 binding site (Appendix 10.2.2) therefore it is possible that the ΔMEF2 mutation may alter SRF binding, either directly or by affecting site availability through the binding of other proteins. As blistered mutants have defects in rhabdomere development (a structure of the *Drosophila* photoreceptor, Figure 1.5, Gambis *et al.* (2011)) similar to those observed upon HDAC4^{3SA} overexpression (Tan (2022), Appendix 10.4.2) it is possible that HDAC4 may act through SRF to mediate disruption of eye development.

Overall, these data again highlight how the effect of HDAC4 overexpression differs depending on the availability of binding partners that regulate its subcellular distribution and activity. Further investigation into the distribution of MEF2 within the adult eye in *Drosophila*, as well as examination of its expression in the pupal eye, will be of interest to determine whether it may have conserved roles in retinal development and visual function.

5.6.5. The role of MEF2 in promoting and stabilising aggregation of HDAC4

In the model of the full-length HDAC4 tetramer that was extrapolated from the AlphaFold-predicted structure of the HDAC4 monomer and the N-terminal tetramer as described by Guo *et al.* (2007), the site that mediates MEF2 binding is situated on the outside of the tetramer (Figure 4.28), suggesting that MEF2 binding is compatible with tetramerisation and possibly higher order oligomer formation (Figure 5.31). Both the hydrophobic core and MEF2 binding site contribute to aggregation of HDAC4, as HDAC4$^{3SA\text{-}F65A}$ and HDAC4$^{3SA\text{-}\Delta MEF2}$ were decreased in aggregate number compared to HDAC4^{3SA}, and the reduction in HDAC4$^{3SA\text{-}\Delta MEF2}$ aggregates was only in the number that co-localised with MEF2, confirming that this site is not required for aggregation. Moreover, MEF2 overexpression increased nuclear localisation of HDAC4^{WT} and appeared to increase aggregation. Therefore, while the interaction between MEF2 and HDAC4 does not appear to be required for aggregate formation, binding of MEF2 to HDAC4 reinforces nuclear localisation and stabilises aggregation; these data support a model in which MEF2 may stabilise higher order oligomer formation to promote aggregation of HDAC4 (Figure 5.31).

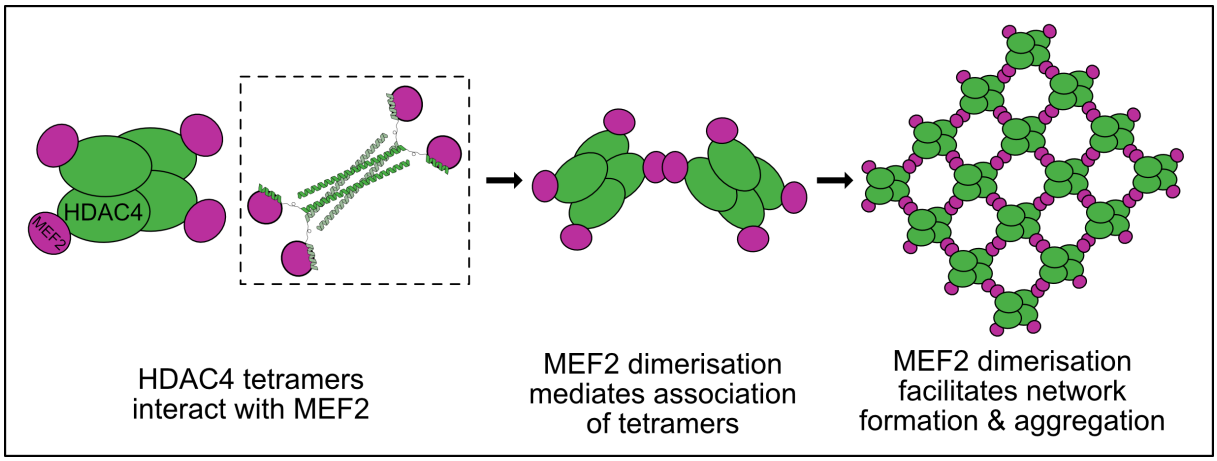

Figure 5.31 A model depicting how dimerisation of MEF2 may facilitate formation of higher order oligomers of HDAC4 that stabilise aggregation
Schematic diagram depicting a model in which HDAC4 aggregation is stabilised by MEF2. Each tetramer of HDAC4 is bound by four monomers of MEF2. Dimerisation of MEF2 facilitates association of HDAC4 tetramers, resulting in network formation and aggregation. *This figure is an original artwork.*

The HDAC4 binding region within MEF2 is highly conserved between the four human isoforms (MEF2A-D), as well as with the single isoform in *Drosophila* (Lu *et al.*, 2000). This region also mediates dimerisation of MEF2 (Molkentin *et al.*, 1996). It is unclear whether dimerisation of MEF2 and HDAC4 binding are mutually exclusive events, however HDAC4 binding is not necessary for MEF2 dimerisation (Molkentin *et al.*, 1996), and it is thought that interaction of MEF2 with HDACs does not affect MEF2 dimerisation (Lu *et al.*, 2000). In light of these findings, as well as the data presented here, this leads to the development of a model where dimerisation of MEF2 may facilitate formation of higher-order oligomers of HDAC4 (Figure 5.31). Each monomer within the MEF2 dimer could bind to a tetramer of HDAC4, resulting in formation of a network of HDAC4-MEF2 multimers, and this may in part facilitate aggregation of HDAC4 in Kenyon cells. It is acknowledged that this is a simplistic model, and the actual mechanism is likely to be more biologically complex. For example, it is possible that only one dimer of MEF2 may be able to interact with HDAC4, and in this case higher order structure formation may be facilitated by an additional protein.

The study by Dai *et al.* (2024) was published during the final stages of writing of this thesis, and sheds light on this hypothesis. In this study, the authors demonstrate that two monomers of the HDAC-binding region of MEF2 (that are DNA-bound) bind one monomer of the N-terminus HDAC4, and that the N-terminus of HDAC4 dimerises to bring two MEF2-bound regions of DNA together (Figure 5.32A-B). The authors suggested that binding of MEF2 to HDAC4 causes a conformational change within the N-terminus of HDAC4 that makes

tetramerisation unfavourable due to steric clashes, as this dimer was not compatible with the tetramer organisation previously observed (Figure 5.32C, Guo *et al.* (2007)). Instead, the N-terminus of HDAC4 was found to dimerise (predominantly via interface I, Figure 5.32A), and these dimers have the potential to form higher order complexes through an additional interaction interface (interface II, Figure 5.32B, D-E). Although these studies do not consider the hindrances presented by the C-terminus of HDAC4, it is possible that increased MEF2 binding to HDAC4 potentiates aggregation *in vivo* via these interaction interfaces.

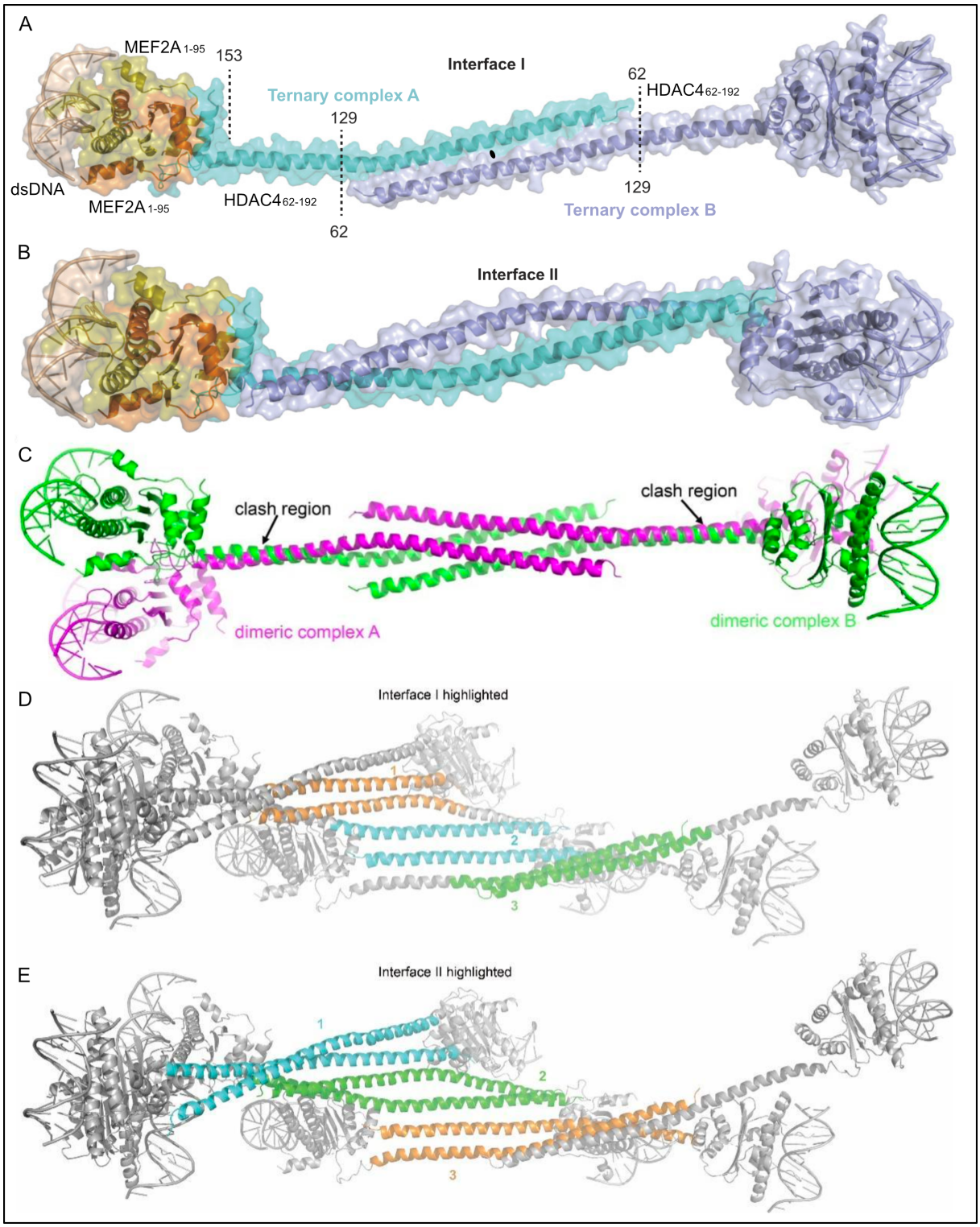

Figure 5.32 Higher order oligomerisation of HDAC4 may be facilitated by the interaction of HDAC4-MEF2 oligomers

(A-B) Complex formation of hHDAC4$^{62-192}$, hMEF2A$^{1-95}$ and double stranded DNA (dsDNA) as solved by crystal structure analysis (Dai *et al.*, 2024). The ribbon structure is overlaid with the surface presentation. Two monomers of MEF2A bound to dsDNA are bound by one monomer of hHDAC4 to form a ternary complex. Two ternary complexes interact via either interface I (A) or interface II (B). The approximate region of the hydrophobic core is marked by an oval in (A). (C) The HDAC4-MEF2 complex in A was superimposed into a tetramer as per Guo *et al.* (2007), resulting in clashing of the N-terminal α-helices of HDAC4. (D-E) Interactions of HDAC4 via interface I (D) and interface II (E)

result in formation of higher order HDAC4-MEF2A-DNA oligomers. *This figure is reproduced with modifications from Dai et al. (2024) (doi: 10.1093/nar/gkae036) which is distributed under CC BY-NC 4.0.*

Although the specifics of MEF2-dependent stabilisation of HDAC4 aggregation are a working hypothesis that is to be subject to further investigation, it is still important to consider that MEF2-dependent stabilisation of HDAC4 aggregation only occurs in cells in which MEF2 is expressed. Aggregation of HDAC4 in the larval eye disc appears largely independent of MEF2 as the protein could not be detected. These data highlight that while MEF2 is not essential for HDAC4 aggregation, it can facilitate it, and it is therefore possible that additional proteins enable aggregation of HDAC4. Further investigation into the interactors of HDAC4 aggregates is warranted. These data also further illustrate the importance of considering protein function in more than one neuronal cell type.

Interestingly, as well as localising within aggregates resulting from HDAC4^{WT} overexpression, MEF2 intensity in Kenyon cells was increased upon HDAC4 overexpression. This was specific to the MEF2 binding site within HDAC4 as ΔMEF2 mutation largely prevented an increase in intensity. It does not appear that altering oligomerisation significantly impacts the ability of HDAC4 to upregulate MEF2 intensity, however it is possible that the upregulation observed upon expression of HDAC4^{F65A} may be an effect of endogenous HDAC4 where HDAC4-overexpression induces nuclear localisation of endogenous HDAC4, which subsequently increases MEF2 intensity through oligomerisation and aggregation. The specific mechanism through which HDAC4-overexpression upregulates MEF2 in Kenyon cells remains unclear. It could be hypothesised that HDAC4 may be upregulating MEF2 at the transcriptional level, however previous work has demonstrated very few changes in transcription via RNA-seq on heads overexpressing HDAC4, including no significant change in transcripts of *MEF2* (Main *et al.*, 2021; Schwartz *et al.*, 2016). Given the sequestration of MEF2 in nuclear aggregates observed in the literature (Fitzsimons *et al.*, 2013; Main *et al.*, 2021; Tan *et al.*, 2024), and in this study, it is possible that such increases may be occurring via stabilisation of MEF2 at the protein level and further investigation of this is warranted.

Modulation of MEF2 levels by HDAC4 is of interest as MEF2 has conserved roles in neuronal development, survival, and function (Section 1.7), and has been identified as a disease-risk loci in Schizophrenia (Mitchell *et al.*, 2018), major depressive disorder (Hyde *et al.*, 2016) and Alzheimer's disease (Lambert *et al.*, 2013). Furthermore, *MEF2* haploinsufficiency is

associated with severe mental retardation and cerebral malformation (Le Meur *et al.*, 2010). *MEF2D* levels are increased in brains of patients with Parkinson's disease (Yang *et al.*, 2009), while expression of *MEF2C* is reduced in brains of Alzheimer's disease patients (Ren *et al.*, 2022). It is unclear whether the increased intensity of MEF2 in Kenyon cells constitutes an increase in functional protein, and thus whether it acts more similarly to increased MEF2 via increased transcription of *MEF2*, or if sequestration impairs or dysregulates MEF2 activity. Further investigation into the role of MEF2 dysregulation mediated by HDAC4 overexpression is warranted as this may shed light on how the interaction between the two may aid in disease onset and or progression. This also poses the question of whether HDAC4 stabilises the nuclear distribution or protein levels of other transcription factors such as CREB and SRF to mediate neuronal dysfunction.

Overall these data illustrate a complex reinforcement of severe neuronal phenotypes once HDAC4 levels exceed a certain threshold. Increasing levels of $HDAC4^{WT}$ result in increasing nuclear localisation. Nuclear HDAC4 results in upregulation of MEF2, which further increases nuclear distribution and stabilises aggregation of HDAC4. Detangling this regulatory network will be essential in overcoming toxicity associated with upregulation of both HDAC4 and MEF2.

5.6.6. The role of serine residues and the HDAC4 nuclear export sequence in nuclear localisation and aggregation dynamics

Neurotoxicity of HDAC4 in both *Drosophila* and human brains has largely been ascribed to the nuclear pool (Fitzsimons (2015), Main *et al.* (2021), Section 1.6.2). However, in both the studies performed in *Drosophila* by Main *et al.* (2021) and those in cell culture by Sando *et al.* (2012) (which are further elaborated on in Section 1.6), HDAC4 was sequestered in nuclei by mutation of three serine residues that are required for 14-3-3 mediated nuclear export and cytoplasmic anchoring of HDAC4 (Section 1.5.1.3). When increased in abundance in the nucleus by the 3SA mutation, aggregation of HDAC4 increased (Tan *et al.*, 2024), however it was unclear whether this was a direct result of increased nuclear localisation, or a secondary effect of the 3SA mutation. Moreover, it was recently determined that 14-3-3 binding sites within proteins contribute to preventing aberrant aggregation (Segal *et al.*, 2023). This suggests that in addition to inducing nuclear localisation, the 3SA mutations may promote aggregation of HDAC4. Therefore, other methods that increased nuclear localisation of HDAC4 were

compared for their effect on HDAC4 aggregation and neuronal phenotypes to further characterise the role of nuclear HDAC4, and determine if 14-3-3 regulates its nuclear aggregation.

MEF2 facilitates nuclear import of HDAC4 (Wang & Yang, 2001), therefore it was hypothesised that MEF2 overexpression would increase nuclear import in addition to stabilising aggregation of HDAC4. Indeed, MEF2 overexpression resulted in increased nuclear localisation of HDAC4, and nuclear aggregation appeared to increase. Concurrently, the severity of β-lobe fusion in the mushroom body was increased. These data further demonstrate that nuclear HDAC4 is deleterious, and increasing nuclear distribution of HDAC4 increases aggregation independent of the 3SA mutation.

Mutation of the nuclear export signal within DmHDAC4 was also hypothesised to increase nuclear localisation, and indeed the ΔNES mutation increased nuclear accumulation of HDAC4 in Kenyon cells similarly to 3SA, consistent with previous studies with hHDAC4 in cell culture (Wang & Yang, 2001). These data also support the evidence that 14-3-3 binding alone is insufficient for the nuclear export of HDAC4, which requires its NES as well (Wang & Yang, 2001). Interestingly the sub-nuclear distribution of HDAC4$^{\Delta NES}$ was strikingly different to HDAC4^{3SA}. The ΔNES and 3SA mutations induce nuclear localisation of HDAC4 via different mechanisms; while the ΔNES mutations prevent nuclear export by inhibiting CRM-1 association (Wang & Yang, 2001), the 3SA mutations impair 14-3-3 binding, which reveals the NLS to promote nuclear import and also prevent cytoplasmic anchoring (Grozinger & Schreiber, 2000; McKinsey *et al.*, 2001; Wang & Yang, 2001). Therefore, accumulation of HDAC4$^{\Delta NES}$ at the nuclear periphery is likely a result of 14-3-3 binding mediating shuttling to the nucleopore complex, however the lack of the functional NES results in the failure of HDAC4$^{\Delta NES}$ to cross the nuclear membrane via CRM-1 (Wang & Yang, 2001), whereas loss of 14-3-3 binding in HDAC4^{3SA} prevents shuttling to the nuclear periphery.

The aggregation of HDAC4^{3SA} and HDAC4$^{\Delta NES}$ in Kenyon cells also differed significantly; HDAC4^{3SA} was granular across the nucleus and formed a range of sizes of aggregates that sequestered MEF2, while HDAC4$^{\Delta NES}$ accumulated at the nuclear periphery and only appeared to form large MEF2-containing aggregates. The relative level of nuclear HDAC4 in each of these mutants has not been investigated, nor have total protein levels been compared, and it is possible that this difference in nuclear aggregation may arise from differences in dose or degree

of nuclear localisation and therefore propensity to aggregate (Figure 5.30). These data should be replicated to confirm differences in aggregation between these mutants, and relative distribution and expression level compared.

It is possible that the different aggregation characteristics between HDAC4^{3SA} and HDAC4$^{\Delta NES}$ may be a result of altered MEF2 binding. While the 3SA mutation does not abolish MEF2 binding (Grozinger & Schreiber, 2000) Ser239, a key residue for 14-3-3 interaction with HDAC4 (Grozinger & Schreiber, 2000; McKinsey *et al.*, 2000; Wang *et al.*, 2000), is in close proximity to the MEF2 binding site both by distance in the primary sequence (Appendix 10.2.2, Figure 5.33A) and in the AlphaFold prediction of the DmHDAC4 structure. Therefore, loss of 14-3-3 binding could reduce competition for this region, thus increasing the association of HDAC4 with MEF2, leading to stabilisation of aggregation (Figure 5.33B). In comparison, the NES of HDAC4 is at the C-terminus (Figure 5.33A) and is predicted to be further from the MEF2 binding site in the AlphaFold structure, therefore HDAC4$^{\Delta NES}$ is less likely to impact MEF2 binding via competition for the binding site than HDAC4^{3SA} (Figure 5.33C). Hence, it is possible that HDAC4^{3SA} undergoes MEF2-dependent stabilisation of aggregation at an increased rate compared to HDAC4$^{\Delta NES}$, which could account for the change in aggregation characteristics between the two.

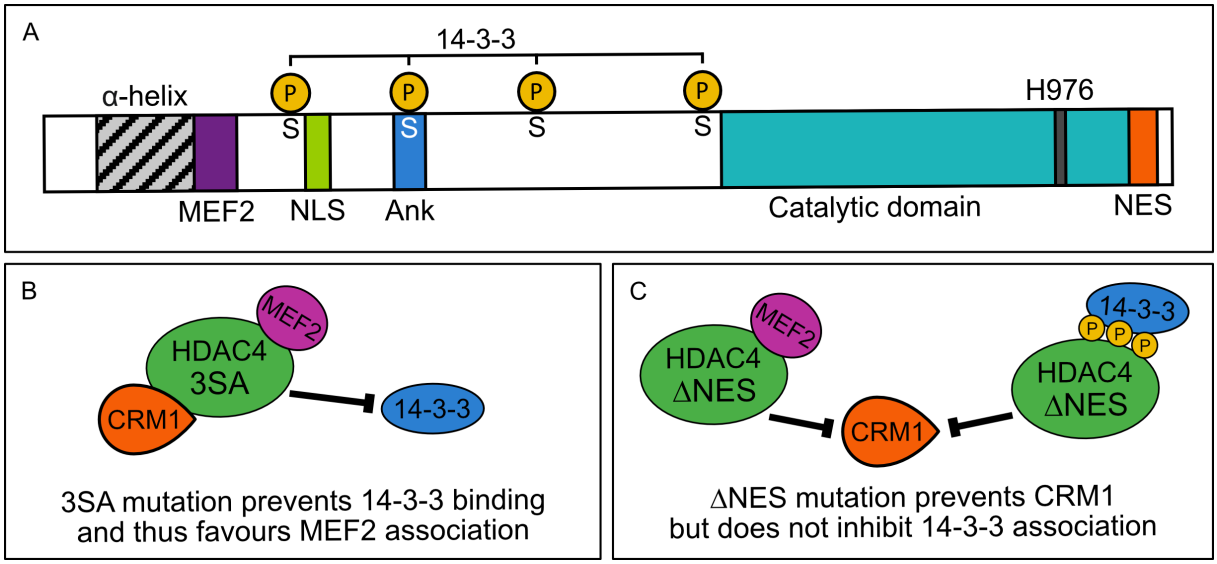

Figure 5.33 Comparison of potential MEF2 binding for 3SA and ΔNES mutants of HDAC4

Schematic diagram depicting a model in which 3SA and NES mutants of HDAC4 differentially affect 14-3-3 and MEF2 association to regulate HDAC4 aggregation. (A) Domain structure of HDAC4, repeated from that in Figure 1.10. The 14-3-3 binding sites are nearer to the MEF2 binding site than the NES, therefore mutations affecting 14-3-3 binding are more likely to affect MEF2 association. (B) 3SA mutation prevents 14-3-3 binding and therefore favours the association of MEF2 (as it was previously

hypothesised that the binding of 14-3-3 to HDAC4 is mutually exclusive to MEF2 association, Figure 5.29), while there is no change in CRM1 binding. (C) ΔNES mutation impairs CRM1 binding but has no impact on either MEF2 or 14-3-3 binding. *This figure is an original artwork.*

Another interaction which may affect HDAC4 aggregation characteristics is that between HDAC4 and 14-3-3. In addition to acting as a molecular chaperone, 14-3-3 proteins have been implicated in protein misfolding and have anti-aggregation activity (Sluchanko & Gusev, 2017). In *Drosophila* cell culture, 14-3-3ζ is upregulated upon heat-stress and dissolves thermal aggregated proteins (Yano *et al.*, 2006). Segal *et al.* (2023) identified the interactome of all 14-3-3 isoforms, and these interactors were enriched in aggregation prone sequences, intrinsic disorder, and had high potential for phase separation. Disruption of 14-3-3 binding resulted in changes in foci formation in 82% of candidate proteins that were altered in subcellular distribution. In most cases, foci were increased upon loss of 14-3-3 binding, and where absolute changes in foci formation were not observed, cellular localisation and dynamics were typically altered. This included a shift to a more nuclear distribution of HDAC4. Moreover, engineering 14-3-3 binding sites into aggregate-prone proteins suppressed their aggregation and increased solubility. It is therefore possible that loss of 14-3-3 binding in HDAC4^{3SA} alters its aggregation dynamics (Figure 5.34).

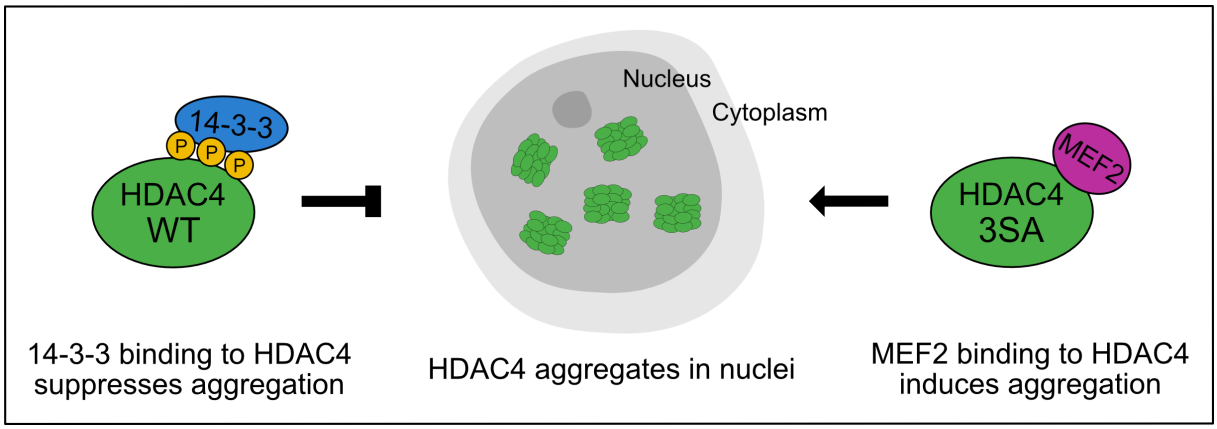

Figure 5.34 Model of the effects of 14-3-3 or MEF2 binding on HDAC4 nuclear aggregation
Schematic diagram illustrating a model in which 14-3-3 binding suppresses nuclear aggregation of HDAC4, while MEF2 binding promotes aggregation. *This figure is an original artwork.*

Together these data demonstrate the importance of considering alternative effects of mutations when trying to elucidate protein function. The 3SA mutations are widely used to induce nuclear localisation of HDAC4 to study the effects of its subcellular distribution on function (Section 1.5.1.3), however it is impossible to dissociate the effects of increased nuclear localisation from

the loss of 14-3-3 binding by examination of the 3SA mutant alone. Many of the studies involving the 3SA mutation also suggest a correlation between nuclear-aggregated HDAC4 and errors in cell function, but loss of 14-3-3 binding may be artificially increasing aggregation, and therefore not representative of increased nuclear HDAC4 in all neuronal disease. It is important to note however that mutation of the 14-3-3 binding site within HDAC4 has been associated with 2q37 deletion syndrome (Wakeling *et al.*, 2021) and therefore exploration of the 3SA mutation will have direct applicability in this context. It is evident that multiple mechanisms may be at play to increase nuclear and aggregated HDAC4 in a disease context. Further studies that examine how HDAC4 aggregates form in a disease context will be essential to understand the mechanism of toxicity, as well as for discovery of effective therapeutic targets.

In summary, the data presented in this chapter highlights the complex nature of effects that result in nuclear aggregation of HDAC4, including dose, oligomerisation and association of binding partners, and how each of these contribute to overexpression-induced neurotoxicity of HDAC4 in *Drosophila.* Specifically, increasing the dose or nuclear abundance of HDAC4 increases both aggregation and neurotoxicity in the mushroom body and eye. These findings are significant when considering the role of HDAC4 in neuronal disease, as both increased expression and nuclear abundance of HDAC4 have been observed. Further investigation of HDAC4 distribution and aggregation in a disease context is therefore warranted to determine whether it may constitute a novel drug target, or biomarker for diagnostic developments. Moreover, this chapter shows that MEF2 facilitates nuclear accumulation and aggregation of HDAC4, therefore disrupting this interaction may be one such drug target to reduce toxicity associated with HDAC4 aggregation. Finally, these data continue to support the hypothesis that aberrant sequestration of HDAC4 binding partners, either canonical or novel, contributes to aggregate-mediated neurotoxicity (Figure 4.29). While sequestration of MEF2 has been characterised and is required for manifestation of phenotypes in the adult mushroom body (Main *et al.*, 2021; Tan *et al.*, 2024), it remains unclear whether there are other proteins present that contribute to neuronal phenotypes. It is therefore essential that the composition of HDAC4 aggregates is investigated to further understand potential mechanisms of toxicity.

Chapter Six

Identifying the composition of HDAC4 aggregates

6. Characterisation of the composition of HDAC4 positive aggregates resulting from overexpression of nuclear restricted HDAC4

The data described in the previous chapters demonstrate that HDAC4 forms multimers *in vivo*, and this oligomerisation is required for aggregation in neuronal nuclei. Mutations that altered oligomerisation and thus aggregation of HDAC4 modified overexpression-induced neurodevelopmental phenotypes, suggesting that these aggregates at least in part mediate neurotoxicity. It is hypothesised that the aggregates prevent the wild-type function of HDAC4, as well as sequester other factors to promote neurotoxicity (Figure 4.29, reproduced below). Indeed it was shown in Section 4.4 that the transcription factor MEF2 co-localises with HDAC4 aggregates in Kenyon cell nuclei, as well as in other studies (Borghi *et al.*, 2001; Chan *et al.*, 2003; Fitzsimons *et al.*, 2013; Main *et al.*, 2021; Miska *et al.*, 1999), and mutations that reduce MEF2 binding to HDAC4 reduced the severity of neuronal phenotypes in *Drosophila* (Tan *et al.*, 2024), while conversely, overexpression of MEF2 stabilises aggregation and exacerbates phenotypes (Section 5.4). Human HDAC4 has a wide interactome (Figure 1.10) but it is unclear whether these interactions are conserved in *Drosophila,* and whether these partners are present in nuclear aggregates and contribute toward neurodevelopmental phenotypes. It is therefore of interest to characterise the composition of nuclear HDAC4 aggregates in *Drosophila* to identify potential mechanisms of neurotoxicity.

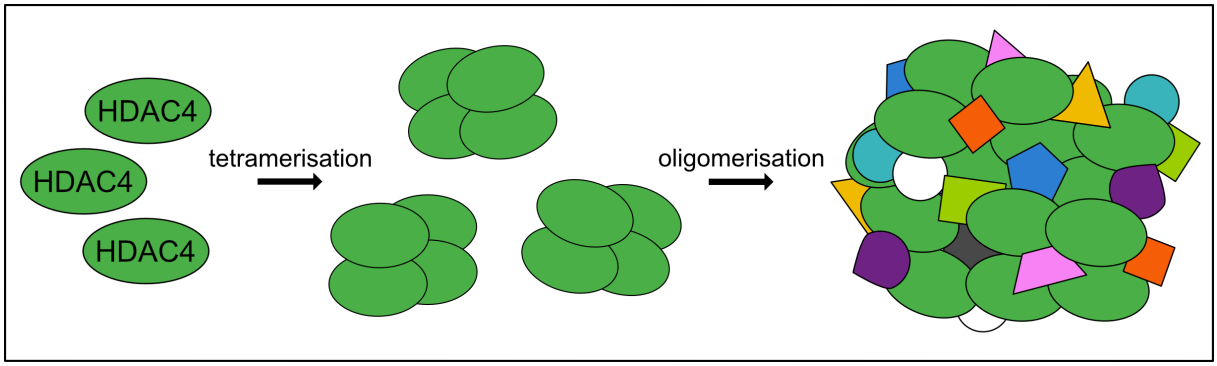

Figure 4.29 HDAC4 aggregates may aberrantly sequester proteins to induce defects in neuronal development and function
Schematic diagram of a model depicting that tetramerisation of HDAC4 results in higher order oligomerisation into aggregates, which sequester additional proteins. Please note this Figure is reproduced from that in Chapter 4 for ease of reference, and therefore has the same figure number. *This figure is an original artwork.*

6.1. Identification of interactors of nuclear-restricted HDAC4 in the *Drosophila* brain

6.1.1. Overview of experimental approach

To identify nuclear binding partners of HDAC4, an immunoprecipitation-coupled mass spectrometry (IP-MS) approach was taken (Figure 6.1). To enrich for nuclear aggregates of HDAC4, immunoprecipitation was performed on heads of flies expressing the nuclear-restricted HDAC4^{3SA} mutant. To complement the functional analyses performed in the mushroom body in this study as well as that by Tan *et al.* (2024), *elav-GAL4* was selected as the driver to mediate pan-neuronal expression of HDAC4^{3SA}. Whole-cell lysates were generated from heads of flies, and HDAC4^{3SA} immunoprecipitated via the Myc tag as per Section 3.2.4. The immunoprecipitate was then electrophoresed in preparation for in-gel digestion (Section 3.2.5). Peptides were separated by reversed phase high-performance liquid chromatography (HPLC) prior to mass spectrometry analysis as described in Sections 3.2.8-3.2.11.

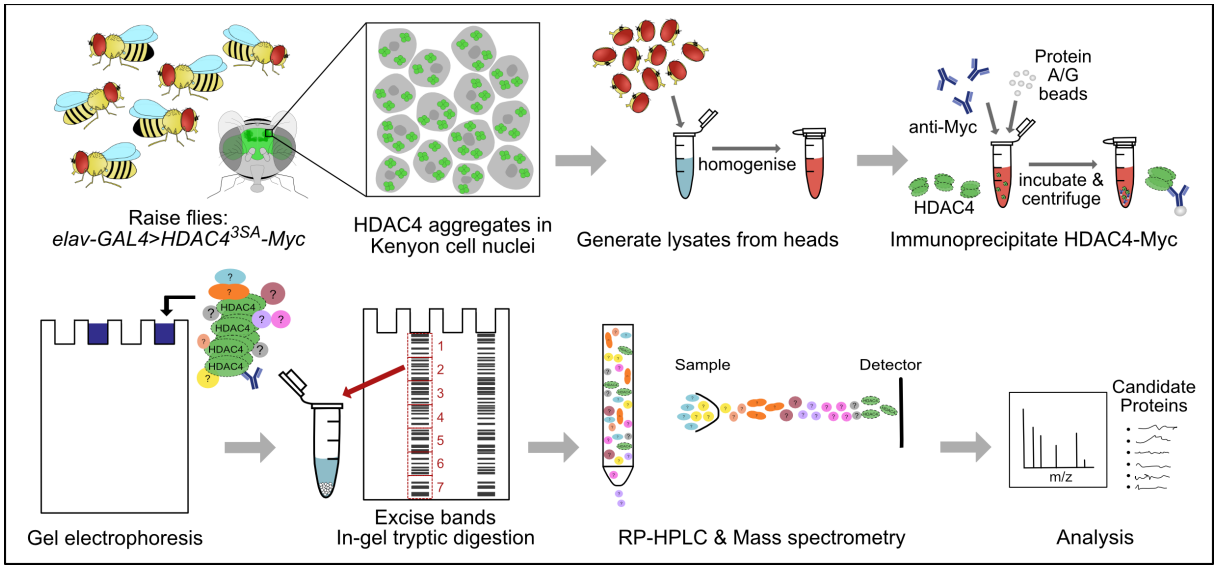

Figure 6.1 Schematic representation of immunoprecipitation-coupled mass spectrometry workflow to identify HDAC4 aggregate binding partners
Flow diagram of the methodology for characterising the composition of nuclear HDAC4 aggregates as described above. RP-HPLC, reversed phase high-performance liquid chromatography. *This figure is an original artwork.*

6.1.2. Optimisation of immunoprecipitation

It was essential that the immunoprecipitation protocol would be sensitive enough to recover intact HDAC4 aggregates to enable detection of co-aggregating proteins. The assumption was made that if oligomers of HDAC4 were recovered, then aggregates would too be isolated, therefore optimisation of the immunoprecipitation protocol was performed to ensure maximal capture of HDAC4 oligomers. Co-immunoprecipitation of GFP- and Myc-tagged HDAC4 was previously described, and successfully used to monitor changes in oligomerisation of HDAC4 (Sections 4.3.3 and 5.2.3). This approach was used here to optimise immunoprecipitation; briefly, whole cell lysates were generated from heads of flies co-expressing wild-type GFP- and Myc-tagged *HDAC4* under the control of *elav-GAL4*. GFP- and Myc-tagged HDAC4^{WT} tetramerise and aggregate *in vivo* given identical sequence similarity (with the exception of the epitope tags). Myc-tagged HDAC4^{WT} was immunoprecipitated and following western blotting, the membrane was probed for GFP-tagged HDAC4^{WT}, and optimisations were made to maximise yield of GFP-HDAC4^{WT}. This included evaluating different brands of protein A/G agarose beads alongside variation of lysis buffers, incubation, wash and elution conditions, and antibody and lysate concentrations. The result of the optimised protocol (protocol 1, Section 3.2.4) is shown in Figure 6.2.

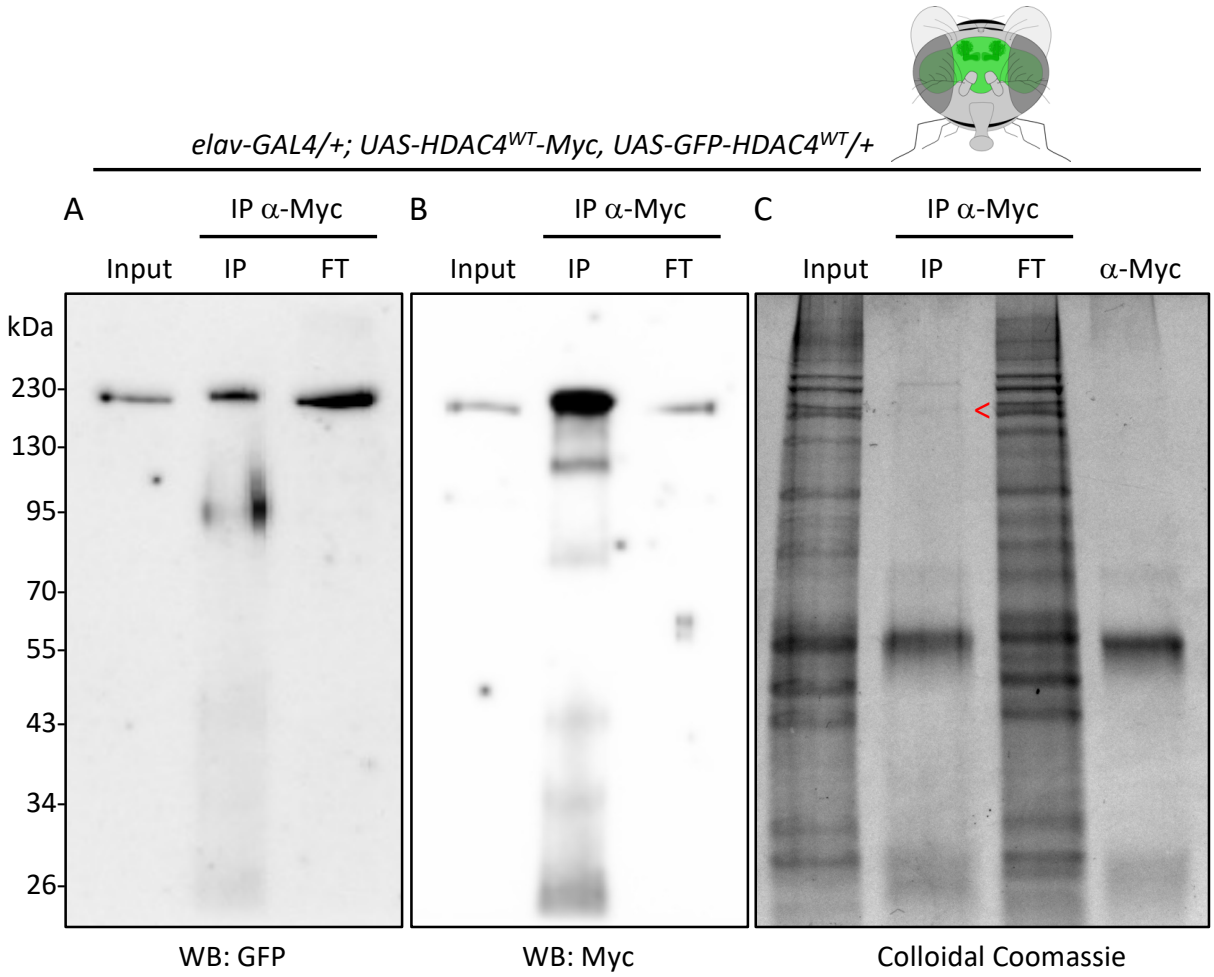

Figure 6.2 Optimised co-immunoprecipitation of GFP-HDAC4^{WT} with HDAC4^{WT}-Myc (Protocol 1)

(A-C) Anti-Myc immunoprecipitation on whole cell lysates made from heads of flies expressing GFP-HDAC4^{WT} and HDAC4^{WT}-Myc under the control of *elav-GAL4*. Input is a sample of the lysate prior to immunoprecipitation (30 µg total protein). Immunoprecipitation (IP) is the eluate from the immunoprecipitation. Flowthrough (FT) is a sample of the lysate immediately after incubation with the antibody-bead complex (non-captured proteins, ~30 µg). (A) Western blot (anti-GFP) detection of GFP-HDAC4^{WT} confirmed co-immunoprecipitation with HDAC4^{WT}-Myc. (B) Western blot (anti-Myc) detection of HDAC4^{WT}-Myc confirmed successful immunoprecipitation. (C) Colloidal Coomassie stained gel showed a significant reduction in the number of bands in the eluate compared to input sample. Red arrow indicates the band at ~144 kDa which is hypothesised to be HDAC4^{WT}-Myc. The anti-Myc antibody was also electrophoresed (1 µg) to compare non-specific bands resulting from antibody leaching from the protein A/G beads. Immunoprecipitation was performed as per protocol 1, Section 3.2.4.

GFP-HDAC4^{WT} was successfully co-immunoprecipitated upon immunoprecipitation of HDAC4^{WT}-Myc (Figure 6.2A), indicating that oligomers were preserved during immunoprecipitation. The flowthrough obtained after incubation of the lysate with antibody-conjugated beads was also electrophoresed, containing non-captured proteins, and presence of HDAC4^{WT}-Myc suggested that the lysate was in excess and maximal saturation of antibody

with protein was achieved (Figure 6.2B). Comparing the relative intensity of the input sample to the IP showed that the proportion of HDAC4^{WT}-Myc obtained was significantly higher than GFP-HDAC4^{WT}; assuming that GFP- and Myc-tagged species of HDAC4^{WT} have equal affinity to oligomerise with each other as they do their own species, this suggests that not all oligomers were being preserved throughout the immunoprecipitation protocol.

Colloidal Coomassie staining was performed to visualise HDAC4 and co-precipitating proteins (Figure 6.2C). The anti-Myc antibody was also denatured and electrophoresed to confirm the identity of bands thought to result from antibody leaching from the A/G beads during elution. A faint band migrating at ~144 kDa was observed in the immunoprecipitate, which was hypothesised to be HDAC4^{WT}-Myc. Significant bands were observed at ~50 and ~25 kDa in both the immunoprecipitate and antibody lanes, and are therefore likely immunoglobulin heavy and light chains, respectively. An additional band was present at ~75 kDa in both immunoprecipitate and antibody lanes which likely represents partially denatured antibody (1x heavy and 1x light chain). Additional bands were observed in the immunoprecipitate not accounted for by the antibody; these may represent proteins that co-precipitated with HDAC4. To confirm the identity of these it was therefore essential to include a negative control sample from which immunoprecipitation has been performed in the absence of HDAC4^{WT}-Myc to identify any non-specific co-precipitating proteins.

Given that HDAC4^{WT}-Myc was successfully immunoprecipitated, and oligomers of GFP- and Myc-tagged HDAC4^{WT} could be isolated, the protocol for immunoprecipitation was deemed acceptable for IP-MS application. It is noted that both GFP- and Myc- tagged species of HDAC4 were co-expressed here, but this was only to confirm the presence of HDAC4 oligomers in the immunoprecipitate, and therefore for the IP-MS subsequently performed, only HDAC4-Myc was expressed.

6.1.3. Interactors detected via IP-MS from whole head lysates of flies expressing HDAC4^{3SA} under the control of *elav-GAL4*

IP-MS was performed on whole cell lysates generated from heads of control flies (*elav-GAL4/+; +*) and heads of flies expressing nuclear-restricted HDAC4 pan-neuronally (*elav-GAL4/+; HDAC4^{3SA}-Myc/+*). Flies were raised at 18 °C to maximise progeny counts; as GAL4 activity is temperature dependent (Duffy, 2002), flies were raised at a low temperature to

prevent HDAC4^{3SA} overexpression-induced lethality during development. Adult flies were then transferred to 30 °C for three days to increase the level of HDAC4^{3SA} expression before harvesting. Heads were collected, lysates generated, and HDAC4^{3SA} immunoprecipitated (Section 3.2.4, Protocol 1) and electrophoresed. Following colloidal Coomassie staining, each lane was divided into seven gel pieces that were trypsin-digested and prepared for mass spectrometry as described in Sections 3.2.9-3.2.11. Peptides were mapped to the *Drosophila melanogaster* database and accessions converted to FBgn identifiers (FlyBase IDs) that correspond to gene names; 28 candidate interactors of HDAC4^{3SA} were identified (Appendix 10.4.1, Table 10.3). Interestingly, few candidates that were previously shown to interact with hHDAC4, such as those presented in Figure 1.10, were detected, consisting only of 14-3-3ε, α-tubulin, and heat shock 70 proteins (Paroni *et al.*, 2008), and there was no detection of MEF2 despite co-localisation in nuclear aggregates.

The Database for Annotation, Visualization, and Integrated Discovery (DAVID) was used to begin functional analyses. DAVID is commonly used for functional annotation of large biological datasets (Dennis *et al.*, 2003; Huang *et al.*, 2009). DAVID 2021 makes use of publicly available databases including UniProt (The UniProt Consortium 2023) and Entrez (Maglott *et al.*, 2005) and compiles and consolidates genes and their linked annotations from these databases into its Knowledgebase (Sherman *et al.*, 2022). Several analytical tools are connected to this Knowledgebase, which allows for comprehensive functional annotation and enrichment analyses. It is noted that in the literature surrounding this tool, inputs and outputs are referred to as genes, whereas here candidate HDAC4 interactors were detected at the protein level. As the input list was submitted via FlyBase IDs (FBgn), this will be referred to as the gene list as annotations are associated at the gene level. When discussing the input into DAVID analyses the HDAC4 candidates will therefore be identified by their gene name, but as these are in the context of a protein-protein interaction the names are not italicised.

To begin to understand the roles of proteins that potentially interact with HDAC4^{3SA}, FBgns of 27/28 candidates as well as HDAC4 were submitted for DAVID Functional Annotation Clustering under the default settings. One candidate was not included, Histone H2B, as it was originally mapped to a protein databank ID that corresponds to the entire Histone H2B gene family, containing 23 individual genes. All 23 genes were mapped to a single FBgn identifier, therefore import via this ID resulted in a list of 50 genes for DAVID analysis, artificially

enriching for histone components. As it is unclear what specific gene/isoform of histone H2B the IP-MS identified, it was not included for DAVID analysis.

The Functional Annotation Clustering tool outputs groupings of annotations that may indicate an enrichment in the gene set for such processes. To do this, all annotations associated with genes from the input list are collated and grouped based on shared gene members. Clusters are further grouped based on similar and redundant annotations, then each cluster is then given an enrichment score, calculated from the annotation p-values, to rank clusters against each other. A high enrichment score typically represents a cluster that has consistently low p-values for its annotation terms, suggesting high biological significance (Huang *et al.*, 2009). Clusters derived from the input gene list that have at least one term with an FDR≤0.05 are summarised in Table 6.1.

Table 6.1 DAVID functional annotation clustering of candidate HDAC4^{3SA} interactors from initial mass spectrometry analysis

Cluster #	Enrichment score	Category	Term	Count	% of input	p-value	Fold change	FDR
1	2.9	UP_KW_DOMAIN	Transit peptide	6	21.4	3.5E-6	20	2.8E-5
		KEGG_PATHWAY	Citrate cycle (TCA cycle)	3	10.7	2.2E-2	12	0.25
		KEGG_PATHWAY	Carbon metabolism	4	14.3	2.5E-2	5.8	0.25
2	2.61	GOTERM_CC_DIRECT	Cytoplasm	15	53.6	2.1E-4	2.7	5.2E-3
		UP_KW_LIGAND	Nucleotide-binding	10	35.7	7.4E-3	2.4	7.4E-2
		UP_KW_CELLULAR_COMPONENT	Cytoplasm	8	28.6	9.5E-3	2.7	3.2E-2
3	2.42	UP_KW_DOMAIN	Transit peptide	6	21.4	3.5E-6	20	2.8E-5
		UP_KW_CELLULAR_COMPONENT	Mitochondrion	7	25.0	2.4E-4	6.7	1.6E-3
		UP_SEQ_FEATURE	TRANSIT:Mitochondrion	4	14.3	3.6E-3	12	0.24
		UP_KW_LIGAND	Flavoprotein	3	10.7	5.0E-2	7.7	0.17
		UP_KW_LIGAND	FAD	3	10.7	7.4E2	6.2	0.19
		UP_KW_MOLECULAR_FUNCTION	Oxidoreductase	4	14.3	0.26	2.1	0.97
4	2.38	UP_KW_CELLULAR_COMPONENT	Mitochondrion	7	25.0	2.4E-4	6.7	1.6E-3
		UP_KW_CELLULAR_COMPONENT	Mitochondrion inner membrane	5	17.9	3.3E-4	13	1.6E-3
		UP_KW_CELLULAR_COMPONENT	Membrane	7	25.0	0.96	0.74	1

Candidate interactors were entered into the DAVID database and functional annotation clustering performed using the default settings. Clusters that contain at least one annotation with an FDR≤0.05 are displayed. All annotations within a cluster are shown. Category is the annotation source; GOTERM was derived from the Gene Ontology resource database: CC, cellular component. KEGG_PATHWAY, Kyoto Encyclopedia of Genes and Genomes pathway database. UP_KW, UniProt keywords database. Count is the number of genes annotated to a term and % of input displays this as the proportion of the 28 input genes. p-values were derived from a modified Fisher's exact test comparing the count of genes enriched here to a database of all genes mapping to this term. Fold enrichment represents the enrichment above the background population (*Drosophila melanogaster*). FDR is the adjusted p-value.

Surprisingly, functional annotation clustering revealed enrichment for cytoplasmic and mitochondrial activities, and further examination of the Gene Ontology term (GOterm) cellular component annotations revealed significant enrichment for cytoplasmic (54%) and mitochondrial (46%) localisation ($p<0.01$). This was unexpected given that HDAC4^{3SA} localises consistently to nuclei within the brain (Tan *et al.* (2024), Chapter 5). Further investigation was sought via GOterm molecular function and biological process annotations, however in both analyses the FDR for each annotation exceeded 0.05, suggesting there was no notable enrichment within the input proteins for any of the molecular function annotations.

To investigate the biological relationship between candidate interactors, these were submitted to the Search Tool for the Retrieval of Interacting Genes/Proteins (STRING), a biological database of known and predicted protein-protein interactions that is used to generate protein interaction networks (Szklarczyk *et al.*, 2023). The 27 candidate proteins that mapped to a single gene, as well as HDAC4, were entered for analysis as FBgn identifiers, resulting in a network with 28 nodes (candidates) and 66 edges (interactions). The expected number of edges for this dataset was 14, with a protein-protein interaction enrichment p-value of <1.0e-16; the network had significantly more interactions than expected, suggesting that the proteins are at least partially biologically connected as a group. The full STRING network is presented in Appendix Section 10.4.1, Figure 10.28. Unexpectedly, no candidates were demonstrated to interact with HDAC4. This network also did not link 14-3-3ε to HDAC4, nor α-tubulin, which are known HDAC4 interactors (Grozinger & Schreiber, 2000; Miska *et al.*, 2001; Paroni *et al.*, 2008). This was not due to a lack of *Drosophila* HDAC4 interactors within the STRING database as when HDAC4 was submitted alone, an abundance of interactors were displayed, including MEF2 and the *Drosophila* orthologues of the HDAC3/SMRT complex, interactions also observed with human HDAC4 (Figure 1.10). Of interest however, alternative splicing was enriched as an annotated keyword associated with eight candidate interactors. Moreover, the reference publication (from PubMed) that associated with the most candidates examined how proteasome dysfunction contributes to defects in protein homeostasis (Tsakiri *et al.*, 2019).

It was expected that HDAC4 would precipitate MEF2, therefore there was concern around the accuracy, significance, and reliability of this dataset. HDAC4^{3SA} was detected at a relatively low abundance, with only eight peptide spectrum matches. It was therefore determined that the immunoprecipitation protocol required further optimisation to increase HDAC4 yield. Indeed, further investigation determined that the agarose beads used in this protocol were unreliable,

and efficacy of immunoprecipitation was batch dependent. It was therefore evident that a new approach was necessary to identify the composition of HDAC4 aggregates.

An initial investigation was made into the co-distribution of two candidate interactors of HDAC4^{3SA} (Appendix 10.4.2). Antibodies against NinaC and Armadillo were obtained and immunohistochemistry performed to examine co-localisation with HDAC4^{3SA}. It is noted that Armadillo is not present within the list of candidate interactors (Appendix Table 10.3); Armadillo was identified as a candidate through IP-MS data not presented here, that was later deemed unreliable, again due to the agarose beads used. Neither NinaC nor Armadillo co-localised with HDAC4^{3SA} nuclear aggregates. These data support the concern around the accuracy of this dataset in identifying components of HDAC4 aggregates and necessitate an alternative approach.

6.2. Determining an approach to enrich for nuclear interactors of HDAC4

Following initial IP-MS analyses it was evident that several factors were contributing to poor isolation of HDAC4 and co-precipitating proteins. Firstly, it was expected that proteins that co-precipitated with HDAC4^{3SA} would be proteins sequestered in nuclear aggregates, however, enrichment of cytoplasmic and mitochondrial proteins was instead observed. While it is possible that cytoplasmic proteins are being sequestered in nuclear aggregates, it is also possible that this represents an artificial interaction that occurred during immunoprecipitation that is not observed *in vivo*.

Secondly, it was expected that MEF2 would co-precipitate with HDAC4^{3SA} since it co-localises with nuclear aggregates of HDAC4 in Kenyon cells, however MEF2 was not detected. *elav-GAL4* was initially selected to drive expression of *HDAC4^{3SA}* to determine interactors that may be responsible for the mushroom body phenotype, as analyses were performed using this driver (Chapters 4-5, Tan *et al.* (2024)). However, endogenous MEF2 expression is primarily detected in Kenyon cells of the adult brain (Crittenden *et al.* (2018), Figure 4.10A), which only make up ~2% of total neuronal cells in the head, and in comparison, *elav-GAL4* has a much wider distribution in the adult brain (Section 4.1). Therefore, when expressed under the control of

elav-GAL4, HDAC4^{3SA} would be expressed in more cells than MEF2, and any HDAC4^{3SA} immunoprecipitated from non-Kenyon cells would not co-precipitate MEF2.

Thirdly, given that HDAC4^{3SA} was only detected at low levels following MS, as indicated by a low number of peptide spectrum matches, co-precipitating proteins would be even more difficult to detect. This suggests that the immunoprecipitation protocol is not yet sensitive enough and needs further optimisation to increase both the yield of HDAC4 and co-precipitating proteins.

To address these concerns, further IP-MS analysis was performed on HDAC4^{3SA} immunoprecipitated from nuclear lysates instead of whole-cell lysates (Section 6.3); validation and optimisation of the subcellular fractionation protocol used to achieve this is described in Appendix 10.4.3.2. The immunoprecipitation protocol was further optimised to increase the yield and sensitivity for detecting HDAC4 oligomers, and this is detailed in Appendix 10.4.3.1.

Given the concern that expression of HDAC4^{3SA} under the control of *elav-GAL4* resulted in an expression pattern that was more widespread than that of MEF2, the aggregation of HDAC4^{WT} when expressed under the control of *OK107-GAL4,* which drives higher expression in Kenyon cells where MEF2 is abundant (Section 4.1), was further examined to determine whether this may be more appropriate for IP-MS studies. To enrich for nuclear aggregates, as aggregation of HDAC4 is dose-dependent (Section 5.6.1), aggregation was investigated in the absence of the TARGET system, and the dose of HDAC4^{WT} was increased by expression from two genomic insertions of the HDAC4^{WT} transgene (Appendix 10.4.4.1). Aggregates resulting from expression of HDAC4^{WT} from one genomic insertion were considerably larger in the absence of the TARGET system, demonstrating that prolonged expression of HDAC4^{WT} influences aggregate size. Increasing the dose of HDAC4^{WT} expression significantly altered HDAC4^{WT} aggregation where the number of aggregates per cell decreased while their size increased. These inclusions maintained co-localisation with MEF2, and had morphology that was reminiscent of aggresomes, which represent overwhelm of the protein homeostasis systems (Johnston *et al.*, 1998).

As these aggregates were not likely to be representative of physiological nuclear accumulation and aggregation of HDAC4 in a disease context, a series of experiments were also carried out to compare the total level of expression and subcellular distribution of HDAC4^{3SA} when driven

by *OK107-GAL4* and *elav-GAL4* (Appendix 10.4.4.2-10.4.4.3). The distribution of HDAC4^{3SA} in the adult brain when expressed under the control of *elav-GAL4* and *OK107-GAL4* was also examined, with particular respect to co-localisation with endogenous MEF2, and aggregate formation in Kenyon cells and other neurons (Appendix 10.4.4.4-10.4.4.5). For brevity and flow of this chapter, these experiments are described in detail in the Appendix.

The findings of these analyses were that while *OK107-GAL4* drives expression in a smaller proportion of neurons compared to *elav-GAL4*, the overall level of HDAC4^{3SA} expression was much higher under the control of *OK107-GAL4*. This is attributed to increased expression in Kenyon cells (Section 4.1), which also results in increased aggregate size likely due to coalescence (Section 5.6.2). Endogenous MEF2 was most abundant in Kenyon cells as expected, but it was also expressed at a much lower level in many other neuronal types. Interestingly, in many neuronal cell types HDAC4^{3SA} still formed aggregates, but these did not always sequester MEF2, indicating that in order to enrich for the MEF2-HDAC4 interaction in aggregates, a high level of expression of HDAC4^{3SA} is desirable in Kenyon cells, but not in other cell types. Furthermore, a pool of cytoplasmic HDAC4^{3SA} was observed, especially in the lobes of the mushroom body, suggesting it is not entirely restricted to nuclei; this may account for the detection of cytoplasmic interactors in the initial analysis. The TARGET system was also included to avoid developmental effects of expression of HDAC4^{3SA}, and this was shown to not compromise the overall level of induced expression in mature Kenyon cells. Finally, when expressed under the control of *OK107-GAL4* in the presence of the TARGET system, HDAC4^{3SA} aggregates were punctate and localised within the nuclear envelope, and large aggregates or aggresome-like inclusions were not observed. Based on these data, *OK107-GAL4* +TARGET was used to drive expression of *HDAC4^{3SA}* for IP-MS from nuclear lysates.

6.3. Identification of interactors of nuclear-restricted HDAC4 in Kenyon cells

6.3.1. IP-MS on nuclear lysates expressing HDAC4^{3SA} in Kenyon cells

IP-MS was performed on nuclear lysates generated from heads of control flies (*tubulin-GAL80ts/+; OK107-GAL4/+*) and flies expressing nuclear-restricted HDAC4 within Kenyon cells (*tubulin-GAL80ts/+; HDAC4^{3SA}-Myc/+; OK107-GAL4/+*). Flies were raised at 18 °C to

prevent transgene expression and maximise progeny counts. Following eclosion, adult flies were transferred to 30 °C for three days to induce HDAC4^{3SA} expression before harvesting. Heads were collected, nuclear lysates generated and HDAC4^{3SA} immunoprecipitated (Section 3.2.4, Protocol 2) and electrophoresed. Following colloidal Coomassie staining, each lane was divided into seven gel pieces that were trypsin-digested and prepared for MS as described in Sections 3.2.9-3.2.11. Peptides were mapped to the *Drosophila melanogaster* database and accessions converted to FBgn identifiers and further filtered; 344 candidate interactors of HDAC4^{3SA} were identified (Appendix Section 10.4.5, Table 10.4), an order of magnitude higher than previously. Comparison of protein hits to the initial round of IP-MS revealed five proteins (including HDAC4) that were shared between the two (Figure 6.3). Comparison of candidate interactors of HDAC4^{3SA} with those known to interact with hHDAC4 in the literature revealed enrichment of several proteins including CtBP (Zhang *et al.*, 2001) and subunits of PP2A (Paroni *et al.*, 2008), however MEF2 was not detected. Heat shock proteins were again detected; while there may be concern that this interaction could be induced due to raising flies at 30 °C, the presence of these in analyses by Paroni *et al.* (2008) suggests this is a specific interaction with HDAC4. Moreover, the heat shock proteins detected here were largely heat shock cognates, which are constitutively expressed (Miller & Fort, 2018).

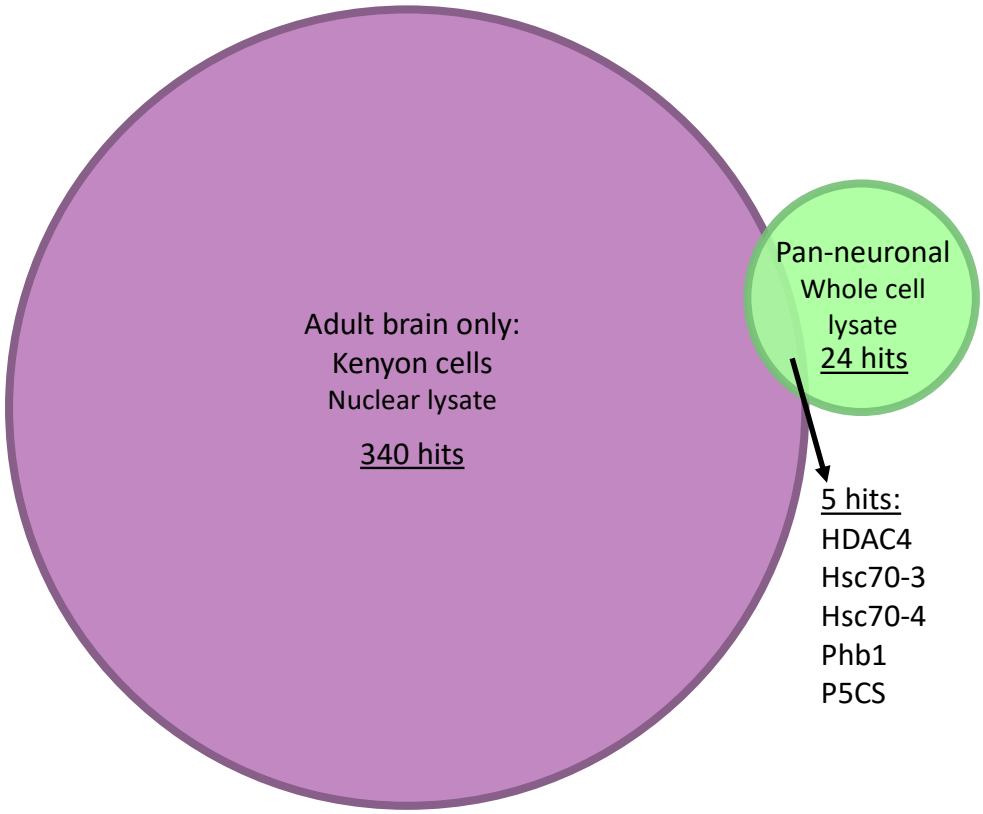

Figure 6.3 Six proteins were common between IP-MS studies

Area proportional Venn diagram illustrating the overlap between IP-MS performed on nuclear lysates of flies expressing HDAC4^{3SA} in Kenyon cells (*OK107-GAL4* +TARGET, purple) or from whole cell lysates expressing HDAC4^{3SA} pan-neuronally (*elav-GAL4*, green). Six hits were common between the two: HDAC4, histone deacetylase four; Hsc70-3, heat shock protein 70 cognate 3; Hsc70-4, heat shock protein 70 cognate 4; phb1, prohibitin 1; P5CS, Δ^1-pyrroline-5-carboxylate synthase. Diagram was made using BioVenn (Hulsen *et al.*, 2008), and further manually annotated.

All 344 candidate proteins plus HDAC4 were entered into the STRING database for network analysis, resulting in a network with 345 nodes and 1237 edges. The expected number of edges for this dataset was 787, with a protein-protein interaction enrichment p-value of <1.0e-16; the network had significantly more interactions than expected, suggesting the proteins are at least partially biologically connected as a group.

Candidate interactors and HDAC4 were then submitted to DAVID for functional annotation clustering. Clusters with at least one term with an FDR≤0.05 are summarised in Table 6.2. Given redundancy of terms within a cluster only those with an FDR≤0.05 are shown. Cluster one annotations related to splicing, suggesting HDAC4^{3SA} aggregates may represent traditional splicing speckles. Cluster two comprised annotations relating to protein folding and refolding, suggesting HDAC4^{3SA} aggregates are affecting neuronal protein homeostasis. Cluster three contained ATPase activity and ATP binding annotations; these annotations encompass a broad range of proteins. Examination of candidate proteins associated with these demonstrated enrichment of chaperones, heat-shock proteins, kinases, and helicases, again implicating HDAC4^{3SA} aggregates in protein homeostasis. Cluster four showed enrichment of proteins containing the WD repeat, which is recognised as a domain that facilitates protein-protein interactions, enabling WD repeat-containing proteins to act as scaffolds for complex formation (reviewed by Xu and Min (2011)). Cluster five contained annotations for vacuolar acidification, all five proteins of which were vacuolar ATPases that are important for neurotransmission (reviewed in Song *et al.* (2020)). Oxidative phosphorylation was also in cluster five, for which candidates were predominantly components of the mitochondrial electron transport chain; mitochondrial dysfunction has been linked to a number of neurodegenerative diseases (reviewed in Johri and Beal (2012)) therefore HDAC4^{3SA} aggregates may be affecting mitochondrial function.

Table 6.2 DAVID functional annotation clustering of candidate HDAC4^{3SA} interactors

Cluster	Enrichment score	Category	Term	Count	% of input	P-value	Fold change	FDR
1	4.52	GOTERM_CC_DIRECT	precatalytic spliceosome	24	7.0	9.9E-12	6	3.7E-09
		GOTERM_CC_DIRECT	catalytic step 2 spliceosome	20	5.8	2.0E-09	5.6	3.8E-07
		GOTERM_MF_DIRECT	RNA binding	40	11.6	3.4E-08	2.7	1.4E-05
		GOTERM_BP_DIRECT	mRNA splicing, via spliceosome	25	7.2	3.8E-08	3.8	4.4E-05
		KEGG_PATHWAY	Spliceosome	19	5.5	3.1E-05	3.1	2.6E-03
		UP_KW_MOLECULAR_FUNCTION	RNA-binding	21	6.1	7.2E-05	2.7	4.1E-03
		GOTERM_MF_DIRECT	nucleic acid binding	25	7.2	2.5E-04	2.3	2.1E-02
2	4.13	GOTERM_MF_DIRECT	unfolded protein binding	15	4.3	9.6E-08	6.2	1.9E-05
		GOTERM_BP_DIRECT	protein folding	14	4.1	2.2E-06	5.3	1.2E-03
		GOTERM_CC_DIRECT	chaperonin-containing T-complex	5	1.4	3.9E-05	22	2.4E-03
		INTERPRO	Chaperonin TCP-1, conserved site	5	1.4	5.0E-05	21	1.8E-02
		INTERPRO	Chaperone tailless complex polypeptide 1 (TCP-1)	5	1.4	5.0E-05	21	1.8E-02
		GOTERM_MF_DIRECT	ATPase activity	20	5.8	2.7E-04	2.6	2.1E-02
		INTERPRO	TCP-1-like chaperonin intermediate domain	5	1.4	3.2E-04	14	4.6E-02
		INTERPRO	GroEL-like equatorial domain	5	1.4	3.2E-04	14	4.6E-02
		INTERPRO	GroEL-like apical domain	5	1.4	4.5E-04	13	4.6E-02
		INTERPRO	Chaperonin Cpn60/TCP-1	5	1.4	4.5E-04	13	4.6E-02
3	2.98	GOTERM_MF_DIRECT	ATPase activity	20	5.8	2.7E-04	2.6	2.1E-02
		GOTERM_MF_DIRECT	ATP binding	41	11.9	4.0E-04	1.8	2.7E-02
4	2.2	INTERPRO	WD40/YVTN repeat-like-containing domain	19	5.5	9.5E-05	2.9	2.2E-02
		UP_KW_DOMAIN	WD repeat	8	2.3	7.2E-03	3.5	4.6E-02
5	1.94	GOTERM_BP_DIRECT	vacuolar acidification	5	1.4	2.6E-04	15	4.2E-02
		KEGG_PATHWAY	Oxidative phosphorylation	16	4.6	1.6E-03	2.5	4.4E-02

Category is the annotation source; GOTERM was derived from the Gene Ontology resource database: CC, cellular component; BP, biological process; MF, molecular function. KEGG_PATHWAY, Kyoto Encyclopedia of Genes and Genomes pathway database. UP_KW, UniProt keywords database. INTERPRO, InterPro database. Terms are only displayed if they have an FDR≤0.05. Count is the number of genes annotated to a term and % of input displays this as the proportion of the 345 input genes. p-values were derived from a modified Fisher's exact test comparing the count of genes enriched here to a database of all genes mapping to this term. Fold enrichment represents the enrichment above the background population (*Drosophila melanogaster*). FDR is the adjusted p-value.

Cellular component annotation from Gene Ontology (GO, GOTERM) clustering revealed that an equal proportion of proteins were associated with the cytoplasm and nucleus (28.7%, Table 6.3). The proportion of hits annotated as nuclear was significantly increased compared to that observed in the initial round of IP-MS (given that filtering excluded the nuclear annotation from the output) suggesting that nuclear fractionation has indeed enriched for nuclear binding partners. This suggests that this dataset is more representative of true interactors within nuclear HDAC4 aggregates than the initial dataset.

Table 6.3 DAVID functional annotation chart: GOTERM: Cellular Component

Term	Count	%	P-Value	Fold Enrichment	FDR	Fisher Exact
cytoplasm	99	28.7	1.6E-06	1.6	1.9E-04	9.8E-07
nucleus	99	28.7	2.4E-04	1.4	1.1E-02	1.7E-04
cytosol	66	19.1	2.3E-06	1.8	2.1E-04	1.2E-06
precatalytic spliceosome	24	7.0	9.9E-12	6	3.7E-09	1.4E-12
catalytic step 2 spliceosome	20	5.8	2.0E-09	5.6	3.8E-07	3.1E-10
nucleoplasm	20	5.8	9.1E-04	2.3	3.7E-02	3.7E-04
fusome	9	2.6	1.0E-05	8.2	7.6E-04	1.0E-06
chaperonin-containing T-complex	5	1.4	3.9E-05	22.2	2.4E-03	9.0E-07
Sin3-type complex	5	1.4	1.7E-04	16.1	9.1E-03	6.9E-06

318/345 genes, 92.2% coverage. Ordered by count, displaying all terms with $p \leq 0.05$ and FDR$\leq$0.05.

Cellular component annotation further supported the functional clustering annotation, with enrichment of annotations relating to splicing and protein folding (Table 6.3). Interestingly there was an 8.2-fold enrichment of candidates relating to the fusome, which is defined by the GO organisation as an intracellular spectrin-rich structure within insect germline cells. This was unexpected given that candidate proteins were obtained from head lysates, however the fusome is highly enriched for cytoskeletal proteins (Cooley & Theurkauf, 1994); all nine candidates with this annotation are associated with cytoskeletal regulation, and all have high expression in the head as determined by RNAseq (FlyBase, Gramates *et al.* (2022)), as well as demonstrated neuronal expression (Beaven *et al.*, 2015; Cervantes-Sandoval *et al.*, 2016; Knowles-Barley *et al.*, 2010; Lee *et al.*, 2004; Pilling *et al.*, 2006; Pintér *et al.*, 1998; Rolls *et al.*, 2007; Zhang *et al.*, 2007).

Five candidates were also associated with the Sin3-type complex annotation (Kdm5, htk, Caf1-55, CG15356 and CG8515), which is defined by the GO organisation as an HDAC-containing

complex with at least one protein with a paired amphipathic helix motif, one class I HDAC, and one WD40 repeat protein. This suggests that HDAC4^{3SA} aggregates may be affecting gene expression; indeed HDAC4 has previously been demonstrated to associate with HDAC1 (Chan *et al.*, 2003) as well as HDAC7 (Downes *et al.*, 2000), both of which are present in Sin-3 like complexes.

Examination of GOTERM molecular function and biological process annotations reiterated the enrichment of proteins associated with the annotations listed in the functional clustering. Biological process terms were examined closely for those relating to HDAC4-overexpression induced defects, specifically those relating to mushroom body and eye development, and memory, and genes annotated to these compiled (Appendix Section 10.4.5, Table 10.5). While the annotations themselves were not significantly enriched, they identify promising candidates that may play a role in manifestation of HDAC4-overexpression induced phenotypes. Annotations relating to splicing were also enriched, as were those associated with protein homeostasis; the candidates annotated to each of these are found in Appendix Section 10.4.5, Tables 10.6 and 10.7.

UP SEQ FEATURE utilises the UniProt Knowledgebase (The UniProt Consortium 2023) and includes terms such as REGION and COMPBIAS, which describe characteristics of a region that have been experimentally defined, and amino acid compositional bias within a protein, respectively (Wu *et al.*, 2006). The term with the highest gene count was REGION: Disordered, representing 58% of all hits. Consistent with this, intrinsically disordered regions have a composition bias and are typically enriched in polar and charged amino acids (Romero *et al.*, 2001), which were overrepresented in 37% and 29% of hits respectively. It is important to note that the FDR for each of these annotations was high (and are therefore not presented in a table here), which could indicate inclusion of false positives, however they are described here due to the link between intrinsically disordered proteins and protein aggregation (Ayyadevara *et al.*, 2022).

In summary, from this initial analysis is evident that HDAC4^{3SA} aggregates are affecting major processes of cellular homeostasis, specifically splicing and pathways involved in protein homeostasis. There were also a number of candidate proteins that may be involved in specific HDAC4-overexpression induced phenotypes.

6.4. Discussion

This chapter aimed to identify the composition of HDAC4 aggregates via IP-MS, with the intention of characterising the role these components play in HDAC4 overexpression-induced toxicity. Following identification of shortfalls and optimisations, a list of 344 candidate interactors was obtained. Initial analysis of these revealed links to splicing and protein homeostasis, as well as candidates involved in mushroom body and eye development, and memory. These findings progress knowledge of the mechanisms through which HDAC4 aggregates may impede neuronal function and provide promising avenues for further investigation.

6.4.1. Evaluation of the strategy to determine HDAC4 aggregate composition

It was hypothesised that HDAC4-overexpression induced toxicity occurs via aberrant sequestration of proteins within HDAC4 aggregates, therefore, to characterise what proteins are found in these, an IP-MS approach was taken. Such an approach has previously been used to identify protein interactions associated with intracellular aggregates (Li *et al.*, 2016; Wang *et al.*, 2007), as well as to characterise protein interactions in *Drosophila* neurons (Mukherjee *et al.*, 2014) and investigate interactors of the cytoplasmic pool of HDAC4 (Federspiel *et al.*, 2019). The initial dataset identified 28 candidate interactors of HDAC4^{3SA} when expressed under the control of *elav-GAL4*. Unexpectedly, this did not include MEF2, nor many other known interactors of hHDAC4, and interactors were instead predominantly cytoplasmic proteins with mitochondrial activities. This was of significant surprise given that the 3SA mutation is widely used to restrict HDAC4 to nuclei, and it was therefore expected that a notable proportion of candidate interactors would be typically nuclear proteins. It is unclear whether these findings represent nuclear sequestration of cytoplasmic proteins or are an erroneous detection not representative of an *in vivo* interaction. Interestingly however, a cytoplasmic pool of HDAC4^{3SA} was observed in the lobes of the mushroom body. HDAC4 interacts with cytoplasmic aggregates of huntingtin (Mielcarek, Landles*, et al.*, 2013), as well as ubiquitinated Lewy bodies (Takahashi-Fujigasaki & Fujigasaki, 2006), however it is unclear what the role of HDAC4 is in this context, and whether this is reflective of a general propensity to associate with already aggregated proteins, or an ability to seed cytoplasmic aggregation. It is also unclear whether HDAC4^{3SA} forms cytoplasmic aggregates in Kenyon cells, as visualisation of this is difficult due to the relatively small area of cytoplasm surrounding nuclei, and the bundled nature

of the axons within the lobe structure. However, it is possible that the cytoplasmic interactors in the initial dataset may represent cytoplasmic aggregates of HDAC4, and therefore further investigation around cytoplasmic aggregation of HDAC4 is warranted.

The presence of 14-3-3ε within the initial dataset was also curious. Subcellular shuttling of HDAC4 is regulated by 14-3-3 proteins, which facilitate nuclear export (Section 1.5.1.3). HDAC4 has previously been demonstrated to interact with 14-3-3ε (Grozinger & Schreiber, 2000; Miska *et al.*, 2001), however here an interaction was detected with the HDAC4^{3SA} mutant. Nuclear localisation of HDAC4^{3SA} is achieved by substitution of three serine residues that when phosphorylated mediate 14-3-3 binding (Main *et al.*, 2021; Tan *et al.*, 2024; Wang & Yang, 2001). A possible explanation for the interaction between HDAC4^{3SA} and 14-3-3ε here is the presence of endogenous HDAC4; endogenous *Drosophila* HDAC4 is sequestered into nuclear aggregates in Kenyon cells (Section 4.2), and has the three serine residues intact and could therefore mediate interaction of HDAC4^{3SA} with 14-3-3ε. Moreover, a fourth serine residue that has also been implicated in 14-3-3 binding (Xu *et al.*, 2012) remained intact in the HDAC4^{3SA} mutant; alone this may facilitate some 14-3-3 binding which was detected here, but not so much as to significantly redirect HDAC4^{3SA} to the cytoplasm.

To address the concerns around erroneous detection of cytoplasmic proteins, immunoprecipitation was performed on nuclear lysates, and to focus on a restricted population of neuronal cells, *HDAC4^{3SA}* expression was driven by *OK107-GAL4*. *OK107-GAL4* was specifically chosen for its strong expression in Kenyon cells, where MEF2 is highly expressed. This yielded 344 candidate interactors, and known interactors of hHDAC4 appeared in abundance within this dataset. Proteins with previously characterised interactions with HDAC4 included CtBP (Zhang *et al.*, 2001), PP2A subunits (Pp2A-29B and widerborst, Paroni *et al.* (2008)) and HP1α (Su(var)205, Zhang *et al.* (2002)). In accordance with Paroni *et al.* (2008), β-tubulin also appeared alongside subunits of heat shock proteins. The presence of known interactors of hHDAC4 within this dataset reassures that co-precipitating proteins are likely due to an interaction with HDAC4. Furthermore, almost one third of interactors in this dataset were annotated to associate with the nucleus, confirming the efficacy of nuclear enrichment via fractionation prior to immunoprecipitation. It is noted that this is not an absolute metric to assess efficacy of enrichment components of nuclear HDAC4 aggregates, as these may too sequester proteins typically found in the cytoplasm.

Interestingly, 14-3-3 did not appear as a candidate interactor of HDAC4^{3SA} in the second dataset. Closer inspection of the raw data revealed that 14-3-3 was present in lists of peptides detected from both control and HDAC4^{3SA} immunoprecipitations, suggesting that 14-3-3 interacts non-specifically with the protein A/G beads and/or anti-Myc antibody. This highlights the importance of both appropriate controls to mitigate inclusion of proteins that interact non-specifically with the immunoprecipitation platform, as well as replication of the IP-MS data. Given the recent findings that 14-3-3 proteins alter aggregation of their target substrates (Segal *et al.*, 2023), it remains of interest to investigate whether 14-3-3 is recruited to HDAC4 aggregates, and whether this is dependent or independent of the characterised 14-3-3 binding residues within HDAC4.

6.4.1.1. Limitations of the current dataset

While these data provide interesting avenues for further investigation, these are not without limitations. The most unexpected result was the absence of MEF2 within both candidate HDAC4 interactor datasets. Given the complete co-localisation of MEF2 in HDAC4 aggregates in Kenyon cells, it was expected that MEF2 would be detected as a candidate interactor of HDAC4^{3SA}. It was initially hypothesised that the lack of detection of MEF2 may be due to a dilution effect; *HDAC4^{3SA}* was expressed in the whole brain via *elav-GAL4*, but endogenous MEF2 is largely restricted to Kenyon cells, which only comprise approximately 2% of neurons in the brain (Aso *et al.*, 2009; Balling *et al.*, 1987; Ito *et al.*, 1997), therefore a significant pool of HDAC4^{3SA} would not have the opportunity to interact with MEF2. However, MEF2 was still absent from the dataset obtained when *HDAC4^{3SA}* expression was restricted to mostly Kenyon cells under the control of *OK107-GAL4*. Interestingly, IP-MS was previously performed on human HDAC4-FLAG expressed in HEK293 cells (Paroni *et al.*, 2008), and MEF2 was not detected under these conditions either. The authors did however demonstrate an interaction between HDAC4 and MEF2 via *in vitro* GST-pulldown assays. These data suggest that while the interaction between HDAC4 and MEF2 may be direct, it is highly dynamic and sensitive to experimental conditions, such as cell lysis and wash buffers. Indeed, here the interaction between HDAC4 and MEF2 proved difficult to detect via co-immunoprecipitation; while the data is not shown, a significant amount of time was dedicated to optimising immunoprecipitation conditions to detect HA-tagged MEF2 expressed under the control of the same driver as HDAC4-Myc from fly heads, however this was with limited success. Together these data highlight that it is essential to consider that the absence of a protein from the IP-MS

data does not exclude it from being present within HDAC4 aggregates *in vivo*. Strategies to address dynamic interactors are discussed in Section 8.4.

It is also unclear whether the choice of the 3SA mutation was the most appropriate way to induce nuclear aggregation of HDAC4. The HDAC4^{3SA} mutant was selected as nuclear aggregates were larger and more numerous than HDAC4^{WT} aggregates, and it was hypothesised that enriching samples with HDAC4 aggregates would aid in their capture. At the time of commencement of this study, this was also the only known method to increase nuclear aggregation of HDAC4. Alternative methods are also now established to induce HDAC4 aggregation include increasing level of HDAC4 protein (Section 10.4.4.1), overexpression of MEF2 (Section 5.4.2), stabilising aggregation by inducing the S69F mutation (Section 4.4.2), or increasing nuclear localisation by ΔNES mutation (Section 5.5.2), however each of these have their own set of limitations. For example, MEF2 overexpression affects not only HDAC4 distribution, but disrupts the balance of MEF2 and may disrupt its function, and it is also unclear if stabilising tetramerisation via MEF2 impairs other functions and interactions of HDAC4.

An important limitation of the 3SA mutation is that it was recently determined that mutations that affect 14-3-3 binding (i.e. the 3SA mutation of HDAC4) alter aggregation dynamics of a number of proteins (Segal *et al.*, 2023), and this appears to include *Drosophila* HDAC4 (discussed in Section 5.6.6). Such changes in aggregation dynamics may alter the composition of aggregates and may confound detection of interactions that aid in HDAC4-overexpression induced toxicity. While aggregation of HDAC4 has been observed in neuronal disease (Section 1.6.2), the cause of such aggregation is undetermined. Without the knowledge of how aggregates form in a disease context, it is difficult to select an appropriate method to induce aggregation of HDAC4 to characterise sequestered proteins.

Further studies are needed to investigate the composition of HDAC4 aggregates. Until it is deciphered how and why HDAC4 aggregates form in a disease context, it is most appropriate that studies of composition are performed using wild-type HDAC4, and therefore increasing HDAC4 protein levels would be the most effective way to induce aggregation. This is especially applicable as HDAC4 mRNA levels are increased in patients with autism spectrum disorder, bipolar disorder, and in mouse models of AD (Chen *et al.*, 2021; Hobara *et al.*, 2010; Nardone *et al.*, 2014). Subcellular fractionation to enrich for the nuclear pool of HDAC4 will also be of utility for immunoprecipitation studies. Furthermore, the level of HDAC4 expression must be

carefully optimised in a cell-type specific, or tissue-specific manner prior to IP-MS. When trying to improve the yield of a target protein when immunoprecipitated from a cell lysate, it is tempting to increase the concentration of the target protein, however this is likely to have significant impacts on the dynamics of HDAC4 aggregation given that nuclear aggresome-like inclusions were observed upon extreme overexpression. Optimisations must therefore carefully consider the level of aggregation that is most similar to that observed in a disease context.

The final limitation of this dataset is that it has not been replicated. In light of the above, a change of approach would be most effective in accurately identifying components of HDAC4 aggregates, and therefore replication was not pursued here. Alternative approaches are discussed in Section 8.4.

6.4.2. Pathway analyses reveal processes that HDAC4 aggregates disrupt to mediate neurotoxicity

As the list of candidate HDAC4^{3SA} interactors has not been replicated, the dataset was instead examined as a whole at the pathway level, and this revealed mechanisms through which HDAC4 may be disrupting neuronal function. There was enrichment of clusters of proteins involved in splicing and protein homeostasis, as well as those important in neuronal and retinal development. These are of significant interest due to the neuronal dysfunction mediated by HDAC4 overexpression in *Drosophila* examined in this thesis as well as studies by Fitzsimons *et al.* (2013), Schwartz *et al.* (2016), Main *et al.* (2021) and Tan *et al.* (2024), as well as dysregulation of HDAC4 in the context of neuronal disease (Section 1.6.2). Furthermore, both splicing and protein homeostasis are key pathways disrupted in age-related neurological disease (Douglas & Dillin, 2010; Licatalosi & Darnell, 2006; Sin & Nollen, 2015).

6.4.2.1. Candidate HDAC4^{3SA} interactors have roles in neuronal development and function

A number of proteins with annotations relating to neuronal development and function were detected to interact with HDAC4^{3SA} (Appendix Section 10.4.5, Table 10.5). These can be separated into three clusters based on HDAC4-overexpression induced phenotypes; candidates involved in mushroom body development, memory formation, and eye development. A selection of interactors are presented in Table 6.4, where the literature that demonstrates that disruption of these candidates results in phenotypes similar to HDAC4 overexpression-induced

phenotypes are summarised. It would be pertinent to perform further in-depth literature reviews on additional candidate interactors from the IP-MS data, however this should follow some degree of validation of the current dataset such as either replication of IP-MS or BioID, as described in Section 8.4. Further analysis of candidates in Table 6.4 is promising as they have already been demonstrated to disrupt neuronal processes similarly to HDAC4; these analyses should involve confirmation of the presence of these proteins within HDAC4 aggregates, followed by examination of the phenotypic result of HDAC4 overexpression combined with either knockdown or overexpression of these candidates. If their presence in HDAC4 aggregates is required for HDAC4-overexpression induced defects, it is hypothesised that these may be ameliorated by their knockdown. Conversely, overexpression may exacerbate defects, especially if excess of the candidate stabilises HDAC4 aggregation. However, it is important to consider that given the low abundance of detection of some of these interactors compared to $HDAC4^{3SA}$, it is likely that phenotypes resulting from HDAC4 overexpression are a function of combined sequestration of each of these proteins, resulting in combined loss-of-function, rather than sequestration of a single protein that is responsible for the phenotype. This combined effect is further discussed in Section 6.4.3.1.

Table 6.4 Summary of candidate HDAC4^{3SA} interactors for which disruption has led to defects in the development of the mushroom body and/or eye, and/or impairments in memory

		Disruption to gene impairs		
FBgn	**Candidate**	**MB development**	**Eye development**	**Memory**
FBgn0261797	Dynein heavy chain 64C (Dhc64C)	Liu *et al.* (2000)	McGrail *et al.* (1995)	
FBgn0011661	Moesin (Moe)	Freymuth and Fitzsimons (2017)#	Karagiosis and Ready (2004)	Freymuth and Fitzsimons (2017)*
FBgn0263289	scribble (scrib)		Brumby and Richardson (2003), Courbard *et al.* (2009)	Cervantes-Sandoval *et al.* (2016)#
FBgn0259685	crumbs (crb)		Izaddoost *et al.* (2002), Pellikka *et al.* (2002)	
FBgn0001108	Dynactin 1, p150 subunit (DCTN1-p150)		Fan and Ready (1997)	
FBgn0264975	Neuroglian (Nrg)	Siegenthaler *et al.* (2015)*, Goossens *et al.* (2011)*#		
FBgn0023169	AMP-activated protein kinase alpha subunit (AMPKalpha)		Pletcher *et al.* (2019)	Silva *et al.* (2022)
FBgn0015609	Cadherin-N (CadN)	Kurusu *et al.* (2012)*#		
FBgn0002940	neither inactivation nor afterpotential E (ninaE)		Kumar and Ready (1995), Kang *et al.* (2012)	
FBgn0266098	rugose (rg)	Volders *et al.* (2012)*		Zhao *et al.* (2013)
FBgn0003380	Shaker (Sh) #Rogero *et al.* (1997)			Cowan and Siegel (1986)
FBgn0286784	Transitional endoplasmic reticulum 94 (TER94) #Pintér *et al.* (1998)	Chang *et al.* (2011)*	Higashiyama *et al.* (2002), Chang *et al.* (2011)	
FBgn0030089	Adaptor Protein complex 1, gamma subunit (AP-1gamma)		Kametaka *et al.* (2012)	
FBgn0013749	ADP ribosylation factor 4 (Arf4)		Kametaka *et al.* (2012)	
FBgn0012051	Calpain-A (CalpA)	Haddadi and Ataei (2022)*		Haddadi and Ataei (2022)*
FBgn0267435	chaoptin (chp)		Van Vactor *et al.* (1988)	
FBgn0011217	effete (eff)		Neufeld *et al.* (1998)	
FBgn0266599	Heat shock protein 70 cognate 4 (Hsc70-4)		Kumar and Tiwari (2018)	
FBgn0041210	Histone deacetylase 4 (HDAC4)	Main *et al.* (2021)*, Tan *et al.* (2024)*	Schwartz *et al.* (2016), Main *et al.* (2021), Tan *et al.* (2024)	Fitzsimons *et al.* (2013)*
FBgn0285926	IGF-II mRNA-binding protein (Imp)	Liu *et al.* (2015)*		
FBgn0010051	Inositol 1,4,5,-trisphosphate receptor (Itpr)	Kobayashi *et al.* (2006)*	Raghu *et al.* (2000)	

		Disruption to gene impairs		
FBgn	**Candidate**	**MB development**	**Eye development**	**Memory**
FBgn0266557	kismet (kis)	Melicharek *et al.* (2010)*#	Melicharek *et al.* (2010)	Melicharek *et al.* (2010)
FBgn0001316	klarsicht (klar)			Mosley-Bishop *et al.* (1999)
FBgn0264307	orb2 (orb2)			Keleman *et al.* (2007)*#
FBgn0259210	prominin (prom)		Van Vactor *et al.* (1988), Zelhof *et al.* (2006), Gurudev *et al.* (2014)	
FBgn0026375	Rho GTPase activating protein p190 (RhoGAPp190)	Ng and Luo (2004), Billuart *et al.* (2001)		
FBgn0086357	Sec61 alpha subunit (Sec61alpha)		Kanuka *et al.* (2005)	
FBgn0011259	Semaphorin 1a (Sema1a)	Zwarts *et al.* (2016)*#		
FBgn0003612	Suppressor of variegation 2-10 (Su(var)2-10)		Betz *et al.* (2001)	
FBgn0031030	Tao (Tao)	King *et al.* (2011)	Poon *et al.* (2011)	
FBgn0023518	trithorax-related (trr)		Sedkov *et al.* (2003), Kanda *et al.* (2013)	Koemans *et al.* (2017), Raun *et al.* (2023)*
FBgn0028671	Vacuolar H[+] ATPase 100kD subunit 1 (Vha100-1)		Williamson *et al.* (2010)	
FBgn0260987	verthandi (vtd)	MacPherson *et al.* (2023)*	Schaaf *et al.* (2009)	
FBgn0003996	white (w)		Ferreiro *et al.* (2017)	Sitaraman *et al.* (2008)

Disruption to gene refers to knockdown, overexpression, or mutant forms (i.e. mutations to the endogenous gene which disrupt the wild-type sequence, including those that result in expression of a truncated protein, as well as null mutants). Review was only conducted on *Drosophila* literature and does not consider the role of orthologues.
* indicates references where β lobe fusion or defects in long-term memory were specifically observed
# indicates expression observed in Kenyon cells

6.4.2.2. Candidate HDAC4^{3SA} interactors are involved in splicing

The list of candidate HDAC4^{3SA} interactors was significantly enriched for proteins involved in splicing (Appendix Section 10.4.5, Table 10.6). Splicing is an essential regulated process wherein pre-mRNAs undergo sequential transesterification reactions that result in the ligation of exons and removal of introns to form a mature mRNA (Black (2003), Figure 6.4). Alternative splicing is a consequence of differing combinations of exons, giving rise to multiple mRNA products resulting in divergent functional proteins from a single gene (Kelemen *et al.*, 2013).

Such events are essential in tailoring protein isoforms for a particular tissue type or stage of development to mediate diverse biological processes. Splicing defects give rise to more pathogenic isoforms of proteins involved in neurodegenerative disease; mutations in candidate loci of Alzheimer's disease have been associated with aberrant alternative splicing leading to repression of the unfolded protein response and neurotoxicity (Li *et al.*, 2021), while alternative splicing of SNCA (which encodes α-synuclein) leads to its increased aggregation in Lewy body dementia and Parkinson's disease (Beyer & Ariza, 2013; Beyer *et al.*, 2008; Kalivendi *et al.*, 2010). As dysregulation of HDAC4 has been implicated in these diseases (Section 1.6.2) it is possible it may be imparting neurotoxicity by altering splicing. In support of this, HDAC4 has been associated with regulation of alternative splicing in neuronal cell culture (Kosiorek *et al.*, 2014).

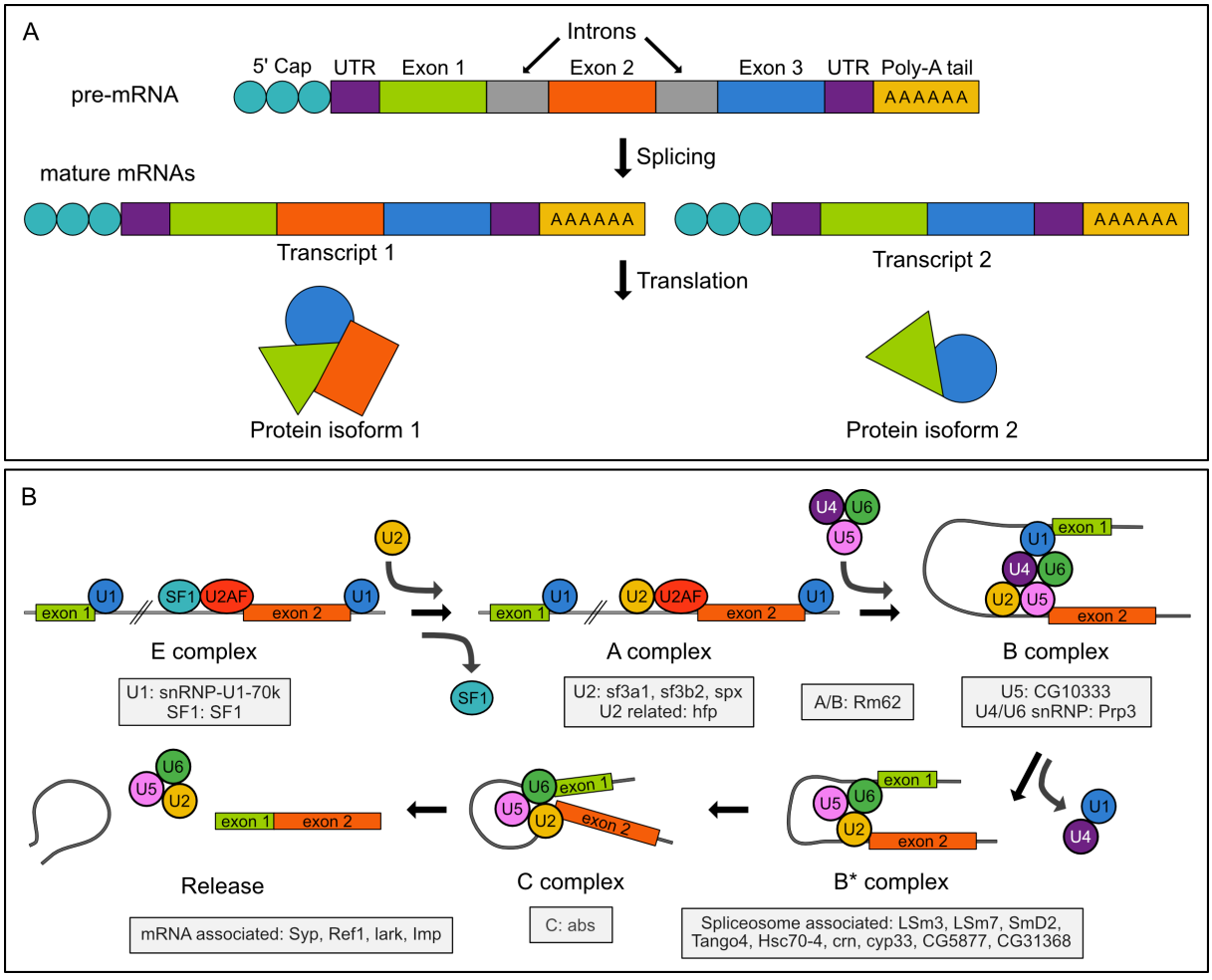

Figure 6.4 HDAC4^{3SA} aggregates may sequester components of the splicing machinery to mediate neurotoxicity

Schematic diagram representing splicing and how HDAC4 aggregates may affect this process. (A) Diagram depicting splicing of a pre-mRNA to yield transcripts with three (transcript 1) and two (transcript 2) exons respectively, resulting in two different isoforms of a protein. (B) Diagram showing the key steps in splicing. Candidate HDAC4^{3SA} interactors are shown in grey boxes below the complexes

in which they are found. A full list of proteins with annotations relating to splicing is found in Appendix Section 10.4.5, Table 10.6. *This figure is an original artwork created with reference to Herold et al. (2009) and Chanarat and Sträßer (2013).*

Splicing is facilitated by the spliceosome, a ribonucleoprotein complex found within nuclei (Matera & Wang, 2014). The spliceosome consists of five ribonucleoprotein (RNP) subunits formed from small nuclear RNPs (U1-2 and U4-6), as well as numerous protein cofactors. A simplified diagrammatic representation of spliceosome assembly and pre-mRNA splicing is presented in Figure 6.4, including notation of components that co-precipitated with HDAC4^{3SA} (boxes in Figure 6.4B). Components of the splicing machinery including spliceosome subunits, splicing factors, and RNA are stored in nuclear condensates termed speckles (Lamond & Spector, 2003). Co-incidentally, HDAC4 aggregates have long been colloquially termed speckles (Chan *et al.*, 2003; Kirsh *et al.*, 2002; Wu *et al.*, 2001), but to date there has been no evidence of such enrichment in HDAC4 aggregates. Given the enrichment of proteins involved in splicing in the candidate HDAC4^{3SA} interactors, it is possible that HDAC4 aggregates may constitute authentic speckles. Moreover, it is possible that sequestration of components of the splicing machinery in HDAC4 aggregates affects splicing of nascent mRNA, thus altering the functional proteome and inducing neuronal dysfunction.

Nuclear splicing speckles are typically identified by co-localisation of SC35 (Spector & Lamond, 2011), a splicing factor encoded by *SRSF2* which mediates spliceosome assembly (Fu & Maniatis, 1990). Although the *Drosophila* orthologue of SC35*,* SRSF2 (Park *et al.*, 2004) was not detected to interact with HDAC4^{3SA} here, it would be of interest to perform anti-SC35 immunohistochemistry on HDAC4 aggregates to determine whether they are splicing speckles. It is important to note however that nuclear aggregates of HDAC5 in fibroblasts did not co-localise with SC35 (Downes *et al.*, 2000), suggesting that HDAC4 aggregates may not constitute authentic speckles, and it is possible that HDAC4 is not contributing to their regulation but is disrupting their function. Nuclear speckles are also observed to sequester lamins A and B1 (Jagatheesan *et al.*, 1999). Interestingly, upon formation of larger aggresome-like structures HDAC4 sequestered lamin (Appendix 10.4.4.1), further suggesting these aggregates may have characteristics of nuclear speckles. If HDAC4 aggregates are confirmed to sequester splicing factors, this may suggest that aggregates alter alternative splicing and cause disruption to the functional proteome, contributing to dysregulation of protein homeostasis.

6.4.2.3. Enrichment of proteins involved in the protein homeostasis network

Protein homeostasis (proteostasis) refers to the processes involved in synthesis, maintenance and degradation of proteins (Balch *et al.*, 2008). Key steps within this pathway include translocation of mRNA from the nucleus to the cytoplasm, initiation of translation, protein folding, protein refolding, and protein degradation (Hipp *et al.*, 2019); proteins involved in each of these processes were immunoprecipitated with HDAC4^{3SA}, directly implicating it in the regulation of proteostasis. These candidates and their broad role in proteostasis are depicted in Figure 6.5. These were identified via parsing of GOterm biological process annotations and are found in Appendix Section 10.4.5, Table 10.7; a more comprehensive list could be generated in the future from a verified dataset by compiling more annotations relating to these processes. Discussion of the implications of involvement of HDAC4 in proteostasis is presented in Section 6.4.3.2.

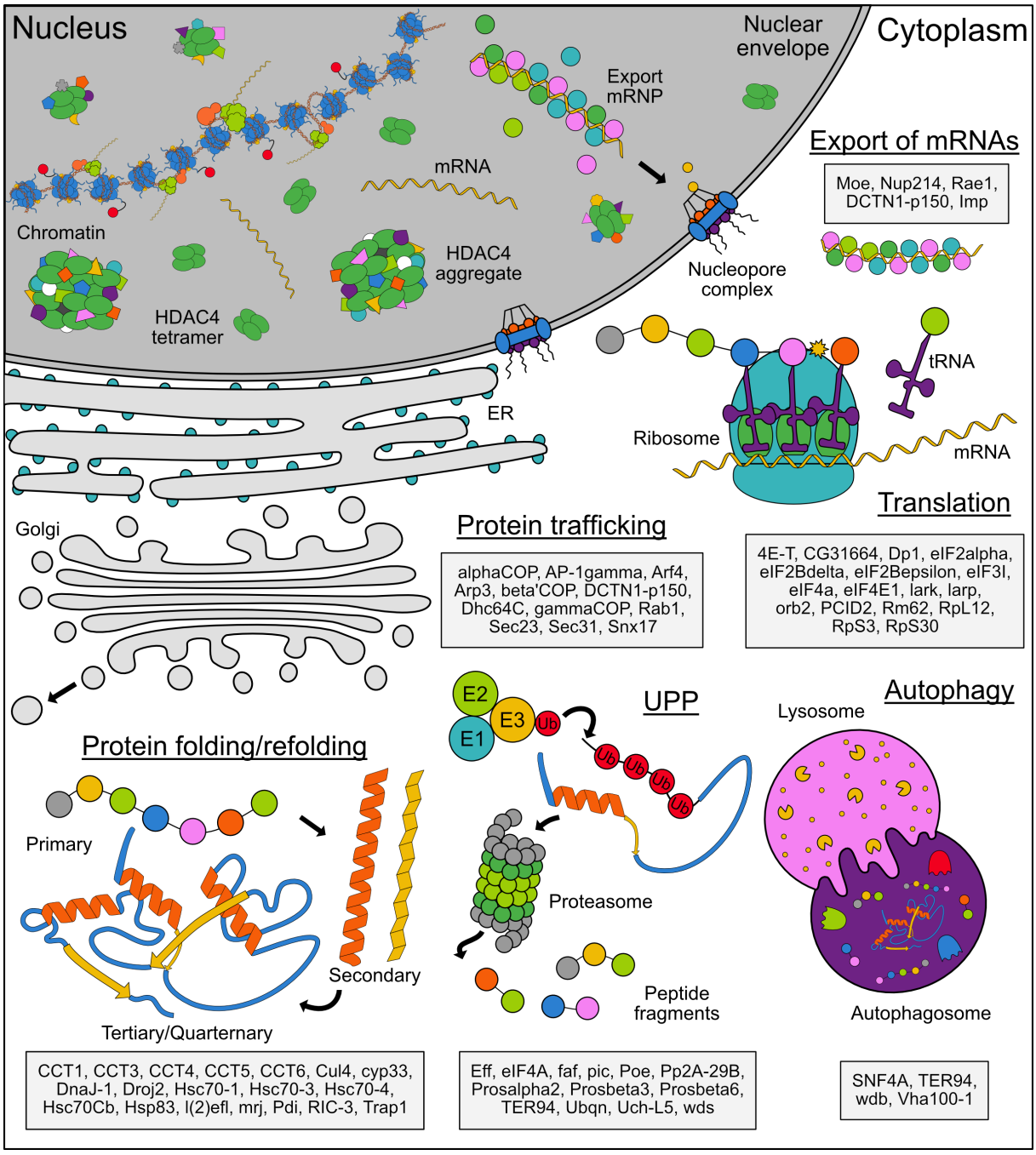

Figure 6.5 HDAC4^{3SA} aggregation may disrupt the proteostasis network
Schematic diagram depicting the key processes that HDAC4 aggregates may disrupt by sequestration of their components in nuclear aggregates. Candidate HDAC4^{3SA} interactors are shown in grey boxes below the processes they relate to. Annotations implicating these proteins in these processes are in Appendix Section 10.4.5, Table 10.7. UPP, the ubiquitin-proteasome pathway. Please note that autophagy is diagrammatically represented as macroautophagy for simplification. *This figure is an original artwork.*

6.4.3. How do HDAC4 aggregates mediate neurotoxicity?

It is acknowledged that sequestration of proteins within HDAC4 aggregates remains a hypothesised mechanism through which these aggregates impart neurotoxicity, and that further investigation of interactors of HDAC4 aggregates is warranted, but it is essential to also consider alternative hypotheses that may describe how the presence of HDAC4 aggregates is associated with neuronal dysfunction.

6.4.3.1. HDAC4 may stochastically sequester proteins with common functions to mediate neurotoxicity

With the exception of MEF2, it is entirely possible that HDAC4 aggregates are relatively homogenous and contain primarily HDAC4, with few additional consistently sequestered proteins. In support of this, three candidate interactors of HDAC4^{3SA} have been investigated in *Drosophila* to date: Armadillo and NinaC (Section 10.4.2), as well as Moesin (Freymuth, 2016). None of these were found to be sequestered in nuclear HDAC4 aggregates. However, from the literature it is evident that disruption to each of these proteins results in a phenotype similar to that associated with HDAC4 overexpression (Barker *et al.*, 2001; Freymuth & Fitzsimons, 2017; Matsumoto *et al.*, 1987; Tan *et al.*, 2013). While further investigation may reveal candidate interactors which co-localise with HDAC4 aggregates, an alternative hypothesis is also proposed; HDAC4 may be stochastically sequestering proteins to mediate neuronal dysfunction (Figure 6.6).

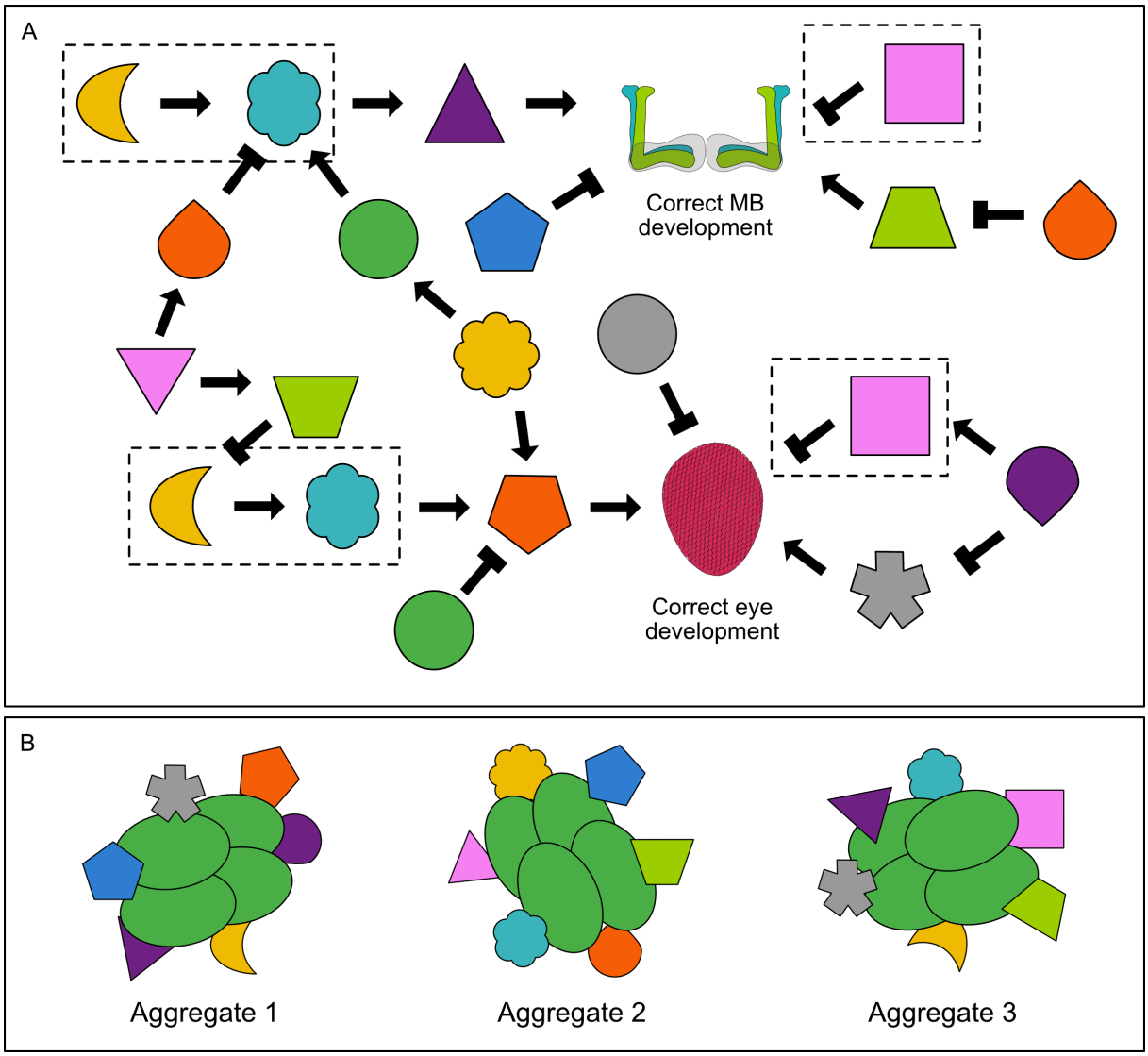

Figure 6.6 HDAC4 aggregates may stochastically sequester proteins to mediate defects in neuronal development and function
Schematic diagram representing the hypothesis that HDAC4 aggregates stochastically sequester proteins to mediate defects in neuronal development. (A) Simplified depiction of a pathway of proteins that regulate mushroom body development, converging with a pathway of proteins that regulate eye development. Boxed processes are shared between the two pathways. (B) Three aggregates of HDAC4 are shown, each sequestering a slightly different sample of the proteins depicted in (A). Each of the aggregates however consistently sequester proteins involved in both processes. *This figure is an original artwork.*

This hypothesis suggests that HDAC4 aggregates sequester many different proteins with low affinity and therefore not consistently, but each of the proteins sequestered acts in an overlapping set of biological processes. Importantly, it is thought that these aggregates still prevent the wild-type function of sequestered proteins to exert neuronal phenotypes. In support of this hypothesis, upon analysis via DAVID, it was evident that HDAC4 interacts with a large proportion of proteins that are enriched for disordered regions. This is of significance as

disordered regions contribute toward protein aggregation in neurodegenerative disease (Ayyadevara *et al.*, 2022). Intrinsically disordered regions (IDRs) of proteins lack a well-defined 3D structure that ultimately drives aggregation due to minimization of free energy (van der Lee *et al.*, 2014). The interactomes of proteins with IDRs are broad and with low affinity (Strodel, 2021), therefore proteins with IDRs that are sequestered in HDAC4 aggregates are likely done so dynamically and will vary widely over time and between cells. This may provide a challenge for the reproducibility of this dataset in terms of proteins consistently identified, or identified with high abundance, therefore it is most appropriate to focus at the pathway level to determine how HDAC4 is disrupting neuronal function.

6.4.3.2. HDAC4 aggregates may disrupt proteostasis to mediate neurotoxicity

The proteostasis network is increasingly dysregulated with age (Hipp *et al.*, 2019), acting as a major risk factor for neurodegenerative disease (Höhn *et al.*, 2020). Careful regulation of proteostasis is essential within the brain over a lifetime to avoid loss of post-mitotic neuronal cells and ensure healthy ageing and longevity (Yerbury *et al.*, 2016). Upon insufficiency and overwhelm of the ubiquitin-proteasome system, a key branch of the proteostasis network, protein aggregates can be actively transported to inclusion bodies termed aggresomes, which are thought to be a protective mechanism as part of the cell stress response pathway for misfolded proteins (Johnston *et al.*, 1998). Interestingly, upon extreme upregulation HDAC4^{WT} formed aggresome-like inclusions within Kenyon cell nuclei. In support of early aggresome formation, components typically enriched in aggresomes such as molecular chaperones including hsc70 (García-Mata *et al.*, 1999), 14-3-3 (Xu *et al.*, 2013) and p97 (TER94 in *Drosophila*, Ju *et al.* (2008)) were detected as candidate interactors of HDAC4^{3SA}. HDAC4 was previously observed to form cytoplasmic aggresome-like structures upon mutation of a key ubiquitination site important in regulating HDAC4 stability (Cernotta *et al.*, 2011). Moreover, HDAC4 localises to cytoplasmic Lewy bodies (Takahashi-Fujigasaki & Fujigasaki, 2006), which are ubiquitinated aggresome-like inclusions observed in the brains of Parkinson's disease patients that form in response to proteolytic stress (McNaught *et al.*, 2002; Olanow *et al.*, 2004). While it is unclear whether the nuclear aggresome-like inclusions observed upon significant HDAC4 overexpression constitute authentic aggresomes, it is evident that these represent widespread disruption of proteostasis.

The implication of nuclear HDAC4 in regulation of proteostasis, either by sequestration of proteins important in regulation of proteostasis, or by overwhelming this network that is trying to minimise the effect of HDAC4 aggregates, suggests a global effect of HDAC4 dysregulation on the cell and may provide a mechanism through which HDAC4 aggregates affect a wide range of neuronal processes. It is therefore hypothesised that the toxicity of HDAC4 aggregates arises not only from loss of function of proteins that may be sequestered within aggregates, but by diversion of critical resources from within the cell for maintaining proper protein function. It is likely that HDAC4 aggregation causes gradual dysregulation and dysfunction of the proteome as protein synthesis, folding, refolding and turnover are each increasingly impaired, and together this enables HDAC4 to impair a range of processes. Given that impairment of proteostasis is frequent in neurodegenerative disease (Höhn *et al.*, 2020) and widespread in ageing (Hipp *et al.*, 2019), it is also evident that HDAC4 aggregation can be both causative and a result of ageing and neurodegenerative processes alike. Irrespective of this, it is clear that mechanisms to decrease HDAC4 aggregation will be of therapeutic benefit for reducing its overall burden on the proteostasis network.

In summary, the data presented in this chapter provides new avenues for investigation of proteins and processes that HDAC4 aggregates may disrupt to mediate defects in neuronal development and function. Proteins identified in this chapter have roles in mushroom body and eye development, as well as memory, and are therefore positioned as promising candidates through which HDAC4 interacts with to mediate neuronal dysfunction when overexpressed in *Drosophila*. Pathways identified converge around the idea of protein homeostasis, and suggest that HDAC4 may be being acted upon by these mechanisms, as well as disrupting them to mediate neuronal dysfunction. These findings have opened new directions for further investigation, and these are discussed in Section 8.4.

Chapter Seven

A strategy to disrupt HDAC4 aggregation

7. Investigation of a mechanism to alter HDAC4 aggregate formation

7.1. A strategy to disrupt HDAC4 aggregation and neurotoxicity

The previous chapters detail the positive correlation between nuclear aggregation of HDAC4 and the severity of HDAC4 overexpression-induced neurodevelopmental phenotypes in the *Drosophila* mushroom body and eye, where mutations hypothesised to reduce tetramerisation reduced aggregation and the severity of phenotypes, and vice versa. This chapter aims to test a strategy to ameliorate defects associated with nuclear aggregation of HDAC4.

Guo *et al.* (2007) examined the formation of the N-terminal α-helix of hHDAC4 from residues 62-153, and determined that this region forms a tetramer in solution (Section 1.8.1). Deletion of the N-terminus of HDAC4 prevents aggregation in HeLa cells (Kirsh *et al.*, 2002), and mutations to this helix disrupt HDAC4 aggregation in neuronal nuclei (Chapter 4). It is hypothesised that expression of the N-terminus of HDAC4 alone is unlikely to significantly disrupt neuronal function as it is devoid of many binding sites present within full-length HDAC4 that may recruit proteins to aggregates (Figure 1.10). This may be of therapeutic advantage as expression of this helix could interfere with the dynamics of tetramerisation and aggregation of full-length HDAC4 (Figure 7.1A). By adjusting the composition of tetramers, and subsequently aggregates, the N-terminus of HDAC4 could reduce the amount of full-length HDAC4 recruited, and thereby reduce the number of proteins sequestered (Figure 7.1B). Ultimately, it could also be possible to tether the helix in the cytoplasm to act as a sink for full-length HDAC4 and reduce nuclear accumulation and aggregation (Figure 7.1C).

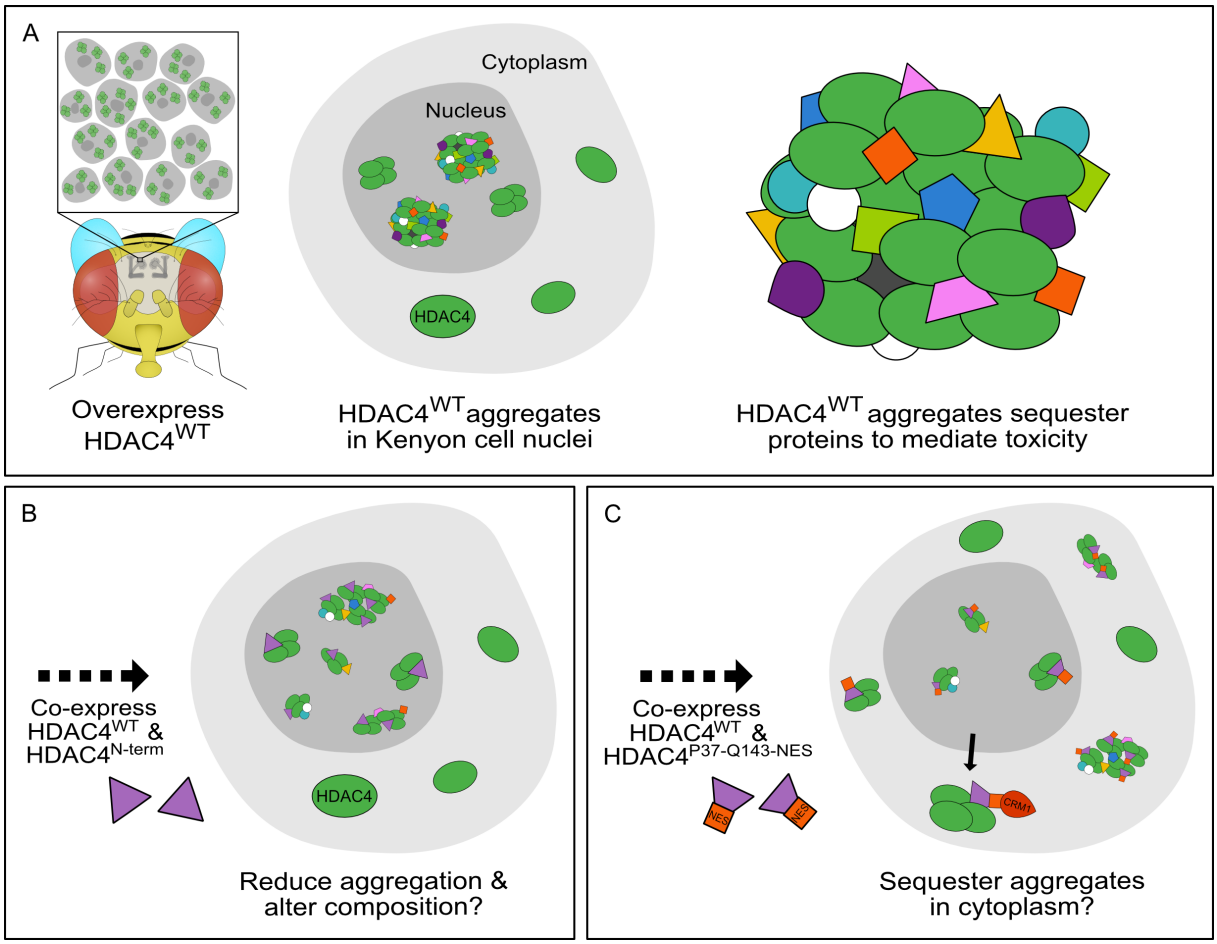

Figure 7.1 Expression of a minimal fragment of HDAC4 including the tetramerisation domain may alter tetramerisation and aggregation of full-length HDAC4
Schematic diagram representing changes in HDAC4^{WT} aggregation upon co-expression of the N-terminus of HDAC4 that includes the tetramerisation domain (HDAC4$^{N\text{-}term}$). (A) Overexpression of HDAC4^{WT} forms nuclear aggregates in Kenyon cells. (B) It is hypothesised that HDAC4$^{N\text{-}term}$ can tetramerise with HDAC4^{WT} when co-expressed, and therefore alter the composition of HDAC4^{WT} aggregates by preventing sequestration of additional proteins. (C) It is hypothesised that co-expression of HDAC4$^{P37\text{-}Q143\text{-}NES}$ or HDAC4$^{NES\text{-}P37\text{-}Q143}$ (not shown) may sequester HDAC4 in the cytoplasm and thus alter phenotypes resulting from nuclear aggregation of HDAC4. *This figure is an original artwork.*

7.1.1. Design of HDAC4$^{N\text{-}term}$ constructs to disrupt oligomerisation of full-length HDAC4^{WT}

To begin to test this strategy, three progressive truncations of the N-terminus of DmHDAC4 were generated (Figure 7.2), herein collectively termed HDAC4$^{N\text{-}term}$. HDAC4$^{M1\text{-}L285}$ begins at the N-terminus of wild-type HDAC4 (Met1) and truncates following residue Leu285. Leu285 was selected as the end point of this construct as it aligns with the caspase cleavage site present in hHDAC4 (which appears not to be conserved in *Drosophila,* Appendix 10.2.2) that generates a functional N-terminal product of HDAC4 (Liu *et al.*, 2004; Paroni *et al.*, 2004), therefore it

was likely that this construct would be tolerated *in vivo*. This construct included the MEF2 binding site (Miska *et al.*, 1999; Sparrow *et al.*, 1999; Wang & Yang, 2001), and endogenous NLS (Wang & Yang, 2001), as well as Ser239, one of the phosphorylation sites important for 14-3-3 binding that facilitates relocation of HDAC4 to the cytoplasm (Grozinger & Schreiber, 2000; Wang *et al.*, 2000). As the aim of this construct was to interfere with nuclear aggregation of HDAC4, Ser239 was mutated to alanine in HDAC4$^{M1\text{-}L285}$ to prevent 14-3-3 binding and thus enforce its nuclear localisation.

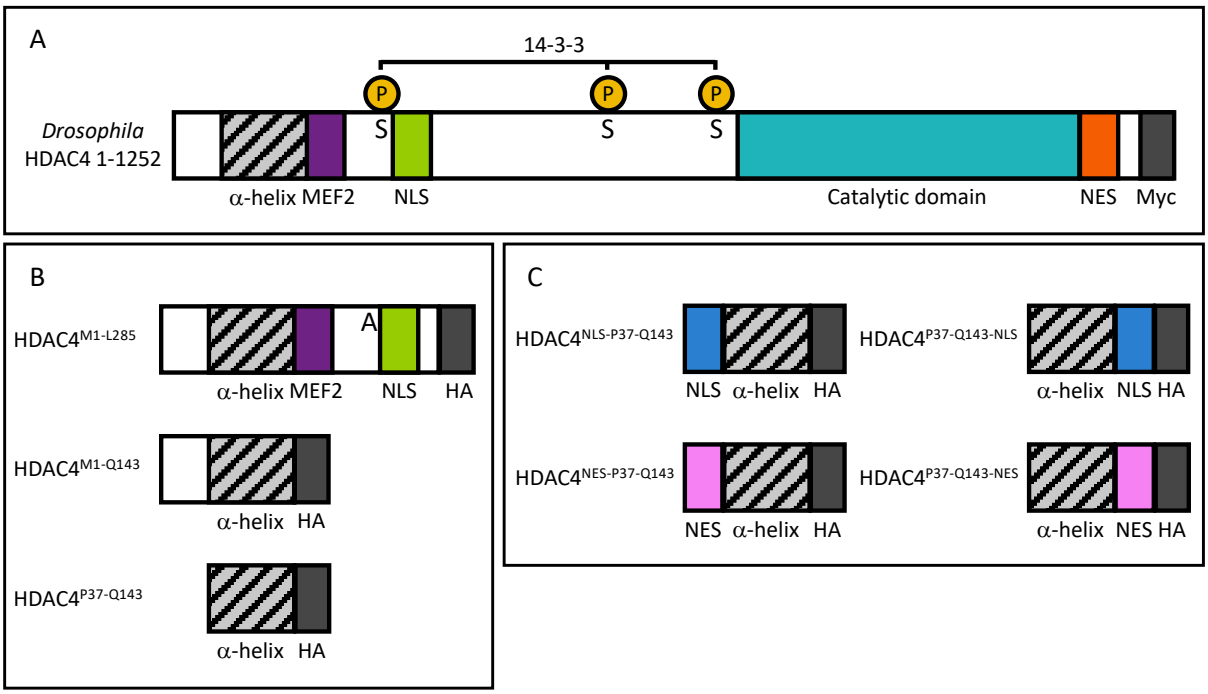

Figure 7.2 N-terminal constructs of HDAC4
(A) Full-length *Drosophila* HDAC4 with domain structure including MEF2 and 14-3-3 binding sites. (B) Three truncations of DmHDAC4 were generated: HDAC4$^{M1\text{-}L285}$, HDAC4$^{M1\text{-}Q143}$, and HDAC4$^{P37\text{-}Q143}$. In HDAC4$^{M1\text{-}L285}$, the serine residue at position 239 has been mutated to alanine. Each have a 3x HA tag to facilitate visualisation. (C) Exogenous nuclear localisation and export sequences (NLS and NES respectively) were added to the α-helix (HDAC4$^{P37\text{-}Q143}$) to assess the role of subcellular distribution in phenotypes. *This figure is an original artwork.*

Transcription factor binding sites within hHDAC4 span the α-helix and downstream regions (Figure 1.10), however with the exception of the MEF2 binding site, it is unknown whether these are conserved in *Drosophila.* HDAC4$^{M1\text{-}Q143}$ truncates at the end of the polyglutamine stretch present in *Drosophila* HDAC4 and does not contain the MEF2 binding site or NLS, and allows examination of the contribution of these domains and regions downstream of the helix to distribution and interaction of this construct with full-length HDAC4 (Figure 7.2B). The

minimal construct HDAC4$^{P37\text{-}Q143}$ corresponds to the region of human HDAC4 used to solve the crystal structure of the four-helix bundle (Guo *et al.*, 2007), with the addition of the downstream non-conserved polyglutamine stretch, and is devoid of the MEF2 binding domain and NLS. Despite its presumed inability to be directly imported into the nucleus via an NLS or MEF2 binding, it is possible that it can oligomerise with endogenous HDAC4 and therefore be shuttled with it.

To characterise the specific nuclear and cytoplasmic effects of this region, nuclear localisation (NLS) and export (NES) sequences were also fused to HDAC4$^{P37\text{-}Q143}$ (Figure 7.2C); fusions were made both upstream (HDAC4$^{NLS\text{-}P37\text{-}Q143}$, HDAC4$^{NES\text{-}P37\text{-}Q143}$) and downstream (HDAC4$^{P37\text{-}Q143\text{-}NLS}$, and HDAC4$^{P37\text{-}Q143\text{-}NES}$) of the helix to account for any effects that this fusion may have on import or oligomerisation. The NLS was derived from the large T antigen of Simian virus 40 (SV40t), and was previously successfully used to target GFP to the nucleus in *Drosophila* (Shiga *et al.*, 1996), while the NES was derived from cAMP-dependent protein kinase inhibitor alpha (PKIA), which has been used in *Drosophila* to target Moesin to the cytoplasm (Bajusz *et al.*, 2021).

To facilitate detection of HDAC4$^{N\text{-}term}$ in these studies, a C-terminal 3x hemagglutinin (HA) tag (previously used to tag MEF2-HA, Main *et al.* (2021)) with a glycine linker has been added. This small flexible linker will distance the helix from the HA tag, allowing better accessibility of the epitope for antibody detection as well as minimising any effect the tag may have on the ability of the helix to oligomerise (Chen *et al.*, 2013). This linker was also used to separate the helix from the NLS/NES sequence.

To investigate the validity of this strategy, expression of each HDAC4$^{N\text{-}term}$ construct was first confirmed and the subcellular distribution and ability to form aggregates characterised. This was followed by analysis of the effects of each HDAC4$^{N\text{-}term}$ construct on neuronal phenotypes in the mushroom body and eye to determine if their expression is neurotoxic. The constructs that are characterised in this chapter are summarised in Table 7.1.

Table 7.1 DmHDAC4$^{N\text{-}term}$ constructs characterised in this chapter

Name	Known domains contained within the construct
HDAC4^{WT}	-
HDAC4$^{M1\text{-}L285}$	N-terminal region, helix, MEF2-binding site, NLS. Ser239 mutated to alanine
HDAC4$^{M1\text{-}Q143}$	N-terminal region, helix
HDAC4$^{P37\text{-}Q143}$	Helix
HDAC4$^{NLS\text{-}P37\text{-}Q143}$	NLS (from SV40t), helix
HDAC4$^{P37\text{-}Q143\text{-}NLS}$	Helix, NLS (from SV40t)
HDAC4$^{NES\text{-}P37\text{-}Q143}$	NES (from PKIA), helix
HDAC4$^{P37\text{-}Q143\text{-}NES}$	Helix, NES (from PKIA)

Transgenic flies harbouring each of these constructs were generated and each are expressed in *Drosophila* under the control of GAL4. Each HDAC4$^{N\text{-}term}$ construct includes an HA-tag.

7.2. Characterisation of the expression of HDAC4$^{N\text{-}term}$

7.2.1. HDAC4$^{N\text{-}term}$ constructs are expressed in *Drosophila*

Transgenic flies harbouring HA-tagged HDAC4$^{N\text{-}term}$ constructs under *UAS*-control were generated (Section 3.1.1). The UAS-GAL4 system (Section 1.2.3) was used to drive pan-neuronal expression of *HDAC4$^{N\text{-}term}$*, facilitated by crossing male flies harbouring *HDAC4$^{N\text{-}term}$* to virgin females carrying *elav-GAL4* (Figure 3.1). Whole cell lysates were generated from heads of these flies and western blotting performed (Figure 7.3). *UAS-MEF2^{WT}-HA* was included as a positive control to demonstrate the specificity of the HA antibody, and was detected as a doublet at approximately 80 kDa as previously observed in our laboratory. No bands of similar size to the HDAC4$^{N\text{-}term}$ constructs were observed in the negative control of lysates generated from the progeny of *elav-GAL4* females crossed to males of the same genetic background as the *HDAC4$^{N\text{-}term}$* constructs, however non-specific bands were consistently observed at approximately 50 and 85 kDa. A single prominent band was detected in each lane corresponding to the N-terminal constructs, and the pattern of banding correlated with their expected molecular weight; HDAC4$^{M1\text{-}L285}$ appeared at the highest molecular weight, HDAC4$^{P37\text{-}Q143}$ the smallest, and a slight increase in size is observed for each NLS/NES-containing construct relative to HDAC4$^{P37\text{-}Q143}$. Each appeared at a slightly increased molecular weight relative to the marker than expected, however this is also observed for MEF2, as well as full-length HDAC4 constructs that were characterised in the previous chapters. There is a

difference in size between the N- and C-terminal fusions of the NLS-containing but not the NES-containing constructs. The lack of a difference between the NES-containing constructs is likely due to duplication (explained in Section 7.2.3) and the reason for that between the NLS-containing constructs is unknown.

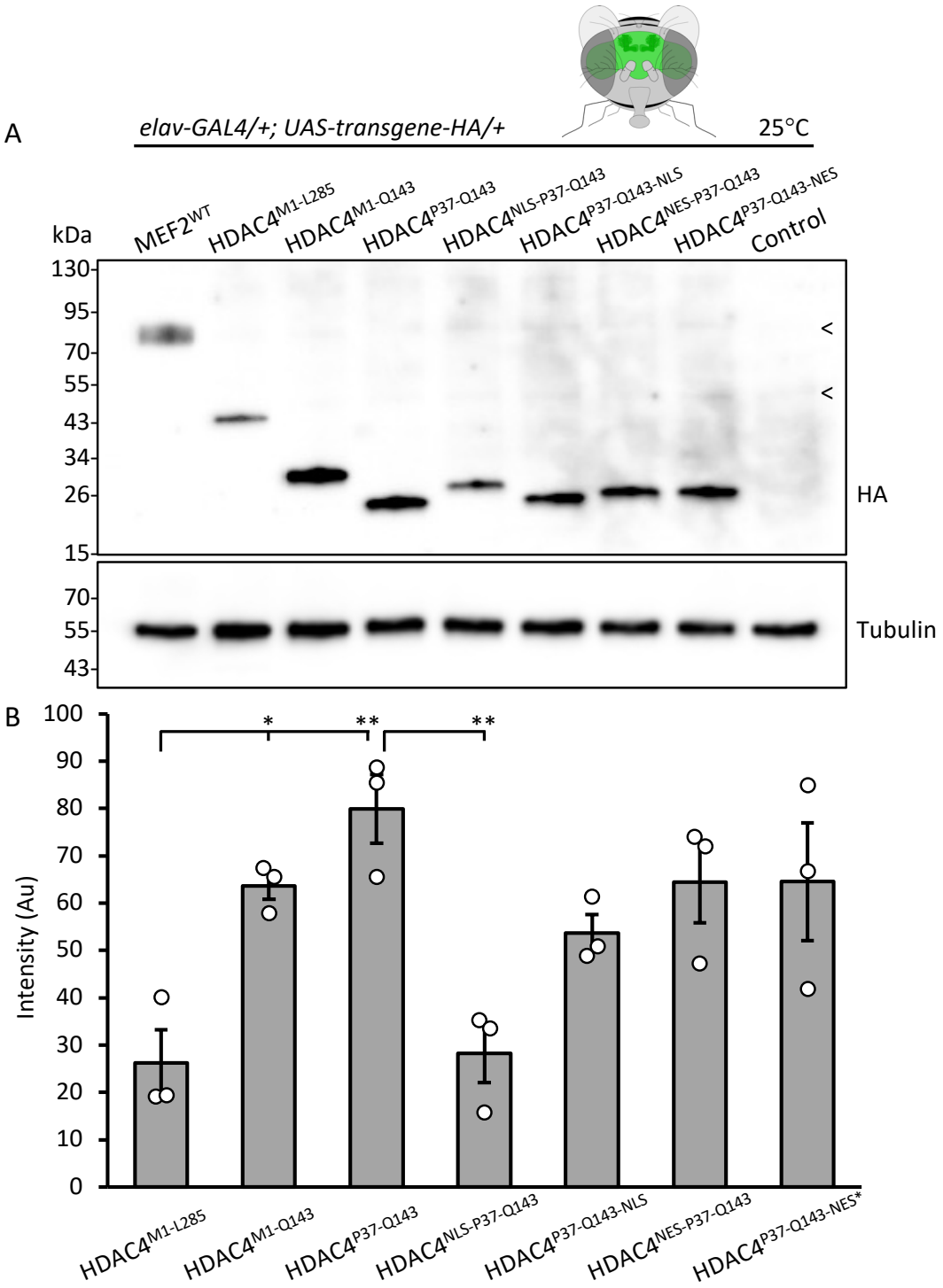

Figure 7.3 HDAC4$^{N\text{-}term}$ constructs are expressed in *Drosophila melanogaster*
(A) Western blot of *elav-GAL4* driven expression of HDAC4$^{N\text{-}term}$ in head whole-cell lysates (30 µg) using anti-HA and anti-alpha-tubulin antibodies. Flies were raised at 25 °C. Control is *elav-GAL4/+*.

MEF2-HA was included as a positive control. The expected molecular weights of the constructs are: MEF2-HA, 57.8 kDa; HDAC4$^{M1\text{-}L285}$, 35.9 kDa; HDAC4$^{M1\text{-}Q143}$, 20.4 kDa; HDAC4$^{P37\text{-}Q143}$, 16.5 kDa; HDAC4$^{NLS\text{-}P37\text{-}Q143}$, HDAC4$^{P37\text{-}Q143\text{-}NLS}$, HDAC4$^{NES\text{-}P37\text{-}Q143}$, HDAC4$^{P37\text{-}Q143\text{-}NES}$, 18.3 kDa. Arrows indicate non-specific bands consistently observed using this antibody. These were present in the negative control lane upon membrane overexposure. (B) Quantification of HDAC4$^{N\text{-}term}$ band intensity. HDAC4$^{N\text{-}term}$-HA intensity was measured and normalised to tubulin (n=3 blots). Intensity was measured in arbitrary units (Au). Mean intensity is plotted with individual data points represented as circles, error bars indicate the SEM. HDAC4$^{M1\text{-}L285}$ was significantly reduced in intensity compared to HDAC4$^{M1\text{-}Q143}$ (ANOVA, $F(6,14)=7.16$, $p=0.0012$, post-hoc Tukey's HSD, $p=0.04129$. *$p<0.05$, **$p<0.01$) and HDAC4$^{P37\text{-}Q143}$ ($p=0.002561$). HDAC4$^{NLS\text{-}P37\text{-}Q143}$ was significantly reduced in intensity compared to HDAC4$^{P37\text{-}Q143}$ ($p=0.00356$). There was no significant difference between HDAC4$^{P37\text{-}Q143}$ and each HDAC4$^{P37\text{-}Q143\text{-}NLS}$, HDAC4$^{NES\text{-}P37\text{-}Q143}$, HDAC4$^{P37\text{-}Q143\text{-}NES}$, or between each HDAC4$^{NLS\text{-}P37\text{-}Q143}$ and HDAC4$^{P37\text{-}Q143\text{-}NLS}$ or HDAC4$^{NES\text{-}P37\text{-}Q143}$ and HDAC4$^{P37\text{-}Q143\text{-}NES}$. Full blots used for quantification are found in Appendix 10.5.1. * denotes that this was the construct that was thought to be HDAC4$^{P37\text{-}Q143\text{-}NES}$, but was later found to be HDAC4$^{NES\text{-}P37\text{-}Q143}$ (Section 7.2.3).

As HDAC4 overexpression-induced phenotypes are dose-dependent, band intensity of each of the HDAC4$^{N\text{-}term}$ constructs was quantified (Figure 7.3B). Notably, HDAC4$^{M1\text{-}L285}$ was significantly reduced in intensity compared to both HDAC4$^{M1\text{-}Q143}$ and HDAC4$^{P37\text{-}Q143}$, and HDAC4$^{NLS\text{-}P37\text{-}Q143}$ was also reduced compared to HDAC4$^{P37\text{-}Q143}$. These variations may be a result of comparatively increased nuclear distribution (further investigated in Section 7.2.2) coupled with inefficient nuclear lysis, and/or represent changes in total protein level, as the rate at which each construct is turned over and whether this differs between them is unknown. Therefore, it is important to consider that these constructs may be differentially subject to dose-dependent effects on aggregation, distribution, and interaction with full-length HDAC4^{WT}.

7.2.2. HDAC4$^{N\text{-}term}$ constructs have different subcellular distributions in the adult brain

HDAC4$^{N\text{-}term}$ distribution in the adult brain was next characterised. As a readout of cytoplasmic distribution, the intensity of HDAC4 in the mushroom body lobes (Kenyon cell axons) was examined (Figure 7.4). Each of the HDAC4$^{N\text{-}term}$ constructs were expressed in the brain via *elav-GAL4* (magenta) and *OK107-GAL4* +TARGET (green), the latter of which drives comparatively higher expression in the mushroom body (Section 4.1), and brains of flies dissected and prepared for immunohistochemistry. The distribution of HDAC4$^{N\text{-}term}$ was also compared to that of full-length HDAC4^{WT}; as these constructs are HA-epitope and Myc-epitope tagged respectively, direct comparisons of intensity cannot be made. HDAC4^{WT} was present in the lobes of the mushroom body as observed previously (Figure 5.1, Tan *et al.* (2024)). The same pattern of intensity in the lobes was observed across the panel of HDAC4$^{N\text{-}term}$ for both

elav-GAL4 and *OK107-GAL4* drivers, suggesting that dose minimally impacts their subcellular distribution in Kenyon cells (Figure 7.4). HDAC4$^{M1\text{-}L285}$ was entirely absent from the lobes (Figure 7.4B,F) while HDAC4$^{M1\text{-}Q143}$ (Figure 7.4C,G) and HDAC4$^{P37\text{-}Q143}$ (Figure 7.4D,H) were observed in the lobes similarly to HDAC4^{WT} (Figure 7.4A,E). Each of the NLS-containing constructs were reduced in intensity in the lobes relative to HDAC4$^{P37\text{-}Q143}$ (Figure 7.4I-J, M-N); this is likely a result of both decreased protein levels as per Figure 7.3, as well as an increase in nuclear distribution. Interestingly, the intensity of HDAC4$^{NLS\text{-}P37\text{-}Q143}$ in the lobes was consistently lower than HDAC4$^{P37\text{-}Q143\text{-}NLS}$, and this reflected the reduced protein levels observed in Figure 7.3, suggesting that the position of the NLS within the construct may have some subtle effect on the rate of protein turnover, as well as potentially the regulation of its subcellular localisation. In contrast, neither of the NES-containing constructs differed significantly in intensity compared to HDAC4$^{P37\text{-}Q143}$ (Figure 7.4K-L, O-P). The effect of the position of the NES cannot be examined as the identity of HDAC4$^{P37\text{-}Q143\text{-}NES}$ was later confirmed in Section 7.2.3.

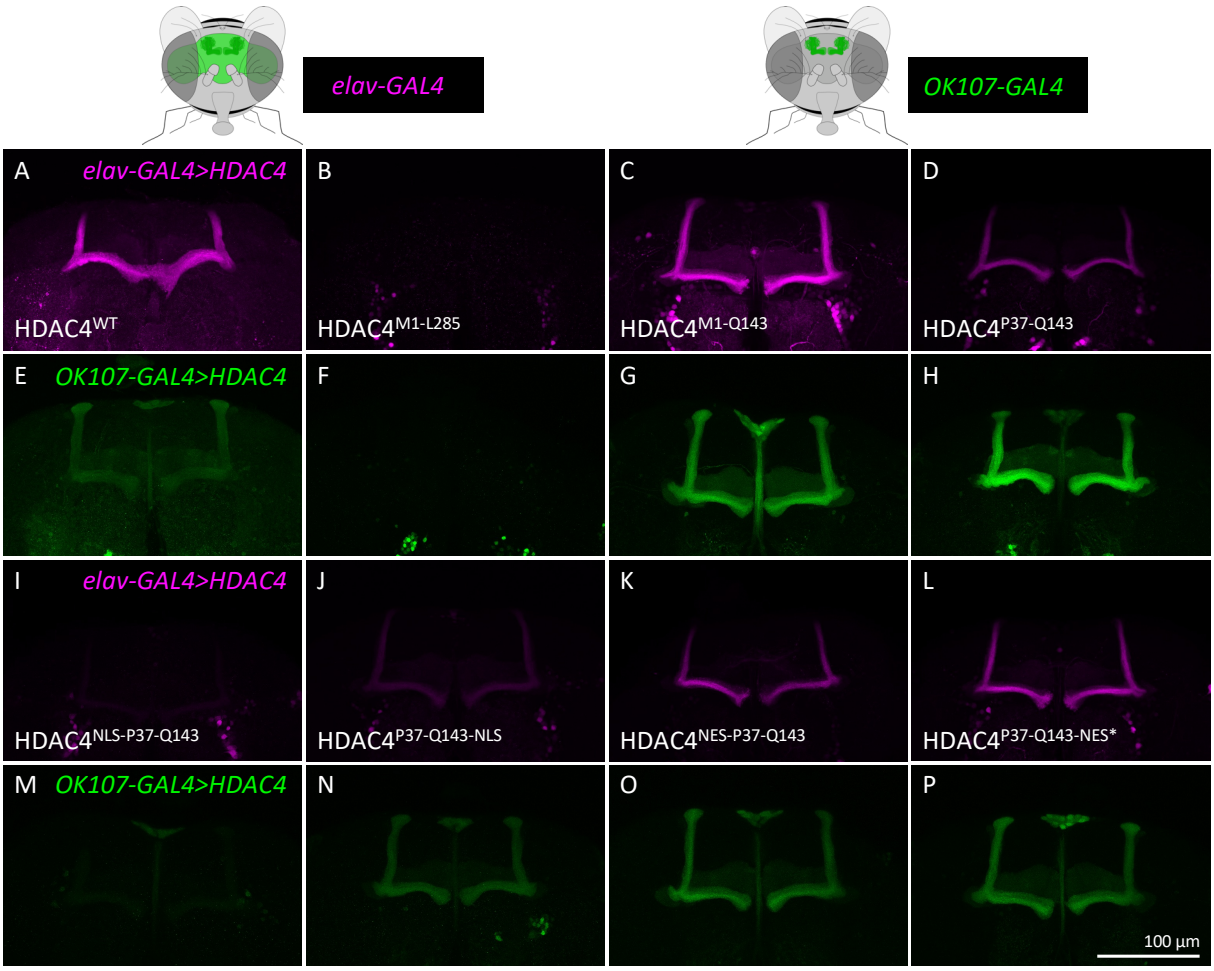

Figure 7.4 Distribution of HDAC4$^{N\text{-}term}$ constructs in the lobes of the adult mushroom body

(A-P) Maximum projections of optical sections (1 µm) through the anterior of the brain demonstrate *elav-GAL4* (magenta, A-D, I-L) or *OK107-GAL4* +TARGET (green, E-H, M-P) driven expression of HDAC4$^{N\text{-}term}$-HA or HDAC4^{WT}-Myc in the adult mushroom body. *elav-GAL4* crosses were raised at 22 °C. *tub-GAL80ts; OK107-GAL4* crosses were raised at 18 °C until adults eclosed, which were then transferred to 30 °C for three days to induce transgene expression. With the exception of HDAC4$^{M1\text{-}L285}$, each construct was detected in the L-shaped lobes of the mushroom body, indicating presence in axons. * denotes that this was the construct that was thought to be HDAC4$^{P37\text{-}Q143\text{-}NES}$, but was later found to be HDAC4$^{NES\text{-}P37\text{-}Q143}$.

The distribution of each construct in the nuclei of Kenyon cells in the posterior of the brain was also examined. Each of the HDAC4$^{N\text{-}term}$ constructs and HDAC4^{WT} were expressed in Kenyon cells under the control of *OK107-GAL4* in the presence of the TARGET system; flies were raised at 18 °C until adults emerged, which were transferred to 30 °C for three days to induce transgene expression. HDAC4^{WT} distributed to the calyx (dendritic field) and Kenyon cell bodies (Figure 7.5A) and was observed in both the nucleus and the cytoplasm surrounding nuclei (Figure 7.5E), forming small nuclear aggregates as observed previously (Figure 4.10). HDAC4^{WT} was absent from intense areas of DAPI staining, which are regions of

heterochromatin (Chiolo *et al.*, 2011). The distribution of the HDAC4$^{N\text{-}term}$ constructs varied; HDAC4$^{M1\text{-}L285}$ was absent from the calyx (Figure 7.5B) and appeared exclusively nuclear in Kenyon cells, with almost complete co-localisation with DAPI (except for regions of heterochromatin, Figure 7.5F), while both HDAC4$^{M1\text{-}Q143}$ and HDAC4$^{P37\text{-}Q143}$ were observed in the calyx (Figure 7.5C-D) and were pan-cellular in Kenyon cells (Figure 7.5G-H) similarly to HDAC4^{WT}. Small nuclear aggregates were occasionally observed for HDAC4$^{M1\text{-}L285}$, and these were not as notable for the two shorter constructs. Interestingly, addition of an NLS or NES to HDAC4$^{P37\text{-}Q143}$ did not result in absolute nuclear and cytoplasmic restriction respectively. Despite decreasing intensity in the calyx (Figure 7.5I-J), addition of an NLS did not increase the nuclear intensity of HDAC4$^{P37\text{-}Q143}$ (Figure 7.5M-N). On the contrary, it appeared reduced, and instead formation of distinct rings surrounding nuclei was observed (Figure 7.5M-N). The rings were observed in both the N- and C-terminal fusion and were not uniform, appearing as accumulations of protein at the nuclear periphery. Addition of an NES also appeared to dull the nuclear intensity of HDAC4$^{P37\text{-}Q143}$ in the Kenyon cells (Figure 7.5K-L compared to D, and O-P compared to H), but did not increase the intensity of cytoplasmic haloes. Again, there was a marked difference between the N- and C-terminal fusions of the NLS-containing constructs (Figure 7.5I-J) but not the NES-containing constructs (Figure 7.5K-L); consistent with increased protein levels (Figure 7.3) HDAC4$^{P37\text{-}Q143\text{-}NES}$ was increased in intensity compared to HDAC4$^{NLS\text{-}P37\text{-}Q143}$.

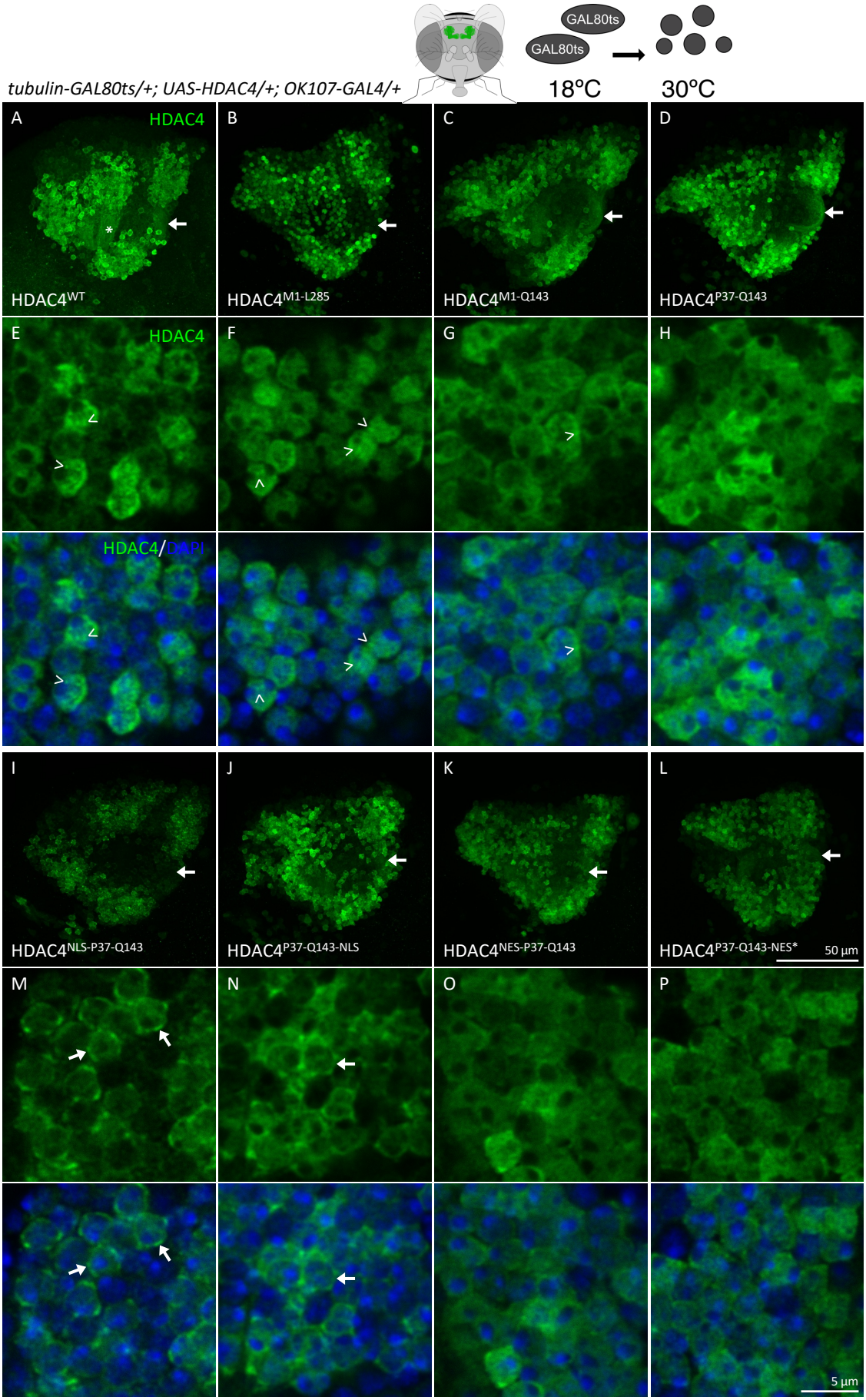

Figure 7.5 Distribution of HDAC4$^{N\text{-}term}$ constructs in the cell bodies of Kenyon cells

(A-D, I-L) Maximum projections of optical sections (0.5 μm) of the Kenyon cell layer in the posterior of the brain demonstrate *OK107-GAL4* +TARGET driven expression of each of the indicated *HDAC4^{WT}-Myc* or *HDAC4$^{N\text{-}term}$-HA* transgenes (green). DAPI highlights nuclei (blue). (E-H, M-P) are magnified single optical sections (0.5 μm). Flies were raised at 18 °C until adults eclosed, which were then transferred to 30 °C for three days to induce transgene expression. *denotes the calyx, arrows point to the right side boundary of the calyx. All of the HDAC4$^{N\text{-term}}$ proteins were detected in nuclei of Kenyon cells, however only HDAC4^{WT} appeared to regularly form small aggregates, with few observed within the other HDAC4$^{N\text{-term}}$ brains (arrowheads). HDAC4$^{NLS\text{-}P37\text{-}Q143}$ and HDAC4$^{P37\text{-}Q143\text{-}NLS}$ were present in rings surrounding nuclei in (M) and (N) (arrows).

7.2.3. Sequencing confirms the identity of HDAC4$^{N\text{-term}}$ constructs

Given that no absolute changes in subcellular distribution were observed for any of the NLS- or NES-containing constructs of HDAC4$^{P37\text{-}Q143}$ compared to HDAC4$^{P37\text{-}Q143}$, the identity of the *HDAC4$^{N\text{-}term}$* constructs was confirmed (Appendix 10.5.2). Genomic DNA was extracted from flies harbouring each N-terminal construct and PCR performed to amplify the sequence corresponding to the HDAC4 transgene. PCR products were electrophoresed and each of *HDAC4$^{M1\text{-}L285}$*, *HDAC4$^{M1\text{-}Q143}$*, and *HDAC4$^{P37\text{-}Q143}$* appeared at their expected size (Figure 10.47). As all *NLS/NES*-containing constructs were of the same size, sequencing was performed on the PCR products to confirm their identity (Figure 10.48). All constructs were of the expected identity apart from *HDAC4$^{P37\text{-}Q143\text{-}NES}$*; unexpectedly the *NES* was N-terminal to the *HDAC4$^{P37\text{-}Q143}$* sequence and was therefore a duplication of *HDAC4$^{NES\text{-}P37\text{-}Q143}$*. Sequences sent for gene synthesis were checked and were of the correct identity, therefore this duplication was not a result of a copy-paste error. It is likely that the duplication arose due to a mix-up of plasmids during preparation for germline transformation, or a mix-up of labelling of transgenic flies when inputting into the laboratory stocks from the overseas shipment. All experiments presented herein will therefore only contain the N-terminal fusions of the NLS and NES-containing constructs (i.e. HDAC4$^{NLS\text{-}P37\text{-}Q143}$ and HDAC4$^{NES\text{-}P37\text{-}Q143}$).

7.3. Characterisation of the neurodevelopmental effects of expression of HDAC4$^{N\text{-term}}$

Following confirmation that each of the HDAC4$^{N\text{-term}}$ constructs were expressed in *Drosophila,* the effects of their overexpression on the development of the mushroom body and eye was examined.

7.3.1. HDAC4$^{N\text{-}term}$ expression does not affect mushroom body development

The effect of HDAC4$^{N\text{-}term}$ expression on mushroom body development was examined as previously (Section 4.5.1). HDAC4^{WT} and HDAC4$^{N\text{-}term}$ were pan-neuronally expressed throughout development under the control of *elav-GAL4*, flies were raised at 22°C, adult flies were dissected, and brains were immunostained for FasII and scored for defects in morphology as per Figure 4.15, and Section 3.4.7. As observed previously (Section 4.5.1, Tan *et al.* (2024)), the predominant phenotype resulting from overexpression of HDAC4^{WT} was β-lobe fusion (Table 7.2). No HDAC4$^{N\text{-}term}$ construct imparted a significant phenotype (Table 7.2), with only a single brain from each of HDAC4$^{M1\text{-}Q143}$, HDAC4$^{P37\text{-}Q143}$, and HDAC4$^{NLS\text{-}P37\text{-}Q143}$ displaying a defect. There was no significant induction of β-lobe fusion for each HDAC4$^{N\text{-}term}$ construct compared to controls (Figure 7.6), suggesting that, as hypothesised, regions downstream of L285 are required to mediate HDAC4-induced mushroom body phenotypes.

Table 7.2 Frequency of mushroom body phenotypes resulting from HDAC4$^{N\text{-}term}$ expression at 22 °C.

(% of brains)	Con	HDAC4 WT	HDAC4 M1-L285	HDAC4 M1-Q143	HDAC4 P37-Q143	HDAC4 NLS-P37-Q143	HDAC4 NES-P37-Q143
α thinning	0	10	0	0	0	0	0
α missing	0	0	0	0	0	0	0
β thinning	0	10	0	0	0	0	0
β missing	0	0	0	5	5	0	0
β fusion	**0**	**100**	**0**	**5**	**0**	**5**	**0**
Mild	0	30	0	5	0	5	0
Severe	0	70	0	0	0	0	0
Guidance	0	10	0	5	5	0	0
N	20	20	20	20	20	20	20

Expression of each denoted *HDAC4* transgene was mediated by *elav-GAL4*; virgin *elav-GAL4* female flies were crossed to males harbouring the *HDAC4* transgene and adult progeny of this cross were dissected and their brains immunostained for FasII to assess mushroom body lobe development. Flies were raised at 22 °C. Instances of defects in morphology were scored for n=20 brains per genotype as per Section 3.4.7 and are displayed as the % of brains with the indicated phenotype. Control (con) is *elav-GAL4/+*. Percentages may not sum to 100 due to rounding.

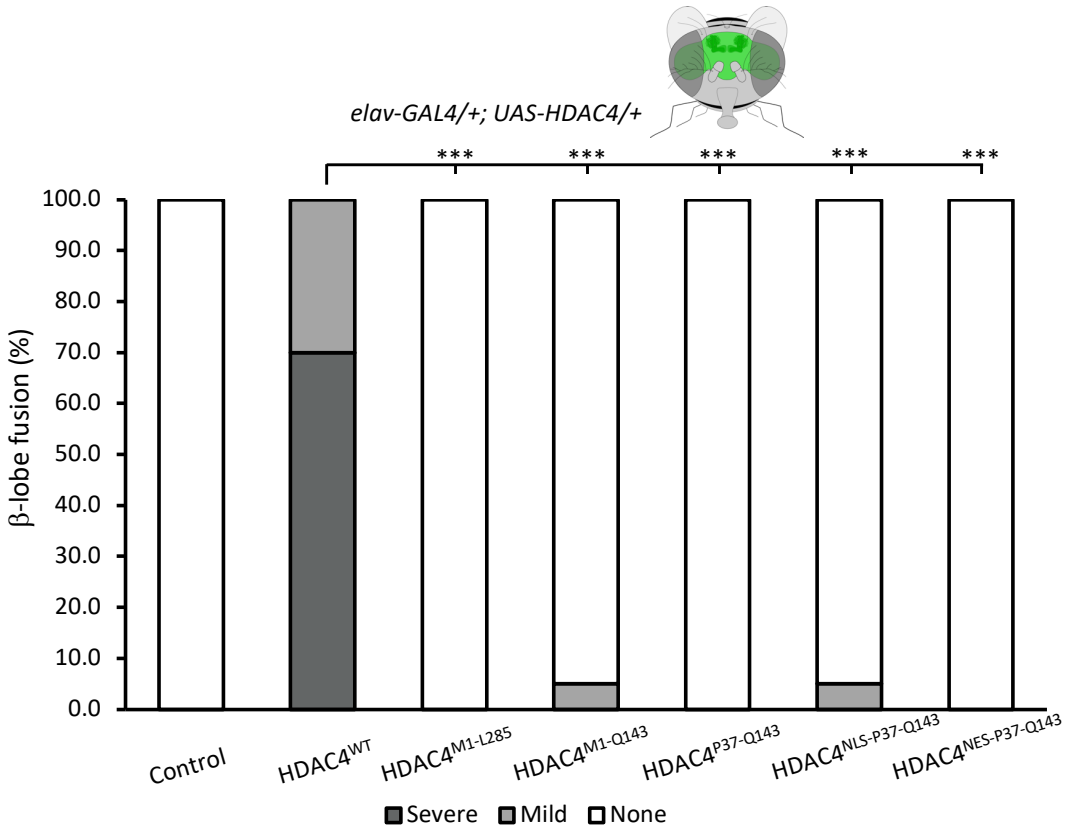

Figure 7.6 HDAC4$^{N\text{-}term}$ constructs do not induce β-lobe fusion of the mushroom body
Quantification of β-lobe fusion resulting from HDAC4$^{N\text{-}term}$ overexpression. HDAC4 expression was mediated by *elav-GAL4* at 22°C, adult brains were processed for anti-FasII immunohistochemistry, and β-lobe fusion was scored. n=20 brains per genotype. All HDAC4$^{N\text{-}term}$ constructs were significantly reduced in severity of β-lobe fusion compared to HDAC4^{WT} (Fisher's exact test, severe β-lobe fusion, ***$p<0.001$). There was no significant difference between HDAC4$^{N\text{-}term}$ and controls ($p=1$).

7.3.2. HDAC4$^{N\text{-}term}$ expression does not affect eye development

To determine whether HDAC4$^{N\text{-}term}$ expression interferes with development of the adult eye, light microscopy was performed on flies expressing each construct under the control of *GMR-GAL4*. No HDAC4$^{N\text{-}term}$ construct induced a phenotype (Figure 7.7C-G), with eyes presenting with a uniform array of ommatidia, while expression of one copy of HDAC4^{WT} (Figure 7.7B) resulted in a mild rough-eye phenotype as observed previously (Section 4.5.2), with mild perturbation of the array.

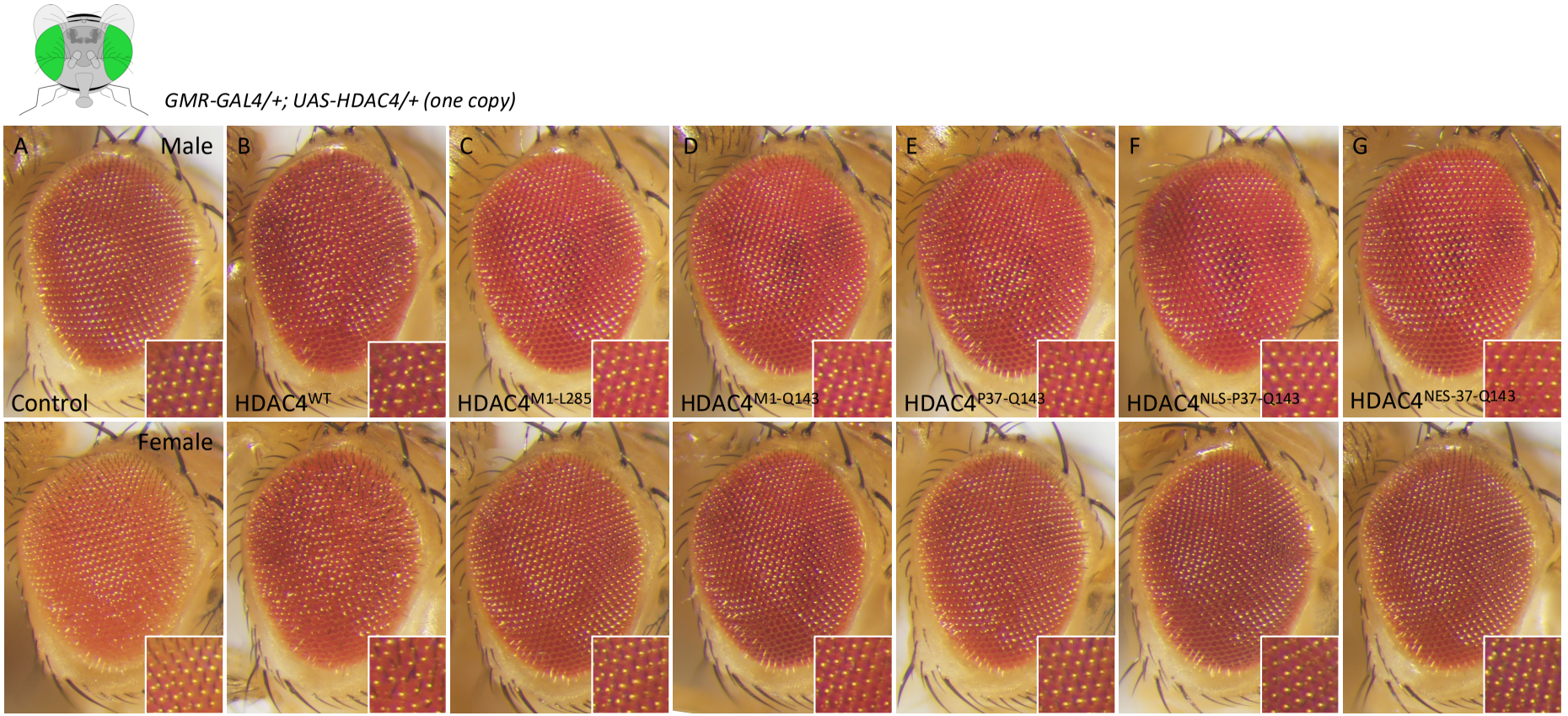

Figure 7.7 Overexpression of HDAC4$^{N\text{-}term}$ mutants does not alter *Drosophila* eye development

(A-G) Light microscopy (110x magnification) images of *Drosophila* eyes raised at 25°C. Top row, males; bottom row, females. Inset shows a magnified image of ommatidia. (A) Control is *GMR-GAL4/+; +/+*. (B-G) Flies harboured one copy of the driver (*GMR-GAL4/+*) and one copy of the *HDAC4* transgene (*UAS-HDAC4/+*). (B) HDAC4^{WT} overexpression induced mild perturbation of the organisation of the adult eye, characterised by misalignment of ommatidia and bristles. (C-G) This was not observed for any of the HDAC4$^{N\text{-}term}$ constructs which had a uniform array of ommatidia like controls in (A).

To exacerbate any phenotype associated with expression of HDAC4$^{N\text{-}term}$, the level of expression was increased (Figure 7.8). Stable lines harbouring the *GMR-GAL4* driver and *HDAC4$^{N\text{-}term}$* were generated (Appendix Section 10.1.6, Figure 10.6). The increased dose of HDAC4^{WT} induced a significant increase in the severity of the eye phenotype, with widespread fusion of ommatidia and loss of pigmentation (Figure 7.8B), as observed previously (Section 4.5.2). The same increase in severity was not observed for any of the HDAC4$^{N\text{-}term}$ constructs (Figure 7.8C-G), the eyes of which remained remarkably organised, and only HDAC4$^{M1\text{-}Q143}$ and HDAC4$^{NES\text{-}P37\text{-}Q143}$ eyes had slight misalignment of ommatidia at the edges. Quantification of these phenotypes was performed as previously described (Section 3.5.1), and corroborated these observations; HDAC4^{WT} had a score of 70.4% severity, while there was no notable score for most of the HDAC4$^{N\text{-}term}$ constructs, with only HDAC4$^{M1\text{-}Q143}$ and HDAC4$^{NES\text{-}P37\text{-}Q143}$ being significantly increased in severity compared to controls (Figure 7.9).

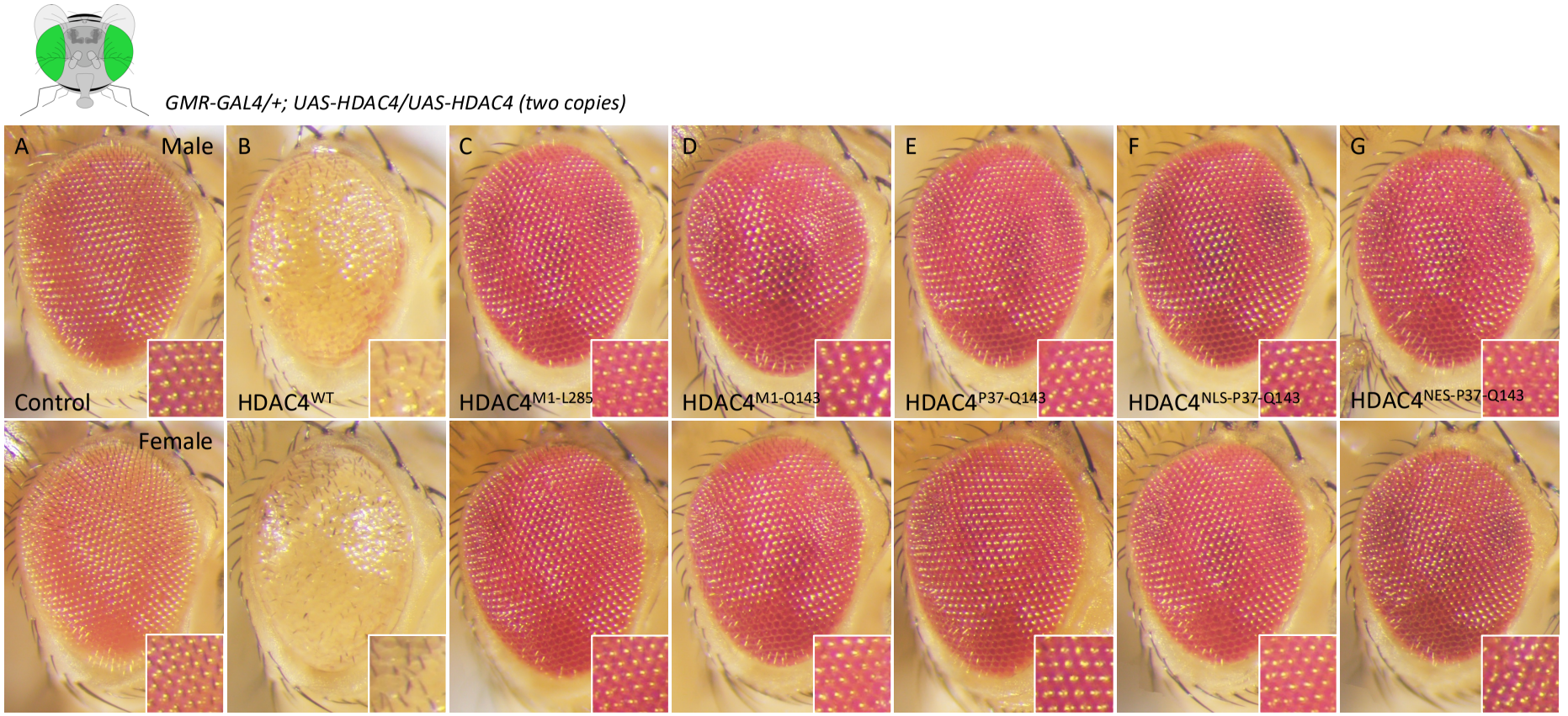

Figure 7.8 Increased dose of HDAC4$^{N\text{-}term}$ does not induce defects in eye development

(A-G) Light microscopy (110x magnification) images of *Drosophila* eyes raised at 25°C. Top row, males; bottom row, females. Inset shows a magnified image of ommatidia. (A) Control is *GMR-GAL4/+; +/+*. (B-G) Flies harboured one copy of the driver (*GMR-GAL4/+*) and two copies of the *HDAC4* transgene (*UAS-HDAC4/UAS-HDAC4*). (B) HDAC4^{WT} overexpression induced severe widespread disorganisation of the adult eye, characterised by ommatidial fusion and loss of pigmentation. (C-G) This was not observed for each indicated HDAC4$^{N\text{-}term}$ construct, with only mild disorganisation observed for HDAC4$^{M1\text{-}Q143}$ and HDAC4$^{NES\text{-}P37\text{-}Q143}$.

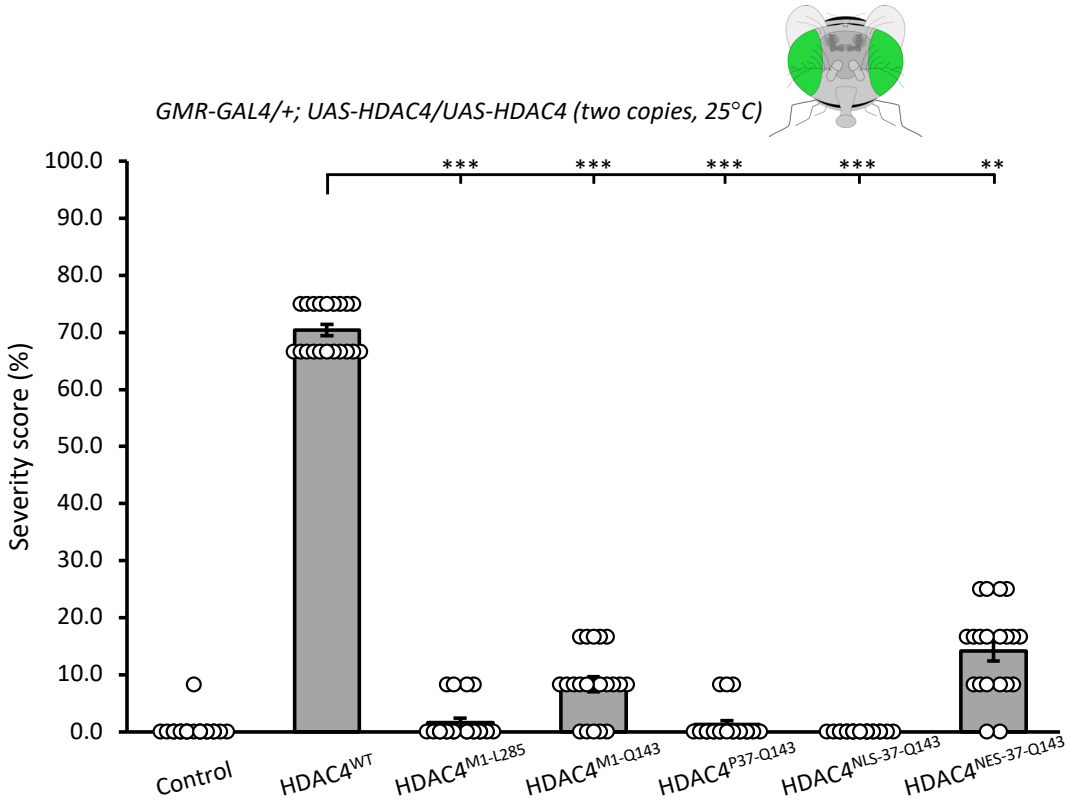

Figure 7.9 Implementation of a scoring system to characterise HDAC4$^{N\text{-}term}$ induced defects in eye development

The severity of eye phenotypes resulting from HDAC4 expression under the control of *GMR-GAL4* at 25°C was scored as per Section 3.5.1. Flies were heterozygous for *GMR-GAL4* and homozygous for *HDAC4* (*GMR-GAL4/+, UAS-HDAC4/UAS-HDAC4*). Control is *GMR-GAL4/+; +/+*. Severity scores were converted to % severity and the average is displayed. Individual data points are represented as circles, and error bars indicate the SEM. n=20 eyes per genotype. HDAC4$^{N\text{-}term}$ did not significantly impact eye development compared to HDAC4^{WT} (Kruskal-Wallis test, $H_{(6)}$=107.88, p<0.001, post-hoc Dunn's test, **p<0.01, ***p<0.001), however HDAC4$^{M1\text{-}Q143}$ and HDAC4$^{NES\text{-}P37\text{-}Q143}$ were significantly increased in severity compared to control (p<0.001).

Together these data demonstrate that the ability of HDAC4^{WT} to mediate developmental phenotypes in the mushroom body and eye upon overexpression is dependent on the presence of domains downstream of L285, as expression of no HDAC4$^{N\text{-}term}$ construct alone mediated significant neuronal phenotypes.

7.4. Characterisation of co-expression of HDAC4^{WT} and HDAC4$^{N\text{-}term}$

Given that expression of each HDAC4$^{N\text{-}term}$ construct alone did not result in significant nuclear aggregate formation, nor did any significantly interfere with neuronal development, it was hypothesised that they may be able to interfere with HDAC4^{WT} aggregation and thus prevent or reduce the neurodevelopmental phenotypes resulting from HDAC4^{WT} expression (Figure 7.1). Therefore, aggregate formation and neuronal phenotypes were examined following co-expression of HDAC4^{WT} and HDAC4$^{N\text{-}term}$. As this involves co-expression of two HDAC4 constructs (HDAC4^{WT} and HDAC4$^{N\text{-}term}$) it is important to compare the effect of each HDAC4$^{N\text{-}term}$ construct on HDAC4^{WT} to flies harbouring both one (heterozygous) and two (homozygous) insertions of full-length *HDAC4^{WT}* to account in part for the effect of dose of HDAC4 expression, as well as determine effects independent of domains downstream of the N-terminus.

7.4.1. HDAC4$^{N\text{-}term}$ expression affects the subcellular distribution and aggregation of HDAC4^{WT} in Kenyon cells

To facilitate co-expression of HDAC4^{WT} and HDAC4$^{N\text{-}term}$, *HDAC4^{WT}* was combined with *OK107-GAL4* into a single fly line (Appendix Section 10.1.6, Figure 10.4) and virgin females of this line were crossed to males harbouring each *HDAC4^{N}-term* construct. Flies were raised at 25 °C and progeny were dissected and brains immunostained with antibodies against the Myc and HA tags to detect HDAC4^{WT} and HDAC4$^{N\text{-}term}$ respectively. The expression of HDAC4^{WT} in combination with each HDAC4$^{N\text{-}term}$ construct was first examined in the mushroom body lobes (Figure 7.10). HDAC4^{WT} was observed in the α-, β- and γ-lobes of the mushroom body (Figure 7.10A), and intensity of Myc staining was increased upon increased dose, as expected (Figure 7.10B). HDAC4^{WT} was also present in the lobes upon co-expression with each HDAC4$^{N\text{-}term}$, however the intensity was significantly reduced in the presence of HDAC4$^{NES\text{-}P37\text{-}Q143}$ (Figure 7.10G), demonstrating that this construct reduces the cytoplasmic distribution of HDAC4^{WT} in Kenyon cells. HDAC4$^{NES\text{-}P37\text{-}Q143}$ also reduced the intensity of HDAC4^{WT} in the calyx while other constructs had little effect (Appendix Section 10.5.3, Figure 10.49). In contrast, the distribution of each HDAC4$^{N\text{-}term}$ did not appear to differ in the presence of HDAC4^{WT} (Figure 7.10) compared to when expressed alone (Figure 7.4); HDAC4$^{M1\text{-}L285}$ was absent from the lobes while varying degrees of intensity were observed for the others, the pattern of which was consistent with those observed previously.

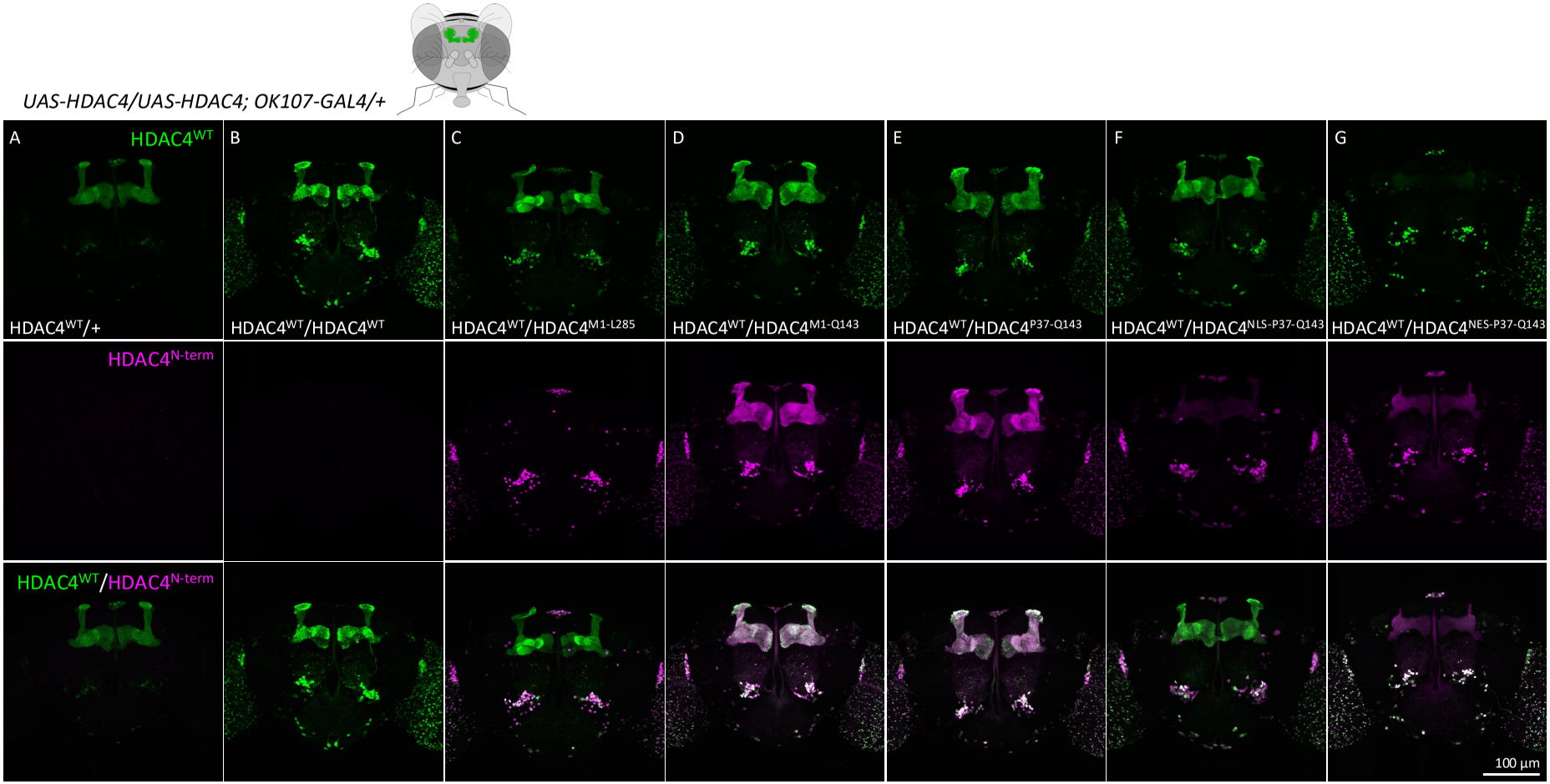

Figure 7.10 Co-expression of HDAC4$^{N\text{-}term}$ differentially affects the subcellular distribution of HDAC4^{WT} in the mushroom body
(A-G) Maximum projections of optical sections (1 µm) through the anterior of the brain demonstrate *OK107-GAL4*-driven expression of HDAC4^{WT}-Myc (green) and HDAC4$^{N\text{-}term}$-HA (magenta) in the adult mushroom body. Flies were raised at 18°C until adults eclosed, which were then transferred to 30°C for three days to induce transgene expression. Each construct was detected in the mushroom body except HDAC4$^{M1\text{-}L285}$.

The effect of expression of each HDAC4$^{N\text{-}term}$ construct on HDAC4^{WT} aggregation in the cell bodies of Kenyon cells was then examined. Expression of one copy of HDAC4^{WT} resulted in formation of punctate aggregates in Kenyon cell nuclei (Figure 7.11A) and increasing the dose of HDAC4^{WT} expression resulted in formation of aggresome-like inclusions (Figure 7.11B). These were reduced in number but increased in size compared to those resulting from expression from one copy of HDAC4^{WT}, as observed previously (Appendix Section 10.4.4.1, Figure 10.36). Strikingly, co-expression of HDAC4$^{M1\text{-}L285}$ significantly altered the distribution of HDAC4^{WT}. While HDAC4$^{M1\text{-}L285}$ remained nuclear (Figure 7.11C) and was relatively unchanged by the co-expression of HDAC4^{WT} (compare Figure 7.11C to 7.5F), HDAC4^{WT} was localised almost exclusively to cytoplasmic haloes. The distribution of HDAC4^{WT} and HDAC4$^{M1\text{-}L285}$ appeared to be mutually exclusive, and nuclear aggregation of HDAC4^{WT} was almost completely eliminated (Figure 7.11C). In contrast, co-expression of HDAC4$^{M1\text{-}Q143}$ or HDAC4$^{P37\text{-}Q143}$ with HDAC4^{WT} did not disrupt HDAC4^{WT} localisation and instead appeared to stabilise aggregation of HDAC4 into aggresome-like inclusions similarly to HDAC4^{WT} homozygotes (Figure 7.11D-E). Aggresome-like inclusions were observed more frequently than punctate aggregates upon co-expression of HDAC4$^{M1\text{-}Q143}$ or HDAC4$^{P37\text{-}Q143}$, however the aggresome-like inclusions were not as large as those in brains of *HDAC4^{WT}* homozygotes. Despite co-localisation with aggregates, both HDAC4$^{M1\text{-}Q143}$ and HDAC4$^{P37\text{-}Q143}$ were still observed within nuclei and in cytoplasmic haloes. The NLS- and NES-containing constructs also stabilised aggregation of HDAC4^{WT}, with aggresome-like inclusions still frequently observed. Interestingly, expression of HDAC4$^{NES\text{-}P37\text{-}Q143}$ reduced cytoplasmic haloes of HDAC4^{WT}, which instead localised within the nucleus and accumulated at the periphery (Figure 7.11G) similarly to HDAC4$^{\Delta NES}$ (Figure 5.25), while HDAC4$^{NES\text{-}P37\text{-}Q143}$ was observed just outside of nuclei. In contrast, both HDAC4^{WT} and HDAC4$^{NLS\text{-}P37\text{-}Q143}$ co-localised in cytoplasmic haloes (Figure 7.11F).

Figure 7.11 Co-expression of HDAC4$^{N\text{-}term}$ affects the aggregation of HDAC4^{WT} in Kenyon cells

(A-G) Single optical sections (0.5 μm) through Kenyon cells in the posterior of the brain demonstrate *OK107-GAL4*-driven expression of HDAC4^{WT}-Myc (green) and HDAC4$^{N\text{-}term}$-HA (magenta). DAPI highlights nuclei (blue). Flies were raised at 18 °C until adults eclosed, which were then transferred to 30 °C for three days to induce transgene expression. Aggregation of HDAC4^{WT} increased with increased dose, resulting in formation of large aggresome-like inclusions within nuclei. All HDAC4$^{N\text{-}term}$ constructs stabilised aggregation of HDAC4^{WT} into aggresome-like inclusions, with the exception of HDAC4$^{M1\text{-}L285}$, which induced cytoplasmic localisation of HDAC4^{WT} and reduced aggregation. Arrowheads in (C) point to punctate HDAC4 aggregates.

These data demonstrate that HDAC4$^{M1\text{-}L285}$ disrupts the aggregation of HDAC4^{WT}, and therefore has significant therapeutic potential in ameliorating phenotypes resulting from HDAC4 aggregation. In contrast, the remaining HDAC4$^{N\text{-}term}$ constructs stabilise aggregation of HDAC4. While this result does not support the utility of these constructs with the original intent of destabilising aggregation, it remains unclear if the composition and dynamics of the aggregates resulting from co-expression of HDAC4^{WT} and HDAC4$^{N\text{-}term}$ differ from those resulting from the expression of only HDAC4^{WT}, and therefore whether these aggregates have the same level of neurotoxicity. Furthermore, it is unclear whether the change in distribution of HDAC4^{WT} has an additional effect. Therefore, all constructs still show a potential for therapeutic benefit, and analysis of the effect of co-expression of these on HDAC4^{WT}-induced neuronal phenotypes remained of interest and was pursued.

7.4.2. HDAC4$^{N\text{-}term}$ constructs differentially modulate HDAC4^{WT}-induced defects in mushroom body development

To facilitate the co-expression of HDAC4^{WT} and HDAC4$^{N\text{-}term}$ for analysis of mushroom body development, *elav-GAL4* and *HDAC4^{WT}* were combined into a single fly line (Appendix Section 10.1.6, Figure 10.8, performed by Dr Helen Fitzsimons). Virgin females of this line were crossed to males harbouring each *HDAC4$^{N\text{-}term}$* construct, progeny were dissected, and mushroom body development assessed via immunostaining for FasII and scored as per Section 3.4.7. All flies were raised at 22 °C. Expression of one copy of HDAC4^{WT} again resulted in significant defects in mushroom body development, the most prominent being β-lobe fusion, as previously observed (Table 7.3, Figure 7.12). The severity of β-lobe fusion increased upon increased dose of HDAC4^{WT}, with 95% of brains from flies homozygous for *HDAC4^{WT}* displaying severe fusion compared to 80% in brains from heterozygous flies. Introduction of a second copy of *HDAC4^{WT}* also resulted in an increase in α-lobe defects. Co-expression of

HDAC4$^{M1\text{-}L285}$ resulted in a reduced percentage of flies displaying total lobe fusion compared to both homozygotes and heterozygotes for *HDAC4^{WT}*, with a significant reduction in severe β-lobe fusion (Figure 7.12), however α-lobe defects remained, and at an increased level compared to *HDAC4^{WT}* heterozygotes (Table 7.3). In contrast, no other HDAC4$^{N\text{-}term}$ construct reduced total lobe fusion compared to brains of flies either hetero- or homozygotes for *HDAC4^{WT}*, and all were increased in severe β-lobe fusion compared to the brains of *HDAC4^{WT}* heterozygotes. Interestingly, addition of an NLS or NES to HDAC4$^{P37\text{-}Q143}$ increased the severity of α-lobe defects compared to HDAC4$^{P37\text{-}Q143}$, suggesting that restriction of nucleocytoplasmic shuttling increases the severity of HDAC4-induced phenotypes.

Table 7.3 Frequency of mushroom body phenotypes resulting from the co-expression of HDAC4$^{N\text{-}term}$ and HDAC4^{WT} at 22°C

(% of brains)	Con	HDAC4^{WT} /+	HDAC4^{WT} /HDAC4^{WT}	HDAC4^{WT} /HDAC4$^{M1\text{-}L285}$	HDAC4^{WT} /HDAC4$^{M1\text{-}Q143}$	HDAC4^{WT} /HDAC4$^{P37\text{-}Q143}$	HDAC4^{WT} /HDAC4$^{NLS\text{-}P37\text{-}Q143}$	HDAC4^{WT} /HDAC4$^{P37\text{-}Q143\text{-}NES}$
α thinning	0	5	40	20	30	20	35	45
α missing	0	0	25	10	5	0	5	5
β thinning	0	0	0	10	0	0	0	0
β missing	0	0	0	5	0	0	0	0
β fusion	**0**	**100**	**100**	**80**	**100**	**100**	**100**	**100**
Mild	0	20	5	30	15	10	0	0
Severe	0	80	95	50	85	90	100	100
Guidance	0	15	5	5	0	0	0	0
n	20	20	20	20	20	20	20	20

Expression of each denoted *HDAC4* transgene was mediated by *elav-GAL4*; virgin *elav-GAL4* female flies that also harboured *HDAC4^{WT}-Myc* were crossed to males harbouring the *HDAC4^{WT}* or *HDAC4$^{N\text{-}term}$* transgene and adult progeny of this cross were dissected and their brains immunostained for FasII to assess mushroom body lobe development. Flies were raised at 22°C. Instances of defects in morphology were scored for n=20 brains per genotype as per methods Section 3.4.7 and are displayed as the % of brains with the indicated phenotype. Control (con) is *elav-GAL4/+*. Percentages may not sum to 100 due to rounding.

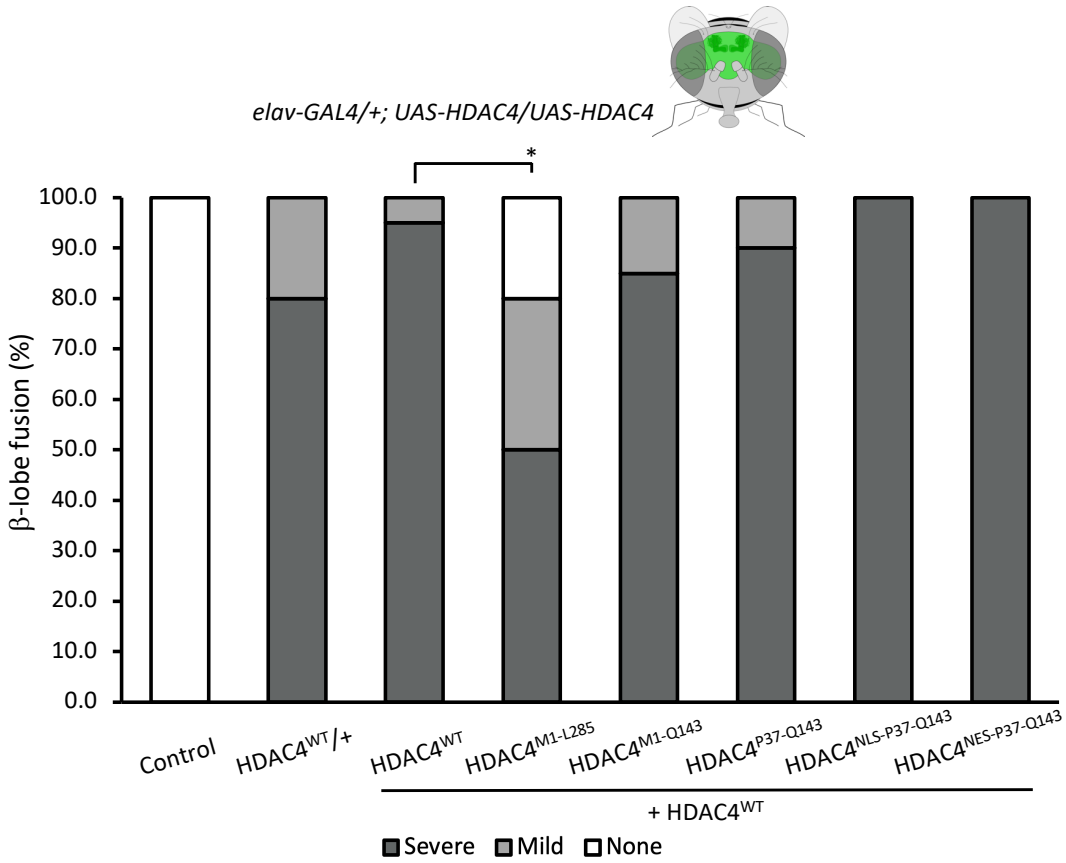

Figure 7.12 Co-expression of HDAC4$^{M1\text{-}L285}$ but no other HDAC4$^{N\text{-}term}$ construct reduces β-lobe fusion induced by HDAC4^{WT} overexpression
Quantification of β-lobe fusion resulting from HDAC4$^{N\text{-}term}$ expression in the presence of HDAC4^{WT}. HDAC4 expression was mediated by *elav-GAL4* at 22°C, adult brains were processed for anti-FasII immunohistochemistry, and β-lobe fusion was scored. Control is *elav-GAL4/+*. n=20 brains per genotype. Severe β-lobe fusion was significantly reduced by co-expression of HDAC4$^{M1\text{-}L285}$ compared to HDAC4^{WT} homozygotes (Fisher's exact test, severe β-lobe fusion, p=0.0033. *p<0.05) but the reduction in severe β-lobe fusion was not significant compared to HDAC4^{WT} heterozygotes (p=0.0958).

7.4.3. HDAC4$^{N\text{-}term}$ constructs differentially modulate HDAC4^{WT}-induced defects in eye development

Each HDAC4$^{N\text{-}term}$ construct was co-expressed with HDAC4^{WT} under the control of *GMR-GAL4* to examine their ability to modulate HDAC4^{WT}-induced defects in eye development. As observed previously, *HDAC4^{WT}* heterozygotes had a mild rough eye phenotype, manifesting predominantly as misalignment of ommatidia (Figure 7.13A), and *HDAC4^{WT}* homozygotes were significantly increased in severity (Figure 7.14), with widespread fusion of ommatidia and loss of pigmentation (Figure 7.13B). Co-expression of HDAC4$^{M1\text{-}L285}$ with HDAC4^{WT} reduced the loss of pigmentation and fusion compared to HDAC4^{WT} homozygotes (Figure 7.13C, Figure 7.14), but loss of pigmentation remained more severe than HDAC4^{WT} heterozygotes, therefore,

unlike in the mushroom body, HDAC4$^{M1\text{-}L285}$ does not reduce the toxicity of HDAC4^{WT} in the eye. The severity of this phenotype increased with the progressive truncations, where co-expression of HDAC4$^{P37\text{-}Q143}$ or HDAC4$^{M1\text{-}Q143}$ with HDAC4^{WT} (Figure 7.13D-E) resulted in a more severe phenotype than with co-expression of HDAC4$^{M1\text{-}L285}$ (Figure 7.14). The progressive increase in severity between these three was consistent with the progressive increases in protein levels detected in Figure 7.3. Interestingly, addition of an NLS significantly reduced the severity of the HDAC4$^{P37\text{-}Q143}$-induced phenotype, almost completely restoring the loss of pigmentation and fusion of ommatidia (Figure 7.13F), but addition of an NES increased the severity of ommatidial fusion (Figure 7.13G).

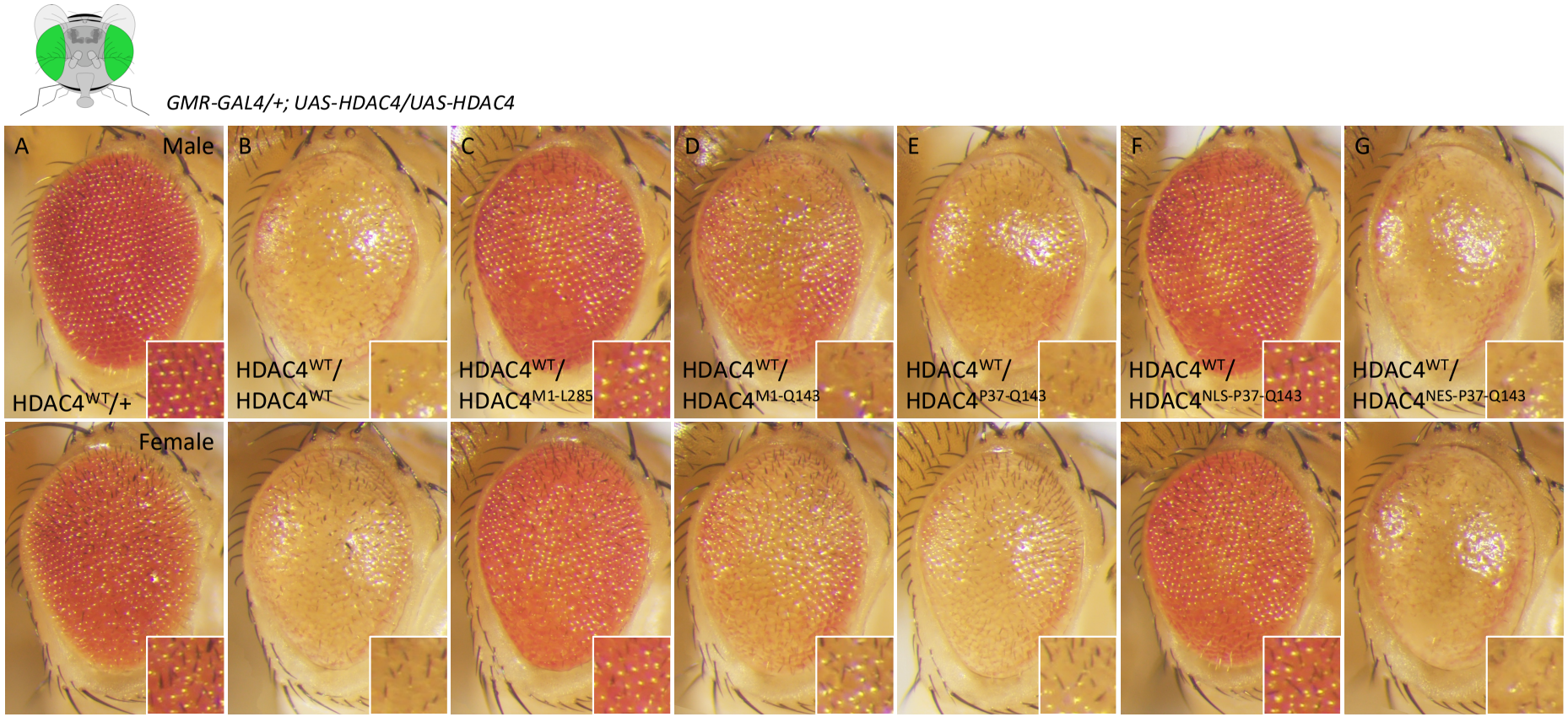

Figure 7.13 Co-expression of HDAC4$^{N\text{-}term}$ increases the severity of HDAC4^{WT}-induced defects in *Drosophila* eye development

(A-G) Light microscopy (110x magnification) images of *Drosophila* eyes raised at 25°C. Inset shows a magnified image of ommatidia. All flies were heterozygous for the *GMR-GAL4* driver (*GMR-GAL4/+*) and copies of *HDAC4* is as noted. (A) Expression of one copy of *HDAC4^{WT}* (*GMR-GAL4/+; UAS-HDAC4^{WT}/+)* induced a mild rough eye phenotype characterised by misalignment of ommatidia and bristles. (B) Increasing the dose of *HDAC4^{WT}* (*GMR-GAL4/+; UAS-HDAC4^{WT}/UAS-HDAC4^{WT}*) increased the severity of the phenotype, where widespread fusion of ommatidia was observed. (C-G) Co-expression of each HDAC4$^{N\text{-}term}$ construct (*GMR-GAL4/+; UAS-HDAC4^{WT}/UAS-HDAC4$^{N\text{-}term}$*) differentially altered the HDAC4^{WT} induced phenotype.

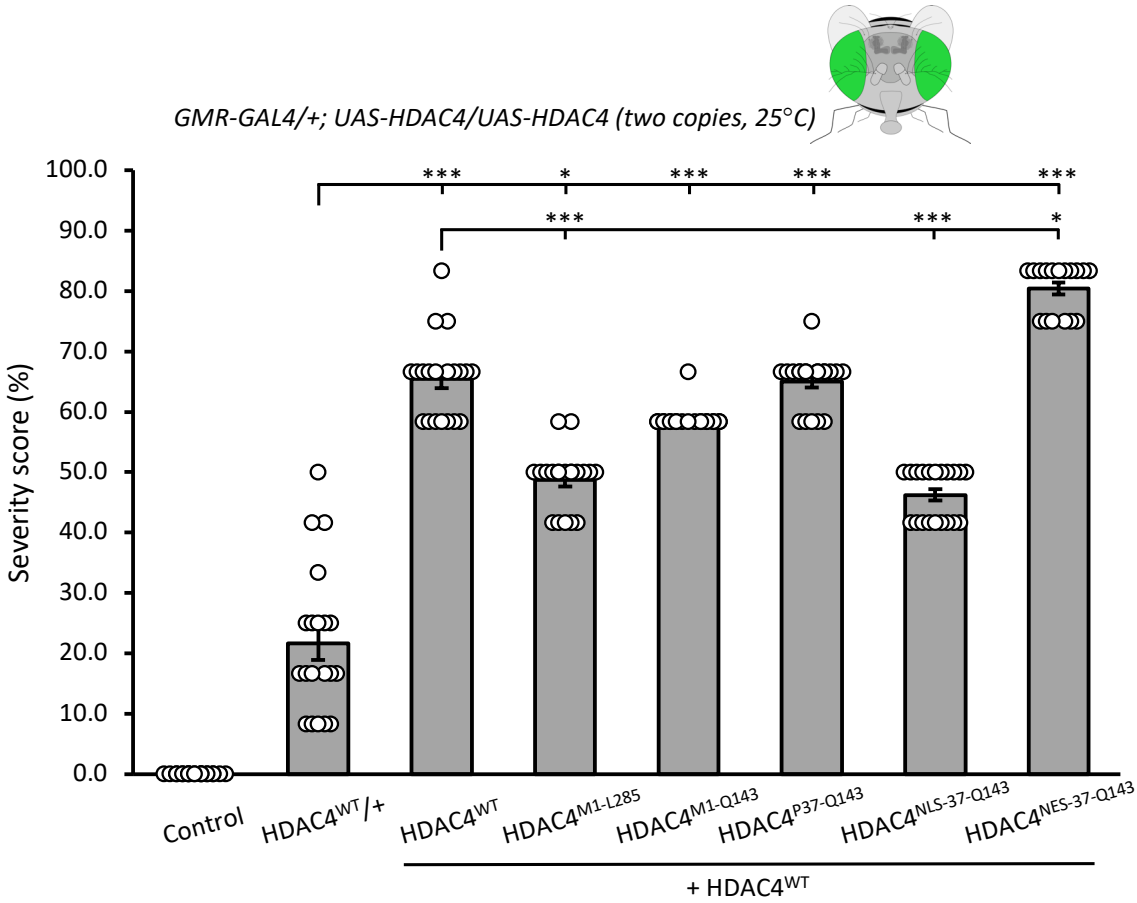

Figure 7.14 Implementation of a scoring system to characterise the modulation of HDAC4^{WT} phenotypes in the adult eye by co-expression of HDAC4$^{N\text{-}term}$

The severity of eye phenotypes resulting from co-expression of HDAC4^{WT} with HDAC4$^{N\text{-}term}$ under the control of *GMR-GAL4* at 25°C was scored as per Section 3.5.1. Flies were heterozygous for *GMR-GAL4* (*GMR-GAL4/+*) and copies of *HDAC4* is as noted. Control is *GMR-GAL4/+; +/+*. Severity scores were converted to % severity and the average is displayed. Individual data points are represented as circles, and error bars indicate the SEM. n≥17 eyes per genotype. There was no significant difference between *HDAC4^{WT}/+* and *HDAC4^{WT}/HDAC4$^{NLS\text{-}P37\text{-}Q143}$* (Kruskal-Wallis test, $H_{(7)}$=146.65, p<0.001, post-hoc Dunn's test, p=0.0879. *p<0.05, **p<0.01, ***p<0.001) or between HDAC4^{WT}/HDAC4^{WT} and HDAC4^{WT}/HDAC4$^{M1\text{-}Q143}$ (p=0.15) and HDAC4^{WT}/HDAC4$^{P37\text{-}Q143}$ (p=0.9622).

The increase in severity of HDAC4^{WT}-induced phenotypes in the eye by co-expression of HDAC4$^{N\text{-}term}$ appears to correlate with the increase in aggregation observed in Kenyon cells (Figure 7.11), therefore it was hypothesised that the increase in severity is related to the stabilisation of HDAC4^{WT} aggregation. To determine whether HDAC4$^{N\text{-}term}$ oligomerises with HDAC4^{WT} to mediate increases in the severity of the eye phenotype, each HDAC4$^{N\text{-}term}$ construct was co-expressed with the F65A mutant of full-length HDAC4 (HDAC4^{F65A}). The F65A mutation alters formation of the hydrophobic core, which is required for oligomerisation and aggregation (Section 1.8.1); it is therefore hypothesised that if HDAC4$^{N\text{-}term}$ constructs exacerbate HDAC4^{WT}-induced phenotypes specifically via oligomerisation, that HDAC4$^{N\text{-}term}$

would not induce an eye phenotype in the presence of HDAC4^{F65A}. As previously observed (Section 4.5.2, Figure 4.18), expression of one copy of HDAC4^{F65A} induced no detectable phenotype (Figure 7.15A, Figure 7.16). Co-expression of HDAC4^{WT} with HDAC4^{F65A} increased the severity of the HDAC4^{F65A} phenotype, and this was more than observed upon expression of one copy of HDAC4^{WT} alone (compare Figure 7.13B and 7.15B). Unlike with HDAC4^{WT}, co-expression of HDAC4$^{N\text{-}term}$ with HDAC4^{F65A} had little impact on the eye development (Figure 7.15C-G, 7.16). Addition of an NES to HDAC4$^{P37\text{-}Q143}$ increased the severity of the HDAC4$^{P37\text{-}Q143}$-induced phenotype in the presence of HDAC4^{F65A} (compare Figure 7.15E 7.15G), however this was very mild and was limited to misalignment of ommatidia with no changes in pigmentation. Together these data confirm that modulation of the HDAC4^{WT} eye phenotypes by HDAC4$^{N\text{-}term}$ is specifically via oligomerisation involving Phe65.

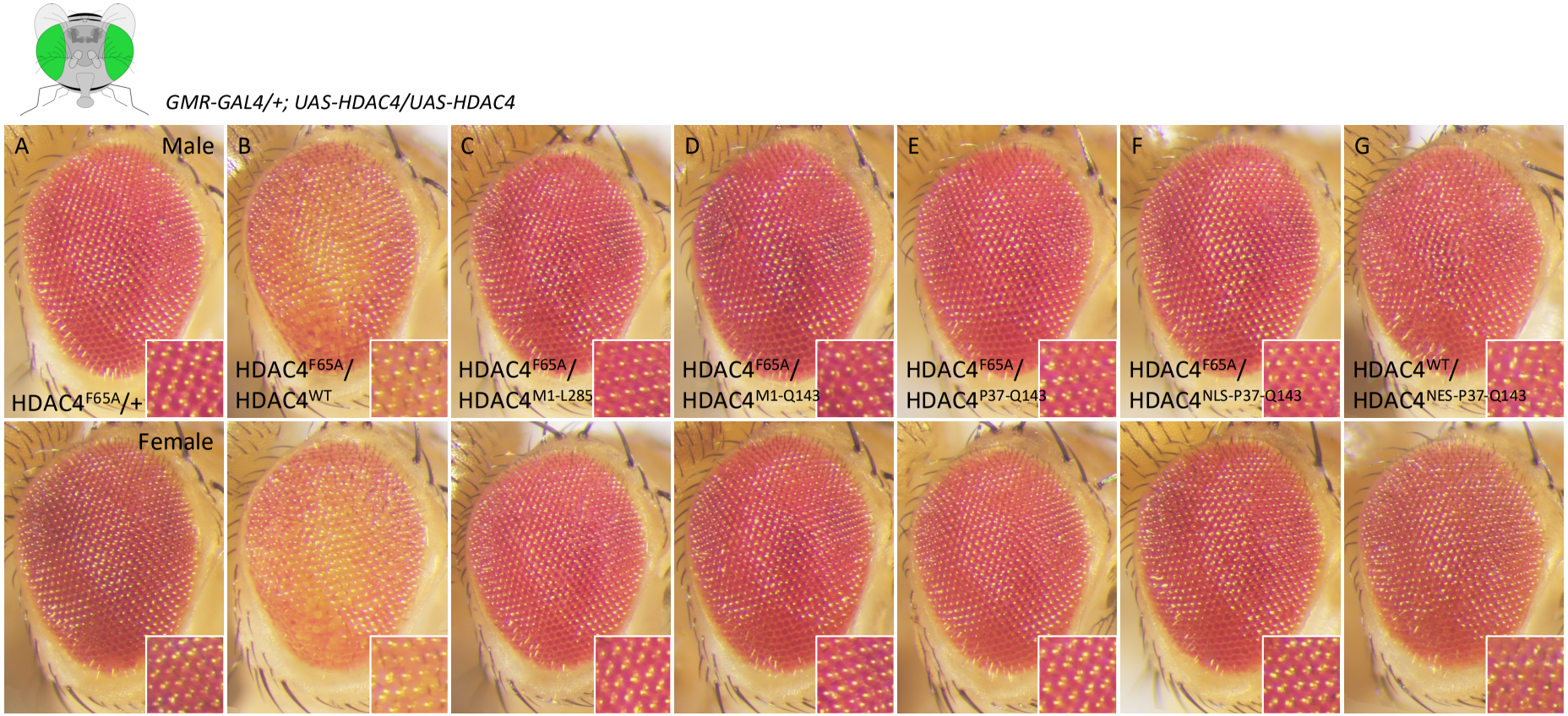

Figure 7.15 Expression of HDAC4$^{N\text{-}term}$ does not significantly alter *Drosophila* eye development in the presence of HDAC4^{F65A}

(A-G) Light microscopy (110x magnification) images of *Drosophila* eyes raised at 25°C. Inset shows a magnified image of ommatidia. All flies were heterozygous for the *GMR-GAL4* driver (*GMR-GAL4/+*) and copies of *HDAC4* is as noted. (A) Expression of one copy of HDAC4^{F65A} (*GMR-GAL4/+; UAS-HDAC4^{F65A}/+)* did not induce a rough eye phenotype. (B) Co-expression of HDAC4^{F65A} and HDAC4^{WT} (*GMR-GAL4/+; UAS-HDAC4^{F65A}/UAS-HDAC4^{WT}*) resulted in a rough eye phenotype consisting of misalignment of ommatidia, fusion, and loss of pigmentation. (C-F) Co-expression of HDAC4$^{N\text{-}term}$ with HDAC4^{F65A} (*GMR-GAL4/+; UAS-HDAC4^{F65A}/UAS-HDAC4$^{N\text{-}term}$)* did not induce a rough eye phenotype, except for HDAC4$^{NES\text{-}P37\text{-}Q143}$ (G), which had slight misalignment of ommatidia.

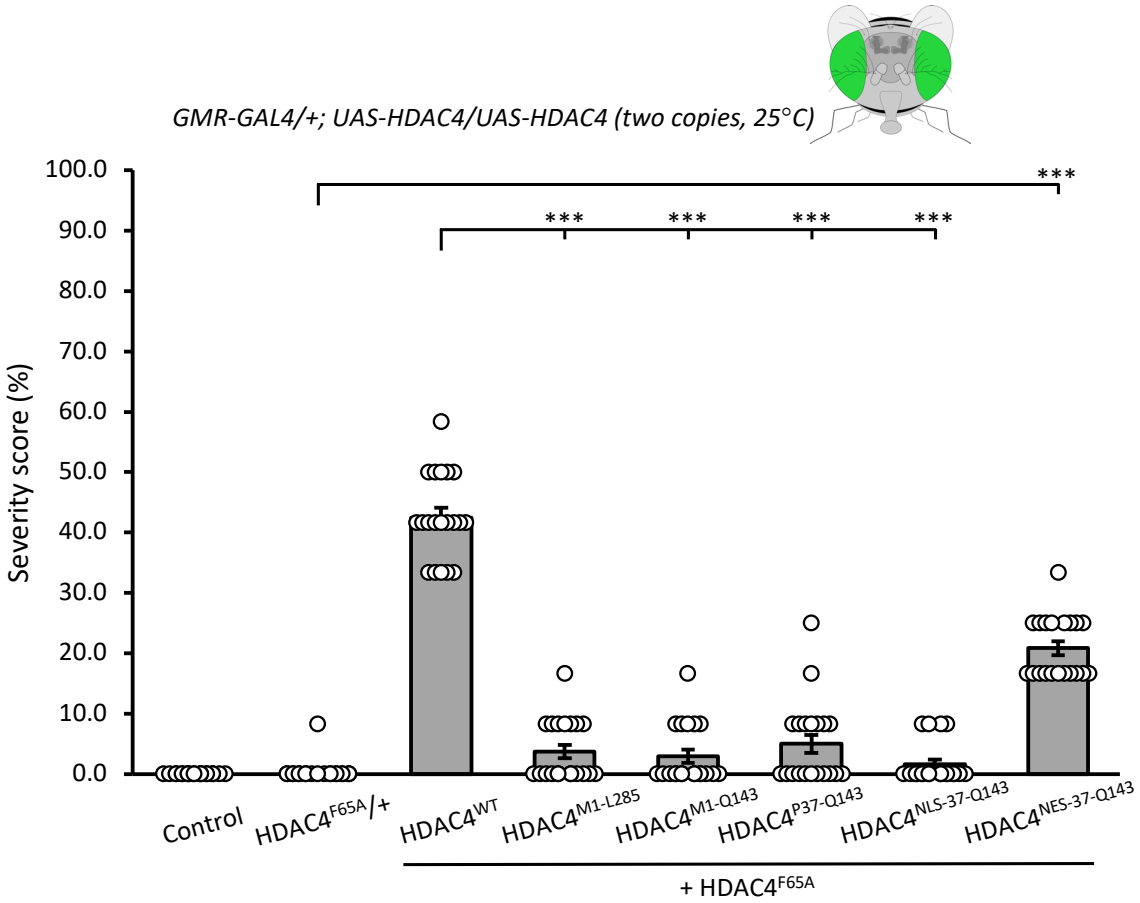

Figure 7.16 Implementation of a scoring system to characterise the modulation of HDAC4^{F65A} phenotypes in the adult eye by co-expression of HDAC4$^{N\text{-}term}$

The severity of eye phenotypes resulting from co-expression of HDAC4^{F65A} with HDAC4$^{N\text{-}term}$ under the control of *GMR-GAL4* at 25°C was scored as per Section 3.5.1. Flies were heterozygous for *GMR-GAL4* (*GMR-GAL4/+*), and copies of *HDAC4* is as noted. Control is *GMR-GAL4/+; +/+*. Severity scores were converted to % severity and the average is displayed. Individual data points are represented as circles, and error bars indicate the SEM. n=20 eyes per genotype. There was no significant difference between HDAC4^{F65A}/+ and HDAC4^{F65A}/HDAC4$^{M1\text{-}L285}$ (Kruskal-Wallis test, $H_{(7)}$=118.40, p<0.001, post-hoc Dunn's test, p=0.1061. ***p<0.001), HDAC4^{F65A}/HDAC4$^{M1\text{-}Q143}$ (p=0.24), HDAC4^{F65A}/HDAC4$^{P37\text{-}Q143}$ (p=0.05087), and HDAC4^{F65A}/HDAC4$^{NLS\text{-}P37\text{-}Q143}$ (p=0.5082), nor between HDAC4^{F65A}/HDAC4^{WT} and HDAC4^{F65A}/HDAC4$^{NES\text{-}P37\text{-}Q143}$ (p=0.1049).

7.5. Discussion

This chapter sought to evaluate an approach to disrupt the nuclear aggregation of HDAC4, in order to ameliorate defects in neuronal development associated with HDAC4 overexpression. To achieve this, a strategy was devised that took advantage of the ability of HDAC4 to oligomerise, and involved expression of progressive N-terminal truncations of HDAC4, each of which were likely to be able to form tetramers with $HDAC4^{WT}$ and were therefore hypothesised to disrupt aggregation (Section 7.1). Expression of $HDAC4^{N\text{-}term}$ alone was not sufficient to induce defects in the development of the mushroom body and eye, however co-expression with $HDAC4^{WT}$ largely increased the severity of phenotypes compared to those resulting from expression of $HDAC4^{WT}$ alone, as $HDAC4^{N\text{-}term}$ stabilised aggregation of $HDAC4^{WT}$. The exception however was $HDAC4^{M1\text{-}L285}$, which induced cytoplasmic localisation of $HDAC4^{WT}$ in Kenyon cells and decreased the severity of β-lobe fusion in the mushroom body upon co-expression.

These data increase understanding of the functions of the N-terminus of HDAC4 as well as downstream regions in the context of dynamics of HDAC4 aggregation, and emphasise that targeting nuclear aggregation of HDAC4 will reduce the severity of neuronal dysfunction. Importantly, they identify that targeting the interaction between HDAC4 and MEF2 will be critical to reducing the degree of HDAC4 nuclear accumulation and aggregation, as well as the severity of aggregation-dependent defects in neuronal development. Moreover, the finding that the N-terminal region of HDAC4 stabilises aggregation of full-length HDAC4 is novel, and given that generation of N-terminal HDAC4 products occurs in response to cellular stress (Section 1.5.1.4), this advances knowledge of a potential way through which HDAC4 aggregation may be induced and/or stabilised in disease.

For ease of reference the data in this chapter are summarised in Table 7.4 below.

Table 7.4 Summary of the data presented in this chapter

	Con	HDAC4 WT	HDAC4 M1-L285	HDAC4 M1-Q143	HDAC4 P37-Q143	HDAC4 NLS-P37-Q143	HDAC4 P37-Q143-NES
Regions contained within construct	-	as below		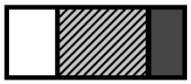		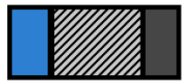	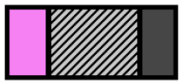
Aggregation Green, HDAC4 Blue, DAPI	-	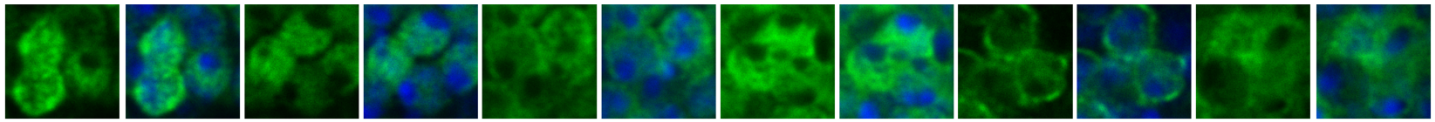					
Aggregation +WT Green, HDAC4^{WT} Magenta, HDAC4$^{N\text{-}term}$	-	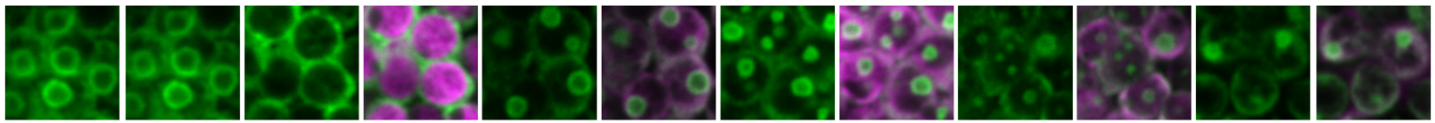					
Severe β-fusion	0.0	**70.0**	0.0	0.0	0.0	0.0	0.0
Severe β-fusion +WT	0.0	**95.0**	50.0	85.0	90.0	100.0	100.0
Eye defects	0.0	**21.7**	1.7	8.3	1.3	0.0	14.2
Eye defects +WT	0.0	**65.4**	48.8	58.8	65.0	46.3	80.4

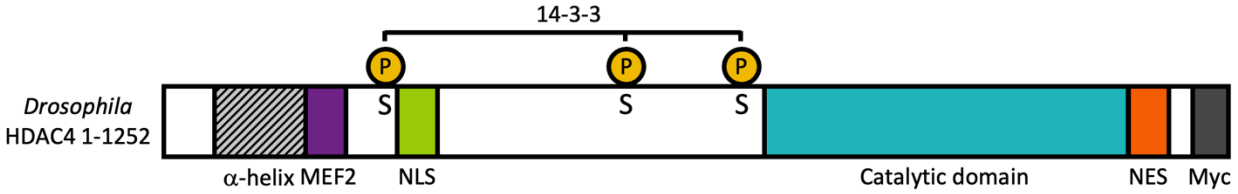

Aggregate images are from Figures 7.5 and 7.11. Severe β-fusion is the % of brains with fusion from Tables 7.2 and 7.3. Eye defects is the average severity score (%) from Figures 7.9 and 7.14. Con is control, and is as denoted in the legends/tables of the aforementioned figures/tables. The A in HDAC4$^{M1\text{-}L285}$ denotes the S239A mutation that was made to prevent 14-3-3 binding of this construct. HDAC4^{WT} + HDAC4^{WT} denotes expression of HDAC4^{WT} from two genomic insertions (homozygotes).

7.5.1. The N-terminal region of HDAC4 stabilises aggregation of full-length HDAC4 in neuronal nuclei

When expressed alone, aggregation of HDAC4$^{N\text{-}term}$ was observed infrequently, and aggregates were smaller and fewer than those resulting from expression of HDAC4^{WT}. It is hypothesised that similarly to the aggregation observed for HDAC4 oligomerisation mutants, aggregation of HDAC4$^{N\text{-}term}$ is stabilised by the presence of endogenous HDAC4 (Section 4.7.1.2). Therefore, it is likely that aggregation of HDAC4$^{N\text{-}term}$ would be even further reduced in the absence of endogenous HDAC4. It is important to note that given that HDAC4 aggregation is dose dependent, as are HDAC4-overexpression induced phenotypes (Section 5.6.1, Tan *et al.* (2024)), it is unclear how appropriate the comparison of HDAC4$^{N\text{-}term}$ aggregation is to HDAC4^{WT} as there is no data comparing the protein levels between the two. It is possible that the protein levels of HDAC4$^{N\text{-}term}$ may be lower than for HDAC4^{WT}, resulting in reduced aggregation and severity of phenotypes. However, increasing the level of HDAC4$^{N\text{-}term}$ expression by increasing the number of transgene copies in the eye did not induce a phenotype, unlike HDAC4^{WT}, suggesting that increased dose may not induce aggregation of HDAC4$^{N\text{-}term}$. Together these data suggest that aggregation of HDAC4 is largely facilitated by regions downstream of L285.

Consistent with the positive correlation between aggregation and neurodevelopmental defects in the mushroom body and eye (Section 4.5), expression of HDAC4$^{N\text{-}term}$ did not impart significant defects in neuronal development compared to full-length HDAC4^{WT}. Therefore, these data support the relationship between HDAC4 aggregation and defects in neuronal development. Moreover, these data demonstrate that in addition to facilitating aggregation, regions downstream of the N-terminus are required for pathogenicity. It is again suggested that this may be mediated in part via the aberrant sequestration of proteins to aggregates.

When co-expressed with HDAC4^{WT}, all HDAC4$^{N\text{-}term}$ constructs except for HDAC4$^{M1\text{-}L285}$ increased HDAC4^{WT} aggregation in Kenyon cells; when only HDAC4^{WT} was expressed, aggregates were punctate and more numerous, but in the presence of HDAC4$^{N\text{-}term}$, most aggregates coalesced into fewer aggresome-like inclusions within nuclei, and this was similar to the aggregation of HDAC4^{WT} observed when the dose of expression was doubled. The effect of HDAC4$^{M1\text{-}L285}$ on aggregation is further discussed in Section 7.5.2. While these data suggest that HDAC4$^{N\text{-}term}$ is capable of oligomerising with HDAC4^{WT}, these data do not support the

original hypothesis that HDAC4$^{N\text{-term}}$ would interfere with aggregation of HDAC4^{WT}, and instead suggest that HDAC4$^{N\text{-term}}$ expression stabilises the formation of HDAC4^{WT} aggregates (summarised in Figure 7.17). It is possible that the presence of HDAC4$^{N\text{-term}}$ in these aggregates may affect their dynamics and therefore modulate neurotoxicity, however this was not sufficient to decrease the severity of neurodevelopmental phenotypes as co-expression of HDAC4$^{N\text{-term}}$ and HDAC4^{WT} increased the severity of phenotypes compared to HDAC4^{WT} overexpression alone. Therefore, these data reinforce the positive correlation between aggregation of HDAC4 and severity of defects in neuronal development. These findings also confirm that oligomerisation of HDAC4 does not require regions downstream of the helix within each monomer, consistent with the tetramerisation observed by Guo *et al.* (2007).

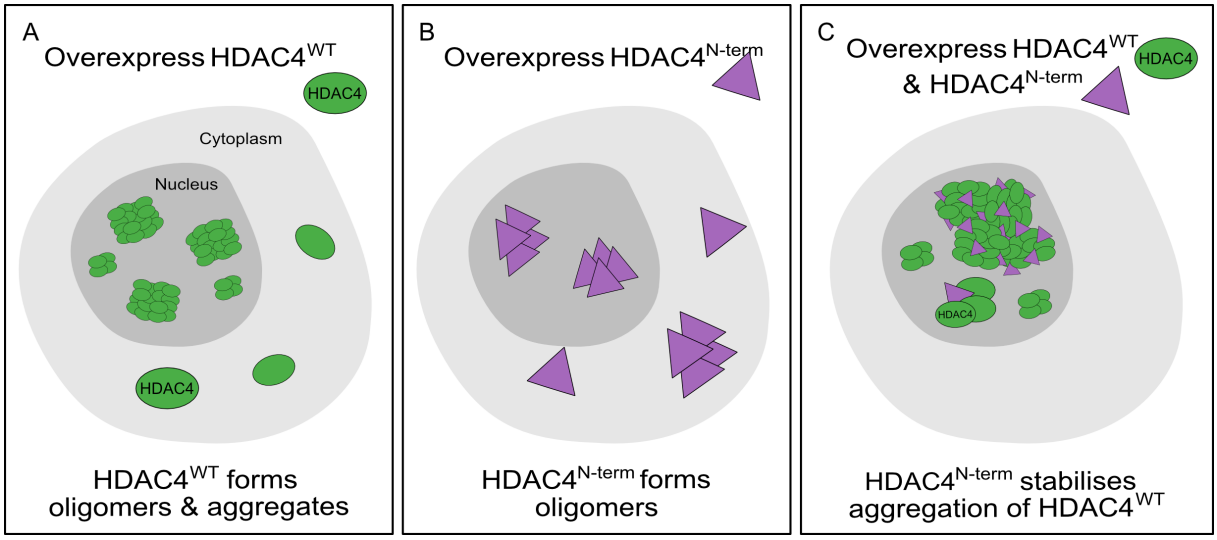

Figure 7.17 HDAC4$^{N\text{-term}}$ has little intrinsic ability to aggregate, but stabilises aggregation of HDAC4^{WT}
Schematic diagram depicting the oligomerisation and aggregation of HDAC4^{WT} and HDAC4$^{N\text{-term}}$. (A) Overexpression of HDAC4^{WT} results in nuclear aggregation. (B) Overexpression of HDAC4$^{N\text{-term}}$ results in nuclear oligomerisation. (C) Co-expression of HDAC4^{WT} and HDAC4$^{N\text{-term}}$ increases nuclear aggregation. *This figure is an original artwork.*

How does HDAC4$^{N\text{-term}}$ stabilise aggregation of HDAC4^{WT}? When measured in solution, HDAC4 N-terminal tetramers are in a dynamic equilibrium between monomeric, dimeric, trimeric and tetrameric states (Guo *et al.*, 2007). It is likely that oligomerisation occurs with full-length HDAC4, as mutations that disrupt tetramerisation in solution (Guo *et al.*, 2007) disrupt oligomerisation *in vivo* (Section 4.3.3), however it is hypothesised that tetramers that contain both full-length HDAC4^{WT} and HDAC4$^{N\text{-term}}$ have altered dynamics of formation compared to those containing only full-length HDAC4^{WT}. While the model of HDAC4

tetramers presented in Section 4.7.5 assembled from the AlphaFold predicted structure suggests that tetramerisation of the N-terminal α-helix of HDAC4 is spatially compatible with the conformation of downstream regions (Section 4.7.5, Figure 4.28), particularly the deacetylase domain, it is likely that tetramers containing $HDAC4^{N\text{-}term}$ are more stable as the absence of downstream domains reduces steric hinderance which may otherwise destabilise tetramer formation. That is to say, tetramers that contain only $HDAC4^{WT}$ may be more dynamic (i.e. less stable) than those that contain both $HDAC4^{WT}$ and $HDAC4^{N\text{-}term}$, which are more stable due to reduced interference of downstream domains with tetramer formation, aiding in finding a stable conformation that results in aggregation. Moreover, in light of the findings by Dai *et al.* (2024), it is possible that $HDAC4^{N\text{-}term}$ may more effectively facilitate higher order oligomerisation via interface II interactions as discussed in Section 5.6.5. Therefore, although $HDAC4^{N\text{-}term}$ lacks downstream regions compared to $HDAC4^{WT}$ that are likely to stabilise aggregation via the recruitment of proteins such as MEF2, the increase in stability by reduction of steric hinderance compensates for this, and therefore $HDAC4^{N\text{-}term}$ stabilises aggregation similarly to increased dose of $HDAC4^{WT}$. Further examination of this is crucial if future investigations focus on disrupting oligomerisation of HDAC4 to reduce aggregation.

While these studies do not support the utility of an N-terminal region of HDAC4 in directly interfering with HDAC4 aggregation and therefore reducing the severity of phenotypes relating to aggregation, this may still be possible with slight modifications. As $HDAC4^{N\text{-}term}$ did not increase the severity of $HDAC4^{F65A}$ phenotypes in the eye, it is likely that $HDAC4^{N\text{-}term}$ does not oligomerise with $HDAC4^{F65A}$ and therefore does not induce its aggregation. Considering this it would be interesting to repeat these studies with $HDAC4^{N\text{-}term}$ constructs that contain the F65A mutation; it is hypothesised that these may instead interfere with oligomerisation of $HDAC4^{WT}$ and would not promote aggregation due to both the F65A mutation, and the absence of downstream regions.

7.5.1.1. Implications of HDAC4 aggregate stabilisation in a disease context

Stabilisation of HDAC4 aggregation by the N-terminus of HDAC4 has implications in the context of cellular homeostasis as HDAC4 undergoes cleavage to produce N-terminal products in response to cellular stress (Section 1.5.1.4). The effect of $HDAC4^{N\text{-}term}$ production on full-length HDAC4 in this context has not been examined; in light of the findings presented here, it

is possible that production of HDAC4$^{N\text{-}term}$ may have a dominant negative effect. When HDAC4 cleavage is stimulated, the N-terminal product enters the nucleus to stimulate a response (Backs *et al.*, 2011; Paroni *et al.*, 2004), therefore, in addition to this characterised protective role, HDAC4$^{N\text{-}term}$ may also induce and/or stabilise aggregation of full-length HDAC4. It is known that both UV-damage and oxidative stress induce this response (Liu *et al.*, 2004; Paroni *et al.*, 2004; Zhang *et al.*, 2014), and given the link between oxidative stress and neurodegenerative disease (reviewed in Uttara *et al.* (2009)) it is possible that this mechanism may in fact aid in disease progression by further inducing cellular stress via HDAC4 aggregation. In light of this, it is essential that future research focuses on further understanding the scenarios in which HDAC4 N-terminal fragments are produced, such as whether this is a common response to cellular stress, and considers their generation in the context of diseases in which HDAC4 is upregulated. This may aid in understanding disease progression and be an important consideration for the development of disease therapeutics.

7.5.2. Targeting the interaction between HDAC4 and MEF2 may be of therapeutic benefit

Interestingly, while HDAC4$^{M1\text{-}Q143}$ and HDAC4$^{P37\text{-}Q143}$ stabilised aggregation of HDAC4^{WT}, the same was not observed for HDAC4$^{M1\text{-}L285}$, which instead accumulated in the nucleus while rendering HDAC4^{WT} largely cytoplasmic, and moreover, few nuclear aggregates were observed. While the lack of stabilisation of aggregation may be a result of HDAC4$^{M1\text{-}L285}$ having a lower protein level than HDAC4$^{M1\text{-}Q143}$ and HDAC4$^{P37\text{-}Q143}$, the protein level was comparable to HDAC4$^{NLS\text{-}P37\text{-}Q143}$, which still stabilised aggregation. Therefore, it is most likely that it is an effect of the presence of the MEF2 binding domain, which is absent from all other HDAC4$^{N\text{-}term}$ constructs.

MEF2 mediates the nuclear import of HDAC4 (Section 1.5.1.2). Studies by Paroni *et al.* (2007) demonstrated that an N-terminal fragment of HDAC4, hHDAC4$^{M1\text{-}D289}$, has a higher binding affinity for MEF2 than full-length HDAC4. It is hypothesised that the HDAC4 N-terminal α-helix undergoes conformational changes upon MEF2 binding (Dai *et al.*, 2024); these may occur more readily with HDAC4$^{M1\text{-}L285}$ than with HDAC4^{WT}, resulting in more effective binding. In light of this, it is hypothesised that HDAC4$^{M1\text{-}L285}$ has a higher affinity for MEF2 than HDAC4^{WT}; when co-expressed, HDAC4$^{M1\text{-}L285}$ therefore undergoes preferential MEF2-dependent nuclear import, thus titrating MEF2 and leaving HDAC4^{WT} in the cytoplasm.

Moreover, the loss of MEF2 binding to HDAC4^{WT} likely prevents MEF2-dependent stabilisation of aggregation (Section 5.6.5). Given the slight reduction in the severity of the mushroom body phenotype observed upon co-expression of HDAC4$^{M1\text{-}L285}$ with HDAC4^{WT}, these data suggest that targeting the interaction between HDAC4 and MEF2 may be a promising avenue to reduce nuclear aggregation and associated neurotoxicity.

It is likely that the residual phenotype of β-lobe fusion resulting from co-expression of HDAC4$^{M1\text{-}L285}$ and HDAC4^{WT} is a result of the nuclear aggregation that still occurred. Indeed, in cell culture, expression of an N-terminal region of HDAC4 including the helix and MEF2 binding region induced aggregation of MEF2 (Chan *et al.*, 2003). Therefore, to further reduce the interaction between HDAC4^{WT} and MEF2 it would be interesting to investigate whether co-expression of the minimal MEF2 binding region within HDAC4 (excluding the helix that mediates oligomerisation, HDAC4^{MEF2}) would out-compete HDAC4^{WT} for MEF2 binding without inducing nuclear aggregation. The MEF2 binding domain of HDAC4 is relatively discrete; short regions of HDAC4 encompassing only the MEF2 binding region have been demonstrated to interact with MEF2 (Jayathilaka *et al.*, 2012) and repress MEF2-dependent transcription (Chan *et al.*, 2003). Importantly, this region was not sufficient to induce nuclear aggregation of MEF2, unlike longer fragments or full-length HDAC4 (Chan *et al.*, 2003). It is therefore possible that expression of HDAC4^{MEF2} may out-titrate HDAC4^{WT} with respect to MEF2 binding, preventing the nuclear import of HDAC4^{WT} as well as MEF2-dependent stabilisation of aggregation, and thus reducing neurotoxicity associated with HDAC4 aggregation.

Alternatively, small molecule inhibitors could be used to target the interaction between HDAC4 and MEF2. BML-210 is thought of as a classical HDAC inhibitor (Wong *et al.*, 2003) and has been identified to disrupt the interaction between HDAC4 and MEF2 *in vitro*, and an analogue of this reduced the abundance of nuclear HDAC4 in cell culture (Jayathilaka *et al.*, 2012). Reduced interaction of HDAC4 and MEF2 following BML-210 administration was also detected in mouse hippocampal lysates, and this correlated with reversion of learning and memory defects in a mouse model of Huntington's disease (Vidal-Sancho *et al.*, 2020). Treatment of flies overexpressing HDAC4^{WT} with BML-210 may therefore reduce the interaction of HDAC4^{WT} with MEF2, reducing nuclear import and aggregation of HDAC4 as well as reducing the associated neurotoxicity.

In addition, HDAC4^{WT} likely displays increased 14-3-3 binding upon co-expression of HDAC4$^{M1\text{-}L285}$ due to both its cytoplasmic distribution and the fact that HDAC4$^{M1\text{-}L285}$ was mutated to prevent 14-3-3 binding (i.e. HDAC4$^{M1\text{-}L285}$ does not compete with HDAC4^{WT} for 14-3-3 binding). This is likely to reinforce the cytoplasmic distribution of HDAC4^{WT} (Section 1.5.1.3), in addition to modulating its aggregation (Segal *et al.* (2023), Section 5.6.6). Therefore, enhancing the interaction between HDAC4 and 14-3-3 may also aid in preventing HDAC4-overexpression induced defects in neuronal function.

The effect of HDAC4$^{M1\text{-}L285}$ on HDAC4^{WT} also provides insight into the MEF2-dependent mechanisms through which HDAC4 disrupts neurodevelopment. The ability of HDAC4 to impair mushroom body development, specifically inducing β-lobe fusion, is dependent on its interaction with MEF2; mutation of the MEF2 binding region of HDAC4 prevents overexpression-induced β-lobe fusion (Main *et al.*, 2021; Tan *et al.*, 2024), as does knockdown of MEF2 in the presence of nuclear HDAC4 (Main *et al.*, 2021), while overexpression of MEF2 alongside HDAC4 overexpression exacerbates β-lobe fusion (Section 5.4.3). It could be hypothesised that HDAC4 is mediating this effect via traditional repression of MEF2, however this is unlikely as knockdown of MEF2 alone does not induce β-lobe fusion (Main *et al.*, 2021), suggesting a novel effect of HDAC4^{WT} on MEF2 function. The fact that HDAC4$^{M1\text{-}L285}$ did not induce β-lobe fusion alone suggests that this region is insufficient to govern the effect that HDAC4^{WT} expression has on MEF2, i.e. in addition to MEF2 binding, HDAC4 requires downstream regions to impair β-lobe development. Moreover, the analogous region of human HDAC4 was still sufficient to repress MEF2-dependent transcription (Paroni *et al.*, 2007) further alluding to an effect of HDAC4^{WT} via MEF2 independent of transcriptional repression. It is possible that this may be related to the upregulation of MEF2 intensity observed in Kenyon cells (Section 5.3), therefore it would be of interest to determine whether HDAC4$^{M1\text{-}L285}$ similarly increases MEF2 in Kenyon cells.

In summary, these data demonstrate that it is essential that further research into the role of HDAC4 in a disease context considers novel effects, independent of both deacetylation and its ability to repress MEF2-dependent transcription.

7.5.3. Modulating the subcellular distribution of HDAC4 may be of therapeutic benefit

The distributions of each of the HDAC4$^{N\text{-}term}$ constructs was consistent with previous studies that examined the distribution of N-terminal products of HDAC4; HDAC4$^{M1\text{-}L285}$ predominantly localised to nuclei similarly to that of the Asp289 cleavage product of hHDAC4 (Paroni *et al.*, 2004), while HDAC4$^{M1\text{-}Q143}$ and HDAC4$^{P37\text{-}Q143}$ were pan-cellular similarly to progressive truncations of hHDAC4 which removed the NLS and MEF2 binding domains (Wang & Yang, 2001). The nuclear localisation of HDAC4$^{M1\text{-}L285}$ is consistent with the presence of the MEF2 binding domain and the NLS, which both mediate nuclear import, and the absence of 14-3-3 binding sites and an NES, which mediate nuclear export, within this construct. The pan-cellular localisation of the remaining constructs is consistent with the absence of intrinsic shuttling signals, but the ability to oligomerise with endogenous HDAC4 which may facilitate nucleocytoplasmic shuttling. However, addition of an exogenous NLS or NES to the minimal HDAC4$^{P37\text{-}Q143}$ truncation did not induce absolute changes in its distribution.

The NLS added to HDAC4$^{P37\text{-}Q143}$ was selected for its previously illustrated efficiency in delivering GFP to the nucleus (Shiga *et al.*, 1996). When individually expressed, HDAC4$^{P37\text{-}Q143}$ was present in both the nucleus and cytoplasm, including the axonal bundles of the mushroom body lobes. HDAC4$^{NLS\text{-}P37\text{-}Q143}$ was reduced in axonal distribution in the lobes, but addition of the NLS did not enforce exclusive nuclear localisation, and it instead accumulated at the nuclear periphery. In contrast, addition of the NES, which was also previously successful in targeting proteins to the cytoplasm in *Drosophila* (Bajusz *et al.*, 2021), did not reduce nuclear localisation of HDAC4$^{NES\text{-}P37\text{-}Q143}$ compared to HDAC4$^{P37\text{-}Q143}$. It is likely that the lack of absolute changes in HDAC4$^{N\text{-}term}$ distribution upon addition of an exogenous NLS/NES is due in part to blocking of HDAC4$^{N\text{-}term}$ shuttling via oligomerisation with endogenous HDAC4. Stable oligomers of HDAC4$^{N\text{-}term}$ and endogenous HDAC4 may not be as efficiently transported through the nucleopore complex compared to monomers due to their size, therefore impeding the action of the exogenous NLS and NES. Endogenous HDAC4 may also confer localisation of HDAC4$^{N\text{-}term}$ dominant to the exogenous NLS/NES by its intrinsic shuttling. It is therefore hypothesised that in the absence of endogenous HDAC4, absolute changes in the distribution of these constructs would have been observed.

However, expression of HDAC4$^{NES\text{-}P37\text{-}Q143}$ had an unexpected dramatic effect on the distribution of HDAC4^{WT}, where HDAC4^{WT} was almost entirely localised to nuclei and gathered at the nuclear periphery while HDAC4$^{NES\text{-}P37\text{-}Q143}$ localised more to cytoplasmic haloes. The distribution of HDAC4^{WT} in the presence of HDAC4$^{NES\text{-}P37\text{-}Q143}$ is reminiscent of that of HDAC4$^{\Delta NES}$ (Figure 5.25). This suggests that the NES of HDAC4$^{NES\text{-}P37\text{-}Q143}$ is acting in trans to compete with the NES within HDAC4^{WT} for nuclear export, which prevents the nuclear export of HDAC4^{WT}, thus functionally rendering HDAC4^{WT} as HDAC4$^{\Delta NES}$. However, the same cannot be said for HDAC4$^{NLS\text{-}P37\text{-}Q143}$, as its distribution and that of HDAC4^{WT} remained relatively unaltered upon co-expression. It is unclear whether a different NLS would be able to more effectively compete with that within HDAC4^{WT} as the NES used here did; further exploration of this is of significant interest as an approach to alter HDAC4 distribution to reduce nuclear aggregation, where expression of a short peptide including a competitor NLS may render HDAC4 cytoplasmic and prevent nuclear aggregation.

Together these data indicate that altering the distribution of HDAC4^{WT} is most effective via competition for the machinery that facilitates such distribution. This includes competing for MEF2 binding, and thus MEF2-dependent nuclear import (as achieved by HDAC4$^{M1\text{-}L285}$, discussed above). HDAC4 also undergoes conformational changes in a redox-dependent manner to reveal its NES for nuclear export (Ago *et al.*, 2008). Therefore, an alternative approach to reduce nuclear localisation of HDAC4 may include treatment with drugs that support the conformation of HDAC4 in which the NES is exposed. LMK235 is a small molecule inhibitor of HDAC4 (Marek *et al.*, 2013), and in a mouse model of CDKL5 disorder in which nuclear accumulation of HDAC4 is observed, LMK235 treatment decreased nuclear localisation of HDAC4 and improved neuronal survival and dendritic outgrowth (Trazzi *et al.*, 2016). LMK235 also reduced lead-induced nuclear accumulation of HDAC4 in PC12 cells (Gu *et al.*, 2020). While the mechanism through which LMK235 affects HDAC4 distribution is unknown, the binding site within the C-terminus is nearby the cysteine residues that regulate redox-dependent conformational changes (Ago *et al.*, 2008; Marek *et al.*, 2013), therefore it is possible that LMK235 supports the NES-exposed conformation of HDAC4 to induce nuclear export. In light of this it would be interesting to treat HDAC4-overexpressing flies with LMK235 and examine the distribution of HDAC4 as well as neurodevelopment of these flies.

Chapter Eight

Summary, reflections & future directions

8. Summary, reflections, & future directions

The data presented in this thesis provide a comprehensive advancement in the knowledge surrounding the mechanisms through which HDAC4 aggregates form in neuronal nuclei, and how these correlate with defects in neuronal development. Together, they also provide many new avenues for investigation of HDAC4 function as well as therapeutic targets for diseases in which HDAC4 is dysregulated. The main findings of this thesis are summarised below, along with avenues for further investigation.

8.1. The utility of *Drosophila* as a model organism

Drosophila provide a powerful model for elucidating molecular pathways and examining their roles in neuronal development and function, and have facilitated the entirety of studies presented in this thesis. The extent of the power of genetic tools already available remains limited however, largely due to a lack of technical data. One of the later experiments performed during this study was a direct comparison of the patterns and levels of expression governed by neuronal GAL4 driver lines (Hawley *et al.*, 2023). This study provided crucial quantification of the level of transgene expression driven by *OK107-GAL4* compared to *elav-GAL4* in the mushroom body, a key structure that has been examined for developmental defects in this thesis. Most importantly, this allowed the interpretation of dose-dependent effects on HDAC4 aggregation, distribution, and neuronal phenotypes. *OK107-GAL4* drove higher expression in the mushroom body, and as a result HDAC4 aggregates were larger under the control of *OK107-GAL4* compared to *elav-GAL4*, giving rise to the hypothesis that HDAC4 aggregates coalesce as they become more numerous. Both *elav-GAL4* and *OK107-GAL4* also drove expression in different subsets of cells, and this finding was essential to understanding the relationship between MEF2 and HDAC4. Specifically, as endogenous MEF2 expression was largely restricted to Kenyon cells, analysis of MEF2-dependent changes in HDAC4 distribution in whole head preparations was most appropriate using *OK107-GAL4*.

Although the data is not presented in this thesis, this study also compared methods to repress GAL4 activity, and revealed that in addition to preventing transgene expression during development, the TARGET system can be used to reduce the level of transgene expression in a temperature-dependent manner (Hawley *et al.*, 2023). This was essential in the decision to utilise the TARGET system to reduce the level of transgene expression for mushroom body

analyses in the latter half of Chapter 5; as the level of $HDAC4^{WT}$ induced β-lobe fusion was already high in the absence of the TARGET system, addition of this reduced the level of HDAC4 expression and enabled examination of increases in severity resulting from $MEF2^{WT}$ or $HDAC4^{\Delta NES}$ overexpression. Selection of the temperature at which flies were raised to induce the appropriate level of HDAC4 overexpression was facilitated by data in Tan *et al.* (2024), which examined the levels of $HDAC4^{WT}$-induced β-lobe fusion at different temperatures.

In summary, in studies that utilise *Drosophila*, and especially the UAS/GAL4 system, informed selection of drivers and conditions under which flies are raised is crucial in good experimental design to give interpretable data. If the data to inform driver selection is not already available, a small amount of time spent on quantifying small details such as these can help explain unexpected phenomena in results, and is therefore absolutely invaluable.

8.1.1. It is essential to consider performing structure-function studies in more than one neuronal cell type

A key observation throughout this thesis, as well as in studies performed by Dr Wei Tan Jun (Tan, 2022), was that there was sometimes discordance in the effect an HDAC4 mutant had on mushroom body development compared to the eye, i.e. there may be a severe phenotype in one but not the other. This is exemplified by the finding that MEF2 is required for HDAC4-overexpression induced phenotypes in the mushroom body, but not the eye (Main *et al.*, 2021; Tan *et al.*, 2024). The discovery that MEF2 protein was negligible at the larval stage supports this. It is hypothesised that the different effects of HDAC4 in the eye and mushroom body is largely to do with the different availability of HDAC4 binding partners, as well as the functions of each cell type. Importantly, this highlights that findings in one neuronal cell type may not be applicable to others. Given that this study aims to increase the understanding of the ways in which HDAC4 aggregates form and how they cause neurotoxicity, examination in a broad range of neuronal types is best to increase understanding of how aggregates contribute to neuronal dysfunction.

8.2. HDAC4 aggregation is dependent on oligomerisation, dose, and nuclear localisation

Upon increased nuclear localisation, HDAC4 aggregation has been observed in cell culture (Borghi *et al.*, 2001; Chan *et al.*, 2003; Miska *et al.*, 1999), and in the *Drosophila* model (Fitzsimons *et al.*, 2013; Main *et al.*, 2021; Tan *et al.*, 2024). Of relevance in the context of disease, increased nuclear abundance has been observed in brains of patients with Alzheimer's disease (Herrup *et al.*, 2013), and the degree of nuclear localisation positively correlated with Braak staging (Shen *et al.*, 2016). Aggregation of HDAC4 has also been observed in nuclei of postmortem brains of patients neuronal intranuclear inclusion disease (Takahashi-Fujigasaki *et al.*, 2006), and in the cytoplasm in patients with Parkinson's disease and Lewy body dementia (Takahashi-Fujigasaki & Fujigasaki, 2006), as well as in a mouse model of Huntington's disease (Mielcarek, Landles*, et al.*, 2013). The relationship that these aggregates have with disease onset and progression is unclear, but it is evident that they do not form in healthy brains, and therefore investigation of the mechanisms through which they form is essential to understand whether they can serve as a biomarker of disease, or a target for therapeutics. In this study, three key factors were identified to contribute to the formation of HDAC4 aggregates in neuronal nuclei.

Firstly, this study has confirmed that oligomerisation of HDAC4 contributes to its ability to aggregate in nuclei. Two previous studies informed the approach to understanding how oligomerisation contributes to HDAC4 aggregation; Kirsh *et al.* (2002) determined that deletion of the N-terminus of HDAC4 prevents its aggregation in HeLa cells, and Guo *et al.* (2007) determined that this region contained an α-helix that assembles into a four-helix bundle. Assembly of the HDAC4 tetramer is dependent on the formation of a hydrophobic core, and is stabilised by polar interaction networks involving a number of glutamine residues. In this study, mutations designed to disrupt either the hydrophobic core (F65A) or stabilising networks (9QA) destabilised HDAC4 oligomer formation and reduced nuclear aggregation, while a mutation to extend the hydrophobic core (S69F) increased oligomerisation and aggregation. The finding that oligomerisation of HDAC4 is critical for its aggregation prompted further investigation of mechanisms to disrupt oligomerisation and subsequent aggregation. It was hypothesised that expression of the N-terminal region of HDAC4 including the α-helix would interfere with oligomerisation of full-length HDAC4, and reduce aggregation *in vivo*. However, the opposite was instead observed, where expression of N-terminal regions of HDAC4 stabilised

aggregation of HDAC4. This is of significant interest in the context of neuronal disease, as N-terminal products of HDAC4 are produced in response to cellular stress (Liu *et al.*, 2004; Paroni *et al.*, 2004; Zhang *et al.*, 2014). It is possible that in a disease context, N-terminal products of HDAC4 are being generated, and this is leading to its nuclear aggregation. Further investigation of the contexts in which these products are generated will be essential to understanding the ways in which HDAC4 aggregation is induced in a disease context.

Secondly, it is clear that dose of HDAC4 contributes to its aggregation. In this study, the level of HDAC4 expression was modulated using different GAL4 driver lines, the TARGET system, and the number of insertions of the HDAC4 transgene. It was consistently observed that increasing the level of HDAC4 expression increased its aggregation in nuclei. Moreover, HDAC4 aggregates were observed to coalesce as they became more numerous. These findings are of significance in neuronal diseases in which increased HDAC4 expression is observed (Chen *et al.*, 2021; Hobara *et al.*, 2010; Nardone *et al.*, 2014). It is possible that nuclear aggregation of HDAC4 may contribute to the pathogenesis of these diseases given the positive correlation of aggregation with impairments in neurodevelopment. The finding that dose of HDAC4 impacts aggregation warrants further investigation into changes in HDAC4 expression levels in healthy and disease brains, and determining whether aggregation is also observed.

Interestingly, the 9QA mutation also provides discussion around the effects of dose of HDAC4, as protein levels of this mutant were reduced compared to wild-type. This meant that it was impossible to separate the contribution of glutamine residues to HDAC4 tetramer stability and aggregation from the effect of reduced total HDAC4, and therefore the reduction in phenotype severity associated with 9QA-containing mutants could not be ascribed to changes in aggregation alone. However this is an important finding in the context of HDAC4 protein turnover. The exact effect that the 9QA mutation has on HDAC4 is unclear; it would therefore be pertinent to perform structural analyses to examine whether this affects HDAC4 conformation. Circular dichroism on the N-terminal region of HDAC4 with and without the 9QA mutation is underway to determine whether these residues affect α-helix formation. Given that glutamine residues contribute to both intra- and inter-helical interactions in the HDAC4 tetramer (Guo *et al.*, 2007) it is expected that HDAC4^{9QA} may have some loss of secondary structure. Further studies of HDAC4 protein half-life would also be of interest, specifically to determine whether glutamine residues contribute to this. If mutations that enrich for glutamine increase the half-life of HDAC4, this may increase dose and therefore level of aggregation and

severity of phenotypes. Given that polyglutamine expansion is not an uncommon phenomenon (Bunting *et al.*, 2022) these findings will be of significance if such mutations in HDAC4 are found in patients with neuronal disease.

Finally, increasing the nuclear localisation of HDAC4 resulted in increased nuclear aggregation. This is significant in the context of 2q37 deletion syndrome as mutations that affect 14-3-3 binding have been observed in patients (Wakeling *et al.*, 2021) and these are therefore likely to increase nuclear localisation and aggregation. This is also interesting in the context of oxidative stress; HDAC4 has been observed to undergo redox-dependent conformational changes that result in altered subcellular shuttling (Ago *et al.*, 2008). Given the link between oxidative stress and neuronal disease (Uttara *et al.*, 2009), it is possible that HDAC4 distribution may be altered in this context, and lead to nuclear aggregation. Further investigation of changes in HDAC4 distribution in healthy and diseased brains is warranted.

8.3. HDAC4 aggregation correlates with defects in neuronal development

HDAC4 overexpression was previously observed to induce defects in the development of the *Drosophila* eye and mushroom body (Main *et al.*, 2021; Schwartz *et al.*, 2016; Tan *et al.*, 2024). This study examined the relationship between HDAC4 aggregation and the induction of these phenotypes. Mutations that disrupted aggregation of HDAC4 reduced the severity of defects in eye and mushroom body development, and the mutation that stabilised aggregation increased the severity of defects. This was independent of the role that HDAC4 oligomerisation has in regulation of HDAC4 subcellular distribution. These findings demonstrate a positive correlation between HDAC4 aggregation and defects in neuronal development, and suggest that HDAC4 aggregates may have some role in mediating impairments, or their formation may correlate with disease onset and/or progression. This positions HDAC4 as an interesting candidate as a biomarker of neurodevelopmental disease, or target for therapeutic developments. This is of significance in the context of neurodevelopmental disease; as mentioned above, mutations that disrupt 14-3-3 binding and thus increase nuclear localisation of HDAC4 were observed in patients with 2q37 deletion syndrome (Wakeling *et al.*, 2021). Investigation of whether HDAC4 aggregation is observed in these patients will be essential in determining how disruption of HDAC4 mediates neuronal toxicity.

These findings are also of interest in the context of changes in neuronal function, and therefore neurodegenerative disease. HDAC4 overexpression in *Drosophila* impairs long-term memory (Fitzsimons *et al.*, 2013) and this is dependent on the nuclear pool of HDAC4 (Main *et al.*, 2021). It is therefore possible that nuclear aggregates of HDAC4 may be contributing to defects in LTM in *Drosophila,* and investigation of the role that aggregation of HDAC4 plays in HDAC4-overexpression induced disruption of LTM in *Drosophila* is currently underway.

As HDAC4 aggregation has been observed in a number of neuronal diseases, continued examination of the neurotoxic roles of HDAC4 is warranted, specifically those that occur in a disease- or age-dependent manner. The *Drosophila* model used here will be extremely useful for these studies as the neurodevelopmental effects of HDAC4 dysregulation are well characterised, and moreover, the genetic tools are available to restrict changes in HDAC4 dose and distribution to only adulthood. *Drosophila* can therefore be manipulated to mimic age-dependent shifts in HDAC4 regulation that may occur during disease onset and/or progression. There are also numerous characterised *Drosophila* models of neurodevelopmental and neurodegenerative disease. Changes in endogenous HDAC4 distribution and aggregation can therefore be quickly examined in these models and correlated with changes in neuronal development and function. These studies may position HDAC4 as a candidate biomarker of disease progression, and/or therapeutic target for the development of drugs to treat neurodegenerative disease. Indeed, new studies are commencing in the lab to investigate shifts in HDAC4 distribution in Alzheimer's and Parkinson's disease models. Preliminary data also demonstrates that increased nuclear HDAC4 impairs the climbing ability of flies, an indicator of motor function (White *et al.*, 2010), and also decreases lifespan (unpublished data, Dr Helen Fitzsimons). These further demonstrate that nuclear HDAC4 is likely to impair both neuronal development, and induce neurodegeneration.

Together these data demonstrate that many factors can contribute to HDAC4 aggregation, and that this aggregation affects neuronal development. In combination with the literature, which positions HDAC4 aggregation as a common feature of diseases that affect neuronal development and function, these findings make HDAC4 a promising candidate for further investigation of correlations between disease severity and nuclear aggregation. Nuclear aggregation of HDAC4 may be an effective biomarker to indicate changes in neuronal homeostasis, which may affect neuronal development and function.

8.4. Towards understanding the mechanism of how HDAC4 aggregates mediate toxicity

The initial hypothesis presented in this thesis to explain how HDAC4 may mediate neurotoxicity was that aggregates of HDAC4 sequester proteins and prevent their wild-type function, and/or gain a new function, resulting in errors in neuronal development. To examine this, an IP-MS approach was taken to identify proteins that interact with nuclear HDAC4. Proteins previously demonstrated to interact with human HDAC4 were identified as interactors of nuclear *Drosophila* HDAC4, suggesting the data is representative of candidates that may be present in nuclear aggregates. However, MEF2 was not detected, which was unexpected given that it completely co-localised with nuclear aggregates of HDAC4 in Kenyon cells. It is evident that the interaction between HDAC4 and MEF2 is highly dynamic; significant optimisations were undertaken on the immunoprecipitation protocol to maximise capture of HDAC4 oligomers, but this did not lead to the detection of MEF2 by IP-MS. While one must consider that it is possible that HDAC4 and MEF2 do not physically and/or directly interact in *Drosophila*, this remains unlikely as MEF2 is found in almost all HDAC4 aggregates in Kenyon cell nuclei, and mutation of the conserved MEF2 binding site reduces nuclear localisation of HDAC4 (Tan *et al.*, 2024), as well as co-localisation of HDAC4 and MEF2 in these aggregates. Moreover, Paroni *et al.* (2008) detected a direct physical interaction between HDAC4 and MEF2, but failed to detect MEF2 following IP-MS of HDAC4. It is therefore concluded that the interaction between HDAC4 and MEF2 is highly dynamic.

The second limitation of the IP-MS studies presented here is that the findings have not yet been replicated. It remains unclear how sensitive the immunoprecipitation protocol is, and whether aggregates of HDAC4 are being obtained. Preliminary data not presented here suggests that detection of the interaction between HDAC4 and MEF2 via co-immunoprecipitation is possible, therefore the sensitivity of the immunoprecipitation protocol could be further optimised to detect the MEF2-HDAC4 interaction. However, it would be more appropriate to take an approach that first fixes HDAC4 interactions prior to immunoprecipitation to overcome the loss of proteins which dynamically interact with HDAC4. Crosslinking followed by IP-MS has been essential to elucidation of three-dimensional protein complex structures (Piersimoni *et al.*, 2022) as well as identification of novel protein complexes (Sutherland *et al.*, 2008; Vasilescu *et al.*, 2004). More recently, specificity of 'crosslinking' has been increased by BioID (Roux *et al.*, 2018), which instead relies on proximity biotinylation of interactors by fusion of

biotin ligase to the target protein. Biotinylated proteins can then be isolated and identified via mass spectrometry. BioID has been further developed by the fusion of biotin ligase to a GFP nanobody (Xiong *et al.*, 2021) enabling biotinylation of interactors of GFP-tagged proteins. This has been adapted for *Drosophila* where fly lines are now available that express GBP-Trbo (biotin ligase fused to a GFP binding protein/nanobody) under the control of the UAS/GAL4 system (Baker *et al.*, 2021). This genetic tool is compatible with those used in this study and is therefore a viable secondary method of validation and extension of the IP-MS data described here. Importantly, BioID would help to dissociate *in vivo* interactions from those that spontaneously occur during immunoprecipitation, and may shed light on the enrichment of cytoplasmic interactors detected here.

Given that the IP-MS data has not been replicated, analyses at the pathway level were undertaken to begin to determine what processes HDAC4 aggregates may interfere with. Splicing was one such process for which proteins involved were co-immunoprecipitated with nuclear HDAC4. It is therefore possible that splicing may be impacted by HDAC4 aggregates, and indeed HDAC4 has already been implicated in regulation of alternative splicing (Kosiorek *et al.*, 2014). Investigation of the effect of HDAC4 aggregates on splicing is a new proposed avenue of investigation in the laboratory, involving RNAseq on wild-type and HDAC4-overexpressing affinity purified Kenyon cell nuclei.

The IP-MS data also identified pathways that converge around protein homeostasis. While it is possible that HDAC4 aggregates sequester these proteins to disrupt these processes and induce neurotoxicity, it also gives rise to a second complementary hypothesis; HDAC4 aggregates disrupt proteostasis by overwhelm of the cellular responses that aberrant protein aggregation invokes. That is to say, HDAC4 aggregates are being acted on by proteostatic mechanisms, and the cell is trying to clear HDAC4 aggregates. This is supported by the formation of nuclear aggresome-like inclusions upon extreme overexpression. Both hypotheses ultimately signal that HDAC4 aggregates are disrupting proteostasis, either by sequestration of proteins or by an overall burden on the mechanism. As a result, these processes are likely unable to maintain cellular homeostasis, resulting in neuronal dysfunction. To further investigate this, assays should be performed to determine whether there is disruption to these processes. This includes examination of proteasome function via colorimetric assays using a fluorogenic proteasome substrate (Vernace *et al.*, 2007), immunohistochemistry to assess co-distribution of HDAC4^{3SA} aggregates with ubiquitin, and immunohistochemistry to assess autophagy by measuring

changes in autophagosome accumulation upon HDAC4^{3SA} expression via the mCherry-GFP-Atg8 reporter (DeVorkin & Gorski, 2014).

8.5. Targeting the interaction between HDAC4 and MEF2 may be of therapeutic benefit in neuronal disease

The data presented in this thesis makes it evident that aggregation of HDAC4 is likely to disrupt neuronal function, and preventing aggregation of HDAC4 is an important target to prevent defects in neurodevelopment associated with upregulation or increased nuclear abundance of HDAC4. As mentioned in Section 8.2, one method that was investigated to interfere with oligomerisation and aggregation of HDAC4 was expression of the N-terminal α-helix, but this instead stabilised aggregation. These data suggest that caution should be taken if development of drugs is sought to interfere with HDAC4 oligomerisation to prevent its aggregation. However, these data also showed the promise of targeting the interaction between HDAC4 and MEF2.

HDAC4 is dependent on MEF2 to mediate defects in mushroom body development (Main *et al.*, 2021; Tan *et al.*, 2024), and moreover, it was shown here that MEF2 appears to stabilise aggregation of HDAC4. Expression of the N-terminal region of HDAC4 that contained the MEF2 binding domain appeared to compete with wild-type HDAC4 for MEF2 binding, preventing its nuclear localisation and aggregation, and reducing HDAC4-induced β-lobe fusion. Therefore, *Drosophila* provides an excellent model to examine methods to disrupt the interaction between HDAC4 and MEF2, and investigate the effect this has on HDAC4 aggregation, neuronal development, and neuronal function.

One option to disrupt the interaction between HDAC4 and MEF2 may be expressing a MEF2-binding peptide. Expression of just the MEF2 binding domain of HDAC4 is hypothesised to compete with wild-type HDAC4 for MEF2 binding similarly to HDAC4$^{M1\text{-}L285}$, but without the risk of stabilising aggregation. This would prevent MEF2-dependent nuclear import of HDAC4 as well as nuclear aggregation. Alternatively, one drug that may achieve this is BML-210; it has already been demonstrated to disrupt the interaction between HDAC4 and MEF2 by binding MEF2 at the site of HDAC4 association (Jayathilaka *et al.*, 2012) and ameliorate defects in learning and memory in a mouse model of Huntington's disease (Vidal-Sancho *et al.*, 2020).

Examination of the effects of the MEF2-binding peptide or drug treatment on HDAC4 aggregation and neurodevelopmental phenotypes in flies overexpressing HDAC4 will be of interest to further investigate the viability of this as a treatment option. A new study investigating this is upcoming.

However, it still remains unclear how the interaction between HDAC4 and MEF2 induces defects in neurodevelopment. Previous RNA-seq studies on *Drosophila* brains upon HDAC4 overexpression revealed few transcriptional changes (Main *et al.*, 2021; Schwartz *et al.*, 2016; Tan, 2022). It is unclear whether this is a result of a dilution effect, where MEF2-dependent transcriptional changes are likely only occurring in Kenyon cells, but samples were prepared from whole heads of which Kenyon cells only make up approximately 2%. MEF2-dependent transcriptional changes can therefore not be excluded as an effect of HDAC4 overexpression, and further RNA-seq studies should be performed on RNA extracted from only Kenyon cells overexpressing HDAC4. Interestingly, increased MEF2 in Kenyon cells was also observed upon HDAC4 overexpression. This is of significance as increased MEF2 also disrupts *Drosophila* eye and mushroom body development (Tan *et al.*, 2024), and MEF2D levels are significantly increased in PD patients (Yang *et al.*, 2009). It is unclear how MEF2 is increased, and whether this represents an upregulation of MEF2 transcription, or stabilisation of protein levels. Furthermore, it is unclear whether the upregulated MEF2 is functional. Given the recent findings that suggest HDAC4 bridges the interaction between MEF2-bound regions of chromatin (Dai *et al.*, 2024), it is of considerable interest to examine whether there is disruption to either HDAC4 or MEF2 chromatin targeting, and whether the transcription of gene targets is altered in the presence of HDAC4 aggregates. New work is commencing in this area in the laboratory and will utilise RNAseq and DamID to investigate this. Specifically, Targeted DamID (TaDa) will be employed, which achieves high specificity in profiling of cell-type specific protein-DNA interactions (Marshall *et al.*, 2016; Southall *et al.*, 2013). Briefly, TaDa involves fusion of bacterial DNA adenine methylase (Dam) to a target protein (HDAC4), which methylates adenine at GATC sequences in close proximity to where the target protein binds (Marshall & Delandre, 2022). Methylated GATC sites are then digested and prepared for sequencing to identify the regions in which the target protein binds. As methylation occurs *in vivo,* this is a highly accurate way to investigate the interaction of HDAC4 with DNA, and profiling whether there are specific genomic loci at which HDAC4 aggregates reside. Moreover, fusion of Dam to MEF2 will enable determination of whether HDAC4 aggregates alter the genomic targets of MEF2, and this can be integrated with RNAseq data to determine

whether expression of chromatin targets of MEF2 and/or HDAC4 are altered in the presence of aggregates.

8.6. Conclusion

In summary, the data and discussions presented in this thesis significantly progress knowledge of the ways in which HDAC4 aggregates, and the roles these aggregates play in defective neuronal development. This study highlights that HDAC4 may be a key upstream regulator of defects in neuronal development and function in neuronal disease, and warrant further investigation into the dysregulation of HDAC4 that occurs with aging and neuronal disease progression. The utility of the *Drosophila* model employed here is clear, and further investigation of neurodegeneration in this will be of great benefit to understanding the HDAC4-dependent mechanisms of both ageing and neurodegeneration. This study also positions HDAC4 as an interesting candidate biomarker of disease, which may also be a therapeutic target to ameliorate defects in neuronal function.

Chapter Nine

References

9. References

Adams, M., D., Celniker, S., E., Holt, R., A., Evans, C., A., Gocayne, J. D., Amanatides, P., G., Scherer, S., E., Li, P., W., Hoskins, R., A., Galle, R., F., George, R., A., Lewis, S., E., Richards, S., Ashburner, M., Henderson, S., N., Sutton, G., G., Wortman, J., R., Yandell, M., D., Zhang, Q., …, & Venter, J., C. (2000). The genome sequence of *Drosophila melanogaster*. *Science, 287*(5461), 2185-2195. https://doi.org/10.1126/science.287.5461.2185

Affolter, M., Montagne, J., Walldorf, U., Groppe, J., Kloter, U., LaRosa, M., & Gehring, W. J. (1994). The *Drosophila* SRF homolog is expressed in a subset of tracheal cells and maps within a genomic region required for tracheal development. *Development, 120*(4), 743-753. https://doi.org/10.1242/dev.120.4.743

Ageing and health. (2022, 1 October 2022). World Health Organisation. Retrieved 11 December 2023 from https://www.who.int/news-room/fact-sheets/detail/ageing-and-health

Ago, T., Liu, T., Zhai, P., Chen, W., Li, H., Molkentin, J. D., Vatner, S. F., & Sadoshima, J. (2008). A redox-dependent pathway for regulating class II HDACs and cardiac hypertrophy. *Cell, 133*(6), 978-993. https://doi.org/10.1016/j.cell.2008.04.041

Aldred, M. A., Sanford, R. O. C., Thomas, N. S., Barrow, M. A., Wilson, L. C., Brueton, L. A., Bonaglia, M. C., Hennekam, R. C. M., Eng, C., Dennis, N. R., & Trembath, R. C. (2004). Molecular analysis of 20 patients with 2q37.3 monosomy: definition of minimum deletion intervals for key phenotypes. *Journal of Medical Genetics, 41*(6), 433. https://doi.org/10.1136/jmg.2003.017202

Allfrey, V. G., Faulkner, R., & Mirsky, A. E. (1964). Acetylation and methylation of histones and their possible role in the regulation of RNA synthesis. *Proceedings of the National Academy of Sciences of the United States of America, 51*(5), 786-794. https://doi.org/10.1073/pnas.51.5.786

American Psychiatric Association. (2013). *Diagnostic and statistical manual of mental disorders* (5th ed.).

Anderson, K. W., Chen, J., Wang, M., Mast, N., Pikuleva, I. A., & Turko, I. V. (2015). Quantification of histone deacetylase isoforms in human frontal cortex, human retina, and mouse brain. *PLOS One, 10*(5), e0126592. https://doi.org/10.1371/journal.pone.0126592

Andzelm, M. M., Cherry, T. J., Harmin, D. A., Boeke, A. C., Lee, C., Hemberg, M., Pawlyk, B., Malik, A. N., Flavell, S. W., Sandberg, M. A., Raviola, E., & Greenberg, M. E. (2015). MEF2D drives photoreceptor development through a genome-wide competition for tissue-specific enhancers. *Neuron, 86*(1), 247-263. https://doi.org/10.1016/j.neuron.2015.02.038

Armstrong, G. A. B., Xiao, C., Krill, J. L., Seroude, L., Dawson-Scully, K., & Robertson, R. M. (2011). Glial Hsp70 protects K+ homeostasis in the *Drosophila* brain during repetitive anoxic depolarization. *PLOS One, 6*(12), e28994. https://doi.org/10.1371/journal.pone.0028994

Aso, Y., Grübel, K., Busch, S., Friedrich, A. B., Siwanowicz, I., & Tanimoto, H. (2009). The mushroom body of adult *Drosophila* characterized by GAL4 drivers. *Journal of Neurogenetics, 23*(1-2), 156-172. https://doi.org/10.1080/01677060802471718

Ayyadevara, S., Ganne, A., Balasubramaniam, M., & Shmookler Reis, R. J. (2022). Intrinsically disordered proteins identified in the aggregate proteome serve as biomarkers of neurodegeneration. *Metabolic Brain Disease, 37*(1), 147-152. https://doi.org/10.1007/s11011-021-00791-8

Backs, J., Backs, T., Bezprozvannaya, S., McKinsey, T. A., & Olson, E. N. (2008). Histone deacetylase 5 acquires calcium/calmodulin-dependent kinase II responsiveness by oligomerization with histone deacetylase 4. *Molecular and Cellular Biology, 28*(10), 3437-3445. https://doi.org/10.1128/MCB.01611-07

Backs, J., Song, K., Bezprozvannaya, S., Chang, S., & Olson, E. N. (2006). CaM kinase II selectively signals to histone deacetylase 4 during cardiomyocyte hypertrophy. *Journal of Clinical Investigation, 116*(7), 1853-1864. https://doi.org/10.1172/jci27438

Backs, J., Worst, B. C., Lehmann, L. H., Patrick, D. M., Jebessa, Z., Kreusser, M. M., Sun, Q., Chen, L., Heft, C., Katus, H. A., & Olson, E. N. (2011). Selective repression of MEF2 activity by PKA-dependent proteolysis of HDAC4. *Journal of Cell Biology, 195*(3), 403-415. https://doi.org/10.1083/jcb.201105063

Bajusz, C., Kristó, I., Abonyi, C., Venit, T., Vedelek, V., Lukácsovich, T., Farkas, A., Borkúti, P., Kovács, Z., Bajusz, I., Marton, A., Vizler, C., Lipinszki, Z., Sinka, R., Percipalle, P., & Vilmos, P. (2021). The nuclear activity of the actin-binding Moesin protein is necessary for gene expression in *Drosophila*. *The FEBS Journal*. https://doi.org/10.1111/febs.15779

Baker, F. C., Neiswender, H., Veeranan-Karmegam, R., & Gonsalvez, G. B. (2021). *In vivo* proximity biotin ligation identifies the interactome of Egalitarian, a Dynein cargo adaptor. *Development, 148*(22). https://doi.org/10.1242/dev.199935

Balch, W. E., Morimoto, R. I., Dillin, A., & Kelly, J. W. (2008). Adapting proteostasis for disease intervention. *Science, 319*(5865), 916-919. https://doi.org/10.1126/science.1141448

Balling, A., Technau, G. M., & Heisenberg, M. (1987). Are the structural changes in adult *Drosophila* mushroom bodies memory traces? Studies on biochemical learning mutants. *Journal of Neurogenetics, 4*(2), 65-73. https://doi.org/10.3109/01677068709167218

Barbosa, A. C., Kim, M.-S., Ertunc, M., Adachi, M., Nelson, E. D., McAnally, J., Richardson, J. A., Kavalali, E. T., Monteggia, L. M., Bassel-Duby, R., & Olson, E. N. (2008). MEF2C, a transcription factor that facilitates learning and memory by negative regulation of synapse numbers and function. *Proceedings of the National Academy of Sciences of the United States of America, 105*(27), 9391. https://doi.org/10.1073/pnas.0802679105

Barker, N., Hurlstone, A., Musisi, H., Miles, A., Bienz, M., & Clevers, H. (2001). The chromatin remodelling factor Brg-1 interacts with β-catenin to promote target gene activation. *The EMBO Journal, 20*(17), 4935-4943-4943. https://doi.org/10.1093/emboj/20.17.4935

Barker, S. J., Raju, R. M., Milman, N. E. P., Wang, J., Davila-Velderrain, J., Gunter-Rahman, F., Parro, C. C., Bozzelli, P. L., Abdurrob, F., Abdelaal, K., Bennett, D. A., Kellis, M., & Tsai, L.-H. (2021). MEF2 is a key regulator of cognitive potential and confers resilience to neurodegeneration. *Science Translational Medicine, 13*(618), eabd7695. https://doi.org/10.1126/scitranslmed.abd7695

Beaven, R., Dzhindzhev, N. S., Qu, Y., Hahn, I., Dajas-Bailador, F., Ohkura, H., & Prokop, A. (2015). *Drosophila* CLIP-190 and mammalian CLIP-170 display reduced microtubule plus end association in the nervous system. *Molecular Biology of the Cell, 26*(8), 1491-1508. https://doi.org/10.1091/mbc.E14-06-1083

Bergbaum, A., & Ogilvie, C. M. (2016). Autism and chromosome abnormalities—a review. *Clinical Anatomy, 29*(5), 620-627. https://doi.org/10.1002/ca.22719

Berman, H. M., Westbrook, J., Feng, Z., Gilliland, G., Bhat, T. N., Weissig, H., Shindyalov, I. N., & Bourne, P. E. (2000). The Protein Data Bank. *Nucleic Acids Research, 28*(1), 235-242. https://doi.org/10.1093/nar/28.1.235

Bertram, L., & Tanzi, R. E. (2005). The genetic epidemiology of neurodegenerative disease. *The Journal of Clinical Investigation, 115*(6), 1449-1457. https://doi.org/10.1172/JCI24761

Betz, A., Lampen, N., Martinek, S., Young, M. W., & Darnell, J. E. (2001). A *Drosophila* PIAS homologue negatively regulates stat92E. *Proceedings of the National Academy of Sciences, 98*(17), 9563-9568. https://doi.org/10.1073/pnas.171302098

Beyer, K., & Ariza, A. (2013). α-Synuclein posttranslational modification and alternative splicing as a trigger for neurodegeneration. *Molecular Neurobiology, 47*(2), 509-524. https://doi.org/10.1007/s12035-012-8330-5

Beyer, K., Domingo-Sàbat, M., Humbert, J., Carrato, C., Ferrer, I., & Ariza, A. (2008). Differential expression of alpha-synuclein, parkin, and synphilin-1 isoforms in Lewy body disease. *Neurogenetics, 9*(3), 163-172. https://doi.org/10.1007/s10048-008-0124-6

Bhambhani, C., Chang, J. L., Akey, D. L., & Cadigan, K. M. (2011). The oligomeric state of CtBP determines its role as a transcriptional co-activator and co-repressor of Wingless targets. *The EMBO Journal, 30*(10), 2031-2043. https://doi.org/10.1038/emboj.2011.100

Bhutani, N., Piccirillo, R., Hourez, R., Venkatraman, P., & Goldberg, A. L. (2012). Cathepsins L and Z are critical in degrading polyglutamine-containing proteins within lysosomes. *The Journal of Biological Chemistry, 287*(21), 17471-17482. https://doi.org/10.1074/jbc.M112.352781

Biancalana, M., & Koide, S. (2010). Molecular mechanism of Thioflavin-T binding to amyloid fibrils. *Biochimica et Biophysica Acta (BBA) - Proteins and Proteomics, 1804*(7), 1405-1412. https://doi.org/10.1016/j.bbapap.2010.04.001

Billuart, P., Winter, C. G., Maresh, A., Zhao, X., & Luo, L. (2001). Regulating axon branch stability: the role of p190 RhoGAP in pepressing a retraction signaling pathway. *Cell, 107*(2), 195-207. https://doi.org/10.1016/S0092-8674(01)00522-0

Bischof, J., Maeda, R. K., Hediger, M., Karch, F., & Basler, K. (2007). An optimized transgenesis system for *Drosophila* using germ-line-specific φC31 integrases. *Proceedings of the National Academy of Sciences of the United States of America, 104*(9), 3312. https://doi.org/10.1073/pnas.0611511104

Black, D. L. (2003). Mechanisms of alternative pre-messenger RNA splicing. *Annual Review of Biochemistry, 72*, 291-336. https://doi.org/10.1146/annurev.biochem.72.121801.161720

Blair, S. S. (1999). *Drosophila* imaginal disc development: patterning the adult fly. In V. E. A. Russo, D. J. Cove, L. G. Edgar, R. Jaenisch, & F. Salamini (Eds.), *Development: Genetics, Epigenetics and Environmental Regulation* (pp. 347-370). Springer Berlin Heidelberg. https://doi.org/10.1007/978-3-642-59828-9_21

Blanchard, F. J., Collins, B., Cyran, S. A., Hancock, D. H., Taylor, M. V., & Blau, J. (2010). The transcription factor Mef2 is required for normal circadian behavior in *Drosophila*. *The Journal of Neuroscience, 30*(17), 5855-5865. https://doi.org/10.1523/jneurosci.2688-09.2010

Bodily, J. M., Mehta, K. P., & Laimins, L. A. (2011). Human papillomavirus E7 enhances hypoxia-inducible factor 1-mediated transcription by inhibiting binding of histone deacetylases. *Cancer Research, 71*(3), 1187-1195. https://doi.org/10.1158/0008-5472.Can-10-2626

Bolger, T. A., & Yao, T.-P. (2005). Intracellular trafficking of histone deacetylase 4 regulates neuronal cell death. *The Journal of Neuroscience, 25*(41), 9544. https://doi.org/10.1523/JNEUROSCI.1826-05.2005

Bolger, T. A., Zhao, X., Cohen, T. J., Tsai, C. C., & Yao, T. P. (2007). The neurodegenerative disease protein ataxin-1 antagonizes the neuronal survival function of myocyte enhancer factor-2. *Journal of Biological Chemistry, 282*(40), 29186-29192. https://doi.org/10.1074/jbc.M704182200

Borghi, S., Molinari, S., Razzini, G., Parise, F., Battini, R., & Ferrari, S. (2001). The nuclear localization domain of the MEF2 family of transcription factors shows member-specific features and mediates the nuclear import of histone deacetylase 4. *Journal of Cell Science, 114*(24), 4477. https://doi.org/10.1242/jcs.114.24.4477

Bottomley, M. J., Lo Surdo, P., Di Giovine, P., Cirillo, A., Scarpelli, R., Ferrigno, F., Jones, P., Neddermann, P., De Francesco, R., Steinkühler, C., Gallinari, P., & Carfí, A. (2008). Structural and functional analysis of the human HDAC4 catalytic domain reveals a regulatory structural zinc-binding domain. *The Journal of Biological Chemistry, 283*(39), 26694-26704. https://doi.org/10.1074/jbc.M803514200

Bour, B. A., O'Brien, M. A., Lockwood, W. L., Goldstein, E. S., Bodmer, R., Taghert, P. H., Abmayr, S. M., & Nguyen, H. T. (1995). *Drosophila* MEF2, a transcription factor that is essential for myogenesis. *Genes & Development, 9*(6), 730-741. https://doi.org/10.1101/gad.9.6.730

Brand, A. H., & Perrimon, N. (1993). Targeted gene expression as a means of altering cell fates and generating dominant phenotypes. *Development, 118*(2), 401. https://doi.org/10.1242/dev.118.2.401

Breijyeh, Z., & Karaman, R. (2020). Comprehensive review on Alzheimer's disease: causes and treatment. *Molecules, 25*(24). https://doi.org/10.3390/molecules25245789

Breitbart, R. E., Liang, C. S., Smoot, L. B., Laheru, D. A., Mahdavi, V., & Nadal-Ginard, B. (1993). A fourth human MEF2 transcription factor, hMEF2D, is an early marker of the myogenic lineage. *Development, 118*(4), 1095. https://doi.org/10.1242/dev.118.4.1095

Bridges, C. B. (1916). Non-disjunction as proof of the chromosome theory of heredity. *Genetics, 1*(1), 1-52. https://doi.org/10.1093/genetics/1.1.1

Broide, R. S., Redwine, J. M., Aftahi, N., Young, W., Bloom, F. E., & Winrow, C. J. (2007). Distribution of histone deacetylases 1-11 in the rat brain. *Journal of Molecular Neuroscience*(1), 47-58. https://doi.org/10.1007/bf02686117

Brumby, A. M., & Richardson, H. E. (2003). *scribble* mutants cooperate with oncogenic Ras or Notch to cause neoplastic overgrowth in *Drosophila*. *The EMBO Journal, 22*(21), 5769-5779. https://doi.org/10.1093/emboj/cdg548

Bunting, E. L., Hamilton, J., & Tabrizi, S. J. (2022). Polyglutamine diseases. *Current Opinion in Neurobiology, 72*, 39-47. https://doi.org/10.1016/j.conb.2021.07.001

Bürli, R. W., Luckhurst, C. A., Aziz, O., Matthews, K. L., Yates, D., Lyons, K. A., Beconi, M., McAllister, G., Breccia, P., Stott, A. J., Penrose, S. D., Wall, M., Lamers, M., Leonard, P., Müller, I., Richardson, C. M., Jarvis, R., Stones, L., Hughes, S., …, & Dominguez, C. (2013). Design, synthesis, and biological evaluation of potent and selective class IIa histone deacetylase (HDAC) inhibitors as a potential therapy for Huntington's disease. *Journal of Medicinal Chemistry, 56*(24), 9934-9954. https://doi.org/10.1021/jm4011884

Burnet, B., Connolly, K., & Beck, J. (1968). Phenogenetic studies on visual acuity in *Drosophila melanogaster*. *Journal of Insect Physiology, 14*(6), 855-860. https://doi.org/10.1016/0022-1910(68)90196-0

Burright, E. N., Clark, H. B., Servadio, A., Matilla, T., Feddersen, R. M., Yunis, W. S., Duvick, L. A., Zoghbi, H. Y., & Orr, H. T. (1995). SCA1 transgenic mice: a model for neurodegeneration caused by an expanded CAG trinucleotide repeat. *Cell, 82*(6), 937-948. https://doi.org/10.1016/0092-8674(95)90273-2

Buszczak, M., Paterno, S., Lighthouse, D., Bachman, J., Planck, J., Owen, S., Skora, A. D., Nystul, T. G., Ohlstein, B., Allen, A., Wilhelm, J. E., Murphy, T. D., Levis, R. W., Matunis, E., Srivali, N., Hoskins, R. A., & Spradling, A. C. (2007). The carnegie protein trap library: A versatile tool for *Drosophila* developmental studies. *Genetics, 175*(3), 1505-1531. https://doi.org/10.1534/genetics.106.065961

Cagan, R. (2009). Principles of *Drosophila* eye differentiation. *Current topics in developmental biology, 89*, 115-135. https://doi.org/10.1016/S0070-2153(09)89005-4

Cagan, R. L., & Ready, D. F. (1989). The emergence of order in the *Drosophila* pupal retina. *Developmental Biology, 136*(2), 346-362. https://doi.org/10.1016/0012-1606(89)90261-3

Campos, E. I., & Reinberg, D. (2009). Histones: annotating chromatin. *Annual Review of Genetics, 43*, 559-599. https://doi.org/10.1146/annurev.genet.032608.103928

Cao, W., Song, H. J., Gangi, T., Kelkar, A., Antani, I., Garza, D., & Konsolaki, M. (2008). Identification of novel genes that modify phenotypes induced by Alzheimer's beta-amyloid overexpression in *Drosophila*. *Genetics, 178*(3), 1457-1471. https://doi.org/10.1534/genetics.107.078394

Caputi, F. F., Candeletti, S., & Romualdi, P. (2017). In G. Chandrika (Ed.), *Neuroblastoma* (pp. Ch. 7). IntechOpen. https://doi.org/10.5772/intechopen.69566

Cernotta, N., Clocchiatti, A., Florean, C., & Brancolini, C. (2011). Ubiquitin-dependent degradation of HDAC4, a new regulator of random cell motility. *Molecular Biology of the Cell, 22*(2), 278-289. https://doi.org/10.1091/mbc.E10-07-0616

Cervantes-Sandoval, I., Chakraborty, M., MacMullen, C., & Davis, R. L. (2016). Scribble scaffolds a signalosome for active forgetting. *Neuron, 90*(6), 1230-1242. https://doi.org/10.1016/j.neuron.2016.05.010

Chan, J. K. L., Sun, L., Yang, X.-J., Zhu, G., & Wu, Z. (2003). Functional characterization of an amino-terminal region of HDAC4 that possesses MEF2 binding and transcriptional repressive activity. *Journal of Biological Chemistry, 278*(26), 23515-23521. https://doi.org/10.1074/jbc.M301922200

Chanarat, S., & Sträßer, K. (2013). Splicing and beyond: The many faces of the Prp19 complex. *Biochimica et Biophysica Acta (BBA) - Molecular Cell Research, 1833*(10), 2126-2134. https://doi.org/10.1016/j.bbamcr.2013.05.023

Chang, Y.-C., Hung, W.-T., Chang, Y.-C., Chang, H. C., Wu, C.-L., Chiang, A.-S., Jackson, G. R., & Sang, T.-K. (2011). Pathogenic VCP/TER94 alleles are dominant actives and contribute to neurodegeneration by altering cellular ATP level in a *Drosophila* IBMPFD model. *PLOS Genetics, 7*(2), e1001288. https://doi.org/10.1371/journal.pgen.1001288

Chapple, J. P., Bros-Facer, V., Butler, R., & Gallo, J. M. (2008). Focal distortion of the nuclear envelope by huntingtin aggregates revealed by lamin immunostaining. *Neuroscience Letters, 447*(2-3), 172-174. https://doi.org/10.1016/j.neulet.2008.09.075

Chawla, S., Vanhoutte, P., Arnold, F. J. L., Huang, C. L. H., & Bading, H. (2003). Neuronal activity-dependent nucleocytoplasmic shuttling of HDAC4 and HDAC5. *Journal of Neurochemistry, 85*(1), 151-159. https://doi.org/10.1046/j.1471-4159.2003.01648.x

Chen, B., & Cepko, C. L. (2009). HDAC4 regulates neuronal survival in normal and diseased retinas. *Science, 323*(5911), 256-259. https://doi.org/10.1126/science.1166226

Chen, H. K., Fernandez-Funez, P., Acevedo, S. F., Lam, Y. C., Kaytor, M. D., Fernandez, M. H., Aitken, A., Skoulakis, E. M., Orr, H. T., Botas, J., & Zoghbi, H. Y. (2003). Interaction of Akt-phosphorylated ataxin-1 with 14-3-3 mediates neurodegeneration in spinocerebellar ataxia type 1. *Cell, 113*(4), 457-468. https://doi.org/10.1016/s0092-8674(03)00349-0

Chen, S., Berthelier, V., Yang, W., & Wetzel, R. (2001). Polyglutamine aggregation behavior *in vitro* supports a recruitment mechanism of cytotoxicity. *Journal of Molecular Biology, 311*(1), 173-182. https://doi.org/10.1006/jmbi.2001.4850

Chen, X., Zaro, J. L., & Shen, W.-C. (2013). Fusion protein linkers: property, design and functionality. *Advanced Drug Delivery Reviews, 65*(10), 1357-1369. https://doi.org/10.1016/j.addr.2012.09.039

Chen, Y., Wang, Y., Modrusan, Z., Sheng, M., & Kaminker, J. S. (2014). Regulation of neuronal gene expression and survival by basal NMDA receptor activity: a role for histone deacetylase 4. *The Journal of Neuroscience, 34*(46), 15327-15339. https://doi.org/10.1523/jneurosci.0569-14.2014

Chen, Y.-A., Lu, C.-H., Ke, C.-C., Chiu, S.-J., Chang, C.-W., Yang, B.-H., Gelovani, J. G., & Liu, R.-S. (2021). Evaluation of class IIa histone deacetylases expression and *in vivo* epigenetic imaging in a transgenic mouse model of Alzheimer's disease. *International Journal of Molecular Sciences, 22*(16). https://doi.org/10.3390/ijms22168633

Cheung, G., To, E., Rivera-Rodriguez, C., Ma'u, E., Chan, A. H. Y., Ryan, B., & Cullum, S. (2022). Dementia prevalence estimation among the main ethnic groups in New Zealand: a population-based descriptive study of routinely collected health data. *BMJ Open, 12*(9), e062304. https://doi.org/10.1136/bmjopen-2022-062304

Chiolo, I., Minoda, A., Colmenares, Serafin U., Polyzos, A., Costes, Sylvain V., & Karpen, Gary H. (2011). Double-strand breaks in heterochromatin move outside of a dynamic HP1a domain to complete recombinational repair. *Cell, 144*(5), 732-744. https://doi.org/10.1016/j.cell.2011.02.012

Cleary, J. P., Walsh, D. M., Hofmeister, J. J., Shankar, G. M., Kuskowski, M. A., Selkoe, D. J., & Ashe, K. H. (2005). Natural oligomers of the amyloid-β protein specifically disrupt cognitive function. *Nature Neuroscience, 8*(1), 79-84. https://doi.org/10.1038/nn1372

Cohen, T. J., Barrientos, T., Hartman, Z. C., Garvey, S. M., Cox, G. A., & Yao, T.-P. (2009). The deacetylase HDAC4 controls myocyte enhancing factor-2-dependent structural gene expression in response to neural activity. *The FASEB Journal, 23*(1), 99-106. https://doi.org/10.1096/fj.08-115931

Cohen, T. J., Waddell, D. S., Barrientos, T., Lu, Z., Feng, G., Cox, G. A., Bodine, S. C., & Yao, T.-P. (2007). The histone deacetylase HDAC4 connects neural activity to muscle transcriptional reprogramming. *Journal of Biological Chemistry, 282*(46), 33752-33759. https://doi.org/10.1074/jbc.M706268200

Cole, C. J., Mercaldo, V., Restivo, L., Yiu, A. P., Sekeres, M. J., Han, J. H., Vetere, G., Pekar, T., Ross, P. J., Neve, R. L., Frankland, P. W., & Josselyn, S. A. (2012). MEF2 negatively regulates learning-induced structural plasticity and memory formation. *Nature Neuroscience, 15*(9), 1255-1264. https://doi.org/10.1038/nn.3189

Cole, S. L., & Vassar, R. (2007). The Alzheimer's disease β-secretase enzyme, BACE1. *Molecular Neurodegeneration, 2*(1), 22. https://doi.org/10.1186/1750-1326-2-22

Colussi, C., Aceto, G., Ripoli, C., Bertozzi, A., Li Puma, D. D., Paccosi, E., D'Ascenzo, M., & Grassi, C. (2023). Cytoplasmic HDAC4 recovers synaptic function in the 3×Tg mouse model of Alzheimer's disease. *Neuropathology and Applied Neurobiology, 49*(1), e12861. https://doi.org/10.1111/nan.12861

Connolly, J. B., Roberts, I. J., Armstrong, J. D., Kaiser, K., Forte, M., Tully, T., & O'Kane, C. J. (1996). Associative learning disrupted by impaired Gs signaling in *Drosophila* mushroom bodies. *Science, 274*(5295), 2104-2107. https://doi.org/10.1126/science.274.5295.2104

Cooley, L., & Theurkauf, W. E. (1994). Cytoskeletal functions during *Drosophila* oogenesis. *Science, 266*(5185), 590-596. https://doi.org/10.1126/science.7939713

Cosgrove, D., Whitton, L., Fahey, L., Ó Broin, P., Donohoe, G., & Morris, D. W. (2021). Genes influenced by MEF2C contribute to neurodevelopmental disease via gene expression changes that affect multiple types of cortical excitatory neurons. *Human Molecular Genetics, 30*(11), 961-970. https://doi.org/10.1093/hmg/ddaa213

Courbard, J. R., Djiane, A., Wu, J., & Mlodzik, M. (2009). The apical/basal-polarity determinant Scribble cooperates with the PCP core factor Stbm/Vang and functions as one of its effectors. *Developmental Biology, 333*(1), 67-77. https://doi.org/10.1016/j.ydbio.2009.06.024

Cowan, T. M., & Siegel, R. W. (1986). *Drosophila* mutations that alter ionic conduction disrupt acquisition and retention of a conditioned odor avoidance response. *Journal of Neurogenetics, 3*(4), 187-201. https://doi.org/10.3109/01677068609106849

Crittenden, J. R., Skoulakis, E. M., Han, K. A., Kalderon, D., & Davis, R. L. (1998). Tripartite mushroom body architecture revealed by antigenic markers. *Learning & Memory, 5*(1-2), 38-51. https://doi.org/10.1101/lm.5.1.38

Crittenden, J. R., Skoulakis, E. M. C., Goldstein, E. S., & Davis, R. L. (2018). *Drosophila* mef2 is essential for normal mushroom body and wing development. *Biology Open, 7*(9). https://doi.org/10.1242/bio.035618

Crocker, A., Guan, X.-J., Murphy, C. T., & Murthy, M. (2016). Cell-type-specific transcriptome analysis in the *Drosophila* mushroom body reveals memory-related changes in gene expression. *Cell Reports, 15*(7), 1580-1596. https://doi.org/10.1016/j.celrep.2016.04.046

Crowther, D. C., Kinghorn, K. J., Miranda, E., Page, R., Curry, J. A., Duthie, F. A. I., Gubb, D. C., & Lomas, D. A. (2005). Intraneuronal Aβ, non-amyloid aggregates and neurodegeneration in a *Drosophila* model of Alzheimer's disease. *Neuroscience, 132*(1), 123-135. https://doi.org/10.1016/j.neuroscience.2004.12.025

Cullum, S., Mullin, K., Zeng, I., Yates, S., Payman, V., Fisher, M., & Cheung, G. (2018). Do community-dwelling Māori and Pacific peoples present with dementia at a younger age and at a later stage compared with NZ Europeans? *International Journal of Geriatric Psychiatry, 33*(8), 1098-1104. https://doi.org/10.1002/gps.4898

Dai, S., Guo, L., Dey, R., Guo, M., Zhang, X., Bates, D., Cayford, J., Jiang, L., Wei, H., Chen, Z., Zhang, Y., Chen, L., & Chen, Y. (2024). Structural insights into the HDAC4–MEF2A–DNA complex and its implication in long-range transcriptional regulation. *Nucleic Acids Research*, gkae036. https://doi.org/10.1093/nar/gkae036

Dai, X., Lin, A., Zhuang, L., Zeng, Q., Cai, L., Wei, Y., Liang, H., Gao, W., Zhang, J., & Chen, X. (2023). Targeting SIK3 to modulate hippocampal synaptic plasticity and cognitive function by regulating the transcription of HDAC4 in a mouse model of Alzheimer's disease. *Neuropsychopharmacology*. https://doi.org/10.1038/s41386-023-01775-1

Darcy, M. J., Calvin, K., Cavnar, K., & Ouimet, C. C. (2010). Regional and subcellular distribution of HDAC4 in mouse brain. *Journal of Comparative Neurology, 518*(5), 722-740. https://doi.org/10.1002/cne.22241

Darling, D. L., Yingling, J., & Wynshaw-Boris, A. (2005). In *Current topics in developmental biology* (Vol. 68, pp. 281-315). Academic Press. https://doi.org/10.1016/S0070-2153(05)68010-6

de Belle, J. S., & Heisenberg, M. (1994). Associative odor learning in *Drosophila* abolished by chemical ablation of mushroom bodies. *Science, 263*(5147), 692-695. https://doi.org/10.1126/science.8303280

del Valle Rodríguez, A., Didiano, D., & Desplan, C. (2011). Power tools for gene expression and clonal analysis in *Drosophila*. *Nature Methods, 9*(1), 47-55. https://doi.org/10.1038/nmeth.1800

Dennis, G., Sherman, B. T., Hosack, D. A., Yang, J., Gao, W., Lane, H. C., & Lempicki, R. A. (2003). DAVID: Database for Annotation, Visualization, and Integrated Discovery. *Genome Biology, 4*(9), R60. https://doi.org/10.1186/gb-2003-4-9-r60

DeVorkin, L., & Gorski, S. M. (2014). Monitoring autophagy in *Drosophila* using fluorescent reporters in the UAS-GAL4 system. *Cold Spring Harbor Protocols, 2014*(9), pdb.prot080341. https://doi.org/10.1101/pdb.prot080341

Dietrich, J.-B. (2013). The MEF2 family and the brain: from molecules to memory. *Cell and Tissue Research, 352*(2), 179-190. https://doi.org/10.1007/s00441-013-1565-2

Dietzl, G., Chen, D., Schnorrer, F., Su, K. C., Barinova, Y., Fellner, M., Gasser, B., Kinsey, K., Oppel, S., Scheiblauer, S., Couto, A., Marra, V., Keleman, K., & Dickson, B. J. (2007). A genome-wide transgenic RNAi library for conditional gene inactivation in *Drosophila*. *Nature, 448*(7150), 151-156. https://doi.org/10.1038/nature05954

Douglas, P. M., & Dillin, A. (2010). Protein homeostasis and aging in neurodegeneration. *Journal of Cell Biology, 190*(5), 719-729. https://doi.org/10.1083/jcb.201005144

Downes, M., Ordentlich, P., Kao, H.-Y., Alvarez, J. G. A., & Evans, R. M. (2000). Identification of a nuclear domain with deacetylase activity. *Proceedings of the National Academy of Sciences of the United States of America, 97*(19), 10330-10335. https://doi.org/10.1073/pnas.97.19.10330

Dubnau, J., Grady, L., Kitamoto, T., & Tully, T. (2001). Disruption of neurotransmission in *Drosophila* mushroom body blocks retrieval but not acquisition of memory. *Nature, 411*(6836), 476-480. https://doi.org/10.1038/35078077

Duffy, J. B. (2002). GAL4 system in *Drosophila*: A fly geneticist's swiss army knife. *Genesis, 34*(1-2), 1-15. https://doi.org/10.1002/gene.10150

Dunwell, T. L., & Pfeifer, G. P. (2014). *Drosophila* genomic methylation: new evidence and new questions. *Epigenomics, 6*(5), 459-461. https://doi.org/10.2217/epi.14.46

Emamian, E. S., Kaytor, M. D., Duvick, L. A., Zu, T., Tousey, S. K., Zoghbi, H. Y., Clark, H. B., & Orr, H. T. (2003). Serine 776 of Ataxin-1 is critical for polyglutamine-induced disease in SCA1 transgenic mice. *Neuron, 38*(3), 375-387. https://doi.org/10.1016/S0896-6273(03)00258-7

Escobedo, S. E., Shah, A., Easton, A. N., Hall, H., & Weake, V. M. (2021). Characterizing a gene expression toolkit for eye- and photoreceptor-specific expression in *Drosophila*. *Fly, 15*(1), 73-88. https://doi.org/10.1080/19336934.2021.1915683

Falk, R. E., & Casas, K. A. (2007). Chromosome 2q37 deletion: Clinical and molecular aspects. *American Journal of Medical Genetics, 145C*(4), 357-371. https://doi.org/10.1002/ajmg.c.30153

Fan, S.-S., & Ready, D. F. (1997). Glued participates in distinct microtubule-based activities in *Drosophila* eye development. *Development, 124*(8), 1497-1507. https://doi.org/10.1242/dev.124.8.1497

Fan, Y., & Bergmann, A. (2008). Distinct mechanisms of apoptosis-induced compensatory proliferation in proliferating and differentiating tissues in the Drosophila eye. *Developmental Cell, 14*(3), 399-410. https://doi.org/10.1016/j.devcel.2008.01.003

Fang, M., Li, J., Blauwkamp, T., Bhambhani, C., Campbell, N., & Cadigan, K. M. (2006). C-terminal-binding protein directly activates and represses Wnt transcriptional targets in *Drosophila*. *The EMBO Journal, 25*(12), 2735-2745. https://doi.org/10.1038/sj.emboj.7601153

Feany, M. B., & Bender, W. W. (2000). A *Drosophila* model of Parkinson's disease. *Nature, 404*(6776), 394-398. https://doi.org/10.1038/35006074

Federspiel, J. D., Greco, T. M., Lum, K. K., & Cristea, I. M. (2019). Hdac4 interactions in Huntington's disease viewed through the prism of multiomics. *Molecular & Cellular Proteomics, 18*(8 suppl 1), S92-s113. https://doi.org/10.1074/mcp.RA118.001253

Fehr, S., Wilson, M., Downs, J., Williams, S., Murgia, A., Sartori, S., Vecchi, M., Ho, G., Polli, R., Psoni, S., Bao, X., de Klerk, N., Leonard, H., & Christodoulou, J. (2013). The CDKL5 disorder is an independent clinical entity associated with early-onset encephalopathy. *European Journal of Human Genetics, 21*(3), 266-273. https://doi.org/10.1038/ejhg.2012.156

Fernandez-Funez, P., Nino-Rosales, M. L., de Gouyon, B., She, W.-C., Luchak, J. M., Martinez, P., Turiegano, E., Benito, J., Capovilla, M., Skinner, P. J., McCall, A., Canal, I., Orr, H. T., Zoghbi, H. Y., & Botas, J. (2000). Identification of genes that modify ataxin-1-induced neurodegeneration. *Nature, 408*(6808), 101-106. https://doi.org/10.1038/35040584

Ferreiro, M. J., Pérez, C., Marchesano, M., Ruiz, S., Caputi, A., Aguilera, P., Barrio, R., & Cantera, R. (2017). *Drosophila melanogaster White* mutant w(1118) undergo retinal degeneration. *Frontiers in Neuroscience, 11*, 732. https://doi.org/10.3389/fnins.2017.00732

Fink, A. L. (1998). Protein aggregation: folding aggregates, inclusion bodies and amyloid. *Folding and Design, 3*(1), R9-R23. https://doi.org/10.1016/S1359-0278(98)00002-9

Fischer, J. A., Giniger, E., Maniatis, T., & Ptashne, M. (1988). GAL4 activates transcription in *Drosophila*. *Nature, 332*(6167), 853-856. https://doi.org/10.1038/332853a0

Fischle, W., Dequiedt, F., Fillion, M., Hendzel, M. J., Voelter, W., & Verdin, E. (2001). Human HDAC7 histone deacetylase activity is associated with HDAC3 *in vivo*. *Journal of Biological Chemistry, 276*(38), 35826-35835. https://doi.org/10.1074/jbc.M104935200

Fischle, W., Dequiedt, F., Hendzel, M. J., Guenther, M. G., Lazar, M. A., Voelter, W., & Verdin, E. (2002). Enzymatic activity associated with class II HDACs is dependent on a multiprotein complex containing HDAC3 and SMRT/N-CoR. *Molecular Cell, 9*(1), 45-57. https://doi.org/10.1016/S1097-2765(01)00429-4

Fitzsimons, H. L. (2015). The class IIa histone deacetylase HDAC4 and neuronal function: nuclear nuisance and cytoplasmic stalwart? *Neurobiology of Learning and Memory, 123*, 149-158. https://doi.org/10.1016/j.nlm.2015.06.006

Fitzsimons, H. L., Schwartz, S., Given, F. M., & Scott, M. J. (2013). The histone deacetylase HDAC4 regulates long-term memory in *Drosophila*. *PLOS One, 8*(12), e83903-e83903. https://doi.org/10.1371/journal.pone.0083903

Fiumara, F., Fioriti, L., Kandel, E. R., & Hendrickson, W. A. (2010). Essential role of coiled coils for aggregation and activity of q/n-rich prions and polyq proteins. *Cell, 143*(7), 1121-1135. https://doi.org/10.1016/j.cell.2010.11.042

Flavell, S. W., Cowan, C. W., Kim, T. K., Greer, P. L., Lin, Y., Paradis, S., Griffith, E. C., Hu, L. S., Chen, C., & Greenberg, M. E. (2006). Activity-dependent regulation of MEF2 transcription factors suppresses excitatory synapse number. *Science, 311*(5763), 1008-1012. https://doi.org/10.1126/science.1122511

Flavell, S. W., Kim, T. K., Gray, J. M., Harmin, D. A., Hemberg, M., Hong, E. J., Markenscoff-Papadimitriou, E., Bear, D. M., & Greenberg, M. E. (2008). Genome-wide analysis of MEF2 transcriptional program reveals synaptic target genes and neuronal activity-dependent polyadenylation site selection. *Neuron, 60*(6), 1022-1038. https://doi.org/10.1016/j.neuron.2008.11.029

Freeman, M. (1996). Reiterative use of the EGF receptor triggers differentiation of all cell types in the *Drosophila* eye. *Cell, 87*(4), 651-660. https://doi.org/10.1016/S0092-8674(00)81385-9

Freeman, M., & Bienz, M. (2001). EGF receptor/Rolled MAP kinase signalling protects cells against activated Armadillo in the *Drosophila* eye. *EMBO Reports, 2*(2), 157-162. https://doi.org/10.1093/embo-reports/kve019

Freymuth, P. S. (2016). *The actin-binding protein Moesin and memory formation in Drosophila : A thesis presented to Massey University in partial fulfillment of the requirements for the degree of Master of Science in Biochemistry, Institute of Fundamental Sciences, Massey University, Manawatu, New Zealand* [Master's, Massey University]. http://hdl.handle.net/10179/9914

Freymuth, P. S., & Fitzsimons, H. L. (2017). The ERM protein Moesin is essential for neuronal morphogenesis and long-term memory in *Drosophila*. *Molecular Brain, 10*(1), 41. https://doi.org/10.1186/s13041-017-0322-y

Fristrom, D. K., & Rickoll, W. L. (1982). The morphogenesis of imaginal discs of *Drosophila*. In R. C. King & H. Akai (Eds.), *Insect Ultrastructure: Volume 1* (pp. 247-277). Springer US. https://doi.org/10.1007/978-1-4615-7266-4_9

Fu, H., Subramanian, R. R., & Masters, S. C. (2000). 14-3-3 proteins: structure, function, and regulation. *Annual Review of Pharmacology and Toxicology, 40*(1), 617-647. https://doi.org/10.1146/annurev.pharmtox.40.1.617

Fu, X. D., & Maniatis, T. (1990). Factor required for mammalian spliceosome assembly is localized to discrete regions in the nucleus. *Nature, 343*(6257), 437-441. https://doi.org/10.1038/343437a0

Fujii, S., Emery, P., & Amrein, H. (2017). SIK3–HDAC4 signaling regulates *Drosophila* circadian male sex drive rhythm *via* modulating the DN1 clock neurons. *Proceedings of the National Academy of Sciences of the United States of America, 114*(32), E6669. https://doi.org/10.1073/pnas.1620483114

Fujisawa, T., & Filippakopoulos, P. (2017). Functions of bromodomain-containing proteins and their roles in homeostasis and cancer. *Nature Reviews Molecular Cell Biology, 18*(4), 246-262. https://doi.org/10.1038/nrm.2016.143

Furumai, R., Komatsu, Y., Nishino, N., Khochbin, S., Yoshida, M., & Horinouchi, S. (2001). Potent histone deacetylase inhibitors built from trichostatin A and cyclic tetrapeptide antibiotics including trapoxin. *Proceedings of the National Academy of Sciences of the United States of America, 98*(1), 87-92. https://doi.org/10.1073/pnas.98.1.87

Gambis, A., Dourlen, P., Steller, H., & Mollereau, B. (2011). Two-color in vivo imaging of photoreceptor apoptosis and development in Drosophila. *Developmental Biology, 351*(1), 128-134. https://doi.org/10.1016/j.ydbio.2010.12.040

Gao, L., Cueto, M. A., Asselbergs, F., & Atadja, P. (2002). Cloning and functional characterization of HDAC11, a novel member of the human histone deacetylase family. *Journal of Biological Chemistry, 277*(28), 25748-25755. https://doi.org/10.1074/jbc.M111871200

Gao, L., She, H., Li, W., Zeng, J., Zhu, J., Jones, D. P., Mao, Z., Gao, G., & Yang, Q. (2014). Oxidation of survival factor MEF2D in neuronal death and Parkinson's disease. *Antioxidants & Redox Signaling, 20*(18), 2936-2948. https://doi.org/10.1089/ars.2013.5399

García-Mata, R., Bebök, Z., Sorscher, E. J., & Sztul, E. S. (1999). Characterization and dynamics of aggresome formation by a cytosolic GFP-chimera. *Journal of Cell Biology, 146*(6), 1239-1254. https://doi.org/10.1083/jcb.146.6.1239

Gatto, C. L., & Broadie, K. (2011). *Drosophila* modeling of heritable neurodevelopmental disorders. *Current Opinion in Neurobiology, 21*(6), 834-841. https://doi.org/10.1016/j.conb.2011.04.009

Gaucherand, L., Porter, B. K., Levene, R. E., Price, E. L., Schmaling, S. K., Rycroft, C. H., Kevorkian, Y., McCormick, C., Khaperskyy, D. A., & Gaglia, M. M. (2019). The influenza A virus endoribonuclease PA-X usurps host mRNA processing machinery to limit host gene expression. *Cell Reports, 27*(3), 776-792.e777. https://doi.org/10.1016/j.celrep.2019.03.063

Gavril, E. C., Nucă, I., Pânzaru, M. C., Ivanov, A. V., Mihai, C. T., Antoci, L. M., Ciobanu, C. G., Rusu, C., & Popescu, R. (2023). Genotype-phenotype correlations in 2q37-deletion syndrome: an update of the clinical spectrum and literature review. *Genes, 14*(2). https://doi.org/10.3390/genes14020465

Gelbart, M. E., & Kuroda, M. I. (2009). *Drosophila* dosage compensation: a complex voyage to the X chromosome. *Development, 136*(9), 1399-1410. https://doi.org/10.1242/dev.029645

Gerlach, M., Riederer, P., Przuntek, H., & Youdim, M. B. (1991). MPTP mechanisms of neurotoxicity and their implications for Parkinson's disease. *European Journal of Pharmacology: Molecular Pharmacology, 208*(4), 273-286. https://doi.org/10.1016/0922-4106(91)90073-q

González, P., Alvarez, V., Menéndez, M., Lahoz, C. H., Martínez, C., Corao, A. I., Calatayud, M. T., Peña, J., García-Castro, M., & Coto, E. (2007). Myocyte enhancing factor-2A in Alzheimer's disease: genetic analysis and association with MEF2A-polymorphisms. *Neuroscience Letters, 411*(1), 47-51. https://doi.org/10.1016/j.neulet.2006.09.055

Goossens, T., Kang, Y. Y., Wuytens, G., Zimmermann, P., Callaerts-Végh, Z., Pollarolo, G., Islam, R., Hortsch, M., & Callaerts, P. (2011). The *Drosophila* L1CAM homolog Neuroglian signals through distinct pathways to control different aspects of mushroom body axon development. *Development, 138*(8), 1595-1605. https://doi.org/10.1242/dev.052787

Gorman, A. M. (2008). Neuronal cell death in neurodegenerative diseases: recurring themes around protein handling. *Journal of Cellular and Molecular Medicine, 12*(6a), 2263-2280. https://doi.org/10.1111/j.1582-4934.2008.00402.x

Gramates, L. S., Agapite, J., Attrill, H., Calvi, B. R., Crosby, M. A., dos Santos, G., Goodman, J. L., Goutte-Gattat, D., Jenkins, V. K., Kaufman, T., Larkin, A., Matthews, B. B., Millburn, G., Strelets, V. B., & the FlyBase, C. (2022). FlyBase: a guided tour of highlighted features. *Genetics, 220*(4), iyac035. https://doi.org/10.1093/genetics/iyac035

Gratz, S. J., Cummings, A. M., Nguyen, J. N., Hamm, D. C., Donohue, L. K., Harrison, M. M., Wildonger, J., & O'Connor-Giles, K. M. (2013). Genome engineering of *Drosophila* with the CRISPR RNA-guided Cas9 nuclease. *Genetics, 194*(4), 1029. https://doi.org/10.1534/genetics.113.152710

Greenspan, R. J. (2004). *Fly pushing: the theory and practice of Drosophila genetics*. CSHL Press.

Grégoire, S., & Yang, X. J. (2005). Association with class IIa histone deacetylases upregulates the sumoylation of MEF2 transcription factors. *Molecular and Cellular Biology, 25*(6), 2273-2287. https://doi.org/10.1128/mcb.25.6.2273-2287.2005

Gregoretti, I., Lee, Y.-M., & Goodson, H. V. (2004). Molecular evolution of the histone deacetylase family: functional implications of phylogenetic analysis. *Journal of Molecular Biology, 338*(1), 17-31. https://doi.org/10.1016/j.jmb.2004.02.006

Groth, A. C., Fish, M., Nusse, R., & Calos, M. P. (2004). Construction of transgenic *Drosophila* by using the site-specific integrase from phage φC31. *Genetics, 166*(4), 1775. https://doi.org/10.1534/genetics.166.4.1775

Grozinger, C. M., Hassig, C. A., & Schreiber, S. L. (1999). Three proteins define a class of human histone deacetylases related to yeast Hda1p. *Proceedings of the National Academy of Sciences of the United States of America, 96*(9), 4868. https://doi.org/10.1073/pnas.96.9.4868

Grozinger, C. M., & Schreiber, S. L. (2000). Regulation of histone deacetylase 4 and 5 and transcriptional activity by 14-3- 3-dependent cellular localization. *Proceedings of the National Academy of Sciences of the United States of America, 97*(14), 7835. https://doi.org/10.1073/pnas.140199597

Gu, X., Huang, X., Li, D., Bi, N., Yu, X., & Wang, H.-L. (2020). Nuclear accumulation of histone deacetylase 4 (HDAC4) by PP1-mediated dephosphorylation exerts neurotoxicity in Pb-exposed neural cells. *NeuroToxicology, 81*, 395-405. https://doi.org/10.1016/j.neuro.2020.10.006

Guenther, M. G., Barak, O., & Lazar, M. A. (2001). The SMRT and N-CoR corepressors are activating cofactors for histone deacetylase 3. *Molecular and Cellular Biology, 21*(18), 6091-6101. https://doi.org/10.1128/mcb.21.18.6091-6101.2001

Guo, L., Han, A., Bates, D. L., Cao, J., & Chen, L. (2007). Crystal structure of a conserved N-terminal domain of histone deacetylase 4 reveals functional insights into glutamine-rich domains. *Proceedings of the National Academy of Sciences of the United States of America, 104*(11), 4297-4302. https://doi.org/10.1073/pnas.0608041104

Gurudev, N., Yuan, M., & Knust, E. (2014). chaoptin, prominin, eyes shut and crumbs form a genetic network controlling the apical compartment of *Drosophila* photoreceptor cells. *Biology Open, 3*(5), 332-341. https://doi.org/10.1242/bio.20147310

Haberland, M., Montgomery, R. L., & Olson, E. N. (2009). The many roles of histone deacetylases in development and physiology: implications for disease and therapy. *Nature Reviews Genetics, 10*(1), 32-42. https://doi.org/10.1038/nrg2485

Haddadi, M., & Ataei, R. (2022). wde, calpA, if, dap160, and poe genes knock down *Drosophila* models exhibit neurofunctional deficit. *Gene, 829*, 146499. https://doi.org/10.1016/j.gene.2022.146499

Halder, G., Callaerts, P., & Gehring Walter, J. (1995). Induction of ectopic eyes by targeted expression of the eyeless gene in *Drosophila*. *Science, 267*(5205), 1788-1792. https://doi.org/10.1126/science.7892602

Hales, K. G., Korey, C. A., Larracuente, A. M., & Roberts, D. M. (2015). Genetics on the fly: a primer on the *Drosophila* model system. *Genetics, 201*(3), 815. https://doi.org/10.1534/genetics.115.183392

Handy, D. E., Castro, R., & Loscalzo, J. (2011). Epigenetic modifications. *Circulation, 123*(19), 2145-2156. https://doi.org/10.1161/CIRCULATIONAHA.110.956839

Hassig, C. A., Tong, J. K., Fleischer, T. C., Owa, T., Grable, P. G., Ayer, D. E., & Schreiber, S. L. (1998). A role for histone deacetylase activity in HDAC1-mediated transcriptional repression. *Proceedings of the National Academy of Sciences of the United States of America, 95*(7), 3519. https://doi.org/10.1073/pnas.95.7.3519

Hawley, H., R. (2020). *Investigating the role of HDAC4 aggregation in neuronal development in Drosophila melanogaster: a thesis presented in partial fulfilment of the requirements for the degree of Bachelor of Science (Honours) in Biochemistry at Massey University, Manawatū, New Zealand.* [Honours, Massey University].

Hawley, H. R., Roberts, C. J., & Fitzsimons, H. L. (2023). Comparison of neuronal GAL4 drivers along with the AGES (auxin-inducible gene expression system) and TARGET (temporal and regional gene expression

targeting) systems for fine tuning of neuronal gene expression in *Drosophila*. *MicroPublication Biology, 2023*. https://doi.org/10.17912/micropub.biology.000885

Hazelrigg, T., Levis, R., & Rubin, G. M. (1984). Transformation of white locus DNA in *Drosophila*: dosage compensation, zeste interaction, and position effects. *Cell, 36*(2), 469-481. https://doi.org/10.1016/0092-8674(84)90240-x

Heisenberg, M., Borst, A., Wagner, S., & Byers, D. (1985). *Drosophila* mushroom body mutants are deficient in olfactory learning. *Journal of Neurogenetics, 2*(1), 1-30. https://doi.org/10.3109/01677068509100140

Helfrich-Forster, C. (2007). Immunohistochemistry in *Drosophila*: sections and whole mounts. *Methods in Molecular Biology, 362*, 533-547. https://doi.org/10.1007/978-1-59745-257-1_42

Hergeth, S. P., & Schneider, R. (2015). The H1 linker histones: multifunctional proteins beyond the nucleosomal core particle. *EMBO Reports, 16*(11), 1439-1453. https://doi.org/10.15252/embr.201540749

Herold, N., Will, C. L., Wolf, E., Kastner, B., Urlaub, H., & Lührmann, R. (2009). Conservation of the orotein composition and electron microscopy structure of *Drosophila melanogaster* and human spliceosomal complexes. *Molecular and Cellular Biology, 29*(1), 281-301. https://doi.org/10.1128/MCB.01415-08

Herrup, K. (2015). The case for rejecting the amyloid cascade hypothesis. *Nature Neuroscience, 18*(6), 794-799. https://doi.org/10.1038/nn.4017

Herrup, K., Li, J., & Chen, J. (2013). The role of ATM and DNA damage in neurons: upstream and downstream connections. *DNA Repair, 12*(8), 600-604. https://doi.org/10.1016/j.dnarep.2013.04.012

Herskovits, A. Z., & Guarente, L. (2013). Sirtuin deacetylases in neurodegenerative diseases of aging. *Cell Research, 23*(6), 746-758. https://doi.org/10.1038/cr.2013.70

Higashiyama, H., Hirose, F., Yamaguchi, M., Inoue, Y. H., Fujikake, N., Matsukage, A., & Kakizuka, A. (2002). Identification of ter94, *Drosophila* VCP, as a modulator of polyglutamine-induced neurodegeneration. *Cell Death & Differentiation, 9*(3), 264-273. https://doi.org/10.1038/sj.cdd.4400955

Hipp, M. S., Kasturi, P., & Hartl, F. U. (2019). The proteostasis network and its decline in ageing. *Nature Reviews Molecular Cell Biology, 20*(7), 421-435. https://doi.org/10.1038/s41580-019-0101-y

Hobara, T., Uchida, S., Otsuki, K., Matsubara, T., Funato, H., Matsuo, K., Suetsugi, M., & Watanabe, Y. (2010). Altered gene expression of histone deacetylases in mood disorder patients. *Journal of Psychiatric Research, 44*(5), 263-270. https://doi.org/10.1016/j.jpsychires.2009.08.015

Höhn, A., Tramutola, A., & Cascella, R. (2020). Proteostasis failure in neurodegenerative diseases: focus on oxidative stress. *Oxidative Medicine and Cellular Longevity, 2020*, 5497046. https://doi.org/10.1155/2020/5497046

Holley, S. A., Jackson, P. D., Sasai, Y., Lu, B., Robertis, E. M. D., Hoffmann, F. M., & Ferguson, E. L. (1995). A conserved system for dorsal-ventral patterning in insects and vertebrates involving sog and chordin. *Nature, 376*(6537), 249-253. https://doi.org/10.1038/376249a0

Holmberg, C. I., Staniszewski, K. E., Mensah, K. N., Matouschek, A., & Morimoto, R. I. (2004). Inefficient degradation of truncated polyglutamine proteins by the proteasome. *The EMBO Journal, 23*(21), 4307-4318. https://doi.org/10.1038/sj.emboj.7600426

Hong, L., Schroth, G. P., Matthews, H. R., Yau, P., & Bradbury, E. M. (1993). Studies of the DNA binding properties of histone H4 amino terminus. *Journal of Biological Chemistry, 268*(1), 305-314. https://doi.org/10.1016/S0021-9258(18)54150-8

Housmans, J. A. J., Wu, G., Schymkowitz, J., & Rousseau, F. (2023). A guide to studying protein aggregation. *The FEBS Journal, 290*(3), 554-583. https://doi.org/10.1111/febs.16312

Huang, D. W., Sherman, B. T., & Lempicki, R. A. (2009). Systematic and integrative analysis of large gene lists using DAVID bioinformatics resources. *Nature Protocols, 4*(1), 44-57. https://doi.org/10.1038/nprot.2008.211

Huang, E. Y., Zhang, J., Miska, E. A., Guenther, M. G., Kouzarides, T., & Lazar, M. A. (2000). Nuclear receptor corepressors partner with class II histone deacetylases in a Sin3-independent repression pathway. *Genes & Development, 14*(1), 45-54. https://doi.org/10.1101/gad.14.1.45

Hubbert, C., Guardiola, A., Shao, R., Kawaguchi, Y., Ito, A., Nixon, A., Yoshida, M., Wang, X.-F., & Yao, T.-P. (2002). HDAC6 is a microtubule-associated deacetylase. *Nature, 417*(6887), 455-458. https://doi.org/10.1038/417455a

Hulsen, T., de Vlieg, J., & Alkema, W. (2008). BioVenn – a web application for the comparison and visualization of biological lists using area-proportional Venn diagrams. *BMC Genomics, 9*(1), 488. https://doi.org/10.1186/1471-2164-9-488

Hurtado, E., Núñez-Álvarez, Y., Muñoz, M., Gutiérrez-Caballero, C., Casas, J., Pendás, A. M., Peinado, M. A., & Suelves, M. (2020). HDAC11 is a novel regulator of fatty acid oxidative metabolism in skeletal muscle. *The FEBS Journal*. https://doi.org/10.1111/febs.15456

Hyde, C. L., Nagle, M. W., Tian, C., Chen, X., Paciga, S. A., Wendland, J. R., Tung, J. Y., Hinds, D. A., Perlis, R. H., & Winslow, A. R. (2016). Identification of 15 genetic loci associated with risk of major depression in individuals of European descent. *Nature Genetics, 48*(9), 1031-1036. https://doi.org/10.1038/ng.3623

Imai, R., Nozaki, T., Tani, T., Kaizu, K., Hibino, K., Ide, S., Tamura, S., Takahashi, K., Shribak, M., & Maeshima, K. (2017). Density imaging of heterochromatin in live cells using orientation-independent-DIC microscopy. *Molecular Biology of the Cell, 28*(23), 3349-3359. https://doi.org/10.1091/mbc.E17-06-0359

Imai, S.-i., Armstrong, C. M., Kaeberlein, M., & Guarente, L. (2000). Transcriptional silencing and longevity protein Sir2 is an NAD-dependent histone deacetylase. *Nature, 403*(6771), 795-800. https://doi.org/10.1038/35001622

Ito, K., Awano, W., Suzuki, K., Hiromi, Y., & Yamamoto, D. (1997). The *Drosophila* mushroom body is a quadruple structure of clonal units each of which contains a virtually identical set of neurones and glial cells. *Development, 124*(4), 761-771. https://doi.org/10.1242/dev.124.4.761

Izaddoost, S., Nam, S.-C., Bhat, M. A., Bellen, H. J., & Choi, K.-W. (2002). *Drosophila* Crumbs is a positional cue in photoreceptor adherens junctions and rhabdomeres. *Nature, 416*(6877), 178-183. https://doi.org/10.1038/nature720

Jacobson, R. H., Ladurner, A. G., King, D. S., & Tjian, R. (2000). Structure and function of a human TAFII250 double bromodomain module. *Science, 288*(5470), 1422. https://doi.org/10.1126/science.288.5470.1422

Jagatheesan, G., Thanumalayan, S., Muralikrishna, B., Rangaraj, N., Karande, A. A., & Parnaik, V. K. (1999). Colocalization of intranuclear lamin foci with RNA splicing factors. *Journal of Cell Science, 112*(24), 4651-4661. https://doi.org/10.1242/jcs.112.24.4651

Jayathilaka, N., Han, A., Gaffney, K. J., Dey, R., Jarusiewicz, J. A., Noridomi, K., Philips, M. A., Lei, X., He, J., Ye, J., Gao, T., Petasis, N. A., & Chen, L. (2012). Inhibition of the function of class IIa HDACs by blocking their interaction with MEF2. *Nucleic Acids Research, 40*(12), 5378-5388. https://doi.org/10.1093/nar/gks189

Jebessa, Z. H., Shanmukha, K. D., Dewenter, M., Lehmann, L. H., Xu, C., Schreiter, F., Siede, D., Gong, X. M., Worst, B. C., Federico, G., Sauer, S. W., Fischer, T., Wechselberger, L., Müller, O. J., Sossalla, S., Dieterich, C., Most, P., Gröne, H. J., Moro, C., Oberer, M., Haemmerle, G., Katus, H. A., Tyedmers, J., & Backs, J. (2019). The lipid droplet-associated protein ABHD5 protects the heart through proteolysis of HDAC4. *Nature Metabolism, 1*(11), 1157-1167. https://doi.org/10.1038/s42255-019-0138-4

Jeibmann, A., & Paulus, W. (2009). *Drosophila melanogaster* as a model organism of brain diseases. *International Journal of Molecular Sciences, 10*(2), 407-440. https://doi.org/10.3390/ijms10020407

Jenett, A., Rubin, G., M, Ngo, T., B., Shepherd, D., Murphy, C., Dionne, H., Pfeiffer, B., D, Cavallaro, A., Hall, D., Jeter, J., Iyer, N., Fetter, D., Hausenfluck, J., H, Peng, H., Trautman, E., T, Svirskas, R., R, Myers, E., W, Iwinski, Z., R, Aso, Y., DePasquale, G., M, Enos, A., Hulamm, P., Lam, S., C, B, Li, H., Laverty, T., R, Long, F., Qu, L., Murphy, S., D, Rokicki, K., Safford, T., Shaw, K., Simpson, J., H, Sowell, A., Tae, S., Yu, Y., & Zugates, C., T. (2012). A GAL4-Driver Line Resource for *Drosophila* Neurobiology. *Cell Reports, 2*(4), 991-1001. https://doi.org/10.1016/j.celrep.2012.09.011

Jenuwein, T., & Allis, C. D. (2001). Translating the histone code. *Science, 293*(5532), 1074. https://doi.org/10.1126/science.1063127

Johnson, R. L., & Tabin, C. J. (1997). Molecular models for vertebrate limb development. *Cell, 90*(6), 979-990. https://doi.org/10.1016/S0092-8674(00)80364-5

Johnston, J. A., Ward, C. L., & Kopito, R. R. (1998). Aggresomes: a cellular response to misfolded proteins. *Journal of Cell Biology, 143*(7), 1883-1898. https://doi.org/10.1083/jcb.143.7.1883

Johri, A., & Beal, M. F. (2012). Mitochondrial dysfunction in neurodegenerative diseases. *Journal of Pharmacology and Experimental Therapeutics, 342*(3), 619-630. https://doi.org/10.1124/jpet.112.192138

Ju, J. S., Miller, S. E., Hanson, P. I., & Weihl, C. C. (2008). Impaired protein aggregate handling and clearance underlie the pathogenesis of p97/VCP-associated disease. *Journal of Biological Chemistry, 283*(44), 30289-30299. https://doi.org/10.1074/jbc.M805517200

Jumper, J., Evans, R., Pritzel, A., Green, T., Figurnov, M., Ronneberger, O., Tunyasuvunakool, K., Bates, R., Žídek, A., Potapenko, A., Bridgland, A., Meyer, C., Kohl, S. A. A., Ballard, A. J., Cowie, A., Romera-Paredes, B., Nikolov, S., Jain, R., Adler, J., Back, T., Petersen, S., Reiman, D., Clancy, E., Zielinski, M., Steinegger, M., Pacholska, M., Berghammer, T., Bodenstein, S., Silver, D., Vinyals, O., Senior, A. W., Kavukcuoglu, K., Kohli, P., & Hassabis, D. (2021). Highly accurate protein structure prediction with AlphaFold. *Nature, 596*(7873), 583-589. https://doi.org/10.1038/s41586-021-03819-2

Kalivendi, S. V., Yedlapudi, D., Hillard, C. J., & Kalyanaraman, B. (2010). Oxidants induce alternative splicing of alpha-synuclein: Implications for Parkinson's disease. *Free Radical Biology and Medicine, 48*(3), 377-383. https://doi.org/10.1016/j.freeradbiomed.2009.10.045

Kametaka, S., Kametaka, A., Yonekura, S., Haruta, M., Takenoshita, S., Goto, S., & Waguri, S. (2012). AP-1 clathrin adaptor and CG8538/Aftiphilin are involved in Notch signaling during eye development in *Drosophila melanogaster*. *Journal of Cell Science, 125*(3), 634-648. https://doi.org/10.1242/jcs.090167

Kanda, H., Nguyen, A., Chen, L., Okano, H., & Hariharan, I. K. (2013). The *Drosophila* ortholog of MLL3 and MLL4, trithorax related, functions as a negative regulator of tissue growth. *Molecular and Cellular Biology, 33*(9), 1702-1710. https://doi.org/10.1128/MCB.01585-12

Kang, M.-J., Chung, J., & Ryoo, H. D. (2012). CDK5 and MEKK1 mediate pro-apoptotic signalling following endoplasmic reticulum stress in an autosomal dominant retinitis pigmentosa model. *Nature Cell Biology, 14*(4), 409-415. https://doi.org/10.1038/ncb2447

Kanuka, H., Hiratou, T., Igaki, T., Kanda, H., Kuranaga, E., Sawamoto, K., Aigaki, T., Okano, H., & Miura, M. (2005). Gain-of-function screen identifies a role of the Sec61α translocon in *Drosophila* postmitotic neurotoxicity. *Biochimica et Biophysica Acta (BBA) - General Subjects, 1726*(3), 225-237. https://doi.org/10.1016/j.bbagen.2005.06.020

Kapuscinski, J. (1995). DAPI: a DNA-specific fluorescent probe. *Biotechnic & Histochemistry, 70*(5), 220-233. https://doi.org/10.3109/10520299509108199

Karagiosis, S. A., & Ready, D. F. (2004). Moesin contributes an essential structural role in *Drosophila* photoreceptor morphogenesis. *Development, 131*(4), 725-732. https://doi.org/10.1242/dev.00976

Karim, F. D., Chang, H. C., Therrien, M., Wassarman, D. A., Laverty, T., & Rubin, G. M. (1996). A screen for genes that function downstream of Ras1 during *Drosophila* eye development. *Genetics, 143*(1), 315-329. https://doi.org/10.1093/genetics/143.1.315

Karran, E., Mercken, M., & Strooper, B. D. (2011). The amyloid cascade hypothesis for Alzheimer's disease: an appraisal for the development of therapeutics. *Nature Reviews Drug Discovery, 10*(9), 698-712. https://doi.org/10.1038/nrd3505

Kasai, Y., & Cagan, R. (2010). *Drosophila* as a tool for personalized medicine: a primer. *Personalized Medicine, 7*(6), 621-632. https://doi.org/10.2217/pme.10.65

Keleman, K., Krüttner, S., Alenius, M., & Dickson, B. J. (2007). Function of the *Drosophila* CPEB protein Orb2 in long-term courtship memory. *Nat Neurosci, 10*(12), 1587-1593. https://doi.org/10.1038/nn1996

Kelemen, O., Convertini, P., Zhang, Z., Wen, Y., Shen, M., Falaleeva, M., & Stamm, S. (2013). Function of alternative splicing. *Gene, 514*(1), 1-30. https://doi.org/10.1016/j.gene.2012.07.083

Kepp, K. P., Robakis, N. K., Høilund-Carlsen, P. F., Sensi, S. L., & Vissel, B. (2023). The amyloid cascade hypothesis: an updated critical review. *Brain, 146*(10), 3969-3990. https://doi.org/10.1093/brain/awad159

Kim, G. S., Jung, H.-E., Kim, J.-S., & Lee, Y. C. (2015). Mutagenesis study reveals the rim of catalytic entry site of HDAC4 and -5 as the major binding surface of SMRT corepressor. *PLOS One, 10*(7), e0132680. https://doi.org/10.1371/journal.pone.0132680

Kim, M.-S., Akhtar, M. W., Adachi, M., Mahgoub, M., Bassel-Duby, R., Kavalali, E. T., Olson, E. N., & Monteggia, L. M. (2012). An essential role for histone deacetylase 4 in synaptic plasticity and memory formation. *The Journal of Neuroscience, 32*(32), 10879. https://doi.org/10.1523/JNEUROSCI.2089-12.2012

King, I., Tsai, L. T. Y., Pflanz, R., Voigt, A., Lee, S., Jäckle, H., Lu, B., & Heberlein, U. (2011). *Drosophila tao* controls mushroom body development and ethanol-stimulated behavior through *par-1*. *The Journal of Neuroscience, 31*(3), 1139. https://doi.org/10.1523/JNEUROSCI.4416-10.2011

Kirsh, O., Seeler, J.-S., Pichler, A., Gast, A., Müller, S., Miska, E., Mathieu, M., Harel-Bellan, A., Kouzarides, T., Melchior, F., & Dejean, A. (2002). The SUMO E3 ligase RanBP2 promotes modification of the HDAC4 deacetylase. *The EMBO Journal, 21*(11), 2682-2691. https://doi.org/10.1093/emboj/21.11.2682

Klement, I. A., Skinner, P. J., Kaytor, M. D., Yi, H., Hersch, S. M., Clark, H. B., Zoghbi, H. Y., & Orr, H. T. (1998). Ataxin-1 nuclear localization and aggregation: role in polyglutamine-induced disease in SCA1 transgenic mice. *Cell, 95*(1), 41-53. https://doi.org/10.1016/s0092-8674(00)81781-x

Knowles-Barley, S., Longair, M., & Armstrong, J. D. (2010). BrainTrap: a database of 3D protein expression patterns in the *Drosophila* brain. *Database (Oxford), 2010*. https://doi.org/10.1093/database/baq005

Kobayashi, M., Michaut, L., Ino, A., Honjo, K., Nakajima, T., Maruyama, Y., Mochizuki, H., Ando, M., Ghangrekar, I., Takahashi, K., Saigo, K., Ueda, R., Gehring, W. J., & Furukubo-Tokunaga, K. (2006). Differential microarray analysis of *Drosophila* mushroom body transcripts using chemical ablation. *Proceedings of the National Academy of Sciences of the United States of America, 103*(39), 14417-14422. https://doi.org/10.1073/pnas.0606571103

Koemans, T., Kleefstra, T., Chubak, M., Stone, M., Reijnders, M., Munnik, S., Willemsen, M., Fenckova, M., Stumpel, C., Bok, L., Saenz, M., Byerly, K., Baughn, L., Stegmann, A., Pfundt, R., Zhou, H., Bokhoven, H., Schenck, A., & Kramer, J. (2017). Functional convergence of histone methyltransferases EHMT1 and KMT2C involved in intellectual disability and autism spectrum disorder. *PLOS Genetics, 13*, e1006864. https://doi.org/10.1371/journal.pgen.1006864

Kopito, R. R. (2000). Aggresomes, inclusion bodies and protein aggregation. *Trends in Cell Biology, 10*(12), 524-530. https://doi.org/10.1016/s0962-8924(00)01852-3

Kosiorek, M., Podszywalow-Bartnicka, P., Zylinska, L., & Pikula, S. (2014). NFAT1 and NFAT3 Cooperate with HDAC4 during Regulation of Alternative Splicing of PMCA Isoforms in PC12 Cells. *PLOS One, 9*(6), e99118. https://doi.org/10.1371/journal.pone.0099118

Kramer, J. M., & Staveley, B. E. (2003). GAL4 causes developmental defects and apoptosis when expressed in the developing eye of *Drosophila melanogaster*. *Genetics and Molecular Research, 2*(1), 43-47.

Kronlage, M., Dewenter, M., Grosso, J., Fleming, T., Oehl, U., Lehmann, L. H., Falcão-Pires, I., Leite-Moreira, A. F., Volk, N., Gröne, H. J., Müller, O. J., Sickmann, A., Katus, H. A., & Backs, J. (2019). O-GlcNAcylation of histone deacetylase 4 protects the diabetic heart from failure. *Circulation, 140*(7), 580-594. https://doi.org/10.1161/circulationaha.117.031942

Kumar, A., & Tiwari, A. K. (2018). Molecular chaperone Hsp70 and its constitutively active form Hsc70 play an indispensable role during eye development of *Drosophila melanogaster*. *Molecular Neurobiology, 55*(5), 4345-4361. https://doi.org/10.1007/s12035-017-0650-z

Kumar, J. P. (2012). Building an ommatidium one cell at a time. *Developmental Dynamics, 241*(1), 136-149. https://doi.org/10.1002/dvdy.23707

Kumar, J. P., & Ready, D. F. (1995). Rhodopsin plays an essential structural role in *Drosophila* photoreceptor development. *Development, 121*(12), 4359-4370. https://doi.org/10.1242/dev.121.12.4359

Kurusu, M., Katsuki, T., Zinn, K., & Suzuki, E. (2012). Developmental changes in expression, subcellular distribution, and function of Drosophila N-cadherin, guided by a cell-intrinsic program during neuronal differentiation. *Developmental Biology, 366*(2), 204-217. https://doi.org/10.1016/j.ydbio.2012.04.006

Kwon, D. H., Ryu, J., Kim, Y. K., & Kook, H. (2020). Roles of histone acetylation modifiers and other epigenetic regulators in vascular calcification. *International Journal of Molecular Sciences, 21*(9). https://doi.org/10.3390/ijms21093246

Lahm, A., Paolini, C., Pallaoro, M., Nardi, M. C., Jones, P., Neddermann, P., Sambucini, S., Bottomley, M. J., Lo Surdo, P., Carfí, A., Koch, U., De Francesco, R., Steinkühler, C., & Gallinari, P. (2007). Unraveling the hidden catalytic activity of vertebrate class IIa histone deacetylases. *Proceedings of the National Academy of Sciences of the United States of America, 104*(44), 17335. https://doi.org/10.1073/pnas.0706487104

Lambert, J.-C., Ibrahim-Verbaas, C. A., Harold, D., Naj, A. C., Sims, R., Bellenguez, C., Jun, G., DeStefano, A. L., Bis, J. C., Beecham, G. W., Grenier-Boley, B., Russo, G., Thornton-Wells, T. A., Jones, N., Smith, A. V., Chouraki, V., Thomas, C., Ikram, M. A., Zelenika, D., …, & Amouyel, P. (2013). Meta-analysis of 74,046 individuals identifies 11 new susceptibility loci for Alzheimer's disease. *Nature Genetics, 45*(12), 1452-1458. https://doi.org/10.1038/ng.2802

Lamond, A. I., & Spector, D. L. (2003). Nuclear speckles: a model for nuclear organelles. *Nature Reviews Molecular Cell Biology, 4*(8), 605-612. https://doi.org/10.1038/nrm1172

Lang, C., Campbell, K. R., Ryan, B. J., Carling, P., Attar, M., Vowles, J., Perestenko, O. V., Bowden, R., Baig, F., Kasten, M., Hu, M. T., Cowley, S. A., Webber, C., & Wade-Martins, R. (2019). Single-cell sequencing of iPSC-dopamine neurons reconstructs disease progression and identifies HDAC4 as a regulator of Parkinson cell phenotypes. *Cell Stem Cell, 24*(1), 93-106.e106. https://doi.org/10.1016/j.stem.2018.10.023

Le Meur, N., Holder-Espinasse, M., Jaillard, S., Goldenberg, A., Joriot, S., Amati-Bonneau, P., Guichet, A., Barth, M., Charollais, A., Journel, H., Auvin, S., Boucher, C., Kerckaert, J. P., David, V., Manouvrier-Hanu, S., Saugier-Veber, P., Frébourg, T., Dubourg, C., Andrieux, J., & Bonneau, D. (2010). *MEF2C* haploinsufficiency caused by either microdeletion of the 5q14.3 region or mutation is responsible for severe mental retardation with stereotypic movements, epilepsy and/or cerebral malformations. *Journal of Medical Genetics, 47*(1), 22. https://doi.org/10.1136/jmg.2009.069732

Le, T. N., Williams, S. R., Alaimo, J. T., & Elsea, S. H. (2019). Genotype and phenotype correlation in 103 individuals with 2q37 deletion syndrome reveals incomplete penetrance and supports HDAC4 as the primary genetic contributor. *American Journal of Medical Genetics, 179*(5), 782-791. https://doi.org/10.1002/ajmg.a.61089

Leader, D. P., Krause, S. A., Pandit, A., Davies, S. A., & Dow, J. A T. (2018). FlyAtlas 2: a new version of the *Drosophila melanogaster* expression atlas with RNA-Seq, miRNA-Seq and sex-specific data. *Nucleic Acids Research, 46*(D1), D809-D815. https://doi.org/10.1093/nar/gkx976

Lee, H., Engel, U., Rusch, J., Scherrer, S., Sheard, K., & Van Vactor, D. (2004). The microtubule plus end tracking protein Orbit/MAST/CLASP acts downstream of the tyrosine kinase Abl in mediating axon guidance. *Neuron, 42*(6), 913-926. https://doi.org/10.1016/j.neuron.2004.05.020

Lee, P.-T., Zirin, J., Kanca, O., Lin, W.-W., Schulze, K. L., Li-Kroeger, D., Tao, R., Devereaux, C., Hu, Y., Chung, V., Fang, Y., He, Y., Pan, H., Ge, M., Zuo, Z., Housden, B. E., Mohr, S. E., Yamamoto, S., Levis, R. W., Spradling, A. C., Perrimon, N., & Bellen, H. J. (2018). A gene-specific T2A-GAL4 library for *Drosophila*. *eLife, 7*, e35574. https://doi.org/10.7554/eLife.35574

Lee, T., Lee, A., & Luo, L. (1999). Development of the *Drosophila* mushroom bodies: sequential generation of three distinct types of neurons from a neuroblast. *Development, 126*(18), 4065. https://doi.org/10.1242/dev.126.18.4065

Lee, T., & Luo, L. (1999). Mosaic analysis with a repressible cell marker for studies of gene function in neuronal morphogenesis. *Neuron, 22*(3), 451-461. https://doi.org/10.1016/S0896-6273(00)80701-1

Lehmann, L. H., Jebessa, Z. H., Kreusser, M. M., Horsch, A., He, T., Kronlage, M., Dewenter, M., Sramek, V., Oehl, U., Krebs-Haupenthal, J., von der Lieth, A. H., Schmidt, A., Sun, Q., Ritterhoff, J., Finke, D., Völkers, M., Jungmann, A., Sauer, S. W., Thiel, C., …, & Backs, J. (2018). A proteolytic fragment of histone deacetylase 4 protects the heart from failure by regulating the hexosamine biosynthetic pathway. *Nature Medicine, 24*(1), 62-72. https://doi.org/10.1038/nm.4452

Leifer, D., Krainc, D., Yu, Y. T., McDermott, J., Breitbart, R. E., Heng, J., Neve, R. L., Kosofsky, B., Nadal-Ginard, B., & Lipton, S. A. (1993). MEF2C, a MADS/MEF2-family transcription factor expressed in a laminar distribution in cerebral cortex. *Proceedings of the National Academy of Sciences of the United States of America, 90*(4), 1546-1550. https://doi.org/10.1073/pnas.90.4.1546

Li, D., McIntosh, C. S., Mastaglia, F. L., Wilton, S. D., & Aung-Htut, M. T. (2021). Neurodegenerative diseases: a hotbed for splicing defects and the potential therapies. *Translational Neurodegeneration, 10*(1), 16. https://doi.org/10.1186/s40035-021-00240-7

Li, F., Lindsey, J. W., Marin, E. C., Otto, N., Dreher, M., Dempsey, G., Stark, I., Bates, A. S., Pleijzier, M. W., Schlegel, P., Nern, A., Takemura, S.-y., Eckstein, N., Yang, T., Francis, A., Braun, A., Parekh, R., Costa, M., Scheffer, L. K., Aso, Y., Jefferis, G. S. X. E., Abbott, L. F., Litwin-Kumar, A., Waddell, S., & Rubin, G. M. (2020). The connectome of the adult *Drosophila* mushroom body provides insights into function. *eLife, 9*, e62576. https://doi.org/10.7554/eLife.62576

Li, J., Chen, J., Ricupero, C. L., Hart, R. P., Schwartz, M. S., Kusnecov, A., & Herrup, K. (2012). Nuclear accumulation of HDAC4 in ATM deficiency promotes neurodegeneration in ataxia telangiectasia. *Nature Medicine, 18*(5), 783-790. https://doi.org/10.1038/nm.2709

Li, M., Linseman, D. A., Allen, M. P., Meintzer, M. K., Wang, X., Laessig, T., Wierman, M. E., & Heidenreich, K. A. (2001). Myocyte enhancer factor 2A and 2D undergo phosphorylation and caspase-mediated degradation during apoptosis of rat cerebellar granule neurons. *Journal of Neuroscience, 21*(17), 6544-6552. https://doi.org/10.1523/jneurosci.21-17-06544.2001

Li, Y., Collins, M., An, J., Geiser, R., Tegeler, T., Tsantilas, K., Garcia, K., Pirrotte, P., & Bowser, R. (2016). Immunoprecipitation and mass spectrometry defines an extensive RBM45 protein-protein interaction network. *Brain Research, 1647*, 79-93. https://doi.org/10.1016/j.brainres.2016.02.047

Licatalosi, D. D., & Darnell, R. B. (2006). Splicing regulation in neurologic disease. *Neuron, 52*(1), 93-101. https://doi.org/10.1016/j.neuron.2006.09.017

Lilly, B., Galewsky, S., Firulli, A. B., Schulz, R. A., & Olson, E. N. (1994). D-MEF2: a MADS box transcription factor expressed in differentiating mesoderm and muscle cell lineages during *Drosophila* embryogenesis.

Proceedings of the National Academy of Sciences of the United States of America, 91(12), 5662. https://doi.org/10.1073/pnas.91.12.5662

Linkert, M., Rueden, C. T., Allan, C., Burel, J.-M., Moore, W., Patterson, A., Loranger, B., Moore, J., Neves, C., MacDonald, D., Tarkowska, A., Sticco, C., Hill, E., Rossner, M., Eliceiri, K. W., & Swedlow, J. R. (2010). Metadata matters: access to image data in the real world. *Journal of Cell Biology, 189*(5), 777-782. https://doi.org/10.1083/jcb.201004104

Litke, C., Bading, H., & Mauceri, D. (2018). Histone deacetylase 4 shapes neuronal morphology via a mechanism involving regulation of expression of vascular endothelial growth factor D. *Journal of Biological Chemistry, 293*(21), 8196-8207. https://doi.org/10.1074/jbc.RA117.001613

Litke, C., Hagenston, A. M., Kenkel, A.-K., Paldy, E., Lu, J., Kuner, R., & Mauceri, D. (2022). Organic anion transporter 1 is an HDAC4-regulated mediator of nociceptive hypersensitivity in mice. *Nature Communications, 13*(1), 875. https://doi.org/10.1038/s41467-022-28357-x

Liu, F., Dowling, M., Yang, X.-J., & Kao, G. D. (2004). Caspase-mediated specific cleavage of human histone deacetylase 4. *Journal of Biological Chemistry, 279*(33), 34537-34546. https://doi.org/10.1074/jbc.M402475200

Liu, Y., Peng, L., Seto, E., Huang, S., & Qiu, Y. (2012). Modulation of histone deacetylase 6 (HDAC6) nuclear import and tubulin deacetylase activity through acetylation. *Journal of Biological Chemistry, 287*(34), 29168-29174. https://doi.org/10.1074/jbc.M112.371120

Liu, Z., Steward, R., & Luo, L. (2000). *Drosophila* Lis1 is required for neuroblast proliferation, dendritic elaboration and axonal transport. *Nature Cell Biology, 2*(11), 776-783. https://doi.org/10.1038/35041011

Liu, Z., Yang, C.-P., Sugino, K., Fu, C.-C., Liu, L.-Y., Yao, X., Lee, L. P., & Lee, T. (2015). Opposing intrinsic temporal gradients guide neural stem cell production of varied neuronal fates. *Science, 350*(6258), 317-320. https://doi.org/10.1126/science.aad1886

Lu, J., McKinsey, T. A., Zhang, C.-L., & Olson, E. N. (2000). Regulation of skeletal myogenesis by association of the MEF2 transcription factor with class II histone deacetylases. *Molecular Cell, 6*(2), 233-244. https://doi.org/10.1016/S1097-2765(00)00025-3

Luckhurst, C. A., Aziz, O., Beaumont, V., Bürli, R. W., Breccia, P., Maillard, M. C., Haughan, A. F., Lamers, M., Leonard, P., Matthews, K. L., Raphy, G., Stott, A. J., Munoz-Sanjuan, I., Thomas, B., Wall, M., Wishart, G., Yates, D., & Dominguez, C. (2019). Development and characterization of a CNS-penetrant benzhydryl hydroxamic acid class IIa histone deacetylase inhibitor. *Bioorganic & Medicinal Chemistry Letters, 29*(1), 83-88. https://doi.org/10.1016/j.bmcl.2018.11.009

Ma, J., & Ptashne, M. (1987). Deletion analysis of GAL4 defines two transcriptional activating segments. *Cell, 48*, 847-853. https://doi.org/10.1016/0092-8674(87)90081-X

Ma'u, E., Cullum, S., Yates, S., Te Ao, B., Cheung, G., Burholt, V., Dudley, M., Krishnamurthi, R., & Kerse, N. (2021). Dementia Economic Impact Report 2020. *University of Auckland, New Zealand*.

MacPherson, R. A., Shankar, V., Anholt, R. R. H., & Mackay, T. F. C. (2023). Genetic and genomic analyses of *Drosophila melanogaster* models of chromatin modification disorders. *Genetics, 224*(4), iyad061. https://doi.org/10.1093/genetics/iyad061

Maglott, D., Ostell, J., Pruitt, K. D., & Tatusova, T. (2005). Entrez Gene: gene-centered information at NCBI. *Nucleic Acids Research, 33*(suppl_1), D54-D58. https://doi.org/10.1093/nar/gki031

Magnin, E. (2021). Neurodevelopmental and neurocognitive similarities and interactions: a point of view about lifelong neurocognitive trajectories. *Journal of Alzheimer's Disease, 79*, 1397-1407. https://doi.org/10.3233/JAD-201207

Main, P., Tan, W. J., Wheeler, D., & Fitzsimons, H. L. (2021). Increased abundance of nuclear HDAC4 impairs neuronal development and long-term memory. *Frontiers in Molecular Neuroscience, 14*(48). https://doi.org/10.3389/fnmol.2021.616642

Main, P. J. (2019). *Investigating the role of HDAC4 subcellular distribution in Drosophila development and memory : a thesis presented in partial fulfilment of the requirements for the degree of Doctor of Philosophy (PhD) in Biochemistry at Massey University, Manawatū, New Zealand.* [Doctoral, Massey University]. http://hdl.handle.net/10179/15578

Maitra, U., Scaglione, M. N., Chtarbanova, S., & O'Donnell, J. M. (2019). Innate immune responses to paraquat exposure in a *Drosophila* model of Parkinson's disease. *Scientific Reports, 9*(1), 12714. https://doi.org/10.1038/s41598-019-48977-6

Majdzadeh, N., Wang, L., Morrison, B. E., Bassel-Duby, R., Olson, E. N., & D'Mello, S. R. (2008). HDAC4 inhibits cell-cycle progression and protects neurons from cell death. *Developmental Neurobiology, 68*(8), 1076-1092. https://doi.org/10.1002/dneu.20637

Mao, Z., Bonni, A., Xia, F., Nadal-Vicens, M., & Greenberg, M. E. (1999). Neuronal activity-dependent cell survival mediated by transcription factor MEF2. *Science, 286*(5440), 785. https://doi.org/10.1126/science.286.5440.785

Marek, L., Hamacher, A., Hansen, F. K., Kuna, K., Gohlke, H., Kassack, M. U., & Kurz, T. (2013). Histone deacetylase (HDAC) inhibitors with a novel connecting unit linker region reveal a selectivity profile for HDAC4 and HDAC5 with improved activity against chemoresistant cancer cells. *Journal of Medical Chemistry, 56*(2), 427-436. https://doi.org/10.1021/jm301254q

Mariño-Ramírez, L., Kann, M. G., Shoemaker, B. A., & Landsman, D. (2005). Histone structure and nucleosome stability. *Expert Review of Proteomics, 2*(5), 719-729. https://doi.org/10.1586/14789450.2.5.719

Markstein, M., Pitsouli, C., Villalta, C., Celniker, S. E., & Perrimon, N. (2008). Exploiting position effects and the gypsy retrovirus insulator to engineer precisely expressed transgenes. *Nature Genetics, 40*(4), 476-483. https://doi.org/10.1038/ng.101

Marshall, O. J., & Delandre, C. (2022). Profiling protein-DNA interactions cell-type-specifically with Targeted DamID. *Methods in Molecular Biology, 2458*, 195-213. https://doi.org/10.1007/978-1-0716-2140-0_11

Marshall, O. J., Southall, T. D., Cheetham, S. W., & Brand, A. H. (2016). Cell-type-specific profiling of protein–DNA interactions without cell isolation using targeted DamID with next-generation sequencing. *Nature Protocols, 11*(9), 1586-1598. https://doi.org/10.1038/nprot.2016.084

Matera, A. G., & Wang, Z. (2014). A day in the life of the spliceosome. *Nature Reviews Molecular Cell Biology, 15*(2), 108-121. https://doi.org/10.1038/nrm3742

Matsumoto, H., Isono, K., Pye, Q., & Pak, W. L. (1987). Gene encoding cytoskeletal proteins in *Drosophila* rhabdomeres. *Proceedings of the National Academy of Sciences of the United States of America, 84*(4), 985. https://doi.org/10.1073/pnas.84.4.985

McBride, S. M. J., Giuliani, G., Choi, C., Krause, P., Correale, D., Watson, K., Baker, G., & Siwicki, K. K. (1999). Mushroom body ablation impairs short-term memory and long-term memory of courtship conditioning in *Drosophila melanogaster*. *Neuron, 24*(4), 967-977. https://doi.org/10.1016/S0896-6273(00)81043-0

McDermott, J. C., Cardoso, M. C., Yu, Y. T., Andres, V., Leifer, D., Krainc, D., Lipton, S. A., & Nadal-Ginard, B. (1993). hMEF2C gene encodes skeletal muscle- and brain-specific transcription factors. *Molecular and Cellular Biology, 13*(4), 2564-2577. https://doi.org/10.1128/mcb.13.4.2564

McGrail, M., Gepner, J., Silvanovich, A., Ludmann, S., Serr, M., & Hays, T. S. (1995). Regulation of cytoplasmic dynein function *in vivo* by the *Drosophila* Glued complex. *Journal of Cell Biology, 131*(2), 411-425. https://doi.org/10.1083/jcb.131.2.411

McGuire, S. E., Le, P. T., Osborn, A. J., Matsumoto, K., & Davis, R. L. (2003). Spatiotemporal rescue of memory dysfunction in *Drosophila*. *Science, 302*(5651), 1765-1768. https://doi.org/10.1126/science.1089035

McGuire, S. E., Mao, Z., & Davis, R. L. (2004). Spatiotemporal gene expression targeting with the TARGET and gene-switch systems in *Drosophila*. *Science, 2004*(220), pl6. https://doi.org/10.1126/stke.2202004pl6

McGurk, L., Berson, A., & Bonini, N. M. (2015). *Drosophila* as an *in vivo* model for human neurodegenerative disease. *Genetics, 201*(2), 377-402. https://doi.org/10.1534/genetics.115.179457

McKinsey, T. A., Zhang, C. L., & Olson, E. N. (2000). Activation of the myocyte enhancer factor-2 transcription factor by calcium/calmodulin-dependent protein kinase-stimulated binding of 14-3-3 to histone deacetylase 5. *Proceedings of the National Academy of Sciences of the United States of America, 97*(26), 14400. https://doi.org/10.1073/pnas.260501497

McKinsey, T. A., Zhang, C. L., & Olson, E. N. (2001). Identification of a signal-responsive nuclear export sequence in class II histone deacetylases. *Molecular and Cellular Biology, 21*(18), 6312-6321. https://doi.org/10.1128/MCB.21.18.6312-6321.2001

McKinsey, T. A., Zhang, C. L., & Olson, E. N. (2002). MEF2: a calcium-dependent regulator of cell division, differentiation and death. *Trends in Biochemical Sciences, 27*(1), 40-47. https://doi.org/10.1016/s0968-0004(01)02031-x

McNaught, K. S., Shashidharan, P., Perl, D. P., Jenner, P., & Olanow, C. W. (2002). Aggresome-related biogenesis of Lewy bodies. *European Journal of Neuroscience, 16*(11), 2136-2148. https://doi.org/10.1046/j.1460-9568.2002.02301.x

Melicharek, D. J., Ramirez, L. C., Singh, S., Thompson, R., & Marenda, D. R. (2010). Kismet/CHD7 regulates axon morphology, memory and locomotion in a *Drosophila* model of CHARGE syndrome. *Human Molecular Genetics, 19*(21), 4253-4264. https://doi.org/10.1093/hmg/ddq348

Meng, E. C., Goddard, T. D., Pettersen, E. F., Couch, G. S., Pearson, Z. J., Morris, J. H., & Ferrin, T. E. (2023). UCSF ChimeraX: Tools for structure building and analysis. *Protein Science, 32*(11), e4792. https://doi.org/10.1002/pro.4792

Meng, E. C., Pettersen, E. F., Couch, G. S., Huang, C. C., & Ferrin, T. E. (2006). Tools for integrated sequence-structure analysis with UCSF Chimera. *BMC Bioinformatics, 7*, 339. https://doi.org/10.1186/1471-2105-7-339

Menzies, F. M., Hourez, R., Imarisio, S., Raspe, M., Sadiq, O., Chandraratna, D., O'Kane, C., Rock, K. L., Reits, E., Goldberg, A. L., & Rubinsztein, D. C. (2010). Puromycin-sensitive aminopeptidase protects against aggregation-prone proteins via autophagy. *Human Molecular Genetics, 19*(23), 4573-4586. https://doi.org/10.1093/hmg/ddq385

Meserve, J. H., & Duronio, R. J. (2017). A population of G2-arrested cells are selected as sensory organ precursors for the interommatidial bristles of the *Drosophila* eye. *Developmental Biology, 430*(2), 374-384. https://doi.org/10.1016/j.ydbio.2017.06.023

Michalik, A., & Van Broeckhoven, C. (2003). Pathogenesis of polyglutamine disorders: aggregation revisited. *Human Molecular Genetics, 12*(suppl_2), R173-R186. https://doi.org/10.1093/hmg/ddg295

Michelitsch, M. D., & Weissman, J. S. (2000). A census of glutamine/asparagine-rich regions: implications for their conserved function and the prediction of novel prions. *Proceedings of the National Academy of Sciences of the United States of America, 97*(22), 11910-11915. https://doi.org/10.1073/pnas.97.22.11910

Mielcarek, M., Landles, C., Weiss, A., Bradaia, A., Seredenina, T., Inuabasi, L., Osborne, G. F., Wadel, K., Touller, C., Butler, R., Robertson, J., Franklin, S. A., Smith, D. L., Park, L., Marks, P. A., Wanker, E. E., Olson, E. N., Luthi-Carter, R., van der Putten, H., Beaumont, V., & Bates, G. P. (2013). HDAC4 reduction: a novel therapeutic strategy to target cytoplasmic huntingtin and ameliorate neurodegeneration. *PLOS Biology, 11*(11), e1001717-e1001717. https://doi.org/10.1371/journal.pbio.1001717

Mielcarek, M., Seredenina, T., Stokes, M. P., Osborne, G. F., Landles, C., Inuabasi, L., Franklin, S. A., Silva, J. C., Luthi-Carter, R., Beaumont, V., & Bates, G. P. (2013). HDAC4 does not act as a protein deacetylase in the postnatal murine brain *in vivo*. *PLOS One, 8*(11), e80849. https://doi.org/10.1371/journal.pone.0080849

Milazzo, G., Mercatelli, D., Di Muzio, G., Triboli, L., De Rosa, P., Perini, G., & Giorgi, F. M. (2020). Histone deacetylases (HDACs): evolution, specificity, role in transcriptional complexes, and pharmacological actionability. *Genes, 11*(5). https://doi.org/10.3390/genes11050556

Miller, D. J., & Fort, P. E. (2018). Heat shock proteins regulatory role in neurodevelopment. *Frontiers in Neuroscience, 12*, 821. https://doi.org/10.3389/fnins.2018.00821

Minatohara, K., Akiyoshi, M., & Okuno, H. (2016). Role of immediate-early genes in synaptic plasticity and neuronal ensembles underlying the memory trace [Review]. *Frontiers in Molecular Neuroscience, 8*. https://doi.org/10.3389/fnmol.2015.00078

Mishra, A. K., Bargmann, B. O., Tsachaki, M., Fritsch, C., & Sprecher, S. G. (2016). Functional genomics identifies regulators of the phototransduction machinery in the *Drosophila* larval eye and adult ocelli. *Developmental Biology, 410*(2), 164-177. https://doi.org/10.1016/j.ydbio.2015.12.026

Miska, E. A., Karlsson, C., Langley, E., Nielsen, S. J., Pines, J., & Kouzarides, T. (1999). HDAC4 deacetylase associates with and represses the MEF2 transcription factor. *The EMBO Journal, 18*(18), 5099-5107. https://doi.org/10.1093/emboj/18.18.5099

Miska, E. A., Langley, E., Wolf, D., Karlsson, C., Pines, J., & Kouzarides, T. (2001). Differential localization of HDAC4 orchestrates muscle differentiation. *Nucleic Acids Research, 29*(16), 3439-3447. https://doi.org/10.1093/nar/29.16.3439

Mitchell, A. C., Javidfar, B., Pothula, V., Ibi, D., Shen, E. Y., Peter, C. J., Bicks, L. K., Fehr, T., Jiang, Y., Brennand, K. J., Neve, R. L., Gonzalez-Maeso, J., & Akbarian, S. (2018). MEF2C transcription factor is associated with the genetic and epigenetic risk architecture of schizophrenia and improves cognition in mice. *Molecular Psychiatry, 23*(1), 123-132. https://doi.org/10.1038/mp.2016.254

Mitchell, K. J. (2011). The genetics of neurodevelopmental disease. *Current Opinion in Neurobiology, 21*(1), 197-203. https://doi.org/10.1016/j.conb.2010.08.009

Molkentin, J. D., Firulli, A. B., Black, B. L., Martin, J. F., Hustad, C. M., Copeland, N., Jenkins, N., Lyons, G., & Olson, E. N. (1996). MEF2B is a potent transactivator expressed in early myogenic lineages. *Molecular and Cellular Biology, 16*(7), 3814-3824. https://doi.org/10.1128/MCB.16.7.3814

Montell, C., & Rubin, G. M. (1988). The *Drosophila* ninaC locus encodes two photoreceptor cell specific proteins with domains homologous to protein kinases and the myosin heavy chain head. *Cell, 52*(5), 757-772. https://doi.org/10.1016/0092-8674(88)90413-8

Moretti, P. N., Figueiredo, A. C. V., Saliba, A., Versiani, B. R., Oliveira, S. F., Pic-Taylor, A., & Mazzeu, J. F. (2020). Genotype and phenotype correlation in a family with a 2q37 deletion downstream of HDAC4. *American Journal of Medical Genetics, 182*(8), 1861-1864. https://doi.org/10.1002/ajmg.a.61620

Morgan, T. H. (1910). Sex limited inheritance in *Drosophila*. *Science, 32*(812), 120. https://doi.org/10.1126/science.32.812.120

Morin, X., Daneman, R., Zavortink, M., & Chia, W. (2001). A protein trap strategy to detect GFP-tagged proteins expressed from their endogenous loci in *Drosophila*. *Proceedings of the National Academy of Sciences of the United States of America, 98*(26), 15050-15055. https://doi.org/10.1073/pnas.261408198

Morris, B., Etoubleau, C., Bourthoumieu, S., Reynaud-Perrine, S., Laroche, C., Lebbar, A., Yardin, C., & Elsea, S. H. (2012). Dose dependent expression of HDAC4 causes variable expressivity in a novel inherited case of brachydactyly mental retardation syndrome. *American Journal of Medical Genetics, 158a*(8), 2015-2020. https://doi.org/10.1002/ajmg.a.35463

Moser, M. A., Hagelkruys, A., & Seiser, C. (2014). Transcription and beyond: the role of mammalian class I lysine deacetylases. *Chromosoma, 123*(1), 67-78. https://doi.org/10.1007/s00412-013-0441-x

Mosley-Bishop, K. L., Qinghong, L., Patterson, K., & Fischer, J. A. (1999). Molecular analysis of the *klarsicht* gene and its role in nuclear migration within differentiating cells of the *Drosophila* eye. *Current Biology, 9*(21), 1211-1220. https://doi.org/10.1016/S0960-9822(99)80501-6

Moujalled, D., Strasser, A., & Liddell, J. R. (2021). Molecular mechanisms of cell death in neurological diseases. *Cell Death & Differentiation, 28*(7), 2029-2044. https://doi.org/10.1038/s41418-021-00814-y

Mukherjee, K., Slawson, J. B., Christmann, B. L., & Griffith, L. C. (2014). Neuron-specific protein interactions of *Drosophila* CASK-β are revealed by mass spectrometry [Original Research]. *Frontiers in Molecular Neuroscience, 7*(58). https://doi.org/10.3389/fnmol.2014.00058

Nakagawa, T., & Guarente, L. (2011). Sirtuins at a glance. *Journal of Cell Science, 124*(6), 833. https://doi.org/10.1242/jcs.081067

Nardone, S., Sharan Sams, D., Reuveni, E., Getselter, D., Oron, O., Karpuj, M., & Elliott, E. (2014). DNA methylation analysis of the autistic brain reveals multiple dysregulated biological pathways. *Translational Psychiatry, 4*(9), e433-e433. https://doi.org/10.1038/tp.2014.70

Narita, T., Weinert, B. T., & Choudhary, C. (2019). Functions and mechanisms of non-histone protein acetylation. *Nature Reviews Molecular Cell Biology, 20*(3), 156-174. https://doi.org/10.1038/s41580-018-0081-3

National population projections: 2022(base)-2073. (2022, 27 July 2022). Statistics New Zealand. Retrieved 11 December 2023 from https://www.stats.govt.nz/information-releases/national-population-projections-2022base2073/

Neufeld, T. P., Tang, A. H., & Rubin, G. M. (1998). A genetic screen to identify components of the sina signaling pathway in *Drosophila* eye development. *Genetics, 148*(1), 277-286. https://doi.org/10.1093/genetics/148.1.277

Neuner, S. M., Wilmott, L. A., Hoffmann, B. R., Mozhui, K., & Kaczorowski, C. C. (2017). Hippocampal proteomics defines pathways associated with memory decline and resilience in normal aging and Alzheimer's disease mouse models. *Behavioural Brain Research, 322*(Pt B), 288-298. https://doi.org/10.1016/j.bbr.2016.06.002

Ng, J., & Luo, L. (2004). Rho GTPases regulate axon growth through convergent and divergent signaling pathways. *Neuron, 44*(5), 779-793. https://doi.org/10.1016/j.neuron.2004.11.014

Nie, J., Mahato, S., & Zelhof, A. C. (2015). Imaging the *Drosophila* retina: zwitterionic buffers PIPES and HEPES induce morphological artifacts in tissue fixation. *BMC Dev Biol, 15*, 10. https://doi.org/10.1186/s12861-015-0056-y

Nishino, T. G., Miyazaki, M., Hoshino, H., Miwa, Y., Horinouchi, S., & Yoshida, M. (2008). 14-3-3 regulates the nuclear import of class IIa histone deacetylases. *Biochemical and Biophysical Research Communications, 377*(3), 852-856. https://doi.org/10.1016/j.bbrc.2008.10.079

Norton, V. G., Imai, B. S., Yau, P., & Bradbury, E. M. (1989). Histone acetylation reduces nucleosome core particle linking number change. *Cell, 57*(3), 449-457. https://doi.org/10.1016/0092-8674(89)90920-3

Nüsslein-Volhard, C., & Wieschaus, E. (1980). Mutations affecting segment number and polarity in *Drosophila*. *Nature, 287*(5785), 795-801. https://doi.org/10.1038/287795a0

O'Kane, C. J., & Gehring, W. J. (1987). Detection *in situ* of genomic regulatory elements in *Drosophila*. *Proceedings of the National Academy of Sciences of the United States of America, 84*(24), 9123-9127. https://doi.org/10.1073/pnas.84.24.9123

Ogen-Shtern, N., Ben David, T., & Lederkremer, G. Z. (2016). Protein aggregation and ER stress. *Brain Research, 1648*(Pt B), 658-666. https://doi.org/10.1016/j.brainres.2016.03.044

Ogienko, A. A., Omelina, E. S., Bylino, O. V., Batin, M. A., Georgiev, P. G., & Pindyurin, A. V. (2022). *Drosophila* as a model organism to study basic mechanisms of longevity. *International Journal of Molecular Sciences, 23*(19). https://doi.org/10.3390/ijms231911244

Olanow, C. W., Perl, D. P., DeMartino, G. N., & McNaught, K. S. (2004). Lewy-body formation is an aggresome-related process: a hypothesis. *Lancet Neurology, 3*(8), 496-503. https://doi.org/10.1016/s1474-4422(04)00827-0

Olzmann, J. A., Li, L., & Chin, L. S. (2008). Aggresome formation and neurodegenerative diseases: therapeutic implications. *Current Medicinal Chemistry, 15*(1), 47-60. https://doi.org/10.2174/092986708783330692

Omori, Y., Kitamura, T., Yoshida, S., Kuwahara, R., Chaya, T., Irie, S., & Furukawa, T. (2015). Mef2d is essential for the maturation and integrity of retinal photoreceptor and bipolar cells. *Genes Cells, 20*(5), 408-426. https://doi.org/10.1111/gtc.12233

Pai, L.-M., Kirkpatrick, C., Blanton, J., Oda, H., Takeichi, M., & Peifer, M. (1996). *Drosophila* β-Catenin and E-cadherin bind to distinct regions of *Drosophila* Armadillo *Journal of Biological Chemistry, 271*(50), 32411-32420. https://doi.org/10.1074/jbc.271.50.32411

Palmer, M. J., & Fitzsimons, H. L. (2023). Herzog is not required for mushroom body development or courtship learning & memory but is required for eye development in *Drosophila melanogaster*. *MicroPublication Biology, 2023*. https://doi.org/10.17912/micropub.biology.000720

Pandey, U. B., & Nichols, C. D. (2011). Human disease models in *Drosophila melanogaster* and the role of the fly in therapeutic drug discovery. *Pharmacological Reviews, 63*(2), 411-436. https://doi.org/10.1124/pr.110.003293

Park, J. W., Parisky, K., Celotto, A. M., Reenan, R. A., & Graveley, B. R. (2004). Identification of alternative splicing regulators by RNA interference in *Drosophila*. *Proceedings of the National Academy of Sciences of the United States of America, 101*(45), 15974-15979. https://doi.org/10.1073/pnas.0407004101

Park, S.-Y., Kim, G. S., Hwang, H.-J., Nam, T.-H., Park, H.-S., Song, J., Jang, T.-H., Lee, Y. C., & Kim, J.-S. (2018). Structural basis of the specific interaction of SMRT corepressor with histone deacetylase 4. *Nucleic Acids Research, 46*(22), 11776-11788. https://doi.org/10.1093/nar/gky926

Park, S.-Y., & Kim, J.-S. (2020). A short guide to histone deacetylases including recent progress on class II enzymes. *Experimental & Molecular Medicine, 52*(2), 204-212. https://doi.org/10.1038/s12276-020-0382-4

Paroni, G., Cernotta, N., Dello Russo, C., Gallinari, P., Pallaoro, M., Foti, C., Talamo, F., Orsatti, L., Steinkühler, C., & Brancolini, C. (2008). PP2A regulates HDAC4 nuclear import. *Molecular Biology of the Cell, 19*(2), 655-667. https://doi.org/10.1091/mbc.e07-06-0623

Paroni, G., Fontanini, A., Cernotta, N., Foti, C., Gupta, M. P., Yang, X. J., Fasino, D., & Brancolini, C. (2007). Dephosphorylation and caspase processing generate distinct nuclear pools of histone deacetylase 4. *Molecular and Cellular Biology, 27*(19), 6718-6732. https://doi.org/10.1128/mcb.00853-07

Paroni, G., Mizzau, M., Henderson, C., Del Sal, G., Schneider, C., & Brancolini, C. (2004). Caspase-dependent regulation of histone deacetylase 4 nuclear-cytoplasmic shuttling promotes apoptosis. *Molecular Biology of the Cell, 15*(6), 2804-2818. https://doi.org/10.1091/mbc.e03-08-0624

Parry, D. A. D. (1982). Coiled-coils in α-helix-containing proteins: analysis of the residue types within the heptad repeat and the use of these data in the prediction of coiled-coils in other proteins. *Bioscience Reports, 2*(12), 1017-1024. https://doi.org/10.1007/BF01122170

Patterson, C. (2018). *World alzheimer report 2018. The state of the art of dementia research: New frontiers*. Alzheimer's Disease International.

Peifer, M., & Wieschaus, E. (1990). The segment polarity gene armadillo encodes a functionally modular protein that is the *Drosophila* homolog of human plakoglobin. *Cell, 63*(6), 1167-1176. https://doi.org/10.1016/0092-8674(90)90413-9

Pellikka, M., Tanentzapf, G., Pinto, M., Smith, C., McGlade, C. J., Ready, D. F., & Tepass, U. (2002). Crumbs, the *Drosophila* homologue of human CRB1/RP12, is essential for photoreceptor morphogenesis. *Nature, 416*(6877), 143-149. https://doi.org/10.1038/nature721

Penrod, R. D., Carreira, M. B., Taniguchi, M., Kumar, J., Maddox, S. A., & Cowan, C. W. (2018). Novel role and regulation of HDAC4 in cocaine-related behaviors. *Addiction Biology, 23*(2), 653-664. https://doi.org/10.1111/adb.12522

Pfeiffer, B. D., Ngo, T.-T. B., Hibbard, K. L., Murphy, C., Jenett, A., Truman, J. W., & Rubin, G. M. (2010). Refinement of tools for targeted gene expression in *Drosophila*. *Genetics, 186*(2), 735. https://doi.org/10.1534/genetics.110.119917

Piersimoni, L., Kastritis, P. L., Arlt, C., & Sinz, A. (2022). Cross-linking mass spectrometry for investigating protein conformations and protein-protein interactions─a method for all seasons. *Chemical Reviews, 122*(8), 7500-7531. https://doi.org/10.1021/acs.chemrev.1c00786

Pilling, A. D., Horiuchi, D., Lively, C. M., & Saxton, W. M. (2006). Kinesin-1 and dynein are the primary motors for fast transport of mitochondria in *Drosophila* motor axons. *Molecular Biology of the Cell, 17*(4), 2057-2068. https://doi.org/10.1091/mbc.e05-06-0526

Pintér, M., Jékely, G., Szepesi, R. J., Attila, F., Theopold, U., Meyer, H. E., Lindholm, D., Nässel, D. R., Hultmark, D., & Friedrich, P. (1998). TER94, a *Drosophila* homolog of the membrane fusion protein CDC48/p97, is accumulated in nonproliferating cells: in the reproductive organs and in the brain of the imago. *Insect Biochemistry and Molecular Biology, 28*(2), 91-98. https://doi.org/10.1016/S0965-1748(97)00095-7

Pletcher, R. C., Hardman, S. L., Intagliata, S. F., Lawson, R. L., Page, A., & Tennessen, J. M. (2019). A genetic screen using the *Drosophila melanogaster* TRiP RNAi collection to identify metabolic enzymes required for eye development. *G3: Genes, Genomes, Genetics, 9*(7), 2061. https://doi.org/10.1534/g3.119.400193

Poewe, W., Seppi, K., Tanner, C. M., Halliday, G. M., Brundin, P., Volkmann, J., Schrag, A.-E., & Lang, A. E. (2017). Parkinson disease. *Nature Reviews Disease Primers, 3*(1), 17013. https://doi.org/10.1038/nrdp.2017.13

Pon, J. R., & Marra, M. A. (2016). MEF2 transcription factors: developmental regulators and emerging cancer genes. *Oncotarget, 7*(3), 2297-2312. https://doi.org/10.18632/oncotarget.6223

Poon, C. L., Lin, J. I., Zhang, X., & Harvey, K. F. (2011). The sterile 20-like kinase Tao-1 controls tissue growth by regulating the Salvador-Warts-Hippo pathway. *Developmental Cell, 21*(5), 896-906. https://doi.org/10.1016/j.devcel.2011.09.012

Port, F., Strein, C., Stricker, M., Rauscher, B., Heigwer, F., Zhou, J., Beyersdörffer, C., Frei, J., Hess, A., Kern, K., Lange, L., Langner, N., Malamud, R., Pavlović, B., Rädecke, K., Schmitt, L., Voos, L., Valentini, E., & Boutros, M. (2020). A large-scale resource for tissue-specific CRISPR mutagenesis in *Drosophila*. *eLife, 9*, e53865. https://doi.org/10.7554/eLife.53865

Porter, J. A., Hicks, J. L., Williams, D. S., & Montell, C. (1992). Differential localizations of and requirements for the two *Drosophila* ninaC kinase/myosins in photoreceptor cells. *Journal of Cell Biology, 116*(3), 683-693. https://doi.org/10.1083/jcb.116.3.683

Quinn, P. M. J., Moreira, P. I., Ambrósio, A. F., & Alves, C. H. (2020). PINK1/PARKIN signalling in neurodegeneration and neuroinflammation. *Acta Neuropathologica Communications, 8*(1), 189. https://doi.org/10.1186/s40478-020-01062-w

Quiquand, M., Rimesso, G., Qiao, N., Suo, S., Zhao, C., Slattery, M., White, K. P., Han, J. J., & Baker, N. E. (2021). New regulators of *Drosophila* eye development identified from temporal transcriptome changes. *Genetics, 217*(4). https://doi.org/10.1093/genetics/iyab007

Raghu, P., Colley, N. J., Webel, R., James, T., Hasan, G., Danin, M., Selinger, Z., & Hardie, R. C. (2000). Normal phototransduction in *Drosophila* photoreceptors lacking an InsP(3) receptor gene. *Molecular and Cellular Neuroscience, 15*(5), 429-445. https://doi.org/10.1006/mcne.2000.0846

Raun, N., Jones, S. G., Kerr, O., Keung, C., Ibrahim, V., Williams, M., Top, D., & Kramer, J. M. (2023). *Trithorax* regulates long-term memory in *Drosophila* through epigenetic maintenance of mushroom body metabolic identity and translation capacity. *bioRxiv*, 2023.2008.2008.549887. https://doi.org/10.1101/2023.08.08.549887

Ready, D. F., Hanson, T. E., & Benzer, S. (1976). Development of the *Drosophila* retina, a neurocrystalline lattice. *Developmental Biology, 53*(2), 217-240. https://doi.org/10.1016/0012-1606(76)90225-6

Reiter, L. T., Potocki, L., Chien, S., Gribskov, M., & Bier, E. (2001). A systematic analysis of human disease-associated gene sequences in *Drosophila* melanogaster. *Genome Research, 11*(6), 1114-1125. https://doi.org/10.1101/gr.169101

Ren, J., Zhang, S., Wang, X., Deng, Y., Zhao, Y., Xiao, Y., Liu, J., Chu, L., & Qi, X. (2022). MEF2C ameliorates learning, memory, and molecular pathological changes in Alzheimer's disease *in vivo* and *in vitro*. *Acta Biochim Biophys Sin (Shanghai), 54*(1), 77-90. https://doi.org/10.3724/abbs.2021012

Ricci, A., Galluzzi, L., Magnani, M., & Menotta, M. (2020). DDIT4 gene expression is switched on by a new HDAC4 function in ataxia telangiectasia. *The FASEB Journal, 34*(1), 1802-1818. https://doi.org/10.1096/fj.201902039R

Richards, M. H., & Furrow, E. Y. (1925). The eye and optic tract in normal and eyeless *Drosophila*. *The Biological Bulletin, 48*(4), 243-[258]-241. https://doi.org/10.2307/1536570

Richmond, T. J., & Davey, C. A. (2003). The structure of DNA in the nucleosome core. *Nature, 423*(6936), 145-150. https://doi.org/10.1038/nature01595

Robinow, S., & White, K. (1988). The locus *elav* of *Drosophila melanogaster* is expressed in neurons at all developmental stages. *Developmental Biology, 126*(2), 294-303. https://doi.org/10.1016/0012-1606(88)90139-X

Rogero, O., Hämmerle, B., & Tejedor, F. J. (1997). Diverse expression and distribution of Shaker potassium channels during the development of the *Drosophila* nervous system. *The Journal of Neuroscience, 17*(13), 5108. https://doi.org/10.1523/JNEUROSCI.17-13-05108.1997

Rolls, M. M., Satoh, D., Clyne, P. J., Henner, A. L., Uemura, T., & Doe, C. Q. (2007). Polarity and intracellular compartmentalization of *Drosophila* neurons. *Neural Development, 2*(1), 7. https://doi.org/10.1186/1749-8104-2-7

Romero, P., Obradovic, Z., Li, X., Garner, E. C., Brown, C. J., & Dunker, A. K. (2001). Sequence complexity of disordered protein. *Proteins, 42*(1), 38-48. https://doi.org/10.1002/1097-0134(20010101)42:1<38::aid-prot50>3.0.co;2-3

Roote, J., & Prokop, A. (2013). How to design a genetic mating scheme: a basic training package for *Drosophila* genetics. *G3: Genes, Genomes, Genetics, 3*(2), 353-358. https://doi.org/10.1534/g3.112.004820

Roser, M., Ortiz-Ospina, E., & Ritchie, H. (2013). *Life expectancy*. https://ourworldindata.org/life-expectancy

Ross, C. A., & Poirier, M. A. (2004). Protein aggregation and neurodegenerative disease. *Nature Medicine, 10*(7), S10-S17. https://doi.org/10.1038/nm1066

Ross, C. A., & Poirier, M. A. (2005). What is the role of protein aggregation in neurodegeneration? *Nature Reviews Molecular Cell Biology, 6*(11), 891-898. https://doi.org/10.1038/nrm1742

Rothblum-Oviatt, C., Wright, J., Lefton-Greif, M. A., McGrath-Morrow, S. A., Crawford, T. O., & Lederman, H. M. (2016). Ataxia telangiectasia: a review. *Orphanet Journal of Rare Diseases, 11*(1), 159. https://doi.org/10.1186/s13023-016-0543-7

Rousset, R., Mack, J. A., Wharton, K. A., Jr., Axelrod, J. D., Cadigan, K. M., Fish, M. P., Nusse, R., & Scott, M. P. (2001). Naked cuticle targets dishevelled to antagonize Wnt signal transduction. *Genes & Development, 15*(6), 658-671. https://doi.org/10.1101/gad.869201

Roux, K. J., Kim, D. I., Burke, B., & May, D. G. (2018). BioID: a screen for protein-protein interactions. *Current Protocols in Protein Science, 91*, 19.23.11-19.23.15. https://doi.org/10.1002/cpps.51

Ruiz, A., Heilmann, S., Becker, T., Hernández, I., Wagner, H., Thelen, M., Mauleón, A., Rosende-Roca, M., Bellenguez, C., Bis, J. C., Harold, D., Gerrish, A., Sims, R., Sotolongo-Grau, O., Espinosa, A., Alegret, M., Arrieta, J. L., Lacour, A., Leber, M., …, & Ramírez, A. (2014). Follow-up of loci from the International Genomics of Alzheimer's Disease Project identifies TRIP4 as a novel susceptibility gene. *Translational Psychiatry, 4*(2), e358. https://doi.org/10.1038/tp.2014.2

Sadigh-Eteghad, S., Talebi, M., & Farhoudi, M. (2012). Association of apolipoprotein E epsilon 4 allele with sporadic late onset Alzheimer's disease. A meta-analysis. *Neurosciences Journal, 17*(4), 321. https://doi.org/10.1212/wnl.43.8.1467

Sage, B. T., Wu, M. D., & Csink, A. K. (2008). Interplay of developmentally regulated gene expression and heterochromatic silencing in trans in *Drosophila*. *Genetics, 178*(2), 749-759. https://doi.org/10.1534/genetics.107.083105

Sando, R., 3rd, Gounko, N., Pieraut, S., Liao, L., Yates, J., 3rd, & Maximov, A. (2012). HDAC4 governs a transcriptional program essential for synaptic plasticity and memory. *Cell, 151*(4), 821-834. https://doi.org/10.1016/j.cell.2012.09.037

Saraf, R., & Marks, R. (2019). *Neurodevelopmental screening and surveillance* (Brief evidence reviews for the well child tamariki ora programme. A better start national science challenge, Issue.

Schaaf, C. A., Misulovin, Z., Sahota, G., Siddiqui, A. M., Schwartz, Y. B., Kahn, T. G., Pirrotta, V., Gause, M., & Dorsett, D. (2009). Regulation of the *Drosophila* enhancer of split and invected-engrailed gene complexes by sister chromatid cohesion proteins. *PLOS One, 4*(7), e6202. https://doi.org/10.1371/journal.pone.0006202

Schlumm, F., Mauceri, D., Freitag, H. E., & Bading, H. (2013). Nuclear calcium signaling regulates nuclear export of a subset of class IIa histone deacetylases following synaptic activity. *The Journal of Biological Chemistry, 288*(12), 8074-8084. https://doi.org/10.1074/jbc.M112.432773

Schmid, B., Schindelin, J., Cardona, A., Longair, M., & Heisenberg, M. (2010). A high-level 3D visualization API for Java and ImageJ. *BMC Bioinformatics, 11*(1), 274. https://doi.org/10.1186/1471-2105-11-274

Schneider, C. A., Rasband, W. S., & Eliceiri, K. W. (2012). NIH Image to ImageJ: 25 years of image analysis. *Nature Methods, 9*(7), 671-675. https://doi.org/10.1038/nmeth.2089

Schneider, J. A., Arvanitakis, Z., Leurgans, S. E., & Bennett, D. A. (2009). The neuropathology of probable Alzheimer disease and mild cognitive impairment. *Annals of Neurology, 66*(2), 200-208. https://doi.org/10.1002/ana.21706

Schor, N. F., & Bianchi, D. W. (2021). Neurodevelopmental clues to neurodegeneration. *Pediatric Neurology, 123*, 67-76. https://doi.org/10.1016/j.pediatrneurol.2021.07.012

Schulz, R. A., Chromey, C., Lu, M. F., Zhao, B., & Olson, E. N. (1996). Expression of the D-MEF2 transcription in the *Drosophila* brain suggests a role in neuronal cell differentiation. *Oncogene, 12*(8), 1827-1831.

Schwartz, S., Truglio, M., Scott, M. J., & Fitzsimons, H. L. (2016). Long-term memory in *Drosophila* is influenced by histone deacetylase HDAC4 interacting with SUMO-conjugating enzyme ubc9. *Genetics, 203*(3), 1249-1264. https://doi.org/10.1534/genetics.115.183194

Schwartz, S., Wilson, S. J., Hale, T. K., & Fitzsimons, H. L. (2023). Ankyrin2 is essential for neuronal morphogenesis and long-term courtship memory in *Drosophila*. *Molecular Brain, 16*(1), 42. https://doi.org/10.1186/s13041-023-01026-w

Scognamiglio, A., Nebbioso, A., Manzo, F., Valente, S., Mai, A., & Altucci, L. (2008). HDAC-class II specific inhibition involves HDAC proteasome-dependent degradation mediated by RANBP2. *Biochimica et Biophysica Acta (BBA) - Molecular Cell Research, 1783*(10), 2030-2038. https://doi.org/10.1016/j.bbamcr.2008.07.007

Sedkov, Y., Cho, E., Petruk, S., Cherbas, L., Smith, S. T., Jones, R. S., Cherbas, P., Canaani, E., Jaynes, J. B., & Mazo, A. (2003). Methylation at lysine 4 of histone H3 in ecdysone-dependent development of *Drosophila*. *Nature, 426*(6962), 78-83. https://doi.org/10.1038/nature02080

Segal, D., Maier, S., Mastromarco, G. J., Qian, W. W., Nabeel-Shah, S., Lee, H., Moore, G., Lacoste, J., Larsen, B., Lin, Z. Y., Selvabaskaran, A., Liu, K., Smibert, C., Zhang, Z., Greenblatt, J., Peng, J., Lee, H. O., Gingras, A. C., & Taipale, M. (2023). A central chaperone-like role for 14-3-3 proteins in human cells. *Molecular Cell, 83*(6), 974-993.e915. https://doi.org/10.1016/j.molcel.2023.02.018

Sen, A., Nelson, T. J., & Alkon, D. L. (2015). ApoE4 and Aβ oligomers reduce BDNF expression via HDAC nuclear translocation. *The Journal of Neuroscience, 35*(19), 7538-7551. https://doi.org/10.1523/JNEUROSCI.0260-15.2015

Seto, E., & Yoshida, M. (2014). Erasers of histone acetylation: the histone deacetylase enzymes. *Cold Spring Harbor Perspectives in Biology, 6*(4). https://doi.org/10.1101/cshperspect.a018713

Shabani, K., & Hassan, B. A. (2023). The brain on time: links between development and neurodegeneration. *Development, 150*(10), dev200397. https://doi.org/10.1242/dev.200397

Shen, X., Chen, J., Li, J., Kofler, J., & Herrup, K. (2016). Neurons in vulnerable regions of the Alzheimer's disease brain display reduced ATM signaling. *eNeuro, 3*(1), ENEURO.0124-0115.2016. https://doi.org/10.1523/ENEURO.0124-15.2016

Sherman, B. T., Hao, M., Qiu, J., Jiao, X., Baseler, M. W., Lane, H. C., Imamichi, T., & Chang, W. (2022). DAVID: a web server for functional enrichment analysis and functional annotation of gene lists (2021 update). *Nucleic Acids Research, 50*(W1), W216-W221. https://doi.org/10.1093/nar/gkac194

Shiga, Y., Tanaka-Matakatsu, M., & Hayashi, S. (1996). A nuclear GFP/β-galactosidase fusion protein as a marker for morphogenesis in living *Drosophila*. *Development, Growth & Differentiation, 38*(1), 99-106. https://doi.org/10.1046/j.1440-169X.1996.00012.x

Siegenthaler, D., Enneking, E. M., Moreno, E., & Pielage, J. (2015). L1CAM/Neuroglian controls the axon-axon interactions establishing layered and lobular mushroom body architecture. *Journal of Cell Biology, 208*(7), 1003-1018. https://doi.org/10.1083/jcb.201407131

Silva, B., Mantha, O. L., Schor, J., Pascual, A., Plaçais, P.-Y., Pavlowsky, A., & Preat, T. (2022). Glia fuel neurons with locally synthesized ketone bodies to sustain memory under starvation. *Nature Metabolism, 4*(2), 213-224. https://doi.org/10.1038/s42255-022-00528-6

Simon, M. A., Bowtell, D. D. L., Dodson, G. S., Laverty, T. R., & Rubin, G. M. (1991). Ras1 and a putative guanine nucleotide exchange factor perform crucial steps in signaling by the sevenless protein tyrosine kinase. *Cell, 67*(4), 701-716. https://doi.org/10.1016/0092-8674(91)90065-7

Simpson, J. H. (2009). In *Advances in Genetics* (Vol. 65, pp. 79-143). Academic Press. https://doi.org/10.1016/S0065-2660(09)65003-3

Sin, O., & Nollen, E. A. (2015). Regulation of protein homeostasis in neurodegenerative diseases: the role of coding and non-coding genes. *Cellular and Molecular Life Sciences, 72*(21), 4027-4047. https://doi.org/10.1007/s00018-015-1985-0

Sitaraman, D., Zars, M., LaFerriere, H., Chen, Y.-C., Sable-Smith, A., Kitamoto, T., Rottinghaus, G. E., & Zars, T. (2008). Serotonin is necessary for place memory in *Drosophila*. *Proceedings of the National Academy of Sciences of the United States of America, 105*(14), 5579-5584. https://doi.org/10.1073/pnas.0710168105

Sivachenko, A., Li, Y., Abruzzi, K. C., & Rosbash, M. (2013). The transcription factor Mef2 links the *Drosophila* core clock to Fas2, neuronal morphology, and circadian behavior. *Neuron, 79*(2), 281-292. https://doi.org/10.1016/j.neuron.2013.05.015

Sjöstedt, E., Zhong, W., Fagerberg, L., Karlsson, M., Mitsios, N., Adori, C., Oksvold, P., Edfors, F., Limiszewska, A., Hikmet, F., Huang, J., Du, Y., Lin, L., Dong, Z., Yang, L., Liu, X., Jiang, H., Xu, X., Wang, J., …, & Mulder, J. (2020). An atlas of the protein-coding genes in the human, pig, and mouse brain. *Science, 367*(6482), eaay5947. https://doi.org/10.1126/science.aay5947

Sluchanko, N. N., & Gusev, N. B. (2017). Moonlighting chaperone-like activity of the universal regulatory 14-3-3 proteins. *The FEBS Journal, 284*(9), 1279-1295. https://doi.org/10.1111/febs.13986

Smialowski, P., Martin-Galiano, A. J., Mikolajka, A., Girschick, T., Holak, T. A., & Frishman, D. (2007). Protein solubility: sequence based prediction and experimental verification. *Bioinformatics, 23*(19), 2536-2542. https://doi.org/10.1093/bioinformatics/btl623

Song, Q., Meng, B., Xu, H., & Mao, Z. (2020). The emerging roles of vacuolar-type ATPase-dependent Lysosomal acidification in neurodegenerative diseases. *Translational Neurodegeneration, 9*(1), 17. https://doi.org/10.1186/s40035-020-00196-0

Southall, Tony D., Gold, Katrina S., Egger, B., Davidson, Catherine M., Caygill, Elizabeth E., Marshall, Owen J., & Brand, Andrea H. (2013). Cell-type-specific profiling of gene expression and chromatin binding without cell isolation: assaying RNA pol II occupancy in neural stem cells. *Developmental Cell, 26*(1), 101-112. https://doi.org/10.1016/j.devcel.2013.05.020

Sparrow, D. B., Miska, E. A., Langley, E., Reynaud-Deonauth, S., Kotecha, S., Towers, N., Spohr, G., Kouzarides, T., & Mohun, T. J. (1999). MEF-2 function is modified by a novel co-repressor, MITR. *The EMBO Journal, 18*(18), 5085-5098. https://doi.org/10.1093/emboj/18.18.5085

Spector, D. L., & Lamond, A. I. (2011). Nuclear speckles. *Cold Spring Harb Perspect Biol, 3*(2). https://doi.org/10.1101/cshperspect.a000646

Spira, P. J., Sharpe, D. M., Halliday, G., Cavanagh, J., & Nicholson, G. A. (2001). Clinical and pathological features of a parkinsonian syndrome in a family with an Ala53Thr α-synuclein mutation. *Annals of Neurology, 49*(3), 313-319. https://doi.org/10.1002/ana.67

Spratford, C. M., & Kumar, J. P. (2014). Dissection and immunostaining of imaginal discs from *Drosophila melanogaster*. *Journal of Visualized Experiments*(91), e51792. https://doi.org/10.3791/51792

St Johnston, D. (2002). The art and design of genetic screens: *Drosophila melanogaster*. *Nature Reviews Genetics, 3*(3), 176-188. https://doi.org/10.1038/nrg751

Strodel, B. (2021). Energy landscapes of protein aggregation and conformation switching in intrinsically disordered proteins. *Journal of Molecular Biology, 433*(20), 167182. https://doi.org/10.1016/j.jmb.2021.167182

Struhl, K. (1998). Histone acetylation and transcriptional regulatory mechanisms. *Genes & Development, 12*(5), 599-606. https://doi.org/10.1101/gad.12.5.599

Sullivan, D. T., & Sullivan, M. C. (1975). Transport defects as the physiological basis for eye color mutants of *Drosophila melanogaster*. *Biochemical Genetics, 13*(9), 603-613. https://doi.org/10.1007/BF00484918

Sullivan, R., Yau, W. Y., O'Connor, E., & Houlden, H. (2019). Spinocerebellar ataxia: an update. *Journal of Neurology, 266*(2), 533-544. https://doi.org/10.1007/s00415-018-9076-4

Sutherland, B. W., Toews, J., & Kast, J. (2008). Utility of formaldehyde cross-linking and mass spectrometry in the study of protein-protein interactions. *Journal of Mass Spectrometry, 43*(6), 699-715. https://doi.org/10.1002/jms.1415

Swingle, M., Ni, L., & Honkanen, R. E. (2007). Small-molecule inhibitors of ser/thr protein phosphatases: specificity, use and common forms of abuse. *Methods in Molecular Biology, 365*, 23-38. https://doi.org/10.1385/1-59745-267-x:23

Szklarczyk, D., Kirsch, R., Koutrouli, M., Nastou, K., Mehryary, F., Hachilif, R., Gable, A. L., Fang, T., Doncheva, N. T., Pyysalo, S., Bork, P., Jensen, L. J., & von Mering, C. (2023). The STRING database in 2023: protein-protein association networks and functional enrichment analyses for any sequenced genome of interest. *Nucleic Acids Research, 51*(D1), D638-d646. https://doi.org/10.1093/nar/gkac1000

Tabrizi, S. J., Flower, M. D., Ross, C. A., & Wild, E. J. (2020). Huntington disease: new insights into molecular pathogenesis and therapeutic opportunities. *Nature Reviews Neurology, 16*(10), 529-546. https://doi.org/10.1038/s41582-020-0389-4

Takahashi-Fujigasaki, J., Arai, K., Funata, N., & Fujigasaki, H. (2006). SUMOylation substrates in neuronal intranuclear inclusion disease. *Neuropathology and Applied Neurobiology, 32*(1), 92-100. https://doi.org/10.1111/j.1365-2990.2005.00705.x

Takahashi-Fujigasaki, J., & Fujigasaki, H. (2006). Histone deacetylase (HDAC) 4 involvement in both Lewy and Marinesco bodies. *Neuropathology and Applied Neurobiology, 32*(5), 562-566. https://doi.org/10.1111/j.1365-2990.2006.00733.x

Takalo, M., Salminen, A., Soininen, H., Hiltunen, M., & Haapasalo, A. (2013). Protein aggregation and degradation mechanisms in neurodegenerative diseases. *American Journal of Neurodegenerative Disease, 2*(1), 1-14.

Takeyari, S., Yamamoto, K., Fujiwara, M., Ohata, Y., Kitaoka, T., Kubota, T., Nagata, M., Ishihara, Y., Miyashita, Y., Asano, Y., & Ozono, K. (2023). A family with brachydactyly mental retardation syndrome with a missense variant in HDAC4. *Clinical Paediatric Endocrinology, 32*(2), 105-109. https://doi.org/10.1297/cpe.2022-0076

Tan, W. J. (2022). *Investigating the role of HDAC4 in Drosophila neuronal function : a thesis presented in partial fulfilment of the requirements for the degree of Doctor of Philosophy (PhD) in Genetics at Massey University, Manawatū, New Zealand* [Doctoral, Massey University]. http://hdl.handle.net/10179/17605

Tan, W. J., Hawley, H. R., Wilson, S. J., & Fitzsimons, H. L. (2024). Deciphering the roles of subcellular distribution and interactions involving the MEF2 binding region, the ankyrin repeat binding motif and the catalytic site of HDAC4 in *Drosophila* neuronal morphogenesis. *BMC Biology, 22*(1), 2. https://doi.org/10.1186/s12915-023-01800-1

Tan, Y., Yu, D., Busto, G. U., Wilson, C., & Davis, R. L. (2013). Wnt signaling is required for long-term memory formation. *Cell Reports, 4*(6), 1082-1089. https://doi.org/10.1016/j.celrep.2013.08.007

Tanaka, M., Kim, Y. M., Lee, G., Junn, E., Iwatsubo, T., & Mouradian, M. M. (2004). Aggresomes formed by alpha-synuclein and synphilin-1 are cytoprotective. *Journal of Biological Chemistry, 279*(6), 4625-4631. https://doi.org/10.1074/jbc.M310994200

The UniProt Consortium (2023). UniProt: the Universal Protein Knowledgebase in 2023. *Nucleic Acids Research, 51*(D1), D523-D531. https://doi.org/10.1093/nar/gkac1052

Thomas, B. J., & Wassarman, D. A. (1999). A fly's eye view of biology. *Trends in Genetics, 15*(5), 184-190. https://doi.org/10.1016/S0168-9525(99)01720-5

Tolwinski, N. S., & Wieschaus, E. (2004). A nuclear function for Armadillo/β-Catenin. *PLOS Biology, 2*(4), e95. https://doi.org/10.1371/journal.pbio.0020095

Tomlinson, A. (1985). The cellular dynamics of pattern formation in the eye of *Drosophila*. *J Embryol Exp Morphol, 89*, 313-331.

Tomlinson, A. (2012). The origin of the *Drosophila* subretinal pigment layer. *Journal of Comparative Neurology, 520*(12), 2676-2682. https://doi.org/10.1002/cne.23063

Trazzi, S., Fuchs, C., Viggiano, R., De Franceschi, M., Valli, E., Jedynak, P., Hansen, F. K., Perini, G., Rimondini, R., Kurz, T., Bartesaghi, R., & Ciani, E. (2016). HDAC4: a key factor underlying brain developmental alterations in CDKL5 disorder. *Human Molecular Genetics, 25*(18), 3887-3907. https://doi.org/10.1093/hmg/ddw231

Tsakiri, E. N., Gumeni, S., Vougas, K., Pendin, D., Papassideri, I., Daga, A., Gorgoulis, V., Juhász, G., Scorrano, L., & Trougakos, I. P. (2019). Proteasome dysfunction induces excessive proteome instability and loss of mitostasis that can be mitigated by enhancing mitochondrial fusion or autophagy. *Autophagy, 15*(10), 1757-1773. https://doi.org/10.1080/15548627.2019.1596477

Tyedmers, J., Mogk, A., & Bukau, B. (2010). Cellular strategies for controlling protein aggregation. *Nature Reviews Molecular Cell Biology, 11*(11), 777-788. https://doi.org/10.1038/nrm2993

Uttara, B., Singh, A. V., Zamboni, P., & Mahajan, R. T. (2009). Oxidative stress and neurodegenerative diseases: a review of upstream and downstream antioxidant therapeutic options. *Current Neuropharmacology, 7*(1), 65-74. https://doi.org/10.2174/157015909787602823

van der Lee, R., Buljan, M., Lang, B., Weatheritt, R. J., Daughdrill, G. W., Dunker, A. K., Fuxreiter, M., Gough, J., Gsponer, J., Jones, D. T., Kim, P. M., Kriwacki, R. W., Oldfield, C. J., Pappu, R. V., Tompa, P., Uversky, V. N., Wright, P. E., & Babu, M. M. (2014). Classification of intrinsically disordered regions and proteins. *Chemical Reviews, 114*(13), 6589-6631. https://doi.org/10.1021/cr400525m

Van Vactor, D., Jr., Krantz, D. E., Reinke, R., & Zipursky, S. L. (1988). Analysis of mutants in chaoptin, a photoreceptor cell-specific glycoprotein in *Drosophila*, reveals its role in cellular morphogenesis. *Cell, 52*(2), 281-290. https://doi.org/10.1016/0092-8674(88)90517-x

Varadi, M., Anyango, S., Deshpande, M., Nair, S., Natassia, C., Yordanova, G., Yuan, D., Stroe, O., Wood, G., Laydon, A., Žídek, A., Green, T., Tunyasuvunakool, K., Petersen, S., Jumper, J., Clancy, E., Green, R., Vora, A., Lutfi, M., …, & Velankar, S. (2021). AlphaFold Protein Structure Database: massively expanding the structural coverage of protein-sequence space with high-accuracy models. *Nucleic Acids Research, 50*(D1), D439-D444. https://doi.org/10.1093/nar/gkab1061

Vasilescu, J., Guo, X., & Kast, J. (2004). Identification of protein-protein interactions using *in vivo* cross-linking and mass spectrometry. *Proteomics, 4*(12), 3845-3854. https://doi.org/10.1002/pmic.200400856

Vega, R. B., Matsuda, K., Oh, J., Barbosa, A. C., Yang, X., Meadows, E., McAnally, J., Pomajzl, C., Shelton, J. M., Richardson, J. A., Karsenty, G., & Olson, E. N. (2004). Histone deacetylase 4 controls chondrocyte hypertrophy during skeletogenesis. *Cell, 119*(4), 555-566. https://doi.org/10.1016/j.cell.2004.10.024

Venkatraman, P., Wetzel, R., Tanaka, M., Nukina, N., & Goldberg, A. L. (2004). Eukaryotic proteasomes cannot digest polyglutamine sequences and release them during degradation of polyglutamine-containing proteins. *Molecular Cell, 14*(1), 95-104. https://doi.org/10.1016/s1097-2765(04)00151-0

Verdin, E., & Ott, M. (2015). 50 years of protein acetylation: from gene regulation to epigenetics, metabolism and beyond. *Nature Reviews Molecular Cell Biology, 16*(4), 258-264. https://doi.org/10.1038/nrm3931

Vernace, V. A., Arnaud, L., Schmidt-Glenewinkel, T., & Figueiredo-Pereira, M. E. (2007). Aging perturbs 26S proteasome assembly in *Drosophila melanogaster*. *The FASEB Journal, 21*(11), 2672-2682. https://doi.org/10.1096/fj.06-6751com

Vidal-Sancho, L., Fernández-García, S., Solés-Tarrés, I., Alberch, J., & Xifró, X. (2020). Decreased myocyte enhancer factor 2 levels in the hippocampus of Huntington's disease mice are related to cognitive dysfunction. *Molecular Neurobiology, 57*(11), 4549-4562. https://doi.org/10.1007/s12035-020-02041-x

Volders, K., Scholz, S., Slabbaert, J. R., Nagel, A. C., Verstreken, P., Creemers, J. W., Callaerts, P., & Schwärzel, M. (2012). *Drosophila* rugose is a functional homolog of mammalian Neurobeachin and affects synaptic architecture, brain morphology, and associative learning. *Journal of Neuroscience, 32*(43), 15193-15204. https://doi.org/10.1523/jneurosci.6424-11.2012

Wagh, D. A., Rasse, T. M., Asan, E., Hofbauer, A., Schwenkert, I., Dürrbeck, H., Buchner, S., Dabauvalle, M.-C., Schmidt, M., Qin, G., Wichmann, C., Kittel, R., Sigrist, S. J., & Buchner, E. (2006). Bruchpilot, a protein with homology to ELKS/CAST, is required for structural integrity and function of synaptic active zones in *Drosophila*. *Neuron, 49*(6), 833-844. https://doi.org/10.1016/j.neuron.2006.02.008

Wakeling, E., McEntagart, M., Bruccoleri, M., Shaw-Smith, C., Stals, K. L., Wakeling, M., Barnicoat, A., Beesley, C., Hanson-Kahn, A. K., Kukolich, M., Stevenson, D. A., Campeau, P. M., Ellard, S., Elsea, S. H., Yang, X. J., & Caswell, R. C. (2021). Missense substitutions at a conserved 14-3-3 binding site in HDAC4 cause a novel intellectual disability syndrome. *Human Genetics and Genomics Advances, 2*(1), 100015. https://doi.org/10.1016/j.xhgg.2020.100015

Walkinshaw, D. R., Weist, R., Kim, G.-W., You, L., Xiao, L., Nie, J., Li, C. S., Zhao, S., Xu, M., & Yang, X.-J. (2013). The tumor suppressor kinase LKB1 activates the downstream kinases SIK2 and SIK3 to stimulate nuclear export of class IIa histone deacetylases. *Journal of Biological Chemistry, 288*(13), 9345-9362. https://doi.org/10.1074/jbc.M113.456996

Wang, A. H., Bertos, N. R., Vezmar, M., Pelletier, N., Crosato, M., Heng, H. H., Th'ng, J., Han, J., & Yang, X. J. (1999). HDAC4, a human histone deacetylase related to yeast HDA1, is a transcriptional corepressor. *Molecular and Cellular Biology, 19*(11), 7816-7827. https://doi.org/10.1128/mcb.19.11.7816

Wang, A. H., Kruhlak, M. J., Wu, J., Bertos, N. R., Vezmar, M., Posner, B. I., Bazett-Jones, D. P., & Yang, X. J. (2000). Regulation of histone deacetylase 4 by binding of 14-3-3 proteins. *Molecular and Cellular Biology, 20*(18), 6904-6912. https://doi.org/10.1128/mcb.20.18.6904-6912.2000

Wang, A. H., & Yang, X. J. (2001). Histone deacetylase 4 possesses intrinsic nuclear import and export signals. *Molecular and Cellular Biology, 21*(17), 5992-6005. https://doi.org/10.1128/mcb.21.17.5992-6005.2001

Wang, B., Moya, N., Niessen, S., Hoover, H., Mihaylova, Maria M., Shaw, Reuben J., Yates, John R., Fischer, Wolfgang H., Thomas, John B., & Montminy, M. (2011). A hormone-dependent module regulating energy balance. *Cell, 145*(4), 596-606. https://doi.org/10.1016/j.cell.2011.04.013

Wang, L., Liu, L., Han, C., Jiang, H., Ma, K., Guo, S., Xia, Y., Wan, F., Huang, J., Xiong, N., & Wang, T. (2023). Histone deacetylase 4 inhibition reduces rotenone-induced alpha-Synuclein accumulation via autophagy in SH-SY5Y cells. *Brain Sciences, 13*(4). https://doi.org/10.3390/brainsci13040670

Wang, W., Nema, S., & Teagarden, D. (2010). Protein aggregation—pathways and influencing factors. *International Journal of Pharmaceutics, 390*(2), 89-99. https://doi.org/10.1016/j.ijpharm.2010.02.025

Wang, Y., Meriin, A. B., Costello, C. E., & Sherman, M. Y. (2007). Characterization of proteins associated with polyglutamine aggregates: a novel approach towards isolation of aggregates from protein conformation disorders. *Prion, 1*(2), 128-135. https://doi.org/10.4161/pri.1.2.4440

Warrick, J. M., Paulson, H. L., Gray-Board, G. L., Bui, Q. T., Fischbeck, K. H., Pittman, R. N., & Bonini, N. M. (1998). Expanded polyglutamine protein forms nuclear inclusions and causes neural degeneration in *Drosophila*. *Cell, 93*(6), 939-949. https://doi.org/10.1016/S0092-8674(00)81200-3

Webster, N., Jin, J. R., Green, S., Hollis, M., & Chambon, P. (1988). The yeast UAS is a transcriptional enhancer in human hela cells in the presence of the GAL4-activator. *Cell, 52*(2), 169-178. https://doi.org/10.1016/0092-8674(88)90505-3

Wheeler, P. G., Huang, D., & Dai, Z. (2014). Haploinsufficiency of HDAC4 does not cause intellectual disability in all affected individuals. *American Journal of Medical Genetics, 164a*(7), 1826-1829. https://doi.org/10.1002/ajmg.a.36542

White, K. E., Humphrey, D. M., & Hirth, F. (2010). The dopaminergic system in the aging brain of *Drosophila*. *Frontiers in Neuroscience, 4*. https://doi.org/10.3389/fnins.2010.00205

Williams, S. R., Aldred, M. A., Der Kaloustian, V. M., Halal, F., Gowans, G., McLeod, D. R., Zondag, S., Toriello, H. V., Magenis, R. E., & Elsea, S. H. (2010). Haploinsufficiency of HDAC4 causes brachydactyly mental retardation syndrome, with brachydactyly type E, developmental delays, and behavioral problems. *American Journal of Human Genetics, 87*(2), 219-228. https://doi.org/10.1016/j.ajhg.2010.07.011

Williamson, W. R., Wang, D., Haberman, A. S., & Hiesinger, P. R. (2010). A dual function of V0-ATPase a1 provides an endolysosomal degradation mechanism in *Drosophila melanogaster* photoreceptors. *Journal of Cell Biology, 189*(5), 885-899. https://doi.org/10.1083/jcb.201003062

Wilson, S. J. (2021). *Teasing apart the interaction between HDAC4 and Ankyrin2 in Drosophila neuronal function : a thesis presented in partial fulfilment of the requirements for the degree of Master of Science in Biochemistry, School of Fundamental Sciences, Massey University, Manawatu, New Zealand* [Master's, Massey University]. http://hdl.handle.net/10179/16298

Wolf, A., Aslanidis, A., & Langmann, T. (2017). Retinal expression and localization of Mef2c support its important role in photoreceptor gene expression. *Biochemical and Biophysical Research Communications, 483*(1), 346-351. https://doi.org/10.1016/j.bbrc.2016.12.141

Wolff, T., & Ready, D. F. (1991). Cell death in normal and rough eye mutants of *Drosophila*. *Development, 113*(3), 825-839. https://doi.org/10.1242/dev.113.3.825

Wolff, T., & Ready, D. F. (1993). Pattern formation in the *Drosophila* retina. In M. Bate & A. Martinez Arias (Eds.), *The development of Drosophila melanogaster* (Vol. 2, pp. 1277-1325). Cold Spring Harbor Laboratory Press.

Wong, J. C., Hong, R., & Schreiber, S. L. (2003). Structural biasing elements for in-cell histone deacetylase paralog selectivity. *Journal of the American Chemical Society, 125*(19), 5586-5587. https://doi.org/10.1021/ja0341440

Wu, C. H., Apweiler, R., Bairoch, A., Natale, D. A., Barker, W. C., Boeckmann, B., Ferro, S., Gasteiger, E., Huang, H., Lopez, R., Magrane, M., Martin, M. J., Mazumder, R., O'Donovan, C., Redaschi, N., & Suzek, B. (2006). The Universal Protein Resource (UniProt): an expanding universe of protein information. *Nucleic Acids Research, 34*(suppl_1), D187-D191. https://doi.org/10.1093/nar/gkj161

Wu, J. S., & Luo, L. (2006). A protocol for dissecting *Drosophila melanogaster* brains for live imaging or immunostaining. *Nature Protocols, 1*(4), 2110-2115. https://doi.org/10.1038/nprot.2006.336

Wu, Q., Yang, X., Zhang, L., Zhang, Y., & Feng, L. (2016). Nuclear accumulation of histone deacetylase 4 (HDAC4) exerts neurotoxicity in models of Parkinson's disease. *Molecular Neurobiology, 54*(9), 6970-6983. https://doi.org/10.1007/s12035-016-0199-2

Wu, X., Li, H., Park, E.-J., & Chen, J. D. (2001). SMRTe inhibits MEF2C transcriptional activation by targeting HDAC4 and 5 to nuclear domains. *Journal of Biological Chemistry, 276*(26), 24177-24185. https://doi.org/10.1074/jbc.M100412200

Wu, Y., Hou, F., Wang, X., Kong, Q., Han, X., & Bai, B. (2016). Aberrant expression of histone deacetylases 4 in cognitive disorders: molecular mechanisms and a potential target [Mini Review]. *Frontiers in Molecular Neuroscience, 9*(114). https://doi.org/10.3389/fnmol.2016.00114

Xiong, Z., Lo, H. P., McMahon, K. A., Martel, N., Jones, A., Hill, M. M., Parton, R. G., & Hall, T. E. (2021). In vivo proteomic mapping through GFP-directed proximity-dependent biotin labelling in zebrafish. *eLife, 10*. https://doi.org/10.7554/eLife.64631

Xu, C., Jin, J., Bian, C., Lam, R., Tian, R., Weist, R., You, L., Nie, J., Bochkarev, A., Tempel, W., Tan, C. S., Wasney, G. A., Vedadi, M., Gish, G. D., Arrowsmith, C. H., Pawson, T., Yang, X. J., & Min, J. (2012). Sequence-specific recognition of a PxLPxI/L motif by an ankyrin repeat tumbler lock. *Science Signaling, 5*(226), ra39. https://doi.org/10.1126/scisignal.2002979

Xu, C., & Min, J. (2011). Structure and function of WD40 domain proteins. *Protein Cell, 2*(3), 202-214. https://doi.org/10.1007/s13238-011-1018-1

Xu, D., Farmer, A., & Chook, Y. M. (2010). Recognition of nuclear targeting signals by Karyopherin-β proteins. *Current Opinion in Structural Biology, 20*(6), 782-790. https://doi.org/10.1016/j.sbi.2010.09.008

Xu, R.-G., Wang, X., Shen, D., Sun, J., Qiao, H.-H., Wang, F., Liu, L.-P., & Ni, J.-Q. (2019). Perspectives on gene expression regulation techniques in *Drosophila*. *Journal of Genetics and Genomics, 46*(4), 213-220. https://doi.org/10.1016/j.jgg.2019.03.006

Xu, Z., Graham, K., Foote, M., Liang, F., Rizkallah, R., Hurt, M., Wang, Y., Wu, Y., & Zhou, Y. (2013). 14-3-3 protein targets misfolded chaperone-associated proteins to aggresomes. *Journal of Cell Science, 126*(Pt 18), 4173-4186. https://doi.org/10.1242/jcs.126102

Yamazaki, Y., Zhao, N., Caulfield, T. R., Liu, C.-C., & Bu, G. (2019). Apolipoprotein E and Alzheimer disease: pathobiology and targeting strategies. *Nature Reviews Neurology, 15*(9), 501-518. https://doi.org/10.1038/s41582-019-0228-7

Yang, Q., She, H., Gearing, M., Colla, E., Lee, M., Shacka, J. J., & Mao, Z. (2009). Regulation of neuronal survival factor MEF2D by chaperone-mediated autophagy. *Science, 323*(5910), 124-127. https://doi.org/10.1126/science.1166088

Yang, Q., Yang, Y., Zhou, N., Tang, K., Lau, W. B., Lau, B., Wang, W., Xu, L., Yang, Z., Huang, S., Wang, X., Yi, T., Zhao, X., Wei, Y., Wang, H., Zhao, L., & Zhou, S. (2018). Epigenetics in ovarian cancer: premise, properties, and perspectives. *Molecular Cancer, 17*(1), 109. https://doi.org/10.1186/s12943-018-0855-4

Yang, X.-J., & Seto, E. (2008). The Rpd3/Hda1 family of lysine deacetylases: from bacteria and yeast to mice and men. *Nature Reviews Molecular Cell Biology, 9*(3), 206-218. https://doi.org/10.1038/nrm2346

Yano, M., Nakamuta, S., Wu, X., Okumura, Y., & Kido, H. (2006). A novel function of 14-3-3 protein: 14-3-3zeta is a heat-shock-related molecular chaperone that dissolves thermal-aggregated proteins. *Molecular Biology of the Cell, 17*(11), 4769-4779. https://doi.org/10.1091/mbc.e06-03-0229

Yasuyama, K., Meinertzhagen, I. A., & Schürmann, F. W. (2002). Synaptic organization of the mushroom body calyx in *Drosophila melanogaster*. *The Journal of Comparative Neurology, 445*(3), 211-226. https://doi.org/10.1002/cne.10155

Yerbury, J. J., Ooi, L., Dillin, A., Saunders, D. N., Hatters, D. M., Beart, P. M., Cashman, N. R., Wilson, M. R., & Ecroyd, H. (2016). Walking the tightrope: proteostasis and neurodegenerative disease. *Journal of Neurochemistry, 137*(4), 489-505. https://doi.org/10.1111/jnc.13575

Yu, Y. T., Breitbart, R. E., Smoot, L. B., Lee, Y., Mahdavi, V., & Nadal-Ginard, B. (1992). Human myocyte-specific enhancer factor 2 comprises a group of tissue-restricted MADS box transcription factors. *Genes & Development, 6*(9), 1783-1798. https://doi.org/10.1101/gad.6.9.1783

Yue, F., Li, W., Zou, J., Chen, Q., Xu, G., Huang, H., Xu, Z., Zhang, S., Gallinari, P., Wang, F., McKeehan, W. L., & Liu, L. (2015). Blocking the association of HDAC4 with MAP1S accelerates autophagy clearance of mutant Huntingtin. *Aging, 7*(10), 839-853. https://doi.org/10.18632/aging.100818

Yun, S. J., Hiraoka, Y., Nishizawa, M., Takio, K., Titani, K., Nogi, Y., & Fukasawa, T. (1991). Purification and characterization of the yeast negative regulatory protein GAL80. *Journal of Biological Chemistry, 266*(2), 693-697. https://doi.org/10.1016/S0021-9258(17)35226-2

Zelhof, A. C., Hardy, R. W., Becker, A., & Zuker, C. S. (2006). Transforming the architecture of compound eyes. *Nature, 443*(7112), 696-699. https://doi.org/10.1038/nature05128

Zeremski, M., Stricker, J. R., Fischer, D., Zusman, S. B., & Cohen, D. (2003). Histone deacetylase dHDAC4 is involved in segmentation of the *Drosophila* embryo and is regulated by gap and pair-rule genes. *Genesis, 35*(1), 31-38. https://doi.org/10.1002/gene.10159

Zhang, C. L., McKinsey, T. A., Lu, J.-r., & Olson, E. N. (2001). Association of COOH-terminal-binding protein (CtBP) and MEF2-interacting transcription repressor (MITR) contributes to transcriptional repression of the MEF2 transcription factor. *Journal of Biological Chemistry, 276*(1), 35-39. https://doi.org/10.1074/jbc.M007364200

Zhang, C. L., McKinsey, T. A., & Olson, E. N. (2002). Association of class II histone deacetylases with heterochromatin protein 1: potential role for histone methylation in control of muscle differentiation. *Molecular and Cellular Biology, 22*(20), 7302-7312. https://doi.org/10.1128/mcb.22.20.7302-7312.2002

Zhang, N., Guo, L., & Simpson, J. H. (2020). Spatial comparisons of mechanosensory information govern the grooming sequence in *Drosophila*. *Current Biology, 30*(6), 988-1001.e1004. https://doi.org/10.1016/j.cub.2020.01.045

Zhang, P., Sun, Q., Zhao, C., Ling, S., Li, Q., Chang, Y.-Z., & Li, Y. (2014). HDAC4 protects cells from ER stress induced apoptosis through interaction with ATF4. *Cellular Signalling, 26*(3), 556-563. https://doi.org/10.1016/j.cellsig.2013.11.026

Zhang, X., Qi, Z., Yin, H., & Yang, G. (2019). Interaction between p53 and Ras signaling controls cisplatin resistance via HDAC4- and HIF-1α-mediated regulation of apoptosis and autophagy. *Theranostics, 9*(4), 1096-1114. https://doi.org/10.7150/thno.29673

Zhang, Y., Guo, H., Kwan, H., Wang, J.-W., Kosek, J., & Lu, B. (2007). PAR-1 kinase phosphorylates Dlg and regulates its postsynaptic targeting at the *Drosophila* neuromuscular junction. *Neuron, 53*(2), 201-215. https://doi.org/10.1016/j.neuron.2006.12.016

Zhao, J., Lu, Y., Zhao, X., Yao, X., Shuai, Y., Huang, C., Wang, L., Jeong, S. H., & Zhong, Y. (2013). Dissociation of rugose-dependent short-term memory component from memory consolidation in *Drosophila*. *Genes, Brain and Behavior, 12*(6), 626-632. https://doi.org/10.1111/gbb.12056

Zhao, X., Ito, A., Kane, C. D., Liao, T.-S., Bolger, T. A., Lemrow, S. M., Means, A. R., & Yao, T.-P. (2001). The modular nature of histone deacetylase HDAC4 confers phosphorylation-dependent intracellular trafficking. *Journal of Biological Chemistry, 276*(37), 35042-35048. https://doi.org/10.1074/jbc.M105086200

Zhao, X., Sternsdorf, T., Bolger, T. A., Evans, R. M., & Yao, T.-P. (2005). Regulation of MEF2 by histone deacetylase 4- and SIRT1 deacetylase-mediated lysine modifications. *Molecular and Cellular Biology, 25*(19), 8456. https://doi.org/10.1128/MCB.25.19.8456-8464.2005

Zhu, Y., Huang, M., Bushong, E., Phan, S., Uytiepo, M., Beutter, E., Boemer, D., Tsui, K., Ellisman, M., & Maximov, A. (2019). Class IIa HDACs regulate learning and memory through dynamic experience-dependent repression of transcription. *Nature Communications, 10*(1), 3469. https://doi.org/10.1038/s41467-019-11409-0

Zwarts, L., Goossens, T., Clements, J., Kang, Y. Y., & Callaerts, P. (2016). Axon branch-specific semaphorin-1a signaling in *Drosophila* mushroom body development. *Frontiers in Cellular Neuroscience, 10*, 210. https://doi.org/10.3389/fncel.2016.00210

Chapter Ten

Appendix

10. Appendix

10.1. Supplementary methods

10.1.1. *Drosophila* lines used in this study

Table 10.1. *Drosophila* lines used in this study

Stock ID Number*	Shorthand name	Genotype	Source	Also combined with
-	WCS10	*Canton S white (w[CS10])*	R. Davis	
	CS	*Canton S*	R. Davis	
H62	Tubulin-GAL80ts	*w[*]; P{w[+mC]=tubP-GAL80ts}10; TM2/TM6B, Tb1*	BDSC 7108	
H565	OK107-GAL4	*w[*]; P{w[+mW.hs]=GawB}OK107 ey[OK107]/In(4)ci[D], ci[D] pan[ciD] sv[spa-pol]*	BDSC 854	
H63	OK107-GAL4; Tubulin-GAL80ts	*w[CS10]; P{w[+mC]=tubP-GAL80ts}10; P{w+mW.hs=GawB}OK107*	H62 and H57	
H83	elav-GAL4	*w[CS10]; P{w[+mW.hs]=GawB}elav[C155]*	BDSC 458	
H184	elav-GAL4; Tubulin-GAL80ts	*w[CS10]; P{w[+mW.hs]=GawB}elav[C155], P{w+mC=tubP-GAL80ts}10; Cantonized*	H62 and H83	
H84	GMR-GAL4	*w[*]; P{w[+mC]=GAL4-ninaE.GMR}12*	BDSC 1104	
H464	GFP-HDAC4^{WT}	*w[1118];PBac{y+-attP-3B}VK37, UAS-GFP-DmHDAC4. Ectopic insertion on 3 (unknown location but not VK37).*	Patrick Main, Main (2019)	
H502	Cy/Bl; TM2/TM6B	*w[1118]/Dp(1;Y)y[+]; CyO/Bl[1]; TM2/TM6B, Tb[1]*	BDSC 3704	
H511	HDAC4::GFP	*y[1] w[*] P{w[+mC]=PTT-GA}HDAC4[CA07134] (Cantonised)*	BDSC 50817	
H736	HDAC4::GFP; OK107-GAL4	*w[CS10] P{w[+mC]=PTT-GA}HDAC4[CA07134] (Cantonised); P{w[+mW.hs]=GawB}OK107 ey[OK107]*	H511 and H565	
H157	MEF2 RNAi #1	*w[1118]; P{GD5039}v15550 CG1429 RNAi*	VDRC #15550	
H408	MEF2 RNAi #2	*w[1118];P{GD5039}v15549 CG1429 RNAi*	VDRC #15549	
H460	MEF2^{WT}	*w[1118]; PBac{y+-attP-3B}VK22, UAS-DmMEF2-HA. Insert into VK22(2R) 57F5*	Genetivision, USA	
H468	HDAC4^{WT}	*w[CS10]; P{y[+t7.7]=CaryP}attP2, UAS-DmHDAC4(WT)-myc. Insert into P2:(3L) 68A4*	Genetivision, USA	H83 H84/H502 H460 H464 H565
H469	HDAC4^{3SA}	*w[CS10]; P{y[+t7.7]=CaryP}attP2, UAS-DmHDAC4-3SA-myc. Insert into P2:(3L) 68A4*	Genetivision, USA	H84/H502
H471	HDAC4$^{\Delta MEF2}$	*w[CS10]; P{y[+t7.7]=CaryP}attP2, UAS-DmHDAC4-dMEF2-myc. Insert into P2:(3L) 68A4*	Genetivision, USA	H84/H502 H460

Stock ID Number*	Shorthand name	Genotype	Source	Also combined with
H562	HDAC4^{9QA}	*w[CS10]; P{y[+t7.7]=CaryP}attP2, UAS-DmHDAC4-9QA-myc. Insert into P2:(3L) 68A4*	Genetivision, USA	H84/H502 H464
H563	HDAC4^{9QAΔQ}	*w[CS10]; P{y[+t7.7]=CaryP}attP2, UAS-DmHDAC4-9QAdQ-myc. Insert into P2:(3L) 68A4*	Genetivision, USA	H84/H502 H464
H564	HDAC4^{F65A}	*w[CS10]; P{y[+t7.7]=CaryP}attP2, UAS-DmHDAC4-F65A-myc. Insert into P2:(3L) 68A4*	Genetivision, USA	H84/H502 H464
H618	HDAC4$^{3SA-ΔMEF2}$	*w[CS10]; P{y[+t7.7]=CaryP}attP2, UAS-DmHDAC4-3A-dMEF2-myc. Insert into P2:(3L) 68A4*	Genetivision, USA	H84/H502
H620	HDAC4^{S69F}	*w[CS10]; P{y[+t7.7]=CaryP}attP2, UAS-DmHDAC4-S69F-myc. Insert into P2:(3L) 68A4*	Genetivision, USA	H84/H502 H464
H621	HDAC4$^{3SA-F65A}$	*w[CS10]; P{y[+t7.7]=CaryP}attP2, UAS-DmHDAC4-3SA-F65A--myc. Insert into P2:(3L) 68A4*	Genetivision, USA	H84/H502 H464
H729	HDAC4$^{9QA-F65A}$	*w[CS10]; P{y[+t7.7]=CaryP}attP2 DmHDAC4-Myc-9QA-F65A. Insert into P2:(3L) 68A4*	Genetivision, USA	H84/H502
H730	HDAC4$^{3SA-9QA}$	*w[CS10]; P{y[+t7.7]=CaryP}attP2 DmHDAC4-Myc-3SA-9QA. Insert into P2:(3L) 68A4*	Genetivision, USA	H84/H502 H464
H731	HDAC4$^{3SA-F65A-ΔMEF2}$	*w[CS10]; P{y[+t7.7]=CaryP}attP2 DmHDAC4-Myc-3A-F65A-dMEF2. Insert into P2:(3L) 68A4*	Genetivision, USA	H84/H502
H734	HDAC4^{ΔNES}	*w[CS10]; P{y[+t7.7]=CaryP}attP2 DmHDAC4-dNES-Myc. Insert into P2:(3L) 68A4*	Genetivision, USA	H84/H502
H722	DmHDAC4$^{P37-Q143}$	*w[CS10]; P{y[+t7.7]=CaryP}attP2 DmHDAC4-P37-Q143. Insert into P2:(3L) 68A4*	Genetivision, USA	H84/H502
H723	DmHDAC4$^{NLS-P37-Q143}$	*w[CS10]; P{y[+t7.7]=CaryP}attP2 DmHDAC4-NLS_P37-Q143. Insert into P2:(3L) 68A4*	Genetivision, USA	H84/H502
H724	DmHDAC4$^{P37-Q143-NLS}$	*w[CS10]; P{y[+t7.7]=CaryP}attP2 DmHDAC4-P37-Q143_NLS. Insert into P2:(3L) 68A4*	Genetivision, USA	H84/H502
H725	DmHDAC4$^{NES-P37-Q143}$	*w[CS10]; P{y[+t7.7]=CaryP}attP2 DmHDAC4-NES_P37-Q143. Insert into P2:(3L) 68A4*	Genetivision, USA	H84/H502
H726	DmHDAC4$^{P37-Q143-NES}$	*w[CS10]; P{y[+t7.7]=CaryP}attP2 DmHDAC4-P37-Q143_NES. Insert into P2:(3L) 68A4*	Genetivision, USA	H84/H502
H727	DmHDAC4$^{M1-Q143}$	*w[CS10]; P{y[+t7.7]=CaryP}attP2 DmHDAC4-M1-Q143. Insert into P2:(3L) 68A4*	Genetivision, USA	H84/H502
H728	DmHDAC4$^{M1-L285}$	*w[CS10]; P{y[+t7.7]=CaryP}attP2 DmHDAC4-M1-L285. Insert into P2:(3L) 68A4*	Genetivision, USA	H84/H502

*stock ID number is specific to the Massey University *Drosophila* Neurogenetics Lab stock list.
H84/H502 notes the stock lines that were *GMR-GAL4/CyO; UAS-HDAC4/UAS-HDAC4.*

10.1.2. Full-length *Drosophila* HDAC4-Myc sequence with mutations characterised in this thesis

Wild-type HDAC4 sequence (nucleotides 461 – 4216, NCBI NM_132640) is displayed with the correct frame translation. Residues mutated in HDAC4^{mutant} are red and are as indicated in margin. 9QA residues are green. Strikethrough indicates the region deleted in 9QAΔQ. The C-terminal glycine linker and 6x Myc tag is red.

```
atg tct agt ccc gac gat aga ata cca ata cac gat ctg cca tca gaa gcc gga agc gat
 M   S   S   P   D   D   R   I   P   I   H   D   L   P   S   E   A   G   S   D
gag cga ttg ctg cac ata acg ccg gcc act ctg aca ttg gac ttc aag ccc cat ccc gcc
 E   R   L   L   H   I   T   P   A   T   L   T   L   D   F   K   P   H   P   A
gtg gat atc gat cag cag atc atg gag ctc aag aag agc cag gag ctg caa aag cag cgg                gcc
 V   D   I   D   Q   Q   I   M   E   L   K   K   S   Q   E   L   Q   K   Q   R         9QA:    A
ctt atc aac tcg ttt cag gag caa tcg aag caa atg gaa ttg gag cat aaa ctt caa ttg        gcc     ttc
 L   I   N   S   F   Q   E   Q   S   K   Q   M   E   L   E   H   K   L   Q   L    F65A: A   S69F: F
gag cac aag tat caa ttt gcg gtg aat tca cat ggc gct ttc cag gaa ttg cga aac gag
 E   H   K   Y   Q   F   A   V   N   S   H   G   A   F   Q   E   L   R   N   E
agc atg gtg aca gcc gcc gct gct gcg gtg gct ~~cag gag caa cat cgc caa cag ttg cat~~
 S   M   V   T   A   A   A   A   A   V   A   ~~Q   E   Q   H   R   Q   Q   L   H~~
~~caa cag cag cag caa cat cag cag cag cag cag cag cag caa cat caa cag cag cag cag~~
 ~~Q   Q   Q   Q   Q   H   Q   Q   Q   Q   Q   Q   Q   Q   H   Q   Q   Q   Q   Q~~
~~cag caa cag~~ gca cgc ggc agg gat ggc atg aaa ctc aag cag aac tgt agt gcc aat gcc
 ~~Q   Q   Q~~   A   R   G   R   D   G   M   K   L   K   Q   N   C   S   A   N   A
agt ccc gag gtc aaa cag att ctc aac tgc ttc atc ctg agc aga aag tcc cag gcg gcg                gcc
 S   P   E   V   K   Q   I   L   N   C   F   I   L   S   R   K   S   Q   A   A       ΔMEF2   3x:    A
gca tcg aat ggc aca acg aca acg tcg ccc tac agg aat cgc ggc gtg gtg aag agc tcc
 A   S   N   G   T   T   T   T   S   P   Y   R   N   R   G   V   V   K   S   S
tcg ggc gaa tcc ctc cca gct gga acc gtg acc agt gcg cat ccg tac aaa ata cct cag
 S   G   E   S   L   P   A   G   T   V   T   S   A   H   P   Y   K   I   P   Q
ccg cca ccc tca ctg ctc aaa tat gaa tct gat ttt ccg ctg agg aag aca gca tcc gaa                gcc
 P   P   P   S   L   L   K   Y   E   S   D   F   P   L   R   K   T   A   S   E       3SA   #1:      A
ccg aac ctg ctg aag atc cgg ctg aag cag agc gtc atc gag cgc aag gcc cgc atc gga
 P   N   L   L   K   I   R   L   K   Q   S   V   I   E   R   K   A   R   I   G
gga ccg gcg gga gcc cgg cgc cac gaa cga ctc ctc cag gcg gcg cag cgt agg cag caa
 G   P   A   G   A   R   R   H   E   R   L   L   Q   A   A   Q   R   R   Q   Q
aag aac tcg gtt ctc aca aac tgc aac agt aca ccg gat tct gga ccc aat tca ccg ccc
 K   N   S   V   L   T   N   C   N   S   T   P   D   S   G   P   N   S   P   P
tcg gca gct gcg ttg gcg gtg ggc gtg gtc ggt agc cgt gga tca ccg aca agt gca ccc
 S   A   A   A   L   A   V   G   V   V   G   S   R   G   S   P   T   S   A   P
att cag gag gaa aac gag gag ggc agc caa tat cag ccg ggc cag agg agc agc atc aac
 I   Q   E   E   N   E   E   G   S   Q   Y   Q   P   G   Q   R   S   S   I   N
gat ttg cca ttg ttc agt tca cca tcg ctg ccg aat att tcg ctc ggg cga ccg cat tta
 D   L   P   L   F   S   S   P   S   L   P   N   I   S   L   G   R   P   H   L
ccc aac tcg gcg cag gcg cat gcc cag gtg aat gcc cag gtt gct gcc cag gct cag gca
 P   N   S   A   Q   A   H   A   Q   V   N   A   Q   V   A   A   Q   A   Q   A
cag gcc cag gca cag gca cag gcg cat gcc atg ttc gcg gca ctg gct gcc gcc cag ggt
 Q   A   Q   A   Q   A   Q   A   H   A   M   F   A   A   L   A   A   A   Q   G
ggc tgc gga cag ccg ggc tac tat aat cca ctg ggc atg gca ttc gtt ggc cgg caa cca
 G   C   G   Q   P   G   Y   Y   N   P   L   G   M   A   F   V   G   R   Q   P
gca ccg ctg gcc atg att ccg gcc acg ggg ata gca ccg cag caa ccg tcg ccg gtg gtg
 A   P   L   A   M   I   P   A   T   G   I   A   P   Q   Q   P   S   P   V   V
cgc agt gca tcg gcc act tcg aca tcg tcg tcg cag gcc tcg ctg gtg ggc gat gtg gcg
 R   S   A   S   A   T   S   T   S   S   S   Q   A   S   L   V   G   D   V   A
cca ccg cag gct cat gcc gcc tcc acc att ctg ccc tcg tca tcg tcc tac atg cag caa
 P   P   Q   A   H   A   A   S   T   I   L   P   S   S   S   S   Y   M   Q   Q
ctg ggc agt gtg gcc ggt tcg ggt gtt aat ctc cat gcc gcc gcc gtt gct gca gcg gca
 L   G   S   V   A   G   S   G   V   N   L   H   A   A   A   V   A   A   A   A
gca gca gca gcc gcc gcc ggt tca ctg cca ccg acc aat agc cat ggt cac gga cac ggt
 A   A   A   A   A   A   G   S   L   P   P   T   N   S   H   G   H   G   H   G
tcc cac gca cat cca cat cca cat gcc cat gga cac ggg cat ggc cat ggc cat ggt atc
 S   H   A   H   P   H   P   H   A   H   G   H   G   H   G   H   G   H   G   I
tac gct ggc cac cag cac aat gtg ccc ata acg gac gcc cag gtg gcg cag gtg cat ctg
 Y   A   G   H   Q   H   N   V   P   I   T   D   A   Q   V   A   Q   V   H   L
cac aaa cag ggc cat cgg ccg ctg gga cga acg cag tcg gca cca ctg ccc ctt gga cat                gcc
 H   K   Q   G   H   R   P   L   G   R   T   Q   S   A   P   L   P   L   G   H       3SA   #2:      A
ccg atg cta acc gga gct gtg caa ctg aat gtg gtc caa acg cac tac gag aat agt gag
 P   M   L   T   G   A   V   Q   L   N   V   V   Q   T   H   Y   E   N   S   E
gcg gag cgc cag gcg tac gag cac cag gtg gtg aac cag aaa gtc cgc cag acc gtc ctg
 A   E   R   Q   A   Y   E   H   Q   V   V   N   Q   K   V   R   Q   T   V   L
act cgc agc gga gct gct gca gca gcc gct gct gcc gcc ggc gtg agc gtg gtg cgt gag
 T   R   S   G   A   A   A   A   A   A   A   A   A   G   V   S   V   V   R   E
gca cag ttg aag gag gag gat gac gac tcg gcc gcc gag gtg atg gac ctc aca gat aag
 A   Q   L   K   E   E   D   D   D   S   A   A   E   V   M   D   L   T   D   K
aaa aaa ccg ccg aag acg gtg cta acc agc acg ata gcc acc agt acg tcc cag aat ctg
 K   K   P   P   K   T   V   L   T   S   T   I   A   T   S   T   S   Q   N   L
```

```
ccc gaa gct ttg gcg gcg gcg gcg gcg gca gcc gcc tac cgt gcc ccg cac aac gcg tcc
 P   E   A   L   A   A   A   A   A   A   A   A   Y   R   A   P   H   N   A   S
agt aac tcc gcc tcc gcc aca aag tcc ggt att aag ctg cgg gac cag gag tat ttg caa
 S   N   S   A   S   A   T   K   S   G   I   K   L   R   D   Q   E   Y   L   Q
cag cag cgg gag caa cta ttg ctc ctt cag cag gag gag gaa ctg gcg aag agc cta atg
 Q   Q   R   E   Q   L   L   L   L   Q   Q   E   E   E   L   A   K   S   L   M
cgt ccg cta tcg cga acg ctt agc agt ccg ctg gtg ccg ctg ggg cca cat ggt ctt agt                 gcc
 R   P   L   S   R   T   L   S   S   P   L   V   P   L   G   P   H   G   L   S       3SA   #3:      A
cag att ccc gac act gga caa cag ccg gca ccg ata gcc aca tcc tcg tcg gcc gat cat
 Q   I   P   D   T   G   Q   Q   P   A   P   I   A   T   S   S   S   A   D   H
ata ccg ccc gtt aac ctc tcg ctg ccg cat cgc cag cac cgc cag cta atg agc aca cta
 I   P   P   V   N   L   S   L   P   H   R   Q   H   R   Q   L   M   S   T   L
tac gcc agc caa ttg cgt aac cac cag cca tcg gcg agt ggt tca ccg ccg cac aag gtc
 Y   A   S   Q   L   R   N   H   Q   P   S   A   S   G   S   P   P   H   K   V
acc acc ggt ttg gcc tac gat ccg ctt atg ctg aag cat tcg tgt att tgc gga gac aat
 T   T   G   L   A   Y   D   P   L   M   L   K   H   S   C   I   C   G   D   N
gcc cag cat ccg gag cac agt ggt cga ctg cag agc gtg tgg gca cgg tta aat gaa acg
 A   Q   H   P   E   H   S   G   R   L   Q   S   V   W   A   R   L   N   E   T
gat ctg gtg aag cgt tgc gat cgc ctg cgc gct cgc aag gcg aca cag gag gag ctg cag
 D   L   V   K   R   C   D   R   L   R   A   R   K   A   T   Q   E   E   L   Q
act gtg cac acc gaa gcg cat gcc atg ctc ttc ggt tcg aat cag tgc cag ctc agc agg
 T   V   H   T   E   A   H   A   M   L   F   G   S   N   Q   C   Q   L   S   R
ccc aag ttg gaa aac acg ttg tcg gcc agc ttt gtg cgt ttg tcg tgc ggc ggc ttg ggt
 P   K   L   E   N   T   L   S   A   S   F   V   R   L   S   C   G   G   L   G
gtg gat ctg gat acc acg tgg aat gag cac cat acg gca acc gct gca cga atg gca gcc
 V   D   L   D   T   T   W   N   E   H   H   T   A   T   A   A   R   M   A   A
ggt tgt gtt atc gat ttg gca ctg aag acg gcc aag ggt gac ctg cgg aat ggc ttt gcc
 G   C   V   I   D   L   A   L   K   T   A   K   G   D   L   R   N   G   F   A
gtt gtc cgg ccg ccg ggc cat cat gcg gag gcc aat ttg gcc atg ggc ttt tgt ttc ttc
 V   V   R   P   P   G   H   H   A   E   A   N   L   A   M   G   F   C   F   F
aat tcg ata gcc att gcg gcc aag ctg ctg cgt cag cgg atg ccc gag gtg cgg cgc atc
 N   S   I   A   I   A   A   K   L   L   R   Q   R   M   P   E   V   R   R   I
ctg atc gtc gat tgg gat gtg cat cac ggc aat ggc aca cag caa gca ttc tac caa agt
 L   I   V   D   W   D   V   H   H   G   N   G   T   Q   Q   A   F   Y   Q   S
ccc gac att cta tat ctt tcc ata cat cga cac gat gac ggt aac ttc ttt ccc ggc aca
 P   D   I   L   Y   L   S   I   H   R   H   D   D   G   N   F   F   P   G   T
ggt gga ccc aca gag tgc ggc tcc ggt gct ggt ctc ggc ttt aac gtg aac atc tca tgg
 G   G   P   T   E   C   G   S   G   A   G   L   G   F   N   V   N   I   S   W
tct ggg gca ctt aat ccg cca ctg ggc gac gcc gag tat atc gct gca ttc cgt acc gtt
 S   G   A   L   N   P   P   L   G   D   A   E   Y   I   A   A   F   R   T   V
gtg atg ccc atc gcg cgg agc ttt aat ccg gac att gtg ctg gta tcc tcc ggc ttc gat
 V   M   P   I   A   R   S   F   N   P   D   I   V   L   V   S   S   G   F   D
gcg gcc acc ggc cat ccg gca ccg ctg ggt ggc tac cat gtc tct ccg gcc tgc ttt ggg
 A   A   T   G   H   P   A   P   L   G   G   Y   H   V   S   P   A   C   F   G
ttc atg acc cgc gaa ctc ctt cag ttg gcc aac ggc aaa gtg gtg ctg gcc ctc gag ggc
 F   M   T   R   E   L   L   Q   L   A   N   G   K   V   V   L   A   L   E   G
ggc tac gat ctg gcc gcc atc tgt gat tcc gcc cag gag tgt gtg cgg gcg ctg ctc ggc
 G   Y   D   L   A   A   I   C   D   S   A   Q   E   C   V   R   A   L   L   G
gat ccc gct gct ccc att gcc aag gcc gag ctg gag cgc ccg cct tgc cag aat gcc atc
 D   P   A   A   P   I   A   K   A   E   L   E   R   P   P   C   Q   N   A   I
aat acg ctc cag aag acg ata gcc ata cag caa acg cat tgg ccc tgc gtg agg atg ctg
 N   T   L   Q   K   T   I   A   I   Q   Q   T   H   W   P   C   V   R   M   L
gag cac acg gtt ggc ttg tct gcg ctg gag acg ctc aag gtg gag cac gac gag tcc gag
 E   H   T   V   G   L   S   A   L   E   T   L   K   V   E   H   D   E   S   E
acg atc aac gcc atg gct ggc ctc tcg atg cag tcg atg cac aga act cta tcc cgc gat                 gcc
 T   I   N   A   M   A   G   L   S   M   Q   S   M   H   R   T   L   S   R   D     ΔNES   4x:      A
gat tcc gag gag ccg atg gat cag gat gaa acc aaa ggc gga ggc gag caa aag ctc att
 D   S   E   E   P   M   D   Q   D   E   T   K   G   G   G   E   Q   K   L   I
tct gaa gag gac ttg aat gaa atg gag caa aag ctc att tct gaa gag gac ttg aat gaa
 S   E   E   D   L   N   E   M   E   Q   K   L   I   S   E   E   D   L   N   E
atg gag caa aag ctc att tct gaa gag gac ttg aat gaa atg gag caa aag ctc att tct
 M   E   Q   K   L   I   S   E   E   D   L   N   E   M   E   Q   K   L   I   S
gaa gag gac ttg aat gaa atg gag caa aag ctc att tct gaa gag gac ttg aat gaa atg
 E   E   D   L   N   E   M   E   Q   K   L   I   S   E   E   D   L   N   E   M
gag agc ttg ggc gac ctc acc atg gag caa aag ctc att tct gaa gag gac ttg                         tag
 E   S   L   G   D   L   T   M   E   Q   K   L   I   S   E   E   D   L   -
```

10.1.3. N-terminal *Drosophila* HDAC4 sequences

Wild-type HDAC4 sequences (NCBI NM_132640.6, nucleotides as indicated) are displayed with the correct frame translation. Ser239 is mutated to alanine in HDAC4$^{M1\text{-}L285}$ and is green. The Exogenous NLS/NES sequences and glycine linker are green. NLS sequence is from Shiga *et al.* (1996) and the NES sequence is from Bajusz *et al.* (2021). The C-terminal glycine linker and 3x HA tag are red.

HDAC4$^{M1\text{-}L285}$ nucleotides 461 – 1315 of NM_132640

```
atg tct agt ccc gac gat aga ata cca ata cac gat ctg cca tca gaa gcc gga agc gat
 M   S   S   P   D   D   R   I   P   I   H   D   L   P   S   E   A   G   S   D
gag cga ttg ctg cac ata acg ccg gcc act ctg aca ttg gac ttc aag ccc cat ccc gcc
 E   R   L   L   H   I   T   P   A   T   L   T   L   D   F   K   P   H   P   A
gtg gat atc gat cag cag atc atg gag ctc aag aag agc cag gag ctg caa aag cag cgg
 V   D   I   D   Q   Q   I   M   E   L   K   K   S   Q   E   L   Q   K   Q   R
ctt atc aac tcg ttt cag gag caa tcg aag caa atg gaa ttg gag cat aaa ctt caa ttg
 L   I   N   S   F   Q   E   Q   S   K   Q   M   E   L   E   H   K   L   Q   L
gag cac aag tat caa ttt gcg gtg aat tca cat ggc gct ttc cag gaa ttg cga aac gag
 E   H   K   Y   Q   F   A   V   N   S   H   G   A   F   Q   E   L   R   N   E
agc atg gtg aca gcc gcc gct gct gcg gtg gct cag gag caa cat cgc caa cag ttg cat
 S   M   V   T   A   A   A   A   A   V   A   Q   E   Q   H   R   Q   Q   L   H
caa cag cag cag caa cat cag cag cag cag cag cag cag caa cat caa cag cag cag cag
 Q   Q   Q   Q   Q   H   Q   Q   Q   Q   Q   Q   Q   Q   H   Q   Q   Q   Q   Q
cag caa cag gca cgc ggc agg gat ggc atg aaa ctc aag cag aac tgt agt gcc aat gcc
 Q   Q   Q   A   R   G   R   D   G   M   K   L   K   Q   N   C   S   A   N   A
agt ccc gag gtc aaa cag att ctc aac tgc ttc atc ctg agc aga aag tcc cag gcg gcg
 S   P   E   V   K   Q   I   L   N   C   F   I   L   S   R   K   S   Q   A   A
gca tcg aat ggc aca acg aca acg tcg ccc tac agg aat cgc ggc gtg gtg aag agc tcc
 A   S   N   G   T   T   T   T   S   P   Y   R   N   R   G   V   V   K   S   S
tcg ggc gaa tcc ctc cca gct gga acc gtg acc agt gcg cat ccg tac aaa ata cct cag
 S   G   E   S   L   P   A   G   T   V   T   S   A   H   P   Y   K   I   P   Q
ccg cca ccc tca ctg ctc aaa tat gaa tct gat ttt ccg ctg agg aag aca gca gcc gaa
 P   P   P   S   L   L   K   Y   E   S   D   F   P   L   R   K   T   A   A   E
ccg aac ctg ctg aag atc cgg ctg aag cag agc gtc atc gag cgc aag gcc cgc atc gga
 P   N   L   L   K   I   R   L   K   Q   S   V   I   E   R   K   A   R   I   G
gga ccg gcg gga gcc cgg cgc cac gaa cga ctc ctc cag gcg gcg cag cgt agg cag caa
 G   P   A   G   A   R   R   H   E   R   L   L   Q   A   A   Q   R   R   Q   Q
aag aac tcg gtt ctc ggc gga ggc tac cca tac gat gtt cct gac tat gcg ggc tat ccc
 K   N   S   V   L   G   G   G   Y   P   Y   D   V   P   D   Y   A   G   Y   P
tat gac gtc ccg gac tat gca gga tcc tat cca tat gac gtt cca gat tac gct tag
 Y   D   V   P   D   Y   A   G   S   Y   P   Y   D   V   P   D   Y   A   -
```

HDAC4$^{M1\text{-}Q143}$ nucleotides 461 – 889 of NM_132640

```
atg tct agt ccc gac gat aga ata cca ata cac gat ctg cca tca gaa gcc gga agc gat
 M   S   S   P   D   D   R   I   P   I   H   D   L   P   S   E   A   G   S   D
gag cga ttg ctg cac ata acg ccg gcc act ctg aca ttg gac ttc aag ccc cat ccc gcc
 E   R   L   L   H   I   T   P   A   T   L   T   L   D   F   K   P   H   P   A
gtg gat atc gat cag cag atc atg gag ctc aag aag agc cag gag ctg caa aag cag cgg
 V   D   I   D   Q   Q   I   M   E   L   K   K   S   Q   E   L   Q   K   Q   R
ctt atc aac tcg ttt cag gag caa tcg aag caa atg gaa ttg gag cat aaa ctt caa ttg
 L   I   N   S   F   Q   E   Q   S   K   Q   M   E   L   E   H   K   L   Q   L
gag cac aag tat caa ttt gcg gtg aat tca cat ggc gct ttc cag gaa ttg cga aac gag
 E   H   K   Y   Q   F   A   V   N   S   H   G   A   F   Q   E   L   R   N   E
agc atg gtg aca gcc gcc gct gct gcg gtg gct cag gag caa cat cgc caa cag ttg cat
 S   M   V   T   A   A   A   A   A   V   A   Q   E   Q   H   R   Q   Q   L   H
caa cag cag cag caa cat cag cag cag cag cag cag cag caa cat caa cag cag cag cag
 Q   Q   Q   Q   Q   H   Q   Q   Q   Q   Q   Q   Q   Q   H   Q   Q   Q   Q   Q
cag caa cag ggc gga ggc tac cca tac gat gtt cct gac tat gcg ggc tat ccc tat gac
 Q   Q   Q   G   G   G   Y   P   Y   D   V   P   D   Y   A   G   Y   P   Y   D
gtc ccg gac tat gca gga tcc tat cca tat gac gtt cca gat tac gct tag
 V   P   D   Y   A   G   S   Y   P   Y   D   V   P   D   Y   A   -
```

HDAC4$^{P37\text{-}Q143}$ nucleotides 569 – 889 of NM_132640

```
atg ccc cat ccc gcc gtg gat atc gat cag cag atc atg gag ctc aag aag agc cag gag
 M   P   H   P   A   V   D   I   D   Q   Q   I   M   E   L   K   K   S   Q   E
ctg caa aag cag cgg ctt atc aac tcg ttt cag gag caa tcg aag caa atg gaa ttg gag
 L   Q   K   Q   R   L   I   N   S   F   Q   E   Q   S   K   Q   M   E   L   E
cat aaa ctt caa ttg gag cac aag tat caa ttt gcg gtg aat tca cat ggc gct ttc cag
 H   K   L   Q   L   E   H   K   Y   Q   F   A   V   N   S   H   G   A   F   Q
gaa ttg cga aac gag agc atg gtg aca gcc gcc gct gct gcg gtg gct cag gag caa cat
 E   L   R   N   E   S   M   V   T   A   A   A   A   A   V   A   Q   E   Q   H
cgc caa cag ttg cat caa cag cag cag caa cat cag cag cag cag cag cag cag caa cat
 R   Q   Q   L   H   Q   Q   Q   Q   Q   H   Q   Q   Q   Q   Q   Q   Q   Q   H
caa cag cag cag cag cag cag caa cag ggc gga ggc tac cca tac gat gtt cct gac tat gcg
 Q   Q   Q   Q   Q   Q   Q   Q   G   G   G   Y   P   Y   D   V   P   D   Y   A
ggc tat ccc tat gac gtc ccg gac tat gca gga tcc tat cca tat gac gtt cca gat tac
 G   Y   P   Y   D   V   P   D   Y   A   G   S   Y   P   Y   D   V   P   D   Y
gct tag
 A   -
```

HDAC4$^{NLS\text{-}P37\text{-}Q143}$: NLS plus nucleotides 569 – 889 of NM_132640

```
atg aga gct cca aag aag aag cgt aag ggc gcc ccg gta caa aaa ggc gga ggc ccc cat
 M   R   A   P   K   K   K   R   K   G   A   P   V   Q   K   G   G   G   P   H
ccc gcc gtg gat atc gat cag cag atc atg gag ctc aag aag agc cag gag ctg caa aag
 P   A   V   D   I   D   Q   Q   I   M   E   L   K   K   S   Q   E   L   Q   K
cag cgg ctt atc aac tcg ttt cag gag caa tcg aag caa atg gaa ttg gag cat aaa ctt
 Q   R   L   I   N   S   F   Q   E   Q   S   K   Q   M   E   L   E   H   K   L
caa ttg gag cac aag tat caa ttt gcg gtg aat tca cat ggc gct ttc cag gaa ttg cga
 Q   L   E   H   K   Y   Q   F   A   V   N   S   H   G   A   F   Q   E   L   R
aac gag agc atg gtg aca gcc gcc gct gct gcg gtg gct cag gag caa cat cgc caa cag
 N   E   S   M   V   T   A   A   A   A   A   V   A   Q   E   Q   H   R   Q   Q
ttg cat caa cag cag cag caa cat cag cag cag cag cag cag cag caa cat caa cag cag
 L   H   Q   Q   Q   Q   Q   H   Q   Q   Q   Q   Q   Q   Q   Q   H   Q   Q   Q
cag cag cag caa cag ggc gga ggc tac cca tac gat gtt cct gac tat gcg ggc tat ccc
 Q   Q   Q   Q   Q   G   G   G   Y   P   Y   D   V   P   D   Y   A   G   Y   P
tat gac gtc ccg gac tat gca gga tcc tat cca tat gac gtt cca gat tac gct tag
 Y   D   V   P   D   Y   A   G   S   Y   P   Y   D   V   P   D   Y   A   -
```

HDAC4$^{P37\text{-}Q143\text{-}NLS}$: nucleotides 569 – 889 of NM_132640 plus NLS

```
atg ccc cat ccc gcc gtg gat atc gat cag cag atc atg gag ctc aag aag agc cag gag
 M   P   H   P   A   V   D   I   D   Q   Q   I   M   E   L   K   K   S   Q   E
ctg caa aag cag cgg ctt atc aac tcg ttt cag gag caa tcg aag caa atg gaa ttg gag
 L   Q   K   Q   R   L   I   N   S   F   Q   E   Q   S   K   Q   M   E   L   E
cat aaa ctt caa ttg gag cac aag tat caa ttt gcg gtg aat tca cat ggc gct ttc cag
 H   K   L   Q   L   E   H   K   Y   Q   F   A   V   N   S   H   G   A   F   Q
gaa ttg cga aac gag agc atg gtg aca gcc gcc gct gct gcg gtg gct cag gag caa cat
 E   L   R   N   E   S   M   V   T   A   A   A   A   A   V   A   Q   E   Q   H
cgc caa cag ttg cat caa cag cag cag caa cat cag cag cag cag cag cag cag caa cat
 R   Q   Q   L   H   Q   Q   Q   Q   Q   H   Q   Q   Q   Q   Q   Q   Q   Q   H
caa cag cag cag cag cag caa cag ggc gga ggc aga gct cca aag aag aag cgt aag ggc
 Q   Q   Q   Q   Q   Q   Q   Q   G   G   G   R   A   P   K   K   K   R   K   G
gcc ccg gta caa aaa ggc gga ggc tac cca tac gat gtt cct gac tat gcg ggc tat ccc
 A   P   V   Q   K   G   G   G   Y   P   Y   D   V   P   D   Y   A   G   Y   P
tat gac gtc ccg gac tat gca gga tcc tat cca tat gac gtt cca gat tac gct tag
 Y   D   V   P   D   Y   A   G   S   Y   P   Y   D   V   P   D   Y   A   -
```

HDAC4$^{NES\text{-}P37\text{-}Q143}$: NES plus nucleotides 569 – 889 of NM_132640

```
atg aat gaa tta gcc ttg aaa tta gca ggt ctt gat atc aac aag aca ggc gga ggc ccc
 M   N   E   L   A   L   K   L   A   G   L   D   I   N   K   T   G   G   G   P
cat ccc gcc gtg gat atc gat cag cag atc atg gag ctc aag aag agc cag gag ctg caa
 H   P   A   V   D   I   D   Q   Q   I   M   E   L   K   K   S   Q   E   L   Q
aag cag cgg ctt atc aac tcg ttt cag gag caa tcg aag caa atg gaa ttg gag cat aaa
 K   Q   R   L   I   N   S   F   Q   E   Q   S   K   Q   M   E   L   E   H   K
ctt caa ttg gag cac aag tat caa ttt gcg gtg aat tca cat ggc gct ttc cag gaa ttg
 L   Q   L   E   H   K   Y   Q   F   A   V   N   S   H   G   A   F   Q   E   L
cga aac gag agc atg gtg aca gcc gcc gct gct gcg gtg gct cag gag caa cat cgc caa
 R   N   E   S   M   V   T   A   A   A   A   A   V   A   Q   E   Q   H   R   Q
cag ttg cat caa cag cag cag caa cat cag cag cag cag cag cag cag caa cat caa cag
 Q   L   H   Q   Q   Q   Q   Q   H   Q   Q   Q   Q   Q   Q   Q   Q   H   Q   Q
cag cag cag cag caa cag ggc gga ggc tac cca tac gat gtt cct gac tat gcg ggc tat
 Q   Q   Q   Q   Q   Q   G   G   G   Y   P   Y   D   V   P   D   Y   A   G   Y
ccc tat gac gtc ccg gac tat gca gga tcc tat cca tat gac gtt cca gat tac gct tag
 P   Y   D   V   P   D   Y   A   G   S   Y   P   Y   D   V   P   D   Y   A   -
```

HDAC4$^{P37\text{-}Q143\text{-}NES}$: nucleotides 569 – 889 of NM_132640 plus NES

```
atg ccc cat ccc gcc gtg gat atc gat cag cag atc atg gag ctc aag aag agc cag gag
 M   P   H   P   A   V   D   I   D   Q   Q   I   M   E   L   K   K   S   Q   E
ctg caa aag cag cgg ctt atc aac tcg ttt cag gag caa tcg aag caa atg gaa ttg gag
 L   Q   K   Q   R   L   I   N   S   F   Q   E   Q   S   K   Q   M   E   L   E
cat aaa ctt caa ttg gag cac aag tat caa ttt gcg gtg aat tca cat ggc gct ttc cag
 H   K   L   Q   L   E   H   K   Y   Q   F   A   V   N   S   H   G   A   F   Q
gaa ttg cga aac gag agc atg gtg aca gcc gcc gct gct gcg gtg gct cag gag caa cat
 E   L   R   N   E   S   M   V   T   A   A   A   A   A   V   A   Q   E   Q   H
cgc caa cag ttg cat caa cag cag cag caa cat cag cag cag cag cag cag cag caa cat
 R   Q   Q   L   H   Q   Q   Q   Q   Q   H   Q   Q   Q   Q   Q   Q   Q   Q   H
caa cag cag cag cag cag caa cag ggc gga ggc aat gaa tta gcc ttg aaa tta gca ggt
 Q   Q   Q   Q   Q   Q   Q   Q   G   G   G   N   E   L   A   L   K   L   A   G
ctt gat atc aac aag aca ggc gga ggc tac cca tac gat gtt cct gac tat gcg ggc tat
 L   D   I   N   K   T   G   G   G   Y   P   Y   D   V   P   D   Y   A   G   Y
ccc tat gac gtc ccg gac tat gca gga tcc tat cca tat gac gtt cca gat tac gct tag
 P   Y   D   V   P   D   Y   A   G   S   Y   P   Y   D   V   P   D   Y   A   -
```

10.1.4. Full-length *Drosophila* MEF2-HA sequence

Wild-type MEF2 sequence (nucleotides 1057 – 2601, NM_057670.5) is displayed with the correct frame translation. The C-terminal glycine linker and 3x HA tag is highlighted in red.

```
atg ggc cgc aaa aaa att caa ata tca cgc atc acc gat gaa cgc aat cgg cag gtg acc
 M   G   R   K   K   I   Q   I   S   R   I   T   D   E   R   N   R   Q   V   T
ttc aac aag cgc aag ttc ggc gtg atg aag aag gcc tac gag ctg tcc gtg ctc tgc gac
 F   N   K   R   K   F   G   V   M   K   K   A   Y   E   L   S   V   L   C   D
tgc gag atc gcc ctg atc atc ttc tcg tcg agc aac aag ctg tac cag tac gcc agc acc
 C   E   I   A   L   I   I   F   S   S   S   N   K   L   Y   Q   Y   A   S   T
gac atg gat cgc gtc ctg ctc aag tac acc gag tac aac gag ccc cac gag tcc ctc acc
 D   M   D   R   V   L   L   K   Y   T   E   Y   N   E   P   H   E   S   L   T
aac aag aac atc atc gag aag gag aac aag aac ggc gtg atg tcg ccg gac tcg ccc gaa
 N   K   N   I   I   E   K   E   N   K   N   G   V   M   S   P   D   S   P   E
gcc gaa acg gac tac aca ctc act ccg cga acg gag gcc aag tac aac aag atc gac gag
 A   E   T   D   Y   T   L   T   P   R   T   E   A   K   Y   N   K   I   D   E
gag ttc cag aac atg atg cag cgc aac cag atg gcc atc ggc ggt gcg ggt gcc cct cgc
 E   F   Q   N   M   M   Q   R   N   Q   M   A   I   G   G   A   G   A   P   R
cag ctt cca aac agc agc tac acg ctg ccc gtt tct gtt ccg gtg ccg gga tct tac ggc
 Q   L   P   N   S   S   Y   T   L   P   V   S   V   P   V   P   G   S   Y   G
gac aac ctg ctg cag gcc agt cca cag atg tcc cac acc aac atc agc ccc cgt cca tcg
 D   N   L   L   Q   A   S   P   Q   M   S   H   T   N   I   S   P   R   P   S
agt tcg gag acg gat tca ggt ggg atg tcc ctg ata att tat cca tcg ggt tcc atg ctg
 S   S   E   T   D   S   G   G   M   S   L   I   I   Y   P   S   G   S   M   L
gag atg tcg aac ggc tat ccg cat tca cac tcg ccg ctt gtg gga tca ccg agt ccg ggt
 E   M   S   N   G   Y   P   H   S   H   S   P   L   V   G   S   P   S   P   G
ccc agt cct ggc ata gcc cac cat ttg tcc att aag cag cag tcg ccg ggc agc cag aac
 P   S   P   G   I   A   H   H   L   S   I   K   Q   Q   S   P   G   S   Q   N
gga cga gct tcc aat cta agg gtc gtc ata ccg ccc aca att gcc ccc ata ccg ccc aat
 G   R   A   S   N   L   R   V   V   I   P   P   T   I   A   P   I   P   P   N
atg tca gcg ccg gat gat gtg gga tat gca gat caa cga cag agc cag aca tcg ctt aac
 M   S   A   P   D   D   V   G   Y   A   D   Q   R   Q   S   Q   T   S   L   N
acg cca gtg gtc acg ctg cag acg ccg att ccc gcc ctc acg agc tat tcc ttt ggg gcg
 T   P   V   V   T   L   Q   T   P   I   P   A   L   T   S   Y   S   F   G   A
cag gac ttc tcc tcc tcc ggc gta atg aac agc gcg gat atc atg agc ctc aac acc tgg
 Q   D   F   S   S   S   G   V   M   N   S   A   D   I   M   S   L   N   T   W
cat cag ggc ctg gtg ccg cac tct agt ctc tcg cac ctg gct gtc tcg aat agc acg ccg
 H   Q   G   L   V   P   H   S   S   L   S   H   L   A   V   S   N   S   T   P
ccg ccc gcc acc tcc ccc gtc tcc ata aag gtc aag gct gag ccg cag tcg ccg ccg aga
 P   P   A   T   S   P   V   S   I   K   V   K   A   E   P   Q   S   P   P   R
gat ctt tcc gcc agc ggt cat cag cag aat agc aat ggt tcc acg ggc agc ggc gga tcc
 D   L   S   A   S   G   H   Q   Q   N   S   N   G   S   T   G   S   G   G   S
agc agc agc acc agt agc aac gcc agc gga gga gca gga ggc ggt gga gcc gtc agc gca
 S   S   S   T   S   S   N   A   S   G   G   A   G   G   G   G   A   V   S   A
gcc aat gtc atc acg cac ttg aac aac gtc agt gtc ctg gcg gga ggt cct tcg ggg cag
 A   N   V   I   T   H   L   N   N   V   S   V   L   A   G   G   P   S   G   Q
gga gga gga ggc gga ggc ggc ggc agc aac gga aat gtc gaa cag gcc acc aat ctt agc
 G   G   G   G   G   G   G   G   S   N   G   N   V   E   Q   A   T   N   L   S
gta ctg agc cac gcg cag caa cat cac ctg ggc atg ccc aac tcg cgt ccc tcg tcc acg
 V   L   S   H   A   Q   Q   H   H   L   G   M   P   N   S   R   P   S   S   T
ggc cac atc aca ccc act cca ggt gcg ccg agc agc gac cag gat gtg cgt ctg gca gcc
 G   H   I   T   P   T   P   G   A   P   S   S   D   Q   D   V   R   L   A   A
gtc gcc gtg cag cag caa cag cag cca cat cag caa cag caa cta ggc gac tac gat
 V   A   V   Q   Q   Q   Q   Q   Q   P   H   Q   Q   Q   Q   L   G   D   Y   D
gcc ccc aac cac aaa cgg ccg aga ata tcg ggc gga tgg ggc aca ggc gga ggc tac cca
 A   P   N   H   K   R   P   R   I   S   G   G   W   G   T   G   G   G   Y   P
tac gat gtt cct gac tat gcg ggc tat ccc tat gac gtc ccg gac tat gca gga tcc tat
 Y   D   V   P   D   Y   A   G   Y   P   Y   D   V   P   D   Y   A   G   S   Y
cca tat gac gtt cca gat tac gct tag
 P   Y   D   V   P   D   Y   A   -
```

10.1.5. Generation of transgenic flies

Stable transformation of *Drosophila* by random P-element mediated insertion mechanisms has been superseded with the advent of PhiC31-mediated site-specific integration, which increases efficacy of transgenesis and minimises off-target effects (Bischof *et al.*, 2007). In this system, transgenic flies are generated by embryo microinjection with a plasmid containing a gene of interest, resulting in stable genomic incorporation of the microinjected DNA (Figure 10.1). The

pUASTattB plasmid has been specifically designed for *Drosophila* transgenesis, incorporating a number of features (HDAC4^{WT}: Figure 10.2, MEF2^{WT}: Figure 10.3) (Groth *et al.*, 2004). pUASTattB harbours an attB donor site, and its complementary landing site attP is present on chromosome 3L at 68A4 within the P2 injection strain (Groth *et al.*, 2004; Markstein *et al.*, 2008). Microinjection of P2 embryos with pUASTattB results in integrase-facilitated homologous recombination between attB and attP (Figure 10.1). The P2 injection strain harbours an endogenous source of bacteriophage PhiC31 integrase under the control of the vasa regulatory element, which can later be excised via surrounding loxP sites (Bischof *et al.*, 2007). Recombination destroys the attB and attP sites, forming two hybrid sites, attR and attL, preventing further recombination. This results in incorporation of the entire contents of the plasmid within the chromosome landing site. The P2 injection strain also has a mutation in the *white* gene (*w*-), resulting in progeny with white eyes. pUASTattB encodes a functional white gene (*mini white, w+*), and complementation allows selection of transgenic flies on the basis of eye colour. Upon outcrossing F0 germline transformed flies into a white-mutated background (*w(CS10)*), transformant F1 progeny with red eyes harbour one copy of *w+* and thus the transgene of interest, whereas non-transformed flies have white eyes. Additional injection strains to mediate integration at different loci are also available (Markstein *et al.*, 2008), allowing recombination of multiple transgenes into one fly line. This includes the VK22 strain that was used to generate MEF2^{WT}.

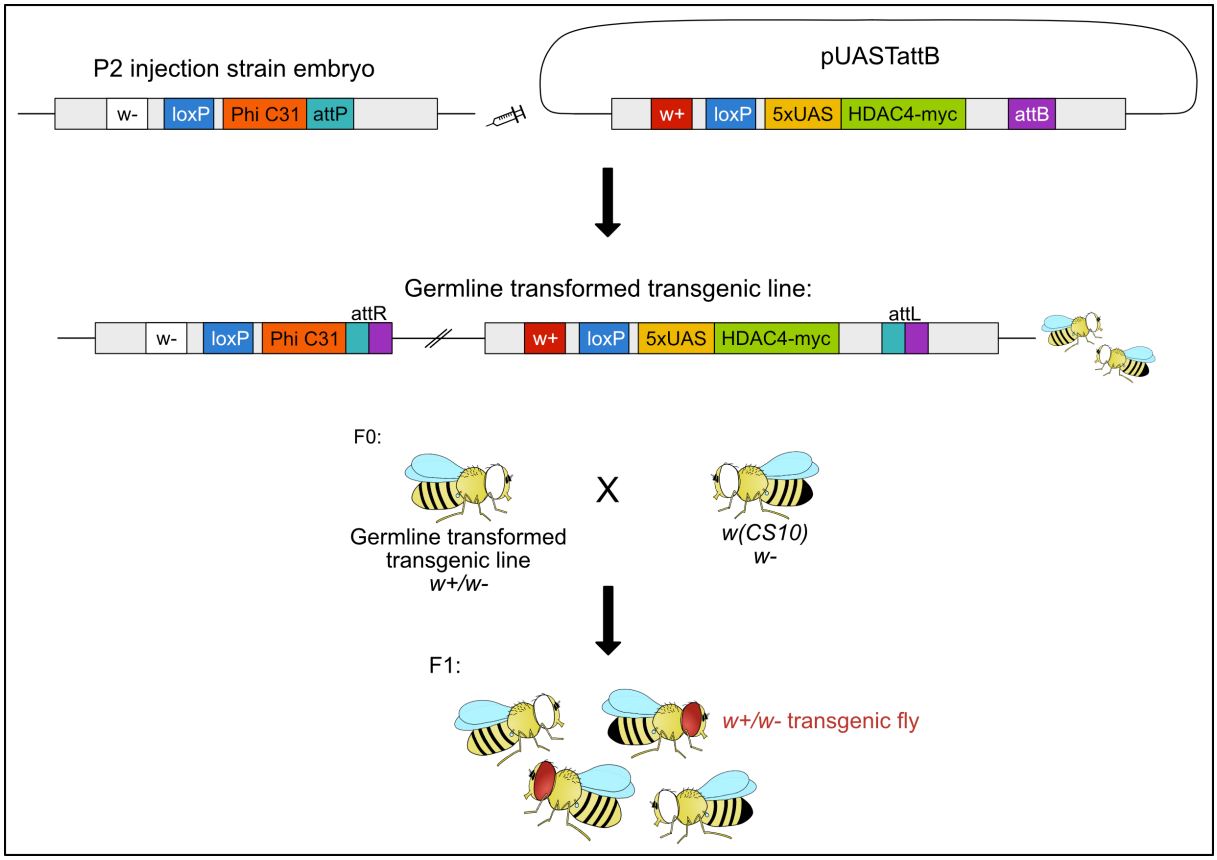

Figure 10.1 Generation of transgenic flies by PhiC31-mediated site-specific integration
P2 injection strain embryos are injected into the posterior of the embryo where the gonads form with the pUASTattB plasmid containing the transgene of interest (*HDAC4-Myc*) and the *w+* gene. PhiC31 integrase mediates recombination of *pUASTattB* into the *attP* landing site. Transgenic flies are selected

by outcrossing germline transformed F0 flies to *w*- mutant flies (*w(CS10)*) and selecting F1 progeny with wild-type red eyes. *LoxP* sites can also be used to excise intervening regions. *This figure is an original artwork created with reference to Bischof et al. (2007).*

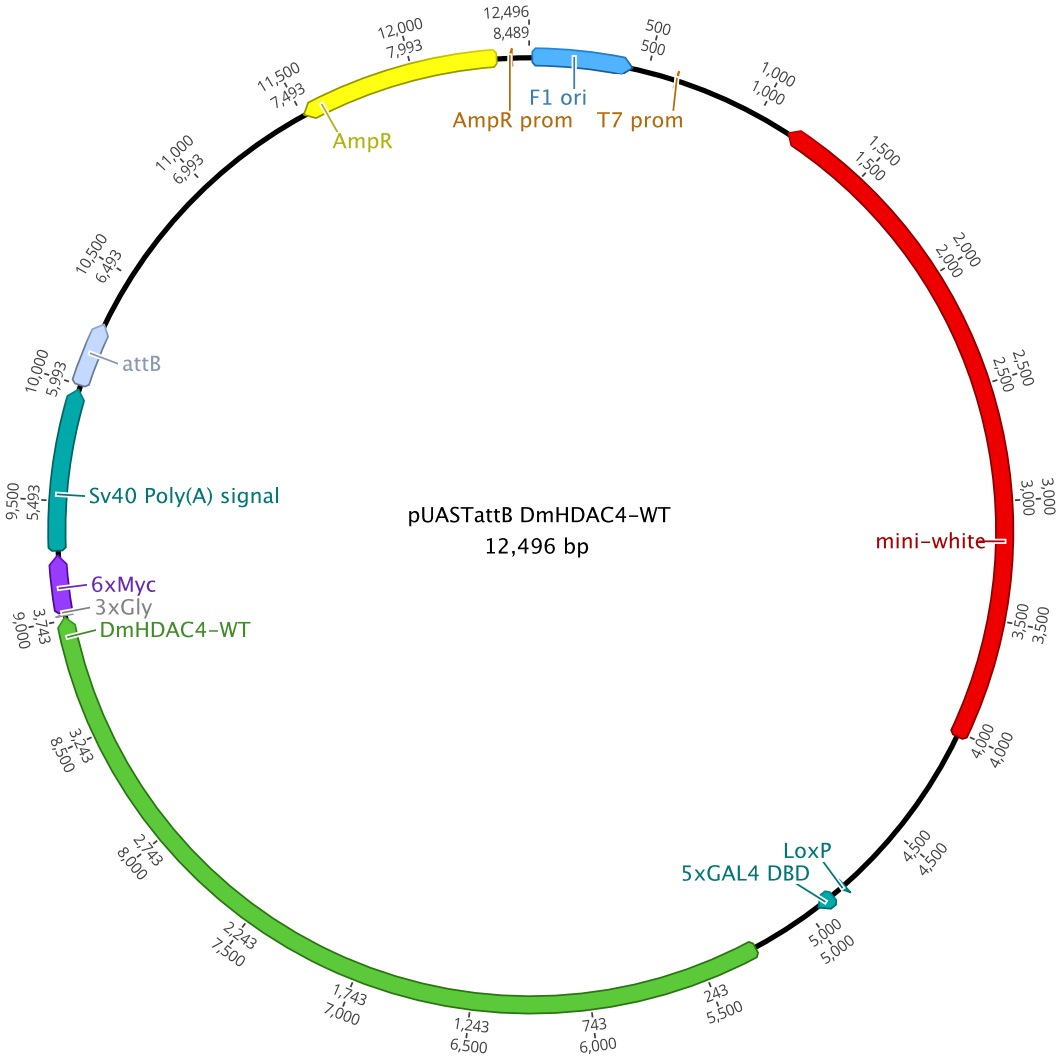

Figure 10.2 Physical map of pUASTattB DmHDAC4-WT
Plasmid map of pUASTattB DmHDAC4^{WT} with annotation of features important for generation of transgenic flies. Figure made in Geneious R9.

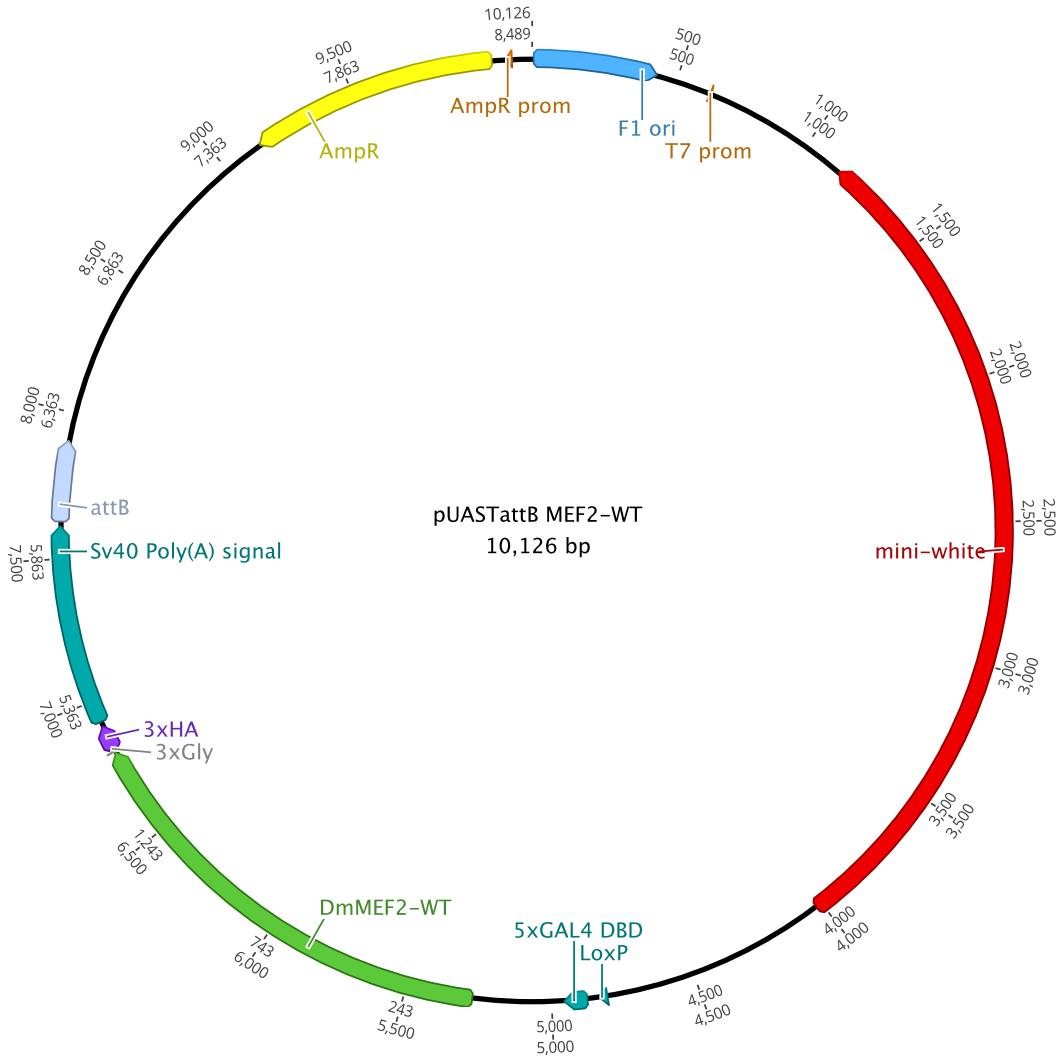

Figure 10.3 Physical map of pUASTattB DmMEF2-WT
Plasmid map of pUASTattB DmMEF2^{WT} with annotation of features important for generation of transgenic flies. Figure made in Geneious R9.

10.1.6. Crossing schemes used to combine transgenes

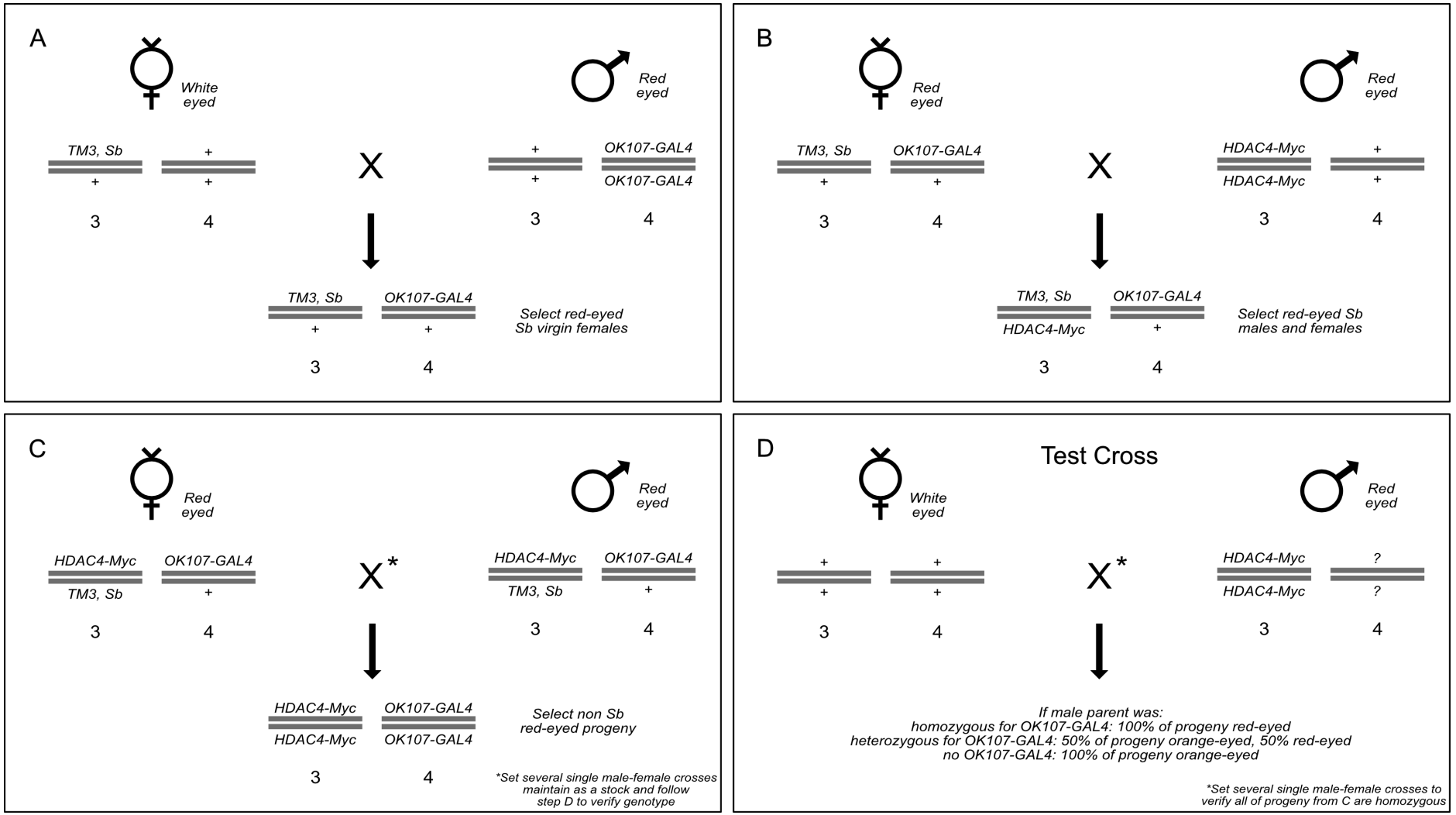

Figure 10.4 Crossing scheme to combine *OK107-GAL4* and *HDAC4^{WT}-Myc* into a single fly line

Female virgin progeny in (A) are used in (B). Male and female progeny in (B) are used in (C). A test-cross is performed in (D) to examine the eye colours of progeny to determine the status of the transgene on the fourth chromosome of the male parent. + indicates a wild-type chromosome. *TM3* denotes a balancer chromosome with multiple inversions to prevent recombination. *Sb,* stubble, dominant marker where flies have blunted bristles on the thorax. *This figure is an original artwork.*

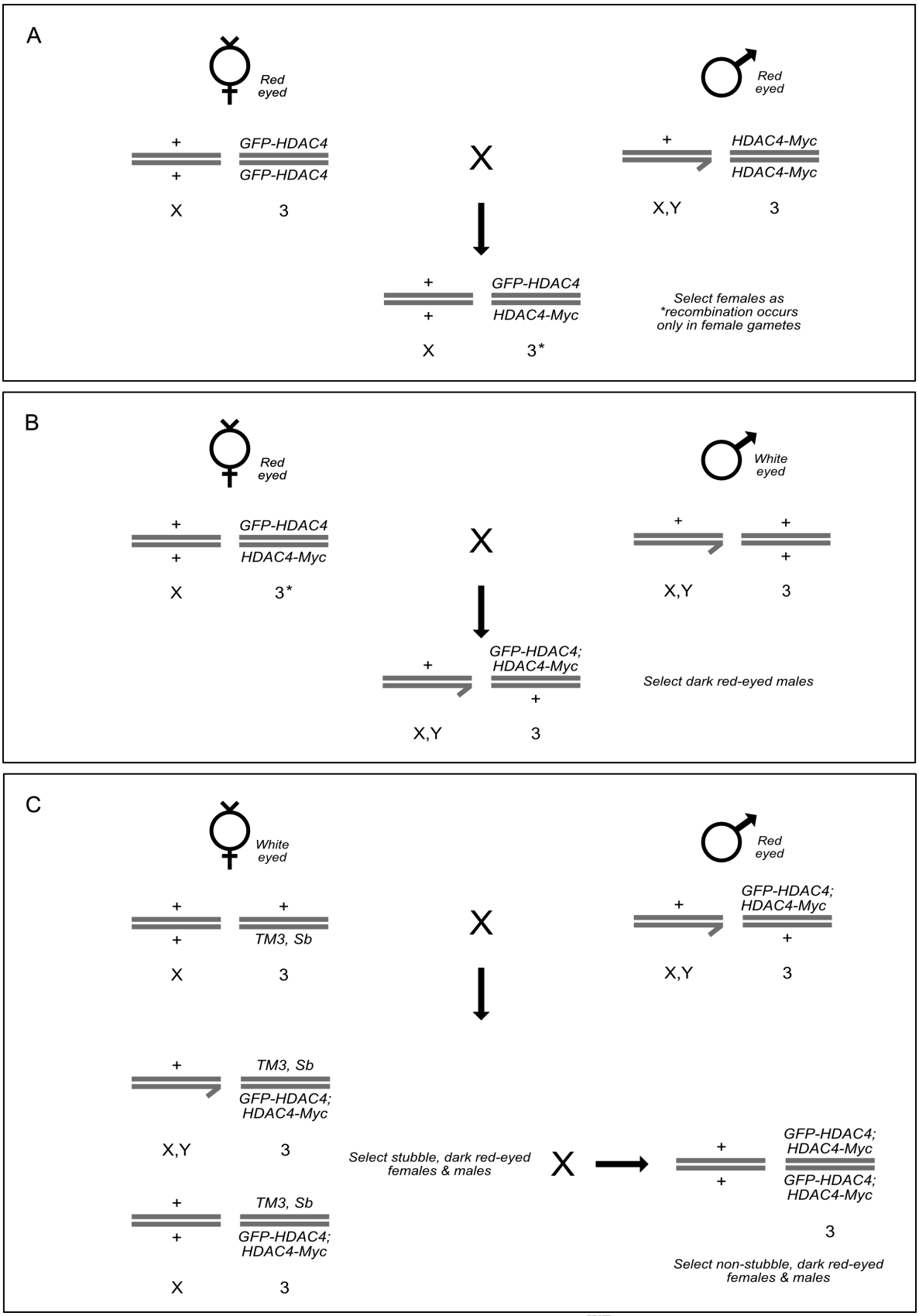

Figure 10.5 Crossing scheme to recombine *GFP-HDAC4^{WT}* and *HDAC4-Myc* transgenes
Female virgin progeny in (A) were used in (B). Male progeny in (B) were used in (C), where selected progeny of this cross were then crossed together. + indicates a wild-type chromosome. *TM3* denotes a balancer chromosome with multiple inversions to prevent recombination. *Sb,* stubble, dominant marker where flies have blunted bristles on the thorax. *This figure is an original artwork.*

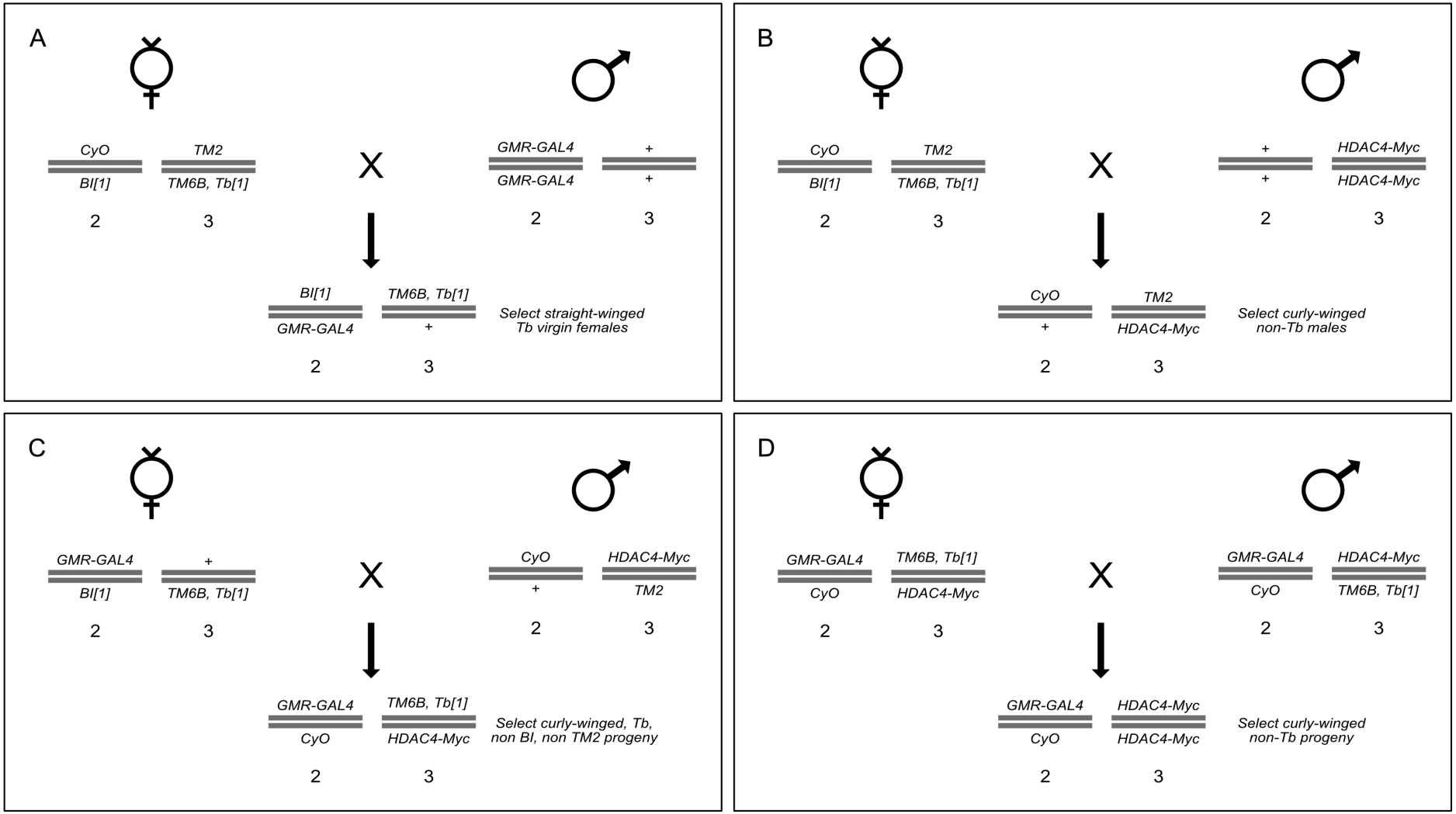

Figure 10.6 Crossing scheme to combine *GMR-GAL4* and *HDAC4* transgenes into a single fly line

Progeny from crosses in (A) and (B) were crossed together in (C). Progeny from (C) are crossed together in (D). + indicates a wild-type chromosome. *CyO*, Curly of Oster, dominant marker where flies have curly wings. *Tb*, tubby, dominant marker where pupae are short and fat, and progeny have rounded abdomens. *Bl[1],* bristle, dominant marker where flies have shorter and thicker bristles on the thorax. *TM2* and *TM6B* denote balancer chromosomes with multiple inversions to prevent recombination. These have additional selectable markers, but the phenotypes are not listed here for simplicity. *This figure is an original artwork.*

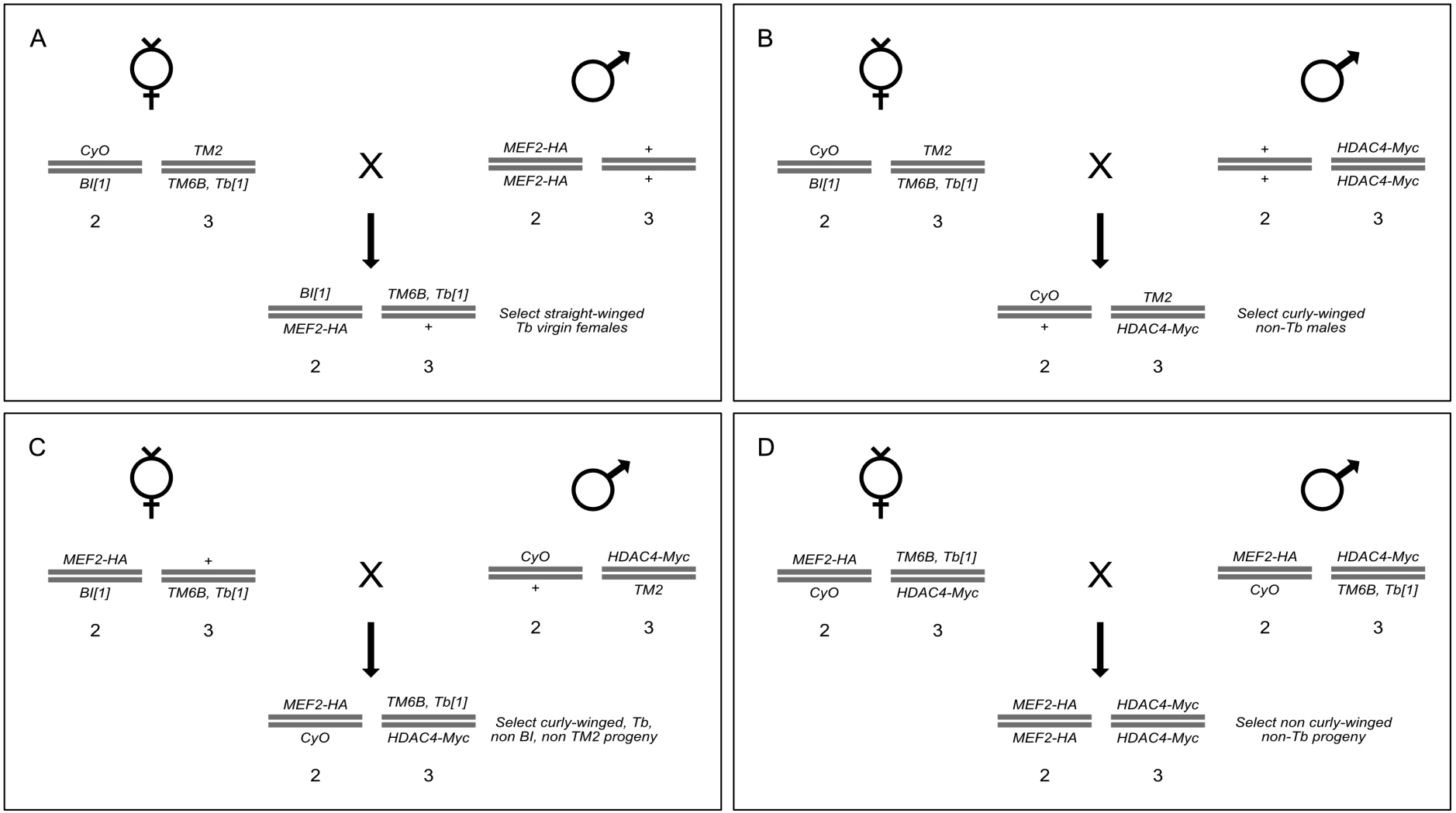

Figure 10.7 Crossing scheme to combine *MEF2-HA* and *HDAC4-Myc* transgenes into a single fly line

Progeny from crosses in (A) and (B) were crossed together in (C). Progeny from (C) were crossed together in (D). + indicates a wild-type chromosome. *CyO*, Curly of Oster, dominant marker where flies have curly wings. *Tb*, tubby, dominant marker where pupae are short and fat, and progeny have rounded abdomens. *Bl[1*], bristle, dominant marker where flies have shorter and thicker bristles on the thorax. *TM2* and *TM6B* denote balancer chromosomes with multiple inversions to prevent recombination. These have additional selectable markers, but the phenotypes are not listed here for simplicity. *This figure is an original artwork.*

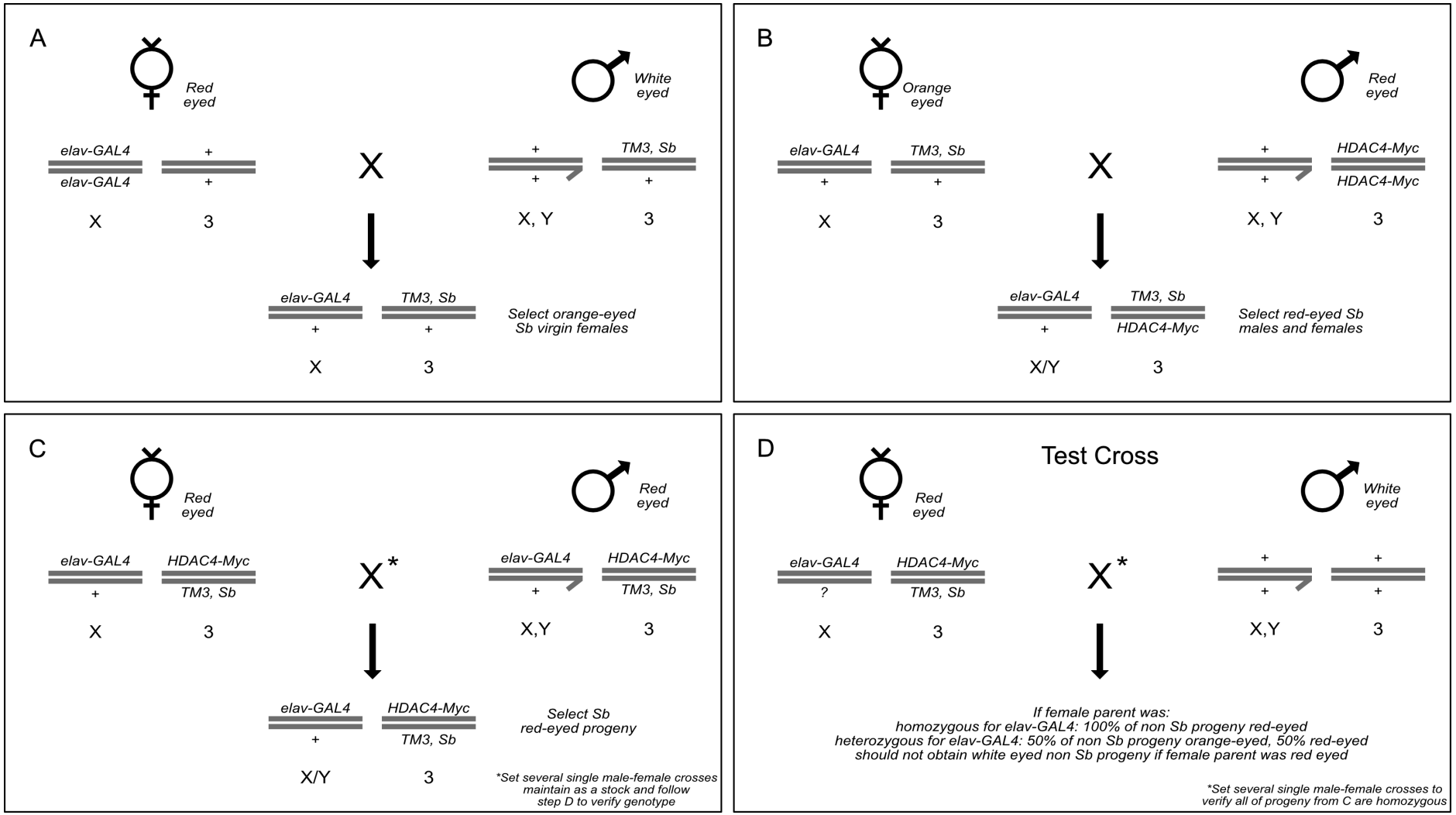

Figure 10.8 Crossing scheme to combine *elav-GAL4* and *HDAC4-Myc* into a single fly line

Female virgin progeny in (A) are used in (B). Male and female progeny in (B) are used in (C). A test-cross is performed in (D) to examine the eye colours of progeny to determine the status of the transgene on the fourth chromosome of the male parent. + indicates a wild-type chromosome. *TM3* denotes a balancer chromosome with multiple inversions to prevent recombination. *Sb,* stubble, dominant marker where flies have blunted bristles on the thorax. *This figure is an original artwork.*

10.1.7. Details of tissue-specific immunofluorescent imaging

For all imaging, all tissues were examined for the most intense fluorescence, and smart gain and offset were set based on this sample, and kept constant for all other samples. Where indicated, maximum projections were generated using ImageJ (Schneider *et al.*, 2012).

For imaging of whole brains, 1 µm sections were obtained from the most anterior point of the brain to the maximum depth accessible. Where the whole brain is shown, images were obtained using a 20x air objective lens. Where only the central brain is shown, images were obtained using a 40x oil objective lens.

For imaging of mushroom bodies, 1 µm optical sections were obtained through the anterior of the brain, commencing at the first emergence of the β-lobe, and ending at the tip of the α-lobe. All images were obtained using a 40x oil objective lens.

For imaging of Kenyon cells, 0.5 µm optical sections were obtained thorough the posterior of the brain, commencing at the first cells observed in the posterior, and ending at the emergence of pedunculus axon bundles. Images for quantitation were obtained using a 40x oil objective lens with 3x optical zoom. Figures are shown as either single sections or maximum projections as indicated. Further images were obtained using a 63x oil objective lens with 8x optical zoom. Single sections of these are presented.

For imaging of larval eye discs, 0.5 µm optical sections were obtained through the entire eye disc using a 40x oil objective lens. Further images were obtained using a 63x oil objective lens with 5x optical zoom. Single sections are presented.

For imaging of adult retina, 0.5 µm optical sections were obtained through the depth of the retina using a 63x oil objective lens. Single sections are presented.

10.2. Supplementary data corresponding to Chapter 4

10.2.1. Generation of the HDAC4::GFP protein trap line

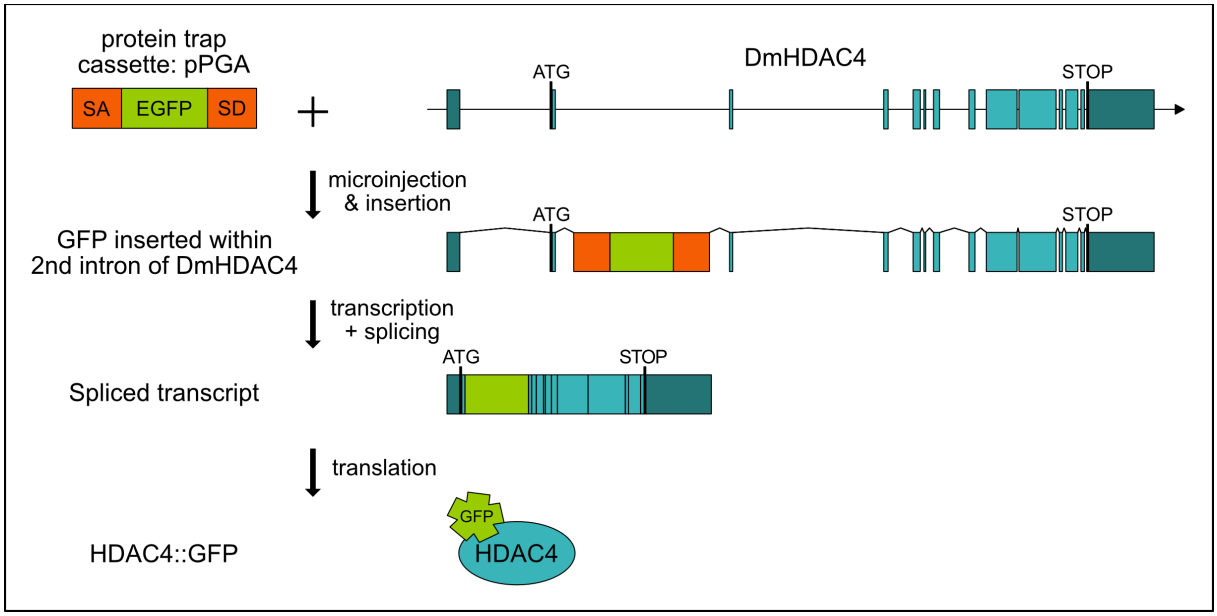

Figure 10.9 Simplified schematic diagram of the generation of the *HDAC4::GFP* protein trap

HDAC4::GFP was generated as part of the Carnegie Protein Trap Library (Buszczak *et al.*, 2007). Flies were microinjected with the pPGA construct, which contains the coding sequence of enhanced green fluorescent protein (*EGFP*) without start or stop codons, flanked by splice acceptor (*SA*) and splice donor (*SD*) sites. The *SA-EGFP-SD* construct was inserted into the second intron of *DmHDAC4* via P-element mediated transposition (not shown) as per Morin *et al.* (2001). Following transcription and splicing, the *EGFP* coding sequence is incorporated within the N-terminus of the *DmHDAC4* transcript, which when translated produces HDAC4::GFP as an internally tagged GFP fusion. *This figure is an original artwork created with reference to Buszczak et al. (2007).*

10.2.2. Protein sequence alignment of *Drosophila* and Human HDAC4 with annotation of key residues important for hHDAC4 function

EMBOSS Water alignment of the glutamine-rich N-terminus of human HDAC4 (hHDAC4, GenBank accession NP_006028), and *Drosophila* HDAC4 (DmHDAC4, GenBank accession NP_572868). Alignment was performed using default parameters: matrix, EBLOSUM62; gap penalty, 10.0; extend penalty, 0.5; identity, 459/1327 (34.6%); similarity, 657/1327 (49.5%); score, 1834.0. Annotations of key residues and DmHDAC4 mutants are as follows: red, 9QA mutations; blue, hydrophobic core; purple, MEF2 binding region (ΔMEF2 mutation); yellow, serine residues involved in 14-3-3 binding (3SA mutation); green, nuclear localisation signal (NLS); orange, nuclear export signal (ΔNES mutant). Ank, Ankyrin-repeat binding domain, CtBP, COOH-terminal binding protein binding site. The sites of the HDAC4$^{N\text{-}term}$ truncations are also indicated.

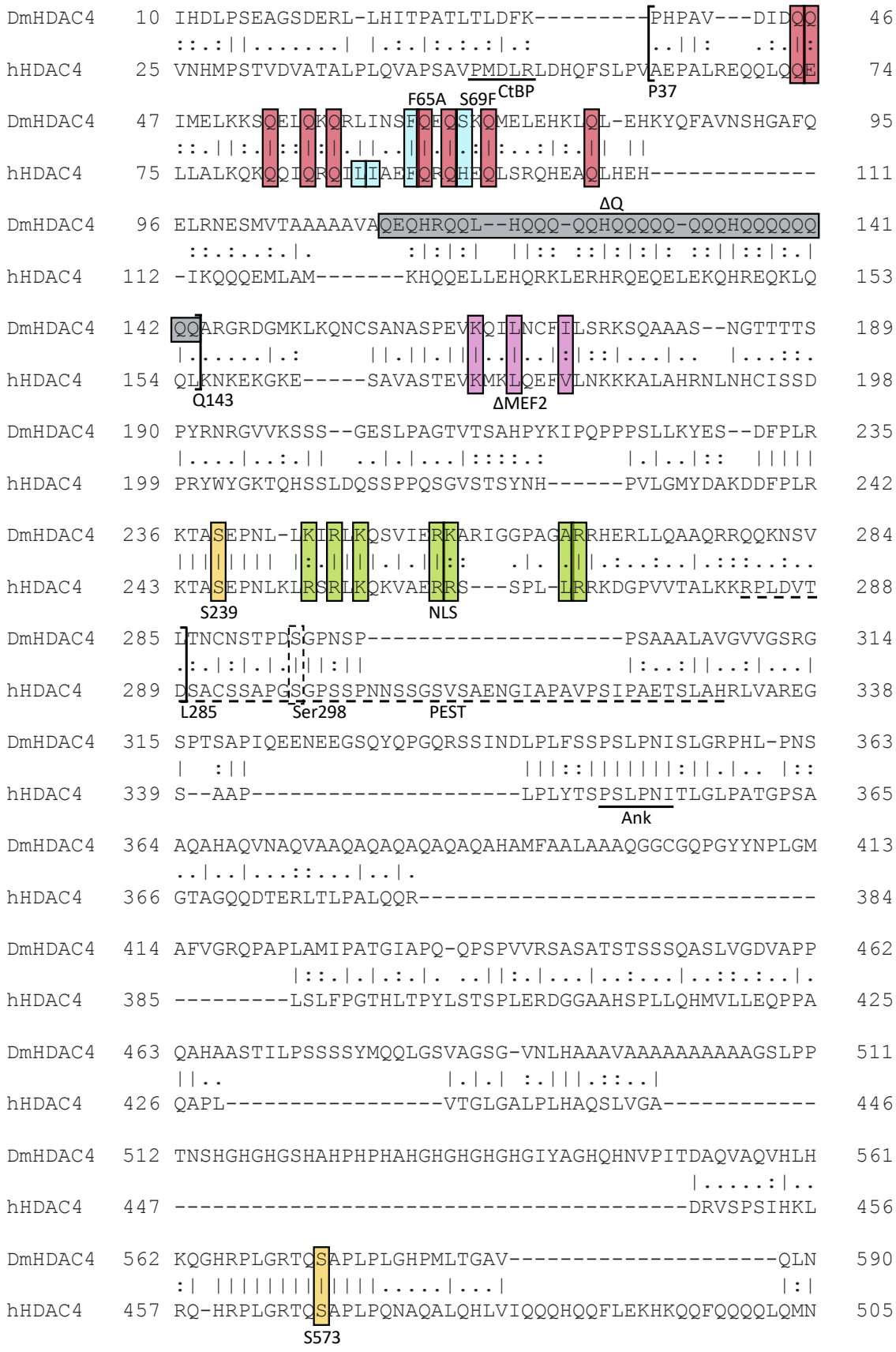
DmHDAC4 10 IHDLPSEAGSDERL-LHITPATLTLDFK---------PHPAV---DIDQQ 46
hHDAC4 25 VNHMPSTVDVATALPLQVAPSAVPMDLRLDHQFSLPVAEPALREQQLQQE 74
CtBP
P37
F65A
S69F
DmHDAC4 47 IMELKKSQELQKQRLINSFQFQSKQMELEHKLQL-EHKYQFAVNSHGAFQ 95
hHDAC4 75 LLALKQKQQIQRQILIAEFQRQHEQLSRQHEAQLHEH------------ 111
ΔQ
DmHDAC4 96 ELRNESMVTAAAAAVAQEQHRQQL--HQQQ-QQHQQQQQ-QQQHQQQQQQ 141
hHDAC4 112 -IKQQQEMLAM-------KHQQELLEHQRKLERHRQEQELEKQHREQKLQ 153
DmHDAC4 142 QQARGRDGMKLKQNCSANASPEVKQILNCFILSRKSQAAAS--NGTTTTS 189
Q143
ΔMEF2
hHDAC4 154 QLKNKEKGKE-----SAVASTEVKMKLQEFVLNKKKALAHRNLNHCISSD 198
DmHDAC4 190 PYRNRGVVKSSS--GESLPAGTVTSAHPYKIPQPPPSLLKYES--DFPLR 235
hHDAC4 199 PRYWYGKTQHSSLDQSSPPQSGVSTSYNH------PVLGMYDAKDDFPLR 242
DmHDAC4 236 KTASEPNL-LKTRLKQSVIERKARIGGPAGARRHERLLQAAQRRQQKNSV 284
S239
NLS
hHDAC4 243 KTASEPNLKLRSRLKQKVAFRRS---SPL-LRRKDGPVVTALKKRPLDVT 288
DmHDAC4 285 LTNCNSTPDSGPNSP--------------------PSAAALAVGVVGSRG 314
L285
Ser298
PEST
hHDAC4 289 DSACSSAPGSGPSSPNNSSGSVSAENGIAPAVPSIPAETSLAHRLVAREG 338
DmHDAC4 315 SPTSAPIQEENEEGSQYQPGQRSSINDLPLFSSPSLPNISLGRPHL-PNS 363
hHDAC4 339 S--AAP----------------------LPLYTSPSLPNITLGLPATGPSA 365
Ank
DmHDAC4 364 AQAHAQVNAQVAAQAQAQAQAQAQAHAMFAALAAAQGGCGQPGYYNPLGM 413
hHDAC4 366 GTAGQQDTERLTLPALQQR------------------------------ 384
DmHDAC4 414 AFVGRQPAPLAMIPATGIAPQ-QPSPVVRSASATSTSSSQASLVGDVAPP 462
hHDAC4 385 ---------LSLFPGTHLTPYLSTSPLERDGGAAHSPLLQHMVLLEQPPA 425
DmHDAC4 463 QAHAASTILPSSSSYMQQLGSVAGSG-VNLHAAAVAAAAAAAAAAGSLPP 511
hHDAC4 426 QAPL-----------------VTGLGALPLHAQSLVGA------------ 446
DmHDAC4 512 TNSHGHGHGSHAHPHPHAHGHGHGHGHGIYAGHQHNVPITDAQVAQVHLH 561
hHDAC4 447 --DRVSPSIHKL 456
DmHDAC4 562 KQGHRPLGRTQSAPLPLGHPMLTGAV---------------------QLN 590
S573
hHDAC4 457 RQ-HRPLGRTQSAPLPQNAQALQHLVIQQQHQQFLEKHKQQFQQQQLQMN 505

```
DmHDAC4   591 VV-----------QTHYENSEAERQAYEHQVVNQKVRQTVLTRSGAAAAA   629
              .:           ::|.|  |.|.:..|||.:   :.:..|.|......|
hHDAC4    506 KIIPKPSEPARQPESHPE--ETEEELREHQAL---LDEPYLDRLPGQKEA   550

DmHDAC4   630 AAAAGVSVVREAQLKEEDDDSAAEVMDLTDKKKPPKTVLTSTIATSTSQN   679
              .|.|||.|.:|   ..|.|:..||         ||:.|       ...|.
hHDAC4    551 HAQAGVQVKQE---PIESDEEEAE---------PPREV-------EPGQR   581

DmHDAC4   680 LPEALAAAAAAAAAYRAPHNASSNSASATKSGIKLRDQEYLQQQREQLLLL   729
              .|.                                 :||.|  .|:|.|||
hHDAC4    582 QPS-------------------------------EQELL--FRQQALLL   597

DmHDAC4   730 QQEEELAKSLMRPLSRTLSSPLVPLGPHGLSQIPDTGQQPAPIATSSSAD   779
              :|:.   ...:|...:::.:..:|        :...|.:|...|.||.|.
hHDAC4    598 EQQR---IHQLRNYQASMEAAGIP--------VSFGGHRPLSRAQSSPAS   636
                                  S748                    S
DmHDAC4   780 HIPPVNLSLPHRQHRQLMSTLYASQLRNHQPSASGSPPHK--VTTGLAYD   827
              ...||::.                          .||.|  .||||.||
hHDAC4    637 ATFPVSVQ---------------------------EPPTKPRFTTGLVYD   659

DmHDAC4   828 PLMLKHSCICGDNAQHPEHSGRLQSVWARLNETDLVKRCDRLRARKATQE   877
              .||||||.|.||.::.||||:||:||:|:||.||.|..:|:.:|.||||.|
hHDAC4    660 TLMLKHQCTCGSSSSHPEHAGRIQSIWSRLQETGLRGKCECIRGRKATLE   709

DmHDAC4   878 ELQTVHTEAHAMLFGSNQCQLSRPKLEN-----TLSASFVRLSCGGLGVD   922
              ||||||:|||.:|:|:|:  .|:|.||::     :|::.||||.|||:|||
hHDAC4    710 ELQTVHSEAHTLLYGTN--PLNRQKLDSKKLLGSLASVFVRLPCGGVGVD   757

DmHDAC4   923 LDTTWNEHHTATAARMAAGCVIDLALKTAKGDLRNGFAVVRPPGHHAEAN   972
              .||.|||.|:|.|||:|.|||::|..|.|.|:|:|||||||||||||.:
hHDAC4    758 SDTIWNEVHSAGAARLAVGCVVELVFKVATGELKNGFAVVRPPGHHAEES   807

DmHDAC4   973 LAMGFCFFNSIAIAAKLLRQRMPEVRRILIVDWDVHHGNGTQQAFYQSPD  1022
              ..||||:|||:|:||||||:|| .|.:|||||||||||||||||..|.
hHDAC4    808 TPMGFCYFNSVAVAAKLLQQRL-SVSKILIVDWDVHHGNGTQQAFYSDPS   856

DmHDAC4  1023 ILYLSIHRHDDGNFFPGTGGPTECGSGAGLGFNVNISWSGALNPPLGDAE  1072
              :||:|:||:||||||||:|.|.|.|:|.|:|||||::::|.|:||:||||
hHDAC4    857 VLYMSLHRYDDGNFFPGSGAPDEVGTGPGVGFNVNMAFTGGLDPPMGDAE   906

DmHDAC4  1073 YIAAFRTVVMPIARSFNPDIVLVSSGFDAATGHPAPLGGYHVSPACFGFM  1122
              |:|||||||||..|.||:|||||||||..|||.|||||::|..|||::
hHDAC4    907 YLAAFRTVVMPIASEFAPDVVLVSSGFDAVEGHPTPLGGYNLSARCFGYL   956

DmHDAC4  1123 TRELLQLANGKVVLALEGGYDLAAICDSAQECVRALLGDPAAPIAKAELE  1172
              |::|:.||.|::|||||||:||.||||:::.||.||||:...|:.:..|:
hHDAC4    957 TKQLMGLAGGRIVLALEGGHDLTAICDASEACVSALLGNELDPLPEKVLQ  1006

DmHDAC4  1173 RPPCQNAINTLQKTIAIQQTHWPCVRMLEHTVGLSALETLKVEHDESETI  1222
              :.|..||:.:::|.:.|...:|.|::....|.|.|.:|....|::|:||:
hHDAC4   1007 QRPNANAVRSMEKVMEIHSKYWRCLQRTTSTAGRSLIEAQTCENEEAETV  1056

DmHDAC4  1223 NAMAGLSMQSMHRTLSRDDSEEPMDQD  1249
              .|||.||:.:.....|.| ||||:::
hHDAC4   1057 TAMASLSV-GVKPAEKRPD-EEPMEEE  1081
                 ΔNES
```

10.2.3. Western blots of HDAC4^{mutant} expression used for intensity quantification

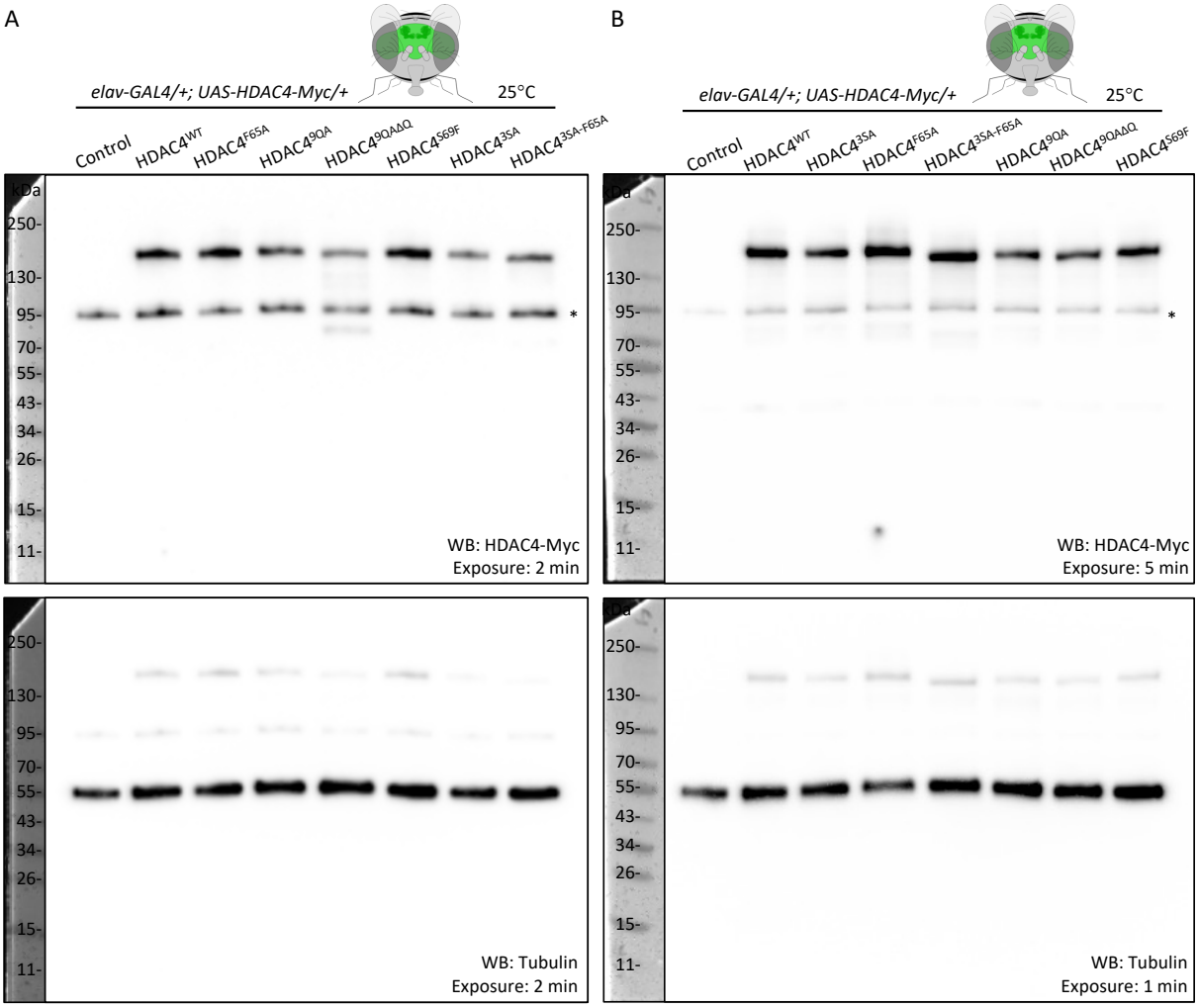

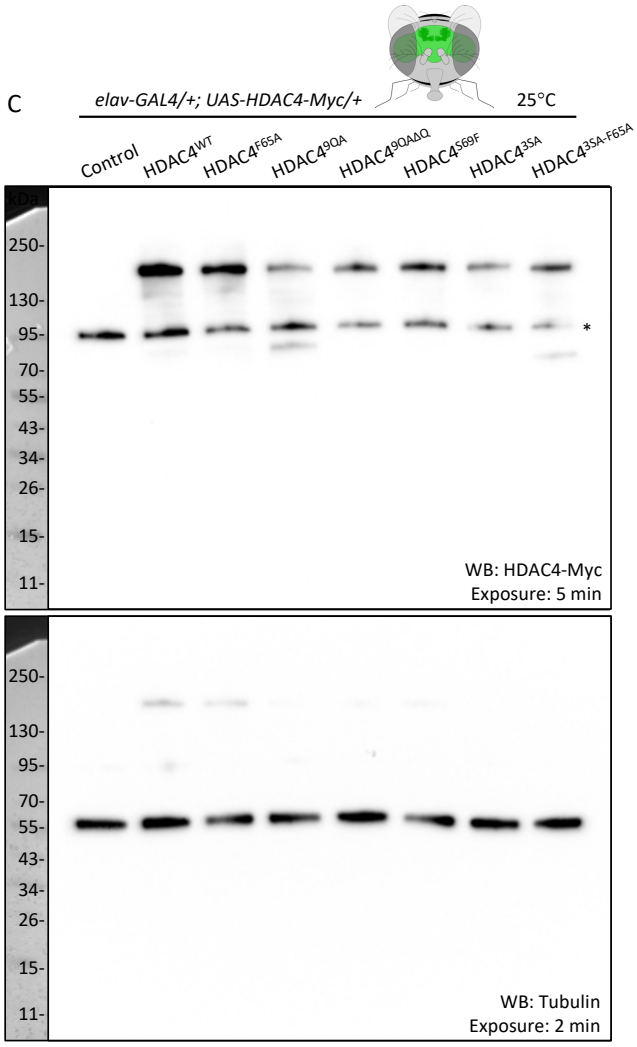

Figure 10.10 Full western blots of HDAC4^{mutant} expression used for intensity quantification in Figure 4.7

(A-C) Western blots of *elav-GAL4* driven expression of HDAC4^{WT} and HDAC4^{mutant} in head whole-cell lysates (30 µg) using anti-Myc and anti-alpha-tubulin antibodies. Flies were raised at 25 °C. Control is *elav-GAL4/+*. The protein bands were of the expected size of ~144 kDa with the exception of HDAC4$^{9QA\Delta Q}$, which has an expected size of ~140 kDa. Additional non-specific bands were observed at ~95 (*) and ~40 kDa in all samples including the control. Western blotting using an antibody that binds endogenous *Drosophila* HDAC4 has previously confirmed that these are a result of non-specific binding of the Myc antibody (Hawley (2020), unpublished data). The identity of the other bands observed has not been confirmed, but it is possible that these are C-terminal cleavage products of HDAC4 due to a shift in height in only HDAC4$^{9QA\Delta Q}$ and HDAC4$^{3SA\text{-}F65A}$ lanes.

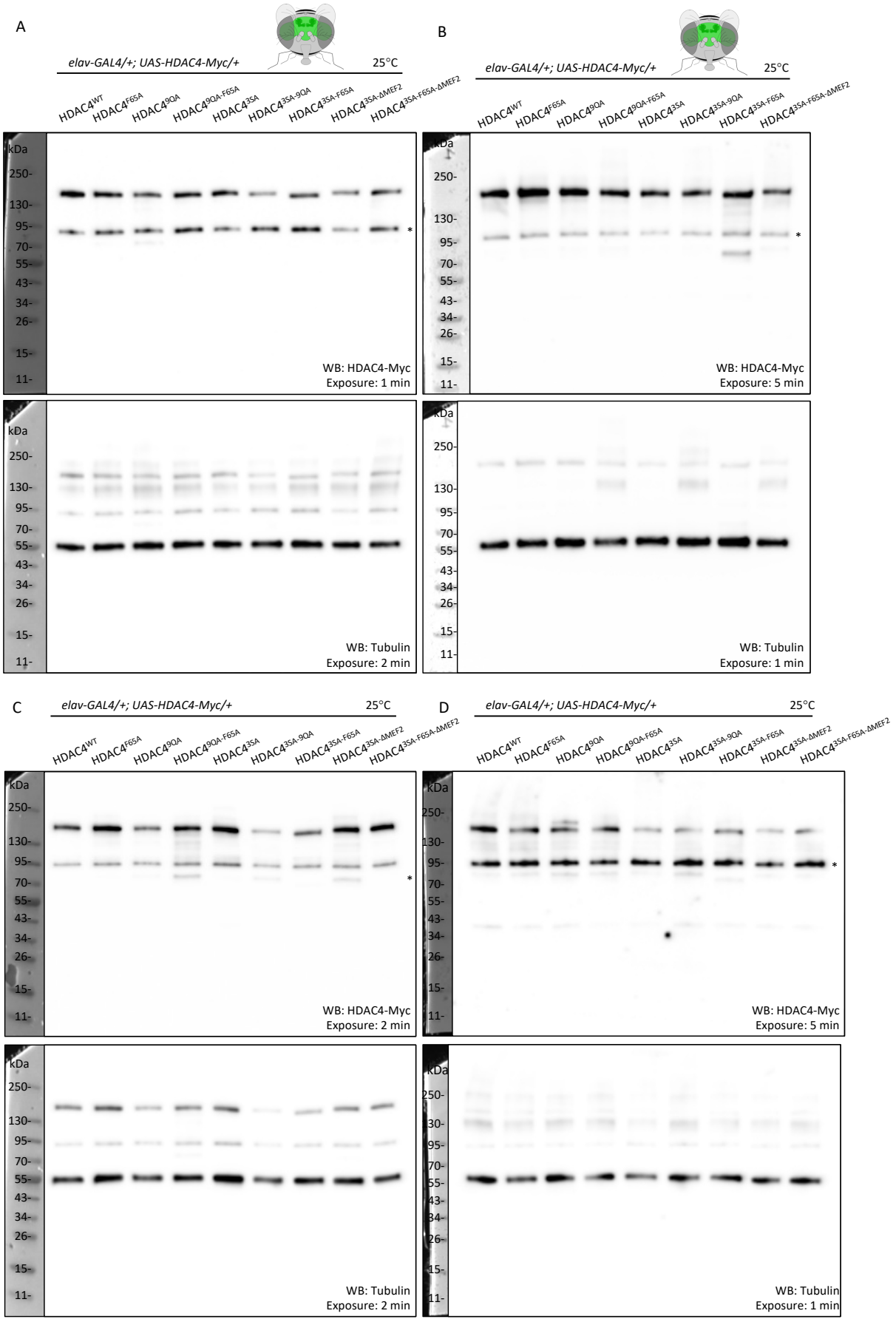

Figure 10.11 Full western blots of HDAC4^{mutant} expression used for intensity quantification in Figure 4.21 and Figure 5.4

(A-D) Western blots of *elav-GAL4* driven expression of HDAC4^{WT} and HDAC4^{mutant} in head whole-cell lysates (30 µg) using anti-Myc and anti-alpha-tubulin antibodies. Flies were raised at 25 °C. Con (control) is *elav-GAL4/+*. The protein bands were of the expected size of ~144 kDa with the exception of HDAC4$^{3SA\text{-}F65A}$. Additional non-specific bands were observed at ~95 (*) and ~40 kDa in all samples including the control. Western blotting using an antibody that binds endogenous *Drosophila* HDAC4 has previously confirmed that these are a result of non-specific binding of the Myc antibody (Hawley (2020), unpublished data). The identity of other bands observed has not been confirmed but it is possible that these are C-terminal cleavage products of HDAC4 due to a shift in height in only HDAC4$^{3SA\text{-}F65A}$ lanes.

10.2.4. Changes in HDAC4^{mutant} intensity in the mushroom body

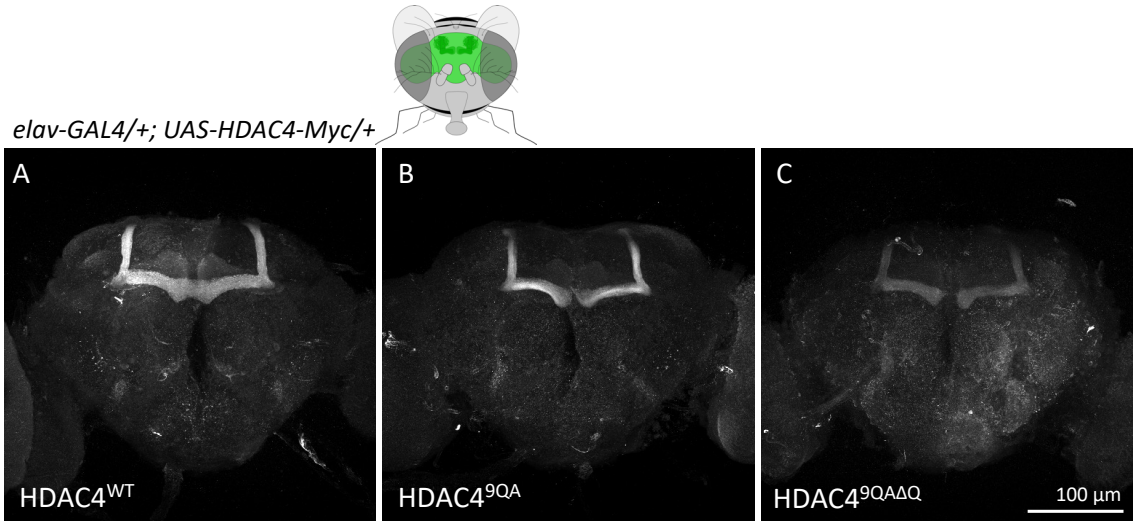

Figure 10.12 HDAC4^{9QA} and HDAC4$^{9QA\Delta Q}$ signal is reduced in the mushroom body compared to HDAC4^{WT}
(A-C) Maximum projections through the anterior of the brain showing expression of HDAC4^{WT} (A), HDAC4^{9QA} (B), and HDAC4$^{9QA\Delta Q}$ (C) driven by *elav-GAL4*. Flies were raised at 25 °C before dissecting and preparing for anti-Myc immunohistochemistry. HDAC4$^{9QA\Delta Q}$ signal intensity was reduced in all lobes, and HDAC4^{9QA} intensity was reduced in the γ lobe compared to HDAC4^{WT}. Images were obtained using constant settings.

10.2.5. Replication of co-immunoprecipitation assays to examine oligomerisation of HDAC4

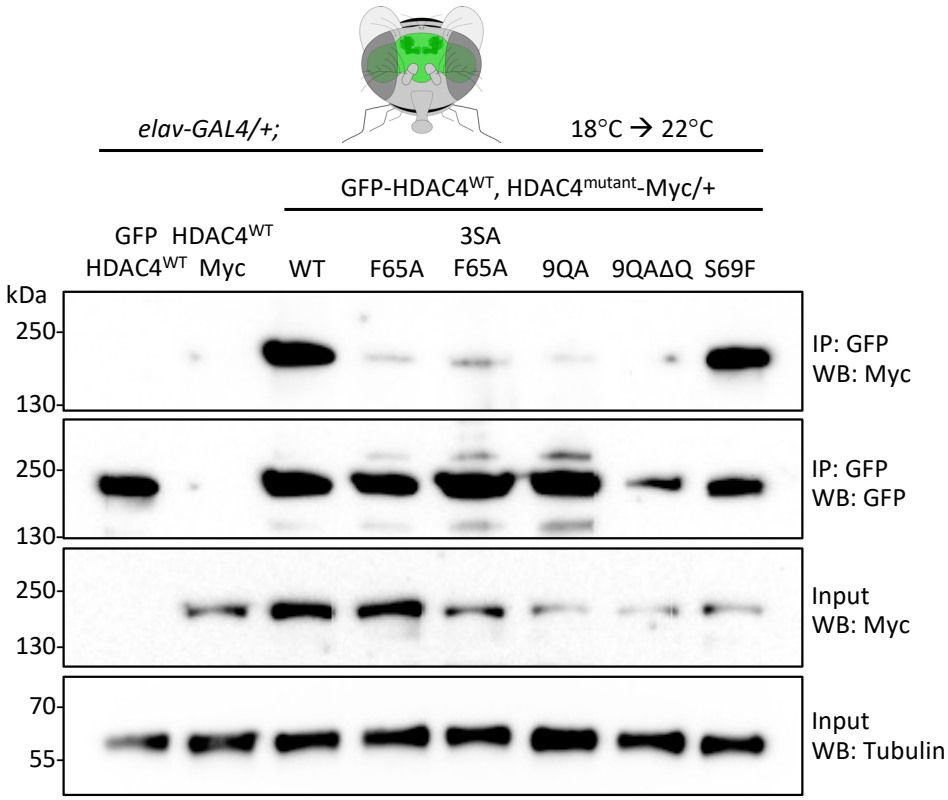

Figure 10.13 Replication of the HDAC4 co-immunoprecipitation assay to assess oligomerisation

The indicated transgenes were expressed pan-neuronally in *Drosophila* under the control of *elav-GAL4*. Flies were raised at 18 °C until adulthood, and then moved to 22 °C for five days to increase the level of transgene expression before harvesting and generation of whole-head lysates. Anti-GFP conjugated agarose beads were used to immunoprecipitate GFP-HDAC4^{WT} from all samples, followed by probing for HDAC4-Myc. HDAC4^{WT} and HDAC4^{S69F} co-immunoprecipitated with GFP-HDAC4^{WT}, while HDAC4^{F65A}, HDAC4$^{3SA-F65A}$, HDAC4^{9QA} and HDAC4^{9QAΔQ} did not despite comparable immunoprecipitation of GFP-HDAC4^{WT} from all samples. Input samples are 30 µg of whole-cell lysate and the level of transgene expression is consistent with previously quantification (Figure 4.7). Protocol 1 was used for this experiment (Methods 3.2.4). Please note a cropped version of this figure is replicated in Figure 5.7. The full membranes are found in Figure 10.25.

10.2.6. Full western blots of co-immunoprecipitation assays to examine oligomerisation of HDAC4

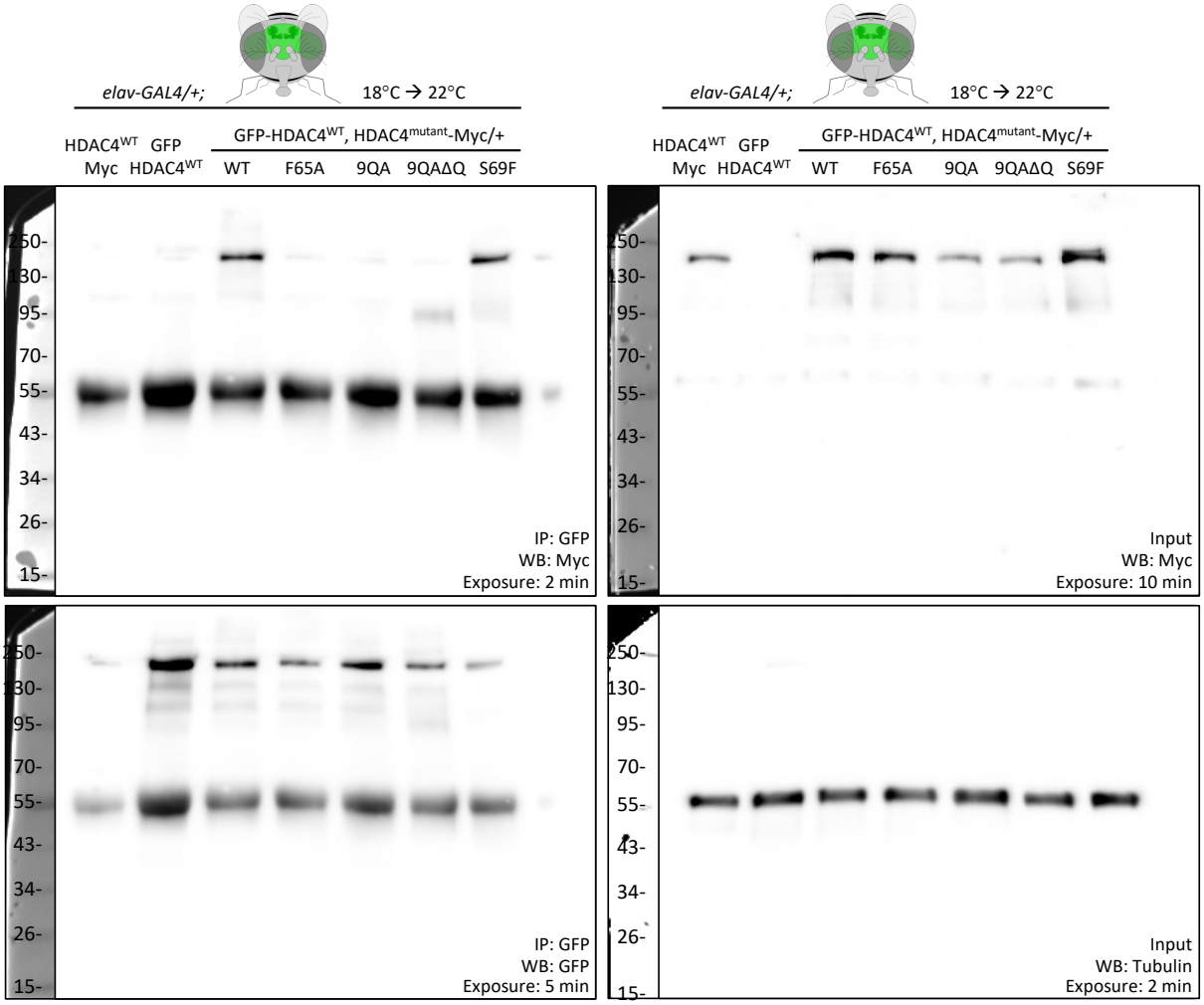

Figure 10.14 Full western blots of the co-immunoprecipitation assay in Figure 4.9
Co-immunoprecipitation experiments to examine the ability of HDAC4^{mutant} to bind HDAC4^{WT} to assess oligomerisation capacity. The indicated transgenes were expressed pan-neuronally in *Drosophila* under the control of *elav-GAL4*. Flies were raised at 18°C until adulthood and then moved to 22°C for five days to increase the level of transgene expression before harvesting and generation of whole-head lysates. Anti-GFP conjugated magnetic beads were used to immunoprecipitate GFP-HDAC4^{WT} from all samples, followed by probing for HDAC4^{WT}-Myc or HDAC4^{mutant}-Myc. HDAC4^{WT} and HDAC4^{S69F} co-immunoprecipitated with GFP-HDAC4^{WT}, while HDAC4^{F65A}, HDAC4^{9QA} and HDAC4^{9QAΔQ} did not despite comparable immunoprecipitation of GFP-HDAC4^{WT} from all samples. Input samples are 30 µg of whole-cell lysate and the level of transgene expression was consistent with previous quantification (Figure 4.7). Protocol 2 (Methods 3.2.4) was used for this experiment.

10.2.7. Optimisation of immunohistochemistry to visualise HDAC4 aggregates

The fixation and staining protocol was optimised for the MEF2 and Myc antibodies, where brains were fixed prior to and following dissection to yield the clearest images of HDAC4 aggregates (Figure 10.15). This resulted in reduced background staining and revealed smaller nuclear aggregates than previously observed, necessitating the use of the Cell Counter plugin within ImageJ (Schneider *et al.*, 2012) for quantification.

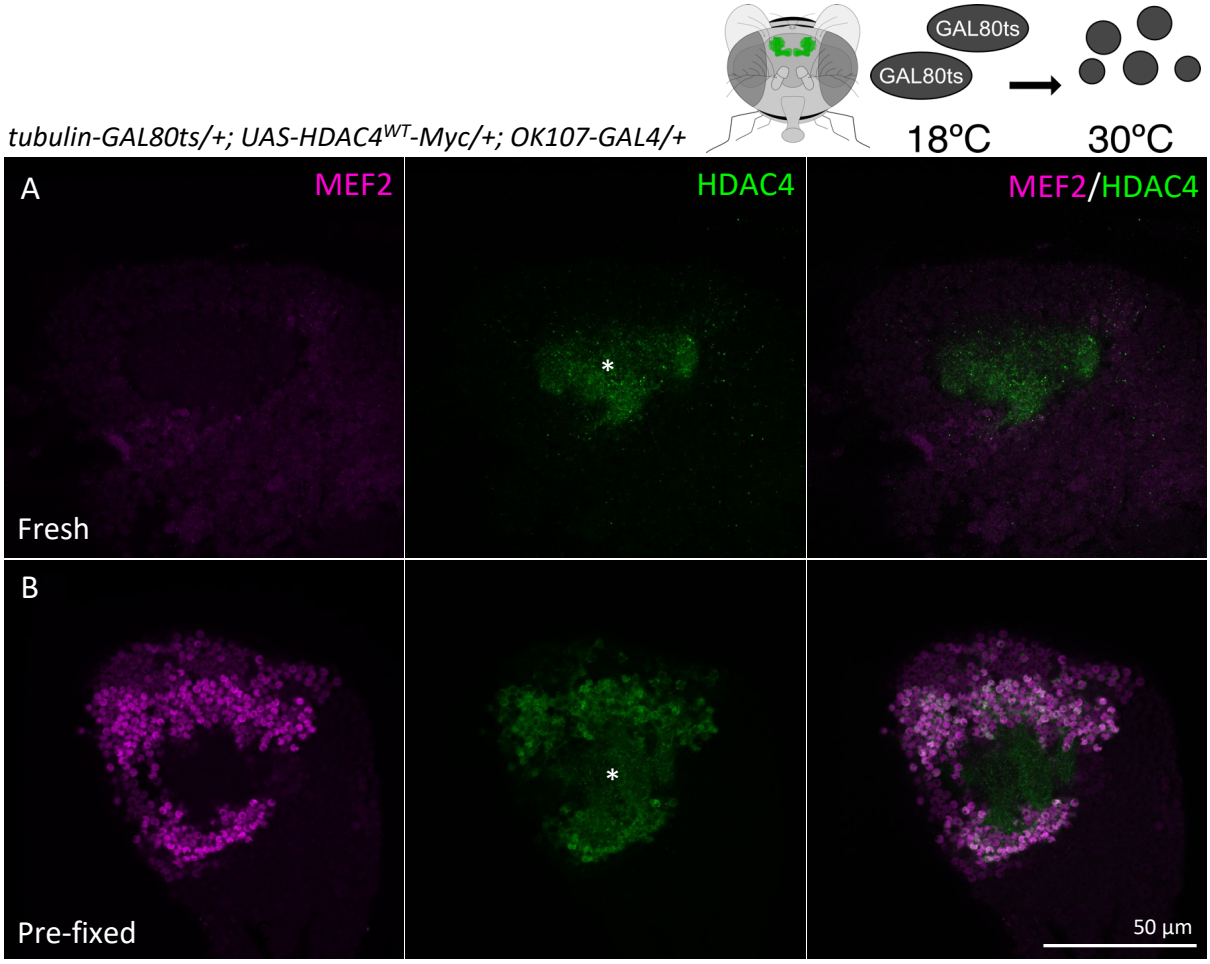

Figure 10.15 Fixation of brains prior to dissection improves the specificity of detection of HDAC4 aggregates containing MEF2 in Kenyon cells
Maximum projection of optical sections through the posterior of the whole-brain of flies expressing HDAC4^{WT} under the control of *OK107-GAL4* in the presence of the TARGET system. Flies were raised at 18°C until eclosion, where adults were transferred to 30°C for three days to induce HDAC4 expression. Brains of flies that were first fixed with PFAT-DMSO prior to dissection (pre-fixed) showed MEF2-containing (magenta) nuclei surrounding the calyx (*) and HDAC4^{WT} (green) within Kenyon cells as well as the calyx (B). Brains of flies that were dissected in the absence of pre-fixation (fresh) only showed HDAC4^{WT} localisation to the calyx (A).

10.2.8. Validation of the specificity of the endogenous MEF2 antibody

Use of the endogenous MEF2 antibody was validated; confocal microscopy was performed on the posterior of brains expressing HA-tagged MEF2 under the control of *OK107-GAL4* (Figure 3.1C) in the presence of the TARGET system, which confirmed specificity (Figure 10.16).

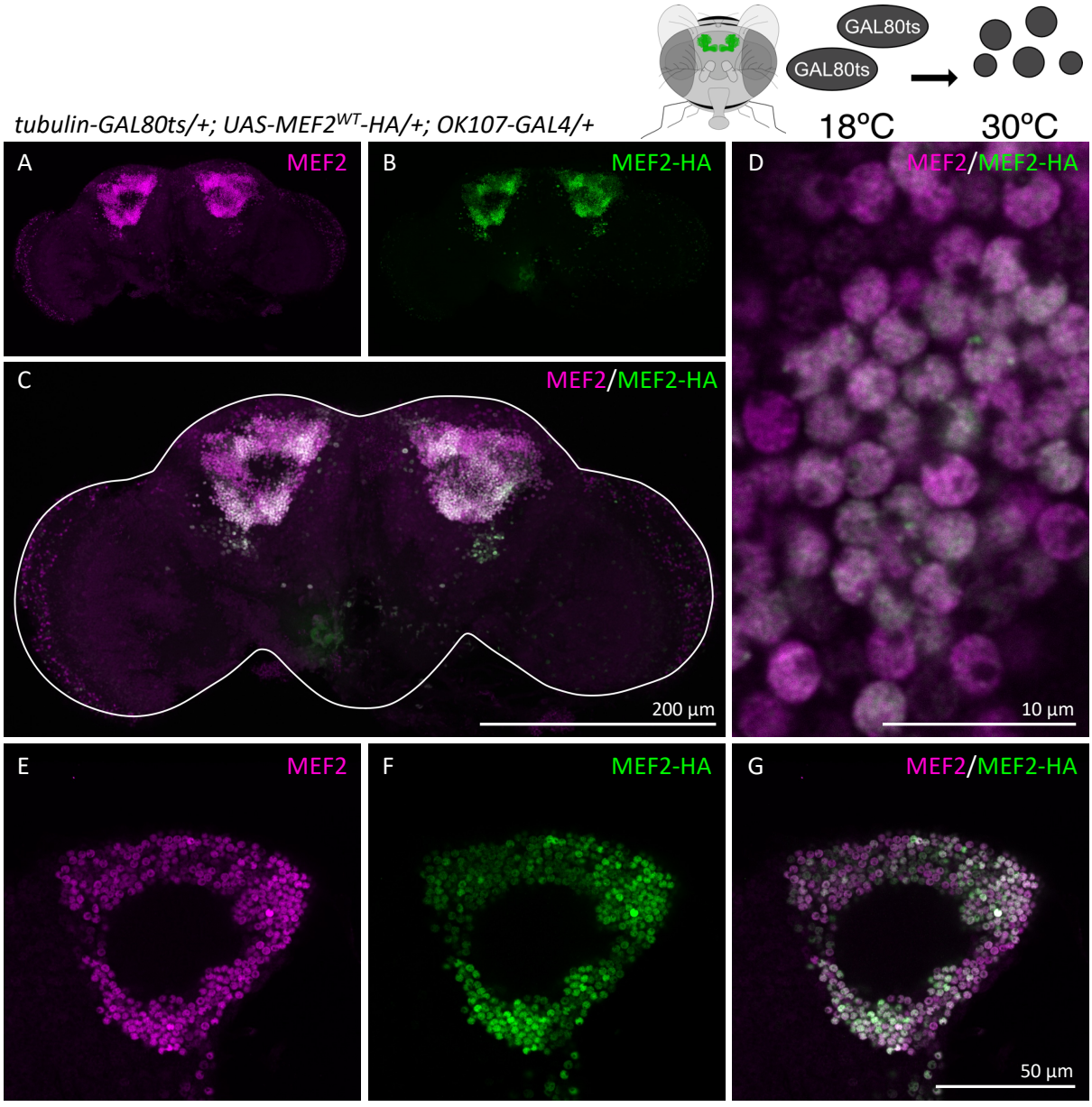

Figure 10.16 The endogenous MEF2 antibody specifically detects MEF2 in Kenyon cells
In flies expressing MEF2^{WT}-HA under the control of *OK107-GAL4*, endogenous MEF2 (magenta) overlaps with MEF2^{WT}-HA (green) indicating specific detection of MEF2. Flies were raised at 18°C until eclosion, where adults were transferred to 30°C for three days to induce MEF2 expression. (A-C) Maximum projection of optical sections through the posterior of the whole brain. (E-G) single optical section through the mid-region of the Kenyon cell layer in the posterior of the brain, Kenyon cells are magnified in (D). *This figure is an adaptation from that found in Tan et al. (2024) (doi: 10.1186/s12915-023-01800-1), which is distributed under CC BY 4.0.*

10.2.9. Confirmation that the circadian clock does not affect HDAC4 aggregation in Kenyon cells

MEF2 expression is known to be regulated in a circadian manner in a subset of cells within the *Drosophila* brain (Blanchard *et al.*, 2010; Sivachenko *et al.*, 2013). In small ventral lateral (s-LNv) neurons, MEF2 is nuclear and levels cycle with the circadian clock, being significantly higher at the end of the night compared to the end of the day (Blanchard *et al.*, 2010). An independent study found that upon overexpression of HDAC4 in these neurons, its subcellular distribution was also regulated in a circadian manner, with nuclear aggregates present in the early hours, and dissipating at the end of the day (Fujii *et al.*, 2017). The identical changes in subcellular distribution of MEF2 and HDAC4 in both these studies is consistent with MEF2 facilitating nuclear import of HDAC4 (Borghi *et al.*, 2001; Wang & Yang, 2001). It was therefore unclear as to whether MEF2 undergoes circadian regulation in Kenyon cells, and if so whether this may affect the quantification of HDAC4 aggregation.

To determine whether HDAC4 aggregation differs in a circadian manner, HDAC4 aggregation at two different time points was compared. $HDAC4^{WT}$ was expressed under the control of the *OK107-GAL4* driver in the presence of the TARGET system, resulting in temperature-inducible expression in Kenyon cells (Aso *et al.*, 2009; Connolly *et al.*, 1996). Flies were pre-fixed and dissected eight hours apart (morning and afternoon) and immunostaining performed with antibodies against the Myc tag, and endogenous MEF2. The whole layer of Kenyon cells was imaged (Figure 10.17) and aggregates of both HDAC4 and MEF2 were counted through ten layers at 1 μm intervals beginning at the first emergence of the calyx. The number of aggregates in Kenyon cell nuclei did not change significantly between those fixed in the morning compared to the afternoon (Figure 10.17C), suggesting that the circadian clock does not influence the formation of these aggregates. The slight increase in aggregate number observed in the afternoon sample could be a result of increased HDAC4 expression due to longer incubation at 30°C where transgene expression is active (as flies were moved to 30°C at the same time). This further validates the use of MEF2 as a counterstain and demonstrates the reliability of the approach in quantifying nuclear aggregates of HDAC4.

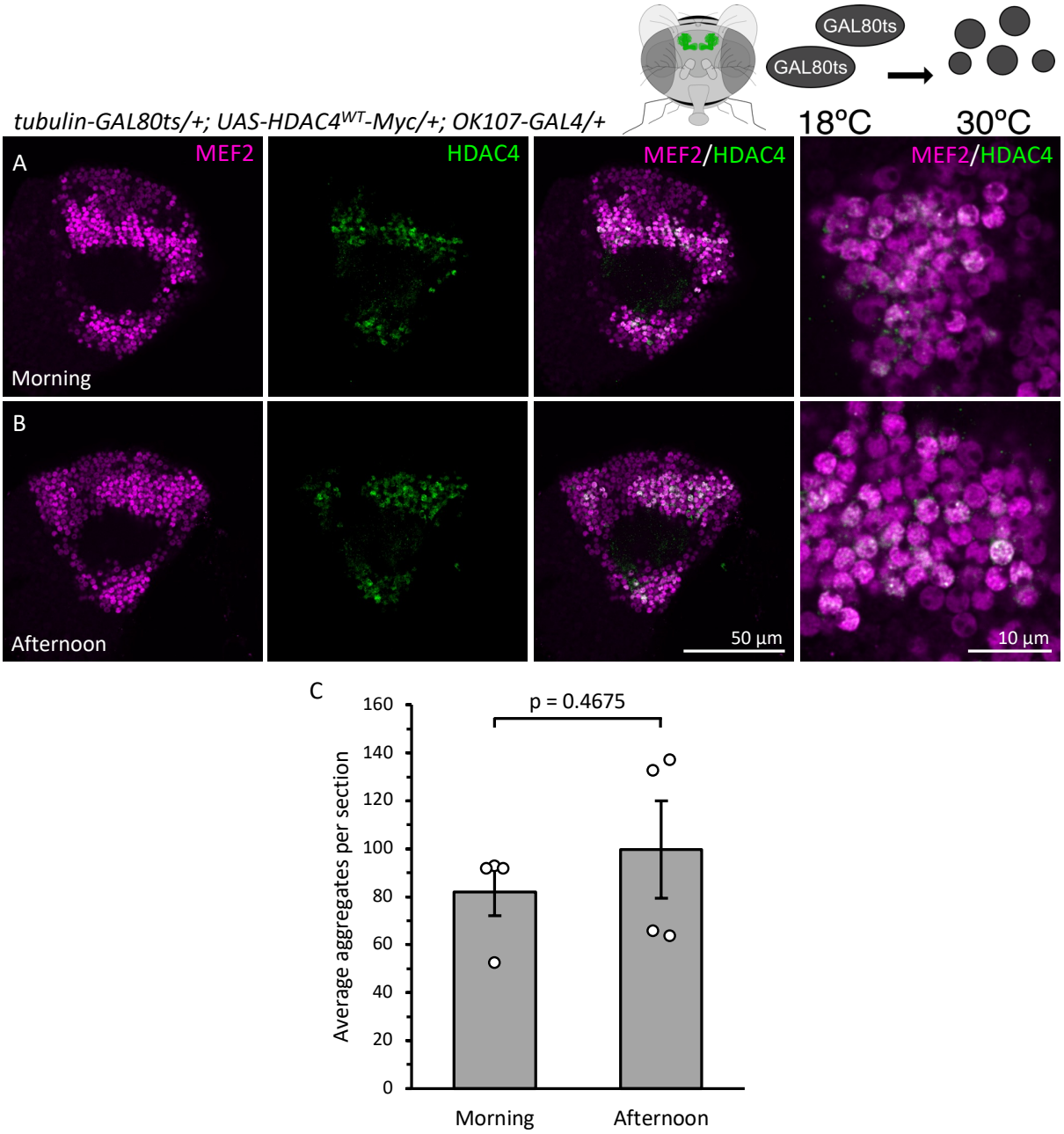

Figure 10.17 The number of nuclear HDAC4-MEF2-containing aggregates does not change with the circadian clock

Single optical sections of the calyx and surrounding Kenyon cells of the posterior of brains expressing HDAC4^{WT} (green) under the control of *OK107-GAL4* in the presence of the TARGET system. Brains were also labelled for endogenous MEF2 (magenta). Flies were raised at 18°C until eclosion, where adults were transferred to 30°C for three days to induce HDAC4 expression. HDAC4^{WT} brains that were fixed in the morning (A) had a slightly decreased average number of aggregates compared to HDAC4^{WT} brains that were fixed in the afternoon (B). (C) Quantification of HDAC4 aggregates. Aggregates of HDAC4 that co-localised with MEF2 were counted through the Kenyon cell layer (as seen in A and B) for 10 optical sections spaced 1µm apart, n=4 brains per genotype. The mean is plotted, and the average number of aggregates per section per brain are plotted as individual points. Error bars indicate the SEM. There was no statistically significant difference between aggregate number in the morning or the afternoon (One-sample t-test, $t_{(6)}$=0.7754, p=0.4675). Please note that parts of this figure are reproduced in Figures 4.10 and 4.11.

10.2.10. Images of *Drosophila* eyes resulting from expression of HDAC4 from one genomic insertion

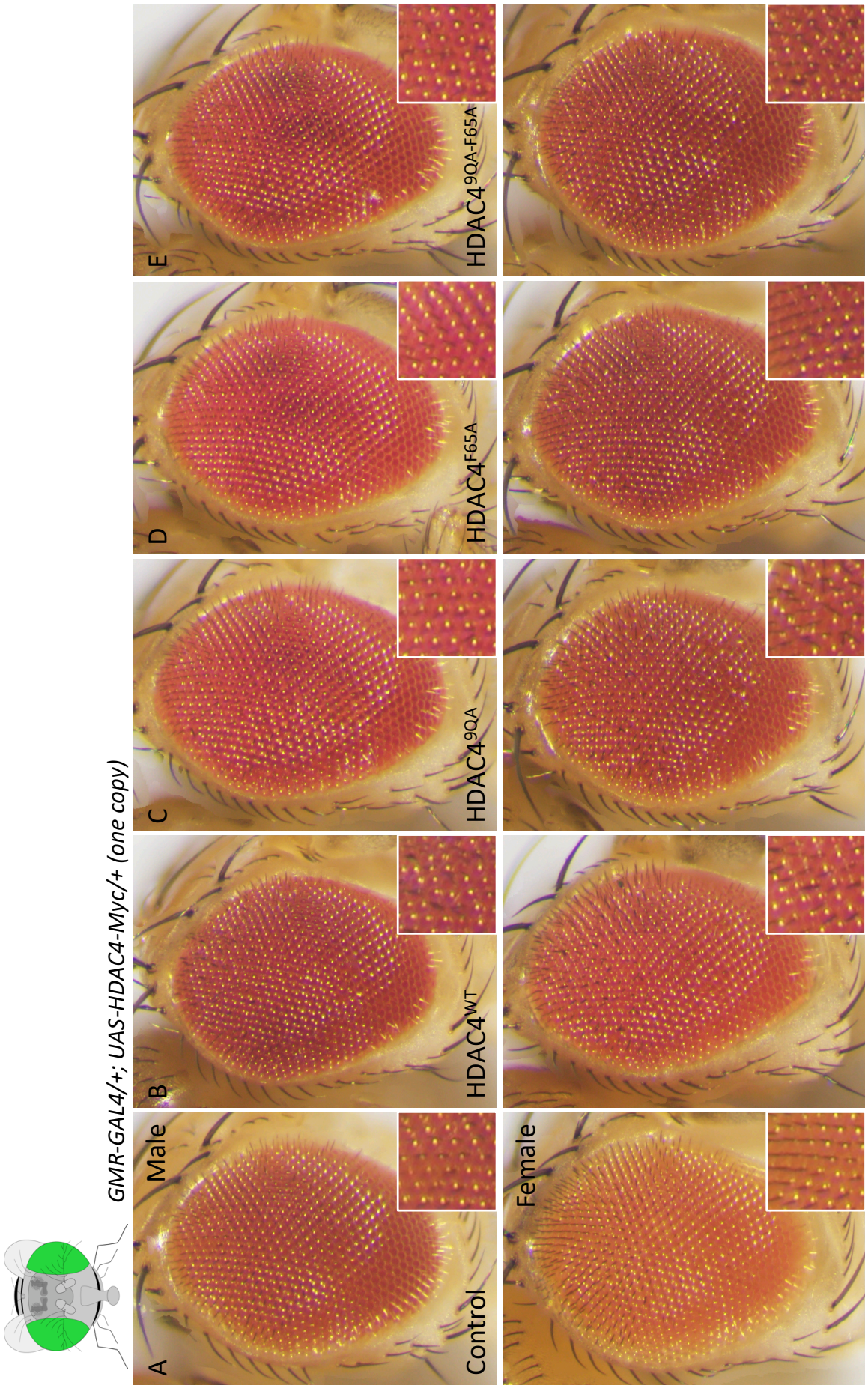

Figure 10.18 Eye phenotypes resulting from of HDAC4$^{9QA-F65A}$ expression from one genomic insertion

(A-E) Light microscopy (110x magnification) images of *Drosophila* eyes raised at 25°C. Subtle differences in eye phenotype are observed upon expression of HDAC4 from one genomic insertion. Flies harboured one copy of the driver and one copy of the HDAC4 transgene (*GMR-GAL4/+; UAS-HDAC4/+*). Control is *GMR-GAL4/+*. Top row, males; bottom row, females. (B) $HDAC4^{WT}$ overexpression induced mild perturbation of the organisation of the adult eye, characterised by misalignment of ommatidia and bristles, which was reduced by $HDAC4^{F65A}$ (C), $HDAC4^{9QA}$ (D), and $HDAC4^{9QA\text{-}F65A}$ (E).

10.3. Supplementary data corresponding to Chapter 5

10.3.1. Further investigation and verification of $HDAC4^{3SA\text{-}F65A}$

As discussed in Section 5.2.1, it was noted that $HDAC4^{3SA\text{-}F65A}$ was detected at a lower molecular weight than expected when western blotting was performed on whole head lysates expressing HDAC4 variants under the control of *elav-GAL4*. This is curious given that the 3SA-F65A mutation does not involve a genomic deletion which would truncate HDAC4 resulting in a smaller protein, and individually the 3SA and F65A mutations do not alter the apparent molecular weight of HDAC4, suggesting it is not a biological effect of one of the mutations. Furthermore, the $HDAC4^{3SA\text{-}F65A\text{-}\Delta MEF2}$ construct was generated via mutagenesis of $HDAC4^{3SA\text{-}F65A}$ and migrates at the full-size, suggesting there is nothing within the plasmid construct which would cause truncation of the protein. It is possible that errors may have occurred during recombination (Section 10.1.5) which could result in an internal deletion. To address this, genomic DNA was extracted from whole flies harbouring $HDAC4^{WT}$ or $HDAC4^{3SA\text{-}F65A}$ and PCR was performed using overlapping primer pairs (A-E) which span the HDAC4 insertion site (Figure 10.19). The primer pairs are listed in Table 10.2. Due to amplification of endogenous *HDAC4*, PCR was also performed on control flies (Canton S) that did not harbour a transgene. The expected transgene-associated amplicon is listed alongside the amplicon associated with amplification of endogenous HDAC4.

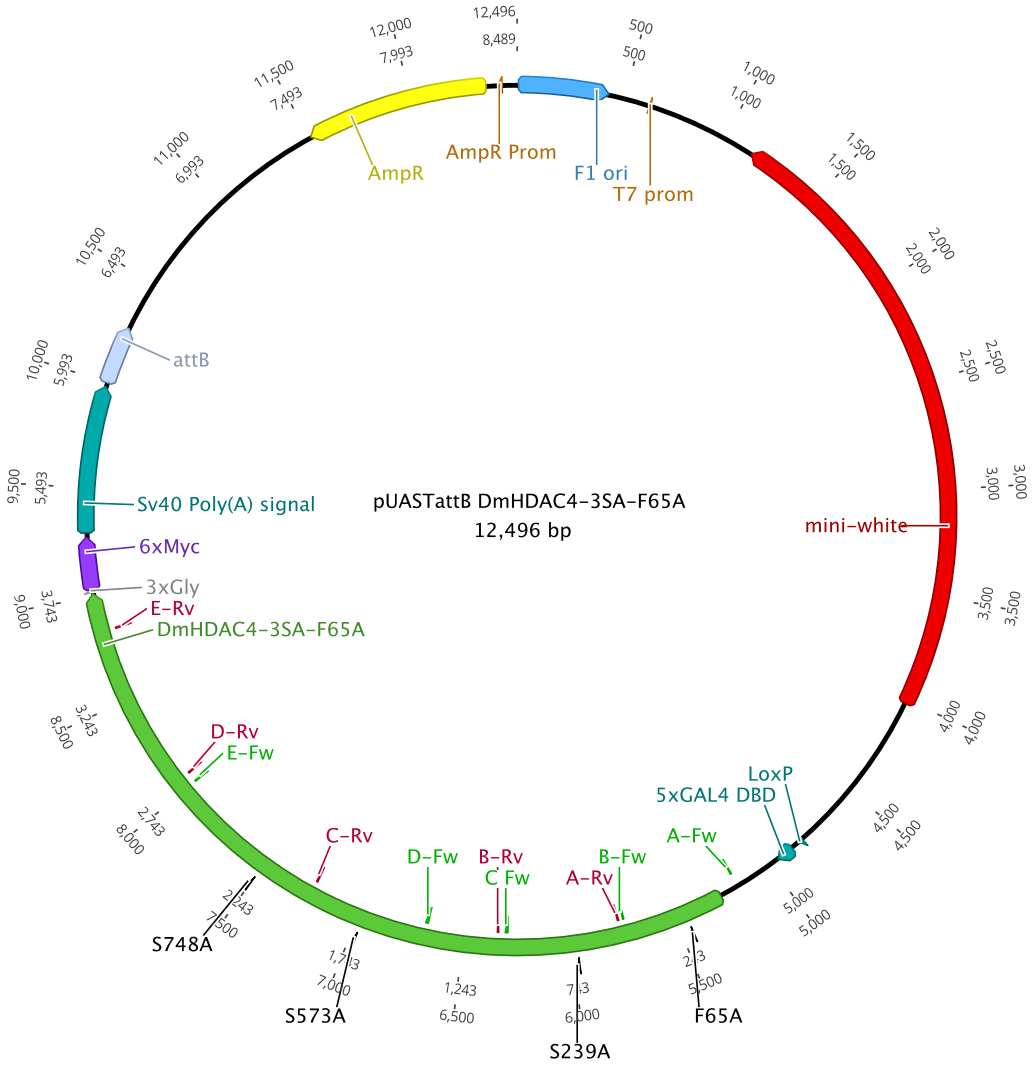

Figure 10.19 Plasmid map of pUASTattB HDAC4$^{3SA-F65A}$

Plasmid map of pUASTattB HDAC4-3SA-F65A with annotation of the primer binding sites used for PCR amplification from genomic DNA in Figure 10.20. This plasmid was used to generate transgenic flies harbouring HDAC4$^{3SA-F65A}$ as described in Section 3.1.1, from which genomic DNA was extracted. Features of the plasmid important for generation of transgenic flies are noted, as well as the sites of the 3SA and F65A mutations, and primer pairs used for verification of the size of HDAC4$^{3SA-F65A}$ as per Table 10.2. Figure made in Geneious R9.

Table 10.2 Primers used for PCR amplification of regions spanning HDAC4$^{3SA\text{-}F65A}$

Pair	Sequence (5'-3')	Expected transgene amplicon (bp)	Expected endogenous amplicon (bp)
A	F: GCAACTACTGAAATCTGCCAAG R: GCAGTTGAGAATCTGTTTGACC	662	-
B	F: TGTAGTGCCAATGCCAG R: AGTTGGGTAAATGCGGTCG	622	2398
C	F: CCATTGTTCAGTTCACCATC R: CGGCGGTTTTTTCTTATCTG	966	1033
D	F: ATTCTGCCCTCGTCATCGTCCTAC R: TGCCGTATGGTGCTCATTC	1392	1459
E	F: TTTGTGCGTTTGTCGTGCG R: ATGCGTTTGCTGTATGGC	849	-

F, forward primer. R, reverse primer.

Gel electrophoresis of PCR products enabled comparison of product size from *HDAC4$^{3SA\text{-}F65A}$* to that from flies harbouring the wild-type construct (WT), and flies that did not harbour an HDAC4 transgene (control) (Figure 10.20). No product from *HDAC4$^{3SA\text{-}F65A}$* flies migrated at a different rate compared to *HDAC4^{WT}*, suggesting that no genomic deletion has occurred. Primer set A was also used on *HDAC4$^{9QA\Delta Q}$*, and demonstrated that a deletion of 96 base pairs could be detected by this method.

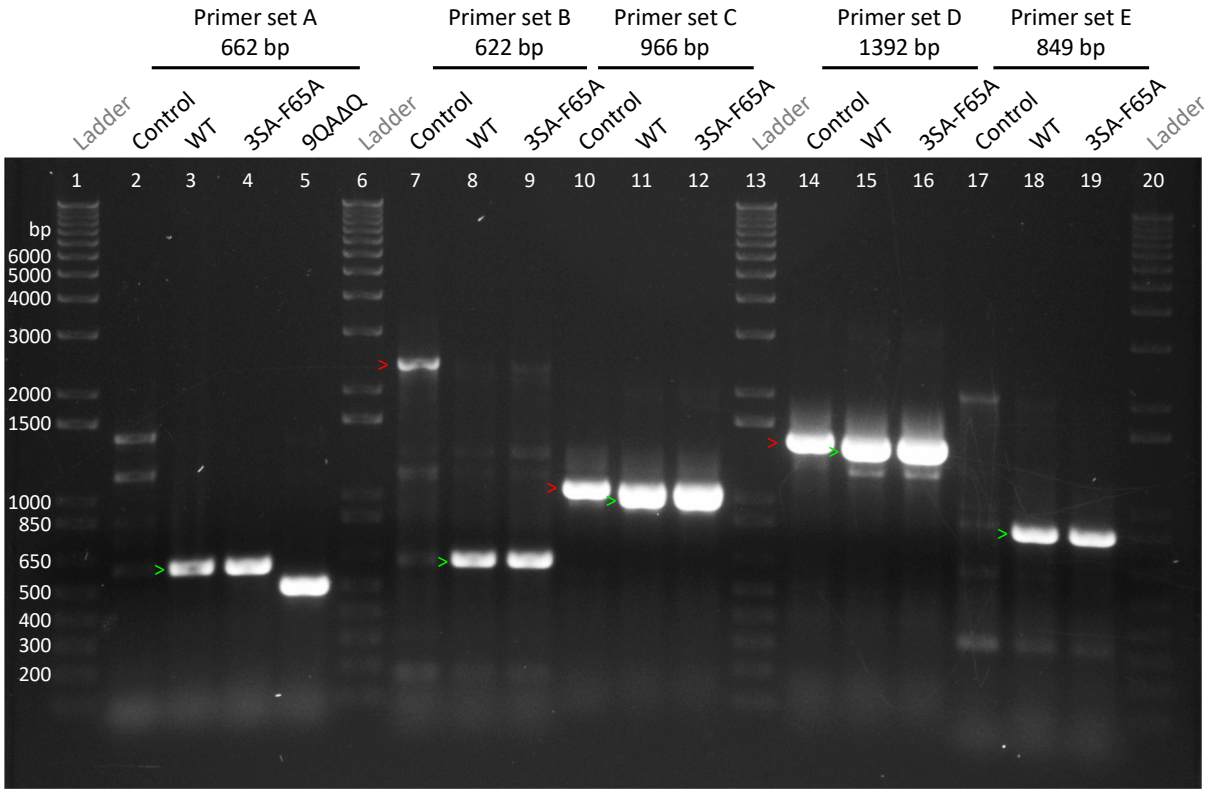

Figure 10.20 Gel electrophoresis of PCR products that span *HDAC4$^{3SA\text{-}F65A}$* show no difference in size compared to *HDAC4^{WT}*

Gel electrophoresis of PCR products amplified from genomic DNA extractions of flies that harboured each of the indicated *HDAC4* constructs. All *HDAC4$^{3SA\text{-}F65A}$* amplicons are of the same size as *HDAC4^{WT}*. *HDAC4$^{9QA\Delta Q}$* appeared at a smaller molecular weight due to the 96 bp ΔQ deletion. As per Table 10.2, the expected transgene-associated bands are marked with a green arrow, and expected endogenous products are marked with a red arrow. Control is Canton S flies.

The detection of HDAC4$^{3SA\text{-}F65A}$ by western blotting via the C-terminal Myc-tag suggests that the C-terminus of the protein remains intact. Based on size comparison with HDAC4$^{9QA\Delta Q}$, HDAC4$^{3SA\text{-}F65A}$ is between 5-7 kDa smaller than HDAC4^{WT}. An internal methionine is present within the N-terminus of HDAC4 that could act as an alternative start site and produce Myc-tagged HDAC4 with an N-terminal truncation. Protein translated from this site would lose 47 amino acids compared to HDAC4^{WT}, corresponding to a deletion of 5.2 kDa. Therefore, the PCR products of *HDAC4^{WT}* and *HDAC4$^{3SA\text{-}F65A}$* from primer set A were subjected to sequencing to determine whether any mutations have occurred that would favour the use of this start site. Alignment of HDAC4^{WT} and HDAC4$^{3SA\text{-}F65A}$ sequences from the PCR products demonstrated that they were identical through this region, with the exception of the F65A mutation (Figure 10.21). Sequencing using the same primers was also performed on the pUASTattB-HDAC4$^{3SA\text{-}F65A}$ plasmid, but did not reveal any unexpected mutations.

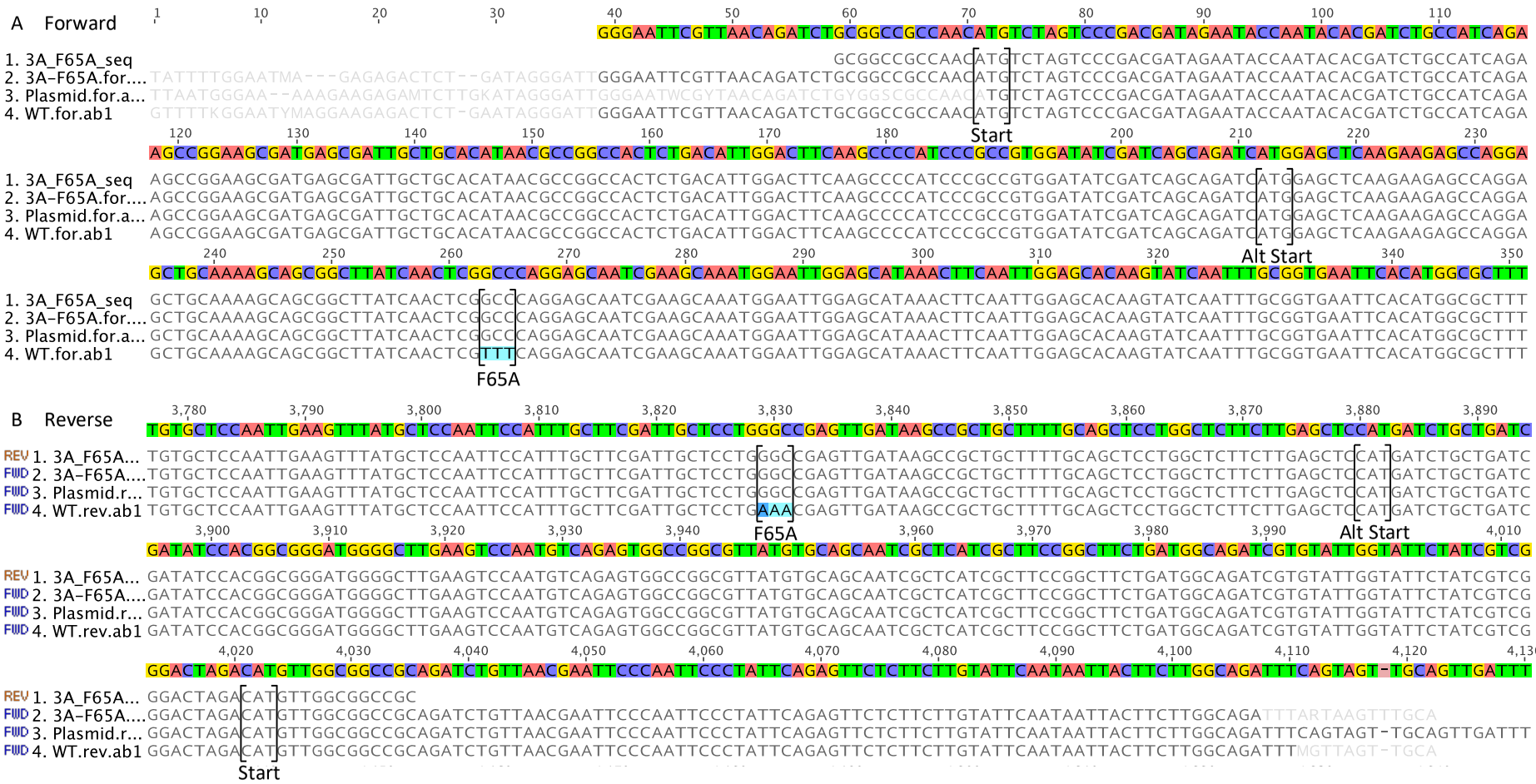

Figure 10.21 Sequence alignment of *HDAC4^{3SA}* expected, plasmid, and genomic sequences shows no mutations near the N-terminus
Pairwise alignment of the expected sequence of HDAC4^{3SA} (1), the genomic sequence obtained of HDAC4$^{3SA-F65A}$ using primer set A (2), the sequence of pUASTattB-HDAC4$^{3SA-F65A}$ obtained using primer set A (3) and the genomic sequence obtained of HDAC4^{WT} using primer set A (4). The forward sequences are shown in (A) and the reverse in (B). Alignments were performed in Geneious R9, version 9.1.8, using Geneious alignment with default settings. The canonical start site is noted, as well as the alternative start site. The only difference observed in this region was with HDAC4^{WT}, which is accounted for the F65A mutation. Greyed regions represent those trimmed under the default settings in Geneious.

Further western blotting was performed on whole-head lysates expressing HDAC4^{WT} and HDAC4^{mutant} under the control of *elav-GAL4* using anti-Myc; adjustment of the light balance revealed three bands between the 95 kDa and 43 kDa marker in HDAC4-expresing samples but not in controls (Figure 10.22). Given detection via the C-terminal Myc tag, these likely correspond to C-terminal cleavage products of HDAC4. A doublet was present at ~80 and ~75 kDa in HDAC4^{WT}, HDAC4^{3SA} and HDAC4^{F65A} lanes, but was shifted in size in HDAC4$^{3SA-F65A}$, suggesting the region responsible for the shift in size of HDAC4$^{3SA-F65A}$ is within the last ~70 kDa of the protein. There is a potential cleavage product at ~50 kDa, and this is not shifted in size for HDAC4$^{3SA-F65A}$, narrowing the region to between 50-70 kDa from the C-terminus of HDAC4.

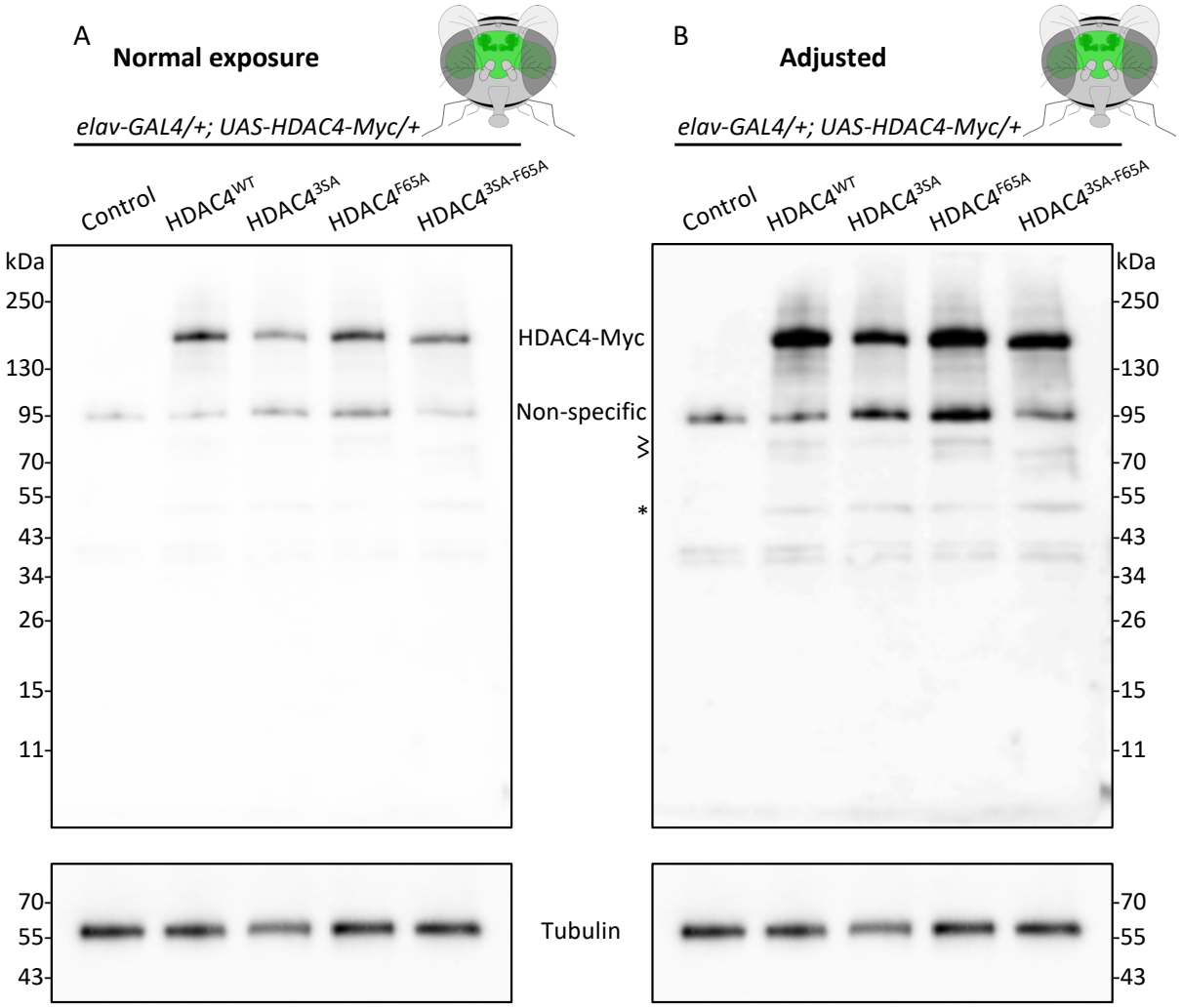

Figure 10.22 Full-length and C-terminal cleavage products of HDAC4$^{3SA-F65A}$ are reduced in apparent molecular weight

(A) Western blot of *elav-GAL4* driven expression of HDAC4^{WT} and HDAC4^{mutant} in head whole-cell lysates using anti-Myc and anti-alpha-tubulin antibodies. Flies were raised at 25°C. The protein bands were of the expected size of ~144 kDa, with the exception of HDAC4$^{3SA-F65A}$. (B) Light intensity levels of the blot in (A) were adjusted to reveal C-terminal cleavage products of HDAC4. Arrowheads denote a doublet detected only in HDAC4-expressing lanes that was reduced in size in the HDAC4$^{3SA-F65A}$ sample. * denotes a band only detected in HDAC4-expressing lanes that was not reduced in size in the HDAC4$^{3SA-F65A}$ sample.

In summary, these data demonstrate that HDAC4$^{3SA\text{-}F65A}$ behaves differently to each HDAC4^{3SA} and HDAC4^{F65A}. Western blotting demonstrated that HDAC4$^{3SA\text{-}F65A}$ migrates at a different molecular weight, but is detected by the Myc tag, confirming that there is no premature termination of translation that would result in a truncated protein without the tag. It was hypothesised that there may be a deletion within *HDAC4$^{3SA\text{-}F65A}$*, however this was not detected by PCR amplification of regions spanning the gene. It was then hypothesised that this may result from alternative start site selection, but sequencing demonstrated no mutation that may favour this. Further western blotting suggested that the region implicated in these changes is towards the C-terminus of HDAC4$^{3SA\text{-}F65A}$, between approximately 50-70 kDa from the C-terminus. It remains unclear why HDAC4$^{3SA\text{-}F65A}$ migrates at a different molecular weight than each of HDAC4^{3SA} and HDAC4^{F65A}. It is possible that the combination of 3SA and F65A mutations may alter protein binding or its conformation to mask or reveal sites that undergo post-translational modifications such as glycosylation or multiple instances of phosphorylation, or favour some biological occurrence such as enzymatic cleavage. However, it is difficult to reason how this would result in an internal deletion, and be reversed upon addition of the ΔMEF2 mutations. In light of this, a change in post-translational modification is more likely. Further investigation of this is required.

10.3.2. Full western blots of subcellular fractionation and co-immunoprecipitation performed on heads of flies expressing HDAC4 mutants

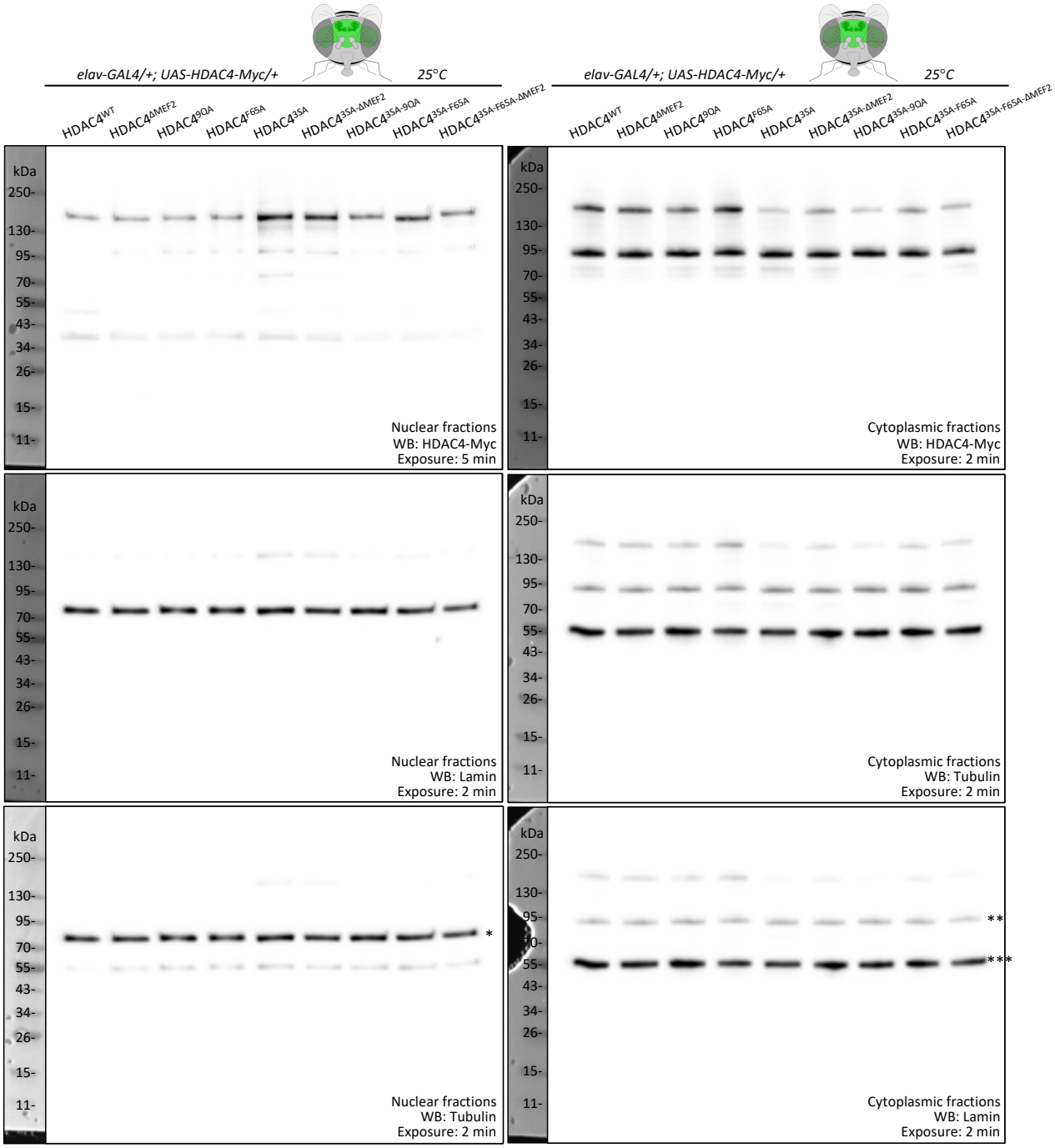

Figure 10.23 Full western blots of the subcellular fractionation assays in Figure 5.5
Subcellular fractionation was performed on the heads of flies expressing HDAC4^{WT} and HDAC4^{mutant} under the control of *elav-GAL4*. Flies were raised at 25°C. Total protein was loaded (20 µg) for both nuclear and cytoplasmic fractions, and each was probed with anti-Myc to detect HDAC4, and anti-lamin and anti-alpha-tubulin to assess nuclear and cytoplasmic abundance respectively in each lysate. Lamin was observed at ~71 kDa and tubulin at ~55 kDa. * indicates residual detection of lamin due to re-probing. ** indicates residual detection of the ~95 kDa non-specific band previously characterised for the anti-Myc antibody due to re-probing. *** indicates residual detection of tubulin due to re-probing. No lamin was observed in the cytoplasmic fractions. Blots were exposed for the same amount of time for each antibody detection and underwent the same adjustments in brightness and contrast between nuclear and cytoplasmic membranes.

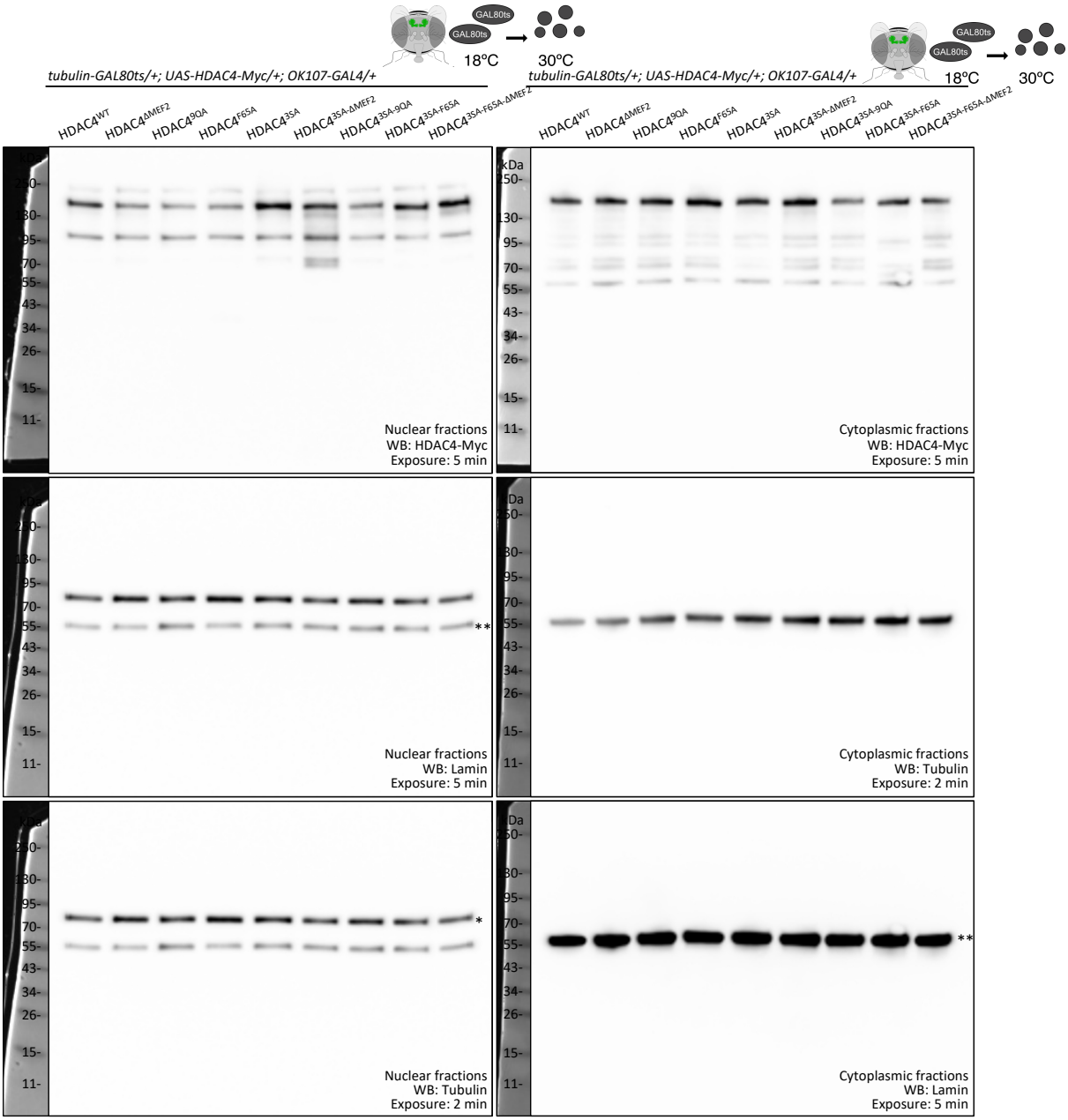

Figure 10.24 Full western blots of the subcellular fractionation assays in Figure 5.6
Subcellular fractionation was performed on the heads of flies expressing *HDAC4*^{WT} and *HDAC4*^{mutant} under the control of *OK107-GAL4* in the presence of the TARGET system. Flies were raised at 18°C until eclosion, and adults were transferred to 30°C for three days to induce expression. Total protein was loaded (20 µg) for both nuclear and cytoplasmic fractions, and each was probed with anti-Myc to detect HDAC4, and anti-lamin and anti-alpha-tubulin to assess nuclear and cytoplasmic abundance respectively in each lysate. Lamin was observed at ~71 kDa and tubulin at ~55 kDa. * indicates residual detection of lamin due to re-probing. ** indicates residual detection of tubulin due to re-probing. No lamin was observed in the cytoplasmic fractions. Blots were exposed for the same amount of time for each antibody detection and underwent the same adjustments in brightness and contrast between nuclear and cytoplasmic membranes. Please note that tubulin and lamin were detected simultaneously, and therefore blots look very similar with the exception of the length of exposure.

A

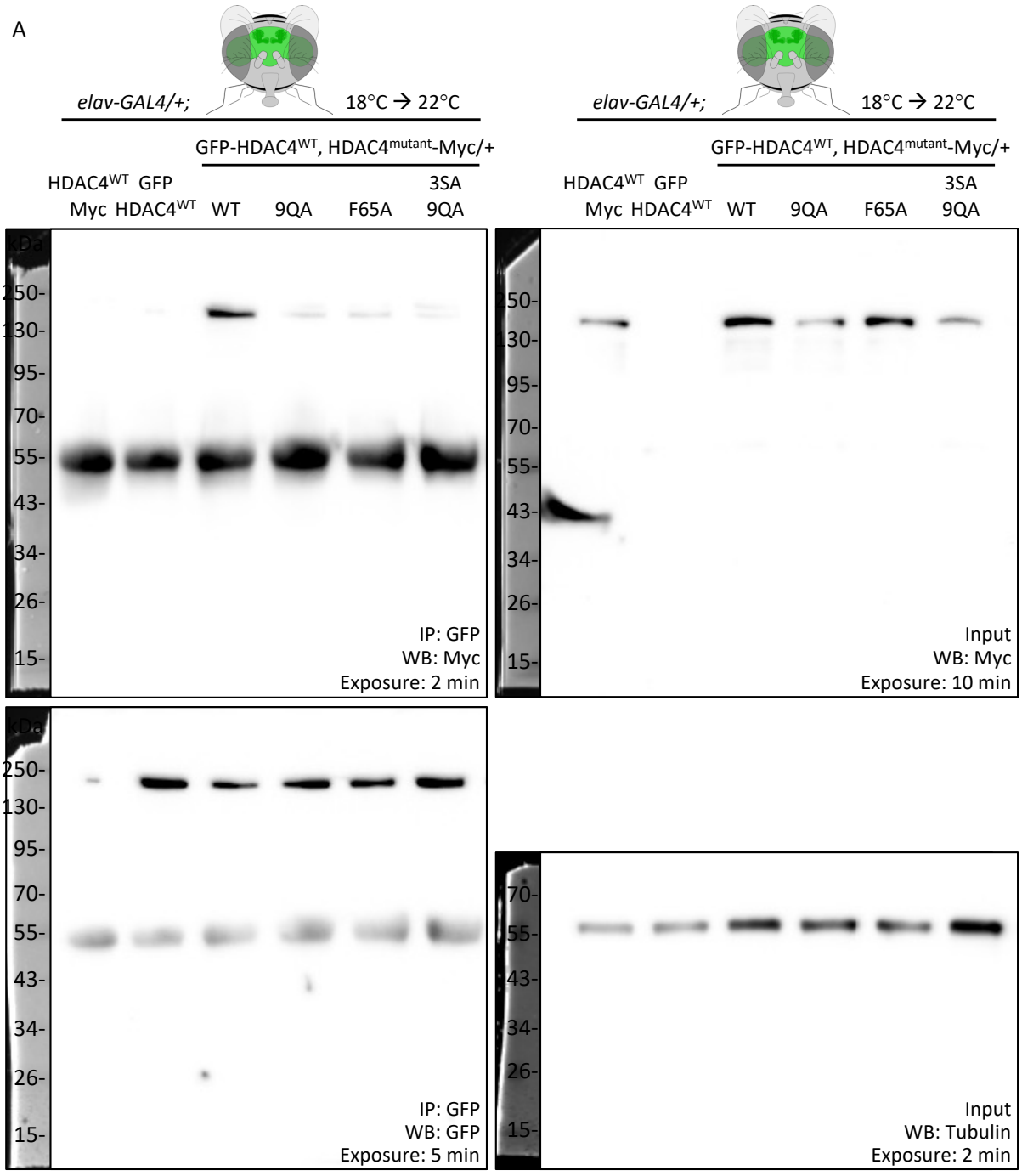
elav-GAL4/+;
18°C → 22°C
GFP-HDAC4WT, HDAC4mutant-Myc/+
HDAC4WT GFP
Myc HDAC4WT WT 9QA F65A 3SA 9QA
kDa
250-
130-
95-
70-
55-
43-
34-
26-
15-
IP: GFP
WB: Myc
Exposure: 2 min
50-
30-
Input
WB: Myc
Exposure: 10 min
IP: GFP
WB: GFP
Exposure: 5 min
Input
WB: Tubulin
Exposure: 2 min

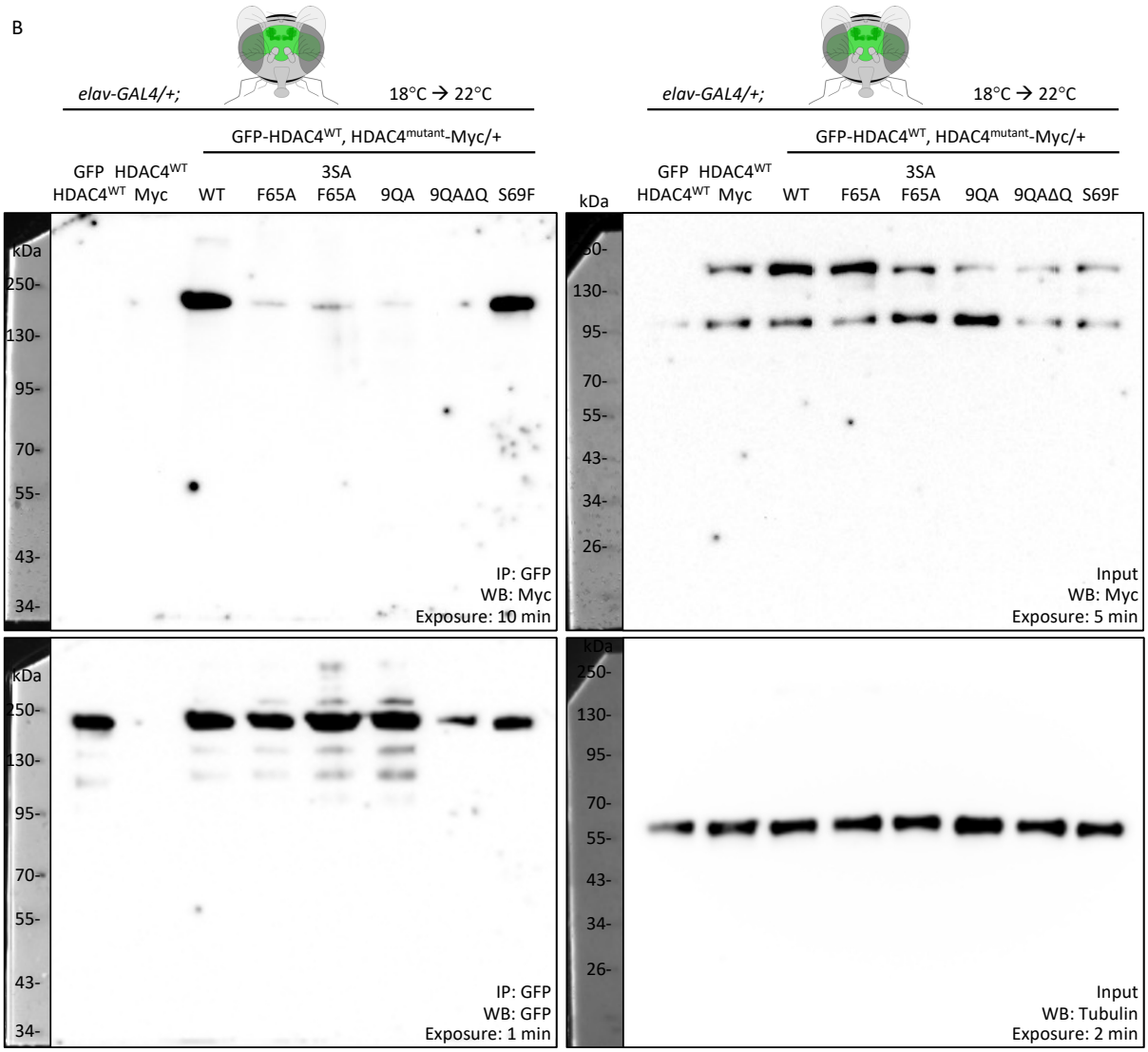

Figure 10.25 Full western blots of the co-immunoprecipitation assay in Figures 5.7 and 10.13

(A, B) Co-immunoprecipitation experiments to examine the ability of HDAC4^{mutant} to bind HDAC4^{WT} to assess oligomerisation capacity. The indicated transgenes were expressed pan-neuronally in *Drosophila* under the control of *elav-GAL4*. Flies were raised at 18°C until adulthood and then moved to 22°C for five days to increase the level of transgene expression before harvesting and generation of whole-head lysates. Anti-GFP conjugated beads were used to immunoprecipitate GFP-HDAC4^{WT} from all samples, followed by probing for HDAC4-Myc. HDAC4^{WT} co-immunoprecipitated with GFP-HDAC4^{WT}, while HDAC4^{9QA}, HDAC4^{F65A}, HDAC4$^{3SA\text{-}9QA}$ and HDAC4$^{3SA\text{-}F65A}$ did not do so significantly despite comparable immunoprecipitation of GFP-HDAC4^{WT} from all samples. Input samples are 30 µg of whole-cell lysate, and the level of transgene expression is consistent with previously quantification (Figures 4.7 and 5.4). Protocol 2 was used for the data shown in (A), and protocol 1 for the data shown in (B).

10.3.3. Eye phenotypes resulting from expression of nuclear-restricted HDAC4 oligomerisation mutants from one genomic insertion

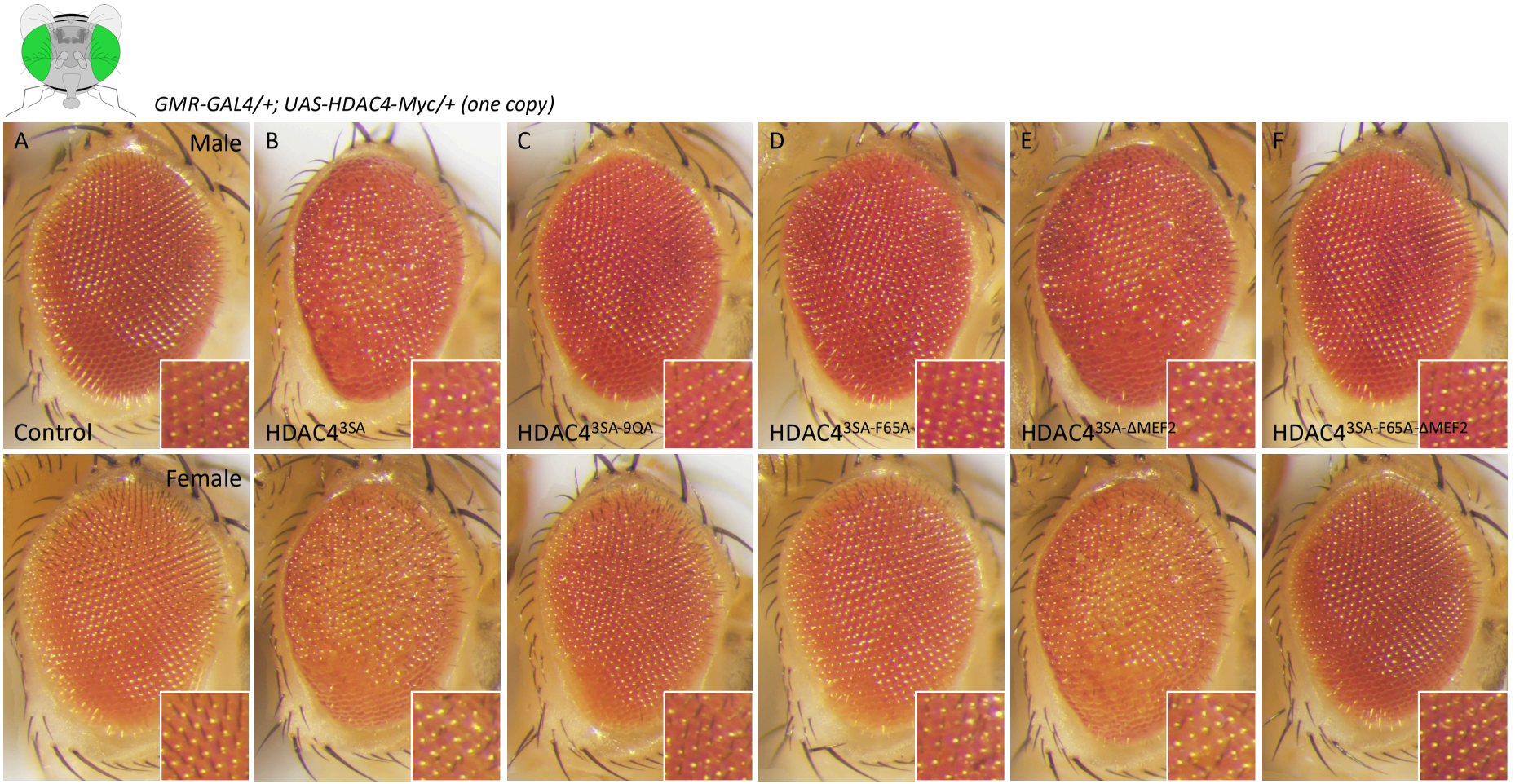

Figure 10.26 Overexpression of nuclear-restricted HDAC4 oligomerisation mutants differentially impacts *Drosophila* eye development

(A-F) Light microscopy images of *Drosophila* eyes raised at 25°C. Top row, males; bottom row, females. Inset shows a magnified image of ommatidia. (A) Control is *GMR-GAL4/+*. (B-F) Flies harboured one copy of the driver (*GMR-GAL4/+*) and one copy of the transgene (*UAS-HDAC4/+*). (B) HDAC4^{3SA} overexpression induced perturbation of the organisation of the adult eye, characterised by misalignment of ommatidia and bristles as well as fusion and loss of pigmentation. This was reduced by HDAC4$^{3SA-9QA}$ (C), HDAC4$^{3SA-F65A}$ (D), and HDAC4$^{3SA-F65A-\Delta MEF2}$ (F). There was little difference between HDAC4^{3SA} and HDAC4$^{3SA-\Delta MEF2}$ (F).

10.3.4. Images of female eyes expressing HDAC4$^{\Delta NES}$

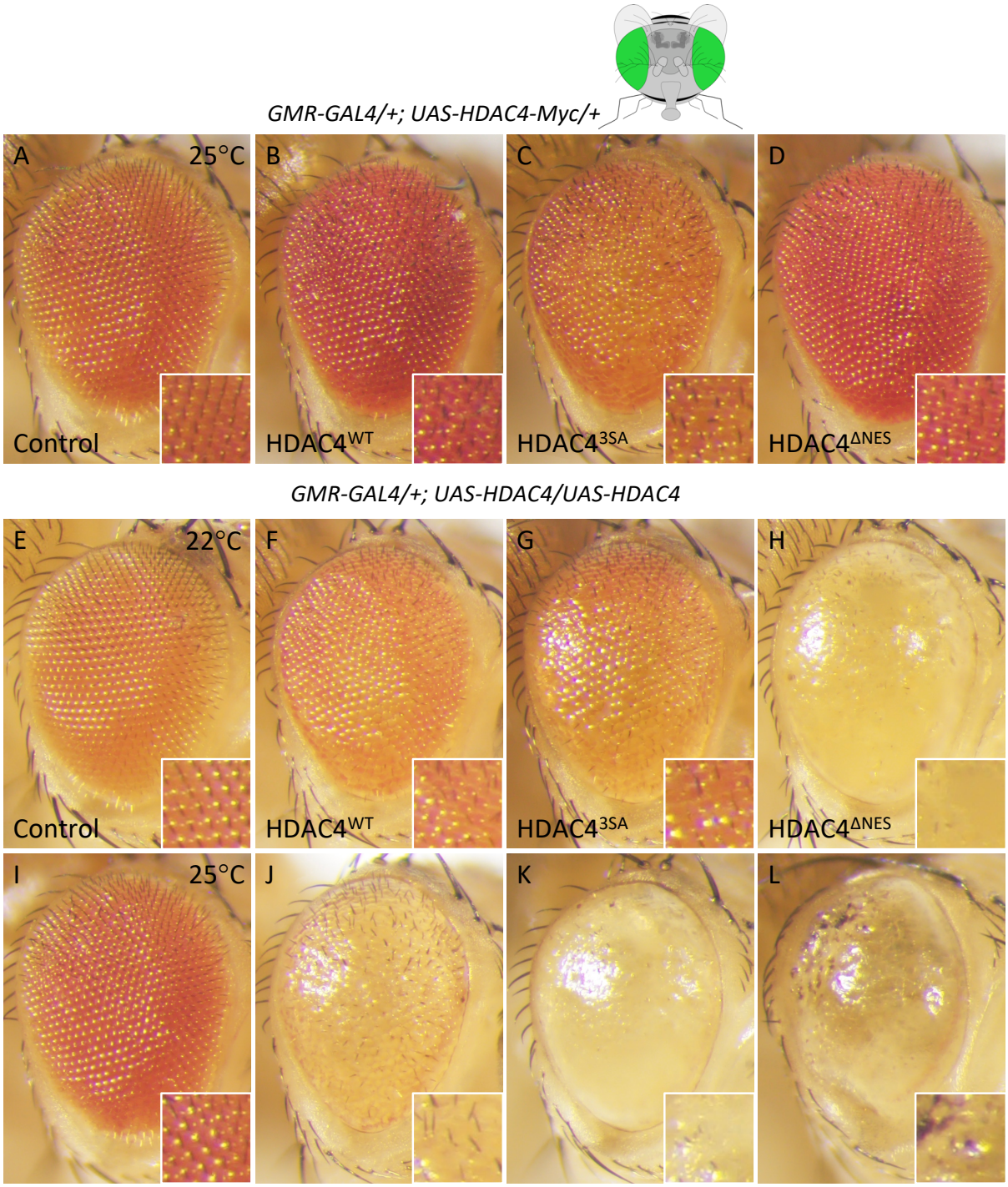

Figure 10.27 Eye phenotypes resulting from enforcing nuclear restriction of HDAC4 via 3SA and ΔNES mutations in females

Light microscopy images of *Drosophila* eyes raised at the indicated temperatures. All eyes shown are from female flies. Inset shows a magnified image of ommatidia. (A, E, I) Control is *GMR-GAL4/+*. (B-D) Flies harboured one copy of the driver (*GMR-GAL4/+*) and one copy of *HDAC4^{WT}* or *HDAC4^{mutant}* (*UAS-HDAC4/+*) and were raised at 25°C. (B) HDAC4^{WT} overexpression induced disorganisation of bristles and ommatidia. This phenotype was increased in severity upon expression of HDAC4^{3SA} (C) which resulted in loss of pigmentation and occasional fusion of ommatidia as well as disorganisation. (D) Expression of HDAC4$^{\Delta NES}$ did not increase phenotype severity compared to HDAC4^{WT}. (F-H) Flies

harboured one copy of the driver (*GMR-GAL4/+*) and two copies of *HDAC4*^{WT} or *HDAC4*^{mutant} (*UAS-HDAC4/UAS-HDAC4*) and were raised at 22°C. (F) Increasing the dose of HDAC4^{WT} overexpression increased the severity of the eye phenotype, with increased loss of pigmentation and fusion of ommatidia, similarly to that of HDAC4^{3SA} (G). (H) Expression of HDAC4$^{\Delta NES}$ resulted in complete fusion of ommatidia and loss of pigmentation. (J-L) Flies harboured one copy of the driver (*GMR-GAL4/+*) and two copies of *HDAC4*^{WT} or *HDAC4*^{mutant} (*UAS-HDAC4/UAS-HDAC4*) and were raised at 25°C. Increasing the temperature at which flies were raised increased the severity of the phenotype. (J) HDAC4^{WT} expressing eyes presented with fusion of ommatidia, and pigment was largely only observed at the edges of the eye. HDAC4^{3SA} expressing eyes (K) presented with total fusion and loss of pigmentation, with necrotic patches. (L) Expression of HDAC4$^{\Delta NES}$ was largely lethal as flies remained in their pupal cases; of the flies that emerged their eyes were small, smooth, and had necrotic patches.

10.4. Supplementary data corresponding to Chapter 6

10.4.1. Identification of interactors of nuclear-restricted HDAC4 in the *Drosophila* brain

Table 10.3 Candidate interactors of HDAC4^{3SA} from initial mass spectrometry analysis

FlyBase ID	Gene name	Gene symbol	#PSMs in Control	#PSMs in HDAC4^{3SA}	Fold Change
FBgn0003360	stress-sensitive B	sesB	10	20	2.0
FBgn0000046	Actin 87E	Act87E	7	17	2.4
FBgn0010551	Prohibitin 2	Phb2	7	15	2.1
FBgn0037138	delta-1-Pyrroline-5-carboxylate dehydrogenase 1	P5CDh1	0	13	-
FBgn0002938	neither inactivation nor afterpotential C	ninaC	0	9	-
FBgn0041210	Histone deacetylase 4	HDAC4	0	8	-
FBgn0003885	alpha-Tubulin at 84D	alphaTub84D	0	8	-
FBgn0037891	-	Dlst	3	7	2.3
FBgn0001218	Heat shock protein 70 cognate 3	Hsc70-3	2	6	3.0
FBgn0002031	Prohibitin 1	Phb1	3	6	2.0
FBgn0264695	Myosin heavy chain	Mhc	0	5	-
FBgn0037146	Delta[1]-pyrroline-5-carboxylate synthase	P5CS	0	5	-
FBgn0261439	Succinate dehydrogenase, subunit A (flavoprotein)	SdhA	0	4	-
FBgn0020653	Thioredoxin reductase 1	Trxr1	0	4	-
FBgn0037607	-	CG8036	0	4	-
FBgn0283658	midline uncoordinated	muc	0	4	-
FBgn0011693	Photoreceptor dehydrogenase	Pdh	0	4	-
FBgn0020238	14-3-3ε	14-3-3ε	0	4	-
FBgn0001198	Histone H2B	His2B	0	4	-
FBgn0003423	sluggish A	slgA	0	3	-
FBgn0031305	Iris	Iris	0	3	-
FBgn0266599	Heat shock protein 70 cognate 4	Hsc70-4	0	3	-
FBgn0001145	Glutamine synthetase 2	Gs2	0	3	-
FBgn0000120	Arrestin 1	Arr1	0	3	-
FBgn0266064	Glycogen synthase	Glys	0	2	-
FBgn0011211	bellwether	blw	0	2	-
FBgn0036927	gamma-aminobutyric acid transaminase	Gabat	0	2	-
FBgn0016687	Nucleosome remodeling factor - 38kD	Nurf-38	0	2	-
FBgn0027786	Mitochondrial carrier homolog 1	Mtch	0	2	-

#PSMs, number of peptide spectrum matches. Candidate interactors of HDAC4^{3SA} are ordered first by #PSMs in HDAC4^{3SA}, then by fold change. HDAC4 is also included here, it is unclear whether peptides detected correspond to wild-type endogenous HDAC4 or HDAC4^{3SA}-Myc.

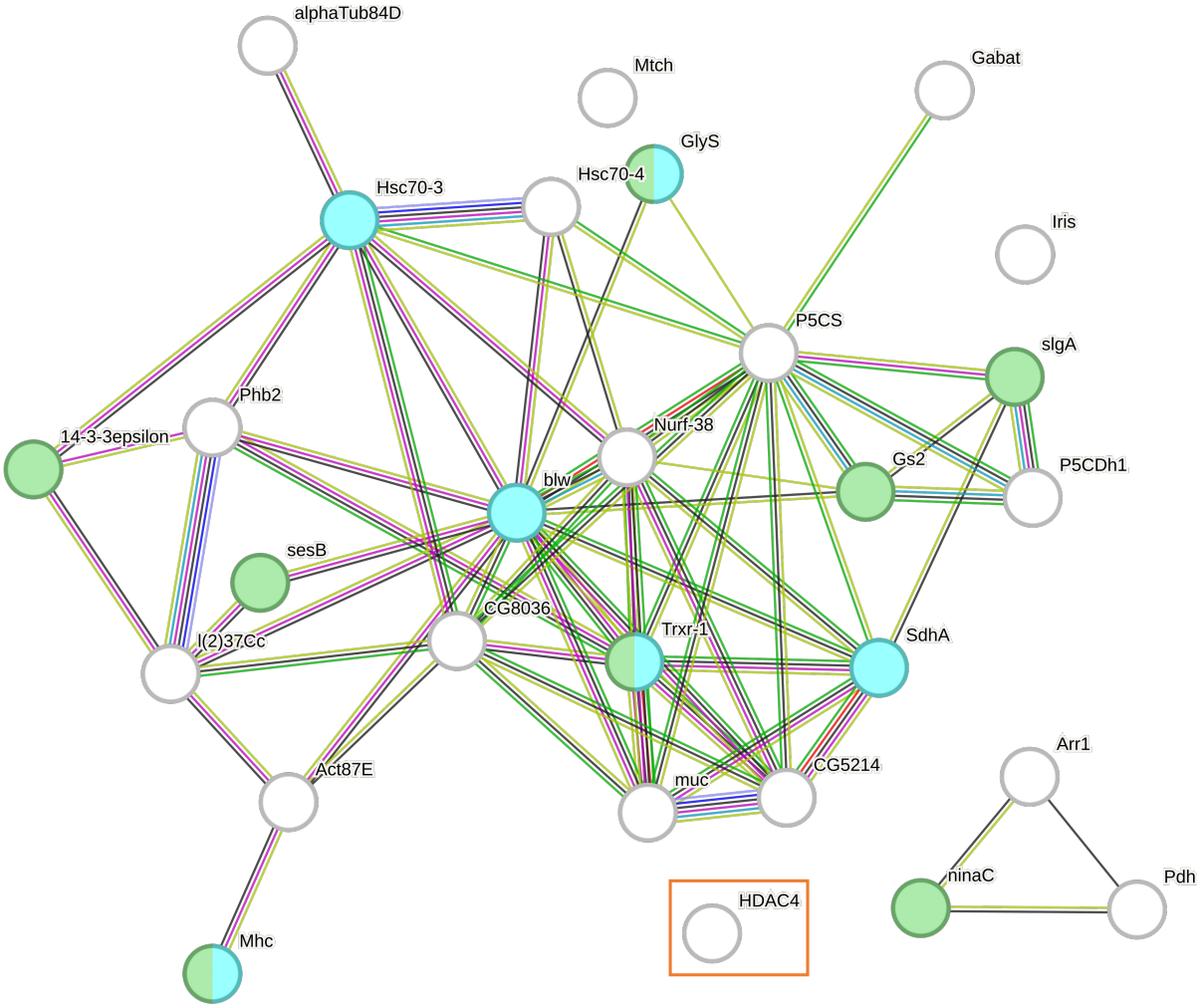

Figure 10.28 STRING interaction network of 27 HDAC4^{3SA} candidate interactors
STRING analysis of predicted interactions between candidate HDAC4^{3SA} interactors. HDAC4 is highlighted in the orange square. The network consists of 28 nodes and 66 edges. The expected number of edges was 14, with a protein-protein interaction enrichment p-value of <1.0e-16 indicating that the network has significantly more interactions than expected, which may indicate that the proteins are at least partially biologically related as a group. Nodes coloured green are associated with the UniProt key words term 'Alternative splicing'. Nodes coloured teal are associated with the study by Tsakiri *et al.* (2019). Edge colours represent the type of interaction: teal, known interaction from curated database; magenta, experimentally determined interaction; dark green, predicted interaction by gene neighbourhood; red, predicted interaction by gene fusion; dark blue, predicted interaction by gene co-occurrence; light green, other interaction based on text mining; black, other interaction based on co-expression; light blue, other interaction based on protein homology.

10.4.2. Preliminary investigation into HDAC4^{3SA} candidate interactors

Two candidates from the initial IP-MS analyses were selected to examine co-distribution with HDAC4^{3SA} aggregates. These candidates were selected for their similarities to HDAC4 with respect to expression pattern in the *Drosophila* brain and roles in eye development and memory, and are briefly described below. The distribution of each of the endogenous proteins was examined in the absence and presence of HDAC4^{3SA} expression under the control of *OK107-GAL4* in the presence of the TARGET system; flies were raised at 18°C until emergence and adults were moved to 30°C for three days before dissecting brains and preparation for immunohistochemistry.

Armadillo is the *Drosophila* orthologue of β-catenin and was first identified for its roles in segment polarity (Peifer & Wieschaus, 1990). While typically cytoplasmic and interacting with cadherins (Pai *et al.*, 1996), nuclear localisation has been demonstrated (Tolwinski & Wieschaus, 2004), suggesting the potential to be sequestered in HDAC4^{3SA} aggregates. Misexpression of armadillo reduced eye size (Freeman & Bienz, 2001) and mutants had a strikingly similar phenotype to HDAC4^{3SA} of ommatidial fusion (Rousset *et al.*, 2001). Armadillo also interacts genetically with CtBP (Bhambhani *et al.*, 2011; Fang *et al.*, 2006), an interactor of human HDAC4 (Zhang *et al.*, 2001). Similarly to HDAC4, expression of Armadillo was observed in the Kenyon cell bodies and calyx in the posterior of the brain, as well as in the lobes of the mushroom body in the anterior, and knockdown impaired long-term but not short-term olfactory memory (Tan *et al.*, 2013). Figure 10.29 depicts Armadillo distribution as imaged through the Kenyon cell layer in the posterior of the brain; Armadillo localised to the calyx and Kenyon cells as observed previously (Tan *et al.*, 2013), however its distribution was punctate and cytoplasmic and did not co-localise with nuclear HDAC4^{3SA} aggregates (Figure 10.29C-D).

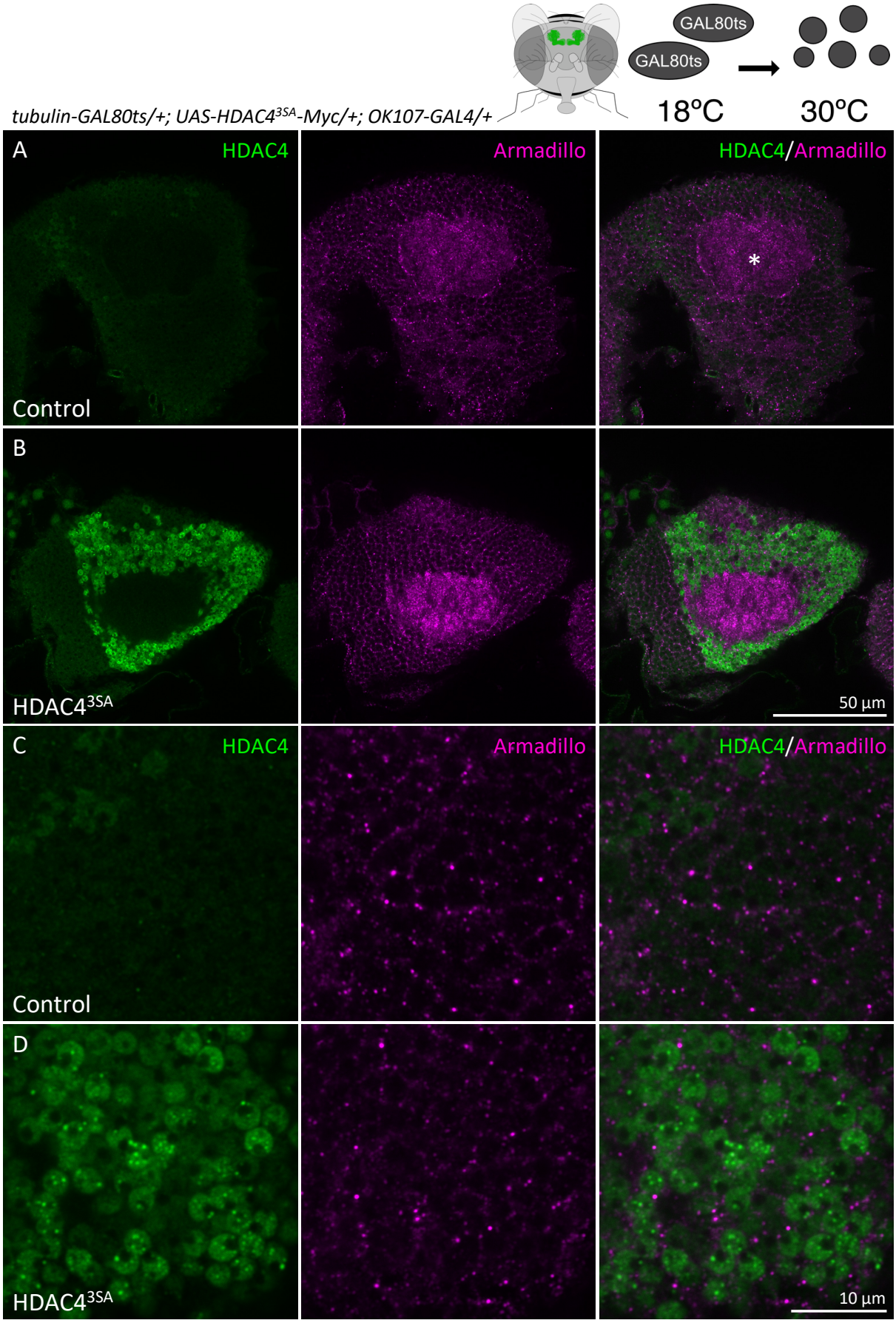

Figure 10.29 Armadillo does not co-localise with HDAC4^{3SA} in Kenyon cell nuclear aggregates

(A-B) Single optical sections (0.5 μm) through the Kenyon cell layer depicting endogenous Armadillo (magenta) and HDAC4^{3SA} (green) expression under the control of *OK107-GAL4* in the presence of the TARGET system; flies were raised at 18°C until eclosion, and adults were transferred to 30°C for three days to induce expression. Control is *tubulin-GAL80ts/+; +; OK107-GAL4/+*. Asterisks denote the calyx. (C-D) Magnified single optical section (0.5 μm) of Armadillo and HDAC4^{3SA} in Kenyon cells above the calyx. Armadillo did not co-localise with HDAC4^{3SA} inclusions.

Neither inactivation nor afterpotential C (NinaC) is a rhodopsin-like protein important in photoreceptor development and function, containing domains with putative serine/threonine kinase and myosin activities (Porter *et al.*, 1992). NinaC mutants have reduced rhabdomere size and impaired structure (Matsumoto *et al.*, 1987), and undergo light-dependent retinal degeneration (Porter *et al.*, 1992). NinaC is also upregulated in mushroom body extrinsic neurons following memory formation (Crocker *et al.*, 2016). Consistent with RNAseq (Leader *et al.*, 2018), immunohistochemistry for NinaC in the adult brain was unsuccessful (data not shown). It is unclear whether this reflected a lack of NinaC, or whether further optimisation of immunohistochemistry was required. *elav-GAL4* drives transgene expression in the adult eye (Sage *et al.*, 2008), suggesting that HDAC4^{3SA} may be interacting with NinaC in this tissue, therefore the distribution of NinaC and HDAC4^{3SA} were investigated in the adult retina (Figure 10.30). NinaC was detected strongly in rhabdomeres as previously described (Montell & Rubin, 1988). NinaC was absent from the interrhabdomeral space, and localised to the cytoplasm of photoreceptor cells. HDAC4^{3SA} aggregates were observed in nuclei surrounding rhabdomeres, however NinaC did not co-localise with these. It is noted however that HDAC4^{3SA} expression resulted in significant disruption to rhabdomere morphogenesis, consistent with that observed upon Nile Red staining by Tan (2022).

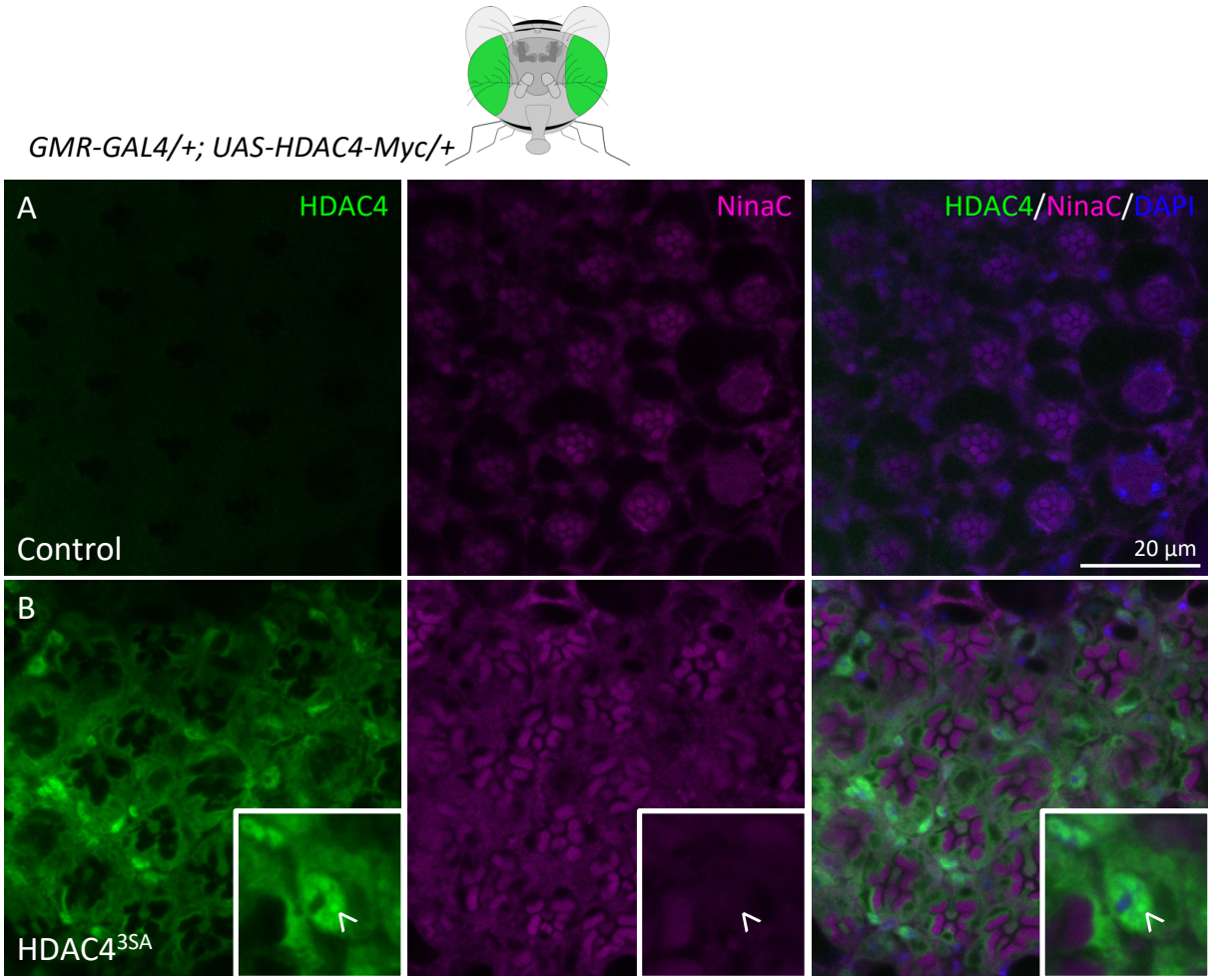

Figure 10.30 NinaC does not co-localise with HDAC4^{3SA} in nuclear aggregates
(A-B) Single optical sections (0.5 µm) through the adult retina at the level of the photoreceptor nuclei depicting endogenous NinaC (magenta) and HDAC4^{3SA} (green) expression driven by *GMR-GAL4*. Flies were raised at 25°C. Control is *GMR-GAL4/+*. Inset, magnified image of a photoreceptor nucleus. Arrowhead denotes a nuclear aggregate of HDAC4. NinaC did not localise to HDAC4^{3SA} inclusions.

10.4.3. Optimisation of protocols for IP-MS analysis

10.4.3.1. Optimisation of the immunoprecipitation protocol

Section 6.1 was performed using immunoprecipitation protocol 1, however it was determined that the protein A/G agarose beads were of variable quality resulting in variable reliability of HDAC4^{3SA} immunoprecipitation. As immunoprecipitation could not always be visualised via western blotting when using these beads, alternative beads were sought. A protocol was tested and optimised for the use of Bio-Rad SureBeads Protein A/G Magnetic Beads, however these were subsequently discontinued. Therefore, Pierce Protein A/G Magnetic Beads (ThermoFisher Scientific) used with anti-Myc antibody (Abcam, ab9106) were compared to Pierce Anti-c-Myc Magnetic Beads (ThermoFisher Scientific) (Figure 10.31).

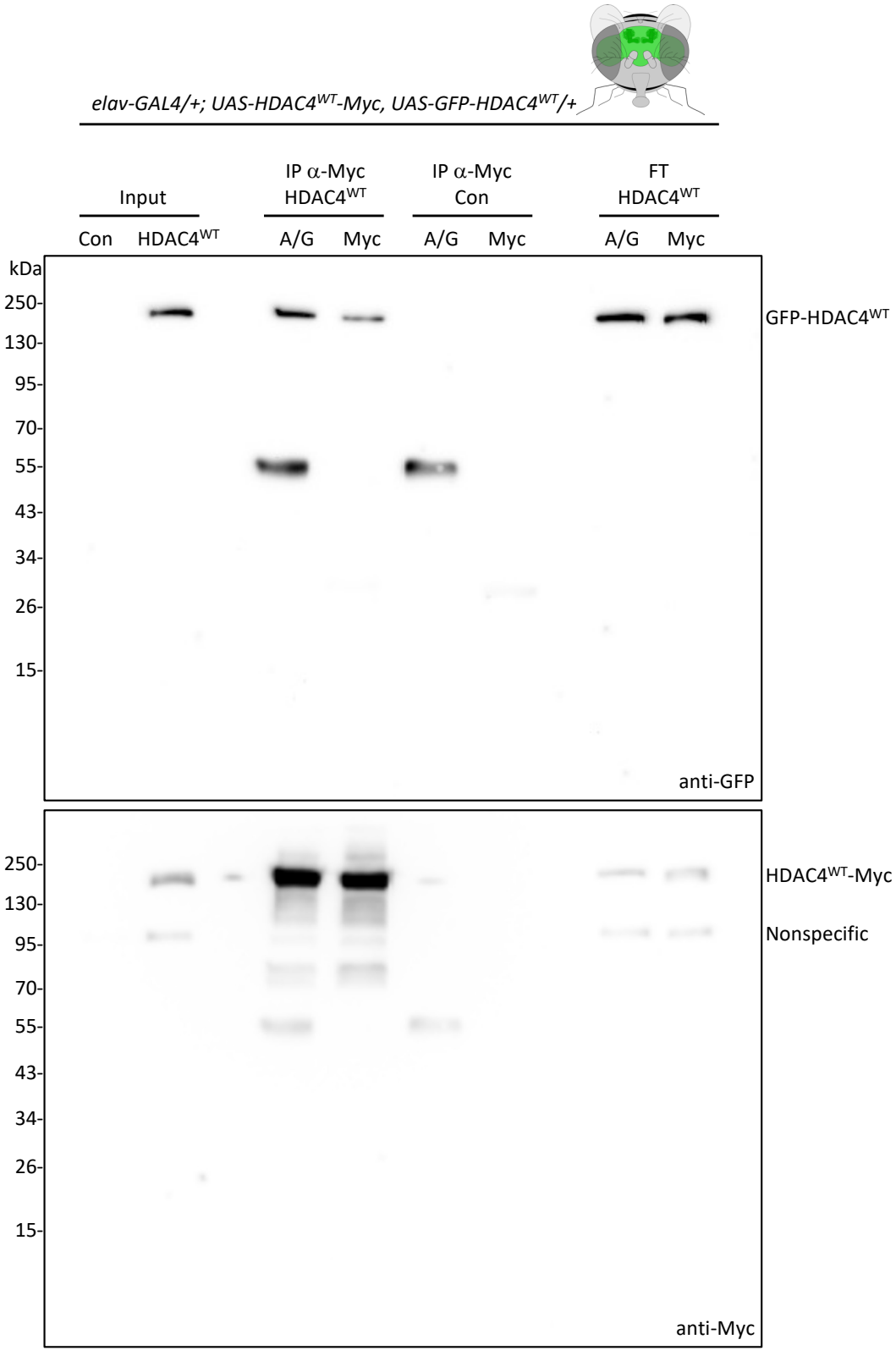

Figure 10.31 Confirming the efficacy and specificity of new protein A/G and anti-Myc beads and respective immunoprecipitation protocols (Protocol 2)

Co-immunoprecipitation experiments to compare the efficacy of Pierce Protein A/G Magnetic beads (ThermoFisher Scientific) using rabbit anti-Myc (ab9106, Abcam) (together abbreviated as A/G) to Pierce Anti-c-Myc Magnetic beads (ThermoFisher Scientific) (abbreviated as Myc). Immunoprecipitation was performed using Protocol 2 with wash conditions as per W1, described below.

Control (con) is *elav-GAL4/+*. GFP-HDAC4^{WT} and HDAC4^{WT}-Myc were expressed pan-neuronally in *Drosophila* under the control of *elav-GAL4*. Flies were raised at 18°C until adulthood and then moved to 22°C for five days to increase the level of transgene expression before harvesting and generation of whole-head lysates. Input samples are 30 µg of whole-cell lysate. Control and GFP/Myc HDAC4^{WT} expressing whole cell lysates were subjected to immunoprecipitation using either the A/G or Myc-conjugated magnetic beads and the total eluate was electrophoresed (IP). Western blotting using anti-GFP confirmed that GFP-HDAC4^{WT} was co-immunoprecipitated, and with anti-Myc confirmed that HDAC4^{WT}-Myc was immunoprecipitated by both A/G and Myc beads. Flowthrough (FT) is a sample of the lysate immediately after incubation with the antibody-bead complex (non-captured proteins, ~30 µg). Two strong bands at ~50 kDa were observed in the anti-GFP blot. Both immunoprecipitation and detection were performed using antibodies raised in rabbit. This band is therefore likely denatured Myc antibody heavy chain as it was absent from inputs as well as from lanes using the Myc conjugated beads. Detection was performed using VeriBlot detection reagent to minimise detection of denatured antibody.

Co-immunoprecipitation of GFP-HDAC4^{WT} was successful for both bead types, as was immunoprecipitation of HDAC4^{WT}-Myc. Similar levels of GFP-HDAC4^{WT} were detected in the flowthrough of both samples, and HDAC4^{WT}-Myc in the IP samples, suggesting a similar level of immunoprecipitation efficiency. The yield of GFP-HDAC4^{WT} was slightly increased in the A/G sample. While it is unclear how reproducible this difference in efficiency is, the A/G beads were selected for further use.

To further improve the efficiency of immunoprecipitation, different immunoprecipitation and wash conditions were tested (Figure 10.32). These were tested across two independent batches of beads (B1 and B2) to satisfy previous concerns about batch-to-batch variability of the beads. Protocol two was followed as per Section 3.2.4 and immunoprecipitation and wash conditions were varied as follows; W1, wash condition one, lysates were incubated for one hour at room temperature with Myc-bound A/G beads, and washes were performed using IP-buffer. W2, wash condition two, lysates were incubated overnight at 4°C with Myc-bound A/G beads, and washes were performed using TBS-T. The change to TBS-T washes and an overnight incubation (W1 B2 vs W2 B2) significantly increased the yield of GFP-HDAC4^{WT} co-immunoprecipitated, and HDAC4^{WT}-Myc immunoprecipitated, therefore these steps were included in the final protocol. Little variation in immuno- and co-immunoprecipitation efficiency was observed between the two bead batches (W1 B1 vs W1 B2).

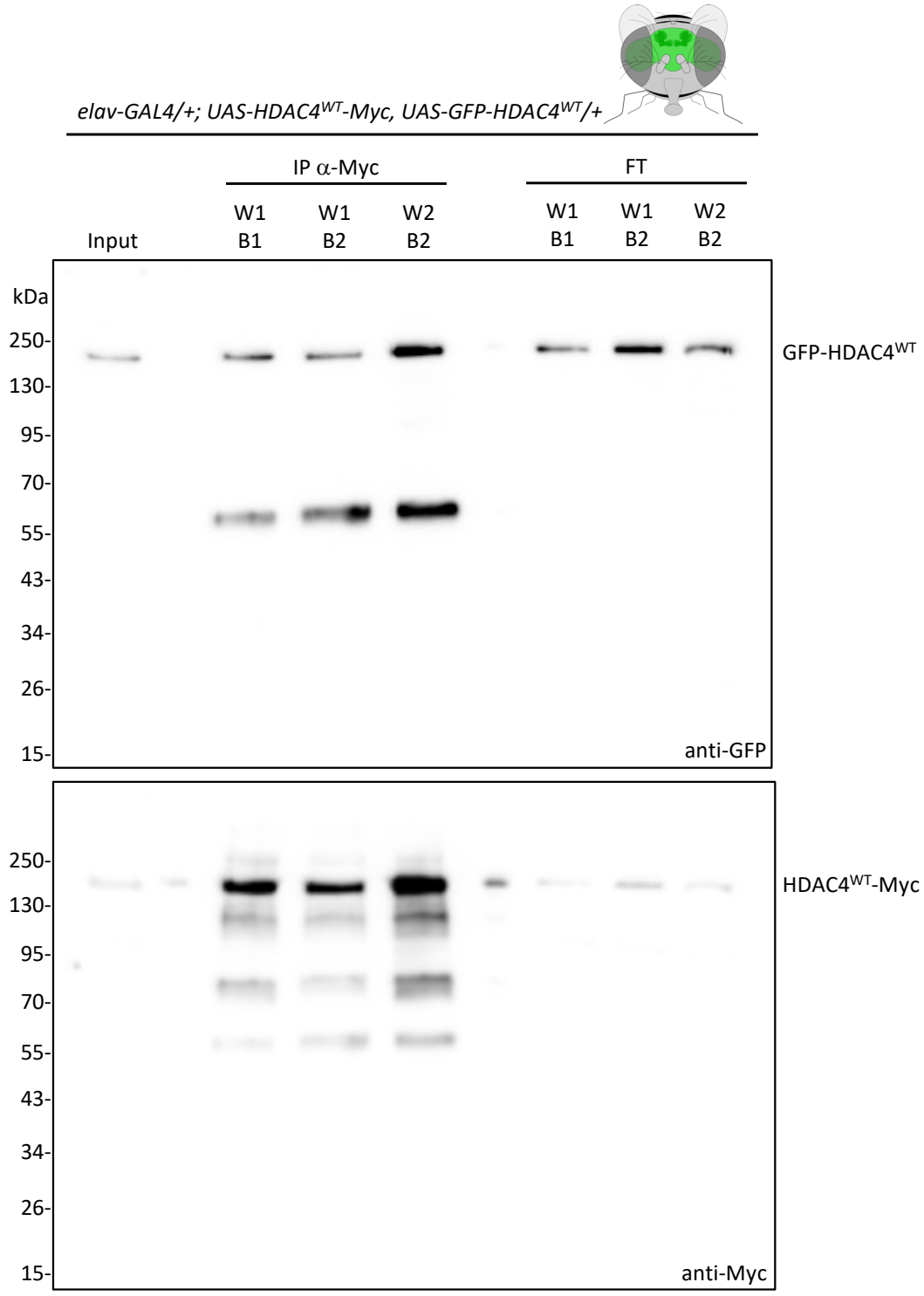

Figure 10.32 Final optimisation of the GFP-HDAC4^{WT} and HDAC4^{WT}-Myc co-immunoprecipitation (Protocol 2)

Co-immunoprecipitation experiments to further optimise immunoprecipitation of HDAC4^{WT}-Myc and co-immunoprecipitation of GFP-HDAC4^{WT}. Immunoprecipitation was performed using Protocol 2 and the A/G beads. GFP-HDAC4^{WT} and HDAC4^{WT}-Myc were expressed pan-neuronally in *Drosophila* under the control of *elav-GAL4*. Flies were raised at 18°C until adulthood and then moved to 22°C for five days to increase the level of transgene expression before harvesting and generation of whole-head lysates. Input sample is 30 µg of whole-cell lysate. GFP/Myc HDAC4^{WT} whole cell lysates were subjected to immunoprecipitation. W1, wash condition one, lysates were incubated for one hour at room

temperature with Myc-bound A/G beads and washes were performed using IP-buffer. W2, wash condition two, lysates were incubated overnight at 4°C with Myc-bound A/G beads and washes were performed using TBS-T. B1, bead batch one. B2, bead batch two. Western blotting using anti-GFP confirmed that GFP-HDAC4^{WT} was co-immunoprecipitated and with anti-Myc confirmed that HDAC4-Myc was immunoprecipitated under all conditions. Maximal yield of GFP-HDAC4^{WT} was obtained with W2, B2. Flowthrough (FT) is a sample of the lysate immediately after incubation with the antibody-bead complex (non-captured proteins, ~30 µg). Strong bands at ~50 kDa were observed in the IP lanes of the anti-GFP blot. Both immunoprecipitation and detection were performed using antibodies raised in rabbit. This band is therefore likely denatured Myc antibody heavy chain as it was absent from inputs. Detection was performed using VeriBlot detection reagent to minimise detection of denatured antibody.

10.4.3.2. Optimisation and validation of the subcellular fractionation protocol

Three different subcellular fractionation protocols (P1-P3) were tested to determine an approach to enrich for the nuclear pool of HDAC4^{3SA}. Fractionations were performed on heads of wild-type flies (Canton S), then cytoplasmic and nuclear fractions were electrophoresed and probed with anti-lamin and anti-tubulin to assess nuclear and cytoplasmic fraction purity, respectively (Figure 10.33). Lamin was not detected in any of the cytoplasmic fractions, suggesting that none of the protocols resulted in inappropriately lysed nuclei. Lamin was most significantly enriched in the nuclear fractions from protocol 1, which also had the least cytoplasmic contamination as deduced from tubulin intensity. Protocol 1 is detailed in the methods, Section 3.2.3, and involves use of the ThermoFisher NE-PER nuclear and cytoplasmic extraction reagents. As these are proprietary, it was unclear whether the nuclear extraction reagent is an appropriate buffer for immunoprecipitation, therefore this was compared to nuclear lysis using IP-buffer (P1.1 vs P1.2). There appeared to be no significant difference in efficiency of nuclear lysis between the two, therefore for immunoprecipitation, nuclear lysis was performed using IP-buffer, and for all other applications nuclear lysis was performed using the nuclear extraction reagent.

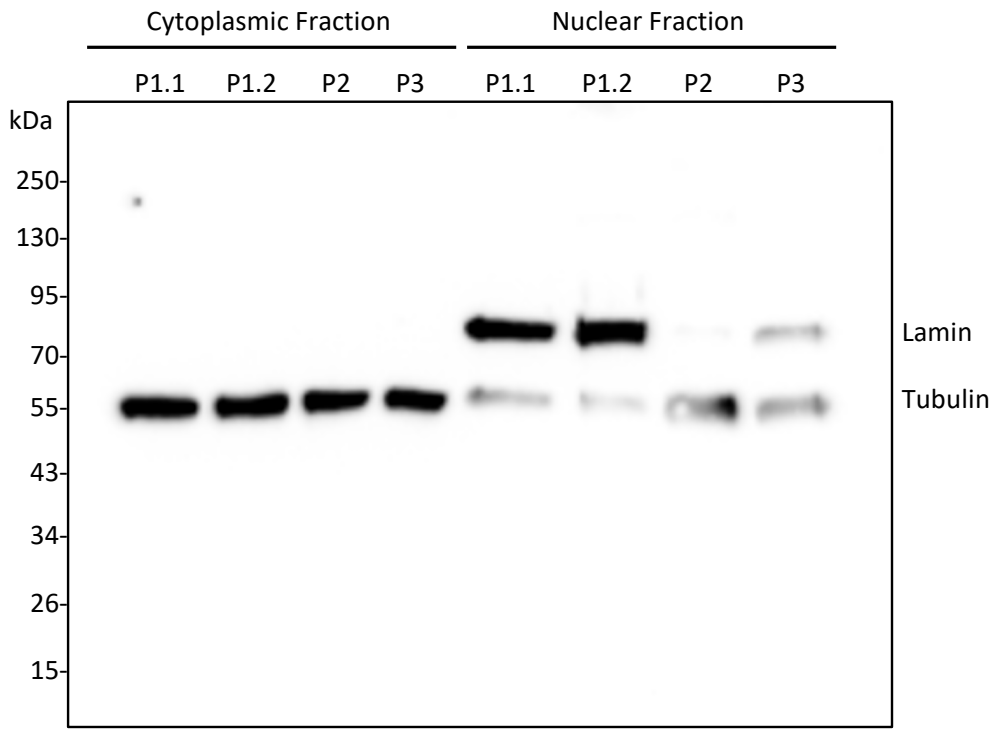

Figure 10.33 Comparison of protocols for subcellular fractionation from *Drosophila* heads

Heads of wild-type flies (*Canton S*) were subjected to fractionation using three different subcellular fractionation protocols (P1-3). P1 was performed as per methods; P1.1 utilised the nuclear extraction reagent while P1.2 utilised IP-buffer. P2 and P3 were alternative ineffective protocols and for brevity are not described here. Nuclear and cytoplasmic lysates were subjected to western blotting using anti-lamin and anti-alpha-tubulin antibodies concurrently and are therefore displayed on the same blot. The highest yield of lamin was obtained for P1, and there was little difference in nuclear lysis for P1.1 and P1.2.

To further reduce cytoplasmic contamination of nuclear fractions, the fractionation protocol was tested using either two or four washes of the nuclear pellet (Figure 10.34). A sample of each of the washes was also electrophoresed to compare changes in tubulin intensity to examine wash efficacy. Across washes 1-4 the intensity of tubulin decreased, where none was detected in the fourth wash, confirming that each wash effectively removed cytoplasmic contamination of the nuclear pellet. The intensity of tubulin in the nuclear lysate produced from the four-wash protocol was significantly reduced compared to that of the two-wash protocol, however some contamination remained. Given that both protocols resulted in a significant enrichment of nuclear proteins compared to the whole cell lysate input (as assessed by comparison of lamin intensity), but still resulted in some cytoplasmic contamination, the 4x wash protocol was not further pursued due to the scale required for IP-MS, and the cost this would impose.

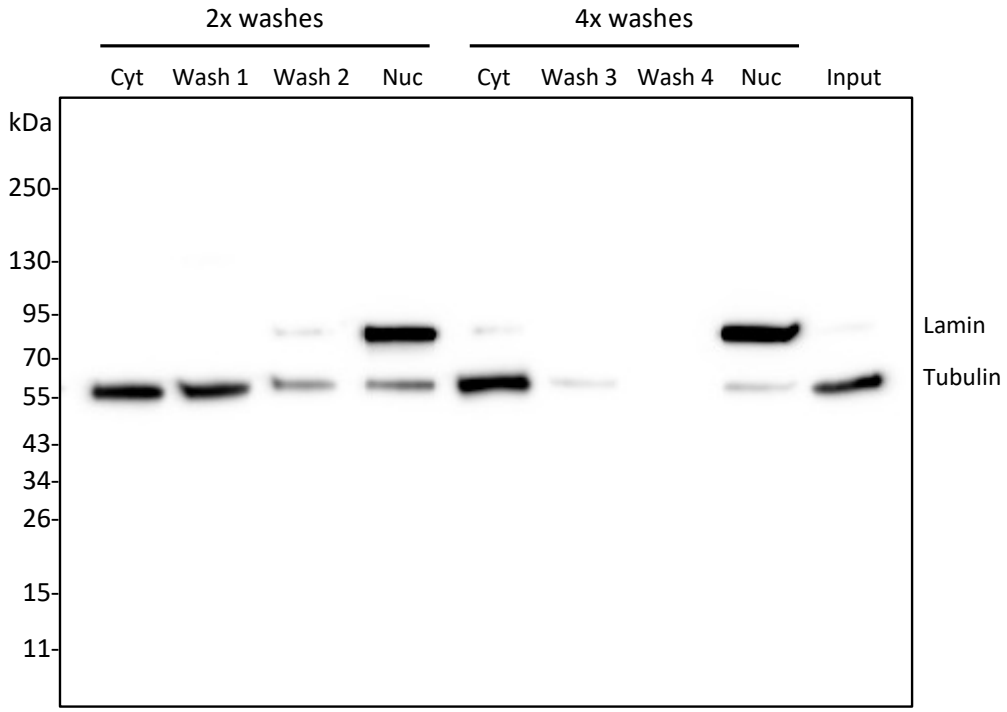

Figure 10.34 Optimisation of wash conditions for effective subcellular fractionation from *Drosophila* heads
Heads of wild-type flies (*Canton S*) were subjected to subcellular fractionation with either two or four wash steps of the nuclear pellet. Nuc and cyt were nuclear and cytoplasmic fractions respectively. Wash 1-4 were samples (same volume) of the wash steps to examine the level of cytoplasmic contamination and nuclear lysis. Input is a whole-cell lysate (30 µg). Lysates were subjected to western blotting using anti-lamin and anti-alpha-tubulin antibodies concurrently and are therefore displayed on the same blot. The 4x wash protocol gave a nuclear sample with less cytoplasmic contamination (as assessed by tubulin intensity) than the 2x wash protocol.

10.4.3.3. Immunoprecipitation of HDAC4^{3SA} from nuclear lysates

Finally, to determine the efficacy of immunoprecipitation from nuclear lysates and relative abundance of co-precipitating proteins, colloidal Coomassie staining was performed on eluates of immunoprecipitations prepared from nuclear lysates of heads of control and HDAC4^{3SA} expressing flies (Figure 10.35). Following selection of the driver and expression conditions (Section 10.4.4) HDAC4^{3SA} expression was driven by *OK107-GAL4* in the presence of the TARGET system; flies were raised at 18°C to maximise progeny counts then transferred to 30°C for three days to induce *HDAC4^{3SA}* expression. The control sample was generated from flies that did not express *HDAC4^{3SA}* but were otherwise of the same genetic background (*tubulin-GAL80ts/+; +; OK107-GAL4/+*). Immunoprecipitation from HDAC4^{3SA}-expressing samples resulted a similar profile of bands to that of controls, suggesting that many of the bands correlate to either antibody leaching from the beads, or non-specific enrichment of proteins. The band at ~144 kDa in the HDAC4^{3SA} lane is significantly more intense than that in the control, and could represent a doublet band, of which one band would be expected to be

immunoprecipitated HDAC4. Band intensity was enriched overall in the HDAC4^{3SA} expressing sample, which may represent candidate HDAC4^{3SA} interactors, or a normal level of variation in immunoprecipitation efficiency.

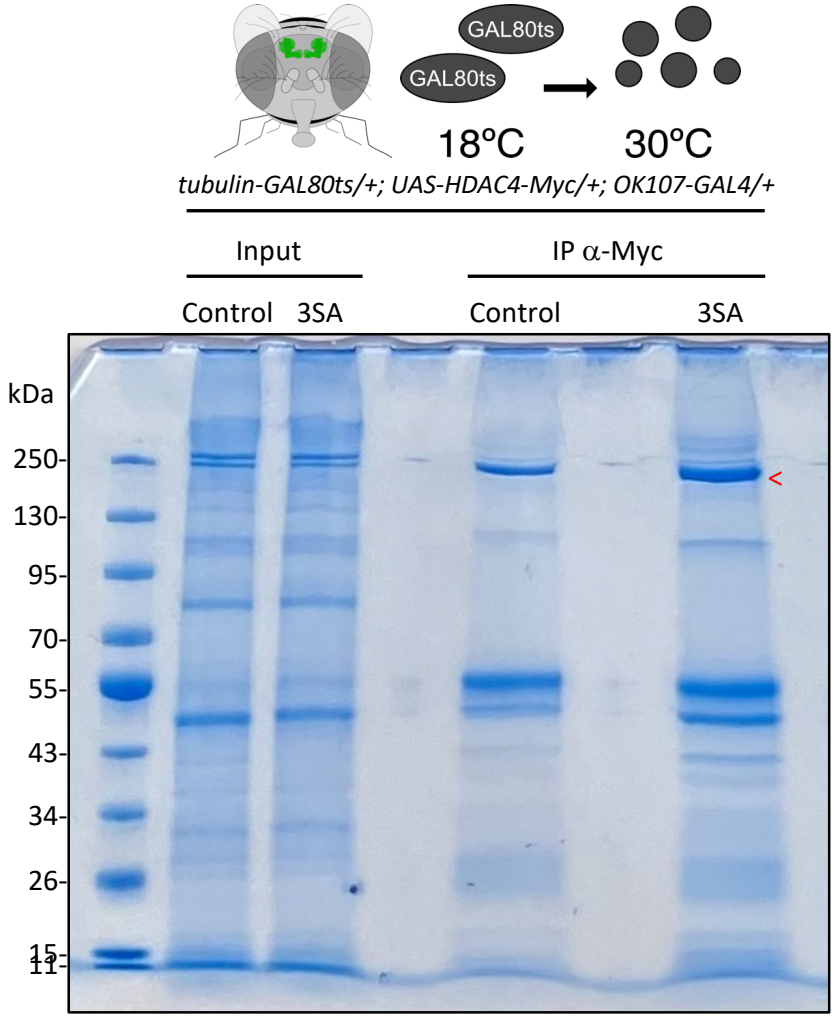

Figure 10.35 Colloidal Coomassie gel of anti-Myc immunoprecipitates from nuclear fractions

Anti-Myc immunoprecipitation (Protocol 2) on heads of flies expressing *HDAC4^{3SA}-Myc* under the control of *OK107-GAL4* in the presence of the TARGET system; flies were raised at 18°C to maximise progeny counts then adults were transferred to 30°C for three days to induce HDAC4^{3SA} expression. Control is *tubulin-GAL80ts/+; +; OK107-GAL4/+*. Input is a sample of the lysate prior to immunoprecipitation (30 µg total protein). Immunoprecipitation (IP) is the eluate from the immunoprecipitation. Colloidal Coomassie staining showed a significant reduction in the number of bands in the eluate compared to the input sample. Red arrow indicates the band at ~144 kDa which was hypothesised to be HDAC4^{3SA}-Myc.

10.4.4. Selection of the driver and conditions in which to raise flies for IP-MS analysis

To best characterise interactors of HDAC4 aggregates, the conditions for transgene expression and subsequent HDAC4 aggregation were further examined. This included examination of $HDAC4^{WT}$ aggregates upon increased dose in Kenyon cells, as well as comparison of expression level and subcellular distribution of $HDAC4^{3SA}$ when expressed under the control of *elav-GAL4* and *OK107-GAL4*, and the resulting distribution and aggregation level in the adult brain.

10.4.4.1. HDAC4 aggregation characteristics alter significantly with increased dose

As increased dose of HDAC4 increases aggregation (Section 5.6.1) the aggregation of $HDAC4^{WT}$ in Kenyon cells was first examined when expressed under the control of *OK107-GAL4* in the absence of the TARGET system. HDAC4 expression level was altered by the number of genomic insertions, where heterozygotes for $HDAC4^{WT}$ (*UAS-HDAC4^{WT}/+; OK107-GAL4/+)* were compared to homozygotes (*UAS-HDAC4^{WT}/UAS-HDAC4^{WT}; OK107-GAL4/+*). $HDAC4^{WT}$ was expressed throughout development in the mushroom body under the control of *OK107-GAL4*; flies were raised at 25°C and brains were dissected from adult flies and immunostained for HDAC4 and DAPI (Figure 10.36).

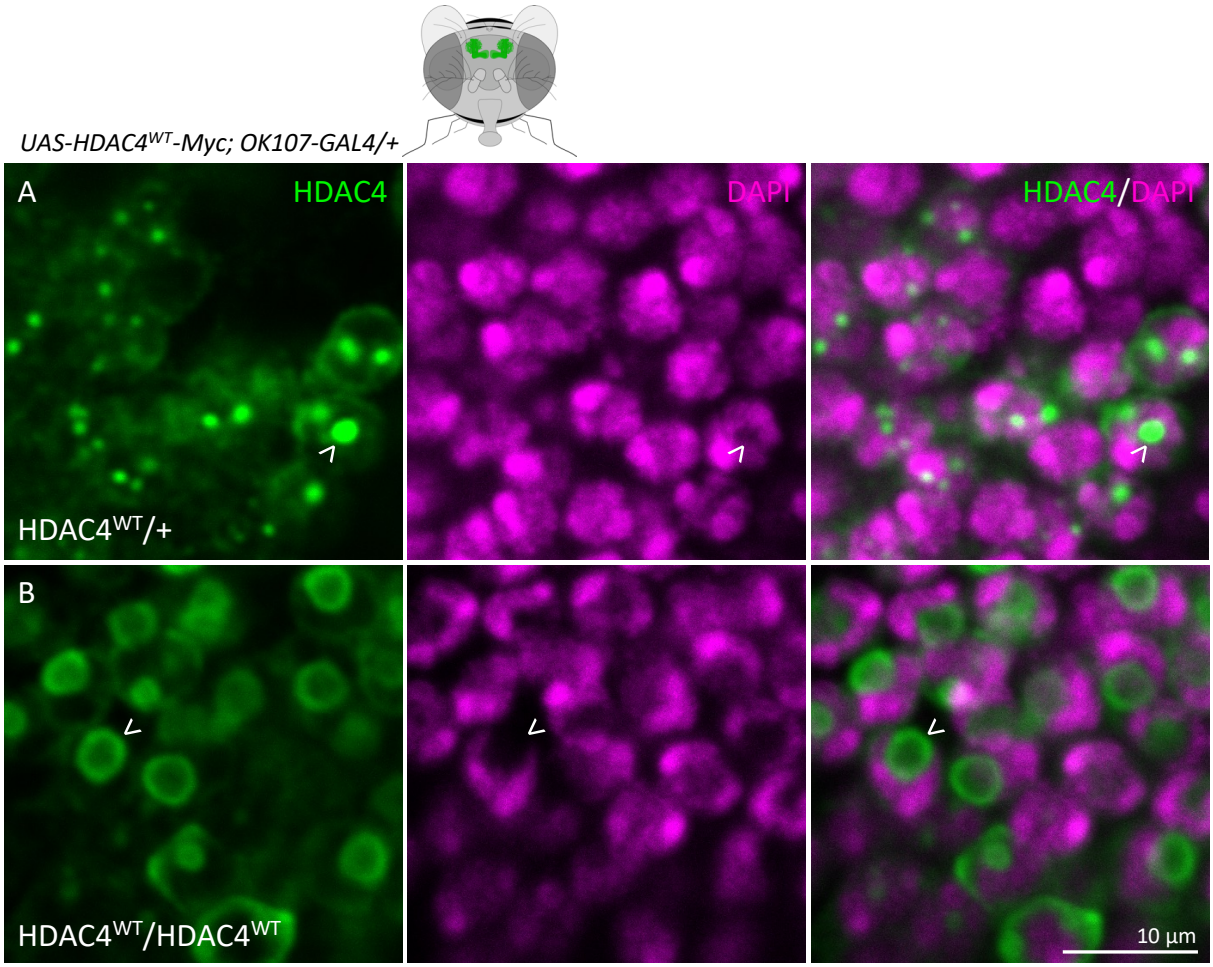

Figure 10.36 HDAC4^{WT} forms aggresome-like inclusions in Kenyon cells upon increased dose

(A-B) Single optical section (0.5 µm) through Kenyon cells in the posterior of the brain of flies expressing HDAC4^{WT} (green) under the control of *OK107-GAL4*. DAPI (magenta) marks nuclei. Flies were raised at 25°C (A) Expression of HDAC4^{WT} from one genomic insertion (*UAS-HDAC4^{WT}*/+) resulted in large punctate aggregates, and (B) increasing the dose of HDAC4^{WT} by increasing the number of transgene insertions (*UAS-HDAC4^{WT}/ UAS-HDAC4^{WT}*) resulted in the appearance of aggresome-like inclusions. Arrowhead indicates an accumulation of HDAC4 that displaced DNA, observed as a loss of DAPI intensity.

Expression of HDAC4^{WT} in Kenyon cells of flies carrying one insertion of the transgene (Figure 10.36A) resulted in large punctate aggregates, significantly larger than those observed in the presence of the TARGET system (Figure 4.10), supporting the idea that prolonged expression of HDAC4 results in increasing severity of aggregation. Smaller aggregates of HDAC4 appeared to co-localise with DAPI, but as they increased in size, they began to displace DAPI staining, suggesting that larger aggregates do not contain DNA. HDAC4^{WT} was also still observed in cytoplasmic haloes surrounding nuclei. Upon increased dose, the number of aggregates per cell decreased while their size increased (Figure 10.36B). Flies harbouring two insertions of *HDAC4^{WT}* presented with more spheroid-like aggregates that were reminiscent of aggresomes (Johnston *et al.*, 1998); there was a ring of more intense HDAC4 staining around the outside of the aggregate and diffuse staining within. When these aggresome-like inclusions

were observed, there was typically only one per cell with few instances of two smaller spheroids, or a single spheroid inclusion with several punctate aggregates.

While the smaller aggregates of HDAC4^{WT} appeared nuclear, it was noted that many larger aggregates excluded DAPI staining, suggesting that they may be altering the organization of DNA and/or the morphology of the nucleus. To further examine this, 3D renderings from serial optical sections were generated, and these demonstrated that spheroid aggregates of HDAC4 displaced DAPI staining (Figure 10.37). However, it remained unclear whether these aggregates were within the nucleus, or perinuclear, similarly to traditional aggresomes (Johnston *et al.*, 1998).

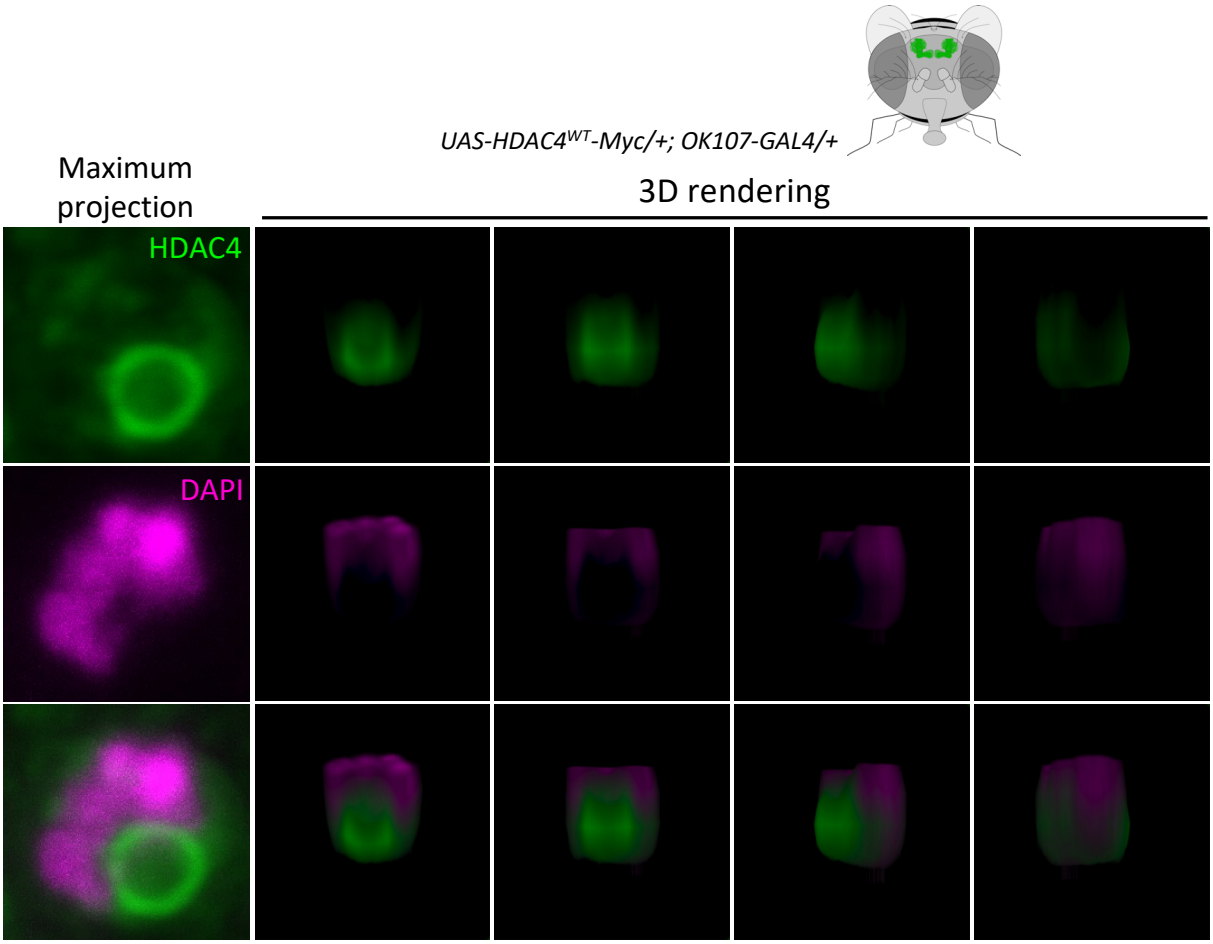

Figure 10.37 3D rendering of an aggresome-like HDAC4 inclusion shows HDAC4^{WT} displacement of DAPI staining
Maximum projection of optical sections (0.5 µm) through a Kenyon cell expressing HDAC4^{WT} (green) from two genomic insertions under the control of *OK107-GAL4*. DAPI (magenta) marks DNA. A 3D rendering of the aggresome-like inclusion was made using the 3D viewer plugin in ImageJ (Schmid *et al.*, 2010), which shows displacement of DAPI staining by the HDAC4 inclusion.

To further investigate the subcellular localisation of these aggregates, immunohistochemistry against lamin, which lines the nuclear envelope, was performed to compare the distribution of HDAC4^{WT} aggregates (Figure 10.38). Lamin counterstaining has previously been used to

determine the subcellular localisation of aggregates (Chapple *et al.*, 2008); it was hypothesised that if rings of lamin surrounded the aggresome-like inclusions as well as surrounding the nuclear periphery, this would indicate cytoplasmic localisation. Lamin was only observed at the nuclear periphery of Kenyon cells expressing $HDAC4^{WT}$ regardless of dose, and did not surround aggresome-like inclusions, suggesting that these were nuclear. Interestingly, lamin staining was observed within the largest aggresome-like inclusions (Figure 10.38C, inset), suggesting they may be sequestering components of the nuclear envelope.

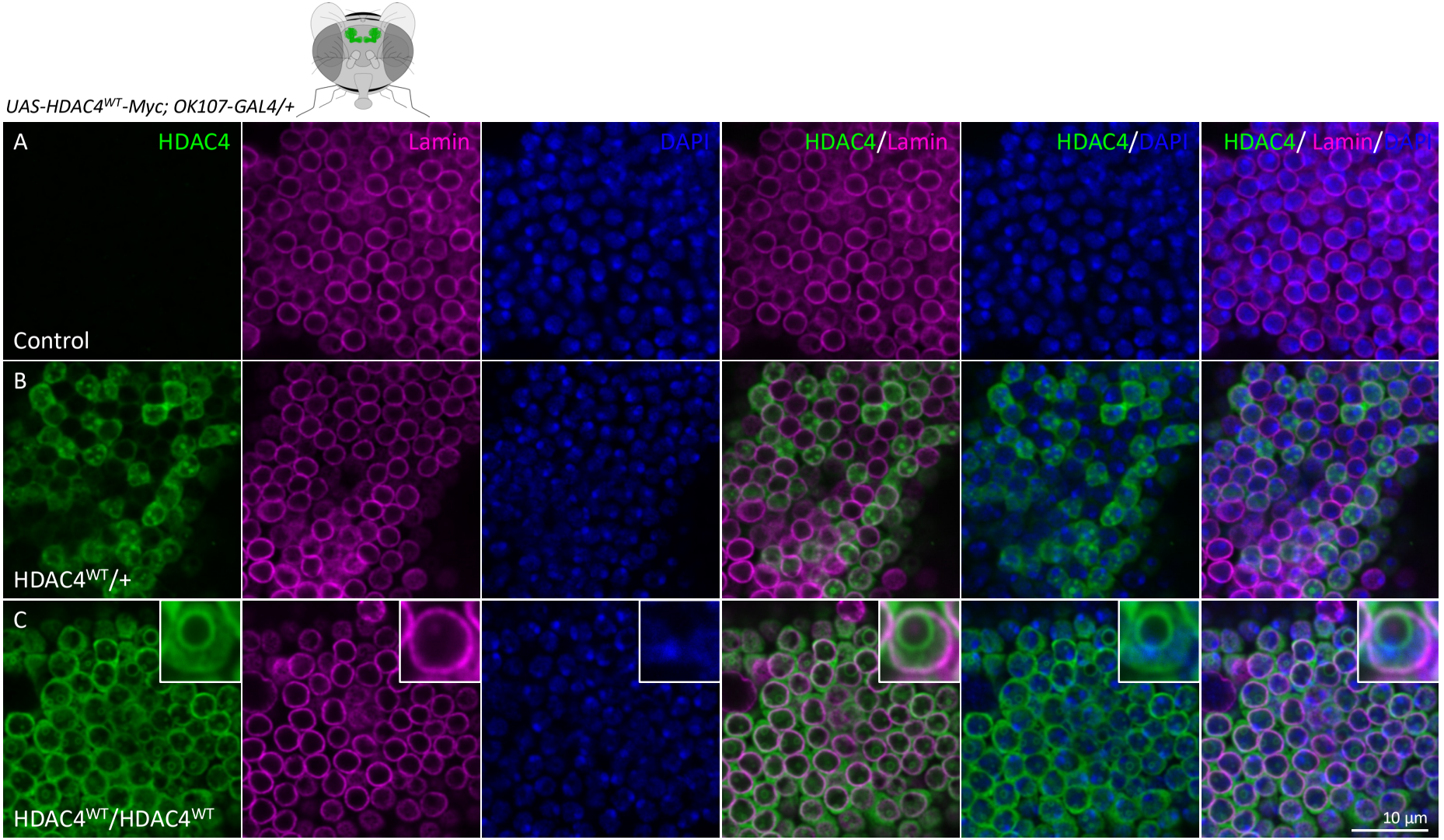

Figure 10.38 Aggresome-like inclusions of HDAC4^{WT} are localised within the nuclear envelope

Single optical sections (0.5 µm) through the Kenyon cells of HDAC4^{WT} (green) expressed under the control of *OK107-GAL4* relative to lamin (magenta), which marks the nuclear envelope. DAPI is shown in blue. Flies were raised at 25°C. (A) Control is *OK107-GAL4/+*. (B) Expression of HDAC4^{WT} from one

genomic insertion (*UAS-HDAC4^{WT}/+*) resulted in large punctate aggregates that were observed within the bounds of lamin staining. (C) Expression of HDAC4^{WT} from two genomic insertions (*UAS-HDAC4^{WT}/UAS-HDAC4^{WT}*) resulted in the formation of aggresome-like spheroids that were observed within the bounds of the nucleus. Inset shows the sequestration of lamin within a large aggresome-like inclusion.

Given the significant change in dynamics of HDAC4^{WT} aggregation upon increased dose, it was of interest to see how this affected sequestration of MEF2. Immunohistochemistry for HDAC4^{WT} and endogenous MEF2 was performed on brains of flies either hetero- or homozygous for *HDAC4^{WT}*, with expression driven by *OK107-GAL4* (Figure 10.39). As previously shown, punctate HDAC4^{WT} inclusions sequestered MEF2, which otherwise remained relatively uniformly distributed within nuclei (Figure 10.39B). MEF2 was absent from regions of intense DAPI staining; these have previously been demonstrated to be distinct nuclear domains of heterochromatin (Chiolo *et al.*, 2011). When HDAC4^{WT} was increased in dose, it formed aggresome-like inclusions (Figure 10.39C). Smaller aggresome-like inclusions had MEF2 within the interior, but as their size increased, MEF2 began to localise with HDAC4 at the periphery. MEF2 intensity elsewhere in the nucleus was significantly reduced where large inclusions were present.

Together these data demonstrate that significant disruption to the cell is occurring upon extreme overexpression of HDAC4, where HDAC4^{WT} aggregates are deposited into nuclear aggresome-like structures. It is unknown how physiological these are, as some studies have suggested that aggresome formation is a cell culture phenomenon and is rarely observed in disease conditions (Olzmann *et al.*, 2008). In light of identifying interactors of HDAC4 aggregates, it is in the best interest to characterise interactors of aggregates that are most representative of those observed in a disease context. Therefore, expression of HDAC4^{3SA} was further characterised (Section 6.3).

Finally, as aggresomes represent disruption of protein homeostasis (Johnston *et al.*, 1998), these findings also support the IP-MS data (presented in Sections 6.1 and 6.3) wherein HDAC4^{3SA} aggregates sequester components of the protein homeostasis machinery. Given that the morphology of HDAC4 aggregates was altered with increasing expression, with the formation of a striking outer ring, it is possible that components of HDAC4 aggregates may too be altered with dose.

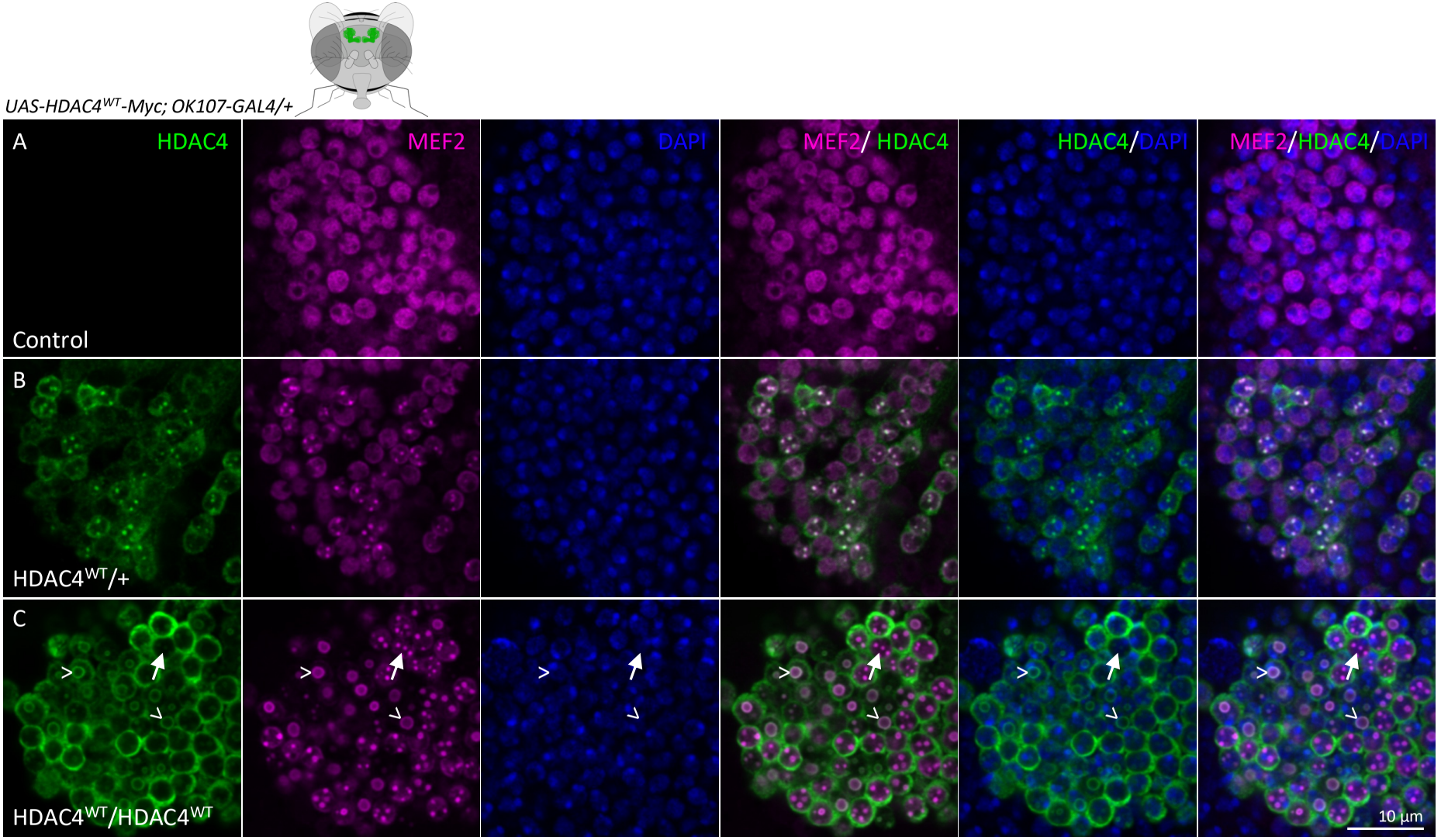

Figure 10.39 Aggresome-like inclusions of HDAC4^{WT} sequester and co-localise with MEF2

Single optical sections (0.5 µm) through the Kenyon cells of brains of flies expressing HDAC4^{WT} (green) under the control of *OK107-GAL4* relative to MEF2 (magenta). DAPI is shown in blue. Flies were raised at 25°C. (A) Control is *OK107-GAL4/+*. (B) Expression of HDAC4^{WT} from one genomic insertion

(*UAS-HDAC4^{WT}/+*) resulted in large punctate aggregates that sequestered MEF2. (C) Expression of HDAC4^{WT} from two genomic insertions (*UAS-HDAC4^{WT}/UAS-HDAC4^{WT}*) resulted in the formation of aggresome-like spheroids that either sequestered MEF2 (arrow), or when increased in size, co-localised with MEF2 (arrowhead).

10.4.4.2. *OK107-GAL4* drives higher total expression of HDAC4^{3SA} compared to *elav-GAL4*

Subcellular fractionation and western blotting were used to determine relative abundance of HDAC4^{3SA} in nuclear and cytoplasmic preparations when expressed under the control of either *elav-GAL4* or *OK107-GAL4* (Figure 10.40). Flies were raised at 18°C to maximise progeny counts and then transferred to 30°C for three days to increase the level of *HDAC4^{3SA}* expression. *OK107-GAL4* drove higher expression of total HDAC4^{3SA} (Figure 10.40B) in both the nuclear and cytoplasmic fractions compared to *elav-GAL4* (Figure 10.40C). However, proportionally, HDAC4^{3SA} was more nuclear under the control of *elav-GAL4* than *OK107-GAL4*, being 66% and 49% nuclear respectively. It is noted that these proportions were derived from only two replicates, therefore no strong conclusions about the significance of these differences can be made. It remains unclear whether this shift in distribution is only occurring in a subset of cells not common between the drivers, or whether this is a dose-dependent effect on distribution (Section 5.6.1). Given that *OK107-GAL4* resulted in a higher total level of HDAC4^{3SA} within the nuclear fraction this driver was selected for further examination.

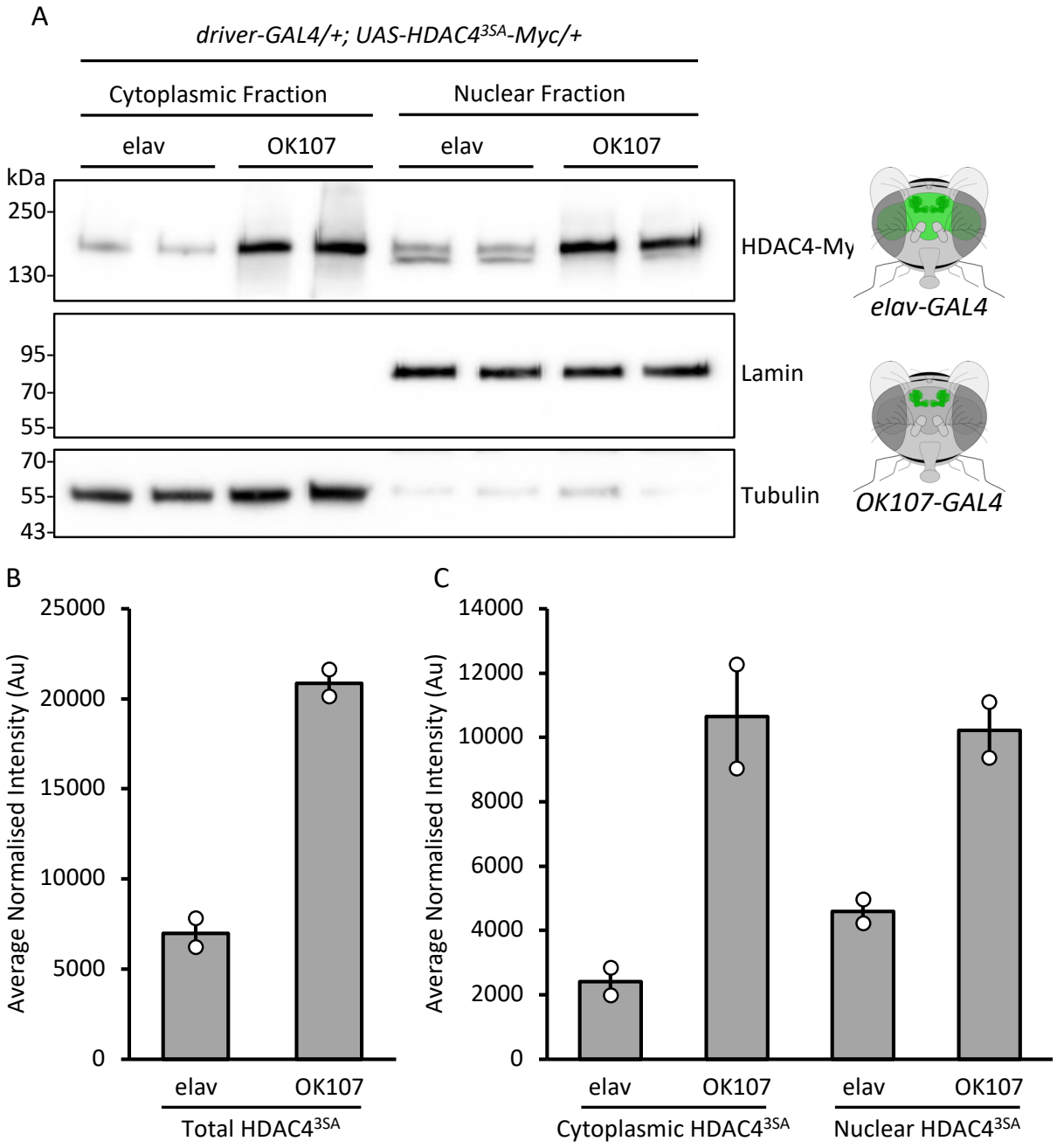

Figure 10.40 Nuclear HDAC4^{3SA} protein levels are increased under the control of *OK107-GAL4* compared to *elav-GAL4*

Subcellular fractionation on heads of flies expressing *HDAC4^{3SA}* under the control of *elav-GAL4* or *OK107-GAL4*. Flies were raised at 18°C to maximise progeny counts. Following eclosion, adult flies were transferred to 30°C for three days to increase HDAC4^{3SA} expression before harvesting. (A) Western blot of cytoplasmic and nuclear fractions. Anti-lamin and anti-alpha-tubulin show relative levels of nuclear and cytoplasmic proteins respectively. (B-C) Quantification of band intensity. elav, *elav-GAL4*; OK107, *OK107-GAL4*. Driver refers to either *elav-GAL4* or *OK107-GAL4*. (B) Quantification of total band intensity. Nuclear and cytoplasmic HDAC4^{3SA} intensity was measured, and normalised to lamin and tubulin respectively, then the normalised values were added (nuc + cyt) for each independent preparation and averaged between preparations to give average normalised intensity. Total HDAC4^{3SA} intensity was increased under the control of *OK107-GAL4* compared to *elav-GAL4*. (C) Quantification of nuclear and cytoplasmic band intensity. Nuclear and cytoplasmic HDAC4^{3SA} intensity was measured, and normalised to lamin and tubulin respectively, then the normalised values

were added for each nuclear and cytoplasmic preparation (nuc + nuc, cyt + cyt) and averaged to give average normalised intensity. HDAC4^{3SA} intensity for each cytoplasmic and nuclear fraction was increased for *OK107-GAL4* compared to *elav-GAL4*.

10.4.4.3. Addition of the TARGET system does not significantly alter the levels or subcellular distribution of HDAC4^{3SA}

While *OK107-GAL4* drives higher levels of transgene expression in both the mushroom body (Section 4.1) and in head lysates compared to *elav-GAL4* (Section 10.4.4.2), it is unclear whether high levels of HDAC4^{3SA} expression affects the development of these cells. Therefore, it was desirable to add the TARGET system to mitigate any developmental effects, however it was unclear whether this would affect total HDAC4 levels. To address this, subcellular fractionation was performed on flies expressing HDAC4^{3SA} under the control of *OK107-GAL4* in the presence and absence of the TARGET system, to induce post-developmental transgene expression (Figure 10.41A). All flies were raised at 18°C until eclosion, then transferred to 30°C for three days to induce/increase transgene expression. Incorporation of the TARGET system had a negligible effect on total HDAC4^{3SA} levels (Figure 10.41B) and did not significantly alter the subcellular distribution of HDAC4^{3SA} (Fig 10.41C), being 60% and 56% nuclear in the absence and presence of the TARGET system respectively. These data agree with McGuire *et al.* (2003), where it was demonstrated that at temperatures exceeding 30°C, the level of transgene expression was no different in the presence or absence of the TARGET system. This confirms that addition of the TARGET system enables post-developmental expression without significantly sacrificing level of HDAC4^{3SA} expression.

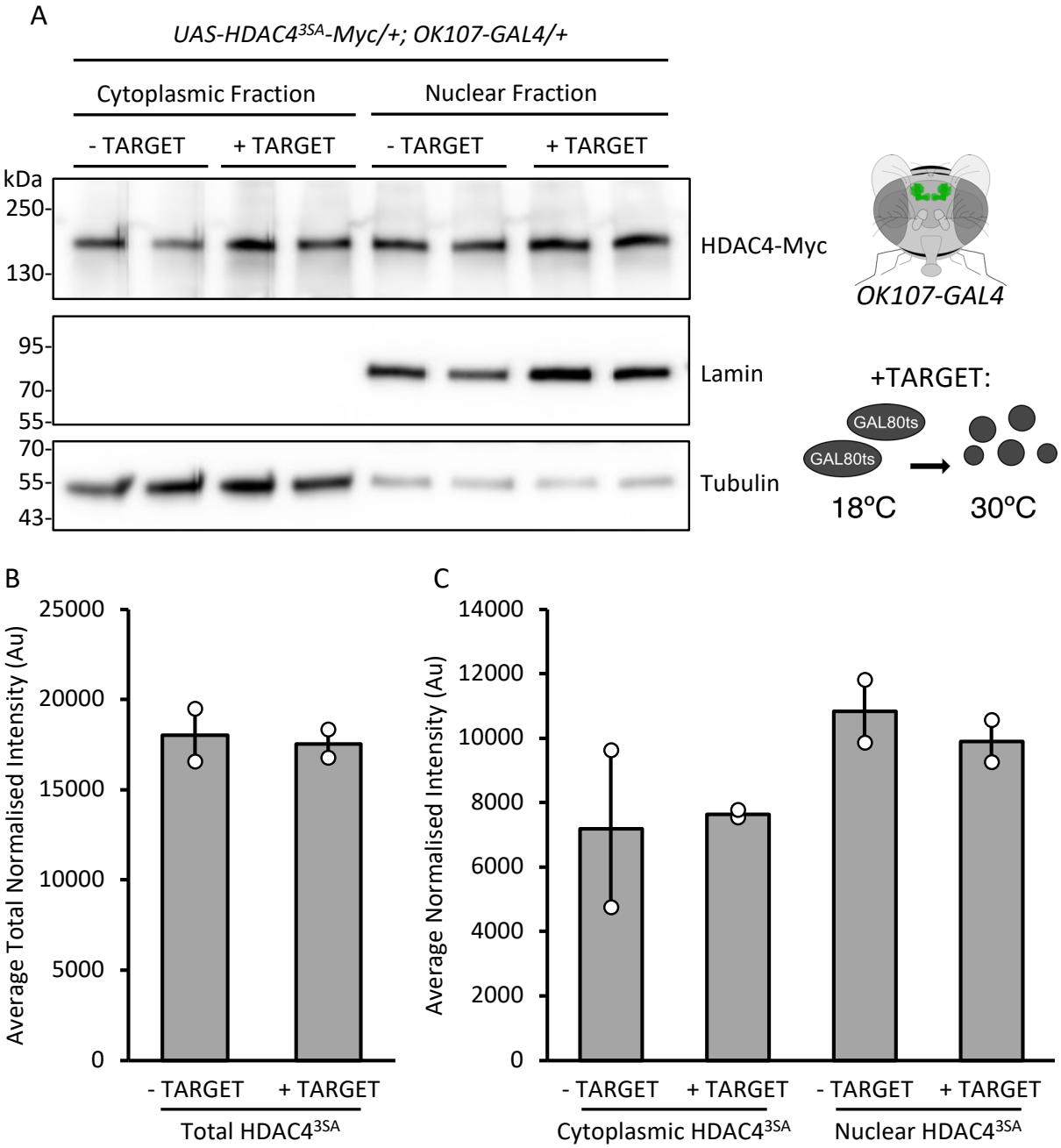

Figure 10.41 There is no significant change in total HDAC4^{3SA} level or subcellular distribution in the presence of the TARGET system

Subcellular fractionation on heads of flies expressing HDAC4^{3SA} under the control of *OK107-GAL4* in the absence (- TARGET) and presence (+ TARGET) of the TARGET system. +TARGET genotype was *tubulin-GAL80ts/+; UAS-HDAC4^{3SA}/+; OK107-GAL4/+*. -TARGET genotype was *+; UAS-HDAC4^{3SA}/+; OK107-GAL4/+*. Flies were raised at 18°C to maximise progeny counts and prevent HDAC4^{3SA} expression in the presence of the TARGET system. Following eclosion, adult flies were transferred to 30°C for three days to induce/increase HDAC4^{3SA} expression before harvesting. (A) Western blot of cytoplasmic and nuclear fractions. Anti-lamin and anti-alpha-tubulin show relative levels of nuclear and cytoplasmic proteins respectively. (B-C) Quantification of band intensity. (B) Quantification of total band intensity. Nuclear and cytoplasmic HDAC4^{3SA} intensity was measured, and normalised to lamin and tubulin respectively, then the normalised values were added (nuc + cyt) for each independent preparation and averaged between preparations to give average normalised intensity. There was no notable difference in total HDAC4^{3SA} intensity in the presence or absence of TARGET.

(C) Quantification of nuclear and cytoplasmic band intensity. Nuclear and cytoplasmic HDAC4^{3SA} intensity was measured, and normalised to lamin and tubulin respectively, then the normalised values were added for each nuclear and cytoplasmic preparation (nuc + nuc, cyt + cyt) and averaged to give average normalised intensity. HDAC4^{3SA} intensity for each cytoplasmic and nuclear fraction varied but there was no significant difference in the presence or absence of the TARGET system.

10.4.4.4. Comparison of HDAC4^{3SA} distribution in the brain and aggregate formation in Kenyon cells resulting from expression under the control of *elav-GAL4* or *OK107-GAL4* in the presence and absence of the TARGET system

To further investigate the distribution and aggregation of HDAC4^{3SA} under different expression conditions, immunohistochemistry was performed on whole brains (Figures 10.42-10.43). Brains were dissected from adult flies expressing HDAC4^{3SA} under the control of *elav-GAL4* or *OK107-GAL4*, as well as *OK107-GAL4* +TARGET. All flies were raised at 18°C until eclosion, then transferred to 30°C for three days to induce/increase transgene expression. Brains were incubated with antibodies against endogenous MEF2, and Myc to detect HDAC4^{3SA}. Gain settings were kept constant between genotypes allowing the direct comparison of intensity and abundance.

As imaged from the anterior of the brain, endogenous MEF2 expression was observed strongly in the nuclei surrounding the antennal lobes as well as within the optic lobes (Figure 10.42A). HDAC4^{3SA} was present in a greater proportion of nuclei in the anterior when expressed under the control of *elav-GAL4* than *OK107-GAL4*, consistent with the previously demonstrated distributions of these drivers (Section 4.1). Localisation of HDAC4^{3SA} to the γ lobe of the mushroom body was also observed when driven by *OK107-GAL4* (Figure 10.42B), which was also evident for *elav-GAL4* and *OK107-GAL4* +TARGET in single optical sections (Figure 10.42F-H). Low level HDAC4^{3SA} expression was also observed in the α and β lobes, and it was also observed to aggregate in nuclei below the antennal lobe (Figure 10.42I-L). MEF2 expression was variable among these cells; expression was low in cells in which HDAC4^{3SA} was expressed, and unlike in Kenyon cell nuclei, MEF2 was not observed to redistribute into HDAC4^{3SA} aggregates. It is unclear whether this staining represents MEF2 protein, or nonspecific antibody binding due to the low intensity of the signal.

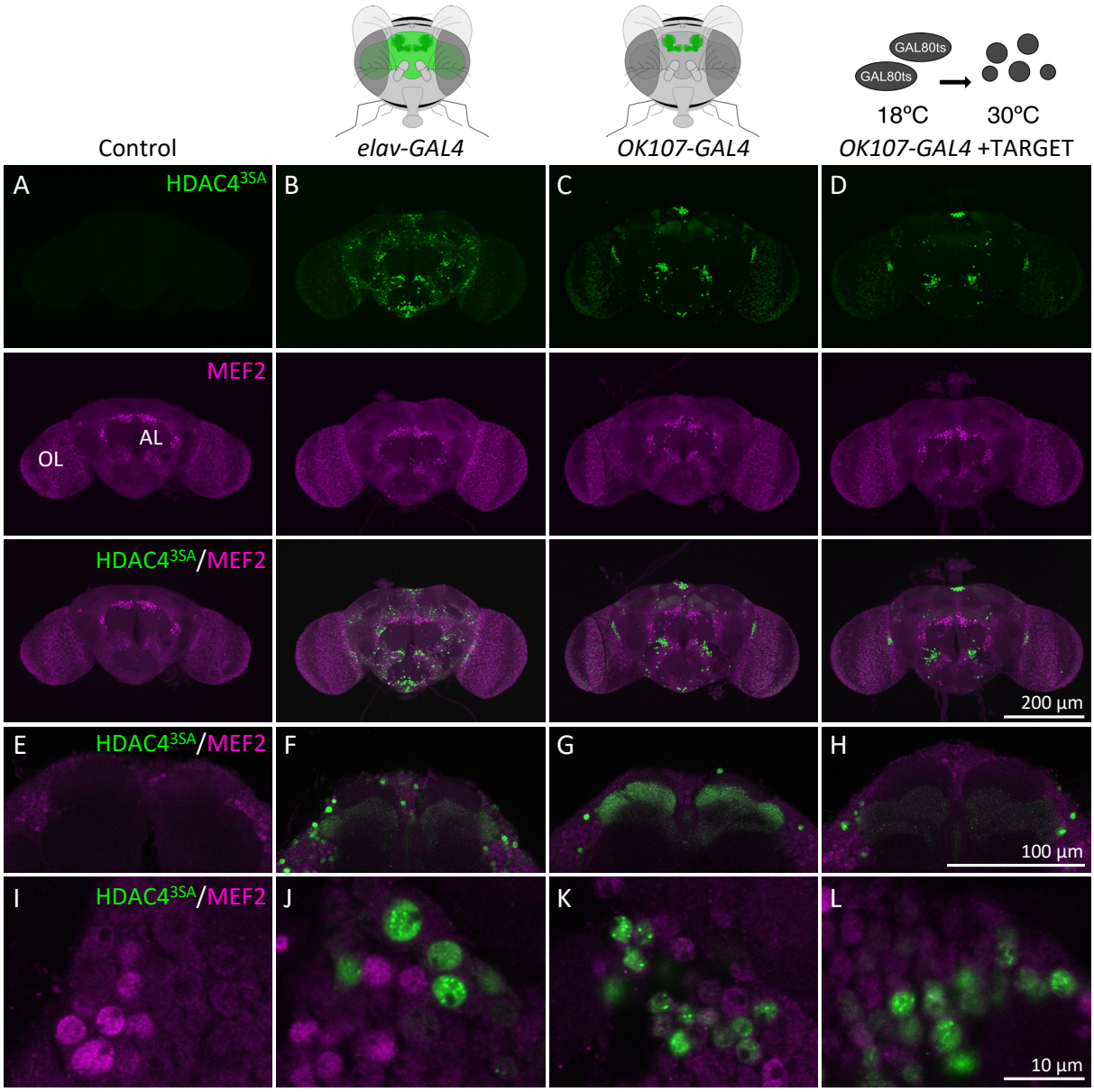

Figure 10.42 Distribution of HDAC4^{3SA} and MEF2 in the anterior of the adult brain
Immunohistochemistry on the anterior of brains expressing HDAC4^{3SA} under the control of *elav-GAL4*, *OK107-GAL4* or *OK107-GAL4* in the presence of the TARGET system. All flies were raised at 18°C until eclosion, where adults were transferred to 30°C for three days to induce/increase HDAC4 expression. Control is wild-type flies (*Canton S*). (A-D) Maximum projection of optical sections (1 µm) through the anterior of the brain. MEF2 (magenta) was observed in nuclei across the brain, while HDAC4 (green) distribution was variable, but consistent with previously demonstrated distributions for each driver (Section 4.1). OL, optic lobe; AL, antennal lobe. (E-H) Single optical sections (1 µm) through the γ lobe of the mushroom body showed distribution of HDAC4^{3SA} to this lobe independent of driver type. (I-L) Single optical sections (0.5 µm) through nuclei below the antennal lobe. HDAC4^{3SA} expression was observed and nuclear aggregates formed, however these did not appear to sequester MEF2.

In the posterior of the brain, MEF2 was primarily localised to nuclei of Kenyon cells and was also observed at the edges of the optic lobe (Figure 10.43A, E). Expression of HDAC4^{3SA}, regardless of the driver, significantly increased total MEF2 intensity in Kenyon cells (Figure 10.43F-H). Under the control of *OK107-GAL4*, HDAC4^{3SA} was observed mainly in Kenyon cells, whereas a wider distribution in the central brain and optic lobes was observed with *elav-GAL4* (compare Figure 10.43C with B), again consistent with their previously observed distributions (Section 4.1). HDAC4^{3SA} aggregate size and number varied widely between the different drivers and conditions, visible in both maximum projections through the Kenyon cell layer as well as in single optical sections (Figure 10.43F-H, J-L). As previously shown, *OK107-GAL4* +TARGET driven expression of HDAC4^{3SA} resulted in a punctate distribution in Kenyon cell nuclei, forming many aggregates that sequestered MEF2 (compare Figures 10.43L and 5.8). In contrast, when driven by *elav-GAL4*, the punctate distribution reduced, and HDAC4^{3SA} was observed in larger nuclear aggregates at a higher frequency (Figure 10.43J). Expression under the control of *OK107-GAL4* resulted in a complete loss of punctate staining and significantly larger aggregates than *elav-GAL4* (Figure 10.43K). Cells with larger aggregates consistently had fewer foci than cells with smaller aggregates. It is unclear whether the aggregate size observed for *OK107-GAL4* may be reflective of physiological aggregation in a disease context, or is simply a result of extreme chronic overexpression, therefore further investigation of HDAC4 aggregate composition was sought using *OK107-GAL4* +TARGET.

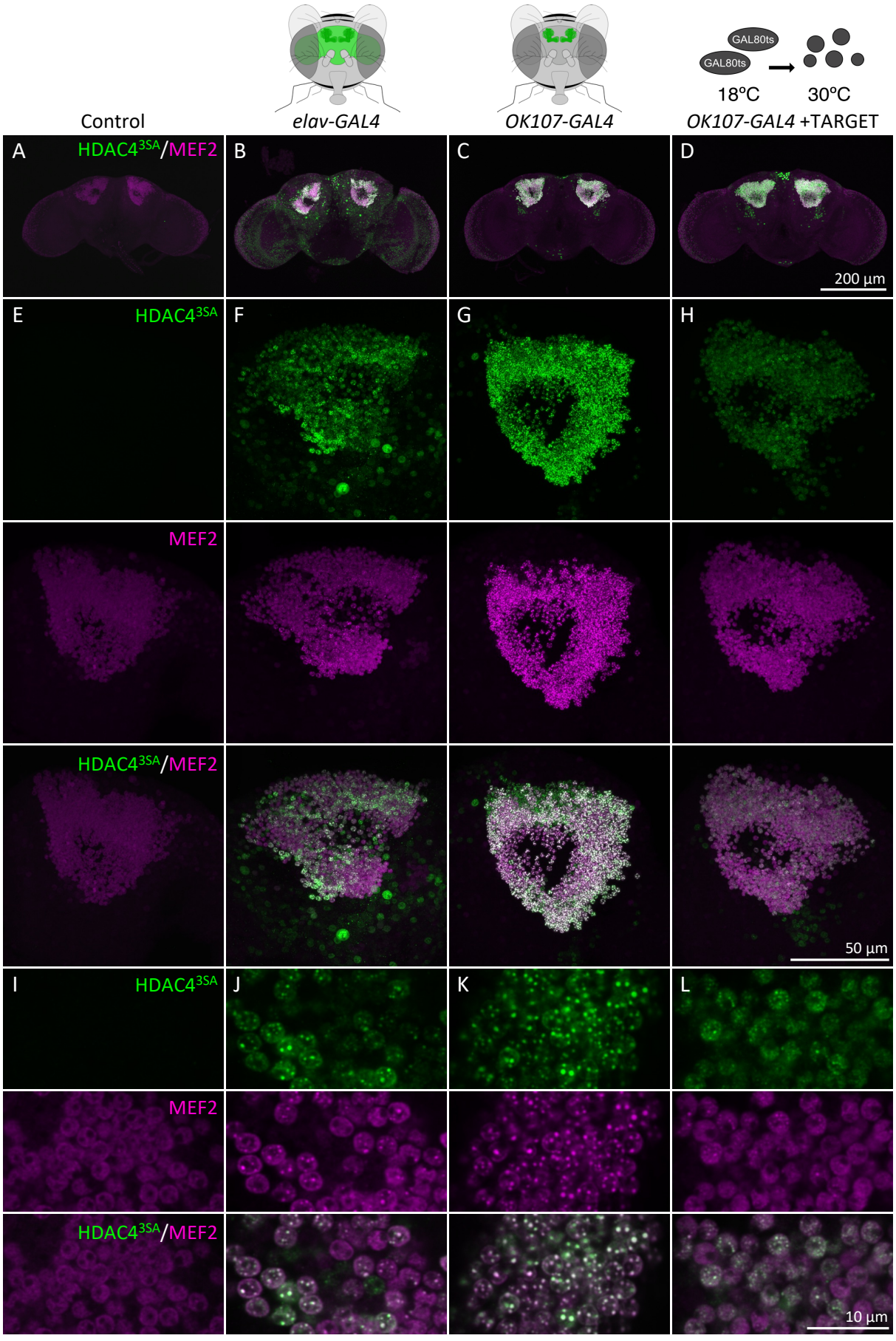

Figure 10.43 Distribution of HDAC4^{3SA} and MEF2 in the posterior of the adult brain

Immunohistochemistry on the posterior of brains expressing HDAC4^{3SA} under the control of *elav-GAL4*, *OK107-GAL4* or *OK107-GAL4* in the presence of the TARGET system. All flies were raised at 18°C until eclosion, where adults were transferred to 30°C for three days to induce/increase HDAC4 expression. Control is wild-type flies (*Canton S*). (A-D) Maximum projection of optical sections (1 μm) through the anterior of the brain. MEF2 (magenta) was observed predominantly in Kenyon cell nuclei, while HDAC4 (green) distribution was variable, but consistent with previously demonstrated distributions for each driver (Section 4.1). (E-H) Maximum projection of single optical sections (0.5 μm) through the Kenyon cell layer showed co-distribution of HDAC4^{3SA} with MEF2 in nuclei and in aggregates. (I-L) Single optical section (0.5 μm) through Kenyon cells above the calyx. HDAC4^{3SA} expression was observed, and nuclear aggregates formed that varied in size and number between the driver conditions.

10.4.4.5. Aggregates in Kenyon cells resulting from HDAC4^{3SA} expression under the control of *OK107-GAL4* +TARGET are within nuclei

As a low level of cytoplasmic distribution of HDAC4^{3SA} was noted by both fractionation and presence in the mushroom body lobes, it was essential to confirm that the HDAC4^{3SA} aggregates in Kenyon cells were within nuclei. Immunohistochemistry was performed on brains of flies expressing HDAC4^{3SA} under the control of *OK107-GAL4* +TARGET to examine aggregation relative to the localisation of lamin, which marks the nuclear lamina on the interior of the nuclear envelope, and DAPI, which binds double stranded DNA and tends to be observed at a higher intensity in regions of heterochromatin (Chiolo *et al.*, 2011; Imai *et al.*, 2017)(Figure 10.44). Flies were raised at 18°C until eclosion, then transferred to 30°C for three days to induce HDAC4^{3SA} expression. HDAC4^{3SA} was observed within the boundary of the nuclear envelope as marked by lamin, and did not co-localise with intense DAPI foci (Figure 10.44B). Nuclear aggregates did not appear to displace DAPI. Larger aggregates were observed toward the periphery of the nucleus and some of these distorted the nuclear lamina (Figure 10.44C) but were never observed outside of it.

These data confirm the nuclear localisation of HDAC4^{3SA} aggregates, but also illustrate that HDAC4^{3SA} can be detected within axons, and therefore has a cytoplasmic distribution too. In light of this, performing immunoprecipitation on nuclear fractions was considered to be the most appropriate method to enrich for the nuclear pool of HDAC4 and identify the composition of HDAC4 aggregates.

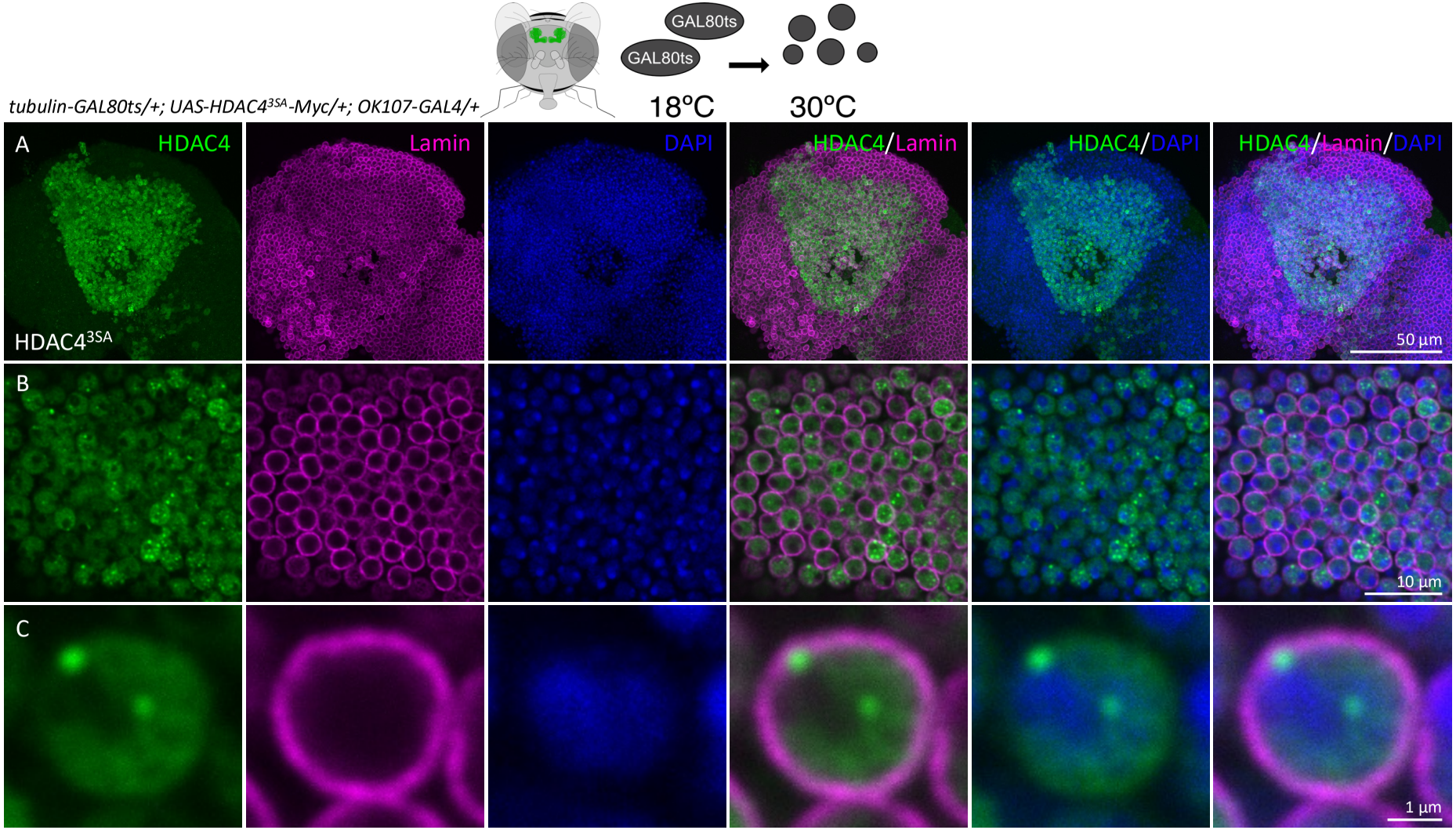

Figure 10.44 HDAC4^{3SA} aggregates are within the bounds of the nuclear envelope in Kenyon cells

(A-C) Immunohistochemistry on the posterior of brains expressing *HDAC4^{3SA}* under the control of *OK107-GAL4* in the presence of the TARGET system. Flies were raised at 18°C until eclosion, where adults were transferred to 30°C for three days to induce HDAC4 expression. Control is *tubulin-GAL80ts/+; OK107-GAL4/+*. (A) Maximum projection of optical sections (0.5 µm) through the Kenyon cell layer of the brain. Lamin (magenta) marks the nuclear envelope while

DAPI (blue) marks double stranded DNA. HDAC4^{3SA} (green) showed localisation to Kenyon cell nuclei and absence from the calyx. (B) Single optical section (0.5 μm) through Kenyon cells above the calyx. HDAC4^{3SA} expression was observed and localised within the lamin boundary and formed nuclear aggregates. HDAC4^{3SA} was absent from intense regions of DAPI staining. (C) Magnified section through a single Kenyon cell showed that HDAC4^{3SA} foci did not occur outside the lamin boundary, but sometimes deformed the edge of the nuclear envelope.

10.4.5. Identification of interactors of nuclear-restricted HDAC4 in Kenyon cells

Table 10.4 Candidate interactors of HDAC4^{3SA} from the secondary mass spectrometry analysis

FlyBase ID	Gene name	Gene symbol	#PSMs in Control	#PSMs in HDAC4 3SA	Fold change
FBgn0000047	Actin 88F	Act88F	685	1394	2.0
FBgn0039897	-	CG1674	51	162	3.2
FBgn0013348	Troponin C at 41C	TpnC41C	76	160	2.1
FBgn0283427	Fatty acid synthase 1	FASN1	71	145	2.0
FBgn0266599	Heat shock protein 70 cognate 4	Hsc70-4	45	92	2.0
FBgn0003890	beta-Tubulin at 97EF	betaTub97EF	26	68	2.6
FBgn0263289	scribble	scrib	32	64	2.0
FBgn0003261	Rm62	Rm62	24	62	2.6
FBgn0052528	parvin	parvin	15	44	2.9
FBgn0011640	lark	lark	19	43	2.3
FBgn0027560	Trehalose-6-phosphate synthase 1	Tps1	19	39	2.1
FBgn0011296	lethal (2) essential for life	l(2)efl	14	36	2.6
FBgn0010397	Lamin C	LamC	11	34	3.1
FBgn0035978	UDP-glucose pyrophosphorylase	UGP	9	33	3.7
FBgn0028427	Integrin linked kinase	Ilk	10	33	3.3
FBgn0039114	Lipid storage droplet-1	Lsd-1	16	33	2.1
FBgn0261797	Dynein heavy chain 64C	Dhc64C	13	28	2.2
FBgn0021906	Rieske iron-sulfur protein	RFeSP	13	28	2.2
FBgn0020908	Sarcoplasmic calcium-binding protein 1	Scp1	13	27	2.1
FBgn0037146	Delta[1]-pyrroline-5-carboxylate synthase	P5CS	11	26	2.4
FBgn0033246	Acetyl-CoA carboxylase	ACC	12	26	2.2
FBgn0024754	Flotillin 1	Flo1	7	21	3.0
FBgn0266448	-	CG45078	0	20	-
FBgn0005671	Vacuolar H[+]-ATPase 55kD subunit	Vha55	5	19	3.8
FBgn0020503	Cytoplasmic linker protein 190	CLIP-190	7	19	2.7

FBgn0259210	prominin	prom	7	19	2.7
FBgn0040078	pontin	pont	8	19	2.4
FBgn0266557	kismet	kis	9	19	2.1
FBgn0004828	Histone H3.3B	His3.3B	0	18	-
FBgn0267435	chaoptin	chp	7	18	2.6
FBgn0013263	Trithorax-like	Trl	8	18	2.3
FBgn0041210	Histone deacetylase 4	HDAC4	0	17	-
FBgn0031977	barrier to autointegration factor	baf	8	17	2.1
FBgn0028544	-	Vajk3	7	16	2.3
FBgn0000116	Arginine kinase 1	Argk1	8	16	2.0
FBgn0001218	Heat shock protein 70 cognate 3	Hsc70-3	8	16	2.0
FBgn0010774	RNA and export factor binding protein 1	Ref1	4	15	3.8
FBgn0260439	Protein phosphatase 2A at 29B	Pp2A-29B	6	15	2.5
FBgn0020279	lingerer	lig	0	13	-
FBgn0038617	WD repeat domain 37	Wdr37	4	13	3.3
FBgn0002622	Ribosomal protein S3	RpS3	2	12	6.0
FBgn0262737	mushroom-body expressed	mub	5	12	2.4
FBgn0051664	-	CG31664	6	12	2.0
FBgn0027835	Dodeca-satellite-binding protein 1	Dp1	6	12	2.0
FBgn0050069	SAXO downstream of blistered	Sdb	3	11	3.7
FBgn0038826	Syncrip	Syp	3	11	3.7
FBgn0011570	capping protein beta	cpb	4	11	2.8
FBgn0027567	Ciz1 zinc finger protein	Ciz1	4	11	2.8
FBgn0002031	Prohibitin 1	Phb1	5	11	2.2
FBgn0014269	proliferation disrupter	prod	5	11	2.2
FBgn0001233	Heat shock protein 83	Hsp83	3	10	3.3
FBgn0020496	C-terminal Binding Protein	CtBP	4	10	2.5
FBgn0035060	Epidermal growth factor receptor pathway substrate clone 15	Eps-15	5	10	2.0
FBgn0033883	Mitochondrial trans-2-enoyl-CoA reductase	Mecr	5	10	2.0
FBgn0001216	Heat shock protein 70 cognate 1	Hsc70-1	0	9	-
FBgn0033194	Vacuolar protein sorting 13	Vps13	0	9	-
FBgn0015268	Nucleosome assembly protein 1	Nap1	3	9	3.0
FBgn0020513	PAICS bifunctional enzyme	Paics	3	9	3.0
FBgn0266917	Splicing factor 3a subunit 1	Sf3a1	3	9	3.0
FBgn0016047	no mechanoreceptor potential A	nompA	4	9	2.3
FBgn0263832	Reduction in Cnn dots 5	Rcd5	4	9	2.3
FBgn0038946	retinol dehydrogenase B	rdhB	4	9	2.3
FBgn0260934	par-1	par-1	2	8	4.0
FBgn0263106	DnaJ-like-1	DnaJ-1	3	8	2.7

FBgn0040066	will die slowly	wds	3	8	2.7
FBgn0032783	-	CG10237	4	8	2.0
FBgn0013749	ADP ribosylation factor 4	Arf4	4	8	2.0
FBgn0001942	eukaryotic translation initiation factor 4A	eIF4A	4	8	2.0
FBgn0050147	Hillarin	Hil	4	8	2.0
FBgn0038072	-	CG6225	0	7	-
FBgn0260972	alicorn	alc	0	7	-
FBgn0025777	homer	homer	0	7	-
FBgn0034646	Rae1	Rae1	0	7	-
FBgn0037958	-	CG6962	3	7	2.3
FBgn0036022	-	CG8329	3	7	2.3
FBgn0263979	Chromatin assembly factor 1, p55 subunit	Caf1-55	3	7	2.3
FBgn0028577	half pint	hfp	3	7	2.3
FBgn0038774	-	CG5023	0	6	-
FBgn0031913	-	CG5958	0	6	-
FBgn0002940	neither inactivation nor afterpotential E	ninaE	0	6	-
FBgn0020249	steamer duck	stck	0	6	-
FBgn0261563	wing blister	wb	0	6	-
FBgn0021760	chromosome bows	chb	2	6	3.0
FBgn0259685	crumbs	crb	2	6	3.0
FBgn0038145	DnaJ-like-2	Droj2	2	6	3.0
FBgn0028671	Vacuolar H[+] ATPase 100kD subunit 1	Vha100-1	2	6	3.0
FBgn0051368	-	CG31368	3	6	2.0
FBgn0285926	IGF-II mRNA-binding protein	Imp	3	6	2.0
FBgn0010051	Inositol 1,4,5,-trisphosphate receptor	Itpr	3	6	2.0
FBgn0039743	JIL-1 anchoring and stabilizing protein	Jasper	3	6	2.0
FBgn0034797	nahoda	nahoda	3	6	2.0
FBgn0035541	-	CG15019	0	5	-
FBgn0031908	-	CG5177	0	5	-
FBgn0261802	-	CG42748	0	5	-
FBgn0262562	-	CG43102	0	5	-
FBgn0086346	ALG-2 interacting protein X	ALiX	0	5	-
FBgn0015019	Chaperonin containing TCP1 subunit 3	CCT3	0	5	-
FBgn0019624	Cytochrome c oxidase subunit 5A	COX5A	0	5	-
FBgn0001122	G protein alpha subunit o	Galphao	0	5	-
FBgn0034598	Insulator su(Hw) mRNA adaptor	Isha	0	5	-
FBgn0027338	karyopherin alpha3	Kap-alpha3	0	5	-
FBgn0035754	Mediator complex subunit 4	MED4	0	5	-
FBgn0287186	scarecrow	scro	0	5	-

FBgn0261789	Small ribonucleoprotein particle protein SmD2	SmD2	0	5	-
FBgn0027779	Vacuolar H[+]-ATPase SFD subunit	VhaSFD	0	5	-
FBgn0261562	-	CG42676	2	5	2.5
FBgn0019830	congested-like trachea	colt	2	5	2.5
FBgn0033260	Cullin 4	Cul4	2	5	2.5
FBgn0027553	NELF-B	NELF-B	2	5	2.5
FBgn0032782	Rab9	Rab9	2	5	2.5
FBgn0262125	Secretory 23	Sec23	2	5	2.5
FBgn0031057	Ubiquilin	Ubqn	2	5	2.5
FBgn0037213	-	CG12581	0	4	-
FBgn0033250	-	CG14762	0	4	-
FBgn0033434	-	CG1902	0	4	-
FBgn0034488	2-hydroxyacyl-CoA lyase	Hacl	0	4	-
FBgn0027348	bubblegum	bgm	0	4	-
FBgn0010621	Chaperonin containing TCP1 subunit 5	CCT5	0	4	-
FBgn0020309	crooked legs	crol	0	4	-
FBgn0036258	eukaryotic translation initiation factor 3 subunit l	eIF3l	0	4	-
FBgn0026439	Excitatory amino acid transporter 1	Eaat1	0	4	-
FBgn0085451	hat-trick	htk	0	4	-
FBgn0026418	Heat shock protein 110	Hsp110	0	4	-
FBgn0051184	Like Sm 3	LSm3	0	4	-
FBgn0036581	Mediator complex subunit 10	MED10	0	4	-
FBgn0002789	Muscle protein 20	Mp20	0	4	-
FBgn0039909	NADH dehydrogenase (ubiquinone) 49 kDa subunit	ND-49	0	4	-
FBgn0052230	NADH dehydrogenase (ubiquinone) MLRQ subunit	ND-MLRQ	0	4	-
FBgn0002930	necrotic	nec	0	4	-
FBgn0024542	Neosin	Neos	0	4	-
FBgn0264975	Neuroglian	Nrg	0	4	-
FBgn0036184	PCI domain-containing protein 2	PCID2	0	4	-
FBgn0044419	Pmi	Pmi	0	4	-
FBgn0039227	polybromo	polybromo	0	4	-
FBgn0034968	Ribosomal protein L12	RpL12	0	4	-
FBgn0003256	rolled	rl	0	4	-
FBgn0031493	Splicing factor 3b subunit 2	Sf3b2	0	4	-
FBgn0028863	stolid	stol	0	4	-
FBgn0262736	Vacuolar H[+] ATPase 16kD subunit 1	Vha16-1	0	4	-
FBgn0039269	veli	veli	0	4	-
FBgn0042111	-	CG18766	2	4	2.0

FBgn0032495	-	CG16820	2	4	2.0
FBgn0032010	-	CG8086	2	4	2.0
FBgn0053303	-	CG33303	2	4	2.0
FBgn0030451	-	CG15717	2	4	2.0
FBgn0034420	-	CG10737	2	4	2.0
FBgn0015331	abstrakt	abs	2	4	2.0
FBgn0262716	Actin-related protein 3	Arp3	2	4	2.0
FBgn0016120	ATP synthase, subunit D	ATPsynD	2	4	2.0
FBgn0000377	crooked neck	crn	2	4	2.0
FBgn0014163	failed axon connections	fax	2	4	2.0
FBgn0052082	Insulin receptor substrate 53 kDa	IRSp53	2	4	2.0
FBgn0027378	MORF-related gene 15	MRG15	2	4	2.0
FBgn0029868	NADH dehydrogenase (ubiquinone) B16.6 subunit	ND-B16.6	2	4	2.0
FBgn0037230	Neprilysin-like 11	Nepl11	2	4	2.0
FBgn0032393	Nfs1 cysteine desulfurase	Nfs1	2	4	2.0
FBgn0259243	Protein kinase, cAMP-dependent, regulatory subunit type 1	Pka-R1	2	4	2.0
FBgn0015799	Retinoblastoma-family protein	Rbf	2	4	2.0
FBgn0038834	Ribosomal protein S30	RpS30	2	4	2.0
FBgn0050296	RIC3 acetylcholine receptor chaperone	RIC-3	2	4	2.0
FBgn0283500	Sac1 phosphatase	Sac1	2	4	2.0
FBgn0286784	Transitional endoplasmic reticulum 94	TER94	2	4	2.0
FBgn0285910	Vacuolar H[+] ATPase AC39 subunit 1	VhaAC39-1	2	4	2.0
FBgn0028879	white walker	wwk	2	4	2.0
FBgn0265180	-	CG44245	0	3	-
FBgn0035033	-	CG3548	0	3	-
FBgn0030625	-	CG5877	0	3	-
FBgn0037016	-	CG13252	0	3	-
FBgn0264894	-	CG44085	0	3	-
FBgn0053098	-	CG33098	0	3	-
FBgn0032218	-	CG5381	0	3	-
FBgn0030870	-	CG6398	0	3	-
FBgn0029861	-	CG3815	0	3	-
FBgn0000083	Annexin B9	AnxB9	0	3	-
FBgn0031089	asperous	aspr	0	3	-
FBgn0004580	Calbindin 53E	Cbp53E	0	3	-
FBgn0022943	cap binding protein 20	Cbp20	0	3	-
FBgn0003676	Chaperonin containing TCP1 subunit 1	CCT1	0	3	-
FBgn0032444	Chaperonin containing TCP1 subunit 4	CCT4	0	3	-
FBgn0025724	Coat Protein (coatomer) beta'	beta'COP	0	3	-

FBgn0028968	Coat Protein (coatomer) gamma	gammaCOP	0	3	-
FBgn0028382	cyclophilin-33	cyp33	0	3	-
FBgn0289579	Dihydrolipoamide dehydrogenase	Dld	0	3	-
FBgn0052016	eIF4E-Transporter	4E-T	0	3	-
FBgn0266758	Extended synaptotagmin-like protein 2	Esyt2	0	3	-
FBgn0039667	F-box involved in polyQ pathogenesis	FipoQ	0	3	-
FBgn0004623	G protein beta subunit 76C	Gbeta76C	0	3	-
FBgn0004507	Glycogen phosphorylase	Glyp	0	3	-
FBgn0034511	GNBP-like 3	GNBP-like3	0	3	-
FBgn0032494	Juvenile hormone binding protein 13	Jhbp13	0	3	-
FBgn0032484	kekkon 4	kek4	0	3	-
FBgn0002121	lethal (2) giant larvae	l(2)gl	0	3	-
FBgn0038578	Mediator complex subunit 17	MED17	0	3	-
FBgn0037301	Mms19	Mms19	0	3	-
FBgn0034091	mrj	mrj	0	3	-
FBgn0023509	Myb-interacting protein 130	mip130	0	3	-
FBgn0038609	Nucleoporin 43kD	Nup43	0	3	-
FBgn0264307	orb2	orb2	0	3	-
FBgn0034789	Phosphatidylinositol 4-phosphate 5-kinase 59B	PIP5K59B	0	3	-
FBgn0003074	Phosphoglucose isomerase	Pgi	0	3	-
FBgn0026380	Proteasome beta3 subunit	Prosbeta3	0	3	-
FBgn0002284	Proteasome beta6 subunit	Prosbeta6	0	3	-
FBgn0285937	Rab1	Rab1	0	3	-
FBgn0031868	Rat1 5'-3' exoribonuclease	Rat1	0	3	-
FBgn0026375	Rho GTPase activating protein p190	RhoGAPp190	0	3	-
FBgn0016715	Rhythmically expressed gene 2	Reg-2	0	3	-
FBgn0051374	sarcomere length short	sals	0	3	-
FBgn0086357	Sec61 alpha subunit	Sec61alpha	0	3	-
FBgn0014029	Septin 2	Septin2	0	3	-
FBgn0038398	sex-specific enzyme 2	sxe2	0	3	-
FBgn0036843	Sideroflexin 2	Sfxn2	0	3	-
FBgn0038810	Signal recognition particle 72	Srp72	0	3	-
FBgn0029975	spidey	spidey	0	3	-
FBgn0015818	Spliceosomal protein on the X	Spx	0	3	-
FBgn0034936	Stomatin like 2	Stoml2	0	3	-
FBgn0010278	Structure specific recognition protein	Ssrp	0	3	-
FBgn0014028	Succinate dehydrogenase, subunit B (iron-sulfur)	SdhB	0	3	-
FBgn0003607	Suppressor of variegation 205	Su(var)205	0	3	-
FBgn0039900	Synaptotagmin 7	Syt7	0	3	-

FBgn0010417	TBP-associated factor 6	Taf6	0	3	-
FBgn0030365	Transport and Golgi organization 4	Tango4	0	3	-
FBgn0023518	trithorax-related	trr	0	3	-
FBgn0011327	Ubiquitin carboxy-terminal hydrolase L5	Uch-L5	0	3	-
FBgn0035147	UDP-galactose 4'-epimerase	Gale	0	3	-
FBgn0027492	widerborst	wdb	0	3	-
FBgn0029990	-	CG2233	0	2	-
FBgn0038146	-	CG9799	0	2	-
FBgn0034027	-	CG8187	0	2	-
FBgn0034030	-	CG8192	0	2	-
FBgn0038058	-	CG5608	0	2	-
FBgn0052407	-	CG32407	0	2	-
FBgn0051207	-	CG31207	0	2	-
FBgn0259715	-	CG42369	0	2	-
FBgn0034417	-	CG15117	0	2	-
FBgn0033989	-	CG7639	0	2	-
FBgn0034403	-	CG18190	0	2	-
FBgn0031377	-	CG15356	0	2	-
FBgn0031914	-	CG5973	0	2	-
FBgn0032685	-	CG10211	0	2	-
FBgn0030081	-	CG7246	0	2	-
FBgn0030100	-	CG12106	0	2	-
FBgn0031023	-	CG14200	0	2	-
FBgn0032690	-	CG10333	0	2	-
FBgn0263355	-	CG31688	0	2	-
FBgn0053138	1,4-Alpha-Glucan Branching Enzyme	AGBE	0	2	-
FBgn0031437	Actin-related protein 2/3 complex, subunit 5	Arpc5	0	2	-
FBgn0030089	Adaptor Protein complex 1, gamma subunit	AP-1gamma	0	2	-
FBgn0023169	AMP-activated protein kinase alpha subunit	AMPKalpha	0	2	-
FBgn0029095	arouser	aru	0	2	-
FBgn0015609	Cadherin-N	CadN	0	2	-
FBgn0012051	Calpain-A	CalpA	0	2	-
FBgn0029093	cathepsin D	cathD	0	2	-
FBgn0004779	Ccp84Ae	Ccp84Ae	0	2	-
FBgn0027329	Chaperonin containing TCP1 subunit 6	CCT6	0	2	-
FBgn0015621	Clipper	Clp	0	2	-
FBgn0025725	Coat Protein (coatomer) alpha	alphaCOP	0	2	-
FBgn0010808	Coiled-coil-helix-coiled-coil-helix domain containing 3	Chchd3	0	2	-

FBgn0036680	Cuticular protein 73D	Cpr73D	0	2	-
FBgn0033188	Death resistor Adh domain containing target	Drat	0	2	-
FBgn0000447	Dihydroorotate dehydrogenase	Dhod	0	2	-
FBgn0001108	Dynactin 1, p150 subunit	DCTN1-p150	0	2	-
FBgn0005640	Ecdysone-induced protein 63E	Eip63E	0	2	-
FBgn0011217	effete	eff	0	2	-
FBgn0037305	Enolase-phosphatase	Enoph	0	2	-
FBgn0261609	eukaryotic translation initiation factor 2 subunit alpha	eIF2alpha	0	2	-
FBgn0034858	eukaryotic translation initiation factor 2B subunit delta	eIF2Bdelta	0	2	-
FBgn0023512	eukaryotic translation initiation factor 2B subunit epsilon	eIF2Bepsilon	0	2	-
FBgn0015218	eukaryotic translation initiation factor 4E1	eIF4E1	0	2	-
FBgn0005632	fat facets	faf	0	2	-
FBgn0027657	globin 1	glob1	0	2	-
FBgn0001112	Glucose dehydrogenase	Gld	0	2	-
FBgn0001124	Glutamate oxaloacetate transaminase 1	Got1	0	2	-
FBgn0262117	Integrator 3	IntS3	0	2	-
FBgn0039081	Inwardly rectifying potassium channel 2	Irk2	0	2	-
FBgn0036004	Jumonji, AT rich interactive domain 2	Jarid2	0	2	-
FBgn0039155	Kallmann syndrome 1	Kal1	0	2	-
FBgn0027596	Kank	Kank	0	2	-
FBgn0001316	klarsicht	klar	0	2	-
FBgn0261618	La related protein	larp	0	2	-
FBgn0010238	Lachesin	Lac	0	2	-
FBgn0086451	lethal (2) k09022	l(2)k09022	0	2	-
FBgn0263605	lethal (3) 72Dn	l(3)72Dn	0	2	-
FBgn0261068	Like Sm 7	LSm7	0	2	-
FBgn0030608	Lipid storage droplet-2	Lsd-2	0	2	-
FBgn0031759	Lysine demethylase 5	Kdm5	0	2	-
FBgn0262782	Malate dehydrogenase 1	Mdh1	0	2	-
FBgn0034962	MAN1	MAN1	0	2	-
FBgn0024326	MAP kinase kinase 4	Mkk4	0	2	-
FBgn0010100	Mitochondrial aconitase 1	mAcon1	0	2	-
FBgn0038662	Mitochondrial pyruvate carrier	Mpc1	0	2	-
FBgn0028530	mitochondrial transcription termination factor	mTTF	0	2	-
FBgn0011661	Moesin	Moe	0	2	-
FBgn0013576	mustard	mtd	0	2	-
FBgn0031505	NADH dehydrogenase (ubiquinone) B14.5 B subunit	ND-B14.5B	0	2	-

FBgn0034576	NADH dehydrogenase (ubiquinone) B14.7 subunit	ND-B14.7	0	2	-
FBgn0031145	Nuclear transport factor-2	Ntf-2	0	2	-
FBgn0010660	Nucleoporin 214kD	Nup214	0	2	-
FBgn0250871	papillote	pot	0	2	-
FBgn0013726	peanut	pnut	0	2	-
FBgn0260962	piccolo	pic	0	2	-
FBgn0030317	Pinkman	pkm	0	2	-
FBgn0036915	Precursor RNA processing 3	Prp3	0	2	-
FBgn0086134	Proteasome alpha2 subunit	Prosalpha2	0	2	-
FBgn0286818	Protein disulfide isomerase	Pdi	0	2	-
FBgn0011230	purity of essence	poe	0	2	-
FBgn0017558	Pyruvate dehydrogenase kinase	Pdk	0	2	-
FBgn0265597	radish	rsh	0	2	-
FBgn0031006	rapamycin-insensitive companion of Tor	rictor	0	2	-
FBgn0283666	Ras-associated protein 2-like	Rap2l	0	2	-
FBgn0265605	Ras-related protein interacting with calmodulin	Ric	0	2	-
FBgn0031814	real-time	retm	0	2	-
FBgn0003218	retinal degeneration B	rdgB	0	2	-
FBgn0014380	Rho-like	RhoL	0	2	-
FBgn0039218	RNA polymerase II, I and III subunit L	Polr2L	0	2	-
FBgn0038951	RNA polymerase III subunit F	Polr3F	0	2	-
FBgn0036697	rogdi	rogdi	0	2	-
FBgn0039152	Rootletin	Root	0	2	-
FBgn0266098	rugose	rg	0	2	-
FBgn0035471	Sc2	Sc2	0	2	-
FBgn0033339	Secretory 31	Sec31	0	2	-
FBgn0011259	Semaphorin 1a	Sema1a	0	2	-
FBgn0003380	Shaker	Sh	0	2	-
FBgn0011016	Signal sequence receptor beta	SsRbeta	0	2	-
FBgn0016978	small ribonucleoprotein particle U1 subunit 70K	snRNP-U1-70K	0	2	-
FBgn0264357	SNF4/AMP-activated protein kinase gamma subunit	SNF4Agamma	0	2	-
FBgn0032191	Sorting nexin 17	Snx17	0	2	-
FBgn0025571	Splicing factor 1	SF1	0	2	-
FBgn0262579	Sterile alpha and Armadillo motif	Sarm	0	2	-
FBgn0003612	Suppressor of variegation 2-10	Su(var)2-10	0	2	-
FBgn0031030	Tao	Tao	0	2	-
FBgn0003687	TATA binding protein	Tbp	0	2	-
FBgn0037792	TATA box-binding protein-associated factor RNA polymerase I subunit B	TAF1B	0	2	-

FBgn0010355	TBP-associated factor 1	Taf1	0	2	-
FBgn0022355	Transferrin 1	Tsf1	0	2	-
FBgn0026761	Trap1	Trap1	0	2	-
FBgn0035121	Tudor staphylococcal nuclease	Tudor-SN	0	2	-
FBgn0030733	Ubiquinol-cytochrome c reductase 14 kDa subunit	UQCR-14	0	2	-
FBgn0034061	Ubiquitin-fold modifier conjugating enzyme 1	Ufc1	0	2	-
FBgn0030354	Upf1 RNA helicase	Upf1	0	2	-
FBgn0028670	Vacuolar H[+] ATPase 100kD subunit 2	Vha100-2	0	2	-
FBgn0260987	verthandi	vtd	0	2	-
FBgn0003996	white	w	0	2	-
FBgn0261862	withered	whd	0	2	-
FBgn0260858	YKT6 v-SNARE	Ykt6	0	2	-
FBgn0005391	Yolk protein 2	Yp2	0	2	-

#PSMs, number of peptide spectrum matches. Candidate interactors of HDAC4^{3SA} are ordered first by #PSMs in HDAC4^{3SA}, then by fold change. HDAC4 is also included here, it is unclear whether peptides detected correspond to wild-type endogenous HDAC4 or HDAC4^{3SA}-Myc.

Table 10.5 HDAC4^{3SA} candidate interactors with annotations relating to HDAC4 overexpression-induced phenotypes

FlyBase ID	Gene symbol	Gene name	General neuronal	MB	Eye	Memory
FBgn0260972	alc	alicorn			1	
FBgn0023169	AMPKalpha	AMP-activated protein kinase alpha subunit	1		1	
FBgn0030089	AP-1gamma	Adaptor Protein complex 1, gamma subunit			1	
FBgn0013749	Arf4	ADP ribosylation factor 4			1	
FBgn0262716	Arp3	Actin-related protein 3		1		
FBgn0029095	aru	arouser				1
FBgn0015609	CadN	Cadherin-N	1	1		
FBgn0012051	CalpA	Calpain-A	1			
FBgn0267435	chp	chaoptin			1	
FBgn0259685	crb	crumbs			4	
FBgn0001108	DCTN1-p150	Dynactin 1, p150 subunit	1		2	
FBgn0261797	Dhc64C	Dynein heavy chain 64C	1	1	2	
FBgn0011217	eff	effete	1		1	
FBgn0041210	HDAC4	Histone deacetylase 4				1
FBgn0266599	Hsc70-4	Heat shock protein 70 cognate 4		1		
FBgn0285926	Imp	IGF-II mRNA-binding protein	1			

FBgn0010051	Itpr	Inositol 1,4,5,-trisphosphate receptor		1		
FBgn0266557	kis	kismet	1			
FBgn0001316	klar	klarsicht			1	
FBgn0011661	Moe	Moesin			4	
FBgn0002940	ninaE	neither inactivation nor afterpotential E			2	
FBgn0016047	nompA	no mechanoreceptor potential A	1			
FBgn0264975	Nrg	Neuroglian	2	1		
FBgn0264307	orb2	orb2				1
FBgn0259210	prom	prominin			1	
FBgn0266098	rg	rugose		1	1	
FBgn0026375	RhoGAPp190	Rho GTPase activating protein p190		1		
FBgn0031006	rictor	rapamycin-insensitive companion of Tor	1			
FBgn0263289	scrib	scribble			4	1
FBgn0287186	scro	scarecrow	1			
FBgn0086357	Sec61alpha	Sec61 alpha subunit	1			
FBgn0011259	Sema1a	Semaphorin 1a	1			
FBgn0003380	Sh	Shaker	1		1	
FBgn0003612	Su(var)2-10	Suppressor of variegation 2-10			1	
FBgn0031030	Tao	Tao		1		
FBgn0286784	TER94	Transitional endoplasmic reticulum 94	2			
FBgn0023518	trr	trithorax-related			1	
FBgn0028671	Vha100-1	Vacuolar H[+] ATPase 100kD subunit 1			1	
FBgn0260987	vtd	verthandi	1			
FBgn0003996	w	white				1

Annotation terms from GOTERM_BP_DIRECT (GOterm Biological process, via DAVID) were selected for relation to HDAC4 overexpression-induced phenotypes in the mushroom body, including reduced FasII intensity, eye phenotypes including surface morphology and rhabdomere development, and memory including long-term memory. Genes annotated for each term were pooled, and then terms were narrowed to minimise redundancy. A number of terms relating to cell polarity were included in the eye category due to the role of determination of apical/basal polarity in rhabdomere morphogenesis. General neuronal: regulation of neuron apoptotic process, axon extension, neuron remodeling, dendrite morphogenesis. MB, mushroom body: mushroom body development, axonal fasciculation. Memory: memory, long-term memory. Eye: compound eye development, compound eye morphogenesis, eye photoreceptor cell development, rhabdomere development, detection of visible light, establishment or maintenance of epithelial cell apical/basal polarity, establishment or maintenance of apical/basal cell polarity, maintenance of apical/basal cell polarity.

Table 10.6 HDAC4^{3SA} candidate interactors with annotations relating to splicing

FlyBase ID	Gene symbol	Gene name
FBgn0015331	abs	abstrakt
FBgn0022943	Cbp20	cap binding protein 20
FBgn0032690	CG10333	uncharacterised protein
FBgn0051368	CG31368	uncharacterised protein
FBgn0030625	CG5877	uncharacterised protein
FBgn0000377	crn	crooked neck
FBgn0028382	cyp33	cyclophilin-33
FBgn0027835	Dp1	Dodeca-satellite-binding protein 1
FBgn0261609	eIF2alpha	eukaryotic translation initiation factor 2 subunit alpha
FBgn0001942	eIF4A	eukaryotic translation initiation factor 4A
FBgn0015218	eIF4E1	eukaryotic translation initiation factor 4E1
FBgn0028577	hfp	half pint
FBgn0266599	Hsc70-4	Heat shock protein 70 cognate 4
FBgn0285926	Imp	IGF-II mRNA-binding protein
FBgn0011640	lark	lark
FBgn0051184	LSm3	Like Sm 3
FBgn0261068	LSm7	Like Sm 7
FBgn0262737	mub	mushroom-body expressed
FBgn0024542	Neos	Neosin
FBgn0264307	orb2	orb2
FBgn0036915	Prp3	Precursor RNA processing 3
FBgn0010774	Ref1	RNA and export factor binding protein 1
FBgn0003261	Rm62	Rm62
FBgn0025571	SF1	Splicing factor 1
FBgn0266917	Sf3a1	Splicing factor 3a subunit 1
FBgn0031493	Sf3b2	Splicing factor 3b subunit 2
FBgn0261789	SmD2	Small ribonucleoprotein particle protein SmD2
FBgn0016978	snRNP-U1-70K	small ribonucleoprotein particle U1 subunit 70K
FBgn0015818	Spx	Spliceosomal protein on the X
FBgn0038826	Syp	Syncrip
FBgn0030365	Tango4	Transport and Golgi organization 4
FBgn0030354	Upf1	Upf1 RNA helicase

GOTERM annotation terms (via DAVID) were selected for relation to splicing. Genes annotated for each term were pooled, and then terms were narrowed to minimise redundancy. Proteins were annotated to one or more of the following: Biological process: mRNA splicing via spliceosome, Biological process: regulation of alternative mRNA splicing, via spliceosome.

Table 10.7 HDAC4^{3SA} candidate interactors with annotations relating to protein homeostasis

FlyBase ID	Gene symbol	Gene name	Process
FBgn0001108	DCTN1-p150	Dynactin 1, p150 subunit	Export of mRNAs
FBgn0285926	Imp	IGF-II mRNA-binding protein	Export of mRNAs
FBgn0011661	Moe	Moesin	Export of mRNAs
FBgn0010660	Nup214	Nucleoporin 214kD	Export of mRNAs
FBgn0034646	Rae1	Rae1	Export of mRNAs
FBgn0052016	4E-T	eIF4E-Transporter	Translation
FBgn0051664	CG31664	uncharacterised protein	Translation
FBgn0027835	Dp1	Dodeca-satellite-binding protein 1	Translation
FBgn0261609	eIF2alpha	eukaryotic translation initiation factor 2 subunit alpha	Translation
FBgn0034858	eIF2Bdelta	eukaryotic translation initiation factor 2B subunit delta	Translation
FBgn0023512	eIF2Bepsilon	eukaryotic translation initiation factor 2B subunit epsilon	Translation
FBgn0036258	eIF3l	eukaryotic translation initiation factor 3 subunit l	Translation
FBgn0001942	eIF4A	eukaryotic translation initiation factor 4A	Translation
FBgn0015218	eIF4E1	eukaryotic translation initiation factor 4E1	Translation
FBgn0011640	lark	lark	Translation
FBgn0261618	larp	La related protein	Translation
FBgn0264307	orb2	orb2	Translation
FBgn0036184	PCID2	PCI domain-containing protein 2	Translation
FBgn0003261	Rm62	Rm62	Translation
FBgn0034968	RpL12	Ribosomal protein L12	Translation
FBgn0002622	RpS3	Ribosomal protein S3	Translation
FBgn0038834	RpS30	Ribosomal protein S30	Translation
FBgn0025725	alphaCOP	Coat Protein (coatomer) alpha	Protein trafficking
FBgn0030089	AP-1gamma	Adaptor Protein complex 1, gamma subunit	Protein trafficking
FBgn0013749	Arf4	ADP ribosylation factor 4	Protein trafficking
FBgn0262716	Arp3	Actin-related protein 3	Protein trafficking
FBgn0025724	beta'COP	Coat Protein (coatomer) beta'	Protein trafficking
FBgn0001108	DCTN1-p150	Dynactin 1, p150 subunit	Protein trafficking
FBgn0261797	Dhc64C	Dynein heavy chain 64C	Protein trafficking
FBgn0028968	gammaCOP	Coat Protein (coatomer) gamma	Protein trafficking
FBgn0285937	Rab1	Rab1	Protein trafficking
FBgn0262125	Sec23	Secretory 23	Protein trafficking
FBgn0033339	Sec31	Secretory 31	Protein trafficking
FBgn0032191	Snx17	Sorting nexin 17	Protein trafficking
FBgn0003676	CCT1	Chaperonin containing TCP1 subunit 1	Protein folding
FBgn0015019	CCT3	Chaperonin containing TCP1 subunit 3	Protein folding
FBgn0032444	CCT4	Chaperonin containing TCP1 subunit 4	Protein folding
FBgn0010621	CCT5	Chaperonin containing TCP1 subunit 5	Protein folding

FBgn0027329	CCT6	Chaperonin containing TCP1 subunit 6	Protein folding
FBgn0028382	cyp33	cyclophilin-33	Protein folding
FBgn0263106	DnaJ-1	DnaJ-like-1	Protein folding
FBgn0038145	Droj2	DnaJ-like-2	Protein folding
FBgn0001216	Hsc70-1	Heat shock protein 70 cognate 1	Protein folding
FBgn0001218	Hsc70-3	Heat shock protein 70 cognate 3	Protein folding
FBgn0266599	Hsc70-4	Heat shock protein 70 cognate 4	Protein folding
FBgn0026418	Hsc70Cb	Hsc70Cb	Protein folding
FBgn0001233	Hsp83	Heat shock protein 83	Protein folding
FBgn0011296	l(2)efl	lethal (2) essential for life	Protein folding
FBgn0034091	mrj	mrj	Protein folding
FBgn0286818	Pdi	Protein disulfide isomerase	Protein folding
FBgn0050296	RIC-3	RIC3 acetylcholine receptor chaperone	Protein folding
FBgn0026761	Trap1	Trap1	Protein folding
FBgn0033260	Cul4	Cullin 4	Protein refolding
FBgn0001216	Hsc70-1	Heat shock protein 70 cognate 1	Protein refolding
FBgn0001218	Hsc70-3	Heat shock protein 70 cognate 3	Protein refolding
FBgn0266599	Hsc70-4	Heat shock protein 70 cognate 4	Protein refolding
FBgn0011296	l(2)efl	lethal (2) essential for life	Protein refolding
FBgn0011217	eff	effete	UPP
FBgn0001942	eIF4A	eukaryotic translation initiation factor 4A	UPP
FBgn0005632	faf	fat facets	UPP
FBgn0260962	pic	piccolo	UPP
FBgn0011230	poe	purity of essence	UPP
FBgn0260439	Pp2A-29B	Protein phosphatase 2A at 29B	UPP
FBgn0086134	Prosalpha2	Proteasome alpha2 subunit	UPP
FBgn0026380	Prosbeta3	Proteasome beta3 subunit	UPP
FBgn0002284	Prosbeta6	Proteasome beta6 subunit	UPP
FBgn0286784	TER94	Transitional endoplasmic reticulum 94	UPP
FBgn0031057	Ubqn	Ubiquilin	UPP
FBgn0011327	Uch-L5	Ubiquitin carboxy-terminal hydrolase L5	UPP
FBgn0040066	wds	will die slowly	UPP
FBgn0264357	SNF4Agamma	SNF4/AMP-activated protein kinase gamma subunit	Autophagy
FBgn0286784	TER94	Transitional endoplasmic reticulum 94	Autophagy
FBgn0028671	Vha100-1	Vacuolar H[+] ATPase 100kD subunit 1	Autophagy
FBgn0027492	wdb	widerborst	Autophagy

GOTERM annotation terms (via DAVID) were selected for relation to processes involved in protein homeostasis. BP, biological process. CC, cellular component. Export of mRNAs: BP_RNA export from nucleus, BP_mRNA transport, CC_nuclear pore complex. Translation: BP_translational initiation, BP_translation, BP_cytoplasmic translation, BP_negative regulation of cytoplasmic translation, BP_negative regulation of translation, BP_positive regulation of cytoplasmic translation, BP_positive regulation of translation. Protein trafficking: BP_intracellular protein transport. Protein folding: BP_protein folding, BP_chaperone-mediated protein folding requiring cofactor, BP_chaperone-

mediated protein folding. Protein refolding: BP_protein refolding. UPP, ubiquitin proteasome pathway: BP_ubiquitin-dependent protein catabolic process, BP_proteasome-mediated ubiquitin-dependent protein catabolic process, BP_positive regulation of proteasomal ubiquitin-dependent protein catabolic process, CC_proteasome complex. Autophagy: BP_autophagy, BP_autophagosome maturation.

10.5. Supplementary data corresponding to Chapter 7

10.5.1. Western blots of HDAC4$^{N\text{-}term}$ expression used for intensity quantification

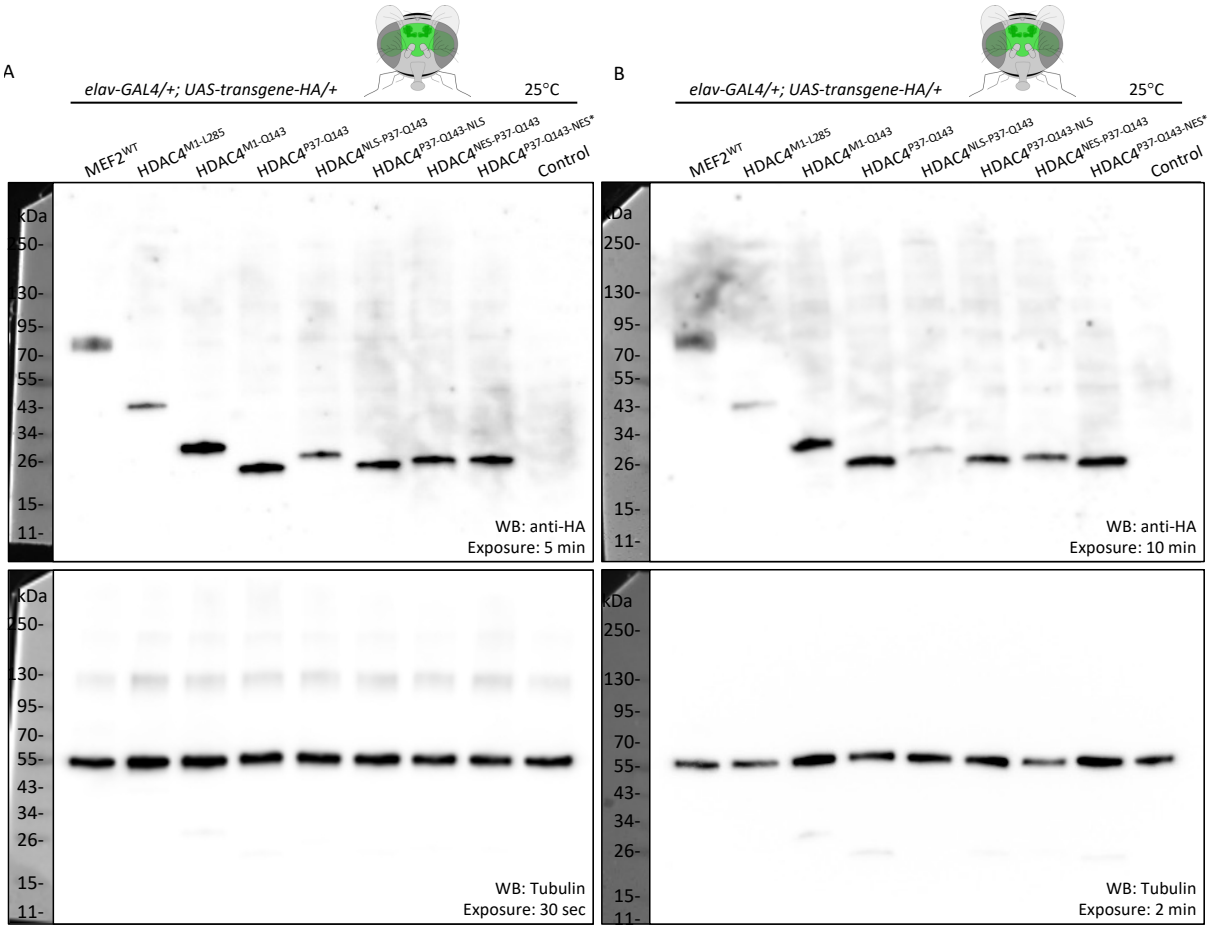

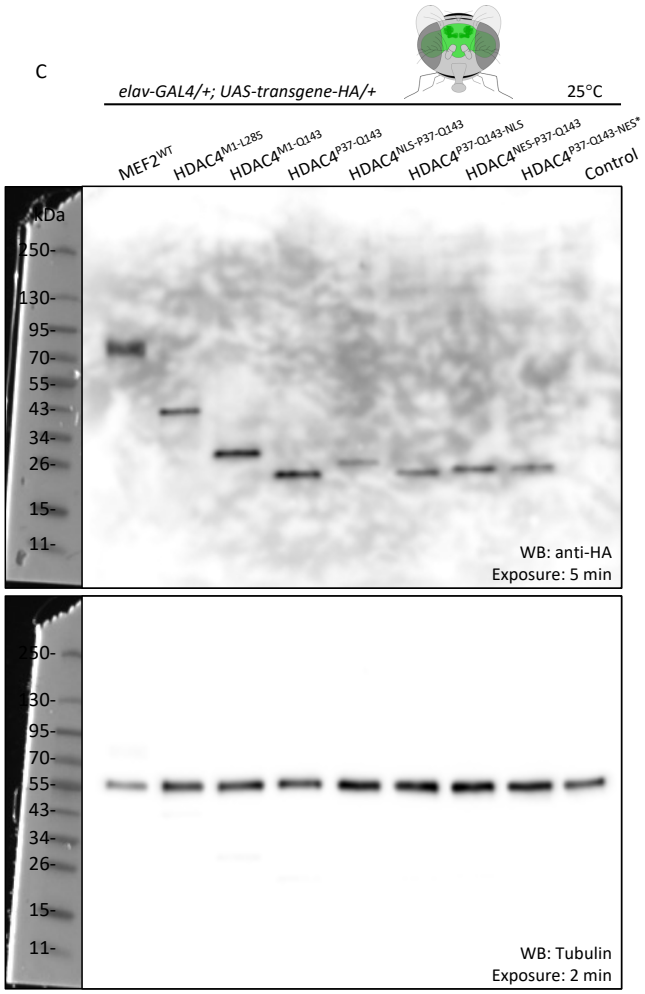

Figure 10.45 Full western blots of HDAC4$^{N\text{-}term}$ expression used for intensity quantification

(A-C) Western blots of *elav-GAL4* driven expression of HDAC4$^{N\text{-}term}$ in head whole-cell lysates (30 µg) using anti-HA and anti-alpha-tubulin antibodies. Flies were raised at 25°C. Control is *elav-GAL4/+*. MEF2-HA was included as a positive control. The expected molecular weight of the constructs are: MEF2-HA, 57.8 kDa; HDAC4$^{M1\text{-}L285}$, 35.9 kDa; HDAC4$^{M1\text{-}Q143}$, 20.4 kDa; HDAC4$^{P37\text{-}Q143}$, 16.5 kDa; HDAC4$^{NLS\text{-}P37\text{-}Q143}$, HDAC4$^{P37\text{-}Q143\text{-}NLS}$, HDAC4$^{NES\text{-}P37\text{-}Q143}$, HDAC4$^{P37\text{-}Q143\text{-}NES}$, 18.3 kDa. Arrows indicate non-specific bands consistently observed using this antibody at ~50 and ~85 kDa in all samples including the control. * denotes that this was the construct that was thought to be HDAC4$^{P37\text{-}Q143\text{-}NES}$, but was later found to be HDAC4$^{NES\text{-}P37\text{-}Q143}$.

10.5.2. Verification of *HDAC4$^{N\text{-}term}$*

Table 10.8 Primers used for PCR amplification of *HDAC4$^{N\text{-}term}$*

Primer pair	Sequence (5'-3')
pUAST	F: GCAACTACTGAAATCTGCCAAG
	R: TCATCAGTTCCATAGGTTGG

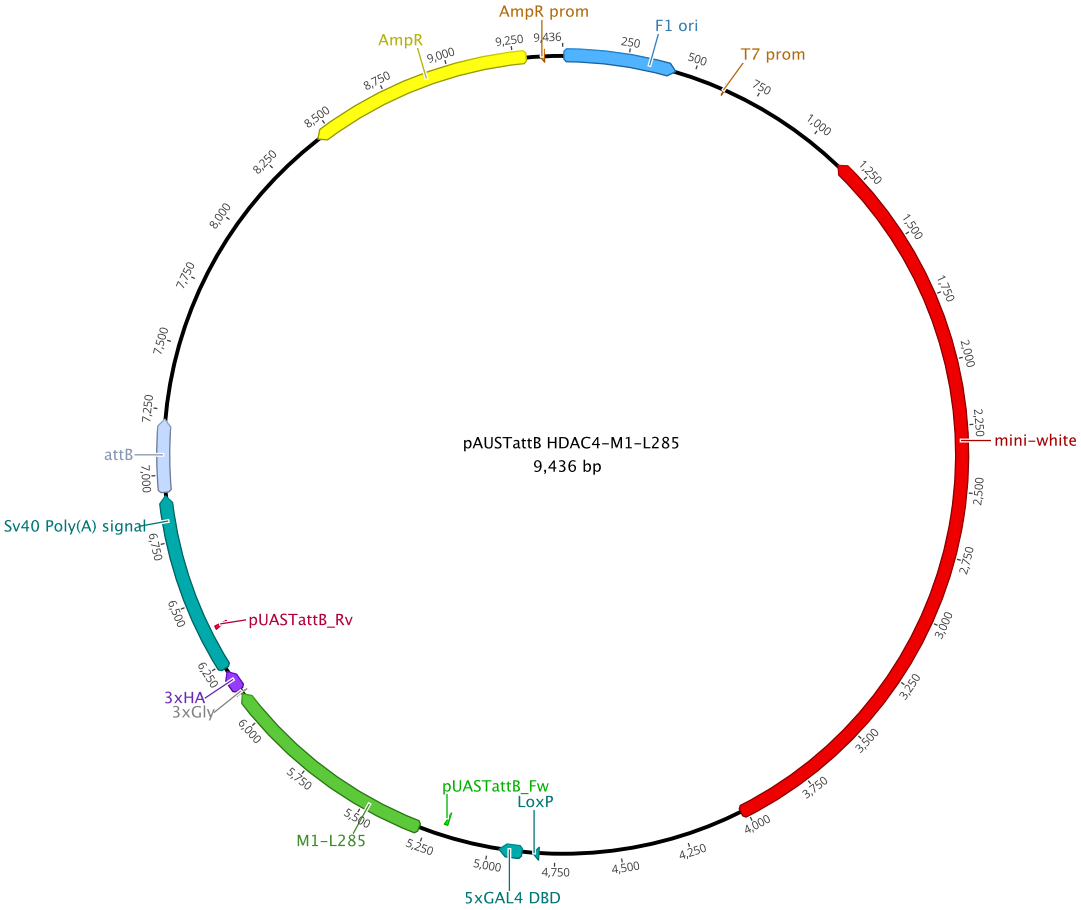
AmpR prom
AmpR
F1 ori
T7 prom
mini-white
pAUSTattB HDAC4-M1-L285
9,436 bp
attB
Sv40 Poly(A) signal
pUASTattB_Rv
3xHA
3xGly
M1-L285
pUASTattB_Fw
LoxP
5xGAL4 DBD

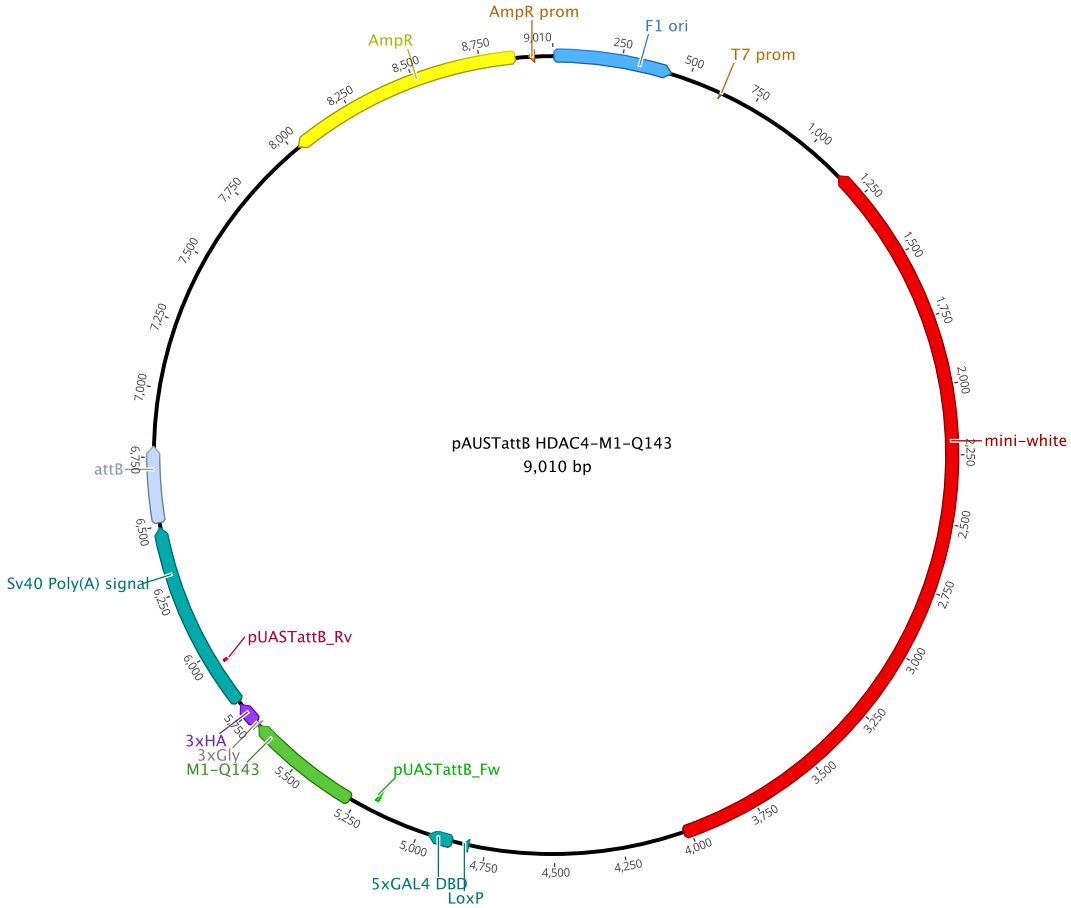
AmpR prom
AmpR
F1 ori
T7 prom
mini-white
pAUSTattB HDAC4-M1-Q143
9,010 bp
attB
Sv40 Poly(A) signal
pUASTattB_Rv
3xHA
3xGly
M1-Q143
pUASTattB_Fw
5xGAL4 DBD
LoxP

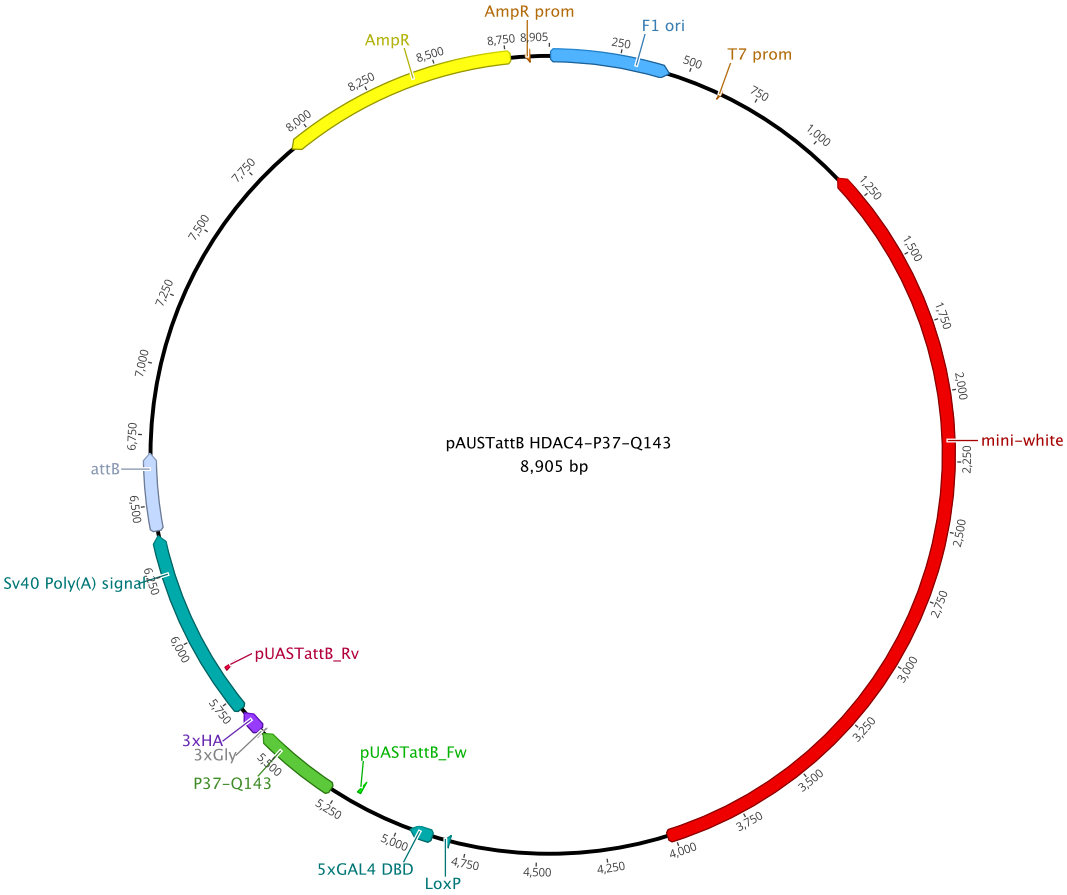
pAUSTattB HDAC4-P37-Q143
8,905 bp
AmpR prom
AmpR
F1 ori
T7 prom
mini-white
attB
Sv40 Poly(A) signal
pUASTattB_Rv
3xHA
3xGly
P37-Q143
pUASTattB_Fw
5xGAL4 DBD
LoxP

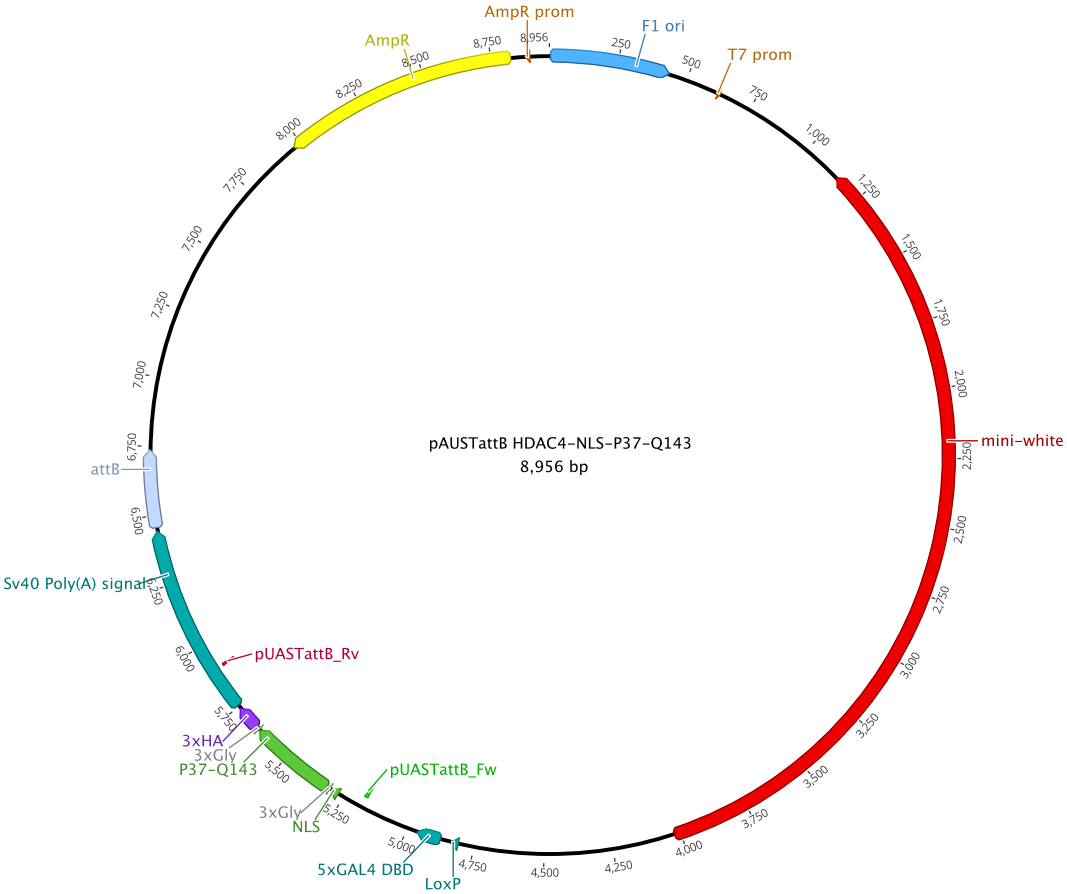
pAUSTattB HDAC4-NLS-P37-Q143
8,956 bp
AmpR prom
AmpR
F1 ori
T7 prom
mini-white
attB
Sv40 Poly(A) signal
pUASTattB_Rv
3xHA
3xGly
P37-Q143
pUASTattB_Fw
3xGly
NLS
5xGAL4 DBD
LoxP

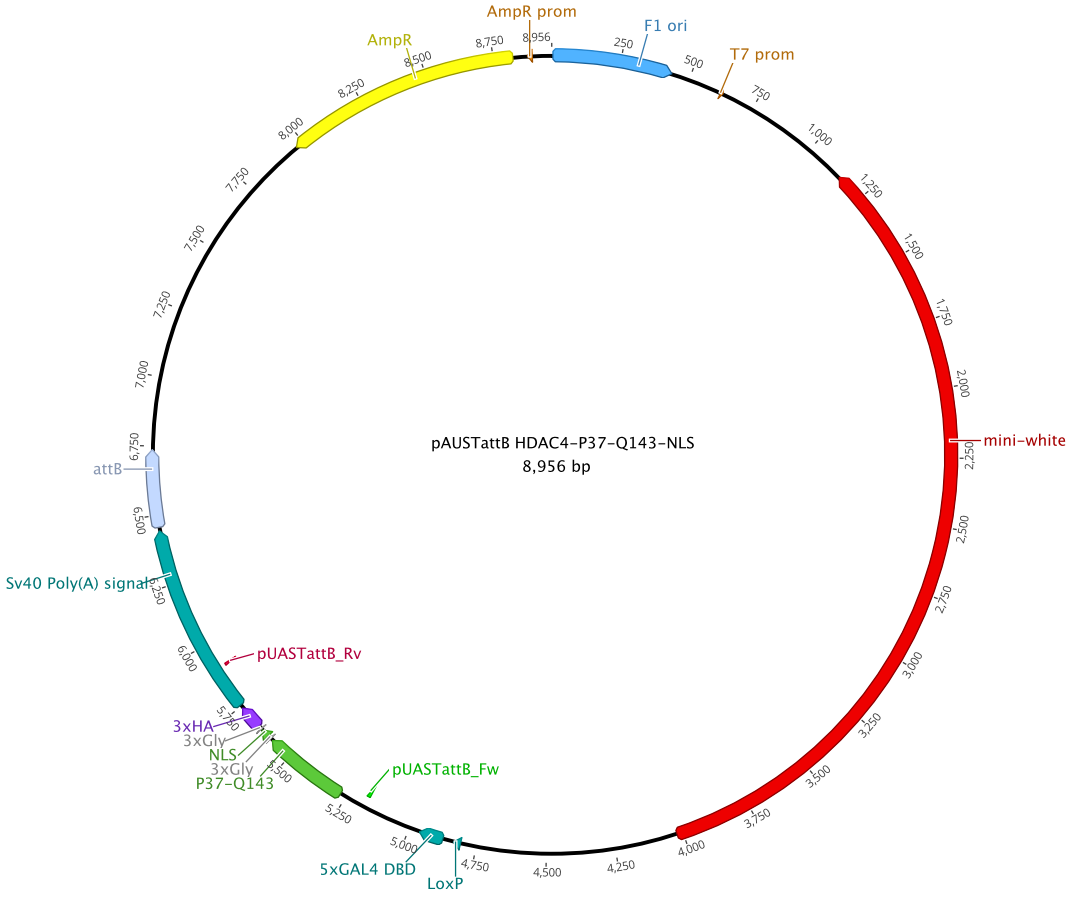
AmpR prom
F1 ori
T7 prom
AmpR
mini-white
pAUSTattB HDAC4-P37-Q143-NLS
8,956 bp
attB
Sv40 Poly(A) signal
pUASTattB_Rv
3xHA
3xGly
NLS
3xGly
P37-Q143
pUASTattB_Fw
5xGAL4 DBD
LoxP

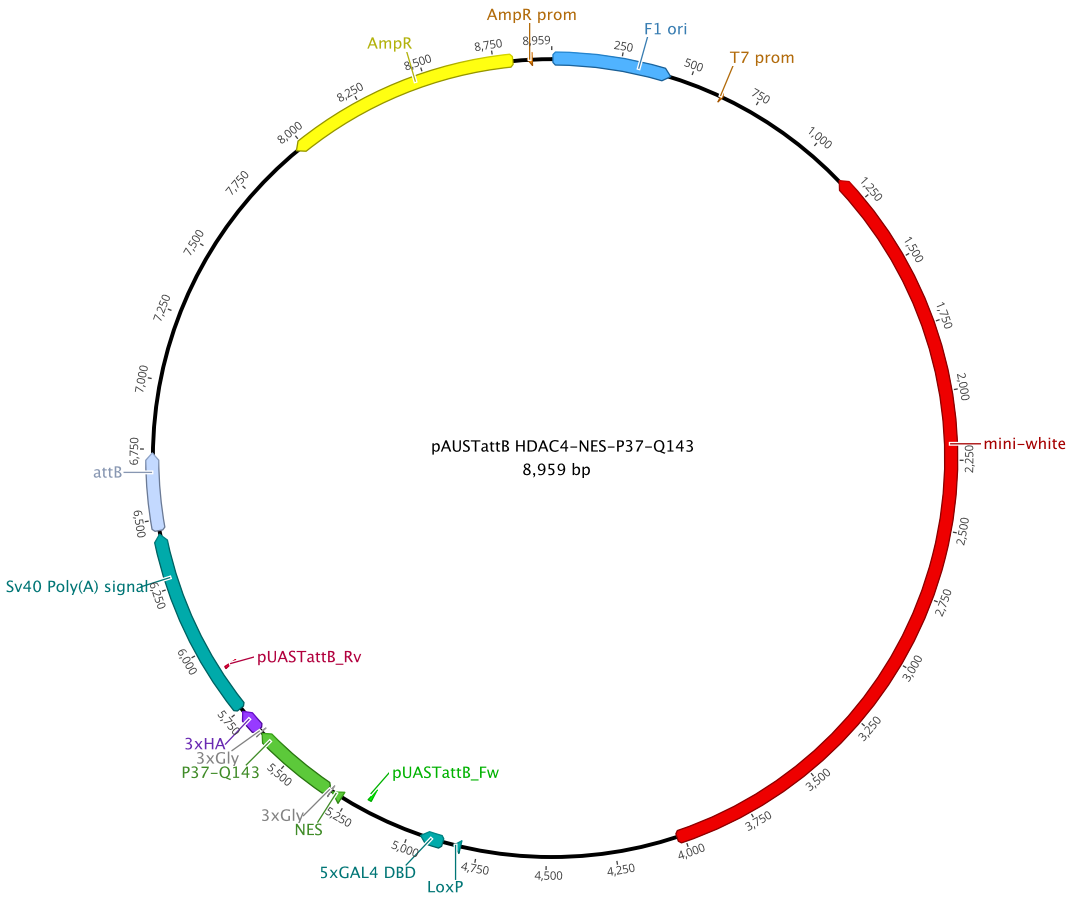
AmpR prom
F1 ori
T7 prom
AmpR
mini-white
pAUSTattB HDAC4-NES-P37-Q143
8,959 bp
attB
Sv40 Poly(A) signal
pUASTattB_Rv
3xHA
3xGly
P37-Q143
pUASTattB_Fw
3xGly
NES
5xGAL4 DBD
LoxP

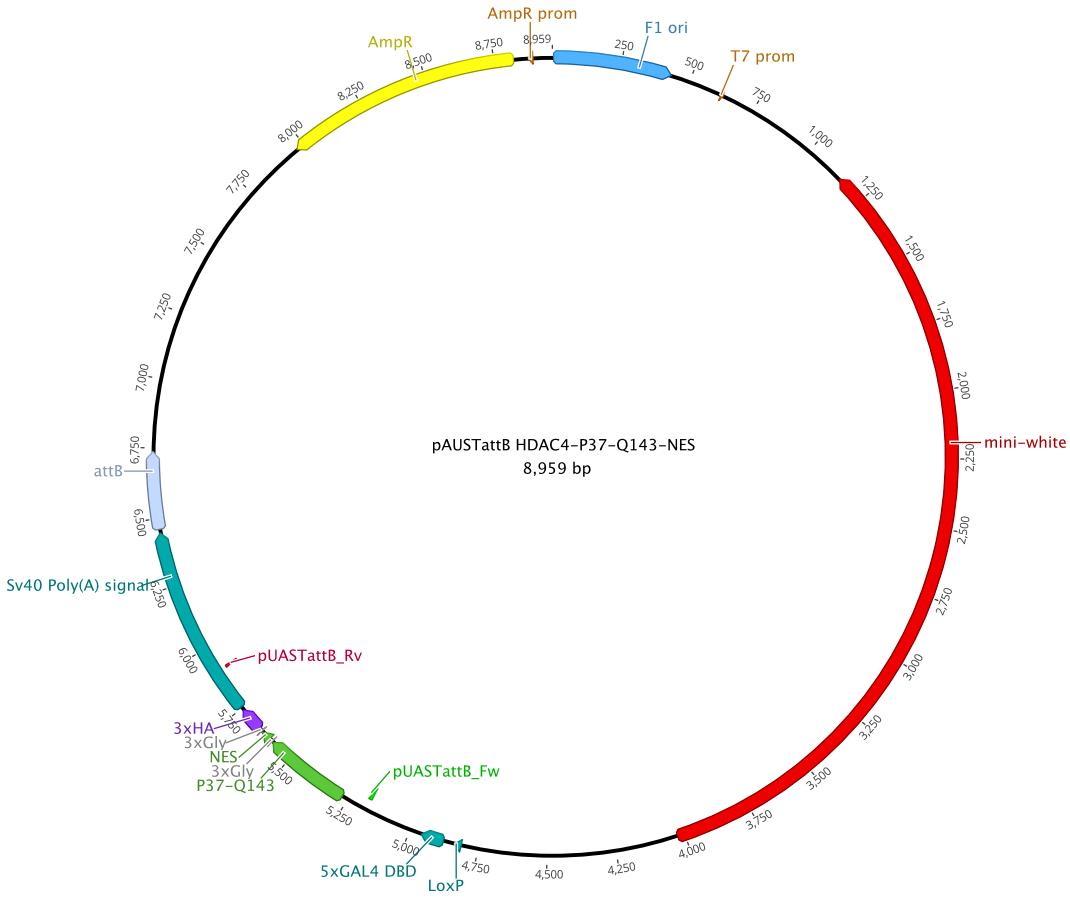

Figure 10.46 Plasmid maps of pUAST used to generate *HDAC4$^{N\text{-}term}$* constructs and notation of primer annealing sites for PCR amplification

Plasmid maps of pUASTattB HDAC4$^{N\text{-}term}$ with annotation of primer binding sites used for PCR amplification from genomic DNA in Figure 10.47. This plasmid was used to generate transgenic flies harbouring HDAC4$^{N\text{-}term}$ as described in Section 3.1.1, from which genomic DNA was extracted. Features of the plasmid important for generation of transgenic flies are noted, as well as the regions of *HDAC4* contained within the constructs, and the location of the exogenous NLS/NES sequences where applicable. Figure made in Geneious R9.

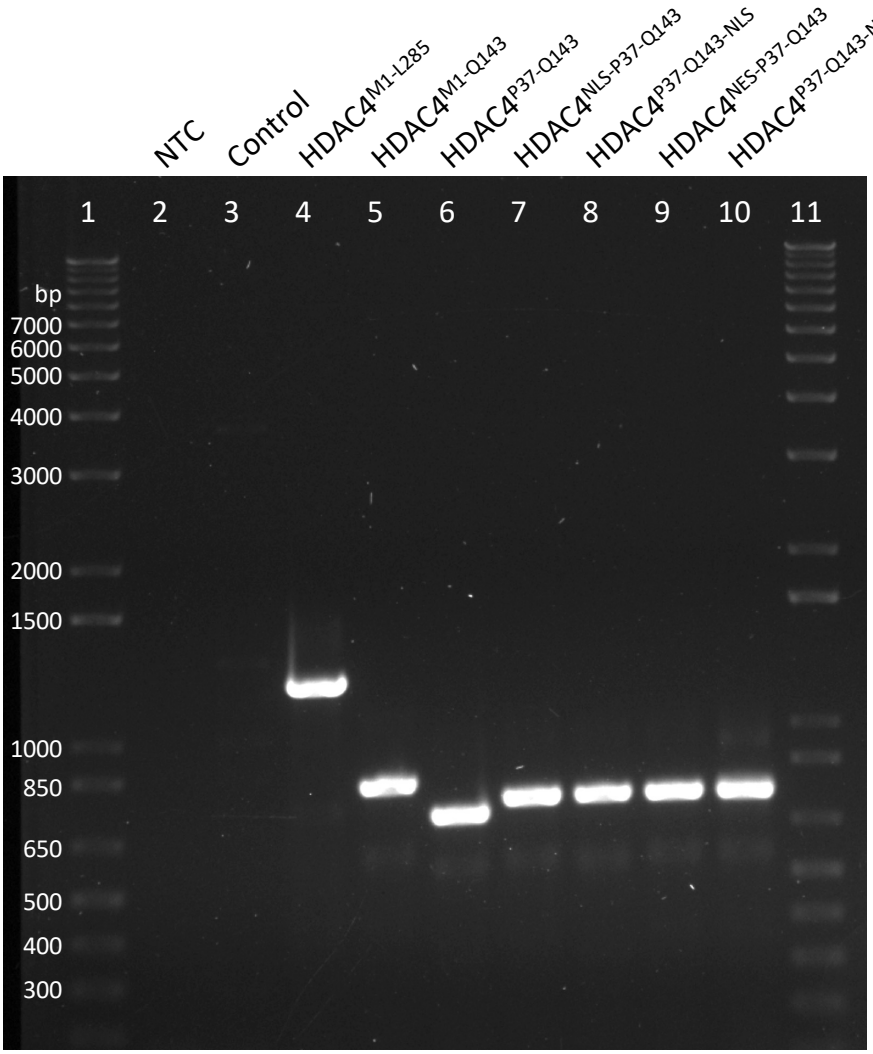

Figure 10.47 Agarose gel electrophoresis of *HDAC4$^{N\text{-}term}$* PCR products
Gel electrophoresis of PCR products amplified from genomic DNA extractions of flies that harboured each of the indicated *HDAC4$^{N\text{-}term}$* constructs. The forward primer annealed immediately upstream of the HDAC4$^{N\text{-}term}$ insertion and the reverse within the polyA tail region (Figure 10.46) therefore the amplicon incorporated the entire HDAC4$^{N\text{-}term}$ insertion. The expected size of each construct is as follows: *HDAC4$^{M1\text{-}L285}$*, 1226 bp; *HDAC4$^{M1\text{-}Q143}$*, 800 bp; *HDAC4$^{P37\text{-}Q143}$*, 695 bp; *HDAC4$^{NLS\text{-}P37\text{-}Q143}$*, 746 bp; *HDAC4$^{P37\text{-}Q143\text{-}NLS}$*, 746 bp; *HDAC4$^{NES\text{-}P37\text{-}Q143}$*, 749 bp; *HDAC4$^{P37\text{-}Q143\text{-}NES}$*, 749 bp. NTC, no template control. Control, negative control of PCR performed on flies that did not harbour *HDAC4$^{N\text{-}term}$* (wCS10, *Canton S white* flies). Ladder, 1 Kb Plus DNA Ladder (Invitrogen) with sizes indicated in base pairs (bp).

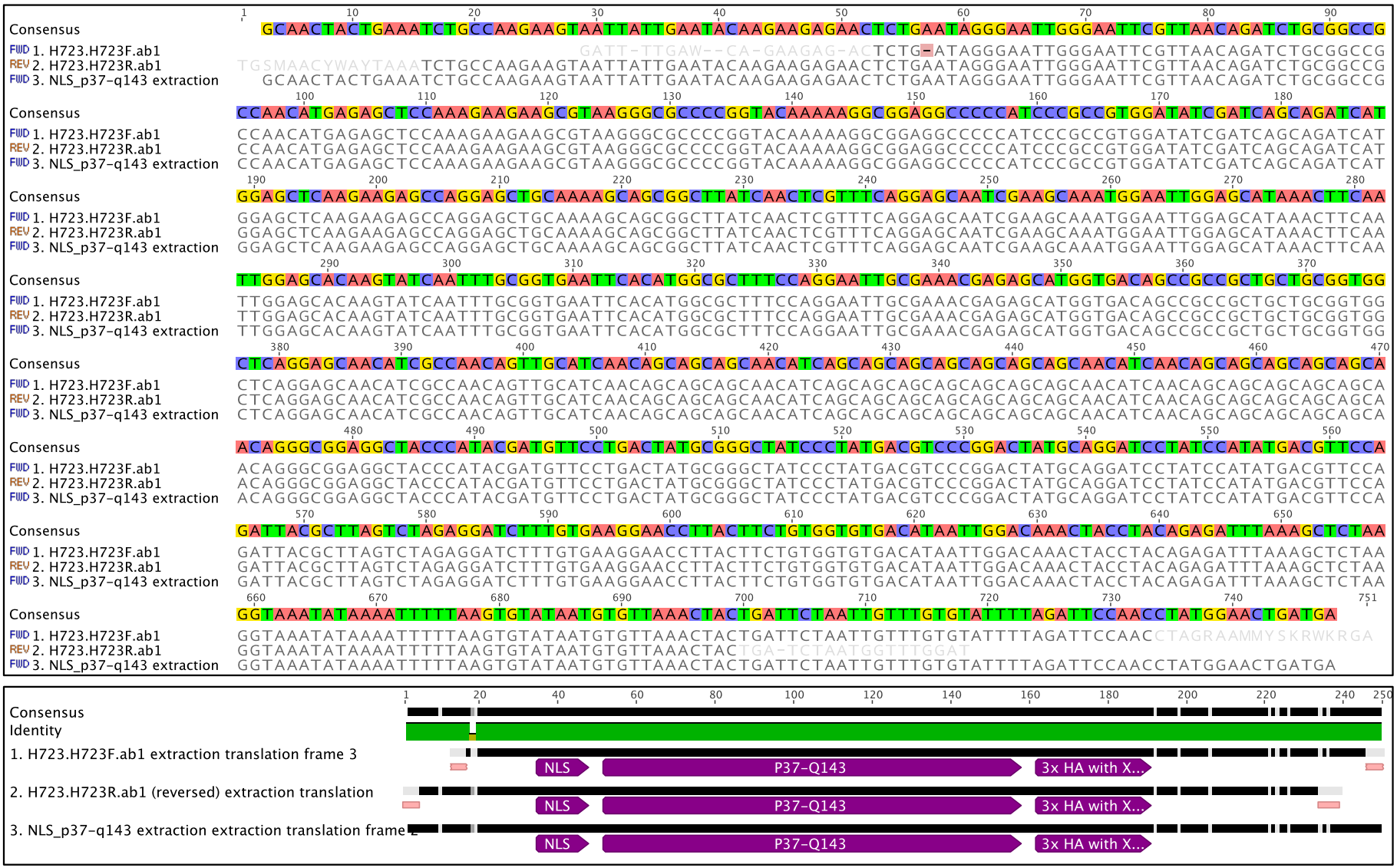
A
Consensus
FWD 1. H723.H723F.ab1
REV 2. H723.H723R.ab1
FWD 3. NLS_p37-q143 extraction
B
Consensus
Identity
1. H723.H723F.ab1 extraction translation frame 3
2. H723.H723R.ab1 (reversed) extraction translation
3. NLS_p37-q143 extraction extraction translation frame 2
NLS
P37-Q143
3x HA with X...

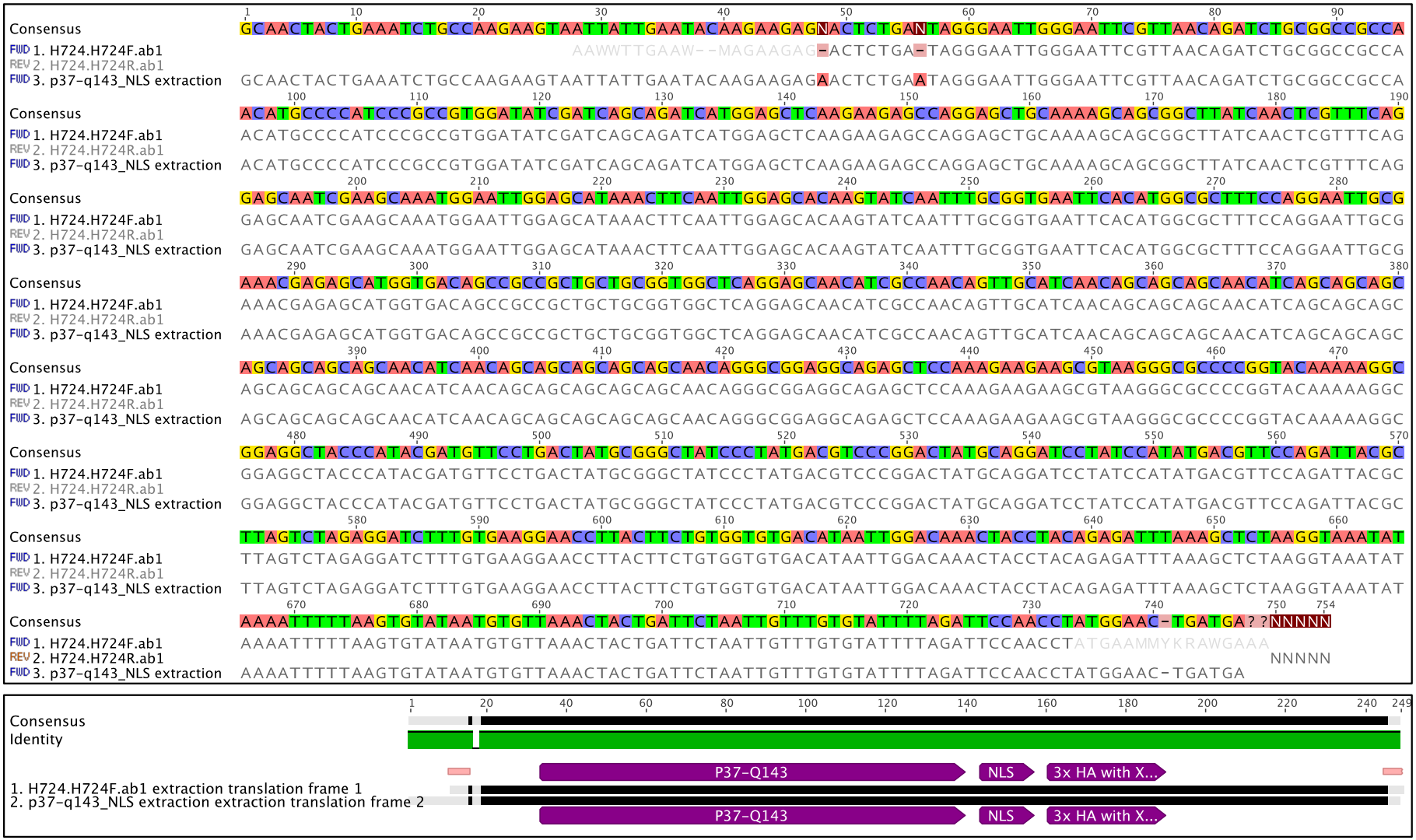
C
Consensus
FWD 1. H724.H724F.ab1
REV 2. H724.H724R.ab1
FWD 3. p37-q143_NLS extraction
D
Consensus
Identity
P37-Q143
NLS
3x HA with X...
1. H724.H724F.ab1 extraction translation frame 1
2. p37-q143_NLS extraction extraction translation frame 2

E
Consensus
FWD 1. H725.H725F.ab1
REV 2. H725.H725R.ab1
FWD 3. NES_p37-q143 extraction
F
Consensus
Identity
1. H725.H725F.ab1 extraction translation frame 1
2. H725.H725R.ab1 (reversed) extraction translation frame 3
3. NES_p37-q143 extraction extraction translation frame 2
NES
P37-Q143
3x HA with X...

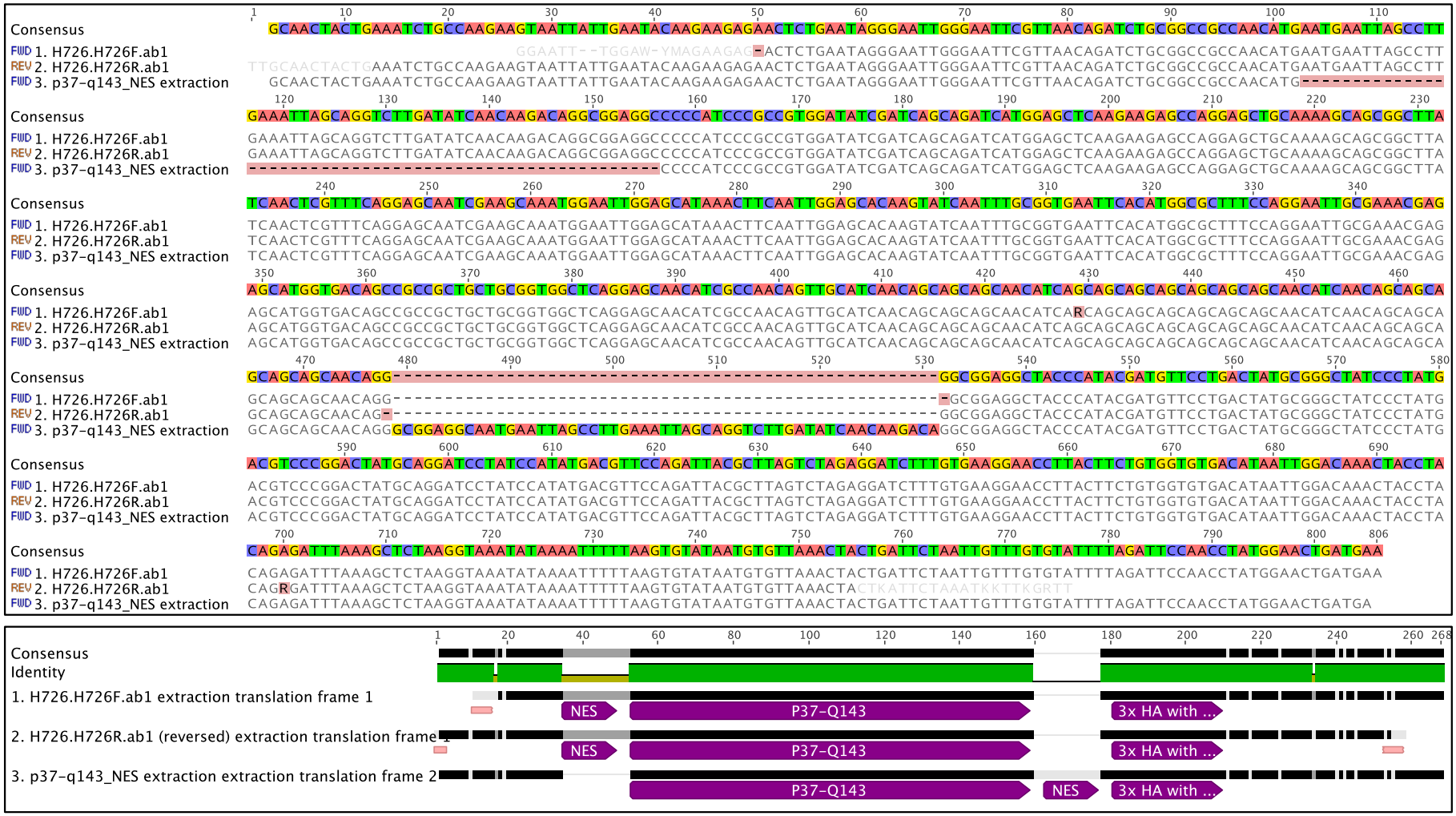

Figure 10.48 Verification *of HDAC4$^{N\text{-}term}$ NLS/NES*-containing construct sequences from genomic DNA

Pairwise alignment of expected (3) and obtained sequences (1-2) for *HDAC4$^{N\text{-}term}$* constructs containing an exogenous NLS or NES. The H-number indicates the stock number of the transgenic fly line sequenced as per Table 10.1. (A, C, E, G) Sequence alignment nucleotide view. The extraction (3) indicates the expected sequence obtained from PCR amplification using the pUAST primer pair. The pairwise identity for each construct was as follows: HDAC4$^{NLS\text{-}P37\text{-}Q143}$, 99.9%*; HDAC4$^{P37\text{-}Q143\text{-}NLS}$, 99.7%*; HDAC4$^{NES\text{-}P37\text{-}Q143}$, 99.9%*; HDAC4$^{P37\text{-}Q143\text{-}NES}$, 89.7%. *indicates that alignment was 100% over the HDAC4

open reading frame; the reduced sequence similarity was due to mismatches in sequencing upstream of *HDAC4*. The reverse sequence for HDAC4$^{P37\text{-}Q143\text{-}NLS}$ failed and is therefore not included. (B, D, F, H) Protein alignment summary showing annotation of the NLS/NES, P37-Q143 region, and the 3xHA tag. Sequences in obtained in A, C, E, and G were each translated, aligned, and annotated to show the location of domains. The lack of alignment of HDAC4$^{P37\text{-}Q143\text{-}NES}$ nucleotides 103-156 and 479-531 as per (H) showed that the NES was not found at the C-terminus of the construct, but was present at the N-terminus. Therefore, sequencing confirmed that H726 was actually HDAC4$^{NES\text{-}P37\text{-}Q143}$, not HDAC4$^{P37\text{-}Q143\text{-}NES}$. Blocks denote the mean pairwise identity: green, 100%; yellow, 30-100%; black line, gap in consensus. Red boxes note regions of automatic trimming at the ends of the sequence reads. Alignments were performed in Geneious R9, version 9.1.8 using Geneious alignment with default settings.

10.5.3. HDAC4$^{N\text{-}term}$ and HDAC4^{WT} distribution in Kenyon cells

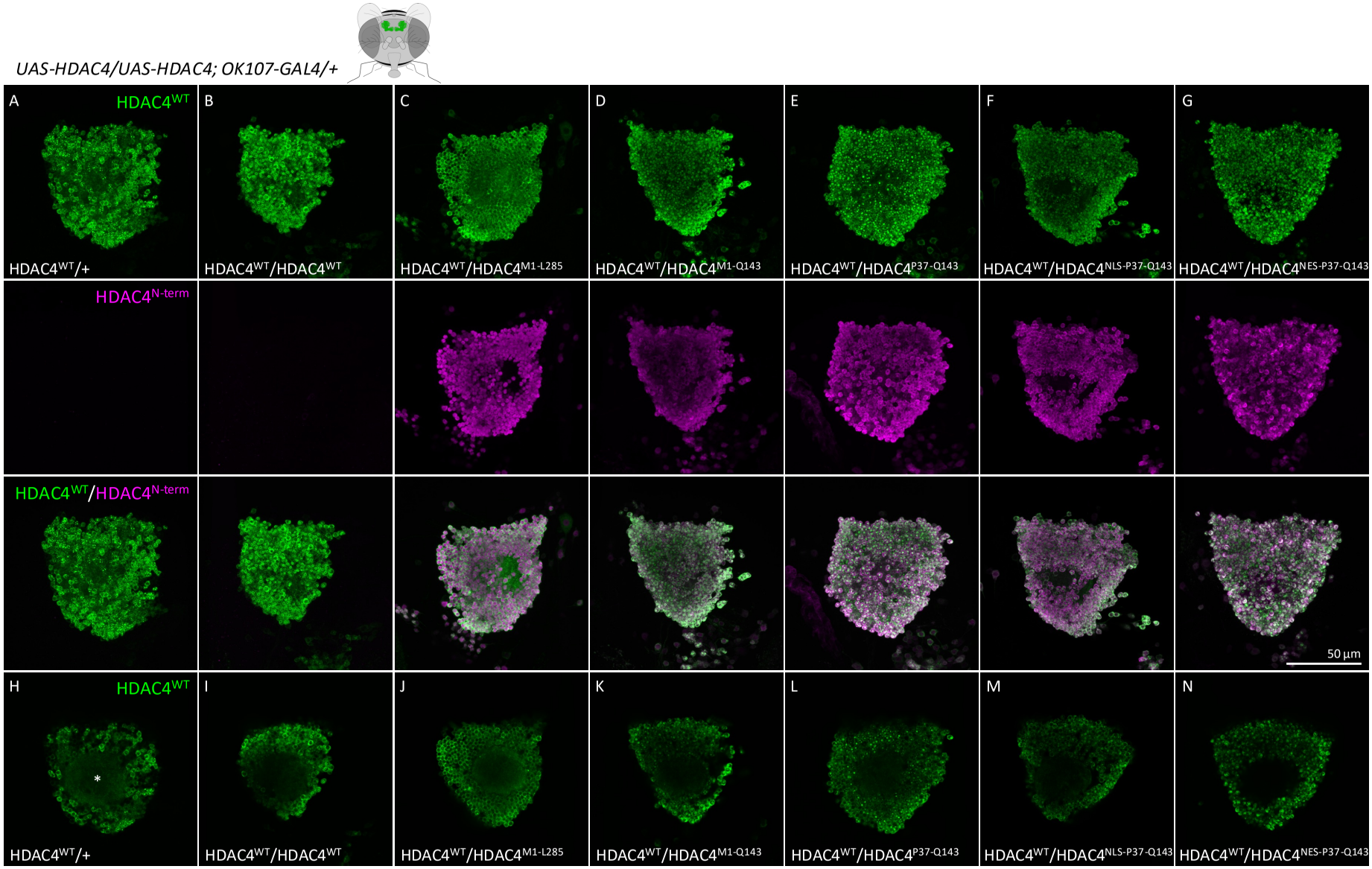

Figure 10.49 Co-expression of HDAC4$^{N\text{-}term}$ differentially affects the subcellular distribution of HDAC4^{WT} in Kenyon cells

(A-G) Maximum projections of optical sections (0.5 µm) through the posterior of the brain demonstrate *OK107-GAL4* driven expression of $HDAC4^{WT}$-Myc (green) and $HDAC4^{N\text{-}term}$-HA (magenta) in Kenyon cells. (H-N) Single optical sections (0.5 µm) through the mid-Kenyon cell layer demonstrate the varied distribution of $HDAC4^{WT}$ upon co-expression with $HDAC4^{N\text{-}term}$, especially in the calyx (*). Flies were raised at 18°C until adults eclosed, which were then transferred to 30°C for three days to induce transgene expression.